

The Cellular Response to Microenvironmental Stress in Barrett's Oesophagus



Christopher Mark Jones

A thesis submitted to the University of Leeds in accordance
with the requirements for the degree of Doctor of Philosophy

May 2021

School of Molecular & Cellular Biology
Faculty of Biological Sciences
University of Leeds

The candidate confirms that the work submitted is his own and that appropriate credit has been given where reference has been made to the work of others.

This copy has been supplied on the understanding that it is copyright material and that no quotation from the thesis may be published without proper acknowledgement.

The right of Christopher Mark Jones to be identified as Author of this work has been asserted by him in accordance with the Copyright, Designs and Patents Act 1988.

© 2021 The University of Leeds and Christopher Mark Jones

Acknowledgements

I am grateful to Wellcome Trust who funded this work via a Clinical Research Training Fellowship distributed from grant 203914/Z/16/Z jointly held by the Universities of Leeds, Manchester, Newcastle and Sheffield. I am also grateful for funding for this work provided by a Bramall Fellowship, by Cancer Research UK through a Pre-Doctoral Bursary Award and a Leeds Centre Future Leader Award and by the Pathological Society via a Small Project Grant jointly awarded to Dr Gordon Hutchins and myself. Finally, I acknowledge receipt of a British Association of Cancer Research NC3Rs training award, which contributed to the development of this work.

Throughout this PhD, I have been afforded considerable freedom to develop and pursue my own ideas. I am grateful to my supervisors - Professors John Ladbury, Andrew Sharrocks, Heike Grabsch and Nick West - for facilitating this independence whilst providing me with support when I have needed it. I am particularly indebted to John for his advice, feedback and encouragement; and for introducing me through his group's work to biophysical and structural biology research approaches that I would otherwise not have encountered. Together, this support and the insight I have received in to new techniques have undoubtedly catalysed my growth as a researcher over the course of this doctorate.

I also wish to extend my thanks to Dr Jax Bond for her exceptionally valuable guidance with technical aspects of the functional genomics screen, and to Sam Ogden and Dr Connor Rogerson for their support conducting, analysing and interpreting the RNA-seq and ATAC-seq aspects of this work. Equally, I am tremendously thankful to Dr Sophie Ketchen, Dr Chi-Chuan Lin, Dr Kin Man Suen, Amy Stainthorp, Eleanor Cawthorne and Dovile Milonaityte for their help and companionship both within, and outside of, the lab.

I would not have undertaken this doctorate, nor have set my sights on clinical academia, were it not for the unfailing mentorship I have received over the past decade from Professor Paul Stewart. I remain deeply indebted and grateful to him for the time and faith he has invested me. I would also perhaps not have reached the end of this doctorate were it not for the close support, advice and friendship of Associate Professors Katie Spencer and Niamh Forde, who have both considerably brightened my time in Leeds but who I suspect will both now be delighted to hear far less about Barrett's oesophagus.

On a personal level, I am deeply grateful for the support of my family; without whom none of this would be possible and from all of whom I have learnt the importance of hard work,

dedication and commitment. Above all else, I am grateful to Rach (who at times has probably felt more like my post-doctoral supervisor than partner) for her constant support at every stage of my career so far, even when between us we have grappled with childcare, a rather long commute and an unexpectedly challenging house renovation; and - with Olivia and, soon, Ralph – for reminding me of how much more important home and family are than work could ever be.

Christopher M. Jones, May 2021

Preface: COVID-19 impact statement

This thesis, and the work it incorporates, has been significantly impacted by the coronavirus disease 2019 (COVID-19) pandemic. The author is a clinician and returned to full-time clinical practice early in his third year of doctoral study, just prior to the first United Kingdom national lockdown period in March 2020. He remained in clinical practice until September 2020, whereafter access to the laboratory was restricted by COVID-19 safety protocols within the Leeds Institute of Cardiovascular & Metabolic Metabolism, University of Leeds to a maximum of 20 hours per week, with no additional out-of-hours access. These significant limitations on laboratory activity persisted until the completion of the author's doctoral studies.

Restrictions elsewhere in the University of Leeds (within the Leeds Institute of Research at St James's on the St James's University Hospital campus of The Leeds Teaching Hospitals NHS Trust) prohibited access to the Operetta microscope used for the siRNA screen described in this work, which prevented completion of a second validation screen. These same limitations to access on this site prevented the planned tissue validation of the data shown here, for which research ethics and governance approvals had been gained by the thesis author.

Further complicating progress, a number of experiments contained within this work were undertaken at the University of Manchester (including RNA-seq and ATAC-seq). No in-person visits to Manchester were possible following the onset of the COVID-19 pandemic, thereby restricting any further collaborative experiments using these techniques.

Finally, a repeat long-course experiment had been in progress at the time of the onset of the first UK national COVID-19-related lockdown. This involved treating cells once a day for five days a week over an intended 12 week period. These cells were sadly lost as a consequence of the restrictions imposed by the lockdown.

Abstract

The incidence of oesophageal adenocarcinoma (OAC) and its metaplastic precursor, Barrett's oesophagus (BO), has increased markedly over recent decades. This is attributed to an increase in the prevalence of environmental risk factors such as gastro-oesophageal reflux disease, which exposes the lower oesophagus to frequent pulses of an acidic, bile-salt containing refluxate. The mechanisms linking stressors that are common to the lower oesophageal micro-environment to the dysplastic progression of BO are, however, unclear. Here, we integrate gene expression, chromatin accessibility and kinase activity profiles to characterise the response of normal squamous epithelial (NSE), non-dysplastic (NDBO) and high-grade dysplastic (HGD) BO cell lines to microenvironmental stress; simulated by a ten minute pulse of bile salts at acidic or neutral pH, acid alone, and a 48-hour period of serum-starvation. We demonstrate that acidic bile salts and serum-starvation both recapitulate gene-regulatory and phenotypic changes that are associated with BO dysplastic progression. In NDBO cells, acidic bile salts result in a gene signature enriched for pro-migratory and pro-inflammatory T_h1 cytokine-mediated processes, whereas serum-starvation gives rise to a pro-autophagic, quiescent, transcriptional response. A number of transcription factors associated with BO dysplastic progression, such as KLF5 and NF- κ B, were linked to these transcriptional changes through analyses of differences in chromatin accessibility. Upstream, kinase activity profiling and a functional genomic screen implicated a number of receptor tyrosine kinases (RTKs) in the BO stress response; most notably including activation of EGFR in response to cytosolic pH normalisation following acid exposure, in a process regulated by acidic sphingomyelinase. These data, and existing evidence for an association of RTK co-overexpression with BO dysplastic progression, together highlight a potential role for a subset of RTKs in mediating the BO dysplastic phenotype in response to microenvironmental stress. This requires further validation but may provide novel biomarkers and targets for risk stratification and chemopreventative strategies in early BO.

Table of Contents

Acknowledgements	iii
Preface: COVID-19 impact statement	v
Abstract	vi
Table of Contents	vii
List of Tables	xi
List of Figures	xii
Chapter 1 Introduction	- 1 -
1.1 Barrett’s oesophagus: a precursor to oesophageal adenocarcinoma	- 1 -
1.1.1. Overview	- 1 -
1.1.2. The BO metaplasia-dysplasia-cancer sequence	- 8 -
1.2 Conceptual overview: stepwise neoplastic transformation and the role of microenvironmental stressors	- 36 -
1.3 Hypothesis	- 37 -
1.4 Aims	- 38 -
Chapter 2 Materials and Methods	- 39 -
2.1. Overview	- 39 -
2.2. Reagents & plasticware	- 39 -
2.3. Cell culture	- 39 -
2.3.1. Cell culture conditions.....	- 39 -
2.3.2. Cell lines	- 39 -
2.3.3. Cell proliferation, experimentation & maintenance	- 42 -
2.3.4. Cryopreservation & recovery	- 43 -
2.4. Protein analysis	- 43 -
2.4.1. Protein extraction	- 43 -
2.4.2. Protein quantification	- 44 -
2.4.3. Immunoblotting	- 45 -
2.5. Transcriptome analyses	- 47 -
2.5.1. RNA extraction & DNase digestion.....	- 47 -
2.5.2. Sample quantification & quality assurance.....	- 48 -
2.5.3. mRNA quantitation by qRT-PCR	- 48 -
2.5.4. RNA-seq.....	- 50 -
2.6. Chromatin accessibility assay	- 52 -

2.6.1. Assay for Transposase-Accessible Chromatin using sequencing (ATAC-seq).....	- 52 -
2.7. Bioinformatics	- 55 -
2.7.1. Enrichment analyses	- 55 -
2.7.2. Pathway and interaction determination	- 56 -
2.8. Viability assays	- 57 -
2.8.1. MTT assay.....	- 57 -
2.8.2. LIVE/DEAD® Viability/Cytotoxicity stain.....	- 57 -
2.8.3. CyQUANT™ Direct Cell Proliferation Assay	- 58 -
2.9. Statistical analyses and representation of data	- 58 -
2.9.1. Statistical analyses	- 58 -
2.9.2. Data representation & images	- 59 -
Chapter 3 Modelling Microenvironmental Stress & its Impact on the Barrett's Transcriptome	- 60 -
3.1. Background	- 60 -
3.1.1. Overview: the dysplastic progression of BO	- 60 -
3.2. Aims.....	- 67 -
3.3. Methods.....	- 67 -
3.3.1. Experimental outline	- 67 -
3.3.2. Treatments & cellular exposures	- 69 -
3.3.3. Functional enrichment	- 70 -
3.4. Results	- 71 -
3.4.1. Characterisation of the basal phenotype of the cell line model of BO	- 71 -
3.4.2. The comparative impact of bile salts at acidic and neutral pH, and acid alone, on the phenotype of cells representing NSE and BO	- 74 -
3.4.3. The comparative impact of serum-starvation on the phenotype of cells representing NSE and BO	- 80 -
3.4.4. The transcriptomic and regulomic response to microenvironmental stress in NDBO	- 83 -
3.5. Discussion	- 100 -
3.5.1. Validation of an <i>in vitro</i> model of BO	- 100 -
3.5.2. The impact of microenvironmental stressors on gene regulatory control	- 104 -
3.5.3. Strengths & limitations	- 109 -
3.6. Conclusions & further work.....	- 111 -
Chapter 4 A Systemic Analysis of the Basal & Stress- Responsive Barrett's Oesophagus Kinome	- 112 -
4.1. Background	- 112 -

4.1.1. Overview	- 112 -
4.1.2. The human kinome	- 113 -
4.1.3. The kinome in BO dysplastic progression	- 114 -
4.2. Aims.....	- 115 -
4.3. Methods.....	- 115 -
4.3.1. Experimental outline	- 115 -
4.3.2. Cell treatments.....	- 115 -
4.3.3. Protein kinase activity profiling.....	- 116 -
4.4. Results	- 122 -
4.4.1. Acidic bile salts result in a significant reduction in PTK but not STK phosphorylation across NSE (Het-1A), NDBO (CP-A) and HGD (CP-B) cell lines	- 122 -
4.4.2. Kinomic analysis of PTK and STK activity reveals a consensus response to acid withdrawal across NSE (Het-1A), NDBO (CP-A) and HGD (CP-B) cell lines	- 124 -
4.4.3. Validation of temporal changes in NDBO (CP-A) and HGD (CP-B) MAPK and PI3K/Akt/mTOR pathway phosphorylation in response to acidic bile salts	- 147 -
4.4.4. An exploration of the relative impact of bile salts on signalling	- 147 -
4.4.5. Upstream mediators of signalling in response to acid and acidic bile salts	- 149 -
4.5. Discussion	- 151 -
4.5.1. Strengths & limitations	- 156 -
4.6. Conclusions & further work.....	- 157 -
<i>Chapter 5 Delineating the RTK-mediated Response to Micro-Environmental Stress in Barrett's Oesophagus.....</i>	- 158 -
5.1. Background	- 158 -
5.1.1. Overview	- 158 -
5.1.2. Cell signalling by RTKs	- 159 -
5.1.3. RTKs in Barrett's and OAC	- 161 -
5.2. Aims.....	- 168 -
5.3. Methods.....	- 168 -
5.3.1. Experimental outline	- 168 -
5.3.2. Phospho-RTK array	- 169 -
5.3.3. Intracellular pH measurement	- 169 -
5.3.4. Oxidative stress detection.....	- 170 -
5.3.5. An siRNA-based functional genomics screen	- 171 -
5.3.6. Sphingomyelinase assays	- 176 -
5.4. Results	- 177 -
5.4.1. RTK activation under conditions of refluxate-exposure.....	- 177 -

5.4.2. RTK activity under stressed serum-starvation and basal proliferative conditions.....	- 185 -
5.4.3. ROS generation under conditions of serum-starvation	- 192 -
5.4.4. Expression of RTKs implicated in mediating the BO basal and stress-responsive phenotype in NSE (Het-1A), NDBO (CP-A) and HGD (CP-B) cells, and matched patient samples	- 192 -
5.5. Discussion	- 193 -
5.5.1. RTK activation under conditions of reflux-mediated stress	- 193 -
5.5.2. RTK control of cellular viability and morphology under basal and serum-starved conditions.....	- 196 -
5.5.3. Limitations.....	- 197 -
5.6. Conclusions & future work.....	- 198 -
<i>Chapter 6 Discussion & conclusions</i>	<i>- 199 -</i>
6.1. Discussion	- 199 -
6.2. Conclusions & further work.....	- 204 -
<i>List of References</i>	<i>- 206 -</i>
<i>List of Abbreviations</i>	<i>- 248 -</i>
<i>Appendix A List of suppliers & manufacturers.....</i>	<i>- 253 -</i>
<i>Appendix B List of antibodies for immunoblotting</i>	<i>- 254 -</i>
<i>Appendix C List of primers for qRT-PCR analyses.....</i>	<i>- 255 -</i>
<i>Appendix D Tyrosine Kinase PamChip®4 Microarray List of Peptide Substrates</i>	<i>- 256 -</i>
<i>Appendix E Serine/Threonine Kinase PamChip®4 Microarray List of Peptide Substrates.....</i>	<i>- 265 -</i>
<i>Appendix F PamGene® Evolve pTyr (PTK) Software Protocol</i>	<i>- 273 -</i>
<i>Appendix G PamGene® Evolve pSer/pThr (STK) Software Protocol</i>	<i>- 274 -</i>
<i>Appendix H Proteome Profiler Human Phospho-RTK Array Kit</i>	<i>- 275 -</i>
<i>Appendix I siGENOME SMARTpool siRNA targeting sequences.....</i>	<i>- 277 -</i>

List of Tables

Table	Page
1.1. A summary of risk factors for the development of BO and OAC.	5
1.2. A summary of luminal, stromal and humoral influences on the BO microenvironment and their relationship with risk factors and BO epithelial phenotype.	14
1.3. An overview of genes and non-coding elements that are implicated in OAC pathogenesis.	17
1.4. A summary of genes implicated in the development of OAC for which promoter methylation is recognised in BO, OAC, or both.	20
1.5. A summary of post-translational protein modifications and their impact on protein structure and function.	22
2.1. Per sample volumes for each master mix component used for cDNA synthesis prior to qRT-PCR.	49
2.2. Per sample volumes for each master mix component used for qRT-PCR.	50
2.3. Per sample volumes for each master mix component used for PCR amplification and qRT-PCR amplification during ATAC-seq library generation.	53
2.4. A list of R packages used for data analysis and representation.	59
3.1. An overview of in vitro studies in which cells resembling Barrett's or OAC are exposed to bile salts at neutral or acidic pH, or acidic pH alone.	64
4.1. A summary of ePK groups.	113
4.2. Characteristics of filters used in the detection of phosphorylated peptides on the PamChip®4 array.	118
4.3. TK Master mix constituents for PTK and STK arrays.	120
4.4. The 10 peptides that showed the largest significant increase in phosphorylation in response to acid and acidic bile salt (BS) exposure in NSE (Het-1A), NDBO (CP-A) and HGD (CP-B) cells.	137
4.5. All peptides that significantly reduced in phosphorylation in response to acid and acidic bile salt (BS) exposure in NSE (Het-1A), NDBO (CP-A) and HGD (CP-B) cells.	138
5.1. A list of RTKs encoded by the human genome, by receptor subfamily.	159
5.2. A list of RTKs for which protein overexpression in NSE, BO or OAC has previously been reported, grouped by receptor subfamily.	162
5.3. Aggregated data showing the direction of morphological change following RTK knockdown in BO cell lines.	191

List of Figures

Figure	Page
1.1. A summary of the endoscopic surveillance regime advocated by the BSG for patients with a confirmed diagnosis of BO in the UK.	7
1.2. A schematic overview of the compartments of the oesophageal NSE barrier.	9
1.3. An overview of signalling pathways implicated in the progression of BO.	24
1.4. The number of publications focussed on the BO genome, proteome, kinome and transcriptome published each year for the past two decades.	37
2.1. A schematic overview of NSE and BO cell lines used in this work.	40
2.2. A representative standard curve for the Pierce™ BCA Protein Assay Kit	45
2.3. A representative example of nucleic acids purified following ATAC library generation and analysed using the Agilent 4200 TapeStation for quality control purposes.	54
3.1. An overview of the proposed starvation and pseudo-starvation states that are implicated in the development of an invasive cellular phenotype.	67
3.2. A schematic representation of the experiments used to characterise NSE and Barrett's cell lines, and to model their response to acute, sustained and repeat microenvironmental stress.	68
3.3. A baseline representation of the morphology of NSE (Het-1A) and Barrett's NDBO (CP-A) and HGD (CP-B, CP-C, CP-D) cells.	71
3.4. An immunoblot showing relative E-cadherin protein expression in NSE (Het-1A), NDBO (CP-A) and HGD (CP-B, CP-C, CP-D) cell lines.	72
3.5. Expression of key markers of columnar and squamous differentiation across (i) patient samples and (ii) cell lines resembling NSE, Barrett's and OAC.	74
3.6. The impact of a ten minute pulse of a 100µM equimolar mix of bile salts at neutral pH (BS) and pH 4.0 (Acidic BS), or pH 4.0 treatment alone (Acid), on (A) cellular proliferation, (B) cellular death and (C) cellular metabolic activity for (i) NSE Het-1A, (ii) NDBO CP-A and HGD (iii) CP-B, (iv) CP-C and (v) CP-D cells.	75
3.7. Representative images detailing the impact of a ten minute pulse of acidic bile salts (100µM equimolar mix at pH 4.0) on the proportion of live and dead (A) Het-1A, (B) CP-A and (C) CP-B cells immediately, 2 hours and 6 hours after exposure.	76
3.8. A representation of the impact of treatment with a ten minute pulse of acidic bile salts (100µM equimolar mix at pH 4.0) for five days a week over twelve weeks on the morphology of cells representing NSE (Het-1A), NDBO (CP-A) and HGD (CP-B).	77
3.9. Fold-change in the expression of key markers of columnar and squamous differentiation across cell lines resembling NSE (Het-1A), NDBO (CP-A) and HGD (CP-B) in response to a ten minute pulse of bile salts (BS; 100µM equimolar mix) at neutral or acidic (4.0) pH, or acidic (pH 4.0) media alone.	78

3.10.	Fold change in the expression of key markers of squamous (KRT4) and intestinal (KRT7, KRT8) markers of differentiation in cells representing NSE (Het-1A), NDBO (CP-A) and HGD (CP-B) that are repeatedly exposed to acidic bile salts over a period of twelve weeks.	79
3.11.	An immunoblot showing relative E-cadherin protein expression in NDBO (CP-A) cell lines under conditions of serum-starvation and after exposure to a ten minute pulse of acidic bile salts.	79
3.12.	The impact of a 48 hour period of serum-starvation on (A) cellular proliferation, (B) cellular death and (C) cellular metabolic activity for (i) NSE Het-1A, (ii) NDBO CP-A and HGD (iii) CP-B, (iv) CP-C and (v) CP-D cells.	80
3.13.	Relative expression of key markers of columnar and squamous differentiation across cell lines representing NDBO (CP-A) following a 48 hour period of serum-starvation.	81
3.14.	A baseline analysis of the morphology of NSE (Het-1A) and Barrett's NDBO (CP-A) and HGD (CP-B, CP-C, CP-D) cells.	82
3.15.	Sample-level quality control outputs for RNA-seq analyses of NDBO (CP-A) cells starved for 48 hours or sampled at 24 and 48 hours following acidic bile salt treatment.	83
3.16.	Sample-level quality control outputs for ATAC-seq analyses of NDBO (CP-A) cells starved for 48 hours or sampled at 24 and 48 hours following acidic bile salt treatment.	84
3.17.	A panel figure illustrating changes in gene expression in NDBO (CP-A) cells 24- and 48- hours following a ten minute exposure to acidified bile salts.	86
3.18.	A panel figure illustrating functional enrichment of differentially expressed genes in NDBO (CP-A) cells at 24 and 48 hours following exposure to a ten minute pulse of acidified bile salts.	88
3.19.	A panel figure illustrating functional enrichment of genes for which expression significantly increased at both 1 and 2 days in NDBO (CP-A) cells following acidic bile salt exposure.	90
3.20.	A panel figure illustrating transcriptional regulators in NDBO (CP-A) cells at days 1 and 2 following acidic bile salt exposure.	92
3.21.	A panel figure illustrating changes in gene expression in NDBO (CP-A) cells after a 48 hour period of starvation.	94
3.22.	A panel figure illustrating functional enrichment of differentially expressed genes in NDBO (CP-A) cells following a 48 hour period of starvation.	96
3.23.	A panel figure illustrating transcriptional regulators in NDBO (CP-A) cells after a 48 hour period of serum-starvation.	98
3.24.	An immunoblot showing relative KLF5 protein expression in NSE (Het-1A), NDBO (CP-A) and HGD (CP-B) cell lines.	99
4.1.	A summary of the experimental approach used to determine the impact of exposure to acidified media or bile salts at either neutral or acidic pH on kinase activity in cells representing NSE (Het-1A), NDBO (CP-A) or HGD (CP-B).	116
4.2.	A typical fluorescent readout generated by FITC-conjugated antibodies on a PamChip®4 array.	117
4.3.	A manually curated summary of the biological function of peptides incorporated within the PTK and STK PamChip®4 microarrays.	119

4.4.	A representative overview of the PamChip®4 layout used for detection of kinase activity.	119
4.5.	Immunoblots demonstrating changes in the relative total (A) tyrosine and (B) serine/threonine phosphorylation in NSE (Het-1A), NDBO (CP-A) and HGD (CP-B) cells during the period following a ten minute exposure to acidic bile salts.	123
4.6.	Sample-level quality control outputs for (A) PTK and (B) STK kinase activity array analyses of NSE (Het-1A), NDBO (CP-A) and HGD (CP-B) cells treated with bile salts (BS) at neutral pH or acidic pH (acidified BS), or with acid alone.	124
4.7.	Violin plots demonstrating the distribution of coefficient of variation (CV) scores for each studied peptide included within the (A) PTK and (B) STK kinase activity arrays for NSE (Het-1A), NDBO (CP-A) and HGD (CP-B) cells treated with bile salts (BS) at neutral pH or acidic pH (acidified BS), or with acid alone.	125
4.8.	A panel figure illustrating kinase activity profiles of NSE (Het-1A), NDBO (CP-A) and HGD (CP-B) cells immediately following exposure to a ten minute pulse of bile salts at neutral or acidic pH, or acid alone.	126
4.9.	A panel figure illustrating a principle components analysis (PCA) to identify the variation in kinase activity profile between NSE (Het-1A), NDBO (CP-A) and HGD (CP-C) cells in their basal state and following exposure to bile salts at neutral or acidic pH, or acid alone.	128
4.10.	A panel figure illustrating differences in the basal kinase activity of NSE (Het-1A), NDBO (CP-A) and HGD (CP-B) cells.	129
4.11.	The top 10 signalling (A) KEGG and (B) REACTOME pathways that significantly enrich in NDBO (CP-A) cells when compared with HGD (CP-B) cells.	130
4.12.	The correlation between change in phosphorylation of (A) all, (B) STK and (C) PTK peptides following a ten minute pulse of bile salts at neutral (Bile salts) or acidified pH (Acidified BS), or acid alone.	131
4.13.	Volcano plots illustrating the differences in peptide phosphorylation between cell lines following exposure to a ten minute pulse of bile salts at neutral (Bile salts) or acidified pH (Acidified BS), or acid alone.	132
4.14.	Kinetic profiles for PTK activity in NSE (Het-1A), NDBO (CP-A) and HGD (CP-B) cells exposed to a ten minute pulse of bile salts at neutral (Bile salts) or acidic (Acidic BS) pH, or acid alone.	134
4.15.	Peptides which significantly (A) increased or (B) decreased in phosphorylation in NSE (Het-1A), NDBO (CP-A) and HGD (CP-B) cells exposed to a ten minute 100µM equimolar mix of bile salts at neutral pH.	135
4.16.	A panel figure illustrating over-represented Gene Ontology (GO) (A) Biological Process and (B) Molecular Function terms in NSE (Het-1A), NDBO (CP-A) and HGD (CP-B) cells following a ten minute pulse of bile salts at neutral (Bile salts) or acidified pH (Acidified BS), or Acid alone.	136
4.17.	A heatmap demonstrating a global view of differences in KEGG and REACTOME pathway enrichment for NSE (Het-1A), NDBO (CP-A) and HGD (CP-B) cells following a a ten minute pulse of bile salts at neutral (Bile salts) or acidified pH (Bile Acid), or acid alone.	139
4.18.	A heatmap demonstrating differences in KEGG pathway enrichment for NSE (Het-1A), NDBO (CP-A) and HGD (CP-B) cells following a ten minute	140

	pulse of bile salts at neutral (Bile salts) or acidified pH (Bile Acid), or acid alone.	
4.19.	A heatmap demonstrating differences in REACTOME pathway enrichment for NSE (Het-1A), NDBO (CP-A) and HGD (CP-B) cells following a ten minute pulse of bile salts at neutral (Bile salts) or acidified pH (Bile Acid), or acid alone.	141
4.20.	A kinome map visualisation of the NDBO (CP-A) response to a ten minute pulse of acidified bile salts.	143
4.21.	Functional grouping of non-redundant over-represented Gene Ontology (GO) Biological Process (BP) terms in peptides that significantly increased in phosphorylation in both NDBO (CP-A) and HGD (CP-B) cells in response to a ten minute pulse of acidic bile salts.	144
4.22.	Conserved signalling response to acidic bile salts in Barrett's epithelia.	145
4.23.	Representative immunoblots detailing the change in PI3K/Akt, mTOR and MAPK activity in NDBO CP-A and HGD CP-B cells during the 60 minute period following a 10-minute exposure to acidic bile salts.	146
4.24.	An immunoblot demonstrating change in phosphorylation of the S473 and T308 Akt epitopes in response to 24 hours exposure to DCA.	148
4.25.	Immunoblots detailing changes in the phosphorylation of (A) ERK, and both the S473 and T308 Akt epitopes, and (B) total tyrosine and serine/threonine residues, in response to bile salts at both neutral and acidic pH.	148
4.26.	Immunoblots detailing changes in the phosphorylation of the S473 and T308 Akt epitopes, ERK, and both AMPK T172 and mTOR in response to a 10 minute pulse of hydrogen peroxide in NSE (Het-1A), NDBO (CP-A) and HGD (CP-B) cells.	149
4.27.	Corresponding upstream mediators of the NSE (Het-1A), NDBO (CP-A) and HGD (CP-B) kinomic response to a ten-minute exposure of acid or acidified bile salts (BS).	150
5.1.	A schematic demonstrating mechanisms of RTK activation.	160
5.2.	A schematic demonstrating the targeted siRNA screen used to determine receptor tyrosine kinase (RTK) contribution to cellular phenotype and viability in NSE (HET-1A), NDBO (CP-A) and HGD (CP-B, CP-D) cells.	171
5.3.	Representative images detailing growth patterns of DAPI-stained NSE (Het-1A), NDBO (CP-A) and HGD (CP-B, CP-D) cells imaged using an Operetta [®] microscope at 10x and 20x magnification.	173
5.4.	A schematic demonstrating morphological parameters analysed from the high-throughput siRNA screen.	174
5.5.	Phospho-RTK array profiling of phosphorylated RTKs in NSE (Het-1A), NDBO (CP-A) and HGD (CP-B) cells following a ten minute pulse of bile salts at neutral (Bile salts) or acidified pH (Bile Acid), or acid alone.	177
5.6.	Immunoblots demonstrating changes in (A) EGFR and (B) IGF1R activation loop phosphorylation immediately following a 10 minute exposure to bile salts, at acidic and neutral pH, and acid alone, in NDBO (CP-A) and HGD (CP-B) cells.	178
5.7.	Immunoblots demonstrating changes in EGFR, IGF1R and HER2 activation loop phosphorylation in NDBO (CP-A) cells during the five minute period following a 10 minute exposure to acidic bile salts.	179

5.8.	A graph plotting intracellular pH against time for NSE (Het-1A), NDBO (CP-A) and HGD (CP-B) cells exposed to pH 4.0 and then neutral media.	180
5.9.	Reactive oxygen species (ROS) production following a 10 minute exposure to bile salts, at acidic (Acidic BS) or neutral pH (BS), acid alone, or positive control (Menadione) in NSE (Het-1A), NDBO (CP-A) and HGD (CP-B, CP-C, CP-D) cells.	181
5.10.	Change in mRNA expression of EGFR, EPHA4, FGFR3 and IGF1R over the 24 hour period following a 10 minute exposure to bile salts at acidic (Acidic BS) or neutral pH (BS), and acid alone.	182
5.11.	Fold change in the expression of EGFR, IGF1R, EPHA4 and FGFR3 in cells representing NSE (Het-1A), NDBO (CP-A) and HGD (CP-B) that are repeatedly exposed to acidic bile salts over a period of twelve weeks.	182
5.12.	A panel figure illustrating (A) the activity of acid sphingomyelinase (ASMase) in response to cellular acid exposure and (B-D) the impact of ASMase inhibition on cellular viability and signalling.	184
5.13.	Plate-well scatter plots for all siRNA screen outputs.	185
5.14.	Representative plate maps for interphase cell number in NSE (Het-1A) cells and nuclear intensity in HGD (CP-B) cells; both of which were maintained in proliferative media.	186
5.15.	A summary of positive and negative control outputs per plate for interphase cell number in (A) NSE (Het-1A), (B) NDBO (CP-A) and (C,D) HGD (CP-B, CP-D) cells.	186
5.16.	A panel illustrating (A) strictly standardised mean difference (SSMD) values for interphase cell number for each replicate (B) their impact on the selection of plates for analysis.	187
5.17.	Robust Z-score cut-off values for each output per cell line, condition and plate.	188
5.18.	Heatmaps demonstrating the impact on cellular viability of siRNA-mediated knockdown of receptor tyrosine kinases (RTKs) under proliferative and serum-starved conditions for NSE (Het-1A), NDBO (CP-A) and HGD (CP-B, CP-D) cells.	189
5.19.	Violin plots demonstrating the differences in baseline morphological characteristics between NSE (Het-1A), NDBO (CP-A) and HGD (CP-B, CP-D) cells maintained in (A) proliferative and (B) serum-starved media.	190
5.20.	A heatmap demonstrating enriched morphological term 'hits' following siRNA-mediated knockdown of all 58 RTKs encoded by the human genome in NSE (Het-1A), NDBO (CP-A) and HGD (CP-B, CP-D) cell lines.	191
5.21.	Reactive oxygen species (ROS) production following a 48-hour culture period within proliferation media (Control) or conditions of serum-starvation (Starved).	192
5.22.	The relative expression of receptor tyrosine kinases in NSE Het-1A, NDBO CP-A and HGD CP-B, CP-C and CP-D cell lines.	193
5.23.	The total mRNA expression of RTKs in normal, NDBO, LGD and OAC tissues in a patient dataset cultivated by Maag et al.	194

Chapter 1 Introduction

1.1 Barrett's oesophagus: a precursor to oesophageal adenocarcinoma

1.1.1. Overview

Oesophageal cancer is a leading cause of cancer-related morbidity and mortality globally.(1) Two main histological subtypes predominate: oesophageal squamous cell carcinoma (OSCC) and oesophageal adenocarcinoma (OAC). Despite their anatomic proximity, these should be regarded as distinct disease entities.(2) Worldwide, more than 85% of diagnoses are OSCC; driven principally by high numbers of cases in central and Eastern Asia and across myriad lower-income countries.(1,3–5) In contrast, rates of OAC have generally now surpassed those of OSCC in higher-income countries following significant increases in age-standardised incidence over recent decades.(1,6)

The diverging patterns of incidence for OAC and OSCC highlight in particular the distinct risk factors implicated in the development of OAC. These include the obesity epidemic and a high prevalence of gastro-oesophageal reflux disease (GORD); both of which are characteristic of industrialised nations.(7–9) Whereas OSCC develops through the malignant transformation of the stratified oesophageal normal squamous epithelium (NSE), OAC has a glandular structure that is not native to the oesophagus. Most, or perhaps all, cases of OAC develop from a premalignant precursor, Barrett's oesophagus (BO); the development and progression of which is similarly linked to environmental risk factors such as smoking, obesity and GORD, as well as a limited number of host genetic factors.(10–12)

Only a small proportion of patients with BO will progress to OAC, and most cases of the latter are identified *de novo*.(12,13) However, mortality to incidence ratios for OAC are high and recent decades have realised only modest improvements in overall survival.(14–16) The multi-modal treatment approaches commonly employed in the management of OAC are

also intensive and have significant long-term sequelae that impair quality of life.(17–19) Strategies to improve primary and secondary prevention are therefore vital; including through enhanced surveillance and screening to ensure those patients most likely to develop progressive BO and OAC are identified in a timely manner.(20)

A comprehensive understanding of the pathogenesis of BO and OAC is important to delivering these improvements in prevention, as well as for informing treatment advances. However, as will be explored here, the cellular origin of BO, the biological basis for its progression and the role environmental stressors such as obesity and GORD play in driving this are all yet to be fully elucidated.

1.1.1.1. The BO lesion

The development of BO – first described in the 1950s - is characterised by the metaplastic replacement of the non-keratinising squamous epithelial lining of the lower oesophagus with a columnar-like epithelium.(21,22) This generally occurs in close proximity to, or overlapping with, the gastro-oesophageal junction (GOJ). The mucosa develops a red velvet appearance due to the presence of a mosaic patch of cells that include gastric fundic-type (oxyntocardiac) epithelia that strongly express *MUC1*, *MUC5AC* and *TFF1*; cardiac-type (transitional) mucous-secreting epithelia that express *MUC6*, *TFF2* and *TFF3* and intestinal-type epithelia formed predominantly of goblet cells that express *MUC2* and *MUC3* (specialised intestinal metaplasia, SIM).(23)

This lesion may evolve in a small proportion of patients from metaplastic but non-dysplastic BO (NDBO) to the development of progressively worsening dysplasia and, in some, intramucosal adenoma or invasive OAC. Although accurate assessment of the cytological and architectural abnormalities that characterise BO is difficult and demonstrates low inter-observer reproducibility amongst pathologists, dysplastic change is generally categorised as low grade (LGD) or high grade (HGD).(21,22,24) SIM has classically been considered the most likely of the mosaic cell types to undergo dysplastic progression and is required for a diagnosis of BO by the American Gastroenterological Association.(25–28) It is not, in contrast, required by the British Society for Gastroenterology (BSG), which presumes its presence even if not directly sampled.(29) There is conflicting evidence regarding the extent to which other cellular types can undergo dysplastic change, though gastric-like foveolar, and cardia, dysplasia have been reported.(30–35) Conflicting with much of this conventional dogma, there is emerging evidence that reduced goblet cell (and thereby SIM) density may in fact confer a greater risk of progression to OAC.(34,35) This is suggested to be a

consequence of the terminally differentiated nature of goblet cells, which may reduce their ability to undergo malignant transformation.(34,35)

1.1.1.2. Epidemiology of BO & OAC

1.1.1.2.1. Incidence

In 2017, there were 473 000 (95% confidence interval, *CI*, 459 000 – 485 000) new cases of oesophageal cancer worldwide.(1) Reflecting the considerable morbidity and mortality associated with this disease, in the same year 9.78 million (95%CI 9.53 – 10.03) disability-adjusted life years (DALYs) were lost and there were 436 000 (95%CI 425 000 – 448 000) deaths across the globe due to oesophageal cancer.(1) It is as a consequence the sixth most common cause of cancer-related death worldwide.(36) However, between 1990 – 2017, the global age-standardised incidence of oesophageal cancer decreased by 22.0% (95%CI 18.6% - 25.2%) to 5.9 (95%CI 5.7 - 6.1)/100 000 population; with an attendant decrease of 33.4% (95%CI 30.4% – 36.1%) in age-standardised oesophageal cancer-related DALYs to 120 (95%CI 117 – 123)/100 000 population and of 29.0% (95%CI 25.8% – 32.0%) to 5.5 (95%CI 5.3 – 5.6)/100 000 population in age-standardised mortality related to oesophageal cancer.(1)

The global decrease in age-adjusted rates of oesophageal cancer over recent decades can be attributed to reductions in age-standardised incidence in populations in which OSCC predominates; including Central and East Asia, and much of Latin America.(1,37) In contrast, over the same period the incidence of OAC has increased considerably in high income countries.(3,4,6,37–39) This ‘*OAC epidemic*’ (as defined by Edgren and others (6)) is most apparent in North America and both Northern and Western Europe, where incidence is particularly high in the United Kingdom (UK) - which has amongst the highest rates in the world - and The Netherlands.(5,40,41) The healthcare burden imposed by OAC in these populations is projected to continue to rise until 2030.(3,4)

Concomitant with rising rates of OAC, an increase in the incidence of its precursor lesion BO has also been reported.(42–44) Data relating to BO incidence and prevalence are however less complete than those for OAC; not least because most cases of BO remain asymptomatic and undiagnosed.(40) There is in addition concern that the reported rise in BO cases is attributable to an increase in surveillance as opposed to reflecting a true increase in prevalence.(43,45) Nevertheless, the general population prevalence of BO in Western countries is now thought to lie between 1-2%, and may be higher amongst a number of at risk populations (see **1.1.1.2.2.**).(46–51)

The rate of increase of the age-standardised incidence of both OAC and BO is slowing across much of the Western world and may have peaked in the UK and The Netherlands in the early 2000s.(52) Conversely, BO is uncommon in lower income and non-Western populations, but may be increasing in prevalence.(53,54)

1.1.1.2.2. Risk factors

The presence of BO confers an eleven-fold increased risk of OAC compared with the general population.(55) As Franklin & Jankowski highlight, this is comparable to the risk of developing breast cancer for a first-degree relative of a person diagnosed with a malignancy secondary to a germline *BRCA1/2* mutation.(56) However, rates of progression to OAC were in the past overestimated and are now thought to be relatively low at between 0.1 - 0.5% per patient year.(22,55,57,58) A higher rate of progression to LGD from NDBO of 4.3% per patient year has been reported, though in this series regression to NDBO occurred in 66% of patients whilst 21% neither progressed or regressed.(59) Estimates for the risk of progression from LGD to HGD or OAC vary from 0.18 - 13.4% per patient year.(55,57,59,60) This substantial range is likely to reflect differences in diagnostic definitions and accuracy.(24) A robust Northern Irish case : control study has reported a relative risk (RR) of malignancy for LGD of 11.8.(61) Overall, the risk of HGD or OAC in patients with baseline NDBO appears to be around 0.33% per patient year or 1.00-5.15 per 1000 patient years.(62)

It is unclear why only a small proportion of patients with BO undergo malignant progression. Nevertheless, BO is thought to be the origin for most, if not all, incident OAC.(11,12) Accordingly, a majority of the risk factors for OAC also apply to the development and progression of BO. As summarised in **Table 1.1.**, these include a number of demographic variables, with older White males at particular risk of developing OAC. Notably, whilst sex-specific differences may reflect hormonal influences on progression, there is evidence that males develop BO earlier and are therefore on average at more prolonged risk of progression, and the factors that drive this, than women.(63) Familial clustering of both BO and OAC has also been reported, with a small number of linkage and genome-wide association studies providing support for a complex genetic trait.(64,65) No monogenic mutations have been reported to contribute to BO or OAC development or progression, though the heritable components of these two lesions are estimated at 35% and 25% respectively.(66) The specific characteristics of the BO lesion may also influence dysplastic progression, with longer lesion length and the development of LGD from NDBO both portending the development of OAC.(67)

	BO OR (95%CI)*	OAC OR (95%CI)*	Evidence level	Refs.
Demographics				
Male sex	2.0 (1.8-2.2)	2.2 (1.8-2.5)	MA/CC	(67–70)
White ethnicity	+	+	MA/CC	(54,71)
Increased age	1.0 (1.0-1.1)	1.0 (1.0-1.1)***	MA/CC	(67,69,70,72)
Medical factors				
Presence of GORD symptoms	2.9 (1.9-4.5)	7.7 (5.3-11.4)	MA/CC	(73–75)
Raised BMI (per unit increase)	1.0 (0.9-1.0)	1.0 (0.9-1.2)***	MA/CC-PA	(67,76,77)
Waist circumference ratio*	1.2 (1.0-1.3)	2.1 (1.3-3.2)	CC-PA	(77)
Hiatus hernia	3.9 (3.0-5.1)	0.9 (0.7-1.2)	MA	(78,79)
Breastfeeding	Unknown	0.6 (0.4-0.9)	CC-PA	(80)
Type 2 diabetes mellitus	1.5 (1.2-1.9)	1.3 (1.0-1.8)	CC/PA	(81–83)
<i>Helicobacter pylori</i> infection	0.7 (0.6-0.8)	0.5 (0.4-0.7)	CC	(84,85)
Family history**	+	+	CS	(86)
Lifestyle factors				
Alcohol intake	1.1 (0.6-1.8)	1.1 (0.8-1.5)***	MA	(67)
Cigarette smoker	1.4 (1.2-1.7)	1.5 (1.1-2.0)***	MA/CC	(67,87,88)
Physical activity	1.2 (0.8-1.7)	0.8 (0.7-0.9)	MA/CC	(89,90)
Medications				
NSAID	1.0 (0.8-1.3)	0.7 (0.5-1.0)***	MA	(67)
PPI	Unknown	0.3 (0.1-0.8)^	MA	(91)
H ₂ RA	Unknown	1.2 (0.8-1.8)	CC	(92)
SSRI	Unknown	-	CS	(93)
Anti-cholinergic drug	Unknown	3.8 (2.2-6.4)	CC	(94)
Corticosteroids	Unknown	0.6 (0.4-0.9)	CC	(95)
Calcium channel blockers	Unknown	2.4 (1.2-5.0)	CC	(96)
Theophylline	Unknown	1.9 (1.3-5.1)	CC	(96)
Statins	0.6 (0.4-0.9)	0.5 (0.3-0.7)	MA/CC	(67)
BO characteristics				
Presence of LGD (vs NDBO)	N/A	4.7 (2.6-8.6)	MA	(67)
Length (per unit cm)	N/A	1.2 (1.1-1.2)	MA	(67)
Right hemispheric lesion	N/A	+	CS	(97,98)

Table 1.1. A summary of risk factors for the development of BO and OAC. The highest level(s) of evidence available are listed. +, positive but quantitatively undefined relationship (i.e. no available, generalisable, odds ratio (OR)); * per unit increase; **, family history of GORD, BO or OAC; *** OR for progression of BO to OAC; 95%CI, 95% confidence interval; BMI, body mass index; CC, case-control study; CS: case series; DM, diabetes mellitus; MA, meta-analysis; NSAID, non-steroidal anti-inflammatory drug; H₂RA, histamine 2 receptor antagonist; N/A, not applicable; PPI, proton pump inhibitor; SSRI, selective serotonin reuptake inhibitor. Table extensively adapted from *Peters et al.*(22)

Beyond these fixed factors, around 70-80% of cases of OAC relate to the modifiable environmental influences of GORD, obesity and smoking.(73,99) Characterised by the refluxate of acidic, bile salt-containing duodenal and gastric contents, GORD is responsible for the development of the initial metaplastic BO lesion. It is in addition amongst the strongest risk factors for the development of OAC, and there is evidence that it plays a major role in promoting dysplastic progression.(9,73,74,100) The presence of a BO lesion in the right oesophageal hemisphere, which is the region most commonly exposed to gastric refluxate, is for instance associated with a greater risk of dysplastic progression.(97,98) Further, medications that relax the lower oesophageal sphincter, and as a consequence lead to an increase in the frequency and severity of gastric reflux, are associated with the

development of OAC.(67,91–96) These include anti-cholinergic drugs, calcium channel blockers and theophylline. Correspondingly, a recent randomised controlled trial confirmed a dose response relationship for the prevention of dysplastic BO progression for acid-suppressant proton pump inhibitors (PPIs) when used in patients with BO.(101) The protection afforded by high dose PPIs was enhanced further by the addition of aspirin. Interestingly, previous studies have identified elevated basal acid production in patients with BO, whilst *Helicobacter Pylori* (*H. Pylori*) may protect against OAC development by reducing gastric acid secretion.(85,102,103) Overall, as many as 36% of cases of OAC have been directly linked to frequent symptomatic acid reflux, and the presence of daily GORD-related symptoms is associated with a seven-fold increased risk of OAC compared with a reduced symptom frequency.(73,104) Nevertheless, a significant proportion of cases are likely to arise in those with silent reflux disease.(22)

Similarly to GORD, obesity is a strong risk factor for the development of both BO and OAC.(67,76,77) In particular, the distribution of fat is a predictor of risk, with central obesity (measured as an increase in waist circumference ratio) independently predicting the development and progression of BO and OAC.(77) This may in part relate to the mechanical promotion of gastric reflux as a consequence of increased pressure secondary to greater abdominal mass.(105,106) However, a number of studies have demonstrated a persistent relationship between obesity and BO when GORD symptoms are controlled for.(77)

The presence of central obesity is closely linked with development of the metabolic syndrome, which may instead constitute the major pathological process underlying BO development and progression in those who are overweight.(107) This disorder is underpinned by a systemic pro-inflammatory state caused by the production of bioactive pro-inflammatory adipocytokines such as leptin, the development of insulin resistance and the presence of a constellation of cardiovascular risk factors.(107) Although understudied in this context, the prevalence of the metabolic syndrome in patients with BO exceeds that of the general population.(108) In addition, raised serum levels of insulin and leptin are independent risk factors for the development and progression of BO, as is Type 2 Diabetes Mellitus (DM), which is partly characterised by profound insulin resistance.(76,82,83) In keeping with these findings, United States (US) Surveillance, Epidemiology and End Results (SEER) analyses have linked the metabolic syndrome to the development of both BO and OAC.(109,110) Physical exercise, which may reverse metabolic syndrome, conversely protects against OAC.(89,90)

1.1.1.3. Clinical characteristics

Despite modest improvements over recent decades, survival rates for OAC remain poor. Overall, less than 20% of patients will live to five years, whilst around half will die from their cancer within a year of diagnosis.(14,16,111) When identified early, OAC is however more treatable and significant improvements in overall survival have been realised for local disease. In a recent analysis using USA SEER data, 73% of patients with stage 0 and 37% with stage 1 disease were alive at five years.(16)

Strategies to promote the prevention and early diagnosis of OAC are therefore integral to delivering improved overall outcomes. Options include screening to detect patients who have BO, the use of effective chemoprevention to limit dysplastic progression, surveillance strategies to identify those who are at risk of or who demonstrate progression, and the use of effective treatments in cases where dysplasia or invasive disease has occurred.

It remains unclear whether community surveillance programmes translate to improved survival.(28,112–114) This may relate in part to a paucity of sensitive and specific biomarkers, and a corresponding failure of current screening and surveillance approaches to identify patients most at risk of neoplastic progression. An additional impact of this is a requirement for intensive, and usually invasive, follow-up regimes (see **Fig. 1.1.**) that place pressure on healthcare resources and put patients at risk of harm.(20) Moreover, there are limited chemopreventative options for BO beyond anti-reflux treatments and no definitive chemotherapeutic option for patients who progress to dysplasia; the development of which instead generally obligates the use of invasive options such as ablative therapy or either endoscopic or surgical resection.

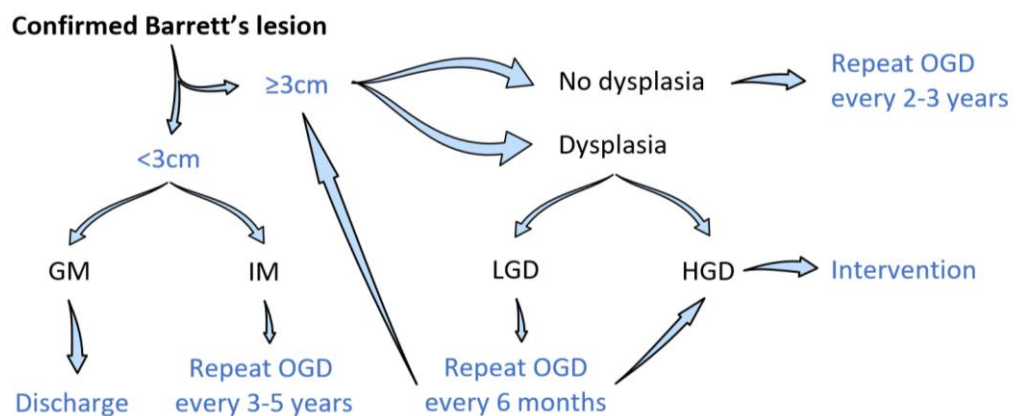


Figure 1.1. A summary of the endoscopic surveillance regime advocated by the BSG for patients with a confirmed diagnosis of BO in the UK.(29) GM: gastric metaplasia; OGD: oesophagogastroduodenoscopy.

It is unlikely that significant improvements will be realised in the prophylaxis and treatment of BO progression, nor in the stratification of and specific approaches advocated for its surveillance, without an improved understanding of the biological basis for the progression of dysplasia towards invasive disease. In particular, it is important to understand how major risk factors for BO progression and the development of OAC act to influence the cellular biology of established BO.

1.1.2. The BO metaplasia-dysplasia-cancer sequence

1.1.2.1. Noxious stimuli and the oesophageal epithelial barrier

The initial metaplastic BO lesion is widely accepted to arise as a consequence of the chronic exposure of the lower oesophagus to gastric refluxate.(9,22,115) This comprises hydrochloric acid-rich gastric acid, bile salts, pepsin, bacteria, proteolytic pancreatic enzymes and ingested foods.(116) The lower oesophageal sphincter (LOS), diaphragmatic sphincter and phrenoesophageal ligament form a lower oesophageal higher pressure zone which, combined with gastric emptying and the peristaltic action of the oesophagus, reduce the frequency and duration of exposure of the oesophageal mucosa to these noxious stimuli.(117,118) Reflux episodes are nevertheless common even in healthy populations, with for instance a median of 44 episodes per 24 hours reported in a previous asymptomatic European cohort monitored by ambulatory impedance-pH studies.(119)

The oesophageal epithelium must therefore maintain a barrier function in order to protect the deep oesophageal mucosa and submucosa from noxious elements within gastroduodenal refluxate. As summarised in **Fig. 1.2**, this is formed by the combined action of a pre-epithelial (luminal), an intrinsic epithelial and a post-epithelial (stromal) compartment.(120) Within the lumen, a pre-epithelial $95\pm 12\mu\text{m}$ mucous buffer layer is formed from bicarbonate, water and mucous swallowed in saliva and produced by submucosal glands.(118,121) This acts to neutralise hydrogen ions and block diffusion of injurious stimuli to the apical cellular membrane, including through the presence of an unstirred water layer that exhibits laminar flow parallel to the apical epithelial surface.(120,122) A number of additional mediators of tissue repair are also present in swallowed saliva, including epidermal growth factor (EGF), prostaglandin E_2 (PGE_2) and transforming growth factor (TGF)- α .(123)

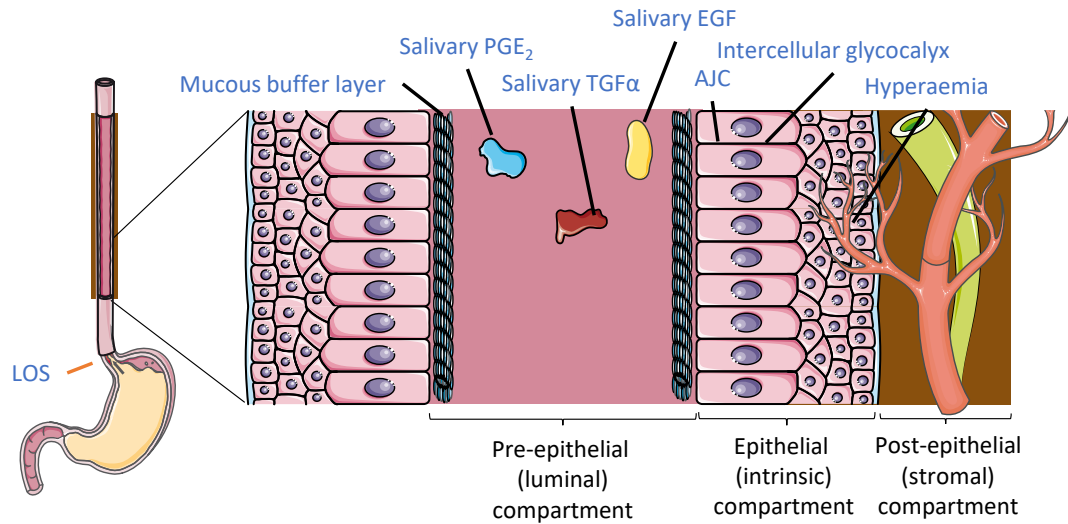


Figure 1.2. A schematic overview of the compartments of the oesophageal NSE barrier. The cross-sectional representation of the oesophagus demonstrates the three protective compartments and their relationship to NSE. AJC: apical junction complex; EGF: epidermal growth factor; LOS: lower oesophageal sphincter; PGE₂: prostaglandin E₂; TGF α : transforming growth factor – α .

These pre-epithelial defences are less effective than their gastric equivalents, which predisposes the oesophageal mucosa to harm.(120) The intrinsic stratified non-squamous epithelial barrier is therefore of great importance in preventing the paracellular intrusion of potentially harmful molecules to deeper mucosal compartments. Central to this function is the presence of an intercellular glycoconjugate as well as an apical junction complex (AJC).(120) This consists of a tight junction complex, adherens junctions and desmosomes. The tetraspan transmembrane claudin and occludin proteins are crucial to the maintenance of the epithelial barrier function.(124,125) Junctional adhesion molecules, which support occludin assembly, are also recognised to be of importance, as is the late epidermal differentiation protein filaggrin, which helps to maintain an intercellular glycoprotein matrix.(126,127) Hydrogen ions that bypass these mechanisms are neutralised in the post-epithelial component by a neutral intercellular glycoconjugate or removed through diffusion into blood, the supply of which increases in response to mucosal acid exposure.(128,129) This hyperaemia also allows for the removal of lactic acid and carbon dioxide, as well as the delivery of acid-neutralising bicarbonate ions.

Despite the presence of these mechanisms, prolonged exposure to hydrochloric acid and other noxious stimuli results in cellular injury and necrosis. Rather than this representing solely a caustic acid effect, work led by Souza indicates a significant injurious impact from cytokine-mediated inflammatory processes.(130) The first step in this process appears to be damage to the AJC, which results in increased permeability of the paracellular space. This is seen morphologically through the presence of dilated intercellular spaces (DIS), which are

sensitive but not specific for GORD.(131,132) Greater hydrogen ion concentrations are as a consequence seen alongside basolateral epithelial cell membranes, which unlike their apical equivalents incorporate a sodium-independent chloride/bicarbonate exchanger.(133) This results in intercellular acidification which in turn leads to acute and chronic inflammation, damage to deoxyribonucleic acid (DNA) and oxidative stress.(120,132)

The epithelium can respond rapidly to cellular injury and necrosis through a process of restitution, during which adjacent healthy cells migrate to a damaged area of epithelium within 30-60 minutes of the initial insult.(134) It is also capable of replicating in order to replace damaged cells, though this process of regeneration is far slower.(135) For some patients with GORD, DIS may occur but without macroscopic mucosal injury, in a process termed non-erosive oesophagitis.(120,122,132) However, prolonged or particularly intense noxious stimuli and the pro-inflammatory processes they provoke may overwhelm slower restorative mechanisms, resulting in mucosal injury through a process termed erosive reflux oesophagitis.

1.1.2.2. The development of the BO lesion

1.1.2.2.1. An adaptive response to an at-risk mucosa

It is in the presence of mucosal injury and erosive reflux oesophagitis that the metaplastic BO lesion develops. In this context, metaplasia should be considered as a change in one tissue type to another, with a number of differentiated columnar epithelial cellular subtypes (as outlined in **1.1.1.1.**) replacing NSE.(136) Rather than representing an entirely maladaptive process, the formation of SIM may provide a mucosal-protective adaptation to an environment rich in acid, reactive oxygen species (ROS), pro-inflammatory cytokines and other noxious stimuli.(115)

Consistent with this theory, *in vitro* studies demonstrate that BO epithelial cells maintain physiological intracellular pH following prolonged exposure to acidic refluxate, whereas NSE do not.(137) BO epithelia also express Claudin-18-dominant tight junctions, which are thought to confer greater intrinsic protection against paracellular acid permeability than the Claudin-18-deficient tight junctions of NSE.(138)

BO epithelia may in addition provide an adapted pre-epithelial barrier function. Unlike NSE, BO is for instance capable of generating a thick adherent mucous layer across which acid can be neutralised.(139) Further, whereas NSE demonstrates relatively low active ion transport,

BO cells are active anion secretors and boast acid-neutralising bicarbonate secretory capacity that is five-fold greater than that of native oesophageal cells.(140)

Bolstering these improved defences, the transcriptional profile of BO epithelium features overexpression of multiple genes involved in defence and repair.(141) Where effective repair cannot occur, the crypt architecture of BO, in which stem cells sit at the base, is such that damaged epithelia are shed into the oesophageal lumen rather than remaining *in situ* and at risk of accumulating further genomic aberrations.(115)

1.1.2.2.2. Cellular origin

The cell from which patches of BO derive is controversial and the murine models on which most relevant research is based are limited.(22,142) It is however accepted that given that intestinal-like cells are not ordinarily present in the stomach or oesophagus, a process of cellular reprogramming must occur in response to GORD.(130) This may happen via transdifferentiation, through which a fully differentiated cell directly transforms to another mature cell, or through the transcommitment of a pluripotent stem cell.(22,130)

Transdifferentiation from NSE may occur directly in a process that is independent of cell division, or indirectly via a mitotic-dependent process that first requires de-differentiation to a transitional non-specialised intermediary.(136) Alternatively, epithelial injury may result in the reprogramming and transcommitment of pluripotent cells in either the oesophageal submucosal layer or gastric cardia, with the latter theorised to migrate to the lower oesophagus in response to tissue damage.(143,144) Interestingly, OAC shares a number of genomic similarities to gastric cancer, which may provide evidence for a gastric origin for BO.(22,145) The presence of a multilayered epithelium (MLE) with characteristics of both squamous and columnar epithelium has long been proposed as another possible precursor and is supported by recent evidence.(146,147) Finally, circulating bone marrow cells and a population of residual embryonic cells have also been suggested as the source of BO progenitor cells, but there is little clinical evidence in support of this theory.(148,149)

Overall, transcommitment is considered to be more likely given the numerous cell lineages that are known to constitute a BO mosaic. It is however possible that there is more than one route through which BO develops.(22,130)

1.1.2.2.3. Molecular mediators of metaplasia

As with the cell of origin for BO, the molecular mechanisms governing the metaplastic process remain uncertain. Significant changes are nevertheless seen in gene regulation and protein expression. This includes the loss, reduced activity or downregulation of transcription factors related to normal oesophageal squamous epithelial development such as tumour protein 63 (p63), transcription factor SOX2 (SOX2) and paired box protein Pax-9 (PAX9).(22,147,150) A concomitant increase in transcription factors related to intestinal development is also seen, including of SOX9, nuclear factor kappa-light-chain-enhancer of activated B cells (NF-κB), GATA binding protein 6 (GATA6), the homeobox proteins CDX1 and CDX2, protein analog homolog 1 (ATOH1), hypoxia inducible factors (HIFs) and the hepatocyte nuclear factors (HNF) 1α, 3α, 3β, 3γ and 4α.(22,147,150–152)

A number of pathways are thought to act upstream of these factors, though most have been studied in the context of transdifferentiation rather than transcommitment. Many are driven by the inflammatory environment induced by GORD, which includes a significant contribution from pro-inflammatory cytokines produced by the lower oesophageal stroma.(153,154) Examples of upstream mediators and signalling cascades implicated in the metaplastic conversion of NSE include the highly-conserved Wnt signalling pathway, the TGFβ superfamily member bone morphogenetic protein (BMP) 4 and the Hedgehog signalling pathway.(155–161) Downregulation of the Notch signalling cascade has in addition been recognised as a probable regulator of both transdifferentiation and transcommitment.(162–164)

1.1.2.3. Dysplastic progression

1.1.2.3.1. A stressful microenvironment

Once established, the BO lesion remains stable in a majority of patients. For most, the metaplastic process is therefore likely to represent successful adaptation in the context of erosive oesophagitis and the microenvironmental stressors that contribute to it.(115,165) However, as summarised in **Table 1.2**, many of the risk factors associated with the development of both BO and OAC continue to shape the luminal, stromal and humoral components of the BO microenvironment; acting as stressors that for a minority of patients contribute to the development and progression of dysplasia.

A key example is GORD, which results in the pulsatile exposure of BO epithelium to gastric refluxate. This is commonly acidic, though pH changes are ameliorated in many patients with BO through the use of PPIs and histamine₂ receptor antagonists (H₂RAs).(166,167) In

addition to the strong epidemiological evidence for a role for GORD in the progression of BO, animal and *in vitro* studies have shown that chronic exposure to gastro-duodenal contents catalyses neoplastic progression.(168,169) Interestingly, there is some evidence that peak bile acid concentration is greater within the refluxate of patients with BO than those with non-erosive oesophagitis or no history of GORD, as is the concentration of potentially more toxic secondary (conjugated) bile salts.(170,171) BO patients are also more frequently exposed to acidic refluxate.(172) The long-term use of PPIs is, in addition, associated with elevated concentrations of gastrin.(173)

For BO lesions proximal to the squamocolumnar junction, exposure to gastric refluxate results in a pro-inflammatory stromal cytokine infiltrate with a T helper 1 (Th1) profile.(154,174) This inflammatory milieu is characterised by the release of cytokines such as tumour necrosis factor (TNF)- α , interferon (IFN)- γ , interleukin (IL)-1 β , IL-6 and IL-8.(153,174–183) The role of inflammation in carcinogenesis is now well established as a general principle yet the mechanism through which these cytokines specifically catalyse dysplastic progression in BO remains unclear. There is however evidence that they contribute to the activation within BO cells of transcription factors implicated in neoplastic progression, as well as promoting oxidative damage and stromal remodelling that favours carcinogenesis.(165,175) The pro-inflammatory BO phenotype may be further potentiated by risk factors such as the metabolic syndrome, which is associated with significant systemic inflammation.(7,105,107,109,110)

The distal oesophageal BO microenvironment, which is in closer proximity to the GOJ and which is the site at which most cancers develop, is in contrast generally characterised by an anti-inflammatory Th₂ profile.(174) This BO lesional inflammatory gradient was first recognised by Fitzgerald and colleagues, who additionally demonstrated a role for oesophageal NSE in maintaining the pro-inflammatory stromal environment of more proximal lesions.(174) Anti-inflammatory cytokines such as IL-10 are recognised to increase in the distal oesophagus during dysplastic progression and may facilitate immune escape processes.(165,174,175,180,184,185)

A recent comprehensive analysis of immune determinants of BO progression suggests that this gradient occurs in the context of an overall increase in immune cell infiltrate during BO progression.(186) This is reversed in the OAC microenvironment, which is relatively depleted of immune cell infiltrate.(186) In keeping with the evidence outlined above, cytokine and cytokine receptors show the largest fold-change increases during progression.(186)

Process	Induced change in microenvironment	Putative impact on BO epithelium	Associations	Refs.
Luminal				
Gastric refluxate exposure	↓ pH ↑ ROS ↑ Bile salts ↑ Nitric oxide	DNA damage ↑ Intracellular signalling ↑ Inflammatory processes	GORD, PPI use	(166,187–195)
Altered saliva composition	↓ Glycoconjugate ↓ HCO ₃ ²⁻	Impaired pH neutralisation	GORD	(196)
	↓ EGF ↑ TGFβ, ↑ PGE ₂	Impaired repair stimulus ↑ Inflammatory processes		
Altered microbiome	↓ Bacterial diversity Altered composition	DNA damage ↑ Inflammatory processes	GORD, PPI use Metabolic syndrome, <i>H. Pylori</i>	(197,198)
Stromal				
Immune cell infiltration	↑ Dendritic cells	↑ Stem cell activation ↑ Regulatory T-cells	GORD, Obesity, Metabolic syndrome, Smoking, PPI use, NSAID use	(199–201)
	↑ Mast cells ↑ Pro-B/plasma cells ↑ Regulatory T-cells ↑ Macrophages	↑ Angiogenesis ↓ Immunosurveillance Matrix remodelling		(174,175, 186,202–204)
Cytokine release*	TGFβ dysregulation	↑ Proliferation, ↑ EMT ECM adaptation		(205,206)
	↑ TNFα ↑ IFNγ, ↑ COX2 ↑ IL-1β, ↑ IL-6 ↑ IL-8, ↑ IL-17A	↑ Inflammatory processes ↑ Intracellular signalling		(153,174–183,207,208)
Hypoxia	↑ IL-23 ↑ IL-21 ↑ IL-10 ↑ IL-4	↓ Inflammatory processes	Smoking, Lesion characteristics	(180,184, 185)
	Vascular remodelling	Oxidative stress Altered metabolism ↑ Proliferation		(175,209, 210)
ECM adaptation	↑ SPARC	↓ Cellular growth	Unclear (partly mediated by cytokine release)	(211)
	↑ Thrombospondin	↑ TGFβ		(212)
	↑ MMP1 ↑ MMP3 ↑ MMP7	Tissue remodelling Migration		(204,213–215)
	↑ MMP9	↑ Angiogenesis		(209)
Humoral				
↑ Adipose tissue*	↑ Adiponectin	↑ Apoptosis	Obesity, Metabolic syndrome, T2DM	(216)
	↑ Grehlin	↓ Inflammation		(216)
Insulin resistance	↑ Leptin	↑ Proliferation ↓ Apoptosis		(217–219)
	↑ Insulin	↑ Leptin ↑ Proliferation		(219–221)

Table 1.2. A summary of luminal, stromal and humoral influences on the BO microenvironment and their relationship with risk factors and BO epithelial phenotype. COX2: cyclo-oxygenase 2; DNA: deoxyribonucleic acid; ECM: extracellular matrix; EGF: epidermal growth factor; EMT: epithelial-mesenchymal transition; GORD: gastro-oesophageal reflux disorder; HCO₃⁻: bicarbonate; IFNγ: interferon γ; IL: interleukin; PGE₂: prostaglandin E₂; PPI: proton pump inhibitor; ROS: reactive oxygen species; SPARC: secreted protein acidic & cysteine rich; T2DM: type 2 diabetes mellitus; TGFβ: transforming growth factor β; TNFα: tumour necrosis factor α.

An increase in immune checkpoints also occurs.(186) Overall, both T_h1 and Th₂ profiles increase during progression, as do pro-B cells.(186) In contrast, the total number of eosinophils appears to fall.(186)

Beyond fuelling changes in the immune infiltrate, gastric refluxate is likely to be directly genotoxic and there is, for instance, evidence that an acidic environment is capable of triggering both the proliferation and apoptosis of BO epithelia.(187–189) Interestingly, a combination of nociceptor activation from reflux-induced damage and chemoreceptor stimulation from acid appears to reduce the secretion within saliva of protective luminal factors such as EGF and pH-neutralising bicarbonate and glycoproteins.(196,222)

In addition to refluxate, the BO microenvironment is further influenced by the presence of humoral factors such as hyperinsulinaemia and the adipokines that characterise the metabolic syndrome and obesity.(216–221) There is in addition evidence that changes to the extracellular matrix (ECM) influence dysplastic progression, though the factors driving these changes remain unclear.(204,209,211–215) The increased metabolic demands of hyperproliferative BO tissue, coupled with the impact of risk factors such as smoking, also result in vascular remodelling, the release of factors known to promote cellular growth, and an increase in oxidative stress.(175,209,210) It is however noteworthy that levels of oxidative stress are also elevated within the proximal stomach of patients with BO, yet this is not a site at which malignancies are frequently seen in this population.(223)

Supporting the importance of the stroma to OAC development and progression, stromal genes discriminate pre-invasive from invasive disease and can predict outcome in OAC.(212) There is evidence in this context that cancer-associated fibroblasts (CAFs) and peri-tumoral adipocytes influence cellular behaviour and epithelial mesenchymal transition (EMT).(224,225) It is not yet known whether these stromal-tumour interactions develop earlier in the development of the BO lesion, nor whether they contribute to worsened dysplasia.(224,225)

Many of the microenvironmental stressors outlined here are active in a majority of patients with BO, yet only a small proportion of patients will progress to cancer. As strikingly, progression can be swift in a significant proportion of those who do develop cancer. For instance, a majority of patients who have OAC are diagnosed within a small number of years from their initial endoscopic BO diagnosis.(55,226–228) Why some patients progress rapidly and most do not remains largely unclear. It may be that progression occurs in the context of a particularly stressful microenvironmental niche.(165) However, the genomic and

molecular changes that are influenced by these microenvironmental stressors and that crucially drive the development of dysplasia are yet to be fully elucidated.

1.1.2.3.2. The genomic landscape

The genomic landscape of both BO and OAC has arguably received the most attention to date, including from researchers seeking to understand the factors underlying the biological instability of some BO lesions.(229,230) It is also perhaps a consequence of the availability of sequential tissue samples that are routinely obtained via surveillance biopsy programmes and which can then be subject to unbiased whole-genome sequencing approaches. Many BO and OAC samples are now collated and characterised prospectively through groups such as the Oesophageal Cancer Clinical and Molecular Stratification (OCCAMS) network and the International Cancer Genome Consortium with which it shares data.

Family studies may also offer insights into the genetic basis for OAC development but are difficult to interpret.(231) Around 7% of cases of BO and OAC in a USA population occurred in family clusters.(231) However, much of the familial risk of BO and its progression appears most closely related to genes implicated in the development of its risk factors such as GORD and the metabolic syndrome.(232,233)

OAC is a heterogenous, structurally unstable, C-class malignancy that is characterised by frequent copy number changes and large scale rearrangements.(229,230,234) It also features a high mutational rate, with around 10 single-nucleotide variations per megabase (Mb).(229) An average of 4.4 driver events are seen in each tumour, with most derived from mutations rather than copy number alterations.(235) As many as 77 driver genes and 21 non-coding driver elements have been suggested (**Table 1.3**).(235) There are, however, few recurrently mutated driver genes and a paucity of clinically-validated prognostic or therapeutic biomarkers.(230,235)

A recent analysis undertaken by Secrier and colleagues has identified three broad patterns of disease in OAC.(236) The first is characterised by enrichment for a defective BRCA-led homologous recombination DNA-damage repair (DDR) pathway. The second is characterised by frequent T:A>G:C transversions seen in the setting of CTT sequences; a change that has been linked to acid-genotoxicity.(234,237) The third appears related to ageing and is reflected by a C>A/T mutational pattern. In this same analysis, Secrier additionally identified amplification of receptor tyrosine kinases (RTKs) in 80-90% of OAC cases, with co-amplification frequently seen.(236)

Coding driver genes	
<i>ABC1B, ACVR2A, ACVR1B, APC, ARID1A, ARID1B, ARID2, AXIN1, B2M, BRAF, C3orf62, CCDC102B, CCND1, CCND3, CCNE1, CD1A, CDH1, CDK6, CDKN1B, CHD4, CHL1, COIL, CRISPLD1, CTNNB1, DNAH7, EGFR, ELF3, EPHA2, EPHA3, ERRB2, FAM196B, FBXW7, GATA4, GATA6, GATAD1, GPATCH8, HIST1H3B, KCNQ3, KRAS, LRRK2, JAK1, KDM6A, LN7A, MAP2K7, MAP3K1, MBD6, MDM2, MET, MSH3, MUC6, MYC, NAV3, NOTCH1, NPBL1, PBRM1, PCDH17, PIK3CA, PIK3R1, POLQ, PPM1D, PTEN, RASA1, RNF43, RPL22, SCN3A, SLIT2, SMAD4, SMARCA4, STK11, TGFB2, TP53, TRP1A, TSHZ3, ZFXH3</i>	
Non-coding driver elements	
Coding gene	
Promoter	<i>MTERFD1, SDCCAG8, HIST1H2BO, HIST1H2AM, RPGRIP1L</i>
5'UTR	<i>PTDSS1, WDR74</i> <i>MMP24, FTO, MTG2</i>
Long non-coding RNA (lncRNA)	
Promoter	<i>AC10127.3, G079632</i>
lncRNA	<i>RNU12</i> <i>G062818, NEAT1</i>
Enhancer	<i>TP53TG1, ABCG2</i>
3'UTR	<i>OPALIN</i>

Table 1.3. An overview of genes and non-coding elements that are implicated in OAC pathogenesis. UTR: untranslated region.

A lower mutational rate of 5.4-6.8 single-nucleotide variations per Mb, or 5.4 mutations per Mb, is recognised in BO.(229,238) This is nevertheless higher than is seen in a number of malignancies, including hepatocellular carcinoma, breast cancer and prostate cancer.(229,238,239) Numerous somatic point mutations, insertions and deletions are seen at all disease stages and it is unclear whether the mutational burden of dysplastic tissue exceeds that of NDBO.(229,235–238)

Underlying this mutational landscape, overall DNA damage levels are raised in BO tissue compared with NSE.(240) *In vitro* and *in vivo* animal analyses have demonstrated that exposure of BO and OAC cells to short pulses of the acid, bile salts and nitric oxide that characterise refluxate can result in DNA damage.(193,241–244) This includes the development of double-stranded DNA breaks in cells treated with acid and nitric oxide.(193) The BO epithelium also appears able to avoid apoptosis despite the presence of DNA damage, potentially contributing to increased genomic instability.(243,245)

Considerable focus has been applied to determining the sequencing of mutations in the dysplastic progression of BO and in identifying mutations responsible for driving malignant progression. It has been recognised for some time that for many patients, loss of protein expression of the tumour suppressor p16 (INK4A) occurs early in progression via promoter methylation or loss of heterozygosity (LoH) of *CDKN2A*.(246,247) Loss of the tumour

suppressor *TP53* has been suggested as a marker for high risk disease and was considered to occur as late as HGD, but has more recently been recognised as early as NDBO.(230,237,238,248) Conflating understanding of the relevance of the mutational landscape further, there is relatively low overlap in the mutations present in BO and OAC tissue, whilst many putative oesophageal driver genes such as *ARID1A* and *SMARCA4* are recurrently mutated in stable, non-progressive BO samples.(229,237,238) Some have even been identified in oesophageal NSE, which is now recognised to be colonised by mutant clones as part of the ageing process.(249)

Similar to the OAC lesion to which it leads BO is, in addition, characterised by early chromosomal instability, reflected by gene-centric focal gains and deletions, and copy number variation termed aneuploidy. These together contribute to significant clonal diversity; the extent of which predicts progression to OAC.(250–252) Li and colleagues have previously demonstrated that chromosomal aberrations, including frequent genome doubling, are seen in 100% of patients biopsied within 48 months of cancer diagnosis.(253) Work from Stachler and colleagues has in addition suggested that in excess of 60% of OACs develop following genome doubling and that tumours with this ‘catastrophic aneuploidy’ feature frequent amplification of oncogenes but infrequent tumour suppressor inactivation.(238) Recent evidence suggests that polyploidy in OAC results from mitotic slippage caused by defective chromosome attachments.(254)

Together, these data indicate that a proportion of patients with BO may develop OAC via a prolonged process of progression involving the gradual loss of tumour suppressor genes such as *TP53* and those important to chromatin remodelling such as *CDKN2A*, *SMAD4* and members of the SWItch/Sucrose non fermentable (SWI/SNF) complex.(237,246–248,255) These likely generate clones that in some cases sweep across the whole BO segment and in other cases undergo branched evolution.(229) Alternatively, patients may instead progress more rapidly to cancer via the loss of *TP53*, catastrophic aneuploidy or chromothripsis, and consequent oncogene amplification.(238,239) Given that there is an inverse association between aneuploidy and the density of goblet cells, this pathway may explain the proposed heightened risk of dysplastic progression for SIM-poor BO lesions.(256)

Interestingly, Paulson and colleagues have very recently reported that progressive BO lesions may be distinguished from those that do not progress by the expansion of populations devoid of cellular tumour antigen p53 (p53) and which have complex structural variation and genomic amplification.(257) These features were detectable up to six years

prior to the development of malignancy. Killcoyne and colleagues have similarly shown that genomic copy number not only predicts the development of OAC, but can do so many years before dysplastic transformation.(258) In their analysis, few of the genomic regions predictive of OAC development clearly relate to cancer-related activity. They therefore predict that ‘the sum of many small changes and the breakdown of gene-regulatory control fuel oncogenicity’.(258) Despite this, the molecular mechanisms that link to microenvironmental BO stressors and that govern gene regulation during dysplastic progression remain vastly understudied.

1.1.2.4. Regulation of genetic expression

1.1.2.4.1. Epigenetic alterations

The epigenome and its constituents play a key role in modifying genetic expression without changing the DNA sequence.(259) The mechanisms through which this is achieved include the differential methylation of DNA, which is almost exclusively seen on cytosines in CpG dinucleotides, and the post-translational modification of histones.(259) CpG rich islands are commonly seen in gene promoters and their methylation results in transcriptional repression.(259) Histone modification, such as through modifying acetylation status, additionally alters the repression of one or multiple genes, but is generally more short lived.(259) Non-coding (nc-) ribonucleic acids (RNA; ncRNA) such as micro-RNAs (miRNAs), long non-coding RNAs (lncRNAs) and piwi-interacting RNAs (piRNA) also act to modulate genetic expression and are regarded as epigenetic regulators.(259,260) Importantly, the epigenome is mitotically stable and changes to it may be inherited across generations via the germline, or may develop somatically in response to environmental pressure.(261)

A number of epigenetic changes are recognised in BO, though it is unclear whether many of these arise as a consequence, or as a cause, of disease progression.(262) Changes to the methylation status, or methylome, of DNA are perhaps the most studied and are recognised to occur early in the progression of BO.(263,264) Within intergenic and non-coding regions, early and widespread hypomethylation is noted.(265) In contrast, hypermethylation of promoter regions is seen and increases from 40-50% of patients with NDBO to around 90% of patients with HGD.(262) This appears to occur as part of a process of age-related methylomic drift, though there is in addition evidence that OAC risk factors such as obesity, tobacco smoking and GORD influence the BO methylome.(266–268)

Importantly, numerous hypermethylated loci map to genes that are implicated in the progression of BO; many of which, as summarised in **Table 1.4**, have tumour suppressor

Gene	Function	Promoter methylation (%)			Associations	Refs
		NDBO	L/HGD	OAC		
AKAP12	B ₂ -adrenergic receptor complex constituent.	39	52-53	52-53	Correlates with lesion length.	(262,269)
APC	Interacts with β-cadherins.	50-95	61-100	61-100	Predicts progression to OAC.	(262,270–272)
CDH13	Cadherin.	70	77.5	76.1	Correlates with lesion length.	(262,273)
CDKN2A	Cell cycle regulator.	7-28	22-55	39-60	Common early event in dysplastic progression.	(262,274)
DAPK1	Mediates programmed cell death.	50	53	60	Correlates with severity of GORD.	(262,268)
GPX/GST	Antioxidants superfamilies	13-90	38-88	15-88	-	(262,275, 276)
MGMT	Repair of DNA alkylation damage	25-89	71-100	23-79	-	(262,268)
NELL1	Signalling molecule controlling mitogenesis	47	53	48	Correlates with lesion length.	(262,277)
RPRM	Regulates p53-mediated G2 cell cycle arrest	36	64	63	Correlate with lesion length.	(262,278)
SFRP	Secreted glycoprotein	73-89	73-89	73-93	Wnt signalling component.	(262,279)
SOCS1	Suppressor of cytokine signalling	-	4/21	42	-	(262,280)
SOCS3	Suppressor of cytokine signalling	13	22/69	74	-	(262,280)
SST	Inhibits gastric acid secretion	70	63/71	72	Correlates with lesion length. Predicts progression to OAC.	(262,281)
TAC1	Neurokinin – proliferative & anti-apoptotic	56	58	61	Correlates with lesion length.	(262,282)
TIMP3	Inhibits tumour growth	54-88	71-78	20-86	-	(272)
WIF1	Wnt antagonist	-	52	83	Wnt signalling component.	(262,279)

Table 1.4. A summary of genes implicated in the development of OAC for which promoter methylation is recognised in BO, OAC, or both.

activity. In their recent analysis, in which they integrated DNA methylation profiles with transcriptomic and genomic data, Jammula and colleagues identified four epigenetically-defined BO subtypes that provide further evidence for the impact of the methylome on disease outcomes.(283) These include a hypermethylated subtype with a high mutation burden, a subtype in which a lack of methylation was seen at transcription factor binding sites as well as expression of genes associated with metabolic processes, an immune-infiltrated subtype in which no changes were seen in methylation compared with controls,

and a DNA hypomethylated subtype characterised by structural changes and copy number variation.

Whether histone post-translational modification also impacts on BO progression has received little attention. Providing at least a proof of principle, histone acetylation status has been identified as a regulator of *INHBA* expression, which is known to increase during BO progression.(284) Histone methylation has been studied in the context of OSCC but not OAC, though in this context the two have unfortunately been conflated within the literature.(285)

Non-coding RNAs have in contrast received rather more focus, particularly over the past decade following the identification in 2008 of distinct miRNA signatures associated with GORD and BO.(286) There are now in excess of 100 miRNAs proposed as contributors to BO progression; though the depth of evidence for these varies significantly.(287) Few studies have determined the target genes for these identified miRNAs, which limits their mechanistic evaluation despite the use of *in silico* analyses to predict miRNA-gene interactions that might be implicated in disease pathogenesis.(287)

The pleiotropic group of lncRNAs, which has a diverse impact on chromatin remodelling and RNA processing, has also been studied. Whilst this remains a relatively immature field, a small number of lncRNAs are implicated in BO progression and OAC development.(288) These include attenuated familial adenomatous polyposis (AFAP)-Antisense RNA 1 (AS1), which contributes to changes in actin filament integrity by facilitating proto-oncogene tyrosine-protein kinase Src (Src) activation.(289) There is a paucity of evidence relating to other ncRNAs in BO progression, though this seems likely to be an area in which research activity significantly increases over the forthcoming decade.

1.1.2.5. Protein pathways in BO progression and their relationship with microenvironmental stressors

1.1.2.5.1. Overview

Signalling cascades and the transcription factors they modulate are key to transducing messages from the extracellular and intracellular environments through to transcriptional, functional and phenotypical responses. Their activity is dependent on the protein expression of proteins within the cascade as well as the influence of post-translational modification (PTM). This enzymatic processing of ribosomally-synthesised proteins broadens the functional diversity of the proteome through an array of reversible and irreversible

Category	Process	Change in protein	Impact on protein
Cleavage	Proteolysis	Breakdown to polypeptide(s)/amino acid(s)	Activation/Inactivation Change in folding/function Neo-protein formation
	Acetylation	Addition of an -acetyl functional group	Change in folding/function Change in localisation
Chemical group addition	Methylation	Addition of a -methyl functional group	Activation/Inactivation Change in localisation
	Phosphorylation	Addition of a -phosphoryl functional group	Activation/Inactivation Change in localisation
Peptide addition	Sumoylation	Addition of a small ubiquitin-like peptide	Changes interaction surfaces
	Ubiquitylation	Addition of a ubiquitin peptide	Targeted for degradation
Complex molecule addition	Glycosylation	Addition of a carbohydrate	Change in folding/function
	Isoprenylation	Addition of hydrophobic molecules	Change in folding/function

Table 1.5. A summary of post-translational protein modifications and their impact on protein structure and function.

processes. These include protein cleavage or the covalent addition to amino acids of peptide side chains, complex molecules or chemical groups via the processes outlined in **Table 1.5**.

As detailed within this table, these actions are vital to either directly regulating protein activity, or to indirectly influencing it by impacting on protein spatial structure, subcellular location or destruction. They may also provide greater protein diversity through the formation of neo-proteins following proteolysis. Crucially, PTMs rarely occur in isolation and it is the network of proteins affected by the multiple impacts of many PTMs that shapes cellular behaviour.

The function and phenotype of BO cells is therefore dependent not just on the genomic factors outlined thus far, but also on the impact of PTMs on the proteins to which these translate, as well as the genes transcribed by the signalling cascades to which these proteins belong. One option for studying these is to analyse snapshots of the presence of PTMs such as phosphorylated residues in target molecules, and the protein expression of these molecules, within fixed tissues at different stages of BO dysplastic progression. Alternatively, the direct impact of microenvironmental stressors linked to BO progression can be studied through the evaluation of induced PTMs, changes in gene expression and corresponding cellular phenotype and behaviour following the *in vitro*, *ex vivo* or even *in vivo* exposure of BO cell lines, primary cultures or *in situ* lesions to the microenvironmental stressors such as acid or bile salts that are linked to disease progression.

The capacity for acid to impact on BO cellular behaviour has for instance been recognised for more than two decades.(189) In *ex vivo* and *in vitro* analyses respectively undertaken using BO tissue and a colorectal carcinoma cell line selected for its intestinal cell derivation, pulsatile acid exposure was found to trigger proliferation and block cellular differentiation.(189,290) In contrast, sustained exposure of BO tissues to acid results in cellular differentiation but abrogates proliferation.(189,290) Adding further layers of complexity, exposure of *ex vivo* BO specimens to bile salts induces proliferation at neutral pH but restricts it at acidic pH.(291)

A number of studies have expanded on this work in an effort to understand the PTM landscape of BO as well as its relationship to microenvironmental stressors. This work has however received relatively little recent focus within the BO literature and existing studies are beset by a raft of limitations. Many are, for example, historical and are accordingly restricted to the biased analysis of a small number of molecules within a limited number of pathways. As a consequence of a previous paucity of well-characterised BO cell lines, a majority of these studies also use cells thought to be representative of NSE or invasive OAC to model the pre-malignant BO epithelium. This includes the SEG-1 and BIC-1 lines, which have formed the backbone of over a decade of research focussed on the BO response to microenvironmental stressors on the basis that they represent OAC, but which are now recognised to derive from extra-oesophageal tissue.(292) SEG-1 cells are instead derived from the large cell lung cancer H460 cell line (American Type Culture Collection (ATCC®)_HTB-177), whilst BIC-1 derives from the colorectal adenocarcinoma cell line SW620 (ATCC®_CCL-227).(292) Further restricting the utility of these analyses, there is such significant variation in the concentrations and pH of treatments used to induce PTMs that it is challenging to compare the PTM response to microenvironmental stressors between disease stages, and between NSE and for instance NDBO and HGD or OAC. The chronicity of exposures also varies, and whilst the signalling pathways underlying pro-proliferative stressor pulses have received significant attention, potentially pro-differentiative but anti-proliferative chronic exposures have not.

Nevertheless, and in spite of this array of limitations, there is evidence for the activation during BO progression and in response to microenvironmental stressors of a number of signalling cascades and the transcription factors on which they converge. There is in addition recognition of a potential role in dictating BO dysplasia for the steroid and peptide hormones that characterise obesity and the metabolic syndrome, the actions of which are respectively

mediated by nuclear receptors or intracellular signalling cascades. These signalling pathways are considered separately below and summarised in **Fig. 1.3**.

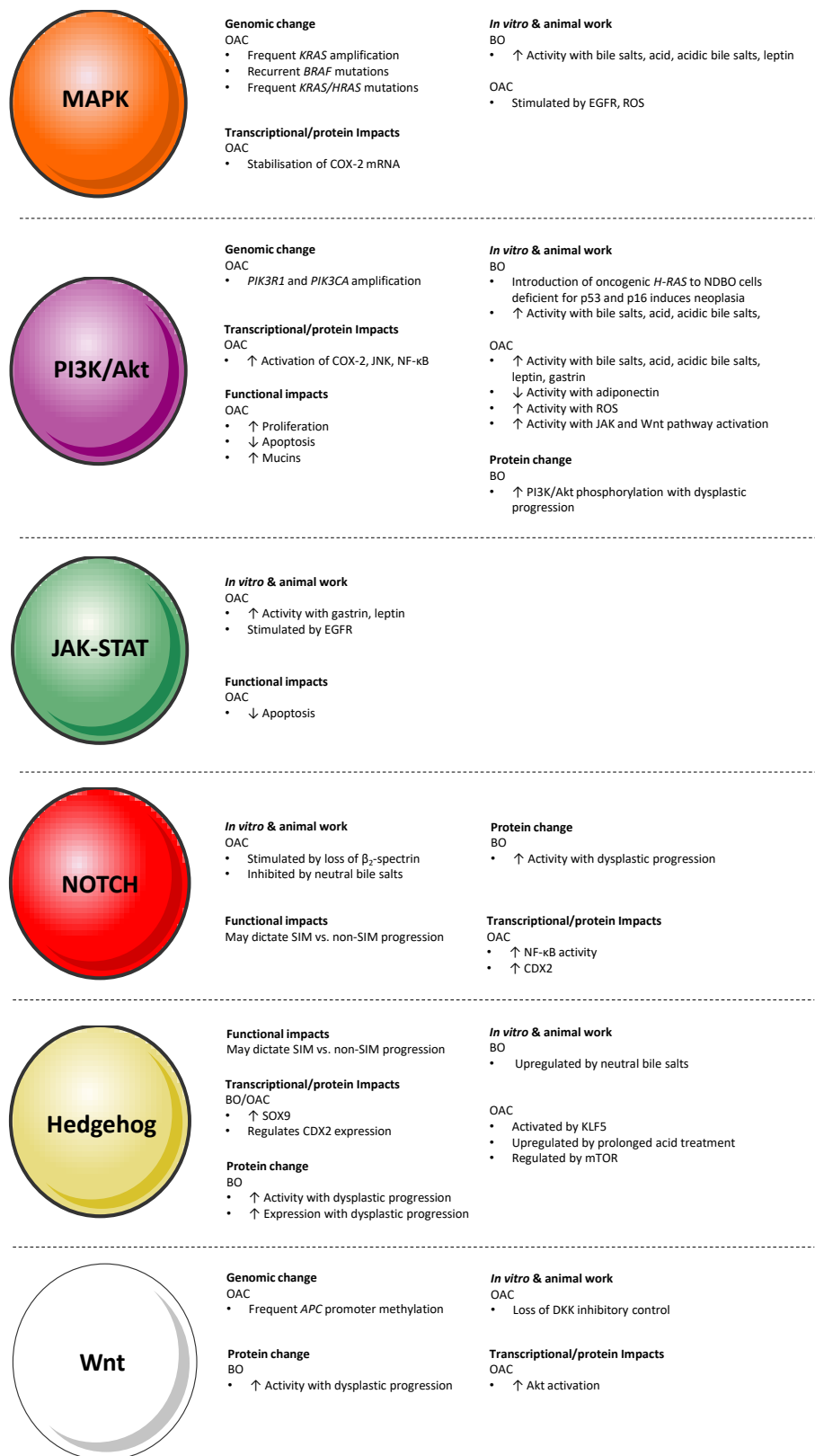


Figure 1.3. An overview of non-inflammatory signalling pathways implicated in the progression of BO and development of OAC. Key aspects of the relationship of each signalling pathway with BO are listed.

1.1.2.5.2. The mitogen-activated protein kinase (MAPK) and phosphatidylinositol 3-kinase (PI3K) – RAC-serine/threonine protein kinase (AKT) pathways

The MAPK pathways are amongst the most well characterised in cancer biology and control cellular proliferation, migration, survival and differentiation.(293) Three signalling cascades exist, each of which comprises at least two, but generally more than three, tiered serine/threonine kinases that each require tandem activation loop phosphorylation for activation. The classical extracellular signal-regulated kinase (ERK) pathway is predominantly activated by transmembrane RTKs, which interact with growth factor receptor bound protein-2 (GRB2) and son-of-sevenless homolog 1 (SOS) to trigger a phosphorylation cascade originating from the small GTPase Ras. In contrast, the p38 MAPK and c-Jun N-terminal kinase (JNK) pathways, which feature considerable cross-talk, respond to cytokine receptors, G-protein coupled receptors (GPCRs, which are also less common activators of the ERK pathway) and stressors that include heat and osmotic shock.(294) Transcription factors downstream of the MAPK pathways include Myc proto-oncogene protein (c-Myc), proto-oncogene c-Fos, cyclic adenosine monophosphate (cAMP) response element-binding protein (CREB), p53 and activator protein-1 (AP-1).

Similarly to the MAPK pathway, PI3K/AKT signalling is highly-conserved and predominantly initiated by activated RTKs, GPCRs and cytokine receptors.(295) These induce activation of PI3K, either directly or via an adapter such as insulin receptor substrate (IRS) 1, which catalyses the conversion of phosphatidylinositol (4,5)-biphosphate (PIP₂) to phosphatidylinositol (3,4,5)-triphosphate (PIP₃) in the plasma membrane. This step can be reversed by the tumour suppressor phosphatase and tensin homolog (PTEN). The MAPK component Ras also influences PI3K activity, thereby providing an avenue for cross-talk between two vital cellular pathways.(296) Once formed, PIP₃ recruits AKT to the plasma membrane, resulting in a conformational change that permits phosphorylation of the threonine (Thr) 308 residue within the AKT activation loop by phosphoinositide-dependent protein kinase 1 (PDK1). This partially activates AKT, resulting in the phosphorylation and consequent inactivation of tuberous sclerosis protein (TSC) 2 and proline-rich AKT substrate of 40kDa (PRAS40). Mammalian target of rapamycin complex 1 (mTORC1) is released as a consequence and acts to promote proliferation, protein synthesis and angiogenesis. Full activation of AKT is achieved by the phosphorylation of the serine (Ser) 473 residue via either released mTOR or the activation of DNA-dependent protein kinase (DNA-PK). Once fully active, AKT inactivates the forkhead transcription factors (FOXO) and results in the

activation of transcription factors such as β -catenin, CREB and NF- κ B; thereby promoting survival, proliferation and migration.

Increased activation of the MAPK pathway by microenvironmental stressors, overexpression or activating mutation are suggested as drivers of BO dysplastic progression and OAC.(297) As described in **1.1.2.3.2.**, Frankell and colleagues recently identified frequent amplification, and therefore overexpression, of *KRAS* and recurrent activating *BRAF* mutations in a large series of OAC cases.(235) Previous studies have suggested that oncogenic mutations of *KRAS* or *HRAS* are acquired in up to 40% of cases of BO dysplasia and OAC, with *BRAF* mutants found in 5-10%.(298–301) Changes to genes encoding for PTEN and PI3K, including *PIK3R1* and *PIK3CA*, are also recognised to drive OAC.(235) However, rates of mutation and amplification are lower than that seen for the MAPK pathway, and as previously described (**1.1.2.3.**), neither mutations of MAPK components nor of PI3K/AKT have been identified as recurrent drivers of dysplastic progression.(297) There is in addition minimal overlap between the proposed genomic drivers of BO and of OAC.

Increased phosphorylation of PI3K/AKT pathway components is nevertheless seen as dysplasia worsens, associating increased activity with dysplastic progression.(302,303) It has in addition been demonstrated that upregulating MAPK and PI3K/AKT activity via the introduction of oncogenic *H-RAS* to a NDBO cell line deficient for p16 and p53 is capable of promoting neoplastic transformation.(304) Perhaps underlining a role for induced MAPK and PI3K/AKT PTM in driving BO progression, the increased activity of both pathways has been reported following exposure to components of the BO microenvironment such as the adipokines leptin and gastrin, as well as acid and both neutral and acidified bile salts.(217,305–314) However, the mechanisms underlying this remain poorly characterised.

In the OAC OE33 cell line, leptin results in direct phosphorylation of the ERK and PI3K/AKT pathways, resulting in activation of cyclooxygenase (COX)-2 and prostaglandin production that feed forward to activation of JNK.(217) These actions together stimulate proliferation and inhibit apoptosis.(217) The peptide hormone gastrin, which may be elevated in patients treated with PPIs, also stimulates proliferation and inhibits apoptosis in the OAC cell lines OE33 and OE19 by first activating the chemokine 2 (CCK₂) receptor.(173,313,314) This induces activity of the PI3K/AKT, janus kinase (JAK) 2 and NF- κ B pathways, which in turn trigger COX-2 activation.(314) In contrast, adiponectin appears to abrogate leptin-induced proliferation and promote apoptosis within the same cells, at least in part by inhibiting AKT activation.(313,315)

Many of the effects of pulsatile bile salt, acid or bile acid exposure are considered to be mediated by increased activation of the MAPK and PI3K/AKT pathways. Stimulation of the former in response to an acid pulse was first reported in SEG-1 cells in 2002.(305) In subsequent studies using this and the BIC-1 cell line, investigators have shown that following a pulse of acid treatment, the phosphorylation of p38 and ERK rapidly increases.(305,307) These together contribute to increased promotion of the COX-2 gene, whilst ERK also acts to stabilise COX-2 messenger RNA (mRNA).(306,308) JNK phosphorylation occurs in response to an acid pulse but occurs later than that of ERK and p38.(305,307) Treatment with bile salts at neutral pH also results in upregulation of COX-2 but this may be mediated by PI3K/AKT pathway activation in addition to increases in the phosphorylation of ERK and p38.(310,316–318) At an acidic pH, bile salt treatment results in expression of MAPK-target genes, potentially demonstrating the prominence of acid-related signals in the cellular response to acidic bile salts.(319) Genes upregulated by acid-induced increases in MAPK activity in SEG-1 cells include cyclin D1, cyclin E, c-Myc, B-cell lymphoma 2 (Bcl-2) and single transducer and activator of proteins (STAT)-3.(308,309) Expression of c-Myc is upregulated in dysplastic BO though this has been attributed to genomic amplification.(320)

Some but not all of these findings have been confirmed in cell lines validated to derive from oesophageal tissue. In the OE33 line, an acid pulse results in MAPK activation via phosphorylation of the epidermal growth factor receptor (EGFR).(218) Interestingly, a synergistic response is generated when these same cells are concomitantly treated with leptin.(218) In contrast, exposure to bile salts for 12-18 hours in OE33 and SK-GT-4 OAC cells results in upregulation of mucins via the PI3K/AKT pathway.(321–323)

There is a paucity of evidence on MAPK and PI3K/AKT activation within validated non-malignant BO cell lines. However, there is evidence that MAPK is frequently phosphorylated in squamous mucosa adjacent to BO lesions, indicating that increased pathway activation in the lower oesophageal environment may be ubiquitous to all cell types, or may occur early in BO progression.(324) Somewhat surprisingly, kinome profiling of *ex vivo* samples has in addition revealed higher MAPK and EGFR activity in NSE than is present in BO tissue.(325) In an *in vivo* feline study, Park and colleagues determined that NSE ERK and PI3K/AKT activation in response to acid were dependent on ROS, whereas p38 upregulation was not.(326) Demonstrating pathway crosstalk, PI3K/AKT activity resulted in activation of the NF-κB pathway.(326)

1.1.2.5.3. The JAK - STAT pathway

The four JAK and seven STAT proteins that can be involved in the JAK-STAT pathway predominantly respond to activation of cytokine receptors but communicate with both the MAPK and the PI3K-AKT pathway, including via phosphorylation of GRB2.(294,295,327) Activated STAT transcription factors regulate cell growth, differentiation and numerous aspects of cellular immunity.(327)

In OAC OE33 and the NDBO QhTRT cell line (erroneously labelled as QhERT by the authors), treatment with gastrin results in activation of JAK2 and STAT3, inhibiting apoptosis as a consequence.(328) Activation of JAK2 in response to both gastrin and leptin also stimulates proliferation of OAC OE33 and OE19 cells, though this is thought to be at least partly dependent on JAK-2 mediated PI3K/AKT, ERK and NF- κ B transactivation.(217,314) STAT3 is nevertheless also reported to promote OAC proliferation and has been suggested as a druggable driver of disease.(329,330) The activity of STAT3 may be modulated by acid and acidic bile salts via a pathway centred on IL-6, though experimental data supporting this derive from SEG-1 cells.(183) There is in addition data drawn from NDBO (CP-A), HGD (CP-B) and OAC (FLO-1, OE33) cell lines that indicates a role for EGFR in activating STAT3 in response to acidic bile salts in a pathway dependent on redox activity and the apurinic/aprimidinic endonuclease 1 enzyme (APE1).(331)

1.1.2.5.4. The Notch pathway

Notch signalling derives from the activation of one of four highly-conserved bipartite single pass transmembrane receptors.(332) Following ligand binding, proteolysis of the receptor results in liberation of its intracellular domain, which subsequently enters the nucleus and modifies gene expression. In the gastrointestinal tract, this includes through promotion of transcription factor HES-1 (HES-1), which inhibits expression of the *ATOH1* gene that drives goblet cell differentiation.(333) This is therefore an important mechanism for stem cell maintenance and for enabling protective intestinal self-renewal. Perhaps unsurprisingly given this, it has also drawn focus as a potential mediator of both the metaplastic origin for BO and its dysplastic progression.

Supporting a potential role in the progression of BO, increased Notch activity during dysplastic progression is reported in patient tissues, a murine model of disease and human cell lines.(143,164,334) In contrast, intact activated Notch signalling is not seen in oesophageal NSE.(164) In a recent parallel human and murine study, Notch activity was found to be inversely proportional to goblet cell density, suggesting that it reduces the

differentiation of gastric cardia progenitor cells to SIM.(335) The authors provide evidence that this is mediated through Notch induction of the NF- κ B pathway.(335) Supporting this role for Notch, *ATOH1* expression is increased in SIM compared with non-SIM BO tissue.(334) Adding further complexity, previous work undertaken in OAC FLO-1, SK-GT-4 and BE3 cell lines suggests that loss of the TGF β signalling adapter β 2-spectrin (β 2SP) facilitates increased Notch activation, which in turn activates SOX9.(336,337) There is in addition evidence that the single-pass transmembrane γ -secretase protein acts to activate Notch signalling in OAC OE33 as well as SK-GT-5 cells, though the latter cell line is now thought to more closely resemble a primary gastric fundal adenocarcinoma.(164,292)

There has been limited analysis of the impact of microenvironmental stressors on this process. However, treatment of OAC OE19 and OE33 cell lines with neutral bile salts results in Notch pathway inhibition, which in OE19 cells led to an increase in ATOH1 and the intestinal marker CDX2.(163,338) Whilst evidence for this is therefore limited, it is possible that the degree of Notch pathway activation dictates whether BO progresses via a differentiated SIM pathway or via an alternative form of dysplastic progression that does not involve SIM.(164,339)

1.1.2.5.5. The Hedgehog signalling pathway

The Hedgehog signalling pathway is characterised by binding of the sonic hedgehog (SHH) ligand to the patched-1 (PTCH1) receptor.(340) This releases PTCH1-mediated smoothed (Smo) inhibition, resulting in activation of the zinc-finger glioma-associated oncogene (GLI) transcription factors which inhibit apoptotic processes and stimulate those relating to migration and proliferation through a variety of target genes, including *BMP4*.(340) The Hedgehog pathway is important to development of the embryonic gastrointestinal tract but is in addition implicated in the development of multiple digestive tract tumours.(341) This includes the oesophagus, where Hedgehog signalling is connected to the development of the BO lesion as well as its dysplastic progression to OAC.(342)

Unlike oesophageal NSE, which does not feature Hedgehog pathway activity, SHH and PTCH1 expression is frequently identified in BO epithelium.(160) In keeping with an active Hedgehog pathway in BO but not NSE, *BMP4* is abundantly expressed in the former but not the latter.(155,343) As with Notch signalling, Hedgehog pathway activity appears to differ between SIM and other BO cells, with lower expression of SHH found in columnar mucosa with goblet cells than those without.(160)

There is evidence that Hedgehog activation (evidenced through increased expression of BMP4) occurs early in the non-SIM epithelia of patients who undergo BO progression.(344) Expression of Hedgehog signalling components nevertheless increases from BO to a maximum in OAC across cell lines, a rat model of BO progression and in patient samples.(345,346) Providing evidence for a causal association, reduction of hedgehog signalling via itraconazole treatment reduced progression to OAC in a rat model of BO dysplasia.(347)

There is some evidence for the action of downstream mediators of Hedgehog signalling in BO progression but it is incomplete. In NSE Het-1A cells, BMP4 activates SOX9; the expression of which is associated with Hedgehog pathway activation in human BO specimens.(159,348) Zinc finger protein GLI1 (GLI1) regulates cyclin dependent kinase (CDK) 2 expression in a rat model of BO oesophagus as well as in NDBO CP-A, HGD CP-C and OAC SK-GT-4 and FLO-1 cells, though its action is thought to be independent of Smo.(345)

Upstream, evidence from OAC (SK-GT-4, OE33) cell lines suggests that Hedgehog signalling is dependent on the activity of the Krüppel-like factor 5 (KLF5) transcription factor.(346) Microenvironmental exposures also impact on pathway components. In NSE Het-1A and OAC OE33 cells, prolonged acid treatment results in upregulation of SHH expression.(159) Bile salts administered at neutral pH similarly upregulate GLI1 and PTCH1 expression in NDBO CP-A and HGD CP-B cells, whilst the expression of BMP4 and PTCH1 are significantly higher in patients exposed to high concentrations of deoxycholic acid (DCA) within refluxate.(160,348) GLI1 expression may also be controlled by mTOR in OAC, reflecting the influence of pathway cross talk.(349)

1.1.2.5.6. The Wnt signalling pathway

Wnt signalling is characterised by ligand binding to the transmembrane GPCR Frizzled (Fz) family of receptors.(350) This can be inhibited by binding of Wnt inhibitory factor 1 (WIF1) to Wnt proteins. In its absence, bound Wnt ligands activate the cytoplasmic protein dishevelled (Dsh) in a process that in some instances requires cooperation from RTKs. Classically, Dsh acts to retain and stabilise β -catenin within the cytoplasm, from where it migrates to the nucleus and acts as a co-activator to the T-cell factor (TCF)/lymphoid enhancer-binding factor 1 (LEF) transcription factor family, dictating cell fate, proliferation and migration. This includes through promoting the transcription of Twist and Slug, which directly inhibit the E-cadherin promoter. This process of Wnt signalling pathway activation is antagonised by dickkopf-related protein (DKK) - 1.

As with the Notch and Hedgehog pathways, Wnt signalling plays an important role in both the embryonic development of the intestine and its maintenance in the adult human. It is, as with these pathways, also implicated in the progression and development of both BO and OAC.(351,352) Increased activity of the Wnt pathway, as evidenced by nuclear accumulation of beta-catenin, appears to be an early feature in the dysplastic sequence and increases as the lesion progresses to OAC.(353–355) Supporting this, increased expression of Wnt target genes is seen as BO lesions progress through worsened dysplasia, with for instance increased expression of TCF4 in LGD versus NDBO.(334,356,357) Significant reduction of E-cadherin expression is also seen during the metaplasia – dysplasia – OAC sequence.(355,358) This may be at least in part attributable to more frequent methylation of the E-cadherin promoter at higher grades of dysplasia but additionally reflects increased Wnt activity.(359) OAC is characterised by significant nuclear accumulation of both beta-catenin and slug, with the latter instead predominantly seen in the cytoplasm in non-invasive disease.(354,355,360) Interestingly, nuclear expression of beta-catenin is reported to be an independent prognostic factor in OAC.(354,355)

It is unclear to what extent Wnt pathway activity is a feature of metaplastic disease. Nuclear beta-catenin was not seen in NDBO human samples or at this disease stage in a mouse model of BO progression.(356) It is however a feature of the NDBO CP-A cell line and both Wnt3a and the products of Wnt target genes, such as AXIN2, c-Myc, Cyclin D1 and DKK1, are overexpressed in NDBO tissues compared with NSE.(357) Interestingly, TCF4 expression and thereby Wnt signalling may be higher in SIM.(361)

This trend to increased Wnt activity during dysplastic progression does not arise through mutational change of its components.(362) Instead, it may be at least in part a consequence of frequent promoter methylation of the *APC* gene and genes encoding for the Wnt antagonists frizzled receptor protein 1 and WIF-1.(363,364) Cell line work has in addition revealed that whilst in NDBO (CP-A) cells, DKK is capable of exerting control over Wnt3a-mediated signalling activation, this is perturbed in OAC OE33 cells.(357,365) DKK expression is nevertheless high in OAC and there is evidence that it instead seems to act through inducing phosphorylation of AKT. In a further example of pathway crosstalk, WNT5A acts as a tumour suppressor in OAC by binding to the RTK-like orphan receptor (ROR)-2, which is frequently overexpressed in invasive disease, though in the absence of ROR2 overexpression instead acts as a tumour promoter.(366) Expression of WNT5A decreases during BO dysplastic progression.(366) It is unclear to what extent, if at all, microenvironmental stressors impact on Wnt activity.

1.1.2.5.7. The NF- κ B pathway

The NF- κ B family of transcription factors comprises of five proteins that form homo- or hetero- dimeric complexes.(367) These are constitutively retained within the cytoplasm by inhibitor of κ B (I κ B) proteins. Stimuli such as genotoxic stress and cytokines cause NF- κ B-mediated transcription by first activating I κ B kinase (IKK) proteins which, through phosphorylating I κ B, cause the release and subsequent nuclear translocation of the NF- κ B dimer. DNA binding of this dimer rapidly controls a raft of immune, cell survival and proliferation processes, including the expression of a raft of pro-inflammatory cytokines.

NF- κ B signalling has been studied in the context of the metaplastic BO step and as a potential mediator of dysplastic progression. Supporting a potential role in the latter process, the expression of NF- κ B proteins increases across the metaplasia-dysplasia-OAC sequence.(368) This may, in part, relate to hyperploidy of NF- κ B-encoding chromosome 4, which is frequently seen as an early event in BO progression.(369) Increased activation of NF- κ B and expression of its target genes is also seen as dysplasia worsens, and may be induced by acid and bile salts.(153,370–374) In the OAC OE19 and OE33 cell lines, prolonged treatment with bile salts at neutral pH resulted in NF- κ B translocation to the nucleus and expression of its target genes.(373,375,376) In contrast, a less convincing change in activity is seen within these same cells following a short pulsatile bile salt treatment and it has been postulated from work undertaken in OAC cell lines that bile salts activate NF- κ B at neutral but not acidic pH.(374,377) However, pulsatile acid exposure, with and without bile salts, did upregulate NF- κ B activity in BO tissue treated *ex vivo*, in the problematic SEG-1 cell line and across NSE (HET-1A), NDBO (BAR-T) and OAC (OE33, FLO-1) cell lines, with an even greater response seen from the addition of bile salts at an acidic pH.(371,372,378)

There has been relatively little focus on the mechanisms linking gastric refluxate to an increase in NF- κ B activity, though in oesophageal NSE it appears to relate to nitric oxide production.(374) In the context of immune cells, nitric oxide is similarly commonly seen to invoke NF- κ B tyrosine phosphorylation but no previous evidence for this has been provided in BO.(379) Instead, the tribbles homolog (TRB) - 3 is reported to regulate NF- κ B in response to bile salts at a neutral pH in both NSE Het-1A and OAC SK-GT-4 cells.(380) Linking with a direct impact from inflammatory mediators, stimulation of toll-like receptor (TLR) 4 with lipopolysaccharide also leads to an increase in NF- κ B activity in NDBO BAR-T cells.(381) A number of cytokines are additionally considered to promote NF- κ B activation, including IL-17A and TNF α , though an association of NF- κ B activation with cytokine upregulation is only evident in patients with OAC.(153,176,208,382,383) In both BO and OAC, upregulation of

NF- κ B activity in response to neutral and acidic bile salts is independent of ROS.(383) Interestingly, exposure to cigarette smoke enhances reflux-induced NF- κ B in a rat model of BO progression.(384)

Downstream, NF- κ B activation increases COX2 and CDX-2 in cell lines and is associated with their increased expression in tissue analyses.(372,376,381) It also results in the activation of DNA methyltransferase, and has therefore been proposed as the cause for the early p16 gene hypermethylation seen in BO.(385) In BO CP-A, HGD CP-B and OAC FLO-1 & OE33 cells, NF- κ B targets silencer of death domain and upregulates Bcl-2, which decreases cell apoptosis.(243,386,387) This process also requires NADPH oxidase, EF-hand calcium binding domain 5 (NOX5)-S and may sustain cells that have genetic damage secondary to reflux and that would otherwise die as a protective mechanism. In NDBO (CP-A), HGD (CP-C) and the non-oesophageal SEG-1 and BE3 cells, bile salts at neutral pH induce and deregulate mTOR and its co-chaperone TSC1 via IKK β signalling. (370)

The NF- κ B pathway is similarly active in NSE, particularly in patients who have developed BO.(388) As with BO, activation results from acid and bile salts, and results in CDX2 induction. (388–391) However, unlike in established BO, the non-classical NF- κ B pathway may be the key pathological mediator of its metaplastic formation.(392)

1.1.2.5.8. The COX-2 – prostaglandin E₂ (PGE₂) pathway

The COX enzymes catalyse the conversion of arachidonic acid into the intermediary prostaglandin H₂, which acts as a substrate for the synthesis of prostaglandins and thromboxanes. These modulate immune responses and inflammation, underlining the rationale for therapeutic inhibition of COX by aspirin and NSAIDs.

The dysplastic progression of BO is marked by increased expression of both COX-2 and PGE₂ receptor 2.(211,393–402) Underlining a potential role for the COX-2 – PGE pathway in BO progression, a number of polymorphisms of the COX-2 gene are associated with an increased risk of progression to OAC.(403–405) COX-2 protein expression is in addition upregulated by a number of microenvironmental stressors common to the BO microenvironment, though it is independent of the degree of local inflammation.(406) These include gastro-duodenal refluxate, which in a rat model of GORD and in *ex vivo* analyses is associated with a significant increase in COX-2 expression within NSE.(407,408) Upregulation of COX-2 and downstream PGE₂ production is also seen following exposure to bile salts at neutral pH and acid in OAC SK-GT-4 cells and the SEG-1 cell

line.(317,318,394,409) Similar findings are seen in the NDBO BAR-T cell line, though acid resulted in greater COX-2 upregulation than was seen with bile salts.(410) It has been suggested that unconjugated bile salts may be more potent upregulators of COX-2 than conjugated bile salts, but this conclusion was drawn from work undertaken in an OSCC cell line.(407) Interestingly, *H. Pylori* is also recognised to cause upregulated COX-2, albeit in NSE.(411)

A number of pathways are reported to contribute to upregulated COX-2 expression. This includes the PI3K/AKT pathway and the cooperative action of p53 and NF- κ B in NSE.(396,407) Interestingly, EGFR is reported to cross-talk with COX-2 and pro-inflammatory cytokines in a rat model of reflux but the mechanism for this is unclear.(412) It is suggested on the basis of work undertaken in SEG-1 cells that bile salts and bile acid result in EGFR phosphorylation, which then leads to CDX2 expression.(311) In OAC SK-GT-4 and OE33 cells, neutral bile salts upregulate COX-2 via PI3K/AKT, ERK, protein kinase C (PKC) and p38, which are reported to result in induction of AP-1 (comprising of Fra-1 and JunB) and CREB.(317,318,409) In OAC FLO and OE33 cells, pulsatile acid treatment results in increased microsomal prostaglandin E synthase 1 (PGES1) via the action of NOX5-S and NF- κ B.(413)

In OAC, COX-2 overexpression is associated with poorer survival and a greater likelihood of lymph node metastases, which has been linked to its induction of angiogenesis and proliferation.(414) Supporting a role for the COX-2-PGE₂ pathway in regulating angiogenesis, PGES expression correlates with vascular endothelial growth factor (VEGF)-A and VEGF-C expression in BO tissue, whilst in NSE tissues examined *ex vivo*, COX-2 directly regulates VEGF production.(398,415) Supporting a role for COX-2 in supporting cellular growth and viability, COX-2 promotes proliferation and antagonises apoptosis in primary BO cultures, OAC FLO, SK-GT-4 and OE33 cells, and in BIC-1 and SEG-1 cells. (318,397,401,416–418) There is evidence that in OAC, PGE₂ may specifically contribute to the inhibition of apoptosis whilst PGE₁ promotes proliferation.(419) In keeping with these functions, inhibition of COX in mice OAC xenografts and a rat model of BO progression decreases disease growth and progression.(420,421) Aspirin is nevertheless insufficient to prevent BO progression when used alone, though it does delay dysplastic progression when used alongside PPIs.(101,422)

1.1.2.5.9. Cell cycle regulators

Loss of the tumour suppressor p53 is widely accepted to denote high-risk disease in BO, though the point in the dysplastic sequence at which genomic aberration of *TP53* occurs remains contested.(229,237,238) In an *in vitro* analysis in which BO cells were treated daily

with bile salts at acidic pH for over 65 weeks, p53 protein expression reduced but the mechanism for this was unclear.(168) In colon tumour cells, bile salts stimulate proteasome-mediated p53 degradation, which though proposed as a possible causative mechanism for p53 downregulation was not seen in a study using BO epithelial cells.(423,424) Instead, acid exposure has in fact been associated with higher expression of p53 in BO epithelium and may act to suppress proliferation.(425) In contrast, the p53 family member p63 is downregulated in response to acid and bile salts at neutral pH, or to a greater extent with bile salts at acidic pH, in NSE and in SEG-1 and BIC-1 cells.(426) Finally, the p53 homologue p73 increases in expression and activity in response to bile salts and is thought to protect against DNA damage in a process regulated by c-Abl.(242,424) A dominant-negative N-terminally truncated p73 isoform, $\Delta Np73$, is overexpressed in OAC and acts as an oncogenic protein, resulting in increased DNA damage.(427)

1.1.2.5.10. Cytokines

The inflammatory gradient to which BO lesions are exposed is summarised in **1.1.2.3.1**. It is also apparent, as outlined in **1.1.2.5.7.**, that cytokines both influence and are influenced by NF- κ B and JAK-STAT signalling. Through this mechanism, there is evidence of upregulation of cytokines including IL-6, IL-8, IL-1b and TNF- α in NDBO BAR-T cells, in a dose-dependent manner, in response to the contents of gastric refluxate.(373) Deregulation of TGF β signalling, which would ordinarily regulate proliferation, is also implicated in Barrett's progression.(205) Work undertaken in tissue and in NSE Het-1A and both NDBO CP-A and OAC OE-33 cell lines shows that TGF β expression is lower in BO and OAC than in NSE.(428) Mutation and loss of heterozygosity of its downstream mediators *SMAD2* and *SMAD4* also occurs during BO progression, as does a reduction in their protein expression.(205,255,429)

1.1.2.5.11. Growth factors

Frequent overexpression of the RTKs to which a wide variety of growth factors bind is seen in both OAC and BO, with a number linked to the activation of the MAPK and PI3K/Akt pathways.(236,430,431) There is in addition emerging but incomplete evidence of a link between activated signalling from RTKs such as EGFR and BO progression.(331) This is explored in greater detail in **Chapter 5**.

1.2 Conceptual overview: stepwise neoplastic transformation and the role of microenvironmental stressors

The development of cancer is characterised by the acquisition of an array of cancer hallmarks.(432) Many of these distinguish OAC from BO yet, as has been evidenced here, a number are acquired during the progression of NDBO through LGD and HGD. Under the terms of the Nowell hypothesis, cancer was previously thought to result from a stepwise selection of genomic mutations.(433) This does not appear to be the case in BO, and indeed there is at present a wider recognition across an array of cancers that malignant transformation may be more complex. It is for instance increasingly recognised that an abundance of mutations, including of classically-considered cancer drivers, are seen in normal somatic tissues; oesophageal NSE alone harbours in excess of 2000 mutations by 60 years of age.(249,434,435) It is also clear that dysplastic progression of BO can be halted or reversed, even following the acquisition of some cancer hallmarks.

Barrett's is therefore more likely to progress in the context of a multitude of genomic changes and, crucially, a breakdown in the regulation of these genes and their protein products.(258) As Balmain highlights in a recent review focused on the broad concept of cancer promotion, it is recognised in the context of skin cancers that whilst mutations are required for carcinogenesis, they are insufficient for the development of cancer in the absence of the action of cancer promoters.(435) Engström and colleagues have also recently identified the potential for environmental chemical mixtures to enable sustained proliferative signalling, which is a key cancer hallmark and which is in turn required for the exhibition of other cancer hallmarks.(436) As outlined here, BO is exposed to a number of potentially cancer promoting agents that may contribute to cellular dysregulation, including most pertinently GORD.

It is therefore crucial to understand the impact of GORD and its constituents on the promotion of dysplastic progression. Key to this is determining the impact of these microenvironmental stressors on the cellular protein constituents (proteome) to which the genome has translated, as well as the activity of these proteins (kinome) and their dynamic impact on the transcriptome and other more direct mediators of the cellular phenotype. However, as this introduction and **Fig. 1.3.** highlight, the BO proteome, kinome and dynamic reprogramming of the transcriptome have received a paucity of attention in comparison with analyses of the genome and transcriptome at fixed stages of disease pathogenesis. Further, and as has been highlighted here, existing analyses of the cellular response to microenvironmental stressors draw from inappropriate cell lines and are biased towards a

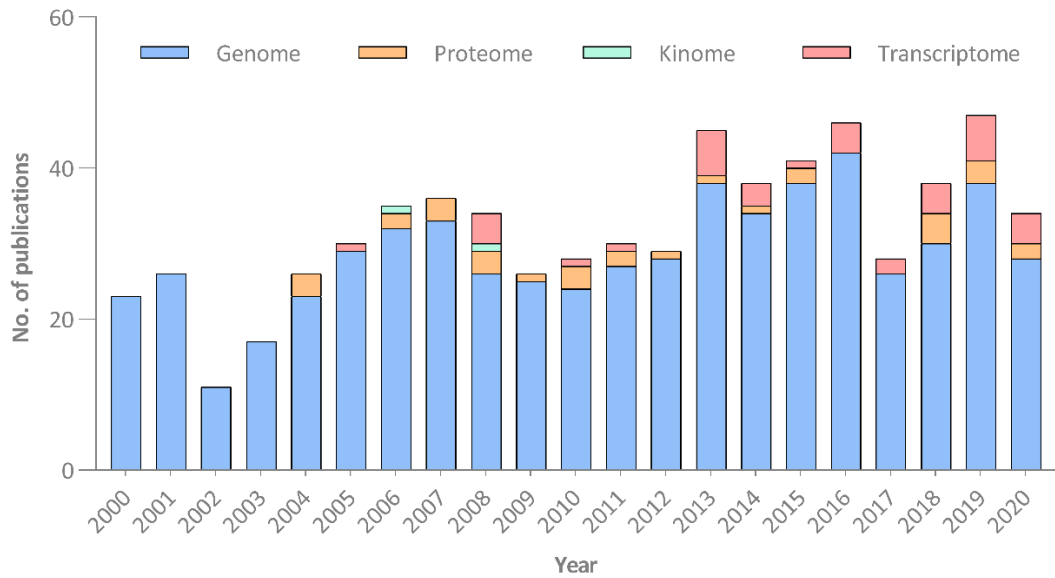


Figure 1.4. The number of publications focussed on the BO genome, proteome, kinome and transcriptome published each year for the past two decades. Published works were identified for each of the four categories by searching PubMed for [Barrett’s oesophagus] AND [Genome] OR [Proteome] OR [Kinome] OR [Transcriptome].

small number of pathways, with limited understanding of the extent to which these cross-talk. They are, in addition, united in their use of a diverse array of stressors; a significant consequence of which is that the cellular response to stressors at different stages of dysplastic progression, which may hold valuable clues to cancer promotion, is currently difficult to elucidate.

To this end, this work establishes standardised *in vitro* stressors that are representative of the microenvironment to which BO belongs. Using a combination of unbiased and targeted approaches, the impact of these on the cellular kinome and both its upstream activators and the transcriptome it promotes is evaluated. The extent to which these differ by stressor, between BO and NSE, and at different stages of BO progression are also determined.

1.3 Hypothesis

That exposure to stressors common to the BO microenvironment results in reprogramming of the BO cellular kinome and transcriptome to promote a pro-dysplastic, pro-oncogenic phenotype, and that the intensity and character of this cellular response is contingent both on the specific stressor and the stage of BO dysplastic progression at which it is applied.

1.4 Aims

1. To recapitulate microenvironmental stressors that are common to the BO microenvironment in an *in vitro* model system representative of NSE and of BO progression. Outlined in **Chapter 3**.
2. To determine the impact of different BO microenvironmental stressors on the Barrett's transcriptome and regulome. Outlined in **Chapter 3**.
3. To evaluate the impact of microenvironmental stressors on the kinome, and to determine the extent to which this differs between different stages, and between BO and NSE. Outlined in **Chapter 4**.
4. To determine the relative contribution of RTKs to the BO phenotype at different stages of dysplastic progression under basal conditions and in response to microenvironmental stressors. Outlined in **Chapter 5**.
5. To identify the causes and consequences of RTK-mediated signalling pathways in BO, particularly with respect to BO dysplastic progression. Outlined in **Chapter 5**.

Chapter 2 Materials and Methods

2.1. Overview

The following chapter provides details relating to materials and methods common to all or a number of the subsequent chapters. Information relating to methods specific to the work contained within a single chapter are presented individually within relevant chapters.

2.2. Reagents & plasticware

Unless otherwise stated, all reagents and chemicals were obtained from Merck KGaA or its subsidiary, MilliporeSigma, and all plasticware sourced from Corning® Incorporated. A full list of suppliers, including their location, is provided in **Appendix A**. Product codes and suppliers are provided in square brackets.

2.3. Cell culture

Unless otherwise stated, all cell culture procedures were performed in a class II biological safety cabinet using sterile tissue culture flasks and reagents. Asepsis was maintained, including through the use of 70% (v/v) ethanol. All cultures were confirmed negative for mycoplasma contamination at least once every two months using the polymerase chain reaction (PCR)-based LookOut® Mycoplasma Detection Kit [MP0035].

2.3.1. Cell culture conditions

Cells were maintained in a humidified incubator at 37°C supplied with 5% carbon dioxide (CO₂)/95% air.

2.3.2. Cell lines

2.3.2.1. NSE: Het-1A (ATCC® CRL-2692™)

The human oesophageal NSE Het-1A cell line was a gift from A Sharrocks (Manchester, UK). This well-characterised, immortalised, adherent cell line was derived from human

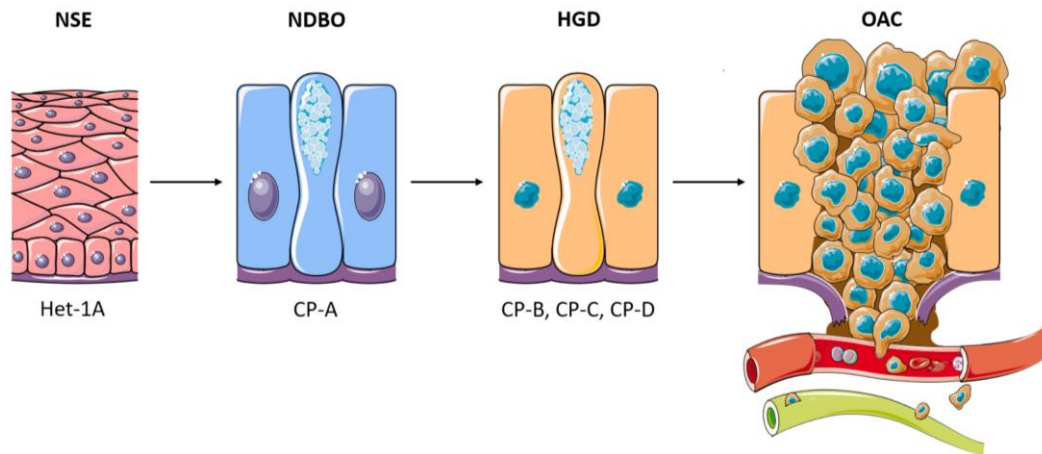


Figure 2.1. A schematic overview of NSE and BO cell lines used in this work. The names of representative cell lines for each disease stage are shown below each image. Disease stages are highlighted at the top of the schematic. The colours used here are used consistently throughout this work to denote the disease stage and cell line to which data representations relate to.

oesophageal tissue excised from a 25 year old Black male donor at autopsy in 1986.(52) It was subsequently transformed by transfection with the pRSV-T plasmid, which contains a Rous sarcoma virus (RSV) long terminal repeat promoter and the sequence encoding simian virus 40 (SV40) early region genes. This hypodiploid line has previously undergone more than 250 population doublings over which it retains epithelial morphology and stains positively for cytokeratins.(437) It is non-tumorigenic in nude mice.(437) *In vitro*, Het-1A cells are stimulated by calcium and, conversely, inhibited by foetal bovine serum (FBS) and both TGF- β 1 and TGF- β 2.(437)

2.3.2.2. BO: CP-A, CP-B, CP-C & CP-D

2.3.2.2.1. NDBO: CP-A (ATCC® CRL-4027™)

The adherent BO cell line, CP-A (also identified as KR-42421), was sourced from ATCC®. This near-diploid immortalised cell line was obtained at endoscopy in 1995 from a patch of NDBO identified in a male donor.(438) A retroviral expression vector (pLXN-hTERT) was used to transduce the cells. The CP-A culture predominately consists of two subclones; one containing i(8)(q10) and trisomy 20 and the other der(1)t(1;18),(q10;q10),i(8,q10), der(13)t(13;22)(q10;q10) and trisomy 20.(438) Non-clonal cells derived from one of these two subclones constitute the remainder of the cellular population and may increase in number at high passages.

2.3.2.2.2. HGD: CP-B (ATCC® CRL-4028™)

Obtained from ATCC® and alternatively known as CP-52731, the immortalised, adherent, hypodiploid CP-B cell line was derived in 1994 from a region of HGD present in a male donor. As with the CP-A cell line, CP-B cells were immortalised via transduction with the pLXN-hTERT expression vector.(438) Numerous derivative chromosomes are present but differ by passage number, with the tetraploid population increasing from approximately 18% to up to 50% at higher passages. These include the derivative chromosomes der(1)t(1;17)(q42;q21), add(8)(p11.2), der(9)t(9;14)(q10;q10), add(12)(q13), add(15)(q24.3), add(17)(p11.2), del(19)(p13.1) and del(21)(q22.1).

2.3.2.2.3. HGD: CP-C (ATCC® CRL-4029™)

CP-C, or CP-94251, cells were sourced from ATCC®. As with CP-B, this adherent line was derived from cells taken at endoscopy from a region of HGD in an adult male and immortalised using the pLXSN-hTERT retroviral expression vector.(438) First obtained in 1995, these cells retain elevated tetraploidy that is similar to their non-transduced parental cells.(438)

2.3.2.2.4. HGD: CP-D (ATCC® CRL-4030™)

Similar to CP-B and CP-C, the adherent CP-D (also known as CP-18821) cell line was derived from a biopsy specimen taken at endoscopy in 1995 from a region of HGD in an adult male. This line was sourced from ATCC® and has been immortalised via transduction with the pLXSN-hTERT retroviral expression vector and is hypotetraploid with consistent loss of one copy of chromosomes X, 10, 13, 14, 15, 19 and 20. Numerous derivative chromosomes are consistently present across passages, including add(2)(q13), der(3)t(3;8)(p10;q10), add(22)(q13)x2, der(7)(q10)dup(q31), der(12)t(12;13)(p10;q10), der(14)t(14;15)(q10;q10) and der(15)t(15;22)(q10;q10).(438)

2.3.2.2.5. Known expression patterns

The NDBO CP-A cell line and HGD CP-B, CP-C and CP-D cell lines are all positive for the epithelial marker pan-cytokeratin and all negative for gastric mucin. All four lines harbour alterations of the sequence encoding p16. *TP53* is wild-type in CP-A cells but demonstrates mutation or LOH in CP-B, CP-C and CP-D cell lines. None of these cell lines are tumourigenic in mice.

2.3.3. Cell proliferation, experimentation & maintenance

All cells were cultured in 10-12ml proliferation media within 75cm³ tissue culture flasks unless otherwise stated. On reaching approximately 70% confluence cells were passaged, with each line cultured to a maximum of 25 passages. At each passage, cells were washed in Dulbecco's Phosphate Buffered Saline (PBS) following removal of proliferation media and then incubated at 37°C in a humidified atmosphere consisting of 5% CO₂/95% air with 3ml 0.05% trypsin-ethylenediaminetetraacetic acid (EDTA; [Thermo Fisher Scientific, TFS]) until cells were seen via light microscopy to detach from the plasticware. Agitation was avoided in order to avoid encouraging cell clumping. Proliferation media was subsequently added to each flask at a 1:1 ratio to trypsin in order to neutralise its action and the cell suspension transferred to a 15ml falcon tube for centrifugation at 150g at room temperature for five minutes. The supernatant was discarded and cells resuspended in media for re-seeding at the required seeding density, as guided through a manual cell count undertaken using a Marienfeld Superior™ Counting Chamber [TFS]. In general, the subcultivation ratio was maintained between 1:5 and 1:8.

2.3.3.1. Proliferation

Cell lines representing NSE (Het-1A) and BO (CP-A, CP-B, CP-C, CP-D) were conditioned to grow in Keratinocyte Serum-Free Medium (KSFM; [TFS]) supplemented with 10% (v/v) FBS, bovine pituitary extract (BPE; 50µg/ml) and EGF (5ng/ml). When not passaged, 50% media changes were undertaken at two-three day intervals.

2.3.3.2. Serum-starvation

Where serum-starvation was used for Het-1A, CP-A, CP-B, CP-C and CP-D lines, cells were initially seeded in proliferation media. After a 24 hour period and once at the required confluency for experimentation, cells were washed twice in PBS and media replaced with KSFM, with no additional supplementation.

2.3.3.3. Experimentation

Unless otherwise stated, cells were seeded at 0.01x10⁶, 0.1x10⁶ and 0.3x10⁶ per well for 96-well, 12-well and 6-well plates respectively, and at 2.2x10⁶ per 10cm² plate. Experimental procedures were undertaken once cells had reached an approximate density of 0.04x10⁶, 0.5x10⁶ and 1.2 x10⁶ per well for 96-well, 12-well and 6-well plates respectively, and at 8.0x10⁶ per 10cm² plate.

2.3.4. Cryopreservation & recovery

2.3.4.1. Cryopreservation

Frozen stocks of each cell line were generated at low passage numbers. Cells were prepared for cryopreservation one day after proliferation media was changed and whilst in the mid log-phase of growth at approximately 70-80% confluency. A cell pellet was prepared as outlined in **2.3.3.** then resuspended in pre-chilled freeze media at $2-4 \times 10^6$ cells/ml. For CP-A, CP-B, CP-C and CP-D cells, freeze media consisted of RPMI-1640 with 10% FBS and 10% dimethyl sulfoxide (DMSO) as a cryoprotectant. Het-1A cells were resuspended in Leibovitz's L-15 medium [TFS] with 2mM L-glutamine [TFS] and 10mM 4-(2-hydroxyethyl)-1-piperazineethanesulfonic acid (HEPES) supplemented with 1% polyvinylpyrrolidone (PVP), 10% FBS and 7.5% DMSO as a cryoprotectant. All cells were cooled to -80°C at a controlled rate using the Corning® CoolCell™ system and frozen ampoules were then stored in the vapour phase of a liquid nitrogen storage tank at approximately -125°C to -200°C .

2.3.4.2. Recovery from cryopreservation

Cryopreserved cell aliquots were removed from liquid nitrogen and rapidly thawed in a 37°C water bath. A matched volume of appropriate pre-warmed proliferation media was added to the defrosted cell solution and then transferred to a 15ml falcon tube. This was centrifuged at 150g for 5 minutes at room temperature and the resulting cell pellet resuspended in 5ml appropriate pre-warmed proliferation media in a 25cm^3 flask.

2.4. Protein analysis

Protein was obtained from cells in order to compare the total expression of target proteins and differences in the phosphorylation of specific amino acid residues across the studied cell lines and between applied treatments.

2.4.1. Protein extraction

Cells from which protein was to be extracted were placed on ice following a defined experimental exposure and time period. Media was removed by pipetting and cells subsequently washed twice in ice-cold PBS. Following the careful and complete removal of any residual PBS and media, lysis was achieved through the addition of Cell Lysis Buffer [#9803, Cell Signalling Technology, CST] supplemented with cOmplete™, Mini, EDTA-free Protease Inhibitor Cocktail (one tablet per 10ml Cell Lysis Buffer [#4693159001, Merck]) at a volume of 25-50 μl or 50-100 μl per well of a 12-well and 6-well plate respectively, or 150-

300µl for a 10cm² dish. Following gentle agitation to distribute the lysis buffer, a cell scraper was used and the resulting lysate transferred to a pre-cooled 1.5ml Pierce™ microcentrifuge tube [#69715, TFS] in which it was stored on ice for 20 minutes. The cell lysate solution was subsequently centrifuged at 13,000 revolutions per minute (RPM) for 20 minutes at 4°C in order to pellet debris, with the resulting supernatant transferred to a clean, pre-cooled 1.5ml Pierce™ microcentrifuge tube. Each lysate was stored at -80°C and each underwent a freeze-thaw cycle prior to quantification of protein concentration.

2.4.2. Protein quantification

The detergent-compatible colorimetric Pierce™ BCA Protein Assay kit [#23225, TFS] was used to measure total protein concentration relative to known protein standards. This utilises bicinchoninic acid (BCA) to detect the Cu¹⁺ cation following its protein-mediated reduction from Cu²⁺. The chelation of two BCA molecules and a single cuprous ion generates an intense purple-coloured water soluble complex with detectable linear absorbance at 562nm.

2.4.2.1. Standards

Bovine Standard Albumin (BSA) samples of known concentration were serially diluted in Cell Lysis Buffer supplemented with cOmplete™ Mini-Protease inhibitor. A 10µL volume of each standard was added in duplicate to a 96-well plate with 200µl freshly prepared Pierce™ BCA Protein Assay working reagent. The plate was mixed thoroughly on a shaker and subsequently incubated at 37°C for 30 minutes whilst protected from light, with regular agitation. The plate was cooled to room temperature and, following a short further period of agitation, absorbance read at room temperature at 590nm using a BioTek™ PowerWave™ Microplate Spectrophotometer. A representative standard curve is shown in **Fig. 2.1**.

2.4.2.2. Samples

The protein concentration of each sample was calculated as per the protocol for standards outlined in **2.4.2.1**. All samples were evaluated at least in duplicate and the mean absorbance used to estimate protein concentration using the standard curve.

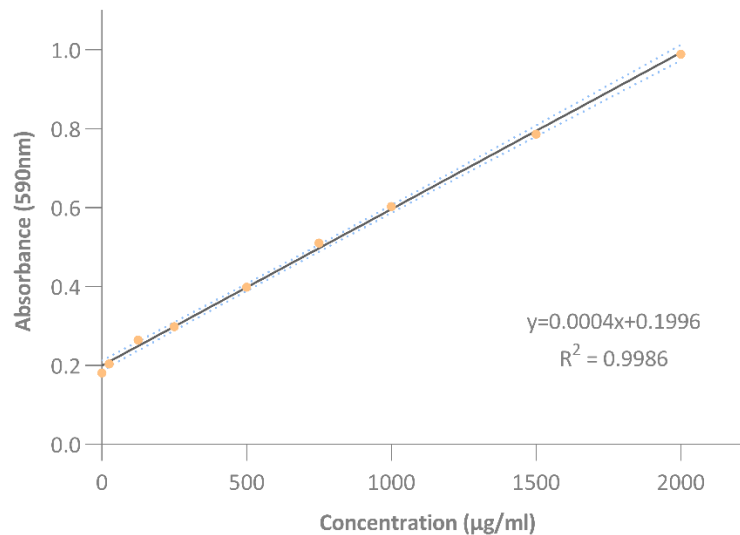


Figure 2.2. A representative standard curve for the Pierce™ BCA Protein Assay Kit. An average of the absorbance readout for at least two technical replicates for each of nine standard protein concentrations in the lysis buffer used for the experimental sample was plotted. The resultant linear relationship is then used to facilitate quantification of the protein concentration of unknown samples. A minimum coefficient of variation, represented by R^2 , of 0.95 was required for the regression model to be used for protein concentration determination.

2.4.3. Immunoblotting

2.4.3.1. Principle

In immunoblotting (Western blotting), proteins are denatured and a standardised quantity separated by molecular weight within each experimental sample using sodium dodecyl sulphate (SDS) – polyacrylamide gel electrophoresis (PAGE). Following transfer to a membrane these are subjected to monoclonal or polyclonal antibodies respectively specific for one or multiple epitopes within a protein's structure. A secondary antibody raised against the primary antibody species, and which is conjugated to an enzymatic label such as horseradish peroxidase, is then applied. This catalyses the oxidation of luminol to 3-aminophthalate in a light-emitting process that through enhanced chemiluminescence (ECL) can be sustained and amplified many-fold to aid detection. The emitted light is compared across samples to demonstrate differences in the relative abundance of the epitope (and therefore protein or PTM to which it belongs) across samples. A protein demonstrated not to vary under the assessed experimental conditions is probed on each blot in order to provide an equal protein loading control.

2.4.3.2. Method

In preparation for SDS-PAGE, a total volume equivalent to 15-30µg of each protein of interest was added at a 1:1 ratio to Laemmli 2x concentrated sample buffer (4% (w/v) SDS,

20% (v/v) glycerol, 10% (v/v) 2-mercaptoethanol, 0.004% (w/v) bromophenol blue, 0.125M Tris HCl). After mixing, each sample was boiled at 95°C for 5 minutes then left to cool on ice for a further 10 minutes. Once cooled, protein samples were added to pre-cast 10-well 10% [#4561033] or 4-20% [#4561096] gradient Mini-PROTEAN® Tris-Glycine Extended (TGX™) precast polyacrylamide gels [Bio-Rad Laboratories Ltd., Bio-Rad]. These were first prepared by removal of the sample comb and fixed within a Mini-PROTEAN® Tetra Vertical Electrophoresis Cell (Bio-Rad) to which Tris-Glycine/SDS running buffer (25mM Tris base, 190mM glycine, 0.1% (w/v) SDS) was added. The first lane of each gel was used to add 8µl Precision Plus Protein™ Dual Colour Standard [#1610374, Bio-Rad] in order to mark specific molecular weights. Each gel was electrophoresed at 70V for 10 minutes followed by 120V until the dye was seen to reach its far end, after which the gel was carefully removed and prepared for wet transfer to a polyvinylidene difluoride (PVDF) membrane via electrophoresis.

The PVDF membrane was activated prior to transfer by incubation in methanol for one minute, after which it was fixed within a stack comprising of two sponges, filter paper and the polyacrylamide gel. This was immersed in wet transfer buffer (25mM Tris base, 190mM glycine, 20% methanol (v/v)) within a pre-cooled Mini Trans-Blot® Electrophoretic transfer cell run at 250mA for 120 minutes.

Following transfer, membranes were blocked for a period of one hour at room temperature with constant rocking in 5% (w/v) milk or - for all instances in which a phosphorylated epitope was probed, 5% (w/v) BSA - in tris-buffered saline (TBS) with 0.1% (v/v) Tween-20 (TBS-T). Membranes were subsequently incubated on a rocker in primary antibody (see **Appendix B**) diluted in 5% milk or 5% BSA, both in TBS-T, within a sealed polythene bag; either for one hour at room temperature or overnight at 4°C. Membranes were then washed on a rocker at room temperature in TBS-T, which was replaced at five minute intervals for a total of 30 minutes. An appropriate secondary antibody (see **Appendix B**) was added as per the primary antibody and incubated on a rocker at room temperature for one hour, followed by a further identical 30 minute wash step.

Clarity™ and Clarity Max™ Western ECL Substrates [Bio-Rad] were used at a volume of 1ml per blot for chemiluminescent development. Following a one minute incubation period, each blot was placed within a saran wrap and any bubbles or excess solution removed. The membrane was subsequently imaged either using either a Syngene G:BOX with an integrated charge-coupled device camera, or a PROTEC Ecomax X-Ray Film developer

following exposure to Amersham™ Hyperfilm™ [GE28-9068-36] for a variable time period dependent on the protein being probed. Blots were retained and re-probed where required following a 15 minute incubation in Restore™ Western Blot Stripping Buffer [#21059, TFS] and a subsequent one hour blocking incubation.

2.4.3.3. Analysis

In addition to the digital image representation of each immunoblot, a densitometric readout of band intensity was obtained using the open source image processing programme ImageJ [National Institutes of Health, USA]. Band density is expressed as relative to the total relevant protein density for phosphorylated epitopes, or as relative to the loading control for epitopes representative of total protein abundance.

2.5. Transcriptome analyses

RNA was extracted from cells for analysis using real-time quantitative reverse transcription polymerase chain reaction (qRT-PCR) and RNA sequencing (RNA-seq).

2.5.1. RNA extraction & DNase digestion

The RNeasy® Mini Kit [#74104, Qiagen] was used to extract and purify RNA from cells. These were seeded in 6- or 12- well plates as outlined in **2.3.3.3.** and subjected to experimentation. At the intended point of RNA sampling, media was removed and the cells washed twice in ice-cold PBS prior to the addition of 350µl buffer RLT to each well. Plates were kept on ice and cells subsequently scraped and transferred to a pre-cooled 1.5ml Pierce™ microcentrifuge tube [#69715, TFS]. One volume of 70% (v/v) ethanol was added to the lysate and mixed well by pipetting. Samples and associated precipitate were transferred to an RNeasy® Mini spin column held within a 2cm collection tube and centrifuged at 8000g for 15 second at 4°C. The flow-through was discarded and centrifugation repeated following the addition of 350µl Buffer RW1. An on-column DNase digestion was subsequently performed through the addition of 80µl DNase I to the spin column followed by 15 minutes incubation at room temperature. Following this, 350µl Buffer RW1 was added prior to centrifugation at 8000g for 15 seconds at 4°C. Flow-through was discarded and 500µl Buffer RPE added followed by further centrifugation at 8000g for 15 second at 4°C. The flow through was again discarded and a further 500µl Buffer RPE added, followed by centrifugation at 8000g for two minutes at 4°C. The RNeasy® Mini spin column was placed in a fresh 2ml collection tube and centrifuged again at 8000g for one minute at 4°C in order to dry the membrane. The spin

column was subsequently transferred to a labelled Pierce™ microcentrifuge tube and 30µl nuclease-free water (NFW; TFS) directly added to the membrane. The RNA was eluted by centrifugation at 8000g for one minute at 4°C. In order to ensure a higher yield, flow-through was added to the membrane of the spin column, which was centrifuged for a further minute at 8000g. Samples were stored at -80°C and thawed on ice prior to use, with freeze-thaw cycles limited.

2.5.2. Sample quantification & quality assurance

The concentration of extracted RNA was measured using a NanoDrop 2000 [TFS] spectrophotometer. Following the addition of 2µl NFW as a blank reference, 2µl of each sample was loaded in order to determine the RNA concentration. The 260/280 and 230/260 ratios were used to assess RNA purity. Since nucleotides and RNA absorb at 260nm, a 260/280 ratio that is appreciably lower than ~1.8 indicates the presence of a contaminant such as protein. Therefore, only samples with a 260/280 ratio of 1.7-2.0, and a 260/230 value of 2.0-2.2, were used in subsequent assays. An aliquot of the each RNA sample was run on a denaturing agarose gel stained with ethidium bromide in order to confirm integrity. Samples were run in 6x DNA-loading buffer (30% (v/v) glycerol, 0.25% (w/v) bromophenol blue and 0.25% (w/v) xylene cyanol) on a 1.8% agarose gel.

2.5.3. mRNA quantitation by qRT-PCR

2.5.3.1. Principle

Relative expression of target genes at the mRNA level was determined by qPCR. This method, often referred to as real-time RT-PCR, utilises intercalation of the fluorescent asymmetrical cyanine SYBR® Green I dye between DNA bases to monitor in real time the amplification of relatively stable complementary DNA (cDNA) synthesised from extracted, purified mRNA. Briefly, this process comprises up to 40 cycles, each of which consists of denaturation, annealing and extension steps. In the denaturation step, incubation at high-temperatures is utilised to melt double-stranded DNA into single-stranded DNA, the secondary structure of which is loosened. An annealing step is then used to hybridize primers to their complementary sequences before primer extension occurs with intercalation of a fluorescent probe. The number of cycles required for fluorescence to pass a fixed signal threshold (the cycle threshold, Ct) is determined for each gene and normalised to an endogenous housekeeping gene, generating the delta Ct (dCt) value. The Ct is inversely proportional to the quantity of target nucleic acid within the sample such that dCt allows for

Reagent	Supplier	Volume (μ l)
SSIV Buffer	TFS	5.0
DTT (100mM)	TFS	2.0
RNAse Inhibitor, Murine	NEB	1.0
SuperScript [®] IV Reverse Transcriptase (200U/ μ l)	TFS	1.0

Table 2.1. Per sample volumes for each master mix component used for cDNA synthesis prior to qRT-PCR.

comparison of the relative abundance of target gene cDNA, and therefore mRNA, between different experimental conditions.

2.5.3.2. cDNA synthesis

A total of 1 μ g of RNA was suspended within a 10 μ l volume of NFW. To this, 1 μ l Oligo dT₂₀ primer [#18418020, New England BioLabs, NEB] and 1 μ l deoxynucleotide triphosphate (dNTP, 10mM) was added and samples incubated for five minutes at 65°C then quick-chilled on ice. A master mix was made up with reagent quantities as listed in **Table 2.1**, plus 10% for pipetting inefficiencies. Eight microlitres of the master mix was added to each sample and the contents gently mixed prior to incubation at 42°C for 50 minutes, 70°C for 15 minutes and 4°C until the samples were transferred for storage at -20°C or -80°C prior to use.

2.5.3.3. Primer design

Primers spanning exon-exon boundaries or flanking introns near the 3' end of target genes were designed using Primer-BLAST [National Centre for Biotechnology Information, NCBI, USA]. Each consisted of a GC content of 40-60%, a melting temperature (T_m) of 60-63°C and a low self-complementarity score. The estimated PCR product size was between 70-200 base pairs. Selected primers of interest were sourced from Integrated DNA Technologies, Inc. (IDT) and are shown in **Appendix C**. Prior to experimental assays, primer efficiency for each gene of interest was confirmed comparable to the housekeeping gene by generating a standard curve from serial primer dilutions. An online qPCR Efficiency Calculator [TFS; accessible via themofisher.com] was subsequently used to confirm primer efficiency from the graph slope. Only primers with an efficiency of 90-110% were selected for further use.

2.5.3.4. qRT-PCR

Prior to each qRT-PCR run, the template cDNA, primers targeted against the gene of interest and master mix reagents were thawed on ice. A separate master mix was made for each primer probe, as shown in **Table 2.2**. All primers were used at a final concentration of 250nM

Reagent	Supplier	Volume (µl)
SensiMix™ SYBR® No-ROX	Meridian BioScience	10.0
Primer Mix	IDT	1.0
NFW	TFS	4.0

Table 2.2. Per sample volumes for each master mix component used for qRT-PCR.

and primer pair constituents were equimolar. Fifteen microlitres of the master mix was added to 5µl cDNA template (100ng per reaction) within a Strip Tube [Qiagen]. All samples were analysed in duplicate and qRT-PCR carried out within a Rotor-Gene Q [Qiagen]. The applied thermal cycling conditions included a 10 minute 95°C polymerase activation step followed by up 40 cycles of 95°C for 15 seconds, 60°C for 30 seconds and 72°C for 30 seconds whilst reading green fluorescence. A final melt curve was included for subsequent analysis of reaction specificity.

2.5.3.5. Data analysis

Two technical replicates of each sample were run. A delta Ct (dCt) value was generated by subtracting the average housekeeping gene Ct value for the experimental condition of interest from the average gene of interest Ct value. Analyses were then undertaken using at least three biological replicates. Arbitrary units (AU) were calculated in order to compare relative mRNA expression values of genes of interest across cell lines. Fold change (FC) was calculated in order to compare the relative increase or decrease in mRNA expression of genes of interest between control and experimental conditions. Relevant formulae are as follows:

$$\text{Arbitrary units} = 1000 * 2^{-dCt}$$

$$\text{Fold change} = 2^{-ddCt} \text{ where } ddCt = dCt (\text{experimental value}) - dCt (\text{control value})$$

All statistical analyses (see 2.8.), including calculation of standard error of the mean (SEM) values, were performed using non-transformed Ct values.

2.5.4. RNA-seq

2.5.4.1. Principle

RNA-seq is an unbiased transcriptomic approach that allows for the analysis of differentially expressed genes (DEGs), in addition to adaptations that allow for the interrogation of the transcriptome, structure and spatiolomics. For the analysis of DEGs, as undertaken using the TruSeq Stranded mRNA [#20020595, Illumina®, Inc.] system here, extracted quality-controlled poly-A containing RNA is first purified and fragmented. Double-stranded cDNA is

subsequently synthesised from cleaved fragments of RNA using reverse transcriptase and random primers. The 3' blunt ends of the cDNA are adenylated with a single nucleotide, which provides a complementary overhang for ligation to a 'T' nucleotide of a sequencing adapter. This synthetic oligonucleotide prepares double-stranded cDNA for hybridisation onto a flow cell but ligated DNA fragments are first enriched with PCR and purified to create a final cDNA library. The DNA attaches to a flow cell using a complementary sequence and both the antisense and sense strand read by paired-end next generation sequencing (NGS). This high throughput approach typically allows for a read depth of 10-30 million reads per sample. Reads are aligned to a transcriptome and normalised between samples so that significant DEGs can be identified. Additional computational steps can be undertaken to identify the pathways, processes and cellular components enriched within these identified genes.

2.5.4.2. Method

Paired-end RNA-seq libraries were generated from 0.1-1.0µg total RNA using the TruSeq Stranded mRNA kit (Illumina®, Inc.), then sequenced on a HiSeq 3000 [Illumina®, Inc.] platform. NGS reads were processed prior to read mapping by using Trimmomatic v0.32 to remove low sequencing quality reads and adapter sequences, and FasQC for sequencing quality assessment.(439,440) The universal RNA-seq aligner Spliced Transcripts Alignment to a Reference (STAR) was used to align sequences to the Reference Sequence (RefSeq) transcript annotation of Genome Reference Consortium Human Build 37 (GRCh37; hg19).(441) Reads aligned to autosomes 1-22 as well as the X-chromosome were retained. These were read by the open source Cufflinks v2.2.1 package, which assembles a parsimonious (containing all fragments required to deliver the splicing event outcomes within the data) transcriptome.(442) Gene expression was determined within Cufflinks by Cuffnorm and DEGs revealed using Cuffdiff.

2.5.4.3. Analysis

Significant DEGs were identified as those with a FC of ± 1.5 (equivalent to a \log_2 FC of 0.58496) and a Q-value (corrected for multiple significance testing) of < 0.05 . The methods used to represent RNA-seq data and to analyse their biological significance are outlined in **2.7.**

2.6. Chromatin accessibility assay

2.6.1. Assay for Transposase-Accessible Chromatin using sequencing (ATAC-seq)

2.6.1.1. Principle

ATAC-seq is an unbiased, high-fidelity technique that provides for the mapping of chromatin accessibility profiles. These may then be compared across samples in order to map nucleosomes, to identify transcription factor binding sites and to review DNA methylation sites. In short, in a process of tagmentation, a hyperactive mutant transposase is used to cleave and tag double-stranded DNA with sequencing adapters. The resulting DNA fragments are then purified, amplified and sequenced by NGS. Alignment of these sequences with a reference genome allows open chromatin stretches to be inferred, and for transcription factor binding sites to be mapped. The Omni-ATAC protocol, used here, improves signal : background ratio compared with conventional ATAC techniques.(443)

2.6.1.2. Method

2.6.1.2.1. Cell lysis & nuclear extraction

Cells were seeded in 6-well plates as per **2.3.3.3.** and harvested post-experimentation, with all experiments undertaken once cells had reached at least 70% confluence. All experimental endpoints were analysed in duplicate. At the intended point of ATAC sampling, media was aspirated and cells washed twice in PBS followed by the addition of 500µl trypsin per well. Once cells had detached, serum-free media was added at a 1:1 ratio and the cell-containing solution pelleted by centrifugation at 150g for five minutes at room temperature. The cell pullet was resuspended in 2ml warm PBS and similarly centrifuged. The supernatant was subsequently aspirated from the resulting cell pellet, which was transferred to a pre-cooled 1.5ml Pierce™ microcentrifuge tube [#69715, TFS] and placed on ice.

In order to isolate nuclei, each sample was resuspended in 250µl of ATAC-resuspension buffer 1 (10mM Tris-HCl [pH 7.4], 10mM NaCl, 10mM MgCl₂, 0.1% NP40, 0.1% Tween-20, 0.01% Digitonin) for three minutes before the subsequent addition of 1ml ATAC-resuspension buffer 2 (10mM Tris-HCl [pH 7.4], 10mM NaCl, 10mM MgCl₂, 0.1% Tween-20), with which it was mixed by gentle agitation of the microcentrifuge tube. Nuclei were pelleted by centrifugation at 500g for 10 minutes at 4°C and, following aspiration of the supernatant, resuspended in 30µl ice-cold PBS. Following a cell count, 50,000 cells were isolated in 16.5µl PBS and the transposition reaction established through their incubation with 0.5µl digitonin 1%, 0.5µl Tween-20 10%, 2.5µl TDE1 Tagment DNA enzyme and 25µl

Tagment DNA buffer in a thermomixer for 30 minutes at 37°C. DNA was purified from this reaction using the silica membrane-based MinElute Reaction Cleanup Kit [#28204, Qiagen] and eluted in to a total of 22µl Buffer EB. Samples of DNA were then stored at -20°C for up to two weeks before further use.

2.6.1.2.2. ATAC library generation

An ATAC library was generated by PCR-based DNA amplification using Illumina indexing/barcoding primers. PCR can introduce GC and size bias, particularly during later PCR cycles that occur with limited reagent concentrations. Libraries should therefore be generated with minimal PCR amplification. This is achieved through a pre-amplification step followed by qRT-PCR, which is used to determine the optimal number of cycles require to amplify the library without reaching PCR saturation.(443)

To achieve this, the amplification mixture was mixed for each sample as shown in **Table 2.3.** and pre-amplification performed via a five minute 72°C step, a 30 second 98°C step and five cycles of 98°C for 30 seconds, 63°C for 30 seconds and 72°C for one minute. From this pre-amplified solution, 5.0µl of sample was added to a qRT-PCR run (**Table 2.3.**) that proceeded via 30 seconds at 98°C then 20 cycles of 98°C for 10 seconds, 63°C for 30 seconds and 72°C for one minute. The number of additional cycles required was determined by identifying the cycle number that correlates to a quarter of maximum fluorescent intensity when linear Rn (reporter dye fluorescence/passive reference dye fluorescence) was plotted against cycle number.

Reagent	Supplier	Volume (µl)
PCR amplification mixture		
Primer Ad1 (25µM)	Illumina	2.5
Primer Ad2 (25µM)	Illumina	2.5
Q5® High-Fidelity 2x Master Mix	NEB	25
Transposed sample	-	20
qRT-PCR amplification mixture		
NFW	TFS	3.76
Primer Ad1 (25µM)	Illumina	0.5
Primer Ad2 (25µM)	Illumina	0.5
Q5® High-Fidelity 2x Master Mix	NEB	5.0
SYBR™ Green PCR Hi-ROX	Meridian BioScience	0.24
Pre-amplified sample	-	5.0

Table 2.3. Per sample volumes for each master mix component used for PCR amplification and qRT-PCR amplification during ATAC-seq library generation.

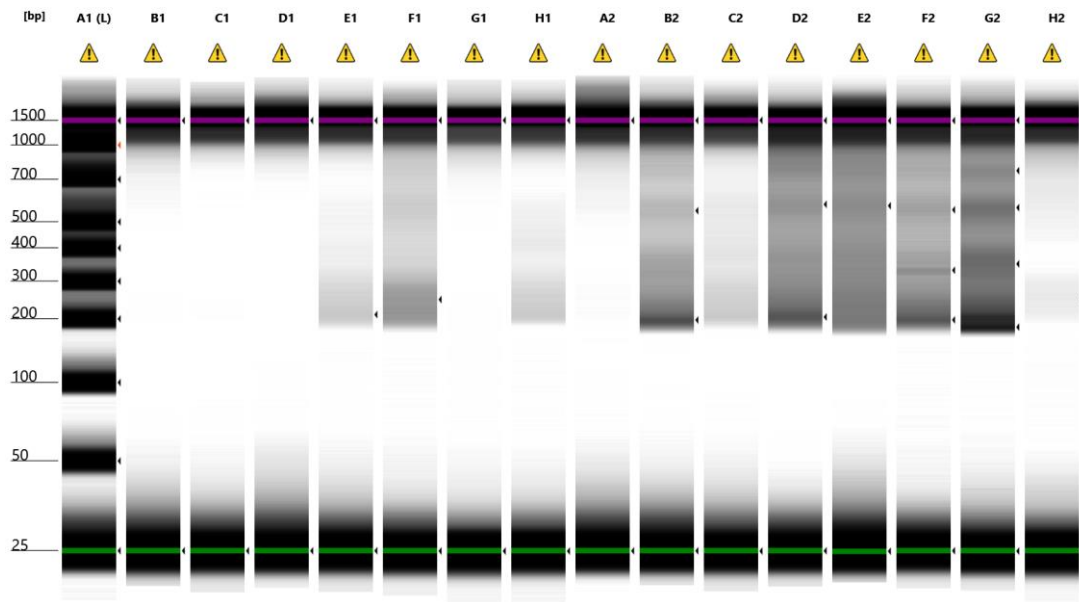


Figure 2.3. A representative example of nucleic acids purified following ATAC library generation and analysed using the Agilent 4200 TapeStation for quality control purposes. Each column represents an individual sample. The periodicity of samples was analysed against markers in A1 with samples showing adequate periodicity such as F1, B2, D2, E2, F2, G2 chosen for further analysis.

2.6.1.2.3. ATAC library purification

Libraries were purified from the minimally amplified PCR products using AMPure XP beads [A63880; Beckman Coulter Life Sciences]. This allows for the removal of primers and large DNA fragments. Briefly, 22.5µl beads were added to 50.0µl PCR products, mixed thoroughly, and incubated at room temperature for 10 minutes, then on a magnetic rack for five minutes. The supernatant was transferred to a new microcentrifuge tube, to which a further 58.5µl beads were added and mixed. The mixture was again incubated at room temperature for 10 minutes then on a magnetic rack for 5 minutes before the supernatant was discarded. The beads were subsequently washed with 200µl 80% ethanol. Once dried, they were resuspended in 10µl NFW, transferred to a magnetic rack and the supernatant transferred to a fresh microcentrifuge tube.

2.6.1.2.4. Quality assurance

Sample quality was assessed by automated electrophoresis using the Agilent 4200 TapeStation. A sample output is provided in **Fig. 2.2**.

2.6.1.2.5. Sequencing

Libraries were sequenced on a HiSeq 4000 (Illumina) platform, as outlined in Britton et al.(444)

2.6.1.3. Analysis

In order to determine differential chromatin accessibility, alignment files for each studied condition were merged and peaks called using Model-based Analysis of ChIP-Seq (MACS) version 2.1.1.(445) Regions were ranked by q-value and a region of ± 250 base pairs reviewed for each of the 50,000 highest-ranking regions, each of which was categorised as promoter or non-promoter. These were assessed for differential accessibility using CuffDiff from the Cufflinks package version 2.1.1.(446) Regions which varied in accessibility by greater than a five-fold linear change in accessibility, with a Q-value of <0.05 , were considered significant.

2.7. Bioinformatics

2.7.1. Enrichment analyses

2.7.1.1. Principle

The large datasets generated by ‘-omics’ analyses such as RNA-seq can, at their simplest level, provide information relating to the differences in the patterns and level of gene or protein expression or activation between samples and conditions. However, to determine the functional impact on the cell of these changes, the differentially regulated genes and proteins can be compared to reference datasets in order to determine which pathways and processes are over-represented. Semantic analyses can then be used to simplify and trim these often long lists of enriched pathways and processes. Enriched terms from a single gene or protein set can be derived from multiple orthogonal databases in order to assess for terms shared across reference sets. It is in addition possible to use bioinformatics approaches to identify functional protein-protein interaction networks within datasets and to predict upstream regulators of these.

2.7.1.2. Gene Ontology (GO) over-representation analyses

Analyses of over-represented GO terms from differentially regulated gene or protein sets derived from RNA-seq (2.5.4) or kinome (4.3.3) analyses were undertaken using Protein Analysis Through Evolutionary Relationships (PANTHER) version 16.0. Functionally enriched GO Biological Process (BP), Molecular Function (MF) and Cellular Component (CC) terms were derived using the reference *Homo Sapiens* gene-set.

2.7.1.3. Gene Set Enrichment Analysis

Gene Set Enrichment Analysis (GSEA) Version 4.1.0. was used to assess for statistically significant differences in gene expression between phenotypes.(447,448) This open-source software utilises *a priori* lists of genes within the Molecular Signatures Database (MSigDB) that are grouped by their involvement in a specific pathway or process. Differentially expressed genes in an input dataset are ranked against this list, with an enrichment score calculated based on the distance from the middle of the list. This provides a Komogorov-Smirnov-like statistic that indicates whether the genes are over-represented towards the top (i.e. over-expressed) or the bottom (i.e. under-expressed) of the list.

2.7.1.4. Pathway enrichment

Pathways enriched within DEGs and differentially-regulated protein sets were identified using the Kyoto Encyclopedia of Genes and Genomes (KEGG), Wiki Pathways (WP) and REACTOME. KEGG and REACTOME were accessed via Search Tool for the Retrieval of Interacting Genes (STRING) version 11.0. WP was accessed via Metascape. Pathways were also identified using Qiagen Ingenuity Pathway Analysis (IPA).

2.7.1.5. Upstream regulator analyses

Putative upstream mediators of DEGs were identified using Qiagen IPA Upstream Regulator analysis. Upstream mediators of differentially phosphorylated peptides were identified using the same database but with peptide sequences as the input, or via Group-based Prediction System (GPS) Version 5.0 (as outlined in **4.3.3.3.4.**).

2.7.1.6. Summary methods used to represent gene-set enrichment

GO term lists were summarised using Reduce & Visualise Gene Ontology (REVIGO). Metascape was used to summarise pathway and gene-set enrichment within a single dataset. Visual representations of over-represented GO data were generated using Cytoscape 3.7.2. with the ClueGo plugin. Functional pathway analyses of kinome data were organised hierarchically and compared across phenotypes using FunMappOne.(449)

2.7.2. Pathway and interaction determination

Gene interaction networks were generated using Metascape. Functional protein interaction networks were generated using STRING version 11.0.

2.8. Viability assays

All viability assays were optimised using a no-cell control, an untreated cell control and positive controls for reduced cell viability, necrosis and apoptosis. Reduced cell viability was established with a 15 minute treatment of digitonin (30µg/ml; MP Biomedicals) or 70% methanol, necrosis with a 4 hour treatment of ionomycin (100µM; BioServ UK Ltd) and apoptosis with a 6 hour treatment with staurosporine (20µM; Caltag Medsystems Ltd). All experimental assays were run with triplicate untreated cell and no cell controls.

2.8.1. MTT assay

2.8.1.1. Principle

The 3-(4,5-dimethylthiazol-2-yl)-2,5-diphenyltetrazolium bromide (MTT) assay is a commonly used colorimetric method for determining metabolic activity, which is used as a surrogate for cellular viability and proliferation. It relies on the reduction by NAD(P)H-dependent oxidoreductase enzymes within viable cells of the yellow MTT tetrazolium salt to purple formazan crystals. These are dissolved and a spectrophotometer used to measure absorbance, with darker solutions indicating a greater number of viable, metabolically active cells.

2.8.1.2. Method

Cells were seeded and subjected to experimentation in 96-well plates as outlined in **2.3.3.3**. At the desired experimentation endpoint, the media was discarded and 10µl MTT (0.5mg/ml) added to each well. The plate was then incubated for four hours at 37°C in a humidified atmosphere supplemented with 5% CO₂/95% air. Following this, 100µl DMSO was added to each well and the plate incubated for two hours at room temperature whilst protected from light. Absorbance was read at 570nm using a BioTek™ PowerWave™ Microplate Spectrophotometer.

2.8.2. LIVE/DEAD® Viability/Cytotoxicity stain

2.8.2.1. Principle

The LIVE/DEAD® Viability/Cytotoxicity kit [L3224, TFS] comprises of cell-permeant calcein-AM and membrane-impermeable ethidium homodimer-1, which simultaneously respectively interact with live and dead cells. Calcein-AM is converted to green-fluorescent

calcein by intracellular esterases, whilst ethidium homodimer-1 enters dying or dead cells via their disrupted cell membranes and binds DNA, fluorescing red.

2.8.2.2. Method

Cells were initially seeded and experimented on in a 96-well plate as per **2.3.3.3**. In line with manufacturer's guidance, 100µl of a mix comprising of 5µl Calcein-AM, 20µl ethidium homodimer-1 and 10ml PBS was added to each well. The plate was incubated for 30 minutes at 37°C in a humidified atmosphere supplemented with 5% CO₂/95% air. Fluorescence was then read at an Ex/Em of 494/517nm for calcein AM and 528/617nm for ethidium homodimer-1 using a BioTek™ PowerWave™ Microplate Spectrophotometer. The percentage of live and dead cells was then determined as a proportion of overall cellular number.

2.8.3. CyQUANT™ Direct Cell Proliferation Assay

2.8.3.1. Principle

The CyQUANT™ Direct Cell Proliferation Assay [C35011, TFS] is a fluorescence-based assay comprising a cell permeable green-fluorescent nucleic acid stain and a cell impermeable background suppression dye. This combination enables for the metabolism-independent quantification of DNA content within viable cells (i.e. that have an intact membrane).

2.8.3.2. Method

Cells were initially seeded and experimented on in a 96-well plate as per **2.3.3.3**. In line with manufacturer's guidance, a 2X working solution was made up by adding 48µl CyQuant® Direct nucleic acid stain to 240µl CyQuant® Direct background suppressor I and 11.7ml PBS. This was added at a 1:1 ratio with KSFM to a total of 200µl per well and cells subsequently incubated for 60 minutes at 37°C in a humidified atmosphere supplemented with 5% CO₂/95% air. Fluorescence was then read at an Ex/Em of 508/527nm using a BioTek™ PowerWave™ Microplate Spectrophotometer.

2.9. Statistical analyses and representation of data

2.9.1. Statistical analyses

Unless otherwise specified, comparisons between two independent samples were performed using the non-parametric Mann-Whitney U test and comparisons between

Package name	Version	Function	Citation
EnhancedVolcano	1.8.0.	Generation and visualisation of volcano plots.	Blighe K, Rana S, Lewis M. 2020.
ggplot2	2.0.0.	Generation and visualisation of graphs.	Wickham H. 2016.
ggpubr	0.4.0.	Modify graph appearances.	Kassambra A. 2020.
ggsci	2.9.0.	Modify graph appearances.	Xiao N. 2018.
gridExtra	2.3.0.	Generation of grid graphics.	Augue B. 2017.
pheatmap	1.0.12.	Generation of heatmaps	Kolde R. 2019.
RColorBrewer	1.1-2.	Modify graph appearances.	Neuwirth E. 2014.

Table 2.4. A list of R packages used for data analysis and representation.

multiple samples undertaken using the non-parametric Kruskal Wallis test with Dunn's post-hoc correction for multiple significance testing. Bonferroni correction for multiple significance testing was employed where multiple two independent sample comparisons were performed. An adjusted p-value of <0.05 was considered significant. All statistical analyses were performed using GraphPad Prism, Version 9.0.2 (GraphPad Software Inc., California, USA) and R 3.6.0 (R Core Team (2020)).

2.9.2. Data representation & images

All data figures were generated using GraphPad Prism, Version 9.0.2, R 3.6.0 and Adobe Illustrator, Version 25.2 (Adobe, California, USA). Schematic figures were adapted from a publicly-available collection of medical images provided by Servier Medical Art (Les Laboratoires Servier, Suresnes, France). **Table 2.4.** lists R packages used in this work.

Chapter 3

Modelling Microenvironmental Stress & its Impact on the Barrett's Transcriptome

3.1. Background

3.1.1. Overview: the dysplastic progression of BO

Most, if not all, cases of OAC arise in patients who have first developed BO.(10–12) However, despite the concomitant rise in the incidence of BO and OAC seen across the Western world over recent decades, only a small proportion of patients with BO will progress to OAC.(1,42–44) In an effort to identify these patients, considerable focus has been directed towards studies of genomic aberrations that may underlie the development and progression of dysplasia in BO.(20,22,230) These have revealed substantial clonal diversity, drawn at least in part from considerable chromosomal instability yet, as outlined in **1.1.2.3.2.**, a paucity of recurrent driver mutations have been identified.(230) There is, however, emerging evidence that the risk of OAC can be predicted by the genomic copy number of NDBO tissues years prior to the development of dysplasia.(258) As such, it is apparent that the onset and evolution of BO dysplasia does not mirror a Darwinian model in which driver events are sequentially acquired in response to environmental pressure. Instead, neoplastic transformation is attributable not just to the genomic instability that characterises BO, but additionally to a breakdown in the regulatory mechanisms that govern genetic expression.(258)

It is increasingly recognised that across a number of tissue types, the phenotype of both preneoplastic and malignant cells is dictated by their dynamic and reversible bidirectional relationship with the tissue microenvironment.(450–457) A pertinent example of this capacity for the cellular environment to shape gene expression is seen in the development of melanoma.(450,458,459) Melanocytes may, for example, acquire the combined driver events of BRAF^{V600E} mutation and *PTEN* loss yet they require additional microenvironmental

influence to breach a threshold beyond which an invasive phenotype is acquired; resulting in only a small proportion of melanocytes with driver genomic events progressing to melanoma.(450,458,459) Similar profound impacts of the microenvironment are seen across a number of tissues, with mounting evidence of genetically uniform cells exhibiting entirely divergent phenotypes in response to environmental pressures, and of cells developing stem-like or EMT phenotypes following microenvironmental change.(451–457,460,461)

In BO, it is recognised that genomic heterogeneity is compounded by considerable phenotypic heterogeneity, and that cells can convert between phenotypes – rather than these exist as binary states - and therefore exist in phenotype space as well as genotype space.(462) This may explain why some cases of dysplasia can regress and highlights that even phenotypes such as EMT, which was previously considered to result from a binary state transition, can be reversed.(454,463,464) It is also clear that, as outlined in **1.1.2.3.1.**, BO cells are exposed to a raft of potentially deleterious microenvironmental influences.(165) It follows that the microenvironment may dictate BO phenotypic space, and therefore risk of dysplastic progression, by shaping the regulatory mechanisms governing gene expression as well as signalling pathways that exert direct control over cellular behaviour.

Studying the impact of microenvironmental stressors on BO gene regulation and signalling is, however, challenging. Firstly, determining their relative impact across disease stages requires analyses of NDBO and dysplastic tissue, yet numerous challenges exist in both establishing and extracting findings from animal, cell and organotypic culture model systems. Secondly, where studies of microenvironmental stressors have been undertaken, the breadth of exposures used to replicate *in vivo* influences is so considerably diverse as to limit comparison of their relative importance to the BO epithelium, whilst the physiological relevance of many of the conditions used is unclear. Thirdly, a majority of existing studies of BO microenvironmental influences use markers of differentiation as a surrogate for dysplastic progression. It is not, however, clear that this approach is appropriate given the prevailing dogma for BO dysplastic progression, which saw differentiated SIM as the cell from which OAC develops, has been challenged. These aspects are outlined in turn here.

3.1.1.1. Modelling stages of BO dysplastic progression

The impact of microenvironmental influences on the development and progression of dysplasia in BO can be studied using *in vitro*, *in vivo* or *ex vivo* model systems. The *ex vivo* use of human BO tissues, either *en-bloc* or as organotypic cultures, provide the most

genetically relevant of these models and can recapitulate tissue heterogeneity. However, there have been few successful attempts at generating three-dimensional (3D) organotypic patient-derived Barrett's organoids and these are additionally limited by constraints on the availability of tissue, by practical considerations when considering high-throughput screening approaches, and on the relatively short length of time over which explants can be successfully cultured.(465–467) Further, whilst a small number of organotypic BO cultures have been generated, these have unfortunately not been made widely available.(467)

Animal models offer an alternative approach but as *Attwood et al.* and *Kapoor et al.* highlight, to be valid these must be genetically and anatomically similar to BO, practically feasible, and to naturally experience GORD with a risk of development of OAC.(142,468) A variety of animals have been used in the hope of meeting these criteria, including baboons, dogs, zebrafish, rats and mice. However, in general, whilst larger animals offer similar upper gastrointestinal anatomy and physiology to humans, they fail to recapitulate their biology; whereas smaller animals are broadly biologically similar to humans but dissimilar in anatomy and physiology.(142) Baboons are the most closely aligned to humans in terms of genomic and structural homology, and additionally naturally develop BO in response to reflux, yet they do not develop OAC even after many years of exposure to refluxate.(142) Surgical models of induced refluxate are therefore more commonly used but these are resource intensive, beset by high rates of mortality and are technically challenging to generate.(142) Separately, genetically-manipulated but non-surgically altered mouse models of progression have been developed through depletion of p63 or overexpression of IL-1 β , yet these respectively fail to survive into maturity and exhibit a low rate of progression to OAC.(143,469)

Given this, it is perhaps unsurprising that the biological effects of the BO microenvironment have in the main been modelled *in vitro* using two dimensional (2D) culture systems.(467) These are adaptable, convenient and relatively easy to use for high-throughput screening approaches. They do not however replicate disease physiology nor tissue heterogeneity and, as has previously been outlined, many cell lines used until recently are now known to derive from extra-oesophageal tissue.(292) Adding to their limitations, there is no genomic characterisation of the host BO lesions from which most of the cells used today derive.(467)

3.1.1.2. Modelling BO microenvironmental stressors

The BO microenvironment is shaped by a multitude of luminal, stromal and humoral stressors, in addition to a number of protective factors. These are summarised in **Table 1.2.**

and include a pro-inflammatory stromal environment in which cells may also be exposed to a relative hypoxia and oxidative stress, as well as the humoral influences of insulin resistance and an excess of adipokines that characterise the metabolic syndrome.

The predominant luminal influence on the cellular microenvironment derives from gastro-oesophageal refluxate, though a relative reduction in salivary EGF and pH-neutralising bicarbonate is also reported in patients with BO.(196) Almost 90% of reflux episodes in patients not managed with PPIs or H₂RAs are acidic, with ambulatory pH monitoring determining that pH levels are less than 4.0 for approximately 20% (less than four hours) of a day.(172,470,471) This corresponds to in excess of 80 single reflux episodes over the same 24 hour period, over 65 of which are acidic, rising to in excess of 100 episodes in more severe disease.(472) Most reflux episodes last ten minutes or less.(473) Treatment with PPIs abrogates, but does not eliminate, the acidity of these episodes by reducing the gastric acid pocket but not the frequency of reflux pulses.(167) Patients with BO who are managed with acid-suppressive therapy are therefore still exposed to intermittent acidic refluxate, albeit at a pH that does not approach that seen in the absence of PPIs.(167,474) Notably, a significant number of patients fail to respond to PPIs altogether and therefore continue to experience strongly acidic reflux pulses.(166) For most patients with BO, bile salt concentration varies between 0.03-0.82 mmol/L.(170,171,475) However, higher concentrations have been reported for some patients and a greater proportion of conjugated bile salts is seen in patients managed with acid suppressive therapy.(475,476)

Combined, these stressors contribute to the spatially-distributed phenotypic heterogeneity that defines BO lesions.(462) This includes an increase in the fraction of proliferating cells and those with SIM differentiation.(462,474,477) The development of both phenotypic states is associated with the direct impacts of refluxate, though a higher proportion of proliferative cells may also represent the presence of a wound-healing response.(462) Accordingly, significant laboratory focus has been applied to the development of these phenotypes in response to acid and bile salt exposure, yet as is outlined in **Table 3.1.**, the exposures used to model refluxate *in vitro* are very variable and in many instances are applied at concentrations or for time periods that do not mirror *in vivo* physiology.

It is noteworthy when considering these prolonged exposures that *in vivo*, BO lesions are directly exposed to acidic refluxate for less than four hours a day.(471) In the absence of direct exposure to refluxate, the BO microenvironment is nevertheless additionally characterised by oxidative stress and a persistent pro-inflammatory state that have been

Author, year	Disease stage (cell line)	Stressors			Exposure time	pH	Bile salts/acids
		BS	Acid	BA			
Fitzgerald, 1996 (189)	-		Y		60min vs 1 hr	3.0-5.0	-
Fitzgerald, 1997 (290)	CRC (HT29)		Y		60 min vs 3 weeks	5.0	-
Kaur, 2000 (291)	-	Y		Y	60 min	3.5	NaGC+NaTC+GCA+TCDCDA 1mM total
Souza, 2002 (305)	OAC* (SEG-1*)		Y		3 min	4.0	-
Jaiswal, 2004 (316)	OAC* (SEG-1*)	Y			20 min	-	GCDCA 50-1000µM
Jenkins, 2004 (377)	OAC (OE33)	Y		Y	0-24 hr	4.0/7.0	DCA 100-300µM
Morgan, 2004 (319)	OAC* (SEG-1*)			Y	20	3.5	-
Souza, 2004 (306)	OAC* (SEG-1*)		Y		0-180 min	6.0	-
Mariette, 2004 (322)	OAC (OE33)	Y			24 hr	-	CDA 100µM + 50µM DCA + CA 500µM + TCDCDA 500µM + NaGC 500µM + GCA 500µM + TCA 500µM + TDC 1000µM + DHC 1000µM + CME 50µM + LC 100µM
Sarosi, 2005 (307)	OAC* (SEG-1*)		Y		3 min	3.0-6.5	-
Jaiswal, 2006 (310)	NSE (NES), NDBO (BAR-T), OAC* (SEG-1*)	Y			5 min	7.4	CDA/GCDCA/TCDCDA 50-1000µM (each)
Beales, 2007 (218)	OAC (OE33)		Y		4 min	4.0	-
Dvorak, 2007 (183)	OAC* (SEG-1*)		Y	Y	10 min	4, 7.4	NaGC+NaTC+GDA+GCDCA+DCA 100µM total (20µM each)
Roman, 2007 (426)	NSE (TE-1, TE-13), OAC* (BIC-1*, SEG-1*)		Y	Y	10-60 min	6.0	DCA 50+100+200µM/CDCA 200µM/TCDCDA 200µM
Song, 2007 (317)	OAC* (SEG-1*, SK-GT-4)	Y			16 hr	-	CDA+DCA (200µM total)/TCA + GCDCA (200µM total)
Si, 2007 (372)	OAC* (SEG-1*)		Y		1 hr	4.0	-
Keswani, 2008 (308)	OAC* (SEG-1*)	Y	Y		5 min	3.0-4.5	TCA 50-100µM
Delgado, 2008 (309)	OAC* (SEG-1*)	Y	Y	Y	5 min	3.5, 5.0	TCA 100µM
Mariette, 2008 (321)	OAC (OE33)	Y			24 hr	-	TCA 500µM + TCDCDA 500µM + GCA 500µM + TDC 1000µM + NaGC 500µM + DCA 50µM
Yen, 2008 (370)	NDBO (CP-A), HGD (CP-C), OAC* (SK-GT-4, SEG-1*, BE3)	Y			2 hr	-	CDA 100µm & 300µM / TCDCDA 200µM
Avissar, 2009 (311)	OAC* (SEG-1*)	Y	Y	Y	0-24 hr	5.0, 7.0	DCA 300µM
Looby, 2009 (318)	OAC (SK-GT-4)	Y			1-24 hr	-	DCA 1-500µM DCA
Morrow, 2009 (163)	OAC (OE19, OE33)	Y			8-24 hr	-	DCA 100-300µM
Burnat, 2010 (376)	OAC (OE-19)	Y			24 hr	7.0	DCA/UDCA 100-300µM

Duggan, 2010 (380)	NSE (HET-1A), OAC (OE-19, OE-33, SK-GT-4)	Y			4-24 hr	-	DCA 300µM
Huo, 2010 (391)	NSE (NES-B, NES-G)	Y	Y	Y	30-60 min 24h	4.0, 7.2 5.0	GCA 175µM + TCA 25µM + GCDCA 125µM + TCDCA 25µM + GDA 50µM + TDA 10µM (400µM total)
Das, 2011 (168)	NDBO (BAR-T)			Y	5 min/day for ≥65 weeks	4.0	200µM GCDA (4.0)
Huo, 2011 (243)	NDBO (BAR-T, BAR-T10)	Y			5, 10, 30 min	7.2	DCA/UDCA 50+250µM
Zaika, 2011 (424)	NSE (HET-1A, EPC2), OAC (SK-GT-4)		Y	Y	30 min	4.0	GCA+TCA+GDA+GCDCA+DCA 100µM total (20µM each)
Song, 2011 (323)	OAC (SK-GT-4)	Y			16 hr	-	GCA+TCA+GCDCA+TCDCA+DCA+CDA (200µM total)
Rawat, 2012 (375)	OAC (OE33)	Y			6 hr	-	DCA 300µM
Tamagawa, 2012 (338)	NSE (HET-1A), OAC (OE33, OE19)	Y					DCA 50-200µM / CA 50-200µM
McAdam, 2012 (374)	OAC (OE33)	Y			4 hr	-	DCA 100-200µM
Hong, 2013 (385)	NDBO (BAR-T, CP-A), OAC (OE33)		Y		24 hr/1 hr	6.0/4.0	-
Zhou, 2013 (413)	OAC (FLO-1, OE33)		Y		1 hr	4.9	-
Zaika, 2013 (427)	NDBO (CP-A, BAR-T1), OAC (SK-GT-4)			Y	30 min	4.0	GCA+TCA+GDA+GCDCA+DCA 100µM total (20µM each)
Peng, 2014 (383)	NSE (HET-1A), NDBO (BAR-T), OAC (FLO-1, OE33)	Y		Y	10 min	4.0/7.0	GCA+TCA+GDA+GCDCA+DCA 100µM total (20µM each)
Park, 2015 (326)	-			Y	0-720 min	4.0-6.0	-
Tamagawa, 2016 (478)	NSE (Het-1A), NDBO (BAR-T, CP-A)	Y			12 hr	-	DCA 50-200µM
Bhardwaj, 2016 (242)	NDBO (BAR-T, CP-A), HGD (CP-B)			Y	5-30 min	4.0	GCA+TCA+GDA+GCDCA+DCA 100µM total (20µM each)
Feng, 2017 (373)	NDBO (BAR-T)	Y			1-12 hr	-	DCA 0-300µM
Li, 2017 (386)	NSE (HET-1A), NDBO (CP-A), HGD (CP-B), OAC (OE33, FLO)		y		1 hr/24 hr	4.0/6.5	-
Bhat, 2018 (331)	NDBO (CP-A), HGD (CP-B), OAC (OE33, FLO-1)			Y	30 min	4.0/7.0	GCA+TCA+GDA+GCDCA+DCA 100µM total (20µM each)
Huo, 2018 (388)	NSE (NES-B, NES-G)	Y	Y	Y	30-60 min 24h	4.0, 7.2 5.0	GCA 175µM + TCA 25µM + GCDCA 125µM + TCDCA 25µM + GDA 50µM + TDA 10µM (400µM total)
Dang, 2019 (392)	NSE (HET-1A)	Y		Y	15 min	4.5	GCA 250µM+TCDCA 100µM+GDCA 150µM + TDA 50µM
Huang, 2019 (348)	NDBO (CP-A), HGD (CP-B)	Y			10 min 3x/day for 3 days	4.0	GCA 175µM + TCA 25µM + GCDCA 125µM + TCDCA 25µM + GDA 50µM + TDA 10µM (400µM total)

Table 3.1. An overview of *in vitro* studies in which cells resembling Barrett's or OAC are exposed to bile salts at neutral (BS) or acidic (BA) pH, or acidic pH (Acid) alone. CA: cholic acid; CDA: chenodeoxycholic acid; CME: cholic methyl ester; DCA: deoxycholic acid; DHC: dehydrocholic acid; GCA: glychocolic acid; GCDCA: glycochenodeoxycholic acid; GDA: glycodeoxycholic acid; LC: lithocholic acid; NaGC: sodium glycocholate; NaTC: sodium taurocholate; TCA: taurocholic acid; TCDCA: taruochenodeoxycholic acid; TDC: taurodeoxycholic acid; UDCA: ursodeoxycholic acid. / = used separately. +used together as a mix.

linked to GORD and the metabolic syndrome.(153,174–183,186,209,210) In higher-grade lesions, regions of BO cells may also reside in regions of hypoxia.(210) It is perhaps then unsurprising that within BO lesions, phenotypic heterogeneity extends to the presence of cells undergoing EMT, cells that are held in quiescence or even dimmed to senescence, cells that have become more stem-like and cells that have entered autophagy.(462,477,479–483) These states have received comparatively little attention in BO modelling, yet inflammation is a known driver of both EMT and stemness, whilst autophagy is likely a protective response to reflux-induced damage and in other contexts is seen to play important tumour-suppressive and tumour-promoting roles.(455,483,484)

Interestingly, there is increasing recognition that a starvation state characterised by nutritional depletion drives the development of intermediate EMT and autophagy phenotypes across a number of tissues and in doing so contributes to the development of invasive disease.(450) These same phenotypic transitions, and the pathways that drive them, can be instigated in nutritionally replete tissues by inflammatory signalling molecules and hypoxia through a process of pseudo-starvation.(450) Correspondingly, the inflammatory environment that pervades BO may contribute to phenotypic transitions towards an invasive or pro-survival phenotype. Given the convergence of signalling pathways implicated in pseudo-inflammation and inflammation, the *in vitro* serum starvation of BO tissue may provide a novel model through which the signalling and transcriptional mediators of inflammation and nutritional depletion can be studied, as summarised in **Fig. 3.1.**

3.1.1.3. The dynamic BO transcriptome

The incubation period between the onset of BO and development of OAC is reported to be around 10 years.(485) It is as a consequence challenging to reliably determine whether *in vitro* exposures translate to a more dysplastic or neoplastic phenotype. Given this, and as illustrated in **Table 3.1.**, some researchers have as a consequence repeatedly exposed cells to potential microenvironmental stressors for in some cases over a year. Whilst this may translate to the development of a more invasive phenotype, there are drawbacks in the requirement to sustain cells at very high passage numbers. Consequently, most investigators instead use markers of differentiation as surrogates for dysplastic progression. This may not though be robust, not least given that it is far from certain that it is the differentiated SIM lesion that undergoes dysplastic progression in BO.

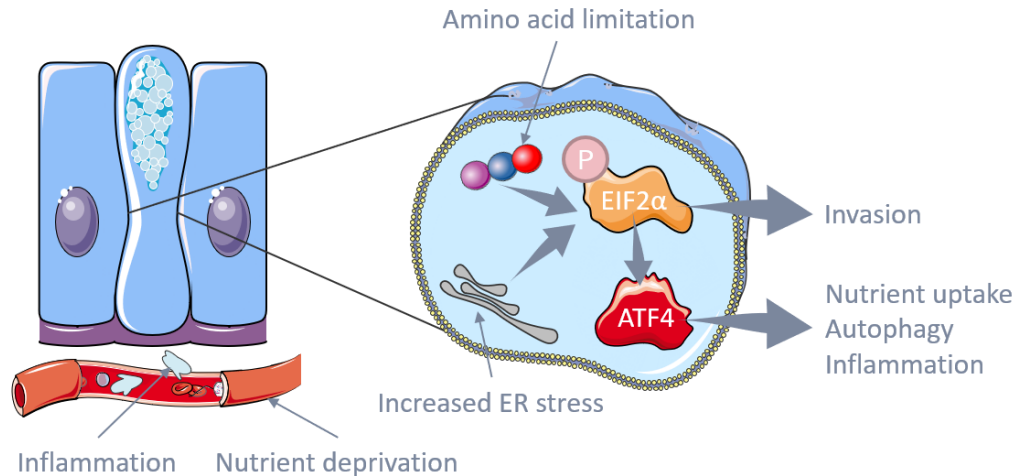


Figure 3.1. An overview of the proposed starvation and pseudo-starvation states that are implicated in the development of an invasive cellular phenotype. A starvation state can result from a relative deprivation of nutrients and a pseudo-starvation state from chronic inflammation, endoplasmic reticulum (ER) stress (such as from oncogene activation) or amino acid limitation. Both states result in phosphorylation of eukaryotic initiation factor (EIF) 2 α , leading to cellular invasion and/or nutrient recycling via autophagy via activation of Activating Transcription Factor 4 (ATF4).(450)

An alternative approach may be to determine the impact of microenvironmental influences on transcriptional regulatory networks. This would allow for the impact of cellular stressors to be mapped to the epigenome, and therefore permits an unbiased assessment of gene regulation that can be mapped on to the genomic changes known to prevail as BO progresses. Supporting this approach, recent work undertaken in both BO and OAC has identified marked changes in chromatin accessibility during BO progression.(444) It is, however, unclear to what extent these relate to the impact of microenvironmental cues.

3.2. Aims

In this work, an *in vitro* model for advancing stages of BO dysplastic progression will be established and validated. Using this, the impact on the BO transcriptome of single or repeat exposure to the contents of gastric refluxate, and of serum-starvation, will be determined in order to evaluate the variable impact of microenvironmental stressors on BO homeostasis.

3.3. Methods

3.3.1. Experimental outline

A summary of the experimental approach is provided in **Fig. 3.2**. Briefly, the baseline morphology and phenotype of cell lines representing NSE (Het-1A), NDBO (CP-A) and HGD (CP-B, CP-C and CP-D) was analysed using light microscopy and through the comparison of

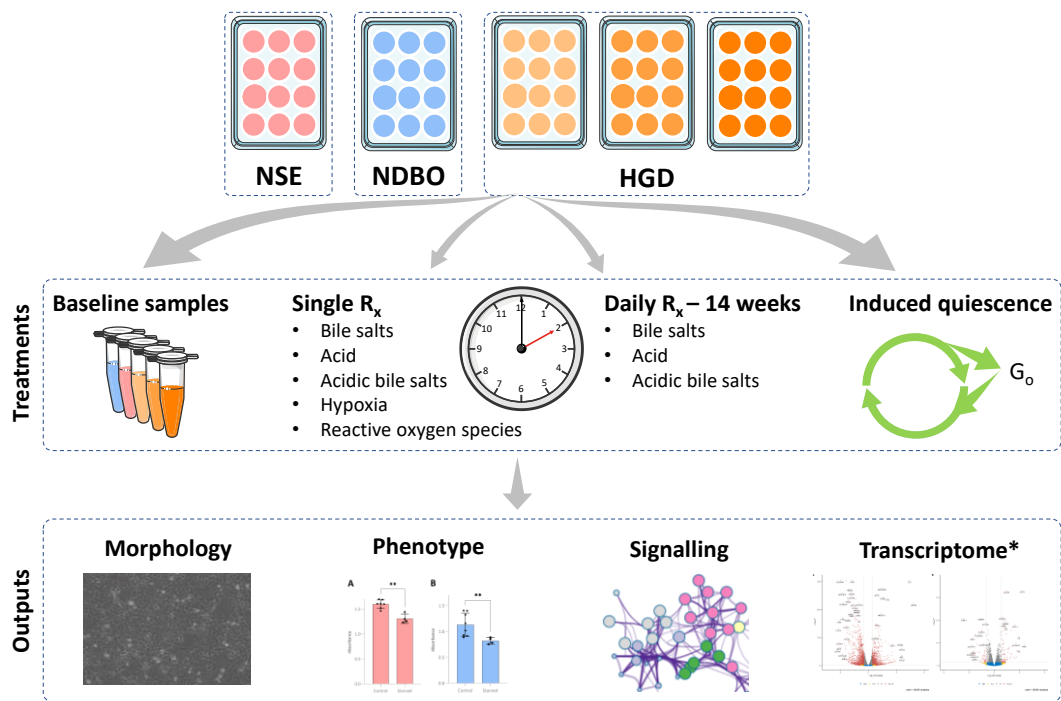


Figure 3.2. A schematic representation of the experiments used to characterise NSE and Barrett's cell lines, and to model their response to acute, sustained and repeat microenvironmental stress. * Transcriptome analyses from the cell lines outlined here were compared to the outputs of whole transcriptome sequencing of NSE, NDBO, LGD and OAC samples performed by *Maag et al.*(486)

mRNA expression of key markers of BO progression with a reference RNA-seq dataset from patients with NSE, NDBO, LGD and OAC.(486) The impact on cell phenotype, viability and markers of BO progression of exposure to bile salts at acidic (pH 4.0) or neutral pH, acid (pH 4.0) alone, and to conditions of serum starvation, was then determined. Finally, an unbiased assessment of changes in the transcriptome and chromatin accessibility of NDBO (CP-A) cells in response to acidic bile salts (pH 4.0) and a 48 hour period of serum starvation was undertaken using RNA-seq and ATAC-seq respectively.

Reagents and plasticware were sourced as outlined in **2.2.** and **Appendix A.** Unless otherwise stated, all reagents and chemicals were obtained from Merck KGaA or its subsidiary, MilliporeSigma, and all plasticware sourced from Corning® Incorporated. Cell culture, immunoblotting, transcriptome analyses (qRT-PCR and RNA-seq), viability assays and ATAC-seq were undertaken as respectively outlined in **2.3., 2.4.3., 2.5., 2.8** and **2.6.,** supported by **Appendix B** and **Appendix C.** Statistical analyses and data representation were undertaken as outlined in **2.9.**

3.3.2. Treatments & cellular exposures

3.3.2.1. Single exposure: acid and bile salts

3.3.2.1.1. Acid

Acidified media (at pH 4.0) was applied to cells for a period of 10 minutes. Media was acidified through the titrated addition of 1M hydrochloric acid immediately prior to use, with pH test strips (range 0-14.0; #P4786) used to confirm pH 4.0 before media was added to cells. At the end of the 10 minute experimental period, cells were washed twice in PBS and lysed for protein and RNA analyses (as outlined in **2.4.1.** and **2.5.1.** respectively) or re-incubated in KSFM (with or without FBS supplementation, depending on the experiment).

3.3.2.1.2. Bile salts

Bile salts were applied to cells within KSFM (without supplementation) as an equimolar 100µM mix comprising of glychocolic acid (GCA [#360512]), taurocholic acid (TCA [T4009, Sigma]), glycodeoxycholic acid (GDCA [sc-280755, Insight Biotechnology]), glycochenodeoxycholic acid (GCDCA [#50534, Sigma]) and deoxycholic acid (DCA [D2510, Sigma]) for a period of 10 minutes, at both neutral (neutral bile salt mix) and acid (pH 4.0, acid bile salt mix) pH. A 5ml sample of bile-salt containing media was centrifuged at 500RPM for 10 minutes prior to use in order to ensure there was no sedimentation and that bile salts were therefore adequately solubilised within both the neutral and acidified KSFM solutions. At the end of the 10 minute experimental period, cells were washed twice in PBS and lysed for protein and RNA analyses (as outlined in **2.4.1.** and **2.5.1.** respectively) or re-incubated in KSFM (with or without supplementation, depending on the experiment).

3.3.2.1.3. Vehicle

Bile salts were solubilised in DMSO prior to their addition to media. An equal volume of DMSO was therefore added to control cells as a vehicle. This did not exceed a 0.1% (v/v) final concentration.

3.3.2.2. Repeat exposure: acidified bile salts

Het-1A, CP-A and CP-B cells were treated with a 10 minute exposure to acidified bile salts, as outlined in **3.3.2.1.2.**, or vehicle, as outlined in **3.3.2.1.3.**, for five consecutive days a week (i.e. with two 'off days') over a period of 12 weeks. Cells were maintained in proliferative media within T75 flasks and passaged on reaching 70% confluence. At two weekly intervals,

the cell pellet was resuspended and, prior to seeding, a proportion removed for protein and RNA extraction, as outlined in **2.4.1.** and **2.5.1.**, respectively.

3.3.2.3. Serum-starvation

Serum-starvation was used both as a source of cellular stress (over 48 hour periods) and for 24 hours prior to all cellular treatments in order to mitigate the impact of ligand supplementation from the FBS within proliferative media. This was achieved by washing cells twice in PBS prior to the addition of non-supplemented KSM. Cells were lysed for protein and RNA analyses at pre-determined timepoints as outlined in **2.4.1.** and **2.5.1.** respectively.

3.3.3. Functional enrichment

Functional enrichment analyses were undertaken as outlined in **2.7.** In all cases, genes that demonstrated a significant change in expression ($p < 0.05$) with a FC of > 1.5 were used as input. Enrichment analyses were undertaken from single directional gene lists only (i.e. upregulated genes were analysed separately to downregulated genes). GSEA was undertaken using default settings, as specifically outlined in **2.7.1.3.**

3.3.3.1. Analysis of over-represented GO terms

GO terms over-represented by genes included within target datasets were identified using PANTHER version 16.0., as outlined in **2.7.1.1.** This generated long lists of GO terms that were summarised by semantic analysis using the REVIGO SimRel semantic similarity measure (revigo.irb.hr). In order to identify only the most significantly over-represented terms, terms were summarised using a dispensability cut-off of 0.05.

3.3.3.2. Metascape

Metascape was used to identify and rank enriched GO, KEGG, REACTOME and WP terms, as well as annotated gene sets within MSigDB.(487) This open-source software first identifies all statistically-enriched terms before filtering based on hypergeometric p-values and enrichment factors. Significant terms are subsequently hierarchically clustered based on Kappa-statistical similarities between the gene memberships for each term. Enriched outputs are provided as lists as well as network representations in which a term representative of each cluster is shown.

3.4. Results

3.4.1. Characterisation of the basal phenotype of the cell line model of BO

The long latency period between the development of BO and progression to OAC poses considerable challenges for studying the impact of microenvironmental stressors on BO dysplastic progression. The use of cell lines derived from NSE, NDBO and HGD may provide an opportunity to determine whether there are BO- or stage- specific factors that contribute to, or protect from, dysplastic progression. A number of 2D cell lines have been derived from NSE and patches of BO in patients with both NDBO and HGD. These are poorly characterised and it is unclear to what extent in particular the BO lines represent different stages of dysplastic progression. In this work, following the workflow outlined in **Fig. 3.2.**, the basal phenotype of commonly used cells representing NSE (Het-1A), NDBO (CP-A) and HGD (CP-B, CP-C, CP-D) is assessed.

3.4.1.1. Morphology

When assessed by light microscopy (**Fig. 3.3.**), both the NSE Het-1A and NDBO CP-A cells are characterised by a polygonal epithelial-like morphology. The growth of Het-1A cells is, however, patchy whereas CP-A cellular growth is more confluent. A similar morphology is

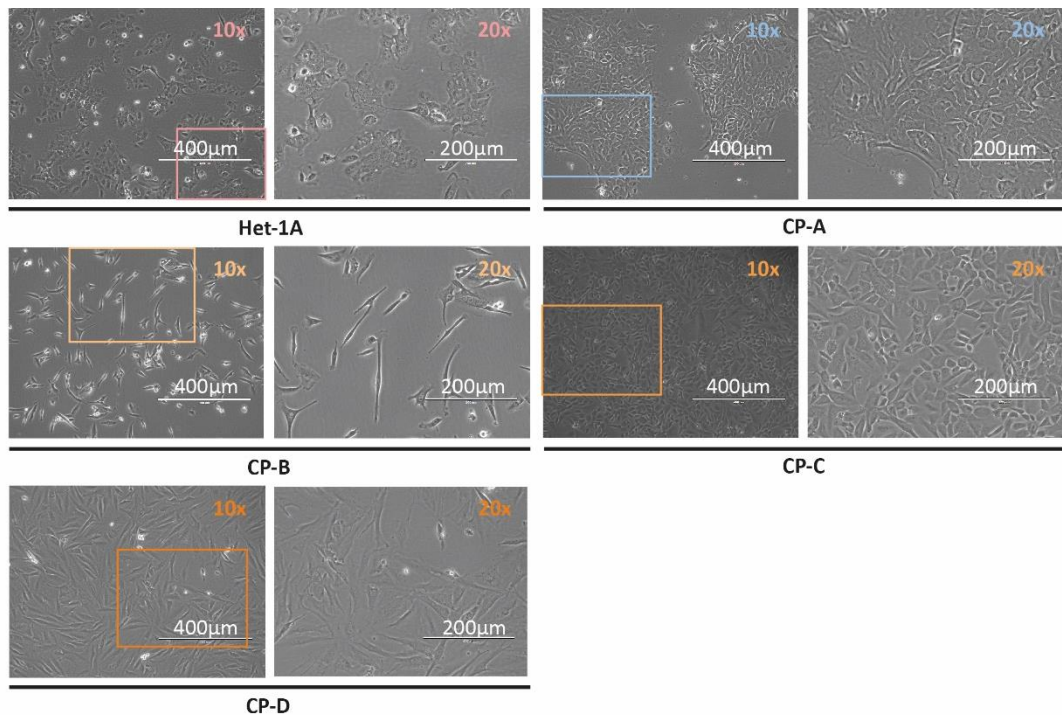


Figure 3.3. A baseline representation of the morphology of NSE (Het-1A) and Barrett's NDBO (CP-A) and HGD (CP-B, CP-C, CP-D) cells. Images are taken via light microscopy whilst suspended in Live Cell Imaging Solution with images taken at 10x and 20x magnification. Cells were previously maintained in proliferative media and all are in adherent cell culture. Scale bars are included within each image, with the highlighted box indicating the region selected for imaging at greater magnification.

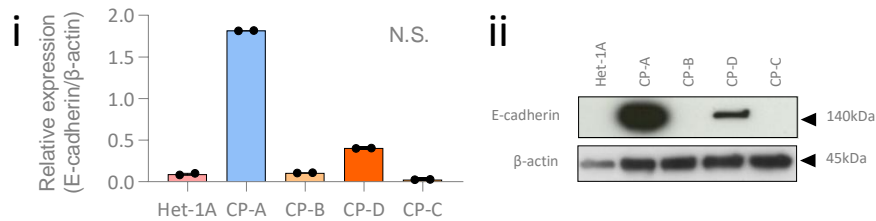


Figure 3.4. An immunoblot showing relative E-cadherin protein expression in NSE (Het-1A), NDBO (CP-A) and HGD (CP-B, CP-C, CP-D) cell lines. A representative immunoblot is presented in (i) and average expression (normalised to β -actin) assessed by densitometry in (ii). $n=2$. Statistical analyses were undertaken using the Kruskal-Wallis test with Dunn's post-hoc correction for multiple significance testing. No difference was found to be statistically significant.

seen for the HGD CP-C cells, which are again polygonal and appear similar to the CP-A cells. This is in contrast to the HGD CP-B and CP-D cells, which are bipolar and characterised by a fibroblastic-like elongated phenotype.

3.4.1.2. EMT

The dysplastic progression of Barrett's correlates with EMT, which is feature common to a number of malignancies and is thought to contribute to increased metastatic potential. In the context of BO, immunohistochemical analyses have identified a significant reduction in E-cadherin through the NDBO-HGD-OAC sequence.(358) E-cadherin is an epithelial marker and is frequently downregulated during EMT as cells instead switch to N-cadherin following the acquisition of a mesenchymal phenotype.(488) Given the fibroblastic (i.e. more mesenchymal) morphology of at least two of the HGD cell lines, we sought to characterise their EMT status by assessment of E-cadherin protein expression. As shown in **Fig. 3.4.**, the NDBO CP-A cells featured the highest protein expression of E-cadherin. This was markedly, albeit not significantly, lower across all HGD lines, with the most pronounced reductions seen in HGD CP-B and CP-C cells. Surprisingly, the epithelial Het-1A line, which would be expected to have similar E-cadherin expression to NDBO CP-A cells, demonstrated relatively minimal protein E-cadherin expression.

3.4.1.3. Markers of cellular differentiation

The morphological characteristics (**3.4.1.1.**) of the cells, coupled with evidence for EMT in the HGD lines, at least in part validates the cell line model as representing two distinct stages of dysplasia. Of the HGD lines, CP-B demonstrates both the greatest loss of E-cadherin protein expression and the most significant morphological transformation, and was therefore selected for further evaluation as a representative cell for HGD.

A particular challenge to determining whether microenvironmental stressors play a role in propagating BO progression is the long latency period between the formation of metaplasia and the development of OAC. Given this, a number of studies have used an increase in intestinal epithelial markers, alongside a concomitant decrease in their squamous equivalents, as surrogate indicators of dysplastic progression. It is, however, less than certain that dysplastic progression is associated with greater differentiation, not least given that it is unclear which specific cell type(s) within the metaplastic mosaic contribute to the formation of OAC. There additionally exists a complex relationship between differentiation and EMT, which is known to associate both with dedifferentiation and differentiation. In light of this, we explored the relationship between BO progression and the mRNA expression of markers of both intestinal (*MUC2*, *SOX9*, *KRT7*, *KRT8*, *KRT18*, *KRT19*) and squamous (*KRT4*, *TP63*) differentiation in patient samples and cells representing NSE (Het-1A), NDBO (CP-A) and HGD (CP-B). Patient-level data were extracted from a RNA-seq dataset curated by *Maag et al.*(486) This did not include patients with HGD so both LGD and OAC data were instead included to represent dysplastic progression.

As shown in **Fig. 3.5.**, most intestinal markers of differentiation (*SOX9*, *KRT7*, *KRT8*, *KRT18*, *KRT19*) were expressed at higher levels in NDBO (CP-A) than in NSE (Het-1A) cells, mirroring changes seen in the patient population. *MUC2* was an exception to this but appears to be expressed at very low levels in all three studied cell lines, which confounds further analysis. Interestingly, the squamous marker *KRT4* was significantly higher in NDBO CP-A cells and corresponding patient NDBO samples than NSE Het-1A cells (0.11 vs. 0.012 arbitrary units (AU); $p < 0.0001$) and patient NSE samples (5.48 vs. 3.40 fragments per kilobase of transcript per million mapped reads (FPKM)+1; $p = 0.0002$). In contrast, expression of the squamous marker *TP63* was significantly lower in patient NDBO samples compared to NSE, but did not significantly differ between any of the studied cell lines.

Surprisingly, none of the intestinal differentiation markers were significantly higher in NDBO CP-A cells when compared with HGD CP-B cells. This *in vitro* finding was for the most part corroborated by the studied patient samples. For instance, the intestinal stem cell marker *SOX9* was significantly higher in NDBO CP-A and patient samples than NSE Het-1A and patient samples, but was of similar expression to that seen in HGD CP-B and both LGD and OAC samples. Similar patterns were seen for *KRT8* and *KRT18*. The expression of the intestinal markers *KRT7* and *KRT19* was significantly lower between NDBO CP-A and HGD CP-B cells, which again correlated with differences seen in the patient samples.

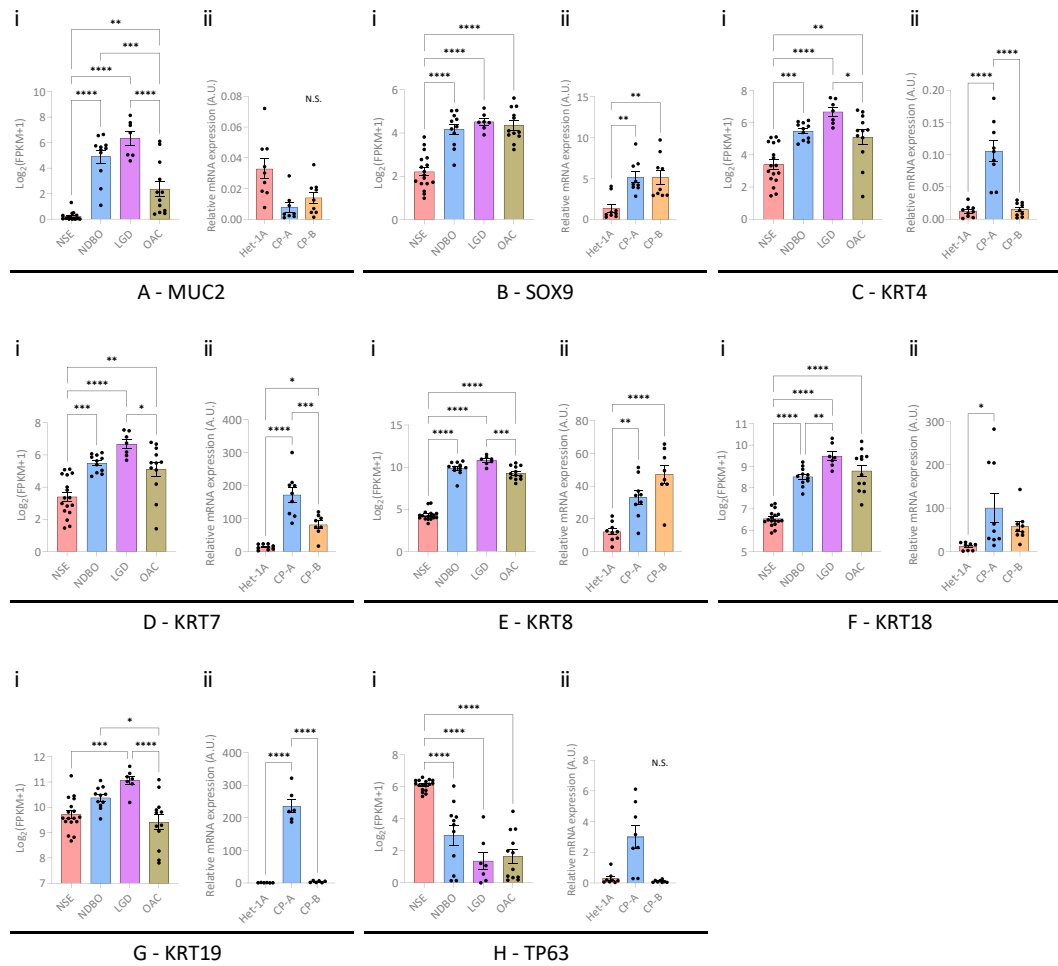


Figure 3.5. Expression of key markers of columnar and squamous differentiation across (i) patient samples and (ii) cell lines resembling NSE, Barrett’s and OAC. For each of the eight genes shown, (i) the relative expression of mRNA expression of each marker was compared between samples from NSE (n=17), NDBO (n=11), LGD (n=7) and OAC (n=12) in a prior analysis performed by *Maag et al.*(486) (ii) Relative mRNA expression for each gene was additionally compared across the Het-1A, CP-A and CP-B cell lines that respectively resemble NSE, NDBO and HGD (n≥6 for all comparisons). Data are presented as mean ± SEM. Statistical analyses were undertaken using a one-way ANOVA with post-hoc Tukey correction for multiple significance testing. Comparisons that reached pre-defined significance thresholds are highlighted, and are distinguished as follows: * p ≤ 0.05; ** p ≤ 0.01; *** p ≤ 0.001; ****p ≤ 0.0001.

3.4.2. The comparative impact of bile salts at acidic and neutral pH, and acid alone, on the phenotype of cells representing NSE and BO

Whilst there is a clear relationship between GORD and both the development and progression of OAC, the specific contribution to this process that is made by each constituent of gastric refluxate remains unclear. In particular, previous analyses have treated cells with a multitude of bile salts at a variety of molar mixes, over variable time periods, at a number of different pH levels. This has resulted in evidence for pro- and anti-proliferative, and both pro- and anti- apoptotic, roles for acid and bile salts. It is in addition unclear to what extent individual components of refluxate influence processes that

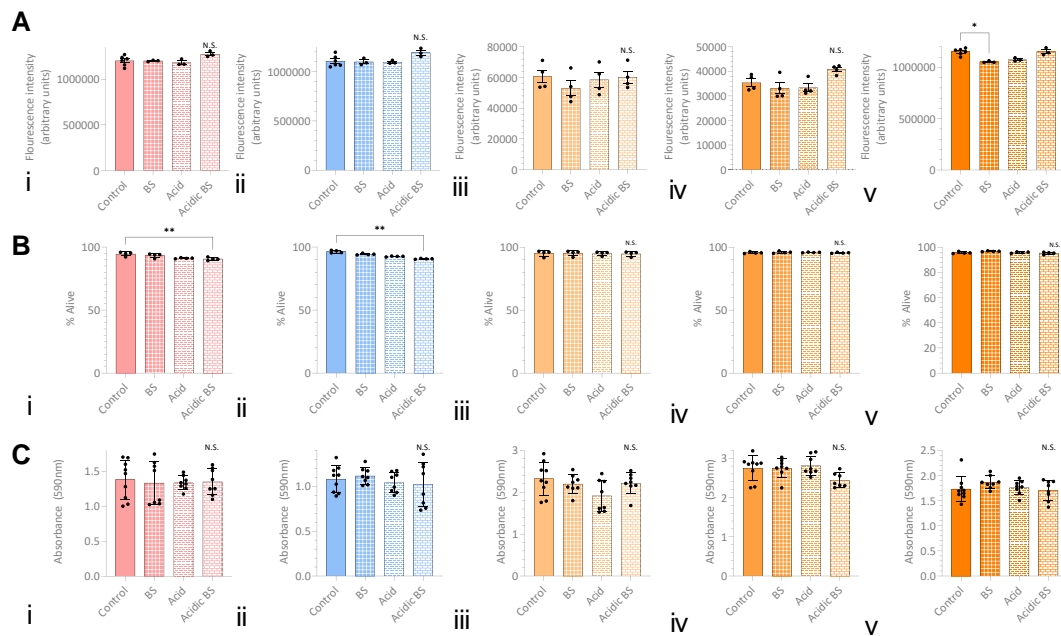


Figure 3.6. The impact of a ten minute pulse of a 100 μ M equimolar mix of bile salts at neutral pH (BS) and pH 4.0 (Acidic BS), or pH 4.0 treatment alone (Acid), on (A) cellular proliferation, (B) cellular death and (C) cellular metabolic activity for (i) NSE Het-1A, (ii) NDBO CP-A and HGD (iii) CP-B, (iv) CP-C and (v) CP-D cells. All cells were assayed at 24 hours post-treatment using (A) Cell prolifer, (B) Live/Dead stain and (C) MTT assays. Individual data points are shown for biological replicates ($n \geq 4$ for all). Statistical analyses were undertaken using the Kruskal-Wallis test with post-hoc Dunn's correction. Comparisons that reached pre-defined significance thresholds are highlighted, and are distinguished as follows: * $p \leq 0.05$; ** $p \leq 0.01$. N.S. refers to non-significant comparisons.

associate with dysplasia, such as EMT. A key hindrance to assessing these studies is that a lack of treatment standardisation means that experiments using acidified bile salts cannot be compared to those using bile salts or acid alone. Given this, we systematically appraised and compared the phenotypic impact of a physiological pulse of acid or bile salts alone, or together, in cells resembling NSE (Het-1A), NDBO (CP-A) and HGD (CP-B, CP-C, CP-D). Acid and bile salts were respectively used at a standardised pH and molar mix that was considered to be near-physiological based on the work explored in 3.1.1.2. and Table 3.1.

3.4.2.1. Cellular viability, proliferation and metabolic activity

The relative impact of bile salts, acid and acidified bile salts on cellular proliferation (as assessed by final viable cell number (Fig. 3.6.A.)), viability (Fig. 3.6.B) and metabolic activity (Fig. 3.6.C.) was assessed across the studied cell line model. In NSE Het-1A (i) and NDBO CP-A (ii) cell lines, a moderate overall increase in cell number was seen following acidic bile salt treatment, though this did not reach significance (1.20×10^6 vs. 1.27×10^6 A.U.; $p=0.1953$ for Het-1A and 1.11×10^6 vs. 1.19×10^6 ; $p=0.0921$ for CP-A). This was associated with a significant reduction in the proportion of viable cells (94.5 vs. 90.6%; $p=0.0089$ for Het-1A and 96.4 vs. 90.7%; $p=0.0011$ for CP-A). Given that the overall metabolic activity of the cells was

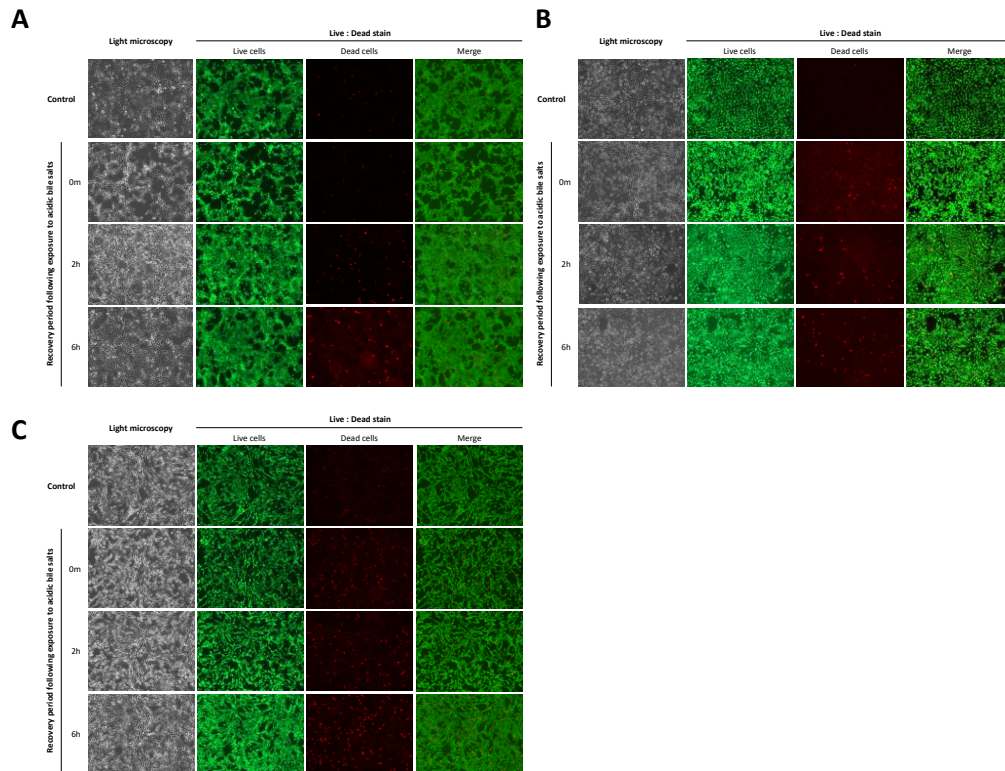


Figure 3.7. Representative images detailing the impact of a ten minute pulse of acidic bile salts (100µM equimolar mix at pH 4.0) on the proportion of live and dead (A) Het-1A, (B) CP-A and (C) CP-B cells immediately, 2 hours and 6 hours after exposure.

unchanged with any treatment, these data indicate that in NSE Het-1A (i) and NDBO CP-A (ii) cells, acidic bile salts but not acid or bile salts alone, resulted in both cellular death and proliferation; leading to a broadly stable or marginally increased overall cellular population. In contrast, all three studied cellular exposures had minimal impact on HGD CP-B, CP-C and CP-D (ii-v) cells, with only a significant reduction in viability with bile salts in CP-D cells (1.15×10^6 vs. 5.30×10^5 ; $p=0.018$) of note.

As shown in **Fig. 3.7.**, the cell death seen in NSE Het-1A (A) and NDBO CP-A (B) cells occurs early, with a small proportion of cells dying by two hours following treatment but little change in cell death to six hours from treatment. This is also seen, albeit to a lesser extent, in HGD CP-B (C) cells, reflecting a similar mechanism but variable intensity of death across the studied cell lines.

3.4.2.2. Cellular morphology

Oesophageal cells *in vivo* are exposed to multiple pulses of refluxate each day, rather than the single exposure that is commonly used to model microenvironmental stress in BO. Given the more pronounced impact of acidified bile salts on cellular phenotype (compared with acid or neutral bile salts alone), we sought to evaluate the impact of long-term daily acidified

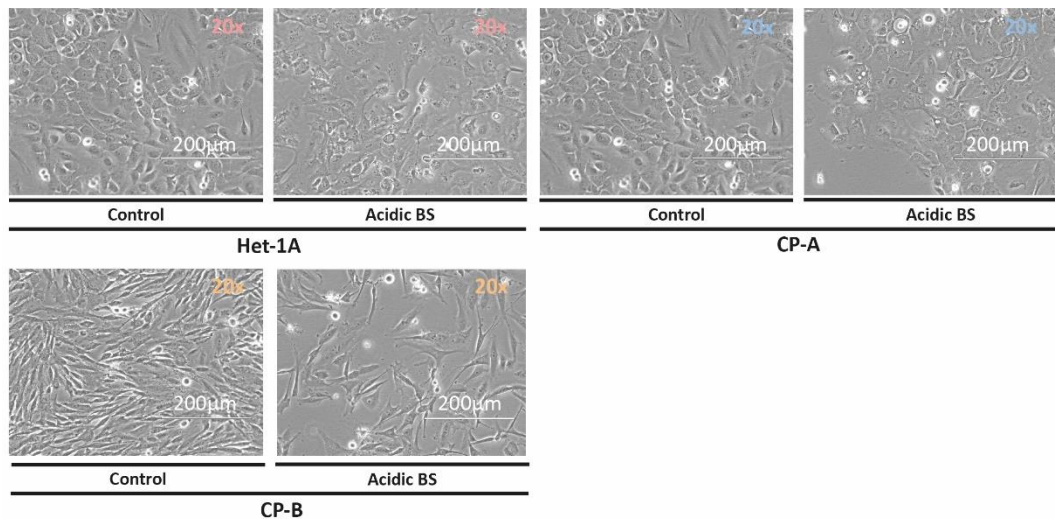


Figure 3.8. A representation of the impact of treatment with a ten minute pulse of acidic bile salts ($100\mu\text{M}$ equimolar mix at pH 4.0) for five days a week over twelve weeks on the morphology of cells representing NSE (Het-1A), NDBO (CP-A) and HGD (CP-B). Images are taken via light microscopy whilst suspended in Live Cell Imaging Solution. Cells were previously maintained in proliferative media and all are in adherent cell culture. Scale bars are included within each image. Acidic bile salt (BS) treated cells are shown alongside passage-matched control cells.

bile salt treatment on NSE (Het-1A), NDBO (CP-A) and HGD (CP-B) cells. As shown in **Fig. 3.8.**, when compared with their basal cellular phenotype (**Fig. 3.3.**), the growth of all three cell lines appeared more disorganised by twelve weeks of treatment. It is in addition noteworthy that though the polygonal morphology of CP-A cells is largely maintained, a greater number of bipolar, elongated cells can be seen at higher magnification. In order to control for passage effects, a separate passage-matched control population was maintained but did not undergo morphological change. These control cells demonstrated similar morphology to the basal morphology of each cell line shown in **Fig. 3.3.** (data not shown).

3.4.2.3. Markers of cellular differentiation

The data outlined in **3.4.1.3.** demonstrates that for the most part, the expression of markers of squamous and intestinal epithelial differentiation poorly discriminates between stages of BO progression. They are nevertheless commonly used as a readout following the *in vitro* exposure of BO cells to stressors within refluxate. Given this, we sought to determine whether a single near-physiological pulse of acidified bile salts would impact on the expression of markers of differentiation, and also to assess for the individual contribution of acid and bile salts to any change in cellular differentiation. Remarkably, and as shown in **Fig. 3.9.**, the only significant change seen was for *KRT7* expression in NSE Het-1A cells following acidic bile salt treatment; demonstrating a 6.8 fold increase versus control; $p < 0.05$). Beyond this, there was generally a trend – albeit not a uniform one - for an increase in the expression of markers of intestinal differentiation (*MUC2*, *SOX9*, *KRT7*, *KRT8*, *KRT18*, *KRT19*) in NSE Het-

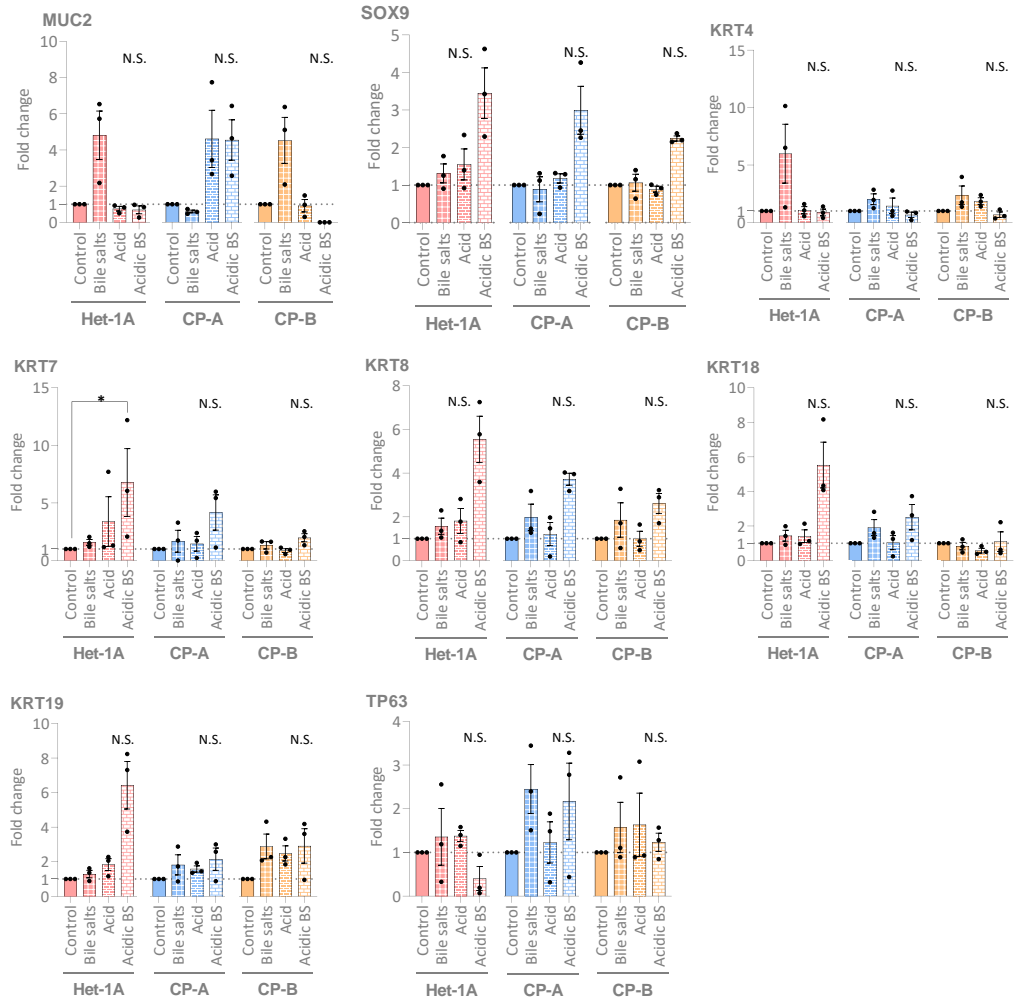


Figure 3.9. Fold-change in the expression of key markers of columnar and squamous differentiation across cell lines resembling NSE (Het-1A), NDBO (CP-A) and HGD (CP-B) in response to a ten minute pulse of bile salts (BS; 100 μ M equimolar mix) at neutral or acidic (4.0) pH, or acidic (pH 4.0) media alone. For each of the eight genes shown, the fold-change in mRNA expression of each gene is shown relative to the control sample for that cell line. Data are presented as mean \pm SEM and all results presented in biological triplicate. Statistical analyses were undertaken with raw Ct values using Kruskal-Wallis test with Dunn’s post-hoc correction for multiple significance testing, with treatment values compared with relevant control samples. Comparisons that reached pre-defined significance thresholds are highlighted, and are distinguished as follows: * $p \leq 0.05$. N.S. refers to non-significant comparisons.

1A and BO CP-A and CP-B cells following treatment with acid or acidic bile salts. In contrast, the impact of bile salts alone appears more modest for markers of intestinal differentiation, regardless of cell type. Alongside, little difference was seen in the expression of markers of squamous differentiation.

Given these limited changes, we sought to determine whether a more differentiated phenotype would result from daily exposure to acidic bile salts over a twelve week period, and whether this would differ by cell line. As shown in **Fig. 3.10.**, expression of the squamous marker *KRT4* was suppressed in all cell lines following two weeks of daily treatment and remained suppressed relative to control over the following ten weeks. In contrast, the

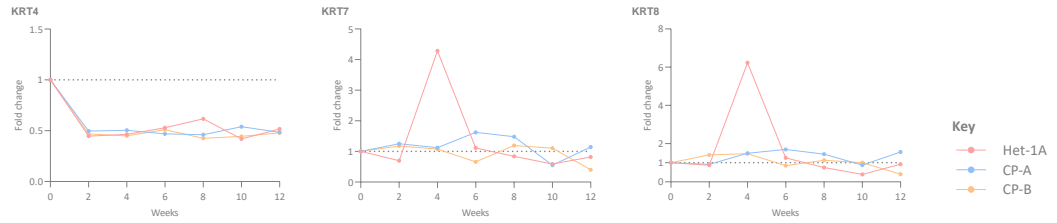


Figure 3.10. Fold change in the expression of key markers of squamous (*KRT4*) and intestinal (*KRT7*, *KRT8*) markers of differentiation in cells representing NSE (Het-1A), NDBO (CP-A) and HGD (CP-B) that are repeatedly exposed to acidic bile salts over a period of twelve weeks. Cells were exposed to an equimolar 100µM mix of bile salts at pH 4.0 or vehicle for ten minutes on five days a week for twelve weeks. Fold-change in mRNA expression of each gene is shown for acidic bile salt treatment relative to control. n=1.

expression of the intestinal markers *KRT7* and *KRT8* remained relatively constant throughout the twelve weeks of treatment. A similar pattern was seen for both markers in the NSE Het-1A cell line, albeit with a significant but isolated increase in both genes at week four of treatment.

3.4.2.4. EMT

Given that differentiation status does not mirror progression (as shown in 3.4.1.3.), it is unclear what the significance is of a lack of clear evidence (as summarised in 3.4.2.3.) for an increase in intestinal differentiation in response to the bile salt and acid constituents of gastric refluxate. However, as shown in 3.4.1.2., there is evidence of an EMT phenotype in the HGD BO cells. We therefore sought to determine whether acidic bile salt treatment of NDBO (CP-A) cells would contribute to EMT by assessing E-cadherin protein expression following acidic bile salt treatment. As shown in Fig. 3.11., a single exposure to acidic bile

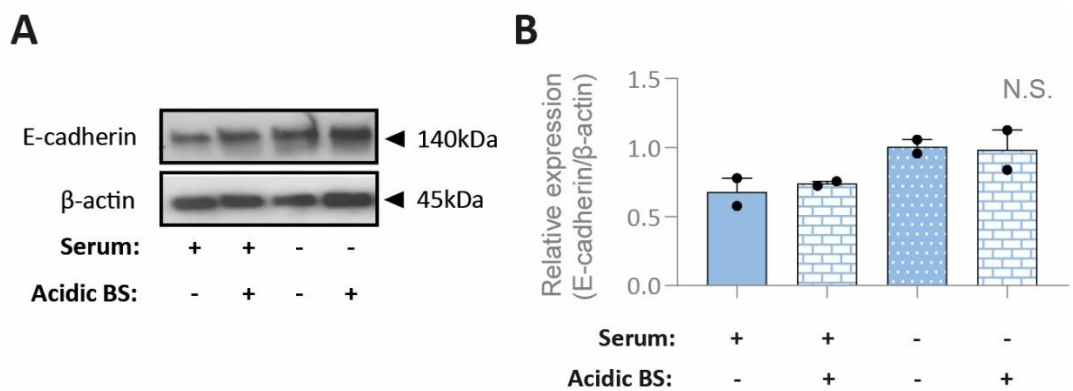


Figure 3.11. An immunoblot showing relative E-cadherin protein expression in NDBO (CP-A) cell lines under conditions of serum-starvation and after exposure to a ten minute pulse of acidic bile salts. A representative immunoblot is presented in (A) and average expression (normalised to β-actin) assessed by densitometry in (B). E-cadherin expression was assessed for cells maintained in proliferative media (FBS+) or after 48 hours of serum starvation (FBS-), with protein lysates measured 24 hours after exposure to a ten minute pulse of vehicle or an equimolar 100µM mix of bile salts at pH 4.0. Statistical analyses were undertaken using the Kruskal-Wallis test with Dunn’s post-hoc correction for multiple significance testing (n=2).

salts did not result in a change in the expression of E-cadherin, even in the presence of an additional serum-starvation stressor.

3.4.3. The comparative impact of serum-starvation on the phenotype of cells representing NSE and BO

As outlined in 3.1.1.2., serum-starvation provides a mechanism through which the signalling and transcriptional mediators of the chronic pro-inflammatory, pro-EMT, pro-autophagic BO microenvironment can be modelled. It has additionally been used in the past as a means to synchronise cells in to the same stage of the cell cycle and to induce quiescence. Most BO and indeed NSE cells will be quiescent unless directly stimulated, meaning that a less proliferative phenotype is likely to more closely mirror *in vivo* conditions in which cells have not recently been exposed to gastric refluxate. Progression into dysplasia commonly results from the conversion from quiescence to a more proliferative cellular phenotype. In order to characterise the factors that contribute to the maintenance of unstimulated cells, as well as non-reflux mediated drivers for their conversion to a proliferative state, we sought to characterise the phenotype of NSE and BO cells under conditions of serum-starvation.

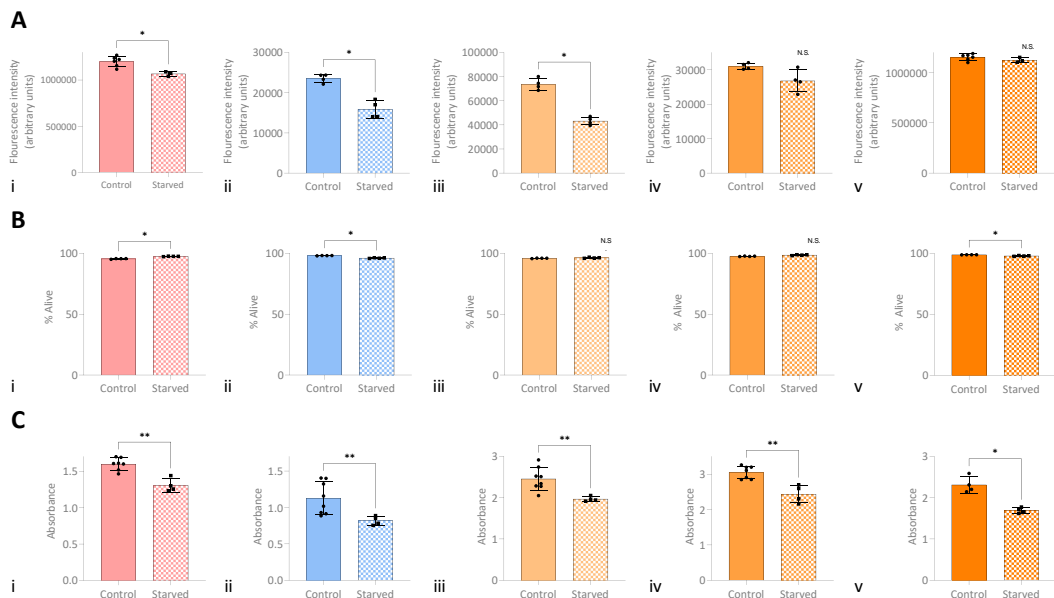


Figure 3.12. The impact of a 48 hour period of serum-starvation on (A) cellular proliferation, (B) cellular death and (C) cellular metabolic activity for (i) NSE Het-1A, (ii) NDBO CP-A and HGD (iii) CP-B, (iv) CP-C and (v) CP-D cells. All cells were assayed at 48 hours following the onset of starvation using (A) Cell prolif, (B) Live/Dead stain and (C) MTT assays. Individual data points are shown for biological replicates (n≥4 for all). Statistical analyses were undertaken using the Kruskal-Wallis test with post-hoc Dunn’s correction. Comparisons that reached pre-defined significance thresholds are highlighted, and are distinguished as follows: * p ≤ 0.05; ** p ≤ 0.01. N.S. refers to non-significant comparisons.

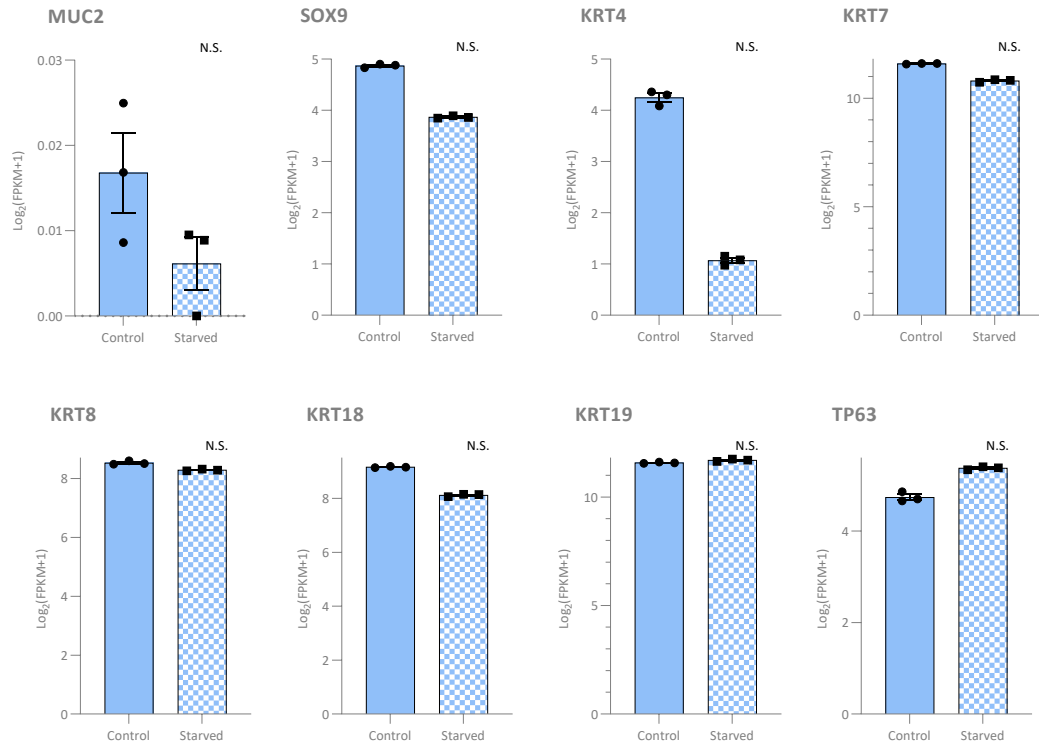


Figure 3.13. Relative expression of key markers of columnar and squamous differentiation across cell lines representing NDBO (CP-A) following a 48 hour period of serum-starvation. Data are taken from RNA-seq analyses. FPKM: Fragments Per Kilobase of transcript per Million mapped reads. Statistical analyses were undertaken using the Kruskal-Wallis test with post-hoc Dunn’s correction. None of the analyses reached a pre-defined threshold for statistical significance of $p \leq 0.05$.

3.4.3.1. Cellular phenotype

In order to validate the impact of serum-starvation, its relative impact on cellular proliferation (as assessed by final viable cell number (**Fig. 3.12A.**)), viability (**Fig. 3.12B.**) and metabolic activity (**Fig. 3.12C.**) was assessed across the studied cell line model. As expected, serum-starvation resulted in a marked decrease in intensity, reflecting a reduction in the final cell number (**Fig. 3.12A.**) of NSE Het-1A (1.20×10^6 vs. 1.07×10^6 A.U.; $p=0.02$), NDBO CP-A (2.4×10^4 vs. 1.5×10^4 ; $p=0.02$) and HGD CP-B (7.4×10^4 vs. 4.3×10^4 A.U.; $p=0.03$) cell lines. A reduction was also seen for HGD CP-C and CP-D cell lines, but was more modest and did not reach significance. Interestingly (**Fig. 3.12B.**), a significantly greater proportion of NSE Het-1A cells were alive following starvation (95.5 vs. 97.5%; $p=0.03$) whereas a significant, albeit minor, decrease in the proportion of live cells was seen for NDBO CP-A (98.0 vs. 96.0%; $p=0.03$) and HGD CP-D (98.8 vs. 97.9%; $p=0.03$) cells. Metabolic activity (**Fig. 3.12C.**) significantly fell across all five studied cell lines following the period of starvation.

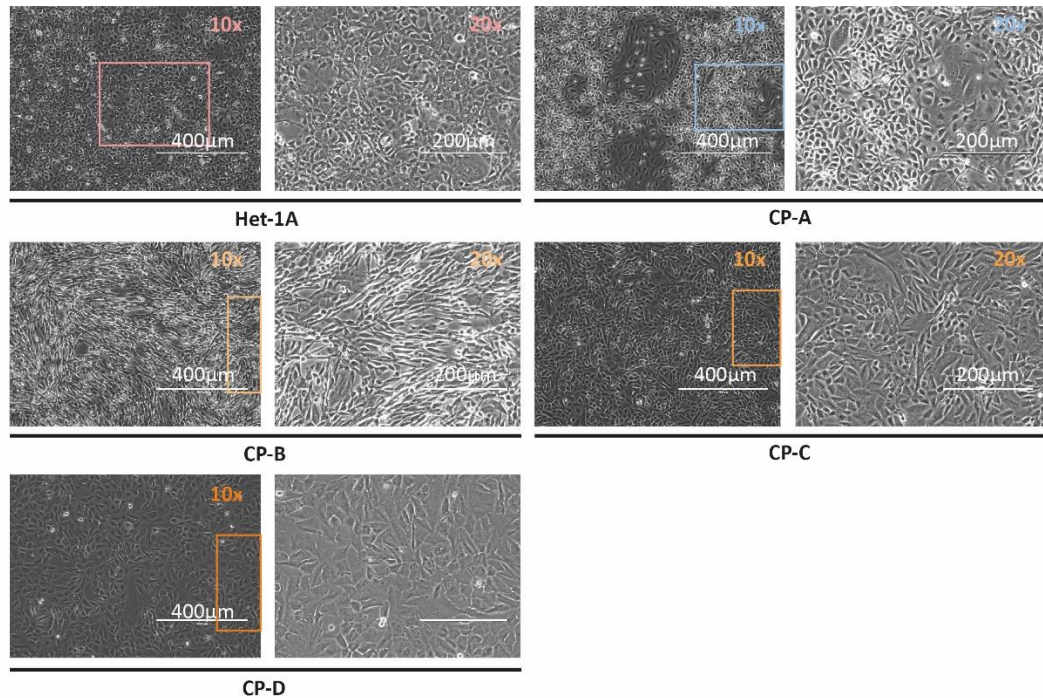


Figure 3.14. A baseline analysis of the morphology of NSE (Het-1A) and Barrett's NDBO (CP-A) and HGD (CP-B, CP-C, CP-D) cells. Images are taken via light microscopy whilst suspended in Live Cell Imaging Solution with images taken at 10x and 20x magnification. Scale bars are included within each image, with the highlighted box indicating the region selected for imaging at greater magnification.

3.4.3.2. Markers of cellular differentiation

The mRNA expression of markers of intestinal and squamous differentiation was evaluated in NDBO CP-A cells following a 48-hour period of serum-starvation in order to provide a comparator to the impact of an alternative stressor (acidic bile salts, as previously outlined in **3.4.2.3**). Data shown in **Fig. 3.13** illustrate that serum-starvation results in a modest fall in the expression of all studied markers of intestinal differentiation other than *KRT19*; albeit with none of the comparisons reaching a pre-defined threshold for statistical significance. The squamous marker *KRT4* also decreased with starvation. Conversely, a modest increase in the expression of the squamous marker *TP63* was seen but did not reach significance.

3.4.3.3. EMT

A state of starvation has been associated with the EMT process. Given this, the impact of starvation on protein E-cadherin expression was evaluated in NDBO CP-A cells by immunoblot, as shown in **Fig. 3.11**. E-cadherin expression was marginally increased following starvation, though this did not reach significance on analysis of repeats by densitometry.

3.4.3.4. Morphology

The most marked change in morphology following serum-starvation, when compared with basal cellular phenotype (**Fig. 3.3.**), was of NDBO CP-A cells. These adopted greater polarity and became more elongated. In contrast, the HGD CP-D cells appear more polygonal following starvation, reflecting that any transition to EMT from starvation may not be uniform. There was minimal change seen in the morphology of NSE Het-1A or HGD CP-B and CP-C cells.

3.4.4. The transcriptomic and regulomic response to microenvironmental stress in NDBO

The work outlined thus far (including most prominently in **3.4.1**) has provided validation for the use of the NDBO CP-A and the HGD CP-B, CP-C and CP-D cells to respectively reflect an early and late stage of BO dysplastic progression. It also appears on the basis of work presented in **3.4.2.** that acidic bile salts impact more significantly on cellular phenotype than acid or bile salts alone, but whilst preserving cellular viability. Further, as evidenced in **3.4.3.**, a 48 hour period of starvation can be used to synchronise cells in a state of quiescence without leading to excess death. From a clinical perspective, the impact of stressors in early BO (i.e. at the level of NDBO) is of perhaps the most significance from the perspective of

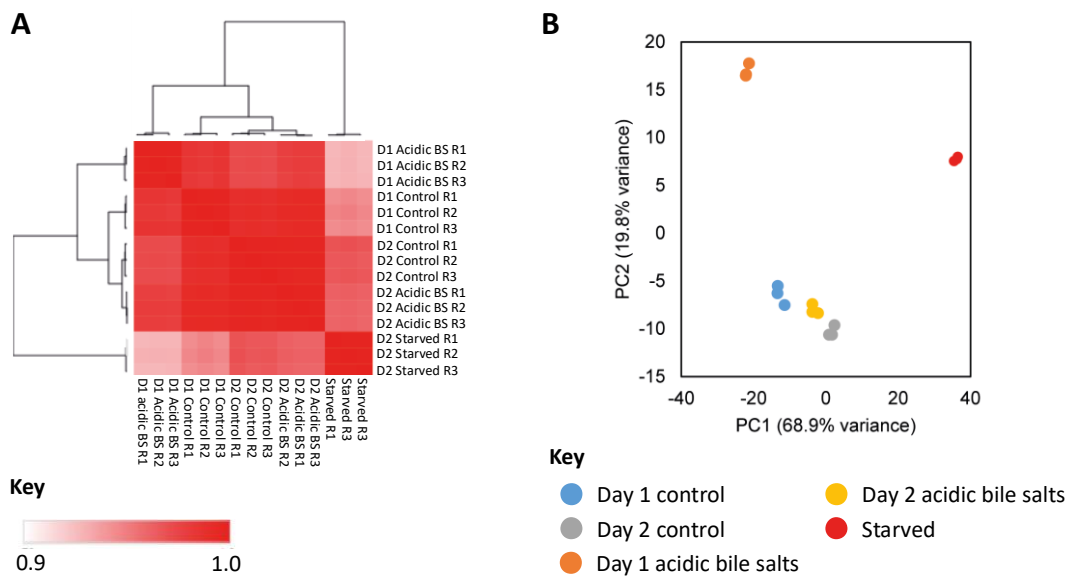


Figure 3.15. Sample-level quality control outputs for RNA-seq analyses of NDBO (CP-A) cells starved for 48 hours or sampled at 24 and 48 hours following acidic bile salt treatment. Pairwise correlation of all replicates is shown in **(A)**, with samples sorted by unsupervised hierarchical clustering following calculation of Pearson's correlation coefficient. Principle component analysis is used in **(B)** to determine the relationship between samples. D1-2: days 1-2; R1-3: repeats 1-3.

identifying chemotherapeutics and biomarkers to respectively prevent or identify dysplastic progression. It is however unclear which cellular processes are initiated by conditions of acute (acidic bile salts) and chronic (serum-starvation) microenvironmental stress in BO, and what relationship these have with the potential for promotion of dysplasia. Given this, we sought to systematically appraise the impact of acidic bile salts and serum-starvation on the NDBO CP-A transcriptome (by RNA-seq) and regulome (by ATAC-seq).

3.4.4.1. Quality control

3.4.4.1.1. RNA-seq

As demonstrated in **Fig. 3.15A**, reproducibility amongst replicates was high, with Pearson's correlation coefficient (PCC) exceeding 0.9 for all pairwise comparisons. This is supported by principal component analysis (PCA; **Fig. 3.15B**), which demonstrated that repeats for each of the assessed experimental conditions closely clustered together.

3.4.4.1.2. ATAC-seq

Fragment size distribution plots for all samples demonstrate decreasing periodical peaks at around 100, 200, 400 and 600bp (**Fig. 3.16A**); correlating well with the expected

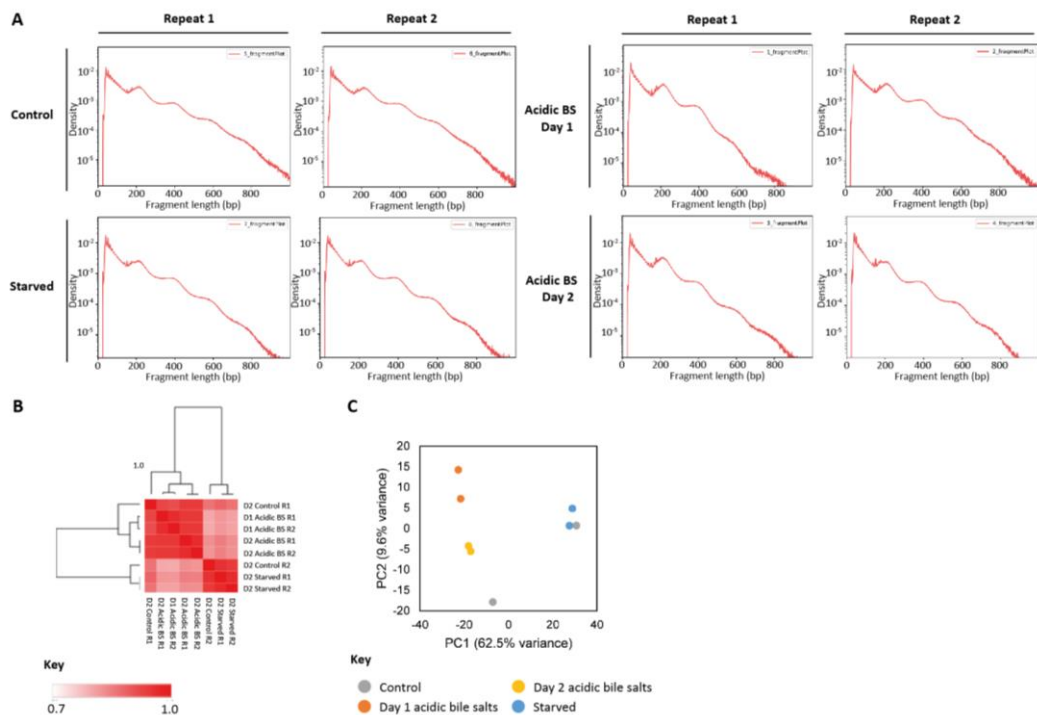


Figure 3.16. Sample-level quality control outputs for ATAC-seq analyses of NDBO (CP-A) cells starved for 48 hours or sampled at 24 and 48 hours following acidic bile salt treatment. Fragment size distribution plots are shown for all samples in (A). Pairwise correlation of all replicates is shown in (B), with samples sorted by unsupervised hierarchical clustering. Principle component analysis is used in (C) to determine the relationship between samples. D1-2: days 1-2; R1-2: repeats 1-2.

nucleosome-free region and mono-, di- and tri- nucleosome sizes. High correlation between replicates was seen for acidic bile salt and 48 hour starved samples, which clustered together when sorted by unsupervised hierarchical clustering and on PCA analysis (**Fig. 3.16B & 3.16C**). However, poorer correlation was seen between control samples, with the second control replicate more closely aligning with starved samples by PCA. This second replicate was therefore excluded from further analyses, which were explored but which are underpowered given that only one control sample was available for analysis.

3.4.4.2. The transcriptome in response to acidic bile salts

3.4.4.2.1. Acidic bile salts rapidly initiate changes in the BO transcriptome

The temporal impact of a ten minute pulse of acidic bile salts was determined by comparing differentially expressed genes (DEGs) after a period of 24 and 48 hours. As illustrated by **Fig. 3.17.**, a dramatic change in gene expression was seen at 24 hours, with fewer DEGs identified at 48 hours. Overall, at 24 hours a similar number of genes were significantly upregulated (n=3305) as were significantly downregulated (n=3593). Of these, 944 genes exhibited greater than a 1.5-fold increase in expression and 1364 genes exhibited a greater than 1.5 fold decrease in expression (**Fig. 3.17A**). In contrast, only 95 genes were significantly upregulated with a fold-change of >1.5 at day 2, and just 59 significantly downregulated with a fold-change of greater than 1.5.

All subsequent analyses considered a change in expression with $p < 0.05$ and a fold-change of greater than 1.5. as significant. As is evident from **Fig. 3.17B** and **Fig. 3.17C**, for a majority of genes the differential expression seen at 24 hours following acidic bile salts did not persist to 48 hours. However, 45 genes were significantly upregulated at both 24 and 48 hours, and 37 significantly downregulated at both time points. Interestingly, the respective significant up- and down- regulation of 37 and 14 genes was seen at 48 hours but not at 24 hours. A small number of genes diverged between the studied timepoints with either an increase in expression at 24 hours followed by a decrease at 48 hours, or vice versa.

At 24 hours post-acidic bile salt exposure, the greatest increase in expression (**Fig. 3.17D**) was seen for *CLU* (\log_2 fold change (LFC) increase of 5.88; $p < 1.0 \times 10^{-300}$), which encodes clusterin; *HSPA6* (LFC increase of 6.46; $p = 1.2 \times 10^{-221}$), which encodes Heat Shock Protein Family A Member 6; and *KRT34* (LFC increase of 4.80; $p = 5.5 \times 10^{-62}$), which encodes cytokeratin 34. In contrast, at 48 hours the vanin-encoding *VNN1* (LFC increase of 2.38; $p = 9.59 \times 10^{-10}$) and the ion-channel encoding *CFTR* (LFC increase of 2.22; $p = 8.75 \times 10^{-34}$) genes demonstrated the largest significant increase in expression.

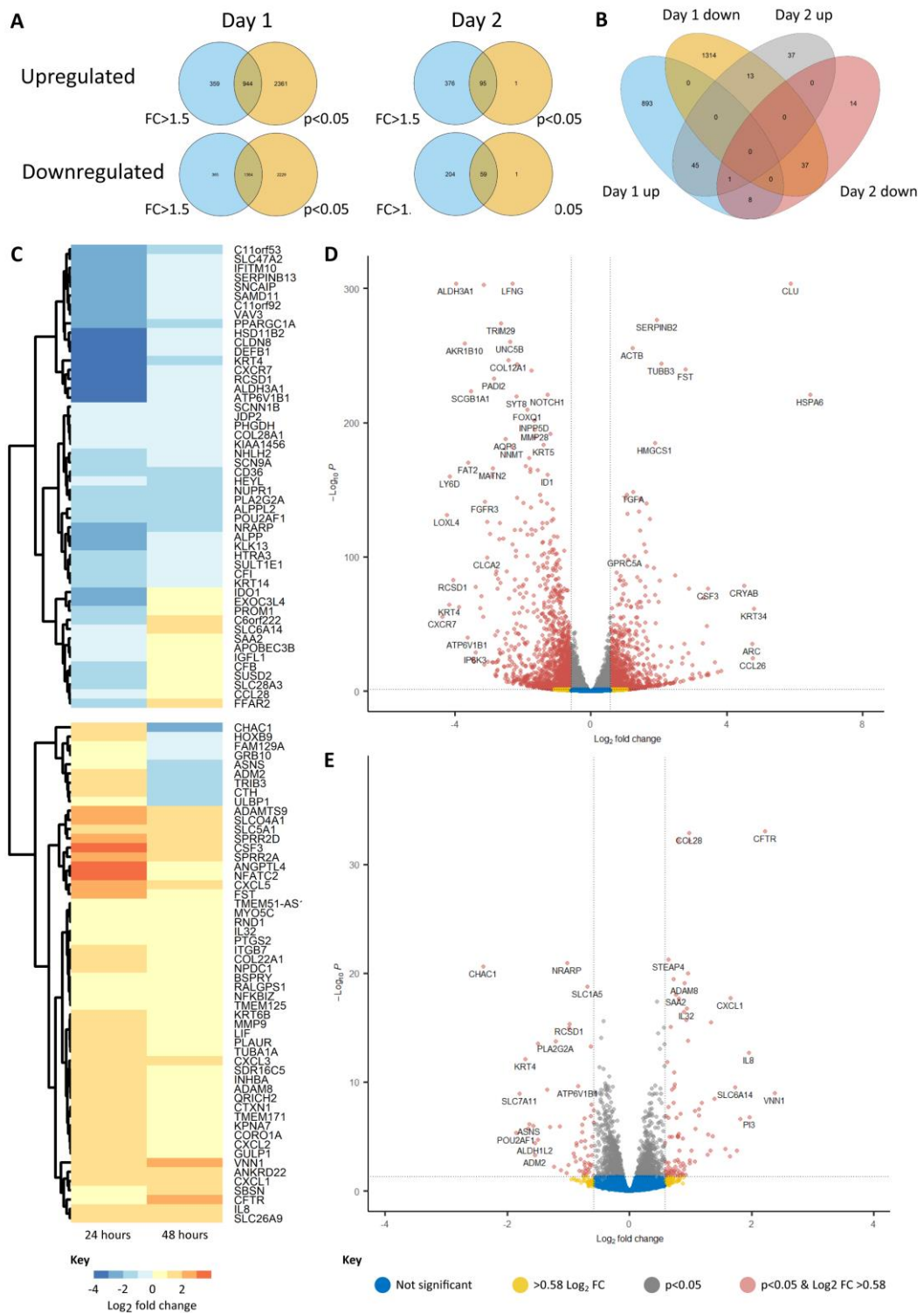


Figure 3.17. A panel figure illustrating changes in gene expression in NDBO (CP-A) cells 24- and 48- hours following a ten minute exposure to acidified bile salts. CP-A cells were exposed to a 100 μ M equimolar mix of bile salts at pH 4.0. The number of genes that exhibited >1.5 log₂ fold change (FC) in expression and for which adjusted p < 0.05 at 24 hours (Day 1) and 48 hours (Day 2) post-exposure is shown in (A). (B) A Venn diagram demonstrating the number of significantly differentially expressed genes with log₂FC >1.5 that were up- or down- regulated at both studied time points. (C) A heatmap demonstrating genes that were significantly differentially expressed at both timepoints. Samples are sorted by Euclidean distance means-based unsupervised hierarchical clustering with complete linkage. Identified relationships are illustrated by the dendrogram. Cell colours represent fold-change. (D,E) Volcano plots illustrating differential gene expression at day 1 (D) and day 2 (E) following acidic bile salt treatment by p-value and log₂FC. Key genes are named within the figure.

The largest fall in expression at 24 hours was seen for the aldehyde dehydrogenase-encoding *ALDH3A1* (LFC decrease of 3.97; $p < 1.0 \times 10^{-300}$) and the chemokine receptor-encoding *CXCR7* (LFC decrease of 4.36; $p = 6.07 \times 10^{-56}$) genes. The squamous cytokeratin-encoding *KRT4* gene also decreased substantially and significantly at both 24 hours (LFC decrease of 4.17; $p = 6.33 \times 10^{-65}$) and 48 hours (LFC decrease of 1.70; $p = 8.01 \times 10^{-13}$). The largest decrease in expression at 48 hours was, however, seen for the endoplasmic reticulum stress-mediating *CHAC1* (LFC decrease of 2.39; $p = 2.23 \times 10^{-21}$) gene, with expression of the cystine/glutamate transporter-encoding *SLC7A11* (LFC decrease of 1.80; $p = 1.18 \times 10^{-9}$) gene also falling considerably.

3.4.4.2.2. Genes upregulated in response to acidic bile salts in NDBO enrich for pro-inflammatory, pro-migratory and RTK-derived signalling processes

Orthogonal functional enrichment analyses were undertaken in order to understand the functional relevance of DEGs that significantly increased or decreased following acidic bile salt exposure (**Fig. 3.18**). Metascape (**Fig. 3.18A**) summarises and ranks overrepresented GO BP terms and enriched pathways (by KEGG, REACTOME and WP) within the same dataset. GSEA (**Fig. 3.18B**) uses a different database to identify signalling and process terms associated with statistically significant differences between phenotypes. Neither identified any enriched processes or pathways for significantly increased or decreased DEGs at 48 hours following acidic bile salt exposure.

However, at 24 hours (day 1), functional enrichment by GSEA and Metascape identified a number of pro-inflammatory and pro-migratory processes within the significantly increased DEG set, in addition to a number of signalling pathways related to RTKs. As well as enrichment of numerous generic inflammatory response-related terms within both the Metascape and GSEA datasets, a number of specific pro-inflammatory pathways were highlighted. These include 'TNF α signalling via NF- κ B' (GSEA), 'IL-18 signalling pathway' (Wiki Pathway, WP, 4754), 'IL2 STAT5 signalling' (GSEA) and 'IL6 JAK STAT3 signalling' (GSEA). A pro-vasculogenic hypoxic-like gene-signature was also apparent, with enrichment of 'GO 0001944: vasculature development' by Metascape and 'Hypoxia' by GSEA.

Beyond the pro-inflammatory processes outlined here, the overall functional cellular response to acidic bile salts is underlined by enrichment of 'GO 0045596: Negative regulation of cell differentiation', 'MTOR1C signalling' (GSEA) and 'Epithelial mesenchymal transition' (GSEA). Upstream of this, there is enrichment of terms relating to RTKs, including by the REACTOME terms 'EGFR interacts with phospholipase C-gamma' and 'Signalling by

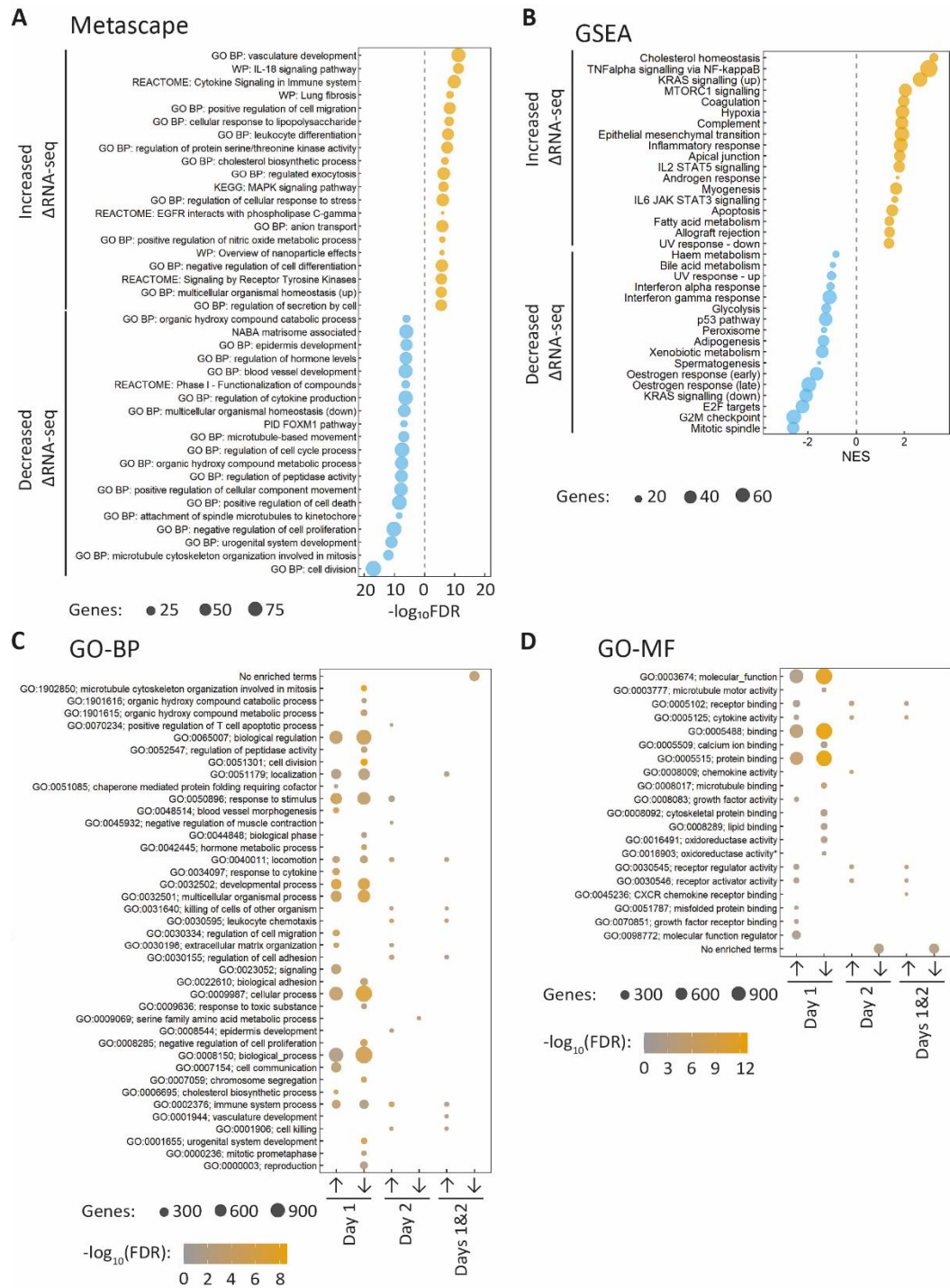


Figure 3.18. A panel figure illustrating functional enrichment of differentially expressed genes in NDBO (CP-A) cells at 24 and 48 hours following exposure to a ten minute pulse of acidified bile salts. CP-A cells were exposed to a 100 μ M equimolar mix of bile salts at pH 4.0 and enrichment of genes for which \log_2 fold change (FC) >1.5 and adjusted $p < 0.05$ analysed following RNA-seq analysis undertaken in biological triplicate. **(A)** Functional enrichment by Metascape and **(B)** gene set enrichment analysis (GSEA) for DEGs significantly up- and down- regulated at day 1 following acidic BS exposure. No classes enriched at day 2 in either Metascape analysis or GSEA. **(C,D)** Over-represented gene ontology (GO) biological process (BP; C) and molecular function (MF; D) terms for DEGs that were significantly upregulated (up-arrow) or downregulated (down arrow) at day 1, day 2 or both days 1 and 2 following acidified bile salt exposure. In all plots, the size of the bubble reflects the number of DEGs contributing to the enriched term. FDR: false discovery rate.

Receptor Tyrosine Kinases'. Enrichment of pathways triggered by RTKs is also seen, including 'KRAS signalling' (GSEA) and 'MAPK signalling pathway' (KEGG).

The terms enriched within significantly downregulated DEGs suggest that the pro-EMT phenotype highlighted from functional enrichment of increased DEGs is mirrored by considerable negative regulation of cell proliferation. This includes enrichment of five GO BP processes and three GSEA terms relating to negative regulation of the cell cycle, including G2M checkpoint (GSEA), E2F targets (GSEA) and mitotic spindle (GSEA). Interestingly, there is also evidence for the activity of hormone nuclear receptors, with enrichment within significantly upregulated genes of an 'Androgen response' (GSEA) and enrichment within significantly downregulated genes of an 'Oestrogen response' (GSEA). Pertinently to BO and its stressors, there is in addition enrichment by GSEA within downregulated genes of a 'p53 pathway response' and 'bile acid metabolism', as well as enrichment within upregulated genes of 'Apical junction' related functions.

This functional enrichment at 24 hours following acidic bile salt exposure is supported by the identification of overrepresented GO BP (**Fig. 3.18C**) and GO MF (**Fig. 3.18D**) terms. At 48 hours following acidic bile salt exposure (day 2), newly represented terms for upregulated genes relate to migration (GO 0030155: regulation of cell adhesion) or an ongoing inflammatory process centred on the action of chemokines (GO 0008009: chemokine activity, GO: 0045236: CXCR chemokine receptor binding). Downregulated genes at 48 hours were enriched for GO BP terms that relate to amino acid and oxo (keto)-acid metabolic processes, including 'GO 0006563: L-serine metabolic processes' (Q (FDR)= 4.71×10^{-2}), 'GO 0089718: amino acid import across the plasma membrane' ($Q=5.55 \times 10^{-3}$), 'GO 1902475: L-alpha-amino acid transmembrane transport' ($Q=1.39 \times 10^{-2}$) and 'GO 0046395: carboxylic acid catabolic process' ($Q=2.11 \times 10^{-2}$). In keeping with these terms, a number of the genes within this downregulated set are essential for mitochondrial function. This includes *PCK2* (-0.74 log₂fold change (LFC) decrease; $p=0.002$), *ALDH1L2* (-1.55 LFC decrease; $p=4.1 \times 10^{-5}$) and *SLC6A9* (-0.91 LFC decrease; $p=3.48 \times 10^{-4}$). There were no enriched terms for the group of 48 hour upregulated genes.

A summary of the process enriched by Metascape for genes upregulated at both 24 and 48 hours following acidic bile salt exposure is provided in **Fig. 3.19A**. This mirrors a majority of the enrichment seen at 24 hours (summarised in **3.19B**) but when the two timepoints are taken together, there is greater enrichment for pro-proliferative ('DNA replication') and pro-migratory ('Regulation of cell adhesion', 'Positive regulation of locomotion') pathways.

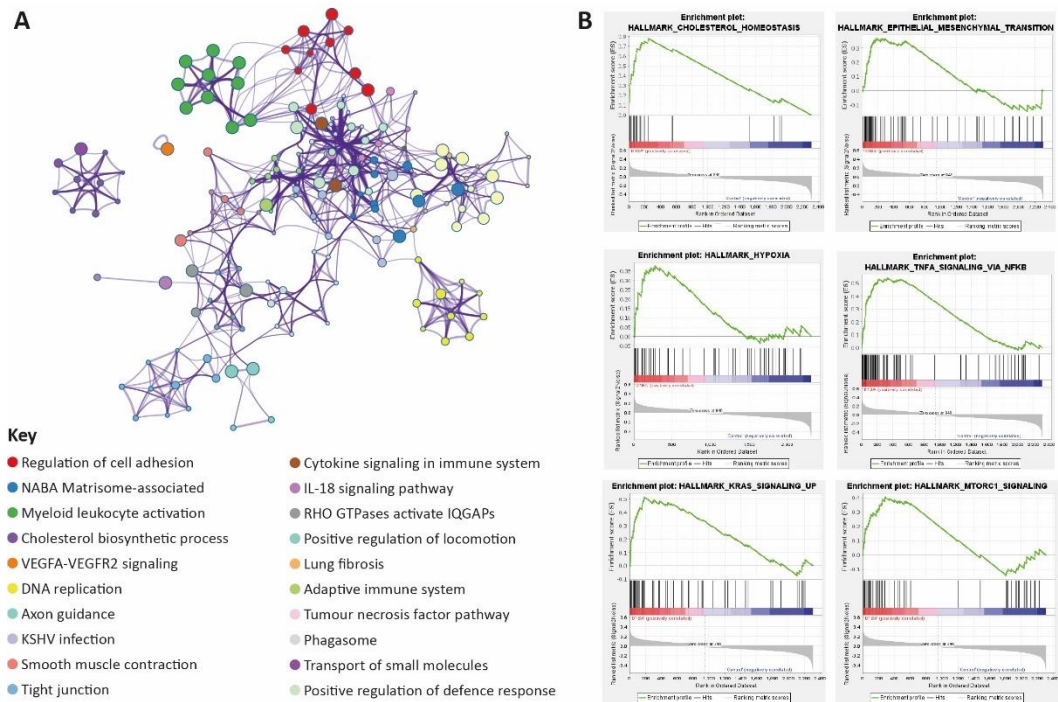


Figure 3.19. A panel figure illustrating functional enrichment of genes for which expression significantly increased at both 1 and 2 days in NDBO (CP-A) cells following acidic bile salt exposure. CP-A cells were exposed to a 100 μ M equimolar mix of bile salts at pH 4.0 and enrichment of genes for which log₂ fold change (FC) >1.5 and adjusted p < 0.05 analysed following RNA-seq analysis undertaken in biological triplicate. **(A)** Network visualisation of enrichment by Metascape for all genes significantly increased at days 1 and 2, with nodes coloured by cluster ID (as shown in the key). Clusters are based on Kappa-statistical similarities amongst the genes representing each enriched term, using a Kappa cut-off value of 0.3. The network plot was generated using Cytoscape v3.1.2. using a force-directed layout and with bundled edges. The size of each node is proportional to the number of input genes. Terms with a similarity score exceeding 0.3 are linked by edges, with edge thickness representing the similarity score. **(B)** Gene set enrichment analysis (GSEA) score curves for a subset of positively-correlated terms enriched from genes significantly upregulated at day 1 following acidic bile salt exposure. In each graph, the green curve represents the weighted score of the enrichment score and the vertical black lines represent the position of each differentially expressed gene in the ordered dataset.

Interestingly, vascular endothelial growth factor receptor (VEGFR) 2 signalling is overrepresented rather than the EGFR signalling enriched at day 1 alone, whilst a gene pattern similar to that seen in lung fibrosis is highlighted.

A separate population of DEGs decreased at 24 hours then increased at 48 hours but did not enrich. However, DEGs that conversely increased at 24 hours then decreased by 48 hours were enriched for 'GO 0034976: response to endoplasmic reticulum stress' (Q=6.22x10⁻⁴). These include a number of genes known to be involved in the unfolded protein response, including the *CHAC1*, asparagine synthetase-encoding *ASNS* and binding protein-encoding *ULBP1* genes.

3.4.4.3. The upstream determinants of genes differentially expressed in response to acidic bile salts in NDBO

A combination of computational analyses and ATAC-seq were used to determine the potential pathways through which genes were differentially regulated in response to acidic bile salts (**Fig. 3.20.**). The candidate signalling components and nuclear receptors with the highest increase and decrease in IPA activation z-score are outlined in **Fig. 3.20A** and **Fig. 3.20B**, respectively. The z-score is a statistical quantity that infers the activation state of biological functions implicated in the differential regulation of gene sets. This is based on an assumption that edges (links) in a network reflect causal relationships, with the direction of effect assigned based on current literature. Identified signalling components are grouped by function.

Potential transcription factors through which these pathways act were identified using orthogonal approaches. Computational methods included prediction by IPA z-score and through the use of the Transcriptional Regulatory Relationships Unravalled by Sentence-based Text-mining (TRRUST) database (**Fig. 3.20C**).⁽⁴⁸⁹⁾ This database includes over 800 human transcription factors and identifies transcription factors that may be mediating increases or decreases in DEGs by sentence-based text mining. Transcription factors were additionally identified experimentally by ATAC-seq, through which changes in chromatin accessibility are profiled and transcription factors complementary to both open and closed chromatin sequences identified (**Fig. 3.20D**).

3.4.4.3.1. The MAPK and PI3L/Akt pathways, and a pro-inflammatory T_h1 cytokine response, are strongly represented in the predicted upstream mediators for differential expression of genes in NDBO in response to acidic bile salts

Overall, the signalling components predicted to mediate DEGs in response to acidic bile salts were similar at 24 hours (day 1) to 48 hours (day 2) following treatment exposure. Reassuringly, most of the predicted signalling components belong to pathways and processes identified in the functional enrichment of DEGs outlined in **3.4.4.2.2**. Amongst the predicted upstream immune pathways, there was strong representation from the NF- κ B pathway, TGF β signalling and TNF α signalling. These, and other cytokines predicted to be activated, including IL-1 β and IL-17A, point to a predominantly T_h1 cytokine response to acidic bile salts. This is supported by the predicted downregulation of T_h2 and anti-inflammatory cytokines such as IL-9, IL-10 and IL-37.

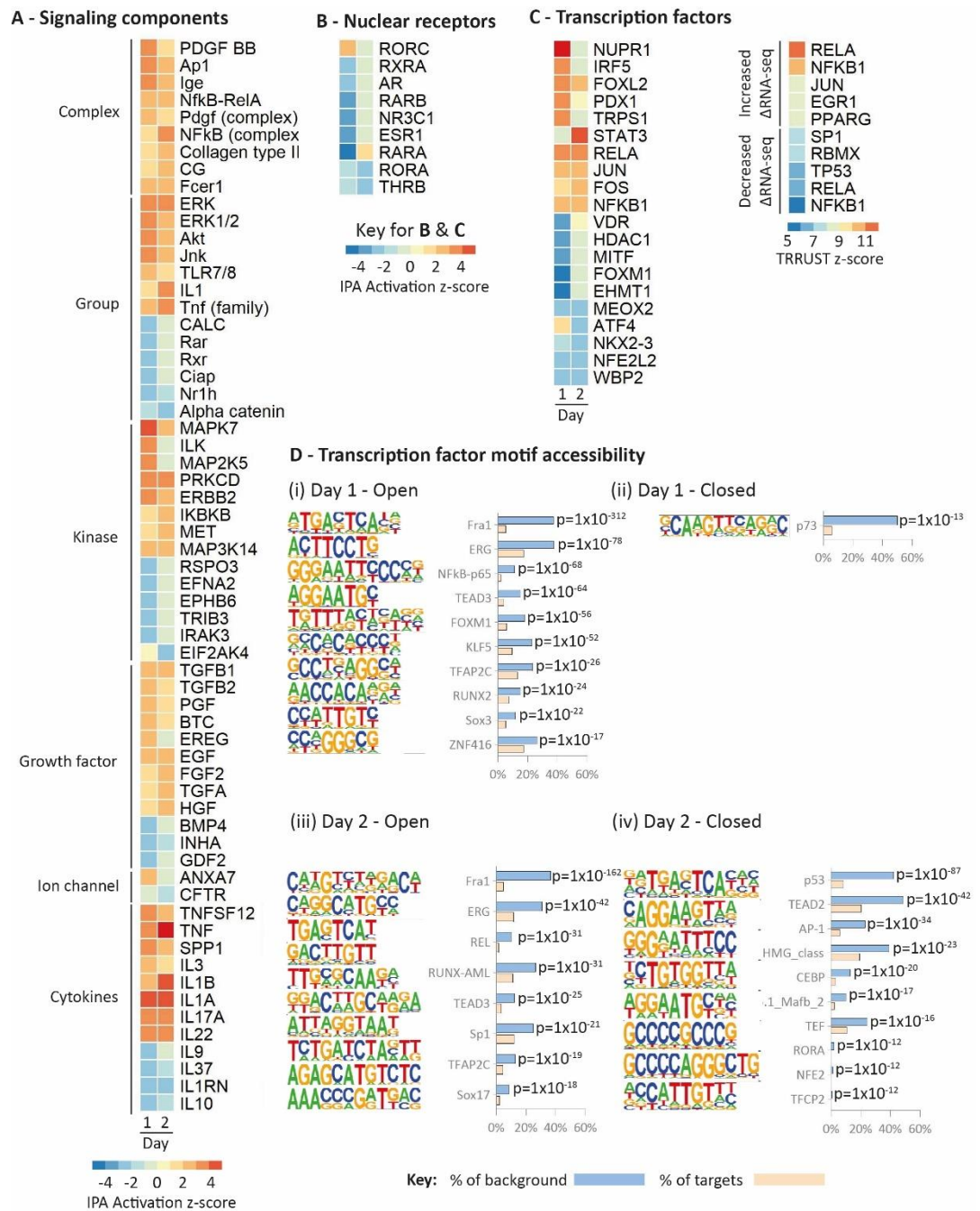


Figure 3.20. A panel figure illustrating transcriptional regulators in NDBO (CP-A) cells at days 1 and 2 following acidic bile salt exposure. CP-A cells were exposed to a 100 μ M equimolar mix of bile salts at pH 4.0. (A-C) Heatmaps demonstrating putative upstream (A) signaling components, (B) nuclear receptors and (C) transcription factors identified from genes for which log₂ fold change (FC) demonstrated a >1.5 increase or decrease, with adjusted p < 0.05, as identified through RNA-seq analysis undertaken in biological triplicate. Potential regulators were identified by (A-C) Ingenuity Pathway Analysis (IPA) and (C) Transcriptional Regulatory Relationships Unraveled by Sentence-based Text mining (TRRUST) analysis. (D,E) Bar charts demonstrating percentage targets and percentage background for *de novo* identified motifs at regions of increased and decreased chromatin accessibility at days 1 and 2 following acidic bile salt exposure, as identified by ATAC-seq. De novo-identified motifs are shown, as are the transcription factors ‘called’ to bin to them, the motif match score and the attributed significance (p-value).

There is in addition strong representation amongst the predicted signalling components for the MAPK and PI3K/Akt pathways. This includes from ERK, Akt, MAPK7 and MAP2K5; all of

which have predicted increased activation z-scores at days 1 and 2 following acidic bile salt treatment. There is also support for a role upstream of these pathways for RTKs, including predicted activation of the RTKs ERBB2 and MET, as well as predicted activation of known RTK ligands such as PDGF, TGF α , EGF, FGF2 and HGF. Amongst the signalling components that have a negative predicted activation z-score are a number of components related to the cellular response to retinoic acid. This includes Rar and Rxr, which is supported by the apparent downregulation of the nuclear receptors RXRA and RORA (**Fig. 3.20B**).

3.4.4.3.2. A consistent regulomic response mediates the NDBO response to acidic bile salts over a 48 hour period

There was considerable correlation between the transcription factors predicted by IPA and TRRUSt (**Fig. 3.20C**) based on RNA-seq data, and those identified based on open and closed chromatin profiling by ATAC-seq (**Fig. 3.20D**). Overall, 1823 open and 50 closed differential chromatin peaks were identified via ATAC-seq at 24 hours following acidic bile salt treatment, and 927 open and 614 closed peaks identified at 48 hours. A majority of the transcription factors for which consensus open chromatin sites were most significantly identified at 24 hours were also reported to bind open chromatin at 48 hours, suggesting that there was no change in the overall 'signal' provided to modulate gene expression over this period. This includes the NF- κ B RELA (p65) subunit, which had activation Z-scores of 2.80 and 2.96 by IPA at day 1 and 2 respectively, and 12 by TRRUSt at day 1. This transcription factor's footprint was overrepresented in 11.35% of target open chromatin sequences, compared with 2.15% of background sequences ($p=1 \times 10^{-68}$) at day 1 and 10.33% of target open chromatin sequences compared with 1.94% of background sequences at day 2 ($p=1 \times 10^{-31}$) following acidic bile salt treatment when assessed by ATAC-seq. The Fos family of transcription factors was also significantly represented as a mediator of the acidic bile salt response by both the predicted IPA set (FOS, z-score of 1.87 and 2.77 at days 1 and 2, respectively) and the ATAC-seq data (Fra1; 37.66% of targets, 5.4% of background, $p=1 \times 10^{-312}$ at day 1 and 36.60% of targets and 4.81% of background, $p=1 \times 10^{-162}$ at day 2). Other transcription factors implicated at day 1 by ATAC-seq include the DNA-damage response protein Forkhead Box M1 (FOXM1, $p=1 \times 10^{-56}$) protein, SOX3 ($p=1 \times 10^{-22}$) and KLF5 ($p=1 \times 10^{-52}$). TEAD3 and ERG, which were not predicted by IPA or TRRUSt, were also identified by ATAC-seq at both day 1 ($p=1 \times 10^{-64}$ and $p=1 \times 10^{-78}$ respectively) and day 2 ($p=1 \times 10^{-25}$ and $p=1 \times 10^{-42}$, respectively).

Despite a number of transcription factor sites predicted by IPA and TRRUST to be downregulated in response to acidic bile salts, only one (p73, 50.0% of targets, 6.0% of background, $p=1 \times 10^{-13}$) was identified as a probable binder by ATAC-seq. At day 2, new closure of consensus chromatin sequences was seen at day 2 for the tumour suppressor p53 (42.2% of targets, 8.6% of background, $p=1 \times 10^{-87}$) and CCAAT/enhancer-binding protein alpha (CEBP; 13.0% of targets, 3.1% of background, $p=1 \times 10^{-20}$).

3.4.4.4. The transcriptome in response to serum starvation

3.4.4.4.1. Serum-starvation results in significant changes in gene expression in NDBO cells

The impact of a 48 hour period of serum-starvation on NDBO cells was determined by identifying DEGs from a control population. As illustrated by **Fig. 3.21A**, similar numbers of genes were significantly upregulated ($n=4,036$) and downregulated ($n=4,383$). Of these, 1742 genes exhibited a greater than 1.5-fold increase in expression and 1932 exhibited a greater than 1.5-fold decrease in expression. All subsequent analyses considered a change in expression with $p < 0.05$ and a fold-change of greater than 1.5 as significant.

The largest increases in expression (**Fig. 3.21B**) were seen for the chemokine-ligand encoding *CXCL14* (LFC increase of 6.91; $p < 1 \times 10^{-84}$) gene, the elastin-encoding *ELN* (LFC increase of 5.87; $p = 3.93 \times 10^{-84}$) gene, the cell-surface glycoprotein-encoding *CD36* (LFC increase of 5.4, $p = 7.07 \times 10^{-127}$) gene and the RTK-ligand encoding *FGF1* (LFC increase of 1.75×10^{-41} ; $p = 1.65 \times 10^{-41}$) gene. The largest decreases in expression were seen for the deiminase-encoding *PADI2* (LFC decrease of 5.73; $p = 2.36 \times 10^{-188}$) gene, the cytokerin-

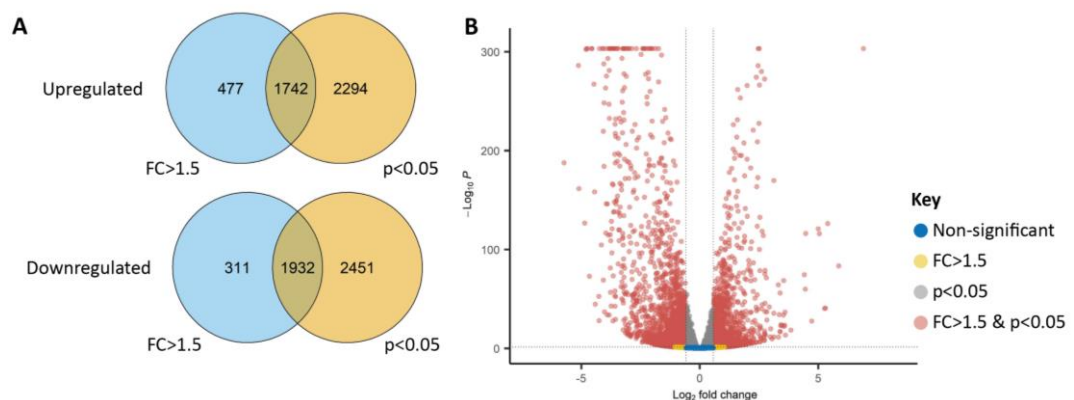


Figure 3.21. A panel figure illustrating changes in gene expression in NDBO (CP-A) cells after a 48 hour period of starvation. (A) A Venn diagram demonstrating the number of significantly differentially expressed genes with $\log_2FC > 1.5$ that were up- or down- regulated. **(B)** A volcano plot illustrating differential gene expression following starvation by p-value and \log_2FC .

encoding *KRT23* (LFC decrease of 5.10; $p=3.17 \times 10^{-162}$) gene, the annexin-encoding *ANXA10* (LFC decrease of 4.86; $p=1.73 \times 10^{-127}$) gene and the uteroglobin-encoding *SCGB1A1* (LFC decrease of 4.80; $p=5.87 \times 10^{-303}$) gene.

3.4.4.4.2. Genes differentially regulated in response to serum-starvation enrich for reduced cell cycle progression, enhanced extracellular matrix remodelling and an increase in growth factor, mTOR and developmental signalling

As in **3.4.4.2.2.**, orthogonal functional enrichment analyses were undertaken in order to understand the functional relevance of DEGs that, in this case, significantly increased or decreased following a 48-hour period of serum-starvation (**Fig. 3.22.**). Analysis by Metascape (**Fig. 3.22A**) revealed a large number of GO BP terms relating to developmental processes that were enriched from significantly upregulated genes. This appeared to reflect a process of increased stem-like and de-differentiative change, with 'GO 0030855: epithelial cell differentiation' enriched amongst significantly decreased DEGs. There was also evidence for extracellular matrix remodelling, including enrichment within significantly increased DEGs of the 'NABA core matrisome', 'REACTOME: Extracellular matrix organisation' and 'GO 0001568: blood vessel development' terms. Unsurprisingly, a number of terms relating to cell proliferation were enriched within the decreased DEGs, highlighting cellular exit from cell cycling following the withdrawal of exogenous growth factor stimulus.

Both the Metascape and the GSEA (**Fig. 3.22B**) analyses point to signalling pathways that potentially regulate these processes. Surprisingly, this includes the 'GO 0071363: Cellular response to growth stimulus' term. This is supported by the over-represented terms identified for singular GO BP (**Fig. 3.22C**) and GO MF (**Fig. 3.22D**) analyses, including 'GO 0048407: platelet-derived growth factor binding', 'GO 0019838: growth factor binding' and 'GO 0030971: receptor tyrosine kinase binding'.

A number of terms relating to an increase in signalling relating to the energy-sensor mTOR1c ('PI3k/AKT/mTOR signalling', 'mTOR1c signalling') were also enriched by GSEA analysis. This may relate to the development of autophagy, which would be supported by the enrichment of a 'TGF β response' by GSEA and the over-representation of 'GO 0071840: cellular component organisation or biogenesis'.

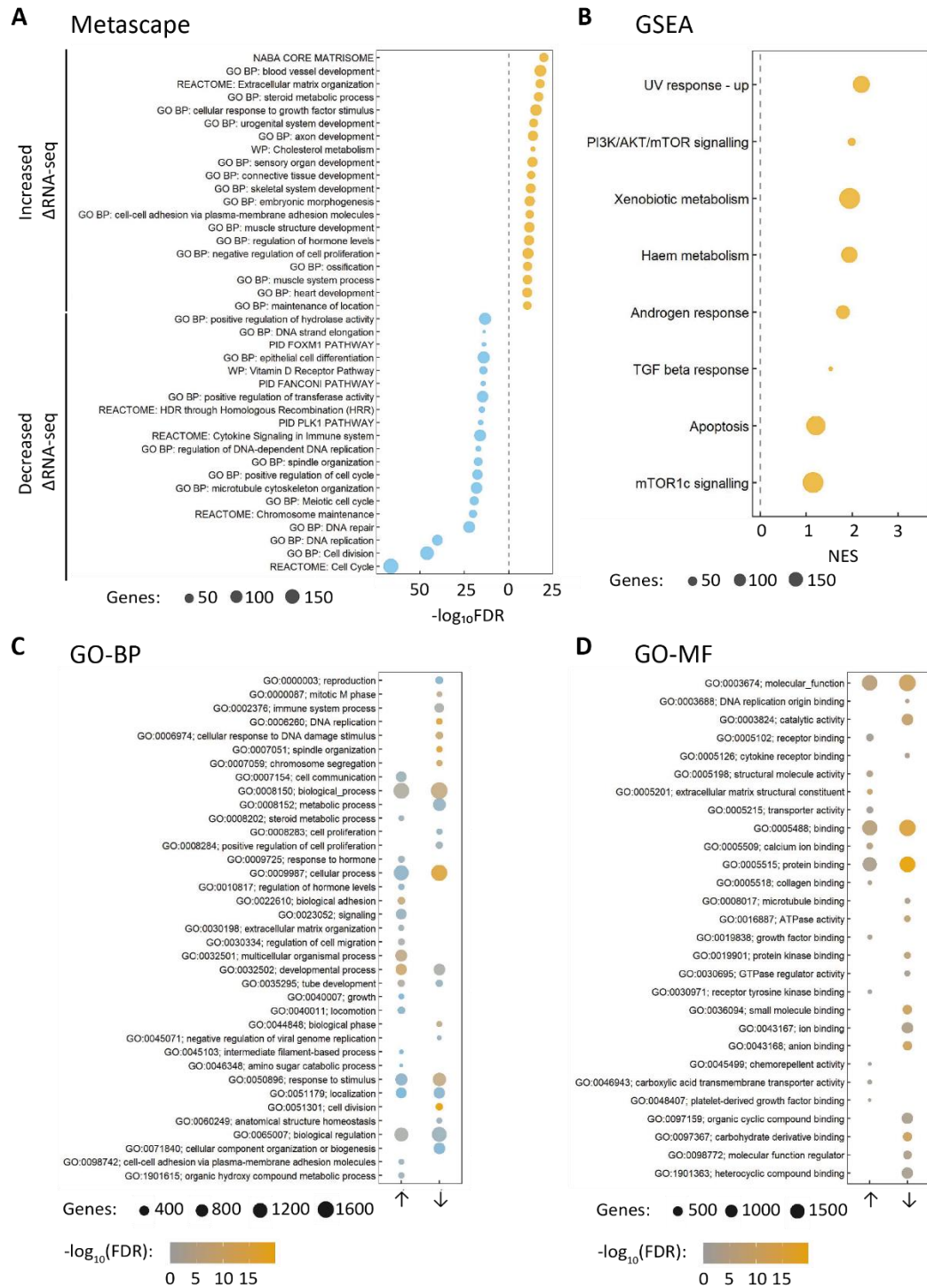


Figure 3.22. A panel figure illustrating functional enrichment of differentially expressed genes in NDBO (CP-A) cells following a 48 hour period of starvation. Enrichment is shown for genes for which \log_2 fold change (FC) >1.5 and adjusted $p < 0.05$ analysed following RNA-seq analysis undertaken in biological triplicate. Functional enrichment by **(A)** Metascape and **(B)** Gene Set Enrichment Analysis (GSEA) for differentially expressed genes (DEGs) significantly up- and down- regulated following 48 hours of serum-starvation. **(C,D)** Over-represented gene ontology (GO) biological process (BP; **C**) and molecular function (MF; **D**) terms for DEGs that were significantly upregulated (up-arrow) or downregulated (down arrow) after 48 hours of serum-starvation. In all plots, the size of the bubble reflects the number of DEGs contributing to the enriched term. FDR: false discovery rate.

3.4.4.5. The upstream determinants of genes differentially expressed in response to serum-starvation

As in **3.4.4.3.**, a combination of computational analyses and ATAC-seq were used to identify potential pathways through which genes were differentially regulated in response to a 48-hour period of serum-starvation (**Fig. 3.23A**), as well as their potential upstream nuclear receptor (**Fig. 3.23B**) and transcription factor (**Fig. 3.23C,D**) drivers.

3.4.4.5.1. Increased activation of G₁ checkpoint, pro-developmental and pro-autophagy components, and decreased activation of pro-inflammatory proteins, is predicted to result in the differentially expressed genes seen in NDBO cells in response to serum-starvation

The signalling components predicted to mediate the DEG response seen after 48 hours of serum-starvation correlated with many of the processes outlined in **3.4.4.2.** This includes predicted activation of a number of genes implicated in autophagy (*IRGM*, *AMPK*, *PRKAA*, *TGF β* , *TGFBR1*, *TGFBR3* and *NODAL*). It also includes a number of genes crucial to developmental processes, such as the de-glycosylating enzyme encoding *NGLY1* gene, the dual specificity tyrosine phosphorylation-regulated kinase-encoding *DYRK1A* gene, the Hippo signalling pathway component-encoding *LATS1* gene and the RTK Ephrin-A2 encoding *EFNA2* gene. There is in addition predicted activation of components of the G₁ cell cycle checkpoint, including *Rb* and *CDKN1A*. In contrast, a large number of inflammatory signalling components have predicted reductions in activity, including the RelA component of NF- κ B, as well as IFN, TNF, IFNL1, IFN γ and IL1 β .

3.4.4.5.2. The serum-starvation regulome in NDBO features changes in multiple developmental and differentiative transcription factors

Overall, 3052 open and 4672 closed differential chromatin peaks were identified via ATAC-seq. As with the day 1 response to acidic bile salts, increased binding of the KLF5 (36.5% of targets, 15.1% of background, $p=1 \times 10^{-169}$) transcription factor was determined by ATAC-seq. Similarly, there is involvement of the TEAD transcription factors in the response to both acidic bile salts and serum-starvation, but for the latter, TEAD1 (10.4% of targets, 3.0% of background, $p=1 \times 10^{-73}$) was identified as a consensus binder to open chromatin rather than TEAD3. Beyond these similarities, many of the sites of open chromatin in response to serum-starvation had been closed in response to acidic bile salt exposure. This includes sites for the binding of AP-1 (represented by its JunB constituent; 11.4% of targets,

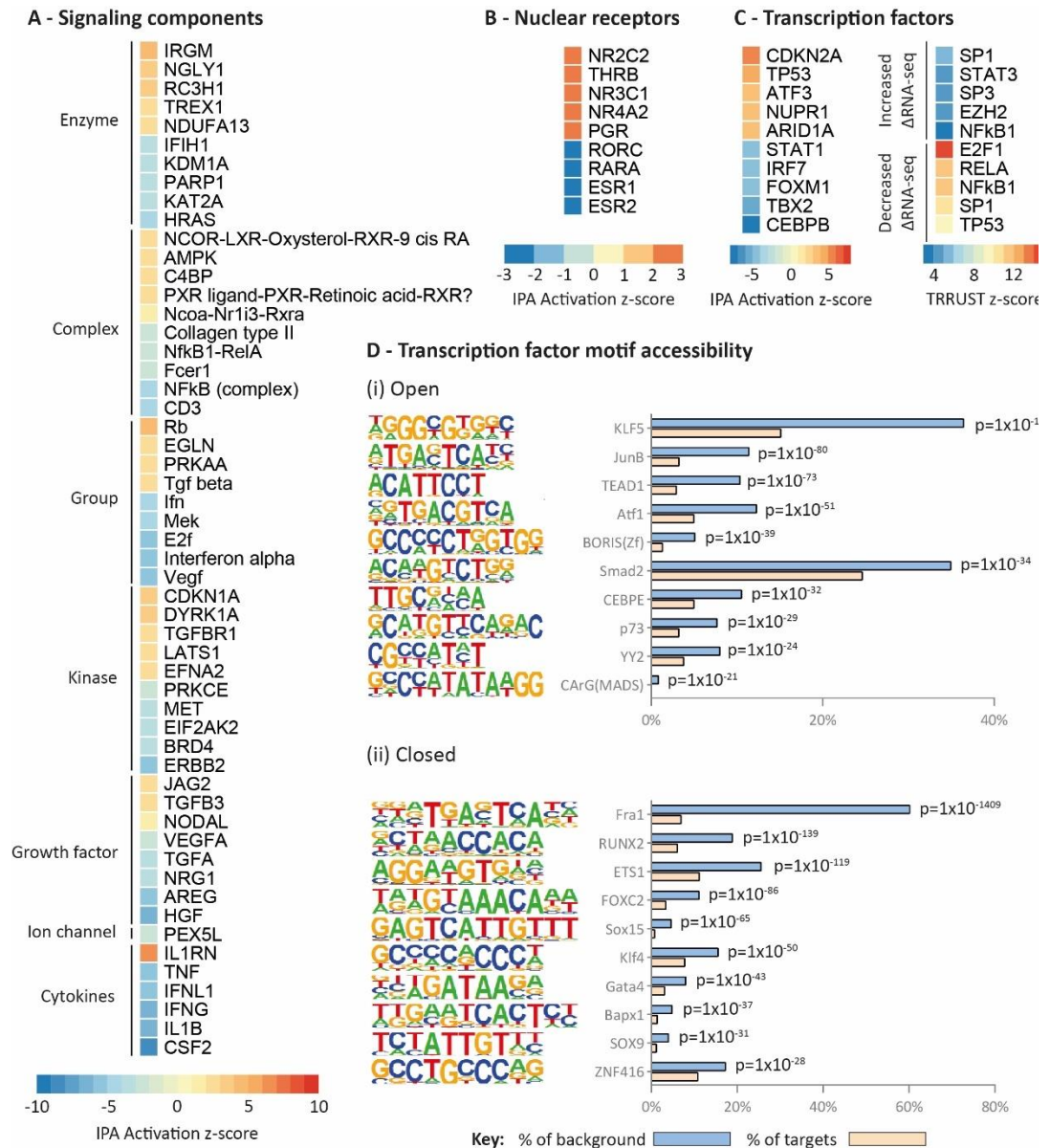


Figure 3.23. A panel figure illustrating transcriptional regulators in NDBO (CP-A) cells after a 48 hour period of serum-starvation. (A-C) Heatmaps demonstrating putative upstream (A) signaling components, (B) nuclear receptors and (C) transcription factors identified from genes for which \log_2 fold change (FC) demonstrated a >1.5 increase or decrease, with adjusted $p < 0.05$, as identified through RNA-seq analysis undertaken in biological triplicate. Potential regulators were identified by (A-C) Ingenuity Pathway Analysis (IPA) and (C) Transcriptional Regulatory Relationships Unraveled by Sentence-based Text mining (TRRUST) analysis. (D,E) Bar charts demonstrating percentage targets and percentage background for *de novo* identified motifs at regions of increased and decreased chromatin accessibility at days 1 and 2 following acidic bile salt exposure, as identified by ATAC-seq. *De novo*-identified motifs are shown, as are the transcription factors ‘called’ to bin to them, the motif match score and the attributed significance (p-value).

3.3% of background, $p=1 \times 10^{-80}$), p73 (7.7% of targets, 3.2% of background, $p=1 \times 10^{-29}$) and CEBP (10.6% of targets, 5% of background, $p=1 \times 10^{-32}$) transcription factors. There is in addition binding of Atf1 ($p=1 \times 10^{-51}$) and Smad2 ($p=1 \times 10^{-34}$).

In keeping with the findings outlined in 3.4.4.4.2. and 3.4.4.5.1., consensus chromatin binding sites for a number of transcription factors implicated in differentiative processes

were closed. This includes SOX15 (4.66% of targets, 0.80% of background, $p=1 \times 10^{-65}$), GATA4 (8.1% of targets, 3.1% of background, $p=1 \times 10^{-43}$), SOX9 (4.1% of targets, 1.2% of background, $p=1 \times 10^{-31}$), RUNX2 (18.9% of targets, 6.1% of background, $p=1 \times 10^{-139}$) and FOXC2 (11.2% of targets, 3.4% of background, $p=1 \times 10^{-86}$). Interestingly, the binding site for Fra1, which was open in response to acidic bile salts, was closed following serum-starvation (60.2% of targets, 7.0% of background, $p=1 \times 10^{-1409}$).

3.4.4.6. Expression of the KLF5 transcription factor is greatest in early BO

The KLF5 transcription factor is implicated in the development of OAC and featured as a mediator of both acidic bile salt and serum-starvation stressors used in this work.(490) Given this, we sought to confirm KLF5 expression within NDBO (CP-A) cells and to compare this with expression seen in NSE (Het-1A) and HGD (CP-B) cells. As shown in **Fig. 3.24A** and **Fig. 3.24B.**, protein expression of KLF5 was highest in NDBO (CP-A) cells but was also present in HGD (CP-B). Interestingly, whilst the same pattern of expression from early to later BO or OAC was seen in patient samples (**Fig. 3.24C**), these also demonstrated significantly greater KLF5 expression in NSE than in BO.

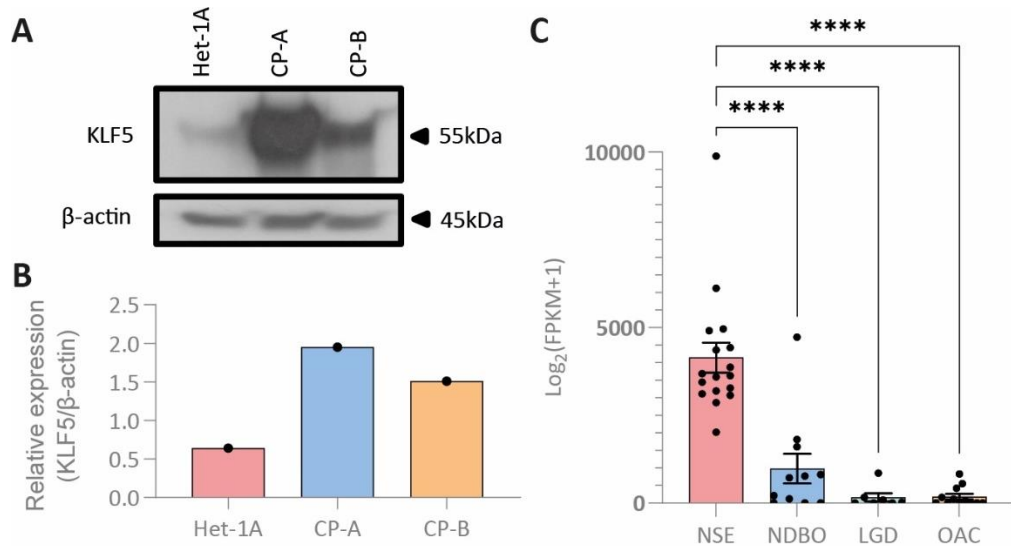


Figure 3.24. Expression of the KLF5 transcription factor (A,B) across cell lines resembling NSE, BO and OAC, and (C) patient samples. (A,B) A representative immunoblot is presented in (A) and expression, normalised to the β -actin loading control, is summarised by densitometry in (B). $n=1$. **(C)** The relative mRNA expression of each marker was compared between samples from NSE ($n=17$), NDBO ($n=11$), LGD ($n=7$) and OAC ($n=12$) in a prior analysis performed by *Maag et al.*(486). Data are presented as mean \pm SEM. Statistical analyses were undertaken using a one-way ANOVA with post-hoc Tukey correction for multiple significance testing. Comparisons that reached pre-defined significance thresholds are highlighted, and are distinguished as follows: **** $p \leq 0.0001$.

3.5. Discussion

3.5.1. Validation of an *in vitro* model of BO

The dysplastic progression of BO and subsequent development of OAC is strongly linked to exposure to the contents of gastric refluxate.(168,169) Foremost amongst these are acid and bile salts, which due to the use of therapeutics such as PPI and H₂RA therapy, may be at a neutral or acidic pH.(166,167,172) Even in the context of persistent exposure to refluxate, progression of BO to OAC can take many years and other than the loss of *TP53* expression, there is no effective biomarker to predict worsening dysplasia.(66,237) Further, direct exposure to refluxate generally occurs for less than 20% of each day, with cells otherwise existing in phenotypic states of proliferation, quiescence, and autophagy, as well as various stages of EMT.(462,477,479–483) Combined, these facets complicate evaluation of the mechanistic contribution made by acid, bile salts and other BO microenvironmental stressors to the development of a more dysplastic phenotype. Nevertheless, it does now appear clear that dysplastic progression in BO occurs predominantly due to a breakdown in gene-regulatory control, rather than for instance the development of specific driving mutations.(258) As such, an enhanced understanding of the role of microenvironmental stressors in modulating gene regulation at different stages of BO progression may provide an opportunity to better comprehend the pathways through which they modulate the BO dysplastic phenotype and, in turn, oncogenicity.

In order to validate the use of an *in vitro* model to explore the impact of these microenvironmental influences on the BO dysplastic phenotype, we evaluated the extent to which a cell line model of BO recapitulated key features of early and late BO. Through analysis of the protein expression of E-cadherin, we identified that the three cell lines representing HGD appear to have undergone a process of EMT. This would be expected on the basis of the current literature, which has underlined that a process of EMT accompanies dysplastic BO progression.(358,488) It is also supported by morphological analysis of the CP-B and CP-D cell lines, which exhibit a mesenchymal or fibroblastic-like bipolar appearance. The more epithelial or polygonal cellular appearance of CP-C cells is less convincing of EMT, but given the relatively lower E-cadherin expression in this cell line it is likely to simply represent an earlier stage in mesenchymal transition, or even that these three cell lines represent at least two different cells of origin from the BO metaplastic mosaic.(23) Concerningly, the NSE Het-1A cell line demonstrated almost a total loss of E-cadherin expression when compared with NDBO CP-A cells. E-cadherin is an epithelial marker and its loss from a squamous epithelial cell line is therefore unexpected.

Given that intestinal and squamous markers of differentiation are frequently used to evaluate for dysplastic progression in response to microenvironmental stressors, we then sought to evaluate the extent to which they demarcate NSE, NDBO and grades of increasing oncogenesis in both the cell line model and patient samples. Broadly, intestinal markers discriminated between NSE and BO in patient samples and the studied cell lines. However, squamous markers were unexpectedly also higher in the NDBO CP-A cell line than in the squamous Het-1A cell line. Further, whilst both studied squamous markers (*KRT4*, *TP63*) discriminated between NDBO CP-A and HGD CP-B cells, they poorly discriminated between NDBO and both LGD and OAC in patient samples. In contrast, no consistent increase in intestinal markers of differentiation was seen between NDBO and dysplasia or OAC in both the cell lines and patient samples.

Together, these findings suggest that the use of intestinal markers as a surrogate marker of dysplastic progression is flawed. They also identify a concerning lack of squamous features in the Het-1A cell line which, when coupled with its surprisingly low expression of the epithelial E-cadherin protein, raises doubts about the extent to which it resembles NSE. Despite the widespread use of this cell line to represent NSE within the literature, this finding supports similar concerns raised by *Underwood et al.* in 2010.(491) In this study, the authors grew Het-1A cells in organotypic culture with normal fibroblasts and identified that the Het-1A cells were highly proliferative but lacked the epithelial E-cadherin or casein kinase 5/6 epithelial markers, but did express the mesenchymal markers vimentin and N-cadherin. These findings, coupled with those presented here, suggest that the Het-1A cell line would be more accurately regarded to represent a dysplastic squamous epithelial cell type. However, despite its apparent dysplastic features, this cell line will continue to be labelled as the NSE-like cell line within this work, albeit with an exploration of appropriate caveats relating to its dysplastic phenotype in instances where it is used as a comparator cell for BO analyses.

Quite apart from their inconsistent relationship with BO progression in these data, it is increasingly clear that cell types other than SIM are likely to undergo dysplastic progression; either as well as or instead of SIM.(30–35) It is then of interest that the HGD CP-B cell line consistently demonstrated lower expression of a number of intestinal differentiation markers than the NDBO cell line. Given this and its bipolar morphology, it is possible that CP-B cells represent a non-SIM lesion, whereas the more polygonal appearance of CP-C cells would be more in keeping with a SIM-like phenotype.

It is nevertheless clear that an analysis of gene regulatory processes would be a more reliable and informative approach for determining the impact of microenvironmental stressors on BO cellular phenotype and propensity to undergo dysplastic progression. We sought to explore these processes in three states; (i) under basal, unstressed and pro-proliferative conditions, (ii) under serum-starved, quiescent pro-autophagic conditions, and (iii) following exposure to the contents of gastric refluxate.

The first of these conditions is likely to be promoted *in vivo* by, amongst other factors, growth factors contained within swallowed saliva.(196,222) It is however noteworthy that key growth factors such as salivary EGF are known to decrease in BO, and that increased metabolic demand and vascular remodelling can result in a relative nutrient deprivation that is akin to serum-starvation, resulting in substantial cellular populations exhibit phenotypic features of autophagy and quiescence.(175,196,209,210,222) The third of these conditions has already been extensively explored within the literature, as highlighted within **Table 3.1**. However, many of the acidic and bile salt exposures used in existing research are supra-physiological, with treatment for as long as 24 hours used to model reflux pulses that *in vivo* last less than ten minutes. Bile salt concentrations are also commonly used at levels that exceed those identified in reflux, and there has been no previous systematic appraisal of the relative contribution to gene regulatory control of acid and bile salts; alone and in combination.

In many of these previous analyses it is also unclear what impact prolonged exposure to stressors such as acid has on viability, and therefore whether the results of these investigations are valid. Complicating this further, previous analyses have identified both pro-proliferative and anti-proliferative, and pro-apoptotic and anti-apoptotic, roles for acid and bile salts.(187–189) Given this, we sought to systematically appraise the relative impact of bile salts at neutral and acidic pH, bile salts and serum-starvation on NSE and BO cellular behaviour.

In summary, these demonstrate that across the studied cell lines, cellular number remains relatively stable, if not a little increased in NSE Het-1A and NDBO cell lines, following exposure to bile salts at neutral and acidic pH, and acid alone. There is however evidence for relatively early cellular death (within two hours) following acidic bile salt exposure, particularly within the NSE and NDBO cell lines. These, therefore, appear particularly susceptible to death from acidic bile salts, but equally able to mount a proliferative recovery response. Given that cell death occurs relatively rapidly, it is possible that it is mediated by

a process other than apoptosis, which would ordinarily be expected to take in excess of 3-4 hours.

These data therefore support the previously reported pro-proliferative and pro-apoptotic effects of acidic bile salts.(187–189) However, a particular strength of the approach taken here is that through assessing final cell number alongside cell death, it is possible to demonstrate that both processes occur simultaneously. It is additionally reassuring, from the perspective of confirming post-acidic bile salt cellular viability, that NSE Het-1A, NDBO CP-A and HGD CP-B cells in this study could be passaged over 12 weeks using the same daily exposure to acidic bile salts. It is likely that the combination of these two processes demonstrates both the cytotoxicity of acidic bile salts and an immediate, compensatory, wound-healing response.

A different pattern in viability, death and metabolism was seen following 48 hours of serum-starvation. As would be expected given the withdrawal of growth factor supplementation, which is known to induce quiescence, cellular number was significantly lower in the NSE Het-1A, the NDBO CP-A and the HGD CP-B cell lines.(492) A relatively lower cell number was also seen for the HGD CP-C and CP-D cell lines following starvation, albeit non-significantly. Further evidence for the cells entering a quiescent phase is provided by both the concomitant significant fall in metabolic activity across all studied cell lines, and the stable or minor change seen in viability. It is unclear why there is seemingly a less dramatic reduction in cell number in CP-C and CP-D cells, but given that these both do exhibit a reduction in metabolic activity on serum-starvation, the lesser difference in cell number to control populations may simply reflect a less proliferative basal phenotype for these cell lines.

Combined, these data support the development of a less-proliferative and metabolically-less active state in response to serum-starvation across cell lines demonstrated to reflect at least two distinct stages of BO progression, and both proliferative and rapid cell death phenotypes following exposure to gastric refluxate contents in the same cell lines. Having validated this model, we sought to establish the relative impact on cellular behaviour of these stressors. Interestingly, there were few significant impacts from either stressor on markers of squamous and intestinal markers of differentiation, even when cells were exposed to acidic bile salts for up to twelve weeks. This contrasts with some of the existing literature that does show substantial fold-change increases in intestinal markers of differentiation in response to bile salts, acid and acidic bile salts. However, these follow

either higher concentrations or more prolonged exposure, indicating that supraphysiological levels of bile salt and acid stressors simply bias towards a more differentiative phenotype.

3.5.2. The impact of microenvironmental stressors on gene regulatory control

Given this and the earlier evidence suggesting that these markers poorly discriminate between stages of BO, we instead sought to systematically appraise the impact of these stressors on gene regulatory control as a means to understanding their potential impact on BO dysplastic progression. These analyses were undertaken using unbiased RNA-seq and ATAC-seq methods, both of which show considerable changes in response to both acidic bile salt and serum-starvation stress.

For acidic bile salt exposure, significant differential gene expression follows within 24 hours and persists, albeit to a lesser extent, to 48 hours from cellular treatment. One of the most significantly upregulated genes was *CFTR*, which was increased in expression at both day 1 and day 2 following acidic bile salt exposure. This ATP-binding cassette is responsible for the transport of chloride ions across epithelial cell membranes, as well as both the secretion of bicarbonate and the inhibition of sodium transport. Mutations of *CFTR* result in the autosomal recessive disease, cystic fibrosis, which amongst a number of multi-system effects results in frequent GORD.⁽⁴⁹³⁾ Interestingly, a locus within *CFTR* (rs17451754) was recently identified to confer a significant risk of the development of OAC through a meta-analysis of genome wide association studies (GWAS) undertaken by *Gharahkani et al.* on behalf of the Barrett's and Esophageal Adenocarcinoma Consortium (BEACON), the Esophageal Adenocarcinoma Consortium (EAGLE) and the Wellcome Trust Case Control Consortium 2 (WTCCC2).⁽⁴⁹⁴⁾ This and eight other terms identified by the authors enriched for muscle-cell differentiation, which has been linked by *Gharahkani* and others to the LOS relaxation that is known to characterise patients with GORD.^(494,495) However, the increase in *CFTR* expression in response to acidic bile salts shown here indicates a potentially more direct role for this gene in mediating the BO cellular response to refluxate. This may relate to its function secreting bicarbonate, which feasibly provides a protective mechanism for oesophageal cells against the presence of luminal acid that patients with relatively less *CFTR* activity, either as a consequence of a polymorphism or through the mutations implicated in the development of cystic fibrosis, would not benefit from. This is supported by work from *Woodley et al*, which identified reduced chemical clearance of acid reflux in children with cystic fibrosis.⁽⁴⁹⁶⁾ It is however noteworthy that genes upregulated at day 2

following acidic bile salt exposure functionally enriched for 'GO 0045932: negative regulation of muscle contraction'.

A second disease process enriched within the dataset is lung fibrosis, the most common clinical form of which is idiopathic pulmonary fibrosis (IPF). IPF is characterised by frequent but often silent GORD for which a majority of patients are managed with PPIs. It has been suggested that the micro-aspiration of gastric material in GORD might result in IPF.(497) The data shown here, and the enrichment of this term, would appear to support this notion and point to the importance of acid suppression in patients with IPF. It also potentially provides new avenues for research; particularly with respect to understanding why lung epithelia becomes fibrotic in response to gastric refluxate whereas BO tissue can undergo malignant change.

Interestingly, the two genes that demonstrated the largest significant increase in expression at day 2 following acidic bile salt exposure, namely *CFTR* and *VNN1*, have both previously been identified to be uniformly present in BO but not present in OAC.(498) Given that these are therefore late acidic bile salt-responsive genes, this finding cautions against the current practice of using OAC cells to model BO responses to gastric refluxate. Amongst other genes that demonstrated the largest fold increase in expression at day 1, *HSPA6* is known to have prognostic value in oesophageal cancer.(499)

Overall, these and other genes for which expression is upregulated in response to acidic bile salts enrich for pro-inflammatory, pro-migratory and RTK-derived signalling processes. This includes enrichment of genes involved in EMT, which has already been extensively described as a feature of dysplastic progression and was noted to be enriched for in the loci identified by *Gharakani et al.*(494) These data are also in keeping with previous *in vitro* evidence for a role for VEGFR2 signalling – enriched in the dataset explored here – in driving EMT in response to acidic bile salts in the NDBO BAR-T cell line.(480)

The enrichment of predominantly pro-inflammatory T_h1 responses is in keeping with the known contribution of inflammation to BO progression. It is however of interest that this develops directly within BO cells, independent of a stromal contribution. This potentially provides an explanation for the BO inflammatory gradient previously reported by *Fitzgerald et al.*(174) This relates to the presence of T_h1 responses in the proximal oesophagus and T_h2 responses in the distal oesophagus. The squamocolumnar junction will be most likely to experience pulsatile rather than continuous exposure to acidic bile salts and it therefore follows that T_h1 responses may result from the pulsatile impact of acid on the BO epithelium.

Importantly, a number of the pathways enriched in response to acidic bile salts have been associated with the dysplastic progression of BO, including TNF α , IL-2 and IL-18.(174,500)

It is otherwise noteworthy that a number of genes essential to mitochondrial function (*PCK2*, *ALDH1L2*, *SLC6A9*) are downregulated at 48-hours post-acidic bile salt exposure, with functional enrichment of terms relating to amino acid and oxo (keto)-acid metabolic processes. Mitochondrial instability and stress is a key feature of BO dysplastic progression.(501) This has previously been attributed to increased susceptibility to damage to mitochondrial DNA. The downregulation here of genes essential for mitochondrial function, and which would in particular help clear the ROS responsible for mitochondrial DNA damage, points to a maladaptive process in the NDBO cells. However, not all of the identified genetic changes are maladaptive. For instance, 'Apical junction upregulation' is conversely likely to be an adaptive response to acidic bile salt treatment, given the known importance of the AJC to the epithelial acid barrier.(120)

Beyond these terms, it is of interest that the p53 response was downregulated. This is a key tumour suppressor and its loss at the level of the genome is one of the few known biomarkers for BO progression. In the cell line model used here, for example, it is recognised that *TP53* is wild-type in NDBO CP-A cells but experiences LOH or mutation in the HGD CP-B, CP-C and CP-D cell lines. Its downregulation in response to acid suggests that even in wild-type cells, there is functional depression of a key molecule responsible for the repair of DNA damage. Importantly, as well as following the loss of p53, progression of BO is recognised to occur more frequently in males and has been linked to androgen excess. This is also known to be a poor prognostic factor in OAC. (502–504) Here, we show that acid upregulates an androgen response and downregulates an oestrogenic response, which would amplify any existing contribution from androgens to BO dysplastic progression.

Finally, the early dramatic effect on protein signalling caused by exposure to acidic bile salts is emphasised by the rapid up, and then down regulation of genes involved in the unfolded protein response, including *CHAC1*, *ASNS*, *ULBP1*. It is suggested that this response is led by RTKs, with significant enrichment of terms relating to EGFR, erbB2 and VEGFR2 signalling. However, the relative contribution of these and other potential upstream regulators to mediating the differential expression of genes shown here in response to acidic bile salts is unclear and requires further work.

Overall, these multiple enriched processes appear to be mediated, at least in part, by MAPK and PI3K/Akt signalling. This is in keeping with a RTK-derived response and occurs as part of

a signalling process that results in genetic change that occurs rapidly and is, for the most part, sustained for at least 48 hours. Given the sustenance of this signal, it would be of interest to identify the impact on gene regulation of repeat pulses of acidic bile salts over a period such as a day, which would be in keeping with the physiological setting.

Nevertheless, the transcription factors for which open consensus chromatin sequences were identified included a number that both sit downstream of RTK signalling and have been linked with either the progression of BO or its cellular response to the constituents of GORD. These include KLF5, which has recently been reported to activate a cell cycle signature during the progression from BO to OAC, in a process at least partly regulated by ErbB2.(490) Other examples of transcription factors already implicated in BO dysplastic progression include FOXM1, which is upregulated in OAC, and NF- κ B; the increased expression and activity of which during the NDBO – dysplasia – OAC sequence has been extensively described, as has its activation through treatment with acid and bile salts.(153,396,413,505,506) Interestingly, binding sites for both the NF- κ B component, RelA, and FOXM1 are present at a susceptibility locus for OAC and BO (SNP rs1325190 ($p=3 \times 10^{-5}$), OR 1.07, that has been identified by two GWAS.(507,508) The TGF β -regulated RUNX2 transcription factor has also been associated with BO dysplastic progression, with a specific role in EMT highlighted that would be in keeping with the EMT terms enriched in the RNA-seq analysis outlined here.(509) The Fra1 transcription factor, which forms part of the AP1 transcription factor complex implicated in the development of OAC, has in addition been previously linked to activation following DCA treatment.(318) TFAP2C is also highlighted by the ATAC-seq analyses but is generally considered to be downregulated during BO progression, though it does form part of a chromatin region that is differentially methylated in oesophageal tissues.(266,510)

Open chromatin regions were also recognised as consensus sites for a number of transcription factors that have not previously been directly implicated in BO progression. This includes ETS related gene (ERG), which forms part of a family recognised to regulate Wnt signalling in cancers such as prostate cancer.(511) This is pertinent given that Wnt signalling has been linked to BO progression and that its related family member, SAM pointed domain-containing ETS transcription factor (Spdef), has been tentatively linked with the development of intestinal epithelium and BO progression.(156,512) The ZNF416 transcription factor is also highlighted and has recently been reported to be a regulator of fibroblast mechano-activation in extra-oesophageal tissue, potentially suggesting a role for it in the BO EMT transition.(513)

Alongside these open chromatin sequences, a smaller number of chromatin sequences were closed at both of the analysed time points. These include a consensus site for p73, which was closed at day 1. As outlined in **1.1.2.5.9.**, p73 is a p53 homologue that increases in expression and activity in response to bile salts and is thought to protect against DNA damage. Its downregulation in response to acidic bile salts is therefore surprising.(242,424) Other transcription factors for which chromatin closed include p53, which is in keeping with the downregulated p53 response outlined from the RNA-seq data, and Retinoic Acid-Related Orphan Receptor A (RORA). This is a putative tumour suppressor gene that has previously been reported to be lost during BO progression but induced by DCA.(514) Its downregulation in response to acidic bile salts here is, again, surprising but is in keeping with the reduced retinoic acid response outlined from the RNA-seq data.

In comparison to the acidic bile salt response, a similar number of genes were differentially regulated following serum-starvation, yet the specific DEGs and the processes that serum-starvation contributed significantly differed to those of acidic bile salts. Amongst the most significantly upregulated genes was *FGF1*, which encodes for the FGFR ligand fibroblast growth factor 1 (FGF1). This has previously been reported to be sequentially upregulated in the NDBO-dysplasia-OAC sequence, though its specific function in this context is unclear.(515,516) Together, these genes contribute to an enrichment for developmental signalling terms and de-differentiative change, which is also evident from the reduction in intestinal differentiation marker expression shown in **Fig. 31.3**. This at least in part models some of the changes known to occur during BO progression, not least given the predominance of developmental signalling pathways that are implicated in both BO development and its dysplastic progression. Unsurprisingly, this change was also accompanied by enrichment for terms indicating a reduction in cell cycle progression, which is a well-known consequence of serum-starvation.

Most pertinently, however, serum-starvation resulted in enhanced remodelling of the ECM and, as indicated by enrichment of mTOR and TGF β signalling, cellular autophagy. Levels of autophagy are known to be increased in BO and have been linked with promoting survival from acidic bile salts.(483) TGF β signalling is also recognised to be dysregulated in BO.(206,336,337,464) Further, ECM remodelling is known to influence BO progression. (204,209,211–215) Importantly, It is not clear on the basis of the results presented here that acidic bile salts directly lead to autophagy; the contributing genes for which were not enriched at day 1 or day 2 following acidic bile salt exposure. In previous reports, autophagy following acidic bile salt exposure has, however, been associated with a more sustained

exposure to ROS. Autophagy has also been linked with an increase in stem-like cells, which is in keeping with the terms enriched for here.(517) The development of autophagy via starvation may therefore provide a model system that enables for the assessment of upstream mediators of the autophagy phenotype that results from sustained stress in BO. Surprisingly, but as emphasised by the significant upregulation of FGF1, growth factor and RTK signalling appears to be an important candidate. However, and in contrast to the acidic bile salt response, immune pathways appear to be downregulated in response to starvation, thereby also providing a model system that allows for the identification of non-immune contributors to BO progression.

Reflecting the different cellular processes induced by serum-starvation when compared with acidic bile salt treatment, a number of transcription factors for which consensus sites were contained within closed chromatin following acidic bile salt treatment were instead matched to open consensus sites in response to serum-starvation. These include p73, the Jun component of AP-1 and CEBP, which has not previously been associated with BO progression but is known to be stress-responsive and is linked with invasive disease in CRC.(518) Conversely, the consensus chromatin site for ZNF416 binding, which was open in response to acidic bile salts, is closed in response to serum-starvation.

An exception to these reversals in chromatin binding is KLF5, which appears to be a more universal mediator of the BO stress-response. In previous reports outlining the role of KLF5 in activating a cell cycle signature during the progression from BO to OAC, its expression was reported to increase during the NSE – dysplasia – OAC sequence.(490) We identified the corollary, with higher protein expression of KLF5 in NDBO CP-A cells, and higher mRNA expression in NDBO patient samples from *Maag et al*, than in their dysplastic equivalents.(486) It is unclear why this discrepancy may exist, but it nevertheless underpins an important role for KLF5 in mediating gene responses in early BO.

3.5.3. Strengths & limitations

This work has a number of strengths and limitations, some of which are addressed in further work in **Chapters 4** and **5**. Amongst its strengths, the experimental approach here systematically appraises a cell line model for BO progression and details key phenotypic aspects that vary between the cells. These are, however, relatively limited in scope, and a full evaluation of this model would include a broader panel of differentiation markers and assessment of comparative phenotypic features such as invasion and migration. It is also

important to note that the assessments of morphology were not systematic and are subject to bias. Nevertheless, all conditions of microenvironmental stress used in this work have been extensively validated to not deleteriously impact on viability, which is a significant reassurance when interpreting their impact on cellular processes. Further, and as outlined in **3.5.1.**, the NSE Het-1A cell appears to more closely resemble a dysplastic squamous cell. This is a limitation from the perspective of concluding on the behaviour of NSE cells in response to conditions of serum-starvation. The Het-1A cell line nevertheless still affords a control vehicle against which the BO cellular response can be compared in order to determine whether it is a ubiquitous or a BO specific cellular response.

Beyond analysis of the cell line model itself, a particular strength of this work is the considerable effort undertaken to define a near-physiological acidic bile salt pulse that would enable for comparison to existing literature. This, and the ability to separately treat cells with the same molar ratio of bile salts but at neutral pH, or acidic pH alone, is a particular positive in terms of allowing for determination of the relative impact on NSE and BO cells of acidic bile salts and its individual acid and bile salt constituents. However, whilst these were compared for analyses of cellular phenotype, their impact on the cellular transcriptome and regulome has not been directly compared due to the considerable resources this would require. An alternative approach to delineating the relative impact of bile salts at neutral and acidic pH, and acid alone, is outlined and evaluated in **Chapter 4.**

This work also benefits from the use of unbiased RNA-seq and ATAC-seq approaches to study the impact of stressors. These are comprehensively analysed and summarised with orthogonal enrichment processes such that multiple databases have contributed to the interpretation of the processes resulting from application of the microenvironmental stressors. Further, the use of ATAC-seq alongside RNA-seq allows for results from the two analyses to be integrated, and for the final component of signalling processes resulting from microenvironmental stress to be extensively explored. The use of just one control sample for ATAC-seq analyses, which followed experimental failure, is however a considerable weakness and limits both the extent of the analyses undertaken with ATAC-seq, and our ability to satisfactorily conclude on these. It is in addition important to note that the suggested binding partners for open chromatin sequences are based on computational analysis and need to be validated using a process such as chromatin immunoprecipitation.

Finally, the relative contribution of the microenvironmental stress-responsive DEGs to dysplastic progression remains unclear from these data, though some aspects can be

extrapolated from the literature. These require exploration within a larger dataset, such as that cultivated by *Maag et al.* (as shown in **Chapter 5**) and such as that held by OCCAMS.(486) This work will be pursued but is beyond the scope of this thesis. It is also apparent that neither RNA-seq or ATAC-seq analyses are able to indicate the precise upstream pathways mediating the response to acidic bile salts and inducing transcription factor activity and differential gene expression. These pathways will be explored in more detail in **Chapter 4**.

3.6. Conclusions & further work

Taken together, the work outlined in this chapter has validated the NDBO CP-A and HGD CP-B, CP-C and CP-D cell lines as representing distinct stages of BO progression. The latter cell lines are in particular characterised by having entered EMT, though the CP-C cell lines are notably morphologically distinct from CP-B and CP-D cells. The data presented here have however also highlighted that the Het-1A cell line, which is reported to represent NSE, more closely resembles a dysplastic squamous cell. Through unbiased RNA-seq and ATAC-seq analyses using the NDBO CP-A cell line, the early BO response to acidic bile salt and serum-starvation stressors was extensively characterised. Acidic bile salt treatment results in a pro-inflammatory T_H1 -like, pro-EMT genetic response that is mediated by a number of transcription factors implicated in BO progression, including NF- κ B, AP1 and FOXM1. In contrast, serum-starvation results in an autophagy-enriched gene response characterised by mTOR and TGF β activation, which is mediated by a number of transcription factors for which consensus chromatin sequences were identified to be closed in response to acidic bile salts; including p73, Jun and CEBP. Nevertheless, RTK signalling is enriched within the gene response to both conditions, as is the transcription factor KLF5, which is known to sit downstream of RTK-derived signalling pathways.

It is, however, unclear on the basis of these data which pathways directly respond to the two cellular stressors outlined here. The relative contribution of the constituents of acidic bile salts is also unclear. These aspects are addressed in **Chapter 4**, in which the pathways mediating the response to bile salts at acidic and neutral pH, and acid alone, are delineated for NSE Het-1A, NDBO CP-A and HGD CP-B cell lines. In further work outlined in **Chapter 5**, the relative contribution of RTKs to the cellular response to both acidic bile salts and serum-starvation, and therefore aspects such as the pro-inflammatory, pro-EMT and pro-autophagy phenotypes respectively outlined here, is undertaken.

Chapter 4

A Systemic Analysis of the Basal & Stress-Responsive Barrett's Oesophagus Kinome

4.1. Background

4.1.1. Overview

Protein phosphorylation is the most commonly observed post-translational modification in eukaryotic cells and provides for the rapid and reversible modulation of protein function.(519) The activity of between a third and up to 90% of the human proteome is regulated by the phosphorylation and dephosphorylation of thousands of target residues.(520–522) This is undertaken by as many as 535 distinct protein kinases that constitute the kinome and 189 phosphatases that reverse their action; together totalling around 3.5% of the human genome.(519,523,524)

Most kinases in eukaryotic cells catalyse the transfer of a γ -phosphate group from adenosine triphosphate (ATP) or guanosine triphosphate (GTP) to a hydroxyl moiety in serine (Ser), threonine (Thr) or tyrosine (Tyr) residues that form part of a target protein's structure.(520,521) This process is rapid and usually occurs as part of complex, highly-coordinated, non-linear signalling networks.(525) These provide the predominant mechanism through which cells can respond to both extracellular and intracellular signals in order to regulate diverse processes that impact on a cell's phenotype, including gene expression, proliferation and migration, motility and apoptosis.

It is, then, perhaps unsurprising that the deregulation or altered activity of kinase signalling networks is recognised to contribute to the development and progression of multiple malignancies.(526) In many instances, this follows an activating mutation of a key kinase node within a signalling network, such as the development of the BRAF^{V600E} mutation that

results in MAPK hyperactivity and that is heavily implicated in the development of melanoma, thyroid and colorectal cancers.(527) However, there is in addition evidence that signalling networks can propagate potentially deleterious responses to signals from the extracellular environment.(528–530) This includes in BO, where changes in the activity and expression of a number of kinases associate with dysplastic progression.(297)

4.1.2. The human kinome

Four hundred and seventy nine of the 535 protein kinases encoded by the human genome incorporate an eukaryotic protein kinase (ePK) domain.(519,531) These are subclassified into seven main families, as summarised in **Table 4.1**. The ePK domain is characterised by the presence of a small N-terminal and a larger C-terminal lobe. The latter aspect binds protein substrates and catalyses the addition of a phosphate group liberated from N-terminal bound ATP. The remaining 56 human protein kinases feature an atypical but nevertheless active protein kinase (aPK) domain.(531) Overall kinase activity is dependent on the expression and degradation of kinase-active proteins, as well as the regulation of kinases via their autoinhibition or phosphorylation, and through their interaction with regulatory proteins.

Fifty two pseudokinases, which lack catalytic machinery, are distributed across the various ePK and aPK groups.(531) Whilst these proteins cannot function as enzymes, their ability to act as scaffolds to which nucleotides can be bound enables them to operate as important molecular switches. A pertinent example is the RTK ErbB3, which can maintain MAPK signalling via interactions with proteins such as ErbB2.(525) Non-catalytic functions of proteins that do have enzymatic capacity have also been reported, including the ability for non-ligand bound RTKs with a cytoplasmic tail proline-rich motif to bind to Src Homology 3 (SH3) domains of intracellular kinases, resulting in their activation.(532,533)

Group	Characteristic	No. of kinases
TK	Phosphorylate Tyr residues.	66
AGC	Basophilic signalling kinases. Phosphorylate Ser/Thr residues in proximity to Lysine and Arginine.	61
CAMK	Mostly modulated by binding of Calcium/Calmodulin C-terminal to catalytic domain	66
GMGC	Includes cyclin-dependent kinases, MAPKs, glycogen synthase kinases	61
STE	Mostly upstream MAPK cascade members.	45
TKL	Similar to TKs but generally specific for Ser/Thr residues.	37
CK1	Dissimilar to other protein kinases.	11
Other	Divergent group that does not fit the above definitions.	81

Table 4.1. A summary of ePK groups. Note that a previously described RGC group has now been reclassified within the 'Other' grouping.(519)

4.1.3. The kinome in BO dysplastic progression

As highlighted in **1.1.2.5.**, the expression of a number of kinases significantly differs between NDBO and varying grades of dysplasia. In some instances, the phosphorylation within tissues of kinases or their target residues has been proposed as indicating higher levels of activity for specific pathways during BO dysplastic progression. These limited studies are complemented by a number of analyses assessing changes in the phosphorylation of kinases and their substrates in response to environmental cues such as acid or bile salt exposure. These are, however, almost exclusively directed towards the biased, static end-point analysis of components of 'linear' signalling pathways. Nevertheless, as is summarised in **Fig. 1.3.** they highlight a potential role in Barrett's pathogenesis for MAPK and PI3K signalling, in addition to a number of developmental and pro-inflammatory pathways. Transcriptomic analyses presented in **Chapter 3** of this thesis additionally implicate pSer/pThr signalling, MAPK activity and RTKs in particular in controlling gene expression in response to pulsatile exposure to acidic bile salts.

It is however noteworthy that – as summarised in **1.1.2.5.** - many of the historical *in vitro* experiments from which the above findings derive were undertaken using cell lines representing OAC or extra-oesophageal tissue, rather than NDBO, LGD or HGD. As has previously been outlined and is summarised in **Table 3.1.**, the exposures modelled also vary considerably meaning that there are a paucity of opportunities to directly compare not just the pathways provoked by specific microenvironmental stressors, but additionally the relative amplitude and chronicity of the signals they generate. One significant result of this is that the relative impact on cell signalling of bile salts at neutral versus acidic pH, and of acidic pH alone, remains unclear.(189,290,291,534)

Traditional approaches to studying protein phosphorylation, such as immunoblotting, provide only a static readout of protein phosphorylation in target molecules. Given the dynamic, complex signalling networks that dictate both physiological and pathological states in a cell, this is insufficient for providing a global assessment of differences in basal kinase activity between differing stages of BO and NSE, and for determining the impact of microenvironmental stressors on this activity. As such, these approaches are also generally insufficient for identifying upstream mediators of kinase activity and the pathways through which it is mediated. Instead, the kinomic study of multiple phosphorylation sites in tandem is an increasingly utilised approach through which a therapeutically-relevant understanding of the molecular mechanisms dictating cellular phenotype can be developed.(535)

4.2. Aims

In this work, high-throughput kinomics approaches will be used to characterise and compare the kinase activity profiles of NSE, NDBO and HGD. The relative impact of stressors common to the lower oesophageal microenvironment on the kinome at each of these disease stages will also be determined, as will the specific pathways through which kinase activity is transmitted and both the upstream regulators and downstream effectors of these networks.

4.3. Methods

4.3.1. Experimental outline

In **Chapter 3**, the transcriptomic and regulomic response of NDBO CP-A cells to a ten minute near-physiological pulse of acidic bile salts was characterised. This implicated a variety of signalling pathways in modulating the resultant differential gene expression. Amongst these, serine/threonine kinase (STK) signalling, MAPK activity and RTK activation featured prominently. Given this, we sought to evaluate protein tyrosine kinase (PTK) and STK phosphorylation in NDBO cells following acidic bile salt exposure. We additionally sought to determine whether similar signalling changes occur in NSE Het-1A and HGD CP-B cells, with the latter chosen from the three available HGD lines because of phenotypic features in keeping with more advanced EMT (as outlined in **Chapter 3**). Signalling was assessed using immunoblotting and, as outlined in **4.3.3.**, using a high-throughput kinome array.

Unless otherwise stated, reagents and plasticware were sourced as outlined in **2.2.** and **Appendix A**. Cell culture and immunoblotting were undertaken as respectively outlined in **2.3.** and **2.4.3.**, supported by **Appendix B**. Graphical representations of data were generated as outlined in **2.9.2.**

4.3.2. Cell treatments

4.3.2.1. Acid, bile salts and acidic bile salts

Cells under investigation were exposed to a ten minute pulse of acid (pH 4.0), bile salts (100µM equimolar mix) or acidified bile salts (100µM equimolar mix at pH 4.0) as outlined in **3.3.2.1.**

4.3.2.2. Hydrogen peroxide

In order to directly stimulate oxidative stress, Barrett's cells were exposed to 300µM hydrogen peroxide in serum-free KSM for a period of one hour. Media was then

removed and plates washed twice in ice-cold PBS prior to lysis for protein and RNA analyses (as outlined in 2.4.1. and 2.5.1. respectively), and subsequent analysis.

4.3.3. Protein kinase activity profiling

4.3.3.1. Overview

A summary of the experimental approach is provided in **Fig. 4.1**. Cells representing NSE (Het-1A), NDBO (CP-A) and HGD (CP-B) were exposed to a ten minute pulse of acidified media (pH 4.0) or a 100 μ M mix of bile salts at either acidic (pH 4.0) or neutral pH, as outlined previously in 3.3.2. The relative impact of these exposures on tyrosine, serine and threonine kinase activity was subsequently assessed using the commercially available PamChip[®] 4 peptide array and PamStation[®] 12 platform [PamGene International B.V.] Bioinformatics analyses were used to identify putative upstream regulators and downstream effectors of the response to the three exposures in each of the studied cell lines.

4.3.3.2. Principle

4.3.3.2.1. Outline

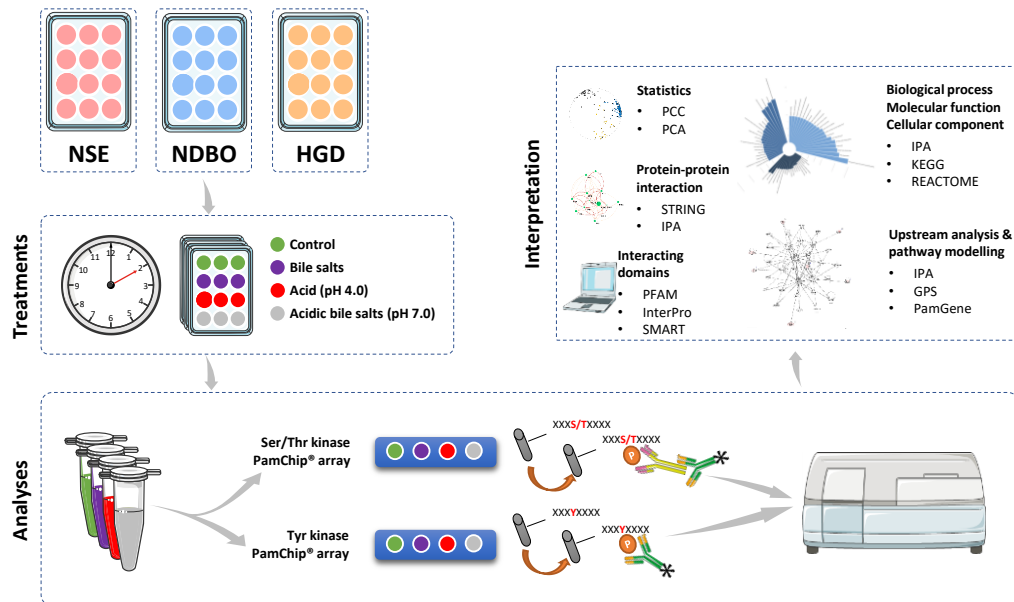


Figure 4.1. A summary of the experimental approach used to determine the impact of exposure to acidified media or bile salts at either neutral or acidic pH on kinase activity in cells representing NSE (Het-1A), NDBO (CP-A) or HGD (CP-B). Cells were lysed following treatment and both PTK and STK activity assayed using the PamStation[®]12 platform. Unlike assessments of STK signalling, which rely on the use of a secondary antibody to generate a signal on recognition of phosphorylated residues, PTK activity is determined using a single FITC-conjugated anti-pTyr antibody, enabling for kinetic profiling of PTK activity. Overall kinome profiles were compared between samples and cell lines. Computational analyses were also undertaken in order to identify putative upstream mediators and downstream effectors of activity.

Each PamChip® 4 module consists of four PTK or STK microarrays that are analysed in parallel using the PamStation® 12 integrated platform. A maximum of twelve microarrays, set over three PamChip® 4 modules, can be analysed at any one time. Each microarray consists of up to 200 oligopeptides immobilised on an aluminium oxide substrate. This is approximately 60µm thick and has a porous structure with long branched interconnected capillaries of around 200nm diameter. Each peptide corresponds to at least one upstream tyrosine or serine/threonine kinase.

Samples are dispensed on to each microarray, supplemented with ATP, and incubated at 30°C within the PamStation®12 platform. The sample is continuously mixed and pumped back and forth through the aluminium oxide substrate in a process controlled by proprietary PamGene® Evolve software. This minimises the reaction time and ensures a maximum distance between target and probe molecules of 100nm, thereby reducing the potential for diffusion to act as a rate-limiting factor in the array. Samples are washed using manufacturer-recommended buffers maintained at 37°C.

4.3.3.2.2. Detection of phosphorylated peptides

Kinase activity is determined by phosphorylation of peptides on the array by kinases within the sampled lysate. Phosphorylated peptides are probed for in real time using an antibody specific for pTyr or pSer/pThr. The pTyr (PTK) PamChip®4 microarray [#86402, PamGene®] consists of 196 immobilised peptides. These are detected in real-time using a fluorescein isothiocyanate (FITC)-conjugated anti-phosphotyrosine (pY20) antibody. The fluorescent signal generated by bound antibodies is quantified for each peptide spot every five minutes, which allows for the kinetic assessment of PTK kinase activity. The pSer/pThr (STK)



Figure 4.2. A typical fluorescent readout generated by FITC-conjugated antibodies on a PamChip®4 array.

Filter designation	Dye	Excitation wavelength (nm)	Emission wavelength (nm)
Filter 1	FITC	460-490	515-550
Filter 2	Cy3	530-560	575-645
Filter 3	Cy5	590-650	665-735

Table 4.2. Characteristics of filters used in the detection of phosphorylated peptides on the PamChip®4 array.

PamChip®4 microarray [#87102, PamGene®] consists of 144 immobilised peptides. Unlike the single antibody PTK array, detection of STK peptides involves a two-step reaction in which antibodies bind to phosphorylated peptides and are in turn bound by a FITC-conjugated secondary antibody. Consequently, kinetic data cannot be generated from STK analyses.

4.3.3.2.3. Signal detection

A typical fluorescent readout generated by bound FITC-conjugated antibodies on each PamChip®4 array is provided in **Fig. 4.2**. This is detected using a filtered excitatory light emitting diode (LED) and a 12-bit charge-coupled device (CCD) digital camera with a pixel resolution of 6.45 x 6.45µm. Filter characteristics are depicted in **Table 4.2**.

4.3.3.2.4. Oligopeptide sequences within the kinase array

A summary of oligopeptide sequences and their corresponding UniProt accession reference for the PTK and the STK PamChip®4 arrays is provided in **Appendix D** and **Appendix E**, respectively. A summary of the peptides contained within the chip and their function is provided in **Fig. 4.3**.

4.3.3.3. Experimental details

4.3.3.3.1. Lysate preparation

Each experimental condition in each cell line was assayed in biological triplicate with two replicates from cells at a passage number of between 5-10 and one replicate from cells at a passage number of 11-15. In order to preserve kinase activity, all lysates were prepared on ice in a temperature-controlled environment set at 4°C. Following treatment, cells were washed twice in ice-cold phosphate buffered saline (PBS) prior to the addition of M-PER™ Mammalian Extraction Buffer [#78503, TFS] with 1% Halt™ Phosphatase Inhibitor Cocktail [#78420, TFS] and 1% Halt™ EDTA-free Protease Inhibitor Cocktail [#78425, TFS]. After a 30 minute incubation rocking on ice, the lysate was transferred from the plate to a pre-cooled microcentrifuge tube by scraping and subsequently centrifuged at 16,000g for 15 minutes

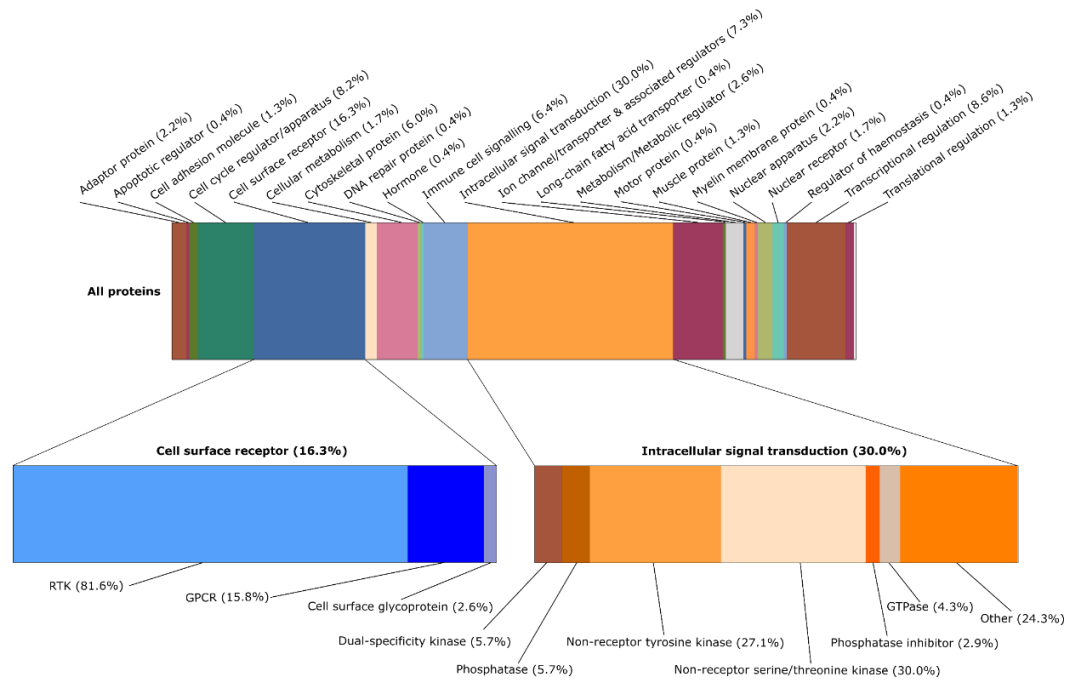


Figure 4.3. A manually curated summary of the biological function of peptides incorporated within the PTK and STK PamChip®4 microarrays.

at 4°C. The supernatant from each sample was divided into equal aliquots within pre-cooled microcentrifuge tubes, each of which was snap frozen using dry ice. Samples were stored at -80°C and underwent only one freeze-thaw cycle prior to kinase activity profiling.

4.3.3.3.2. Measurement of protein concentration

Protein concentration was determined using the detergent-compatible colorimetric Pierce™ BCA Protein Assay kit [#23225, TFS], as previously outlined in **2.4.2**. In order to preserve the accuracy of this assay, a standard curve was generated using M-PER™ Mammalian Extraction Buffer with 1% Halt™ Phosphatase Inhibitor Cocktail and 1% Halt™ EDTA-free Protease Inhibitor Cocktail.

4.3.3.3.3. PamChip®4 preparation

A representative PamChip® 4 sample layout used for each cell line and for both PTK and STK assays is shown in **Fig. 4.4**. All analyses for each cell line were run in parallel so that all three biological replicates for all four conditions were analysed in a single run using the PamStation®12. Lysates prepared from the same biological replicate were used for each PTK and STK analysis in order to permit a global analysis of kinase signalling from each sample. Each PTK and STK PamChip®4 module used in this experiment were generated in the same production batch. As per manufacturer instructions, each was equilibrated at room temperature for ten minutes prior to use. The PamChip®4 modules were subsequently

	PamChip® 4 Number 1	PamChip® 4 Number 2	PamChip® 4 Number 3
A1	Control R1	Control R2	Control R3
A2	Bile salt R1	Bile salt R2	Bile salt R3
A3	Acid R1	Acid R2	Acid R3
A4	Bile Acid R1	Bile Acid R2	Bile Acid R3

Figure 4.4. A representative overview of the PamChip®4 layout used for detection of kinase activity. Samples were run in biological triplicate using simultaneously probed arrays derived from the same batch in order to control for experimental variation. Rn: biological replicate number.

loaded into the PamStation® 12 and to each a 30µl 2% BSA blocking solution was added. PK wash buffer was prepared in a syringe through the addition of 300µl 10x ABL/PK buffer to 2700µl ultrapure water and loaded in to the PamStation® 12. PamChip®4 modules were immediately processed once loaded on to the PamStation®12, as per the manufacturer-recommended pre-set protocols run from proprietary PamGene® Evolve version 2.0.8 software. Each array was blocked and washed for a period of 30 minutes prior to sample addition and kinase activity profiling,

4.3.3.3.4.PTK PamChip®4 Array process

A fresh PTK master mix was prepared for each experimental run as per the volumes outline in **Table 4.3**. As per manufacturer instructions, PTK additive was incubated at 37°C for five minutes prior to use in case of precipitation. The PY20-FITC solution was protected from light. A total of 5µg of sample lysate in 10µl M-PER mammalian extraction buffer with Halt Phosphatase Inhibitor Cocktail and Halt EDTA-free Protease Inhibitor Cocktail, both at 1:100, was used for each PTK array. Assays were prepared to a total volume of 40µl in pre-cooled microcentrifuge tubes through the addition of 30µl TK master mix to the 10µl lysate mix just prior to their addition to the pre-blocked PamChip®4 array. PamChip®4 modules were

Solution	PTK Volume (µl)	STK volume (µl)
Water	16.6	21.14
10x PK buffer	4.0	4
1M DTT solution	0.4	-
10x PTK additive	4.0	-
100x BSA solution	0.4	0.4
PTK antibody solution (PY20-FITC)	0.6	-
STK antibody solution	-	0.46
ATP solution (4mM)	4.0	4.0
Sample	10.0	10.0

Table 4.3. TK Master mix constituents for PTK and STK arrays. All reagents were used from an individual kit supplied by PamGene B.V. and all shared the same batch number.

immediately processed once the lysate-containing mix was loaded, as per the manufacturer-recommended pre-set 1200PTKlysv03.PS12 protocol (**appendix E**). Peptide phosphorylation was repeatedly assessed at five minute intervals over a total of 92 pumping cycles carried out over a one hour period.

4.3.3.3.5. STK PamChip®4 Array process

A fresh STK master mix was prepared for each experimental run as per the volumes outlined in **Table 4.3**. A total of 5µg of sample lysate in 10µl M-PER mammalian extraction buffer with Halt Phosphatase Inhibitor Cocktail and Halt EDTA-free Protease Inhibitor Cocktail, both at 1:100, was used for each STK array. Assays were prepared to a total volume of 40µl in pre-cooled microcentrifuge tubes through the addition of 30µl TK master mix to the 10µl lysate mix just prior to their addition to the pre-blocked PamChip®4 array. PamChip®4 modules were immediately processed once the lysate-containing mix was loaded, as per the manufacturer-recommended pre-set 1300STKlysv08.PS12Protocol (**Appendix F**). STK detection mix was freshly prepared for each experimental run and comprised of 26.6µl water, 3.0µl Ab buffer and 0.4µl STK antibody per sample.

4.3.3.4. Analyses

4.3.3.4.1. Statistical analyses

Data from the kinase array were analysed using ANOVA with post-hoc Dunnett's test to correct for multiple significance testing. All statistical analyses were undertaken within the proprietary Pamgene® Bionavigator software.

4.3.3.4.2. Functional enrichment

Functional enrichment analyses were undertaken as outlined in **2.7.1**. Pathway analyses were organised hierarchically and compared across phenotypes using FunMappOne.(449) This provides a platform through which the intrinsic hierarchy of functional annotations can be presented so that terms and pathways can be rationally and readily compared across conditions at each hierarchical level.

4.3.3.4.3. Protein-protein interaction networks

STRING analysis software was used to generate functional protein-protein interaction networks. Statistically significant proteins were submitted to STRING via the Cytoscape app

with plugin and terms with a minimum interaction of 0.4 shown. GLayer clustering was used to partition proteins into groups across which within-cluster variance is minimised.

4.3.3.4.4. Upstream analyses

Upstream mediators of changes in kinase activity were determined by IPA Upstream Regulator Analysis, as outlined in **2.7.1.5**. Fold-change and significance were used as inputs, as well as the specific peptide sequence to which they relate (i.e. rather than the protein/gene name, as was used when analysing DEGs). Further upstream analyses were undertaken using the kinase-specific GPS version 5.0. This allows for the prediction of cognate kinases from a database of 44,795 protein kinases using position weight determination and scoring matrix optimisation.(536,537)

4.4. Results

4.4.1. Acidic bile salts result in a significant reduction in PTK but not STK

phosphorylation across NSE (Het-1A), NDBO (CP-A) and HGD (CP-B) cell lines

In order to determine the temporal impact of acidic bile salts on signalling, we assessed the change in total tyrosine and total serine/threonine phosphorylation across NSE Het-1A, NDBO CP-A and HGD CP-B cells following exposure to a ten minute pulse of bile salts at neutral or acidic pH, or acid (**Fig. 4.5**). Remarkably, after ten minutes of exposure to both acid alone and acidic bile salt treatment all three cell lines demonstrated a substantial reduction in tyrosine phosphorylation (**Fig. 4.5A**). This reached a pre-determined threshold for significance ($p < 0.05$) for acidic bile salts on analysis of repeat immunoblots for Het-1A and CP-A but not CP-B. Interestingly, the degree to which total tyrosine phosphorylation reduced was similar for acid and acidic bile salts in all three studied cell lines.

In contrast, the intensity of total serine/threonine phosphorylation remained relatively stable following acid and acidic bile salt treatment, but as can be seen in **Fig. 4.5B**, the pattern of phosphorylation (i.e. which molecules are phosphorylated) appeared to change. This was most pronounced for the NSE Het-1A and HGD CP-B cell lines. Neither total tyrosine phosphorylation nor total serine/threonine phosphorylation changed in response to bile salt treatment in any of the studied cell lines.

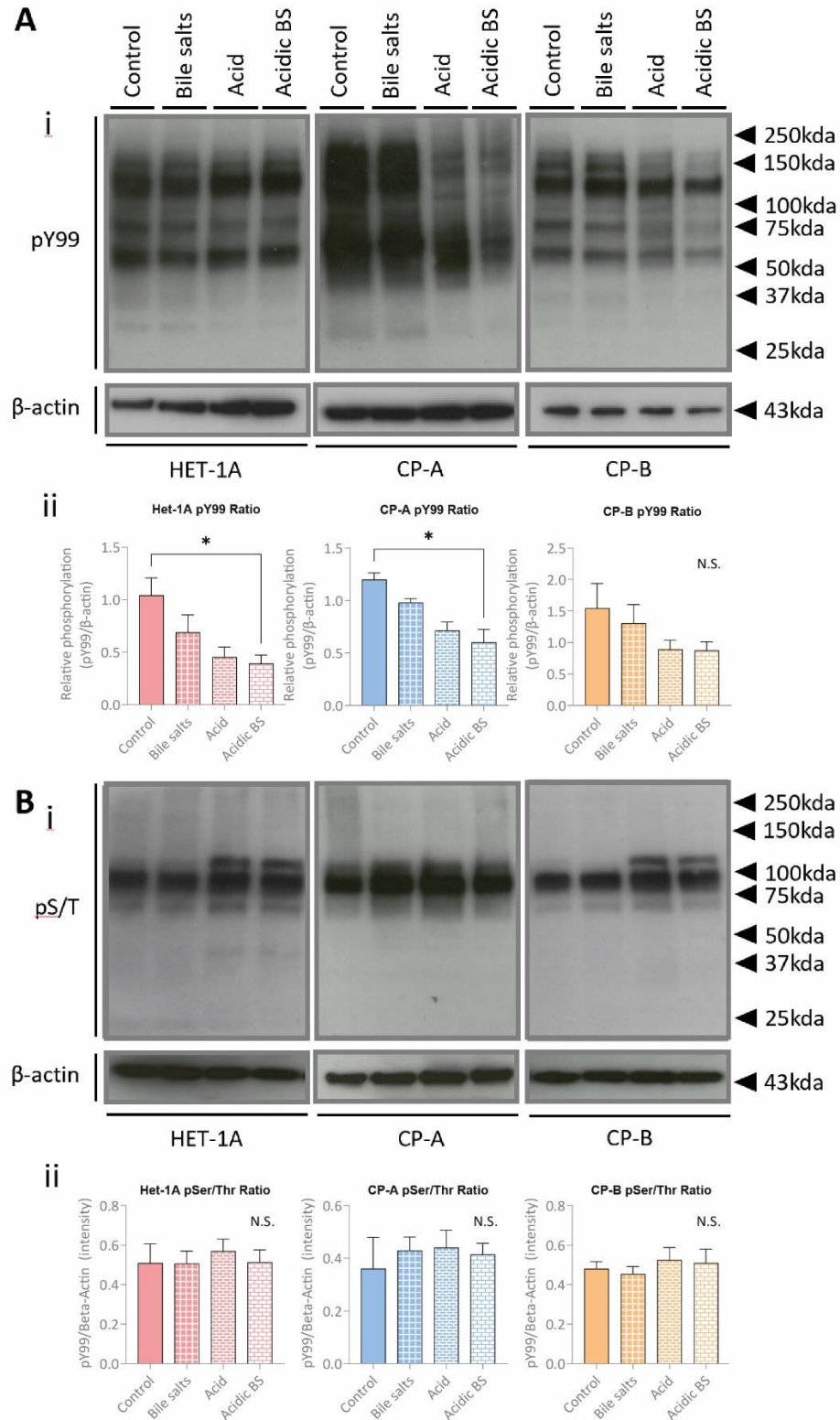


Figure 4.5. Immunoblots demonstrating changes in the relative total (A) tyrosine and (B) serine/threonine phosphorylation in NSE (Het-1A), NDBO (CP-A) and HGD (CP-B) cells during the period following a ten minute exposure to acidic bile salts. Cells were exposed to a 100 μ M equimolar mix of bile salts at pH 4.0 for ten minutes then either sampled or washed and maintained within serum-free media in order to monitor changes in signalling. Cells treated with vehicle only within serum-free media are used as a control population. Representative immunoblots for Het-1A, CP-A and CP-B are presented in (i) and target epitope phosphorylation, normalised to the β -actin loading control, is summarised by densitometry in (ii). Statistical analyses were undertaken using the Kruskal-Wallis test with Dunn's post-hoc correction. n=3

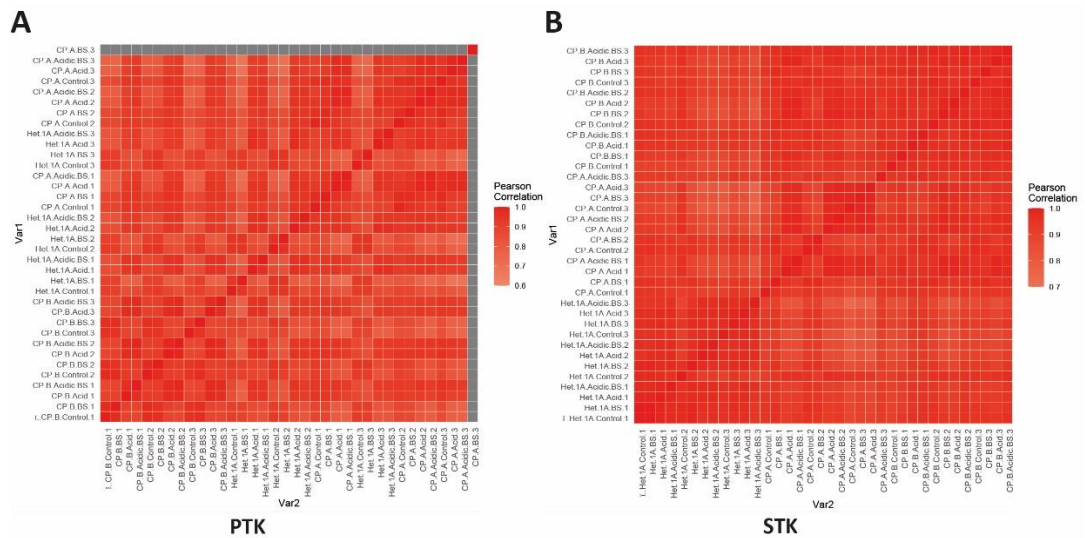


Figure 4.6. Sample-level quality control outputs for (A) PTK and (B) STK kinase activity array analyses of NSE (Het-1A), NDBO (CP-A) and HGD (CP-B) cells treated with bile salts (BS) at neutral pH or acidic pH (acidified BS), or with acid alone. Pairwise correlation of all replicates is shown with samples sorted by unsupervised hierarchical clustering. R1-3: repeats 1-3.

4.4.2. Kinomic analysis of PTK and STK activity reveals a consensus response to acid withdrawal across NSE (Het-1A), NDBO (CP-A) and HGD (CP-B) cell lines

It is apparent from the work undertaken in **Chapter 3** that, at the least, a combination of RTKs and serine/threonine signalling are implicated in the differential regulation of genes following acidic bile salt exposure. However, as outlined in **1.1.2.5.**, there remains significant uncertainty regarding the relative contribution of acid, bile salts and acidic bile salts to signalling processes that may be implicated in the dysplastic progression of BO. This is despite significant evidence for a role for exposure to refluxate in the development of both BO and OAC. The data presented here, in **4.4.1.**, suggest that acid suppresses tyrosine but not serine/threonine signalling, which we predicted then recovers following the restoration of a neutral extracellular pH. In order to identify pathways and processes involved in the NSE and BO response to refluxate, and the relative contribution made by acid and bile salts, we used a kinome activity assay to characterise PTK and STK activity in the period immediately following the withdrawal of these stressors (i.e. as the cell restores tyrosine phosphorylation following its suppression in the presence of acid).

4.4.2.1. Quality control

As demonstrated in **Fig. 4.6.**, reproducibility amongst replicates was high, with Pearson’s correlation coefficient respectively exceeding 0.6 for all but one pairwise PTK comparison (**Fig. 4.6A**). All STK pairwise comparisons (**Fig. 4.6B**) exceeded a Pearson’s correlation value

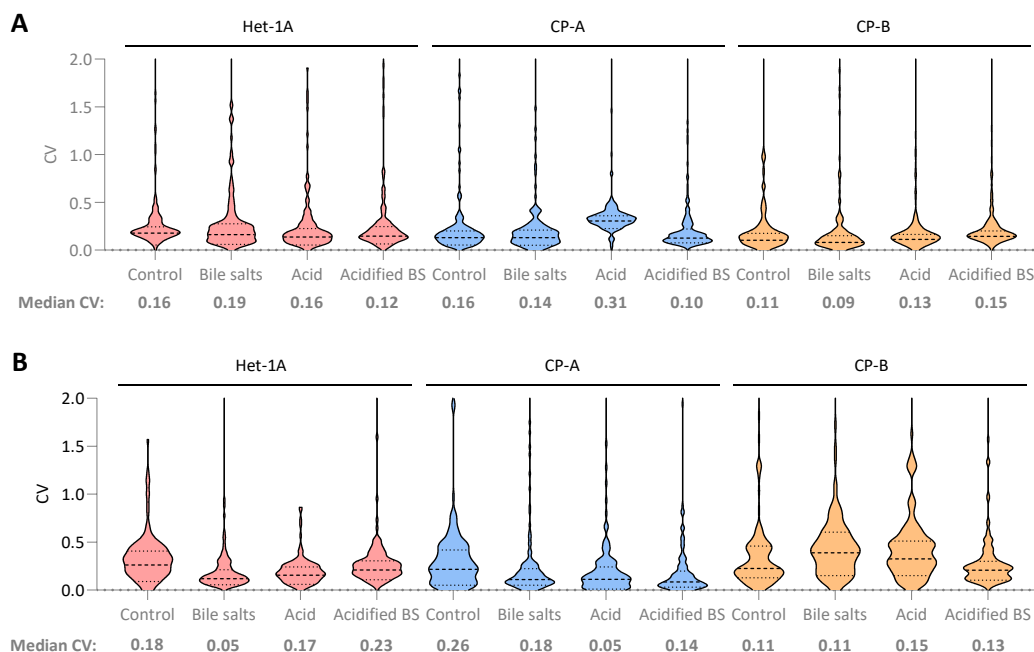


Figure 4.7. Violin plots demonstrating the distribution of coefficient of variation (CV) scores for each studied peptide included within the (A) PTk and (B) STk kinase activity arrays for NSE (Het-1A), NDBO (CP-A) and HGD (CP-B) cells treated with bile salts (BS) at neutral pH or acidic pH (acidified BS), or with acid alone. Cells were assayed using PamChip®4 PTk and STk arrays immediately following a ten minute exposure to a 100µM equimolar mix of bile salts in neutral or acidic (pH 4.0) conditions, or a ten minute pulse of acidified (pH 4.0) media alone. CV values exceeding 0.5 were excluded from further analyses in line with manufacturer guidance.

of 0.7. PTk readings for ‘CP-A bile salts repeat 3’ did not correlate with repeats 1 and 2 for CP-A bile salts and significantly differed from all other readings. This is far more than would be expected given the use of a standardised analysis array and this repeat was therefore excluded from further analyses.

Following analysis of the correlation between repeats, the coefficient of variation (CV) for each peptide within repeats for each specific cell line and condition was assessed, as summarised in **Fig. 4.7**. The raw median CV values for each specific condition within each cell line ranged from 0.05 to 0.31, which are in keeping with array manufacturer recommended limits. As per manufacturer instructions, peptides with a CV value exceeding 0.5 were excluded from further analyses. Following this step, 151 PTk and 98 STk peptides remained for further analysis.

4.4.2.2. NDBO (CP-A) cells exhibit a basal and stress-responsive kinome profile that is distinct from that of NSE (Het-1A) and HGD (CP-B) cells

Overall kinase activity profiles were compared across cell lines and treatment conditions. As shown in **Fig. 4.8.**, the basal and treatment-responsive kinase activity of NDBO (CP-A) cells

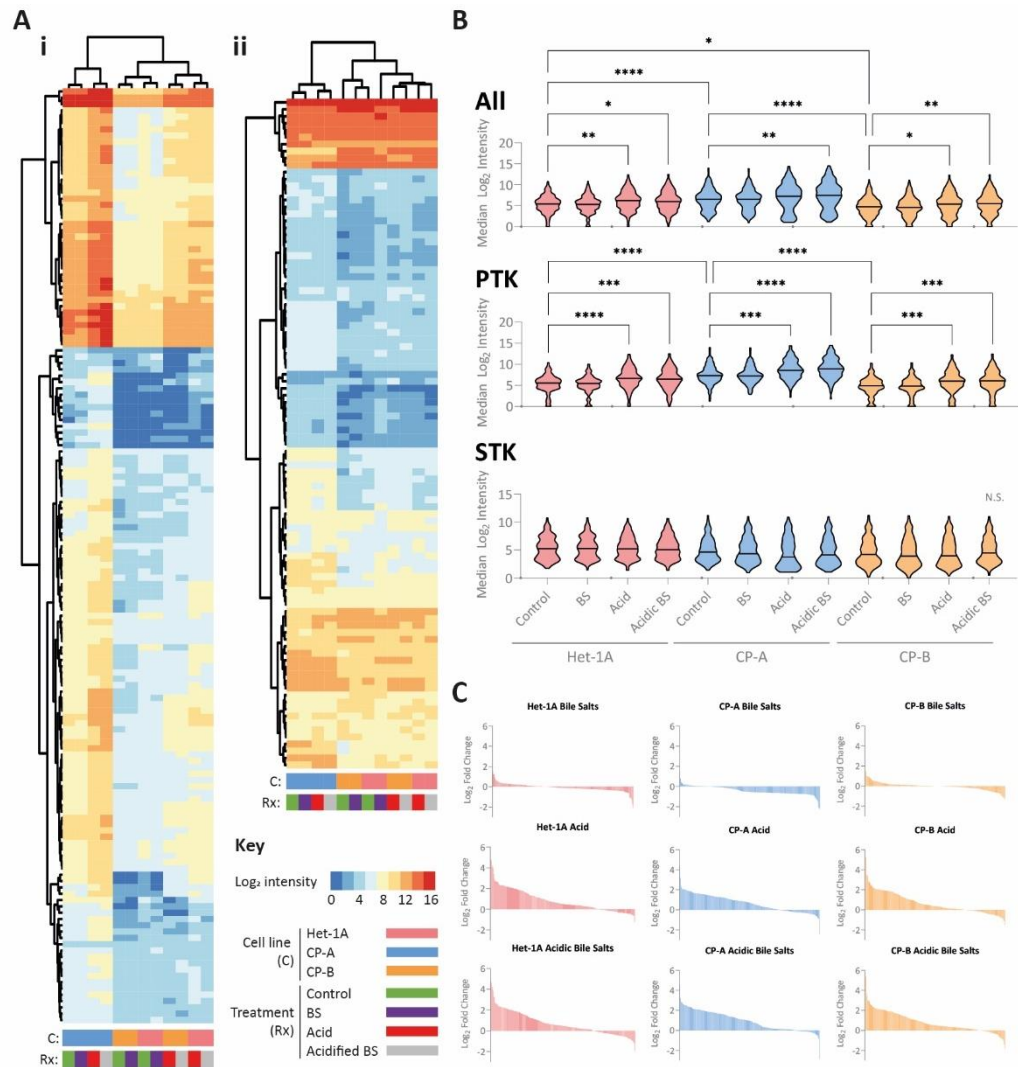


Figure 4.8. A panel figure illustrating kinase activity profiles of NSE (Het-1A), NDBO (CP-A) and HGD (CP-B) cells immediately following exposure to a ten minute pulse of bile salts at neutral or acidic pH, or acid alone. Cells were assayed using PamChip®4 PTK and STK arrays immediately following a ten minute exposure to a 100µM equimolar mix of bile salts in neutral or acidic (pH 4.0) conditions, or a ten minute pulse of acidified (pH 4.0) media alone. Peptide intensity is equivocal to activity; CP-A BS PTK readings are at biological n=2, all others at biological n=3. **(A)** Heatmaps providing an overview of **(i)** PTK and **(ii)** STK peptide intensity with samples sorted by Euclidean distance means-based unsupervised hierarchical clustering with complete linkage. Identified relationships between conditions and studied peptides are illustrated by the dendrograms. **(B)** Violin plots illustrating the distribution of median intensity readings for all peptides, and for PTK and STK peptides separately, in each of the studied conditions. Analyses were undertaken using ANOVA with post-hoc Tukey correction for multiple significance testing. Comparisons that reached pre-defined significance thresholds are highlighted, and are distinguished as follows: * p ≤ 0.05; ** p ≤ 0.01; *** p ≤ 0.001; **** p ≤ 0.0001. **(C)** Waterfall plots demonstrating the distribution of fold-change in peptide intensity versus control for each of the studied conditions. Samples are ordered from greatest positive fold change to greatest negative fold change.

differed from that of NSE (Het-1A) and HGD (CP-B) cells. This is particularly apparent in **Fig. 4.8A**, within which cells and treatment conditions were ordered by unsupervised hierarchical clustering. Here, CP-A cells cluster separately from Het-1A and CP-B cells for all treatments for both the PTK and the STK assays. This is in contrast to Het-1A and CP-B cells,

which are relatively similar both in the basal state and when responding to neutral bile salt, acid or acidic bile salt treatments. Interestingly, the overall basal kinase activity of CP-A cells, as reflected by the median Log_2 intensity of evaluated peptides (**Fig. 4.8B**), is significantly higher for CP-A cells than Het-1A cells (6.49 vs. 5.36 A.U.; $p < 0.0001$). A significantly higher level of activity is also seen in CP-A cells when compared with CP-B cells (6.49 vs. 4.68 A.U.; $p < 0.0001$). The higher basal level of kinase activity exhibited by CP-A cells is driven by PTK signalling, which is significantly greater in CP-A cells than in Het-1A cells (7.46 vs. 5.37 A.U.; $p < 0.0001$). In contrast, the median Log_2 intensity of evaluated STK peptides is marginally lower for CP-A cells compared with Het-1A (4.99 vs. 5.34 A.U.; $p = 0.98$), and marginally higher in CP-A than CP-B (4.99 vs. 4.65 A.U.; $p = 0.34$), though neither comparison reached the pre-determined threshold for significance.

4.4.2.3. Acid and acidic bile salts, but not bile salts alone, upregulated PTK activity

We next sought to evaluate the relative impact on PTK and STK signalling of neutral bile salts, acidic bile salts and acid alone. As shown in **Fig. 4.8B**, acid and acidic bile salts led to significant upregulation of PTK kinase activity across all three cell lines. No similar change in the intensity of PTK activity was seen with bile salts. In contrast, there was no significant change in the overall intensity of STK activity with any of the conditions, though as demonstrated by the changing architecture of the violin plots, the pattern of activity did differ.

Similarly, individual analysis of the change in intensity of all assayed peptides (**Fig. 4.8C**) demonstrated that, though there was no overall change in the intensity of activity following bile salt exposure, the pattern of activity did differ with a number of peptides both increasing and decreasing in activity. In addition, whilst a majority of peptides were upregulated in response to both acid and acidic bile salts across Het-1A, CP-A and CP-B cell lines, a variable number decreased. There is in addition evidence for bile salts modifying the strong changes seen with acid, with the some variation seen in the acid and acidic bile salt waterfall plots for each cell line.

In order to confirm the extent to which basal and treatment-responsive signalling differed between the studied cell lines, a PCA analysis was undertaken using all appraised peptides (**Fig. 4.9**). As outlined in **Fig. 4.9A**, the first three principle components explained in excess of 90% of the variance between the submitted peptides with (**Fig. 4.9B**) three separate clusters of peptides contributing to most of the variance shown between principle components 1 and 2. As shown in **Fig. 4.9C**, the kinase activity of the cell lines was sufficiently

different to mean that they separately clustered (i) regardless of whether they were assayed following treatment or whilst in their basal state. However, (ii) treatment with acid and

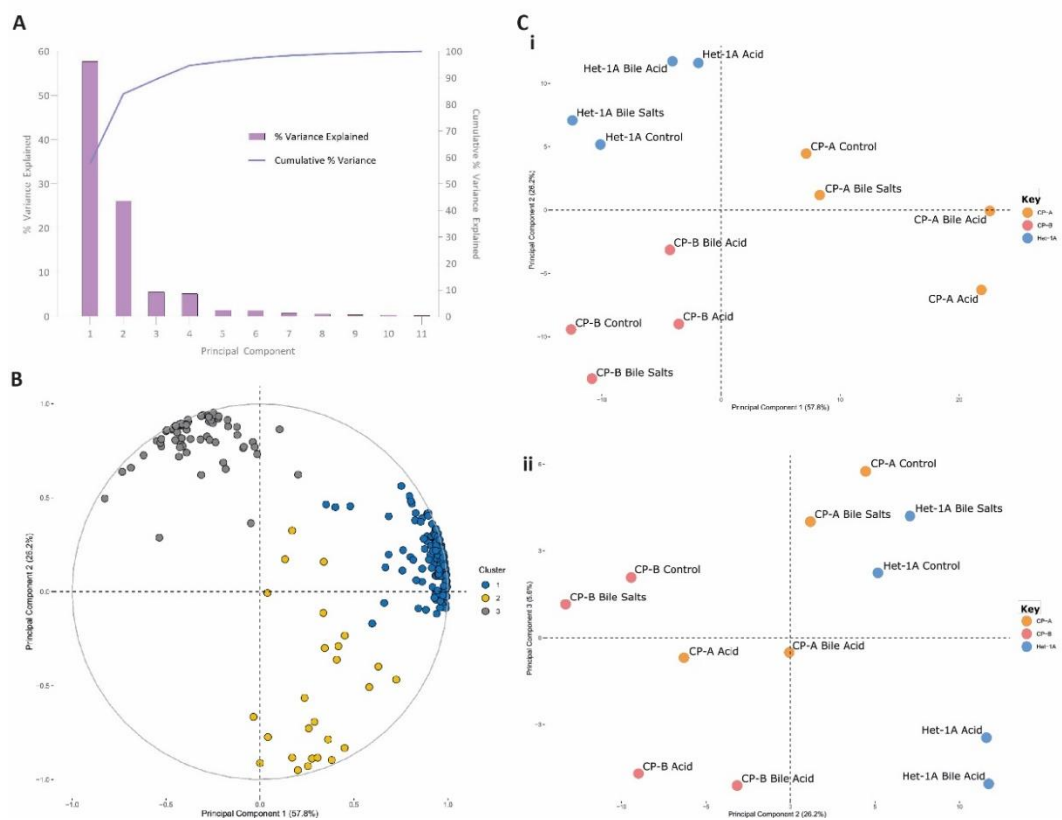


Figure 4.9. A panel figure illustrating a principle components analysis (PCA) to identify the variation in kinase activity profile between NSE (Het-1A), NDBO (CP-A) and HGD (CP-C) cells in their basal state and following exposure to bile salts at neutral or acidic pH, or acid alone. Cells were assayed using PamChip®4 PTK and STK arrays following a ten minute exposure to a 100µM equimolar mix of bile salts in neutral or acidic (pH 4.0) conditions, or a ten minute pulse of acidified (pH 4.0) media alone. CP-A BS PTK readings are at biological n=2, all others at biological n=3. **(A)** A scree plot illustrating the percentage variance in kinase activity explained by each principle component. **(B)** Peptide clusters contributing to principle components 1 and 2. **(C)** PCA results for **(i)** principle component 1 versus principle component 2, and **(ii)** principle component 2 versus principle component 3.

acidic bile salts explained a smaller proportion of the variance, with control and bile salt readings for all three cell lines clustering separately from acid and acidic bile salt readings.

4.4.2.4. The basal NDBO (CP-A) kinome is enriched for migratory terms, immune system processes and RTK signalling

The basal kinome of Het-1A, CP-A and CP-B cells was compared in order to identify the pathways and processes that establish the differences between these cells that were outlined in 4.4.2.2. and 4.4.2.3. When compared with both Het-1A and CP-A cells, CP-B cells had the largest number of peptides for which phosphorylation was significantly lower (**Fig. 4.10A**). In contrast, CP-A had the greatest number of peptides with significantly greater phosphorylation.

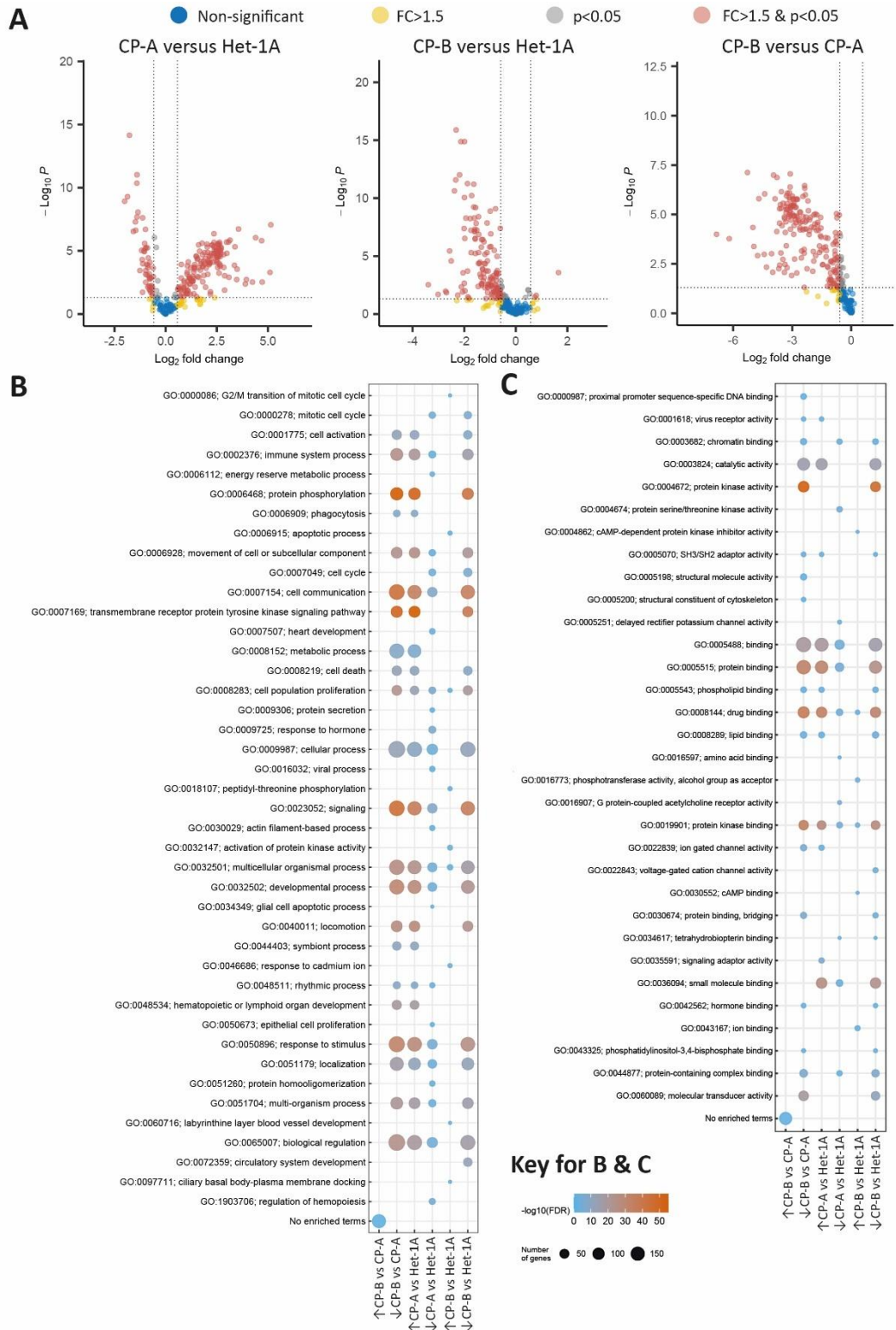


Figure 4.10. A panel figure illustrating differences in the basal kinase activity of NSE (Het-1A), NDBO (CP-A) and HGD (CP-B) cells. Cells were assayed using PamChip® 4 PTK and STK arrays following a 24 hour period of serum-starvation. All samples are in biological triplicate and analyses were undertaken using ANOVA with post-hoc Tukey correction for multiple significance testing. **(A)** Volcano plots illustrating the differences in peptide phosphorylation between cell lines by adjusted p-value and log₂FC. **(B,C)** A summary of overrepresented Gene Ontology (GO) Biological Process (B) and Molecular Function (C) terms from peptides that significantly differed in phosphorylation between the cell lines. GO terms are shown following semantic analysis was applied using REVIGO in order to eliminate redundant terms. FDR; false discovery rate.

In order to determine the processes and pathways contributed to by peptides that had significantly greater basal phosphorylation in one cell line compared with another, functional enrichment was undertaken by analysis of overrepresented GO BP (Fig. 4.10B) and MF (Fig. 4.10C) terms. Compared with CP-B and Het-1A cells, CP-A cells were enriched for a number of migratory terms, including 'GO 0051179: localisation', 'GO 004011: locomotion' and 'GO 0006928: movement of cell or subcellular component'. A number of immune system process and signalling terms were also enriched in CP-A lines when compared with both Het-1A and CP-B cells, including 'GO 002376: immune system process', 'GO 0023052: signalling', 'GO 0007154: cell communication' and 'GO: 0050897: response to stimulus'. Interestingly, and perhaps underlining their apparent increase in basal tyrosine activity, CP-A cells also enriched for RTK signalling ('GO 0007169: transmembrane receptor protein tyrosine kinase signalling pathway').

In contrast, there was minimal enrichment of any terms in CP-B cells when compared with either Het-1A or CP-A cells. However, when compared with CP-A and CP-B cells, Het-1A cells were enriched for a number of processes relating to the circulatory system, including 'GO 1903706: regulation of haemopoiesis', 'GO 0072359: circulatory system development' and 'GO 0007507: heart development'. Further, whilst proliferative terms were seen for both upregulated and downregulated peptides for comparisons across all cell lines, Het-1A cells were enriched for the 'GO 000278: mitotic cell cycle' term when compared with both Het-1A and CP-B cells.

We next sought to determine the specific pathways underlying the stark differences seen in the cellular processes enriched for the BO CP-A and CP-B cell lines (Fig. 4.11). Reflecting the

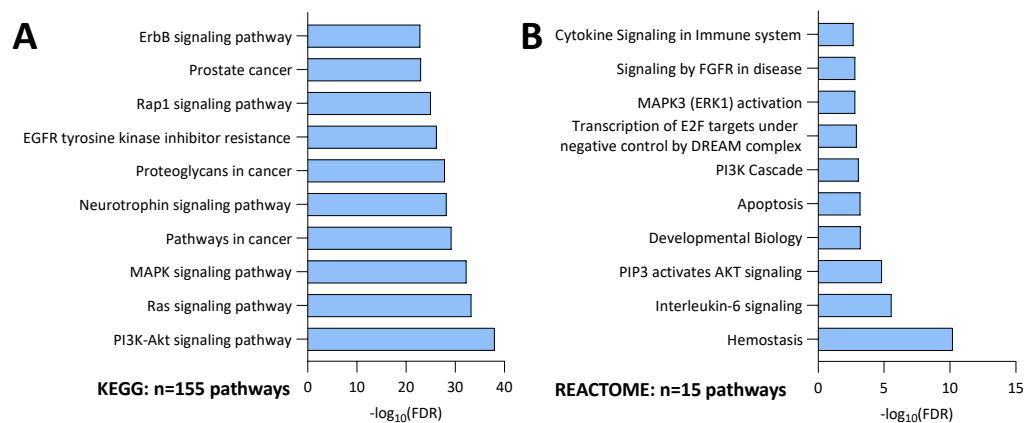


Figure 4.11. The top 10 signalling (A) KEGG and (B) REACTOME pathways that significantly enrich in NDBO (CP-A) cells when compared with HGD (CP-B) cells. Basal kinase activity was determined by PamChip®4 PTK and STK arrays following a 24 hour period of serum-starvation, with all readings undertaken in biological triplicate. Enriched KEGG and REACTOME pathways were identified by Fisher's exact test. FDR: false discovery rate.

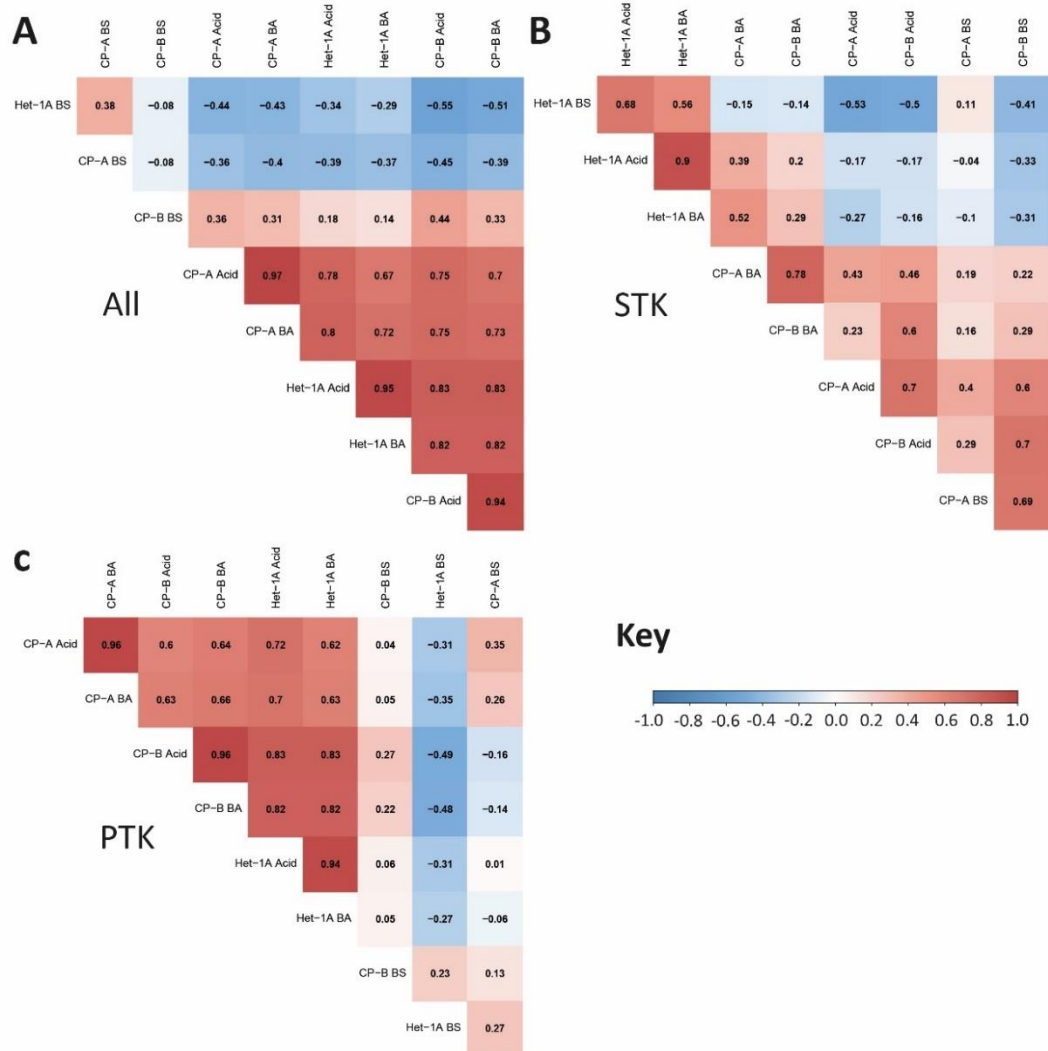


Figure 4.12. The correlation between change in phosphorylation of (A) all, (B) STK and (C) PTK peptides following a ten minute pulse of bile salts at neutral (Bile salts) or acidified pH (Acidified BS), or Acid alone. Cells were assayed using PamChip®4 PTK and STK arrays immediately following a ten minute exposure to a 100µM equimolar mix of bile salts in neutral or acidic (pH 4.0) conditions, or a ten minute pulse of acidified (pH 4.0) media alone. CP-A BS PTK readings are at biological n=2, all others at biological n=3. Pearson correlation coefficients are shown and used to organise cell lines and exposure, with those more similar to one another clustered close together.

over-represented RTK-related term, these included the KEGG ‘ErbB signalling’ and ‘EGFR tyrosine kinase inhibitor resistance’ terms, as well as the REACTOME ‘signalling by FGFR in disease’ term. A number of pathways known to be downstream of RTKs were also enriched, including those relating to MAPK and PI3K/Akt signalling. A number of cytokine-related immune pathways were also enriched. Perhaps most intriguingly, the NDBO CP-A cells were enriched for ‘Pathways in cancer’ when compared with HGD CP-B cells.

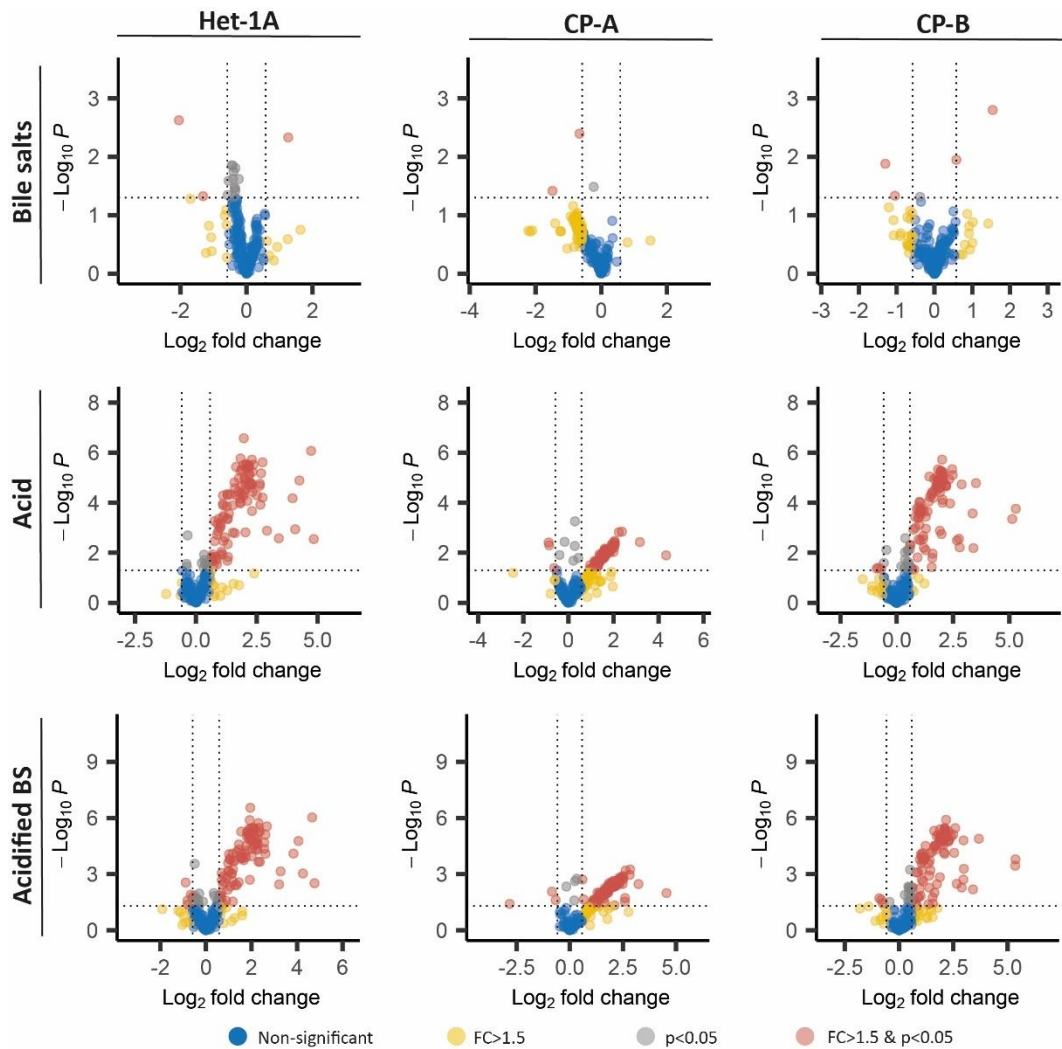


Figure 4.13. Volcano plots illustrating the differences in peptide phosphorylation between cell lines following exposure to a ten minute pulse of bile salts at neutral (Bile salts) or acidified pH (Acidified BS), or Acid alone. Cells were assayed using PamChip®4 PTK and STK arrays immediately following a ten minute exposure to a 100µM equimolar mix of bile salts in neutral or acidic (pH 4.0) conditions, or a ten minute pulse of acidified (pH 4.0) media alone. CP-A BS PTK readings are at biological n=2, all others at biological n=3.

4.4.2.5. The cellular response to acid and acidic bile salts correlates more closely for PTK than STK activity

It is apparent from data outlined in 4.4.2.3. that acid is a significant driver for kinase activity – and in particular PTK signalling - in both NSE and BO cells. We sought to explore the extent to which acid-derived signalling differs between cell lines and in the presence or absence of bile salts. To do this, we compared the correlation in signal change following acid, and both neutral and acidic bile salt treatment between each of the studied lines for all peptides, and for PTK and STK peptides separately.

Across all peptides, and as outlined in Fig. 4.12A., reasonably strong correlation (PCC>0.7) was seen between acidic and acidic bile salt treated cells. This contrasts with neutral bile salts, which delivered an overall kinase activity signal that neither correlated across cell lines

or with acid or acidic bile salt treated cells. When evaluated for STK (**Fig. 4.12B**) signalling alone, a different pattern was seen. Here, PCC between acid and acidic bile salt treated cells varied from a maximum of 0.9 for Het-1A to a minimum of 0.43 for CP-A cells. In contrast, much higher correlation levels of a maximum of 0.96 for both CP-A and CP-B, and a minimum of 0.94 for Het-1A, were seen for PTK signalling alone (**Fig. 4.12C**). Taken together, these results indicate that bile salts exert minimal influence on PTK signalling when in the presence of acid, but have a greater role in influencing STK signalling when delivered with acid.

4.4.2.6. The specific cellular response to bile salts, acid and acidic bile salts

The differences in the number of peptides for which phosphorylation significantly changed, and the magnitude of the change seen, is shown for all cell lines and exposures in **Fig. 4.13**. On the basis of the data presented thus far, it is apparent that though acid is a major driver for PTK activity, the total kinase activity signal generated by acid, acidic bile salts and neutral bile salts differs for each cell line. Given this, we sought to evaluate the pathways and processes generated by these different peptide changes in each cell line, in response to each stressor. This enables for the relative contribution of each microenvironmental stressor to specific signalling processes to be determined, as well as the characterisation of particular aspects of each cell's response to these and their potential upstream mediators, as is outlined later in this chapter.

4.4.2.6.1. The kinetic PTK signalling response to acid and both neutral and acidic bile salts in NSE and BO

As outlined in **4.4.2.3.** and **4.4.2.5.**, acid and acidic bile salts both result in significant upregulation in kinase activity across all studied cell lines. This appears for the most part a consequence of an increase in PTK activity. Assessing the kinetics of this signalling (i.e. the change in PTK activity over time following exposure to acid or acidic bile salts), and comparing these with the signal from bile salts alone (as shown in **Fig. 4.14**) allows for the relative contribution of acid versus acidic bile salts to be assessed over the lifetime of a signalling sequence.

Across all studied cell lines, a significant increase in PTK activity followed both acid and acidic bile salt stimulation. This suggests no additional influence from bile salts in the early phase of signalling given the lack of divergence of the acid and acidic bile salt curves up to and including the onset of increased PTK signalling between cycles 30-40. Beyond this point, minor divergence of the acid and acidic bile salt kinetic curves was seen relatively early for

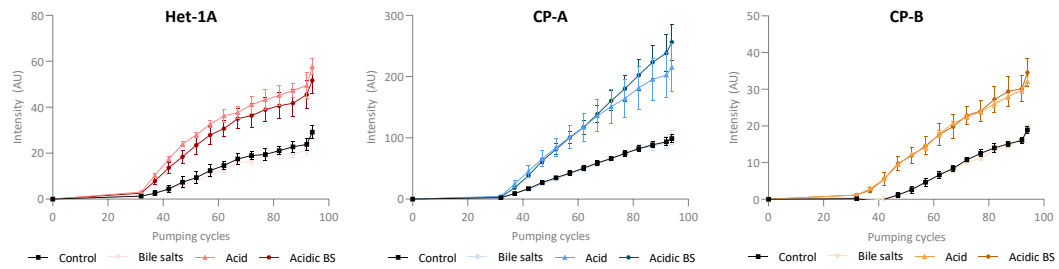


Figure 4.14. Kinetic profiles for PTK activity in NSE (Het-1A), NDBO (CP-A) and HGD (CP-B) cells exposed to a ten minute pulse of bile salts at neutral (Bile salts) or acidic (Acidic BS) pH, or acid alone. Cells were assayed using PamChip®4 PTK arrays immediately following a ten minute exposure to a 100µM equimolar mix of bile salts in neutral or acidic (pH 4.0) conditions, or a ten minute pulse of acidified (pH 4.0) media alone. The kinetic curves capture peptide phosphorylation over each ‘pumping cycle’ in which the substrate was pumped through a porous membrane on which peptides were embedded. CP-A BS PTK readings are at biological n=2, all others at biological n=3.

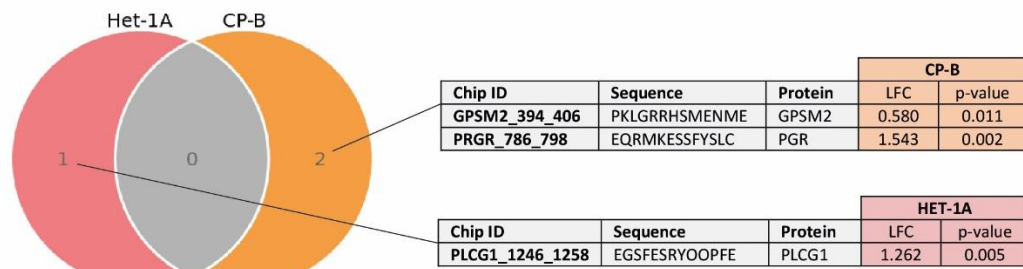
Het-1A, and late for CP-A; suggesting that activation of cellular-specific signalling components enable bile salts to modulate an acid signal. In contrast, the two curves closely tracked one-another for CP-B, with little evidence for significant influence on signalling from either neutral or acidic bile salts.

Interestingly, a marginal reduction in signalling activity is seen for the Het-1A bile salt curve when compared with control. This suggests a role for bile salts in reducing PTK signalling within this cell line, which is supported by the lower intensity curve seen for acidic bile salts compared with acid signalling alone. Of additional note, the final intensity of CP-A signalling far exceeds that of both Het-1A and CP-A signalling.

4.4.2.6.2. The NSE and BO kinome in response to neutral bile salts

As shown in **Fig. 4.15.**, only three peptides significantly increased in phosphorylation in response to bile salts across all of the cell lines. These were a peptide derived from the cell growth factor phospholipase-Cy1 (PLCy1) in Het-1A cells (LFC 1.262; p=0.005), and peptides derived from both G-protein-signalling modulator 2 (GPM2, LFC 0.58; p=0.011) and the progesterone receptor (PGR, LFC 1.543; p=0.002) in CP-B cells. Phosphorylation of two peptides fell in both CP-A and CP-B cells, which both exhibited a significant decrease in the phosphorylation of three peptides. These were derived from the voltage-gated potassium channel potassium voltage-gated channel subfamily A member 1 (KCNA1) and the G₁ cell-cycle checkpoint mediator M-phase inducer phosphatase 1 (CDC25A). Interestingly, the Rb G₁ checkpoint protein was also downregulated in response to bile salts in CP-B cells. As shown in **Fig. 4.15**, the CP-A bile salt response did not enrich, whilst the CP-B response to bile salts was enriched for terms relating to proliferation (GO 0051301: cell division, GO 0090068: positive regulation of cell cycle process).

A - ↑ Phosphorylation



B - ↓ Phosphorylation

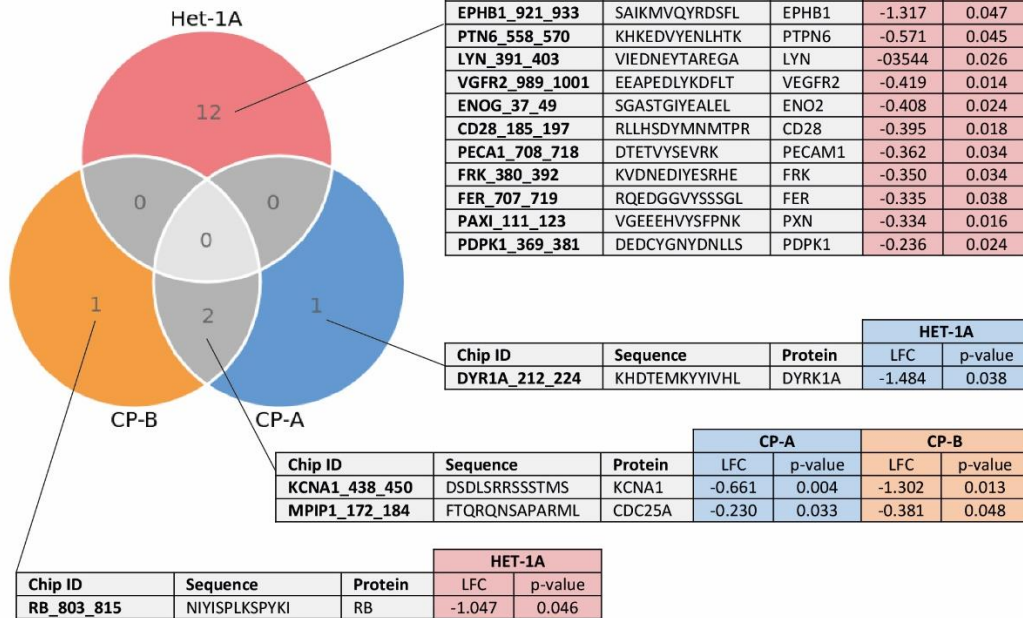


Figure 4.15. Peptides which significantly (A) increased or (B) decreased in phosphorylation in NSE (Het-1A), NDBO (CP-A) and HGD (CP-B) cells exposed to a ten minute 100µM equimolar mix of bile salts at neutral pH. Cells were assayed using PamChip®4 PTK and STK arrays. CP-A BS PTK readings are at biological n=2, all others at biological n=3. Statistical analyses were undertaken using ANOVA with post-hoc Tukey correction for multiple significance testing. LFC: log₂-fold change from baseline.

A greater number of peptides were significantly downregulated in Het-1A cells, including multiple targets within RTKs and their downstream pathways, such as ephrin B1 (EPHB1, LFC decrease of -1.317; p=0.047), VEGFR2 (LFC decrease of -0.419; p=0.014) and the tyrosine protein kinases LYN (LFC decrease of -0.354; p=0.026), FRK (LFC decrease of -0.35; p=0.034) and FER (LFC decrease of -0.335; p=0.038). These enrich (Fig. 4.16) for GO BP terms relating to migration (GO 0016477: cell migration, GO 0007155: cell migration, GO 0051179: locomotion) and immune system function (GO 0002367: immune system process, GO 0016032: viral process, GO 0045321: leucocyte activation). In keeping with the reduction seen in RTK phosphorylation, the GO MF term 'GO 0038023: signalling receptor activity' was also enriched.

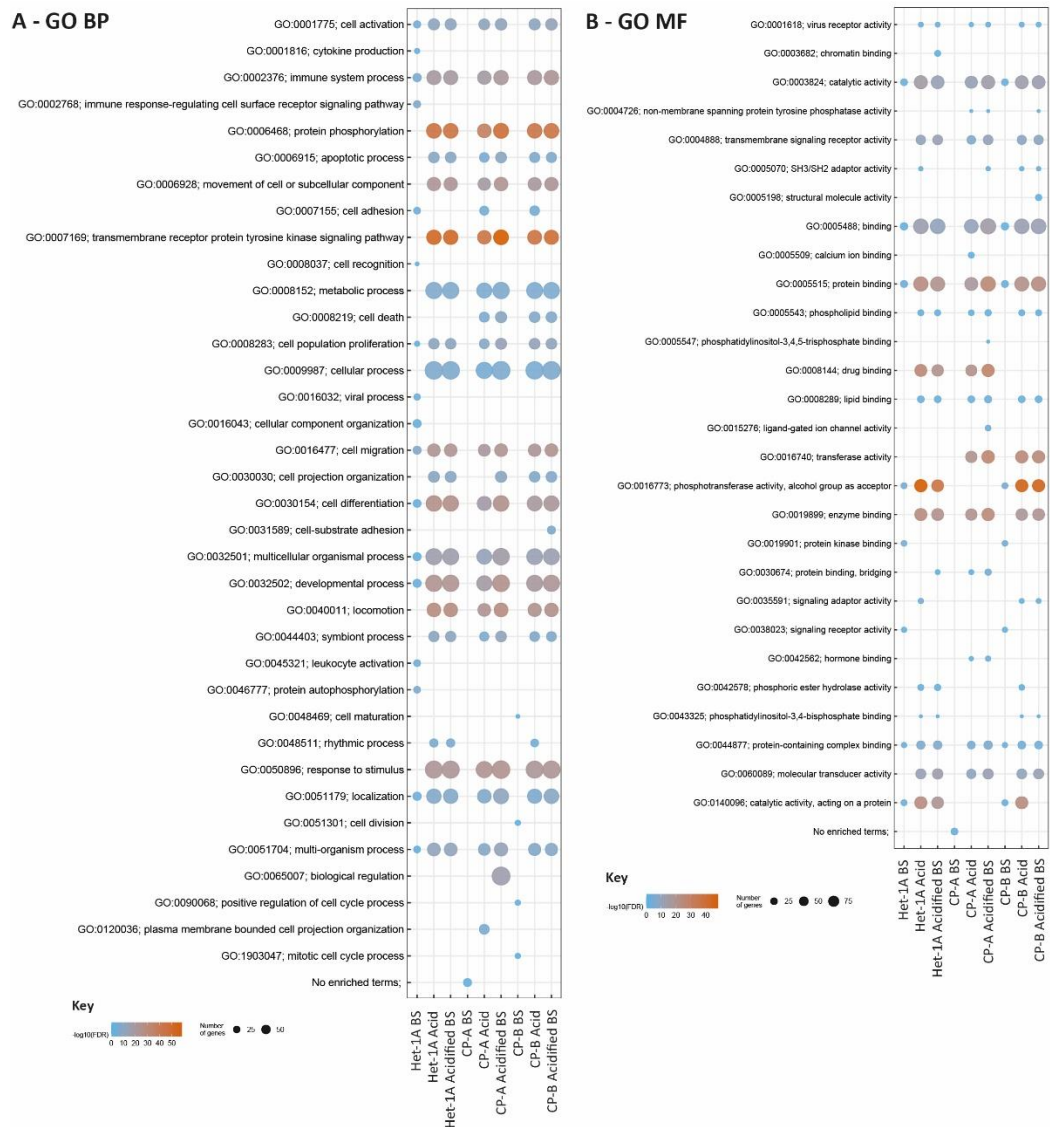


Figure 4.16. A panel figure illustrating over-represented Gene Ontology (GO) (A) Biological Process and (B) Molecular Function terms in NSE (Het-1A), NDBO (CP-A) and HGD (CP-B) cells following a ten minute pulse of bile salts at neutral (Bile salts) or acidified pH (Acidified BS), or Acid alone. Cells were assayed using PamChip®4 PTK and STK arrays following a 24 hour period of serum-starvation. CP-A BS PTK readings are at biological n=2, all others at biological n=3. GO terms are shown following semantic analysis was applied using REVIGO in order to eliminate redundant terms. FDR; false discovery rate.

4.4.2.6.3. The kinase response to acid, alone or with bile salts, enriches for RTK signalling, immune system processes, migration and cell death across NSE (Het-1A), NDBO (CP-A) and HGD (CP-B) cell lines

As can be seen in **Fig. 4.16.**, the addition of bile salts to acid treatment had limited impact on the derived functional enrichment, with most GO BP and MF terms similarly overrepresented for acid and acidic bile salt treatment. These group as four main processes; RTK signalling, immune system processes, migration and cell death. Overrepresented RTK

Sequence	Protein	Acid L ₂ FC	Acidic BS L ₂ FC
Het-1A			
HSTPPSAYGSVKA	Annexin A2	4.08	4.26
GSVQNPVYHNQPL	Epidermal growth factor receptor	3.41	3.21
QALDNPEYHNASN	Receptor tyrosine-protein kinase erbB-4	2.92	3.28
EIGVGAYGTVYKA	Cyclin-dependent kinase 4	2.74	2.61
VADIDGQYAMTRA	Catenin beta-1	2.74	2.68
VIDNEYTAREGA	Tyrosine-protein kinase Lyn	2.68	
LDTSSVLYTAVQP	Platelet-derived growth factor receptor beta	2.65	2.37
LIEDNEYTARQGA	Tyrosine-protein kinase Yes	2.62	
NENTEDQYSLVED	Phosphatidylinositol 3-kinase regulatory subunit alpha	2.36	2.32
HSTPPSAYGSVKA	Annexin A2	4.08	
RLIEDNEYTAREG	Tyrosine-protein kinase Lck		2.37
KVDNEDIYSRHE	Tyrosine-protein kinase FRK		2.31
CP-A			
RHTDDEMTGYVAT	Mitogen-activated protein kinase 14	4.34	4.55
YTATEGQYQQQP	Tyrosine-protein kinase Lyn	3.17	3.23
HSTPPSAYGSVKA	Annexin A2	2.06	
GSVQNPVYHNQPL	Epidermal growth factor receptor	2.06	2.53
VIDNEYTAREGA	Tyrosine-protein kinase Lyn	2.04	
LIEDNEYTARQGA	Tyrosine-protein kinase Yes	2.01	2.49
EIGVGAYGTVYKA	Cyclin-dependent kinase 4	1.94	
ESTNHIYSNLANS	Mast/stem cell growth factor receptor Kit	1.94	2.41
LDIDETEHADGG	Receptor tyrosine-protein kinase erbB-2	1.91	2.36
RLIEDNEYTAREG	Tyrosine-protein kinase Lck	1.83	
NENTEDQYSLVED	Phosphatidylinositol 3-kinase regulatory subunit alpha		2.82
TEATATDYHTTSH	Band 3 anion transport protein		2.60
QALDNPEYHNASN	Receptor tyrosine-protein kinase erbB-4		2.59
CP-B			
EQRMKESFYSLC	Progesterone receptor	3.52	3.68
LDIDETEHADGG	Receptor tyrosine-protein kinase erbB-2	3.41	3.40
VIDNEYTAREGA	Tyrosine-protein kinase Lyn	2.89	2.97
GSVQNPVYHNQPL	Epidermal growth factor receptor	2.80	2.89
HSTPPSAYGSVKA	Annexin A2	2.76	2.96
YMAPYDNYVPSAP	Platelet-derived growth factor receptor beta	2.67	2.66
LIEDNEYTARQGA	Tyrosine-protein kinase Yes	2.49	2.50
EIGVGAYGTVYKA	Cyclin-dependent kinase 4	2.37	2.54
NENTEDQYSLVED	Phosphatidylinositol 3-kinase regulatory subunit alpha	2.33	2.40
RLIEDNEYTAREG	Tyrosine-protein kinase Lck	2.20	
LDDFDGTYETQGG	Ephrin type-A receptor 1		2.32

Table 4.4. The 10 peptides that showed the largest significant increase in phosphorylation in response to acid and acidic bile salt (BS) exposure in NSE (Het-1A), NDBO (CP-A) and HGD (CP-B) cells. Cells were assayed using PamChip®4 PTK and STK arrays. CP-A BS PTK readings are at biological n=2, all others at biological n=3. Statistical analyses were undertaken using ANOVA with post-hoc Tukey correction for multiple significance testing. L₂FC: log₂-fold change from baseline.

signalling GO terms include the GO BP term 'GO 0007169: transmembrane receptor protein tyrosine kinase signalling pathway', which was the most significantly enriched term, and the GO MF term 'GO 0004888: transmembrane signalling receptor activity'. Increased RTK activity was also supported by enrichment of downstream terms, including 'GO 0005070:

Sequence	Protein	Acid	Acidic BS
		L ₂ FC	L ₂ FC
Het-1A			
NIHLEKKYVRRDS	Macrophage colony-stimulating factor 1 receptor	-0.38	-0.42
EPHVTRRTPDYFL	Serine/threonine-protein phosphatase 2A catalytic subunit beta isoform	-0.37	
RRKRKPSTSDSD	DNA topoisomerase 2-alpha	-0.34	
FSGTPEYLAPVL	RAC-alpha serine/threonine-protein kinase (AKT1)		-0.89
IVAENPEYLSEFS	Receptor tyrosine-protein kinase erbB-4		-0.81
EHIERRVSNAGGP	Vasodilator-stimulated phosphoprotein		-0.81
ASLGRRASFHLEC	Voltage-dependent L-type Ca ²⁺ channel subunit alpha-1c		-0.66
GFHPRRSSQGATQ	Hormone-sensitive lipase		-0.59
KMQLRRPSDQEV	Proto-oncogene c-Rel		-0.57
RRKRKPSTSDSD	DNA topoisomerase 2-alpha		-0.49
ELLCLRRSSLKAY	Beta-2 adrenergic receptor		-0.49
SSRRTTLCGLDY	Aurora kinase A		-0.34
CP-A			
GLGRSITPTTLY	Retinoblastoma-like protein 2	-0.87	
VRMRHLSQEFGL	Androgen receptor	-0.85	-0.66
QLFRGFSFVATGL	Ribosomal protein S6 kinase alpha-1	-0.63	
AILRRPTSPVSRE	Early E1A protein	-0.40	
LQARRRQSVLNL	Cystic fibrosis transmembrane conductance regulator	-0.16	-0.16
SLGFKRSYEEHIP	Insulin receptor		-2.83
AAGERRKSQEAQV	Stathmin-2		-0.84
CP-B			
GLGRSITPTTLY	Retinoblastoma-like protein 2	-0.89	
QLFRGFSFVATGL	Ribosomal protein S6 kinase alpha-1	-0.82	
AAGERRKSQEAQV	Stathmin-2	-0.69	-0.82
FGYGRASDYKSA	Myelin basic protein	-0.57	
EPHVTRRTPDYFL	Serine/threonine-protein phosphatase 2A catalytic subunit beta isoform	-0.46	
FSGTPEYLAPVL	RAC-alpha serine/threonine-protein kinase		-0.91
KSFLDSGYRILGA	Vinculin		-0.76
ANRERRPSYLPTP	Potassium voltage-gated channel subfamily A member 6		-0.44

Table 4.5. All peptides that significantly reduced in phosphorylation in response to acid and acidic bile salt (BS) exposure in NSE (Het-1A), NDBO (CP-A) and HGD (CP-B) cells. Cells were assayed using PamChip®4 PTK and STK arrays. CP-A BS PTK readings are at biological n=2, all others at biological n=3. Statistical analyses were undertaken using ANOVA with post-hoc Tukey correction for multiple significance testing. L₂FC: log₂-fold change from baseline.

SH3/SH2 adaptor activity' and 'GO 0004726: non-membrane spanning protein tyrosine phosphatase activity'. Two GO immune system processes were separately enriched, including the BP term 'GO 0002376: immune system process' and the MF term 'GO 0001618: virus receptor activity'. Migratory terms enriched in response to acid included 'GO 0006928: movement of cell or subcellular component', 'GO 0016477: cell migration', 'GO 0030030: cell projection organisation', 'GO 0007155: cell adhesion' and 'GO 0051179: localisation'. Finally, the GO BP term 'GO 0006915: apoptotic process' was also consistently enriched across cell lines following both acid and acidic bile salt treatment.

The proteins showing the largest significant fold increase in response to acid and acidic bile salts reflect in particular the role of RTKs in establishing signalling in response to acid, as outlined in **Table 4.4**. These include a number of members of the EGFR family, such as EGFR itself, which showed a significant LFC increase in activity of greater than 2 with both acid and acidic bile salts in all cell lines. The RTK erbB-2 was also represented amongst the proteins demonstrating the largest increase in phosphorylation in BO cells, whilst erbB-4 featured in the top ten for Het-1A and CP-A, and the EphA1 receptor for CP-B. A number of targets downstream of RTKs also substantially increased in activity, including the tyrosine-protein kinases Lck, FRK, Yes and Lyn.

In contrast, there were few peptides that decreased in activity in response to both acid and acidic bile salts (**Table 4.5**). In CP-A cells, two proteins that did show a reduced activity were the androgen receptor (LFC decrease of 0.85 and 0.66 in response to acid and acidic bile salts, respectively) and CFTR (LFC decrease of 0.16 in response to both acid and acidic bile salts). The microtubule stabiliser Stathmin-2 also showed a consistent decrease in activity (LFC decrease of 0.69 and 0.82 for acid and acidic bile salts, respectively) in CP-B cells. Interestingly, the largest fold-change reduction in activity was seen for the insulin receptor in CP-A cells (LFC decrease of 2.83).

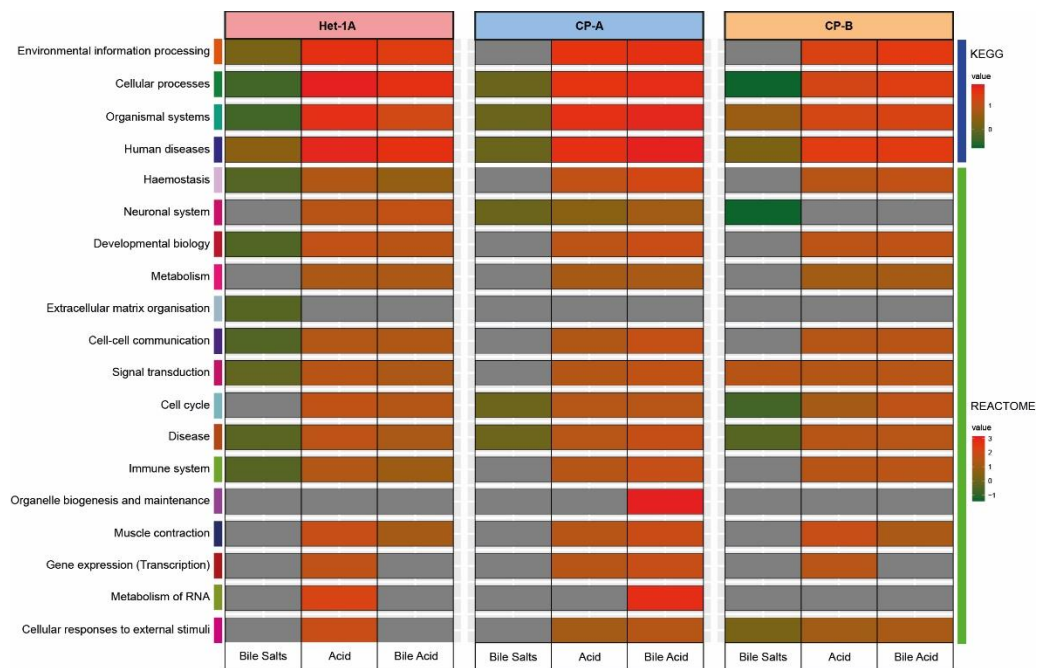


Figure 4.17. A heatmap demonstrating a global view of differences in KEGG and REACTOME pathway enrichment for NSE (Het-1A), NDBO (CP-A) and HGD (CP-B) cells following a ten minute pulse of bile salts at neutral (Bile salts) or acidified pH (Bile Acid), or acid alone. Cells were assayed using PamChip®4 PTK and STK arrays. CP-A BS PTK readings are at biological n=2, all others at biological n=3. Enriched KEGG and REACTOME pathways were determined and hierarchically categorised from global (tier 1 – shown here) to individual signalling (tier 3) categories to allow for comparisons across cell lines and conditions.

4.4.2.6.4. Functional enrichment of signalling networks following exposure to bile salts, at neutral and acidic pH, and acid alone, in NSE (Het-1A), NDBO (CP-A) and HGD (CP-B) cells

In order to validate the functional enrichment of GO BP and GO MF terms, we used an orthogonal approach to enrich KEGG and REACTOME pathways for differentially regulated peptides across the three cell lines following treatment with bile salts, at neutral or acidic pH, and bile salts alone. This additionally allowed for the comparison of functionally enriched pathways not represented in GO BP and MF databases. Pathways enriched by KEGG and REACTOME were organised hierarchically using FunMapOne, as illustrated in **Figs. 4.17-4.19**, and outlined in **4.3.3.4.2**.

Summary data from KEGG and REACTOME analyses are provided in **Fig. 4.17**. This shows activation of a wide array of cellular processes in response to acid and acidic bile salt treatment. In contrast, and in keeping with previously described data, bile salts alone generally result in a suppression in signalling processes. Pertinently, both REACTOME and KEGG enrichment highlights that the pattern of kinase activity seen in response to acid is

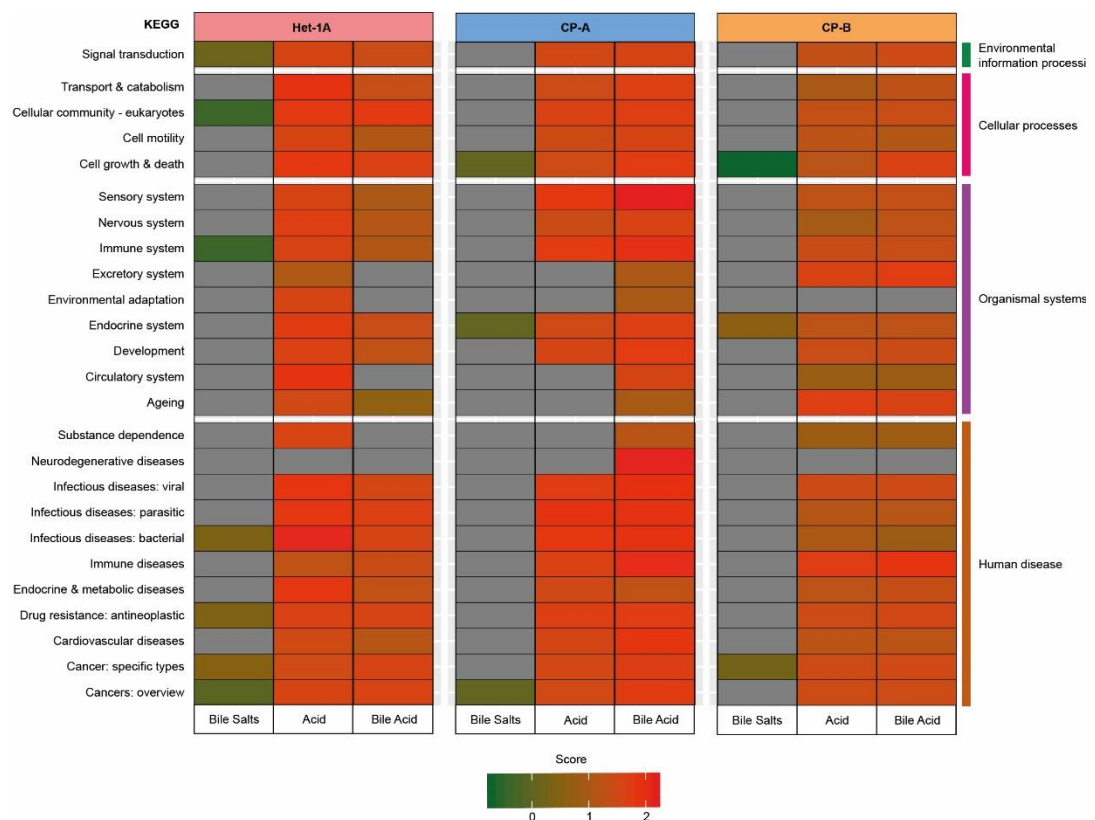


Figure 4.18. A heatmap demonstrating differences in KEGG pathway enrichment for NSE (Het-1A), NDBO (CP-A) and HGD (CP-B) cells following a ten minute pulse of bile salts at neutral (Bile salts) or acidified pH (Bile Acid), or acid alone. Cells were assayed using PamChip®4 PTK and STK arrays. CP-A BS PTK readings are at biological n=2, all others at biological n=3. Enriched KEGG pathways were determined and hierarchically categorised from global (tier 1) to individual signalling (tier 3) categories to allow for comparisons across cell lines and conditions. This tier 2 view focusses on a subset of categories identified to be enriched in tier 1.

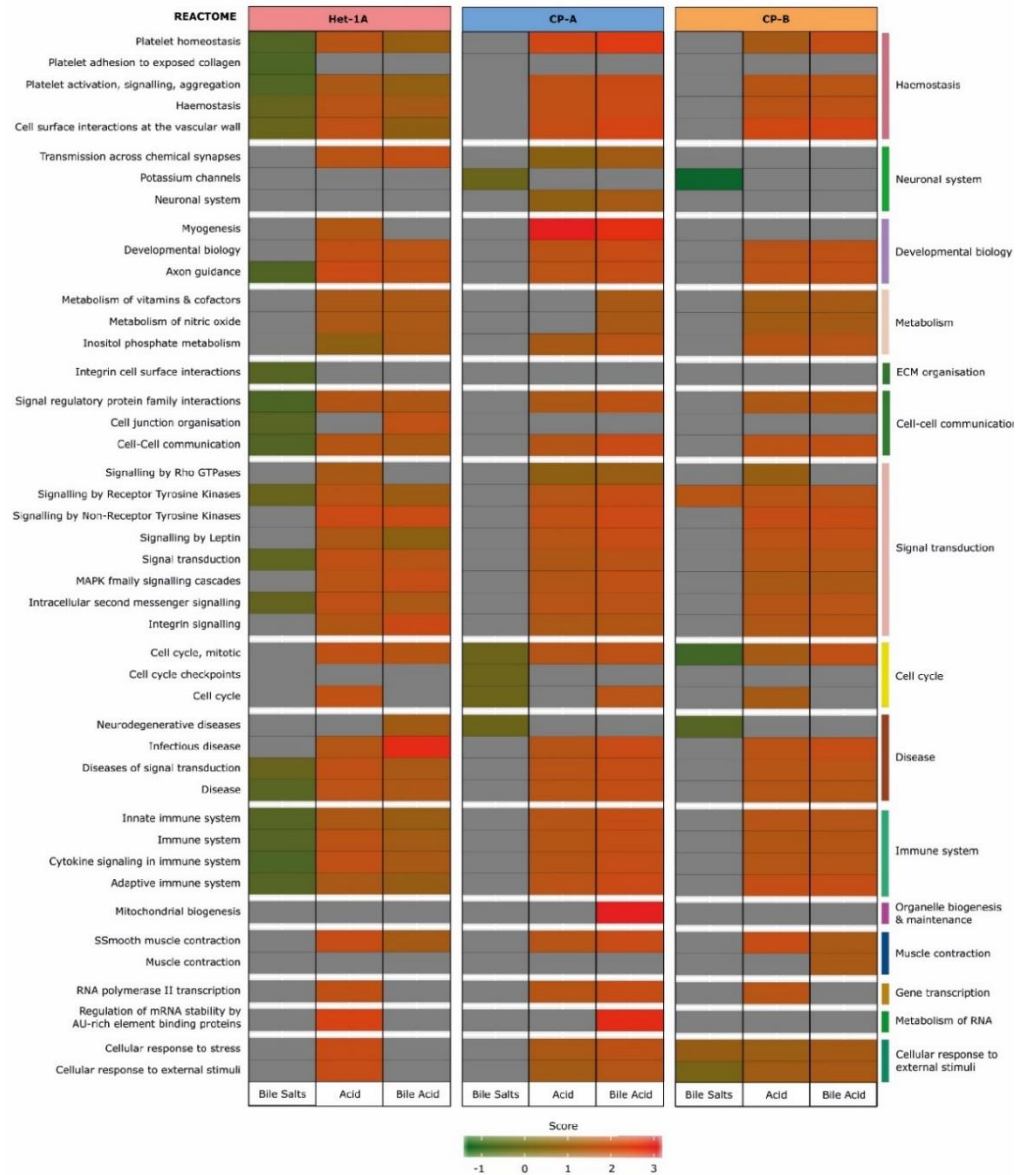


Figure 4.19. A heatmap demonstrating differences in REACTOME pathway enrichment for NSE (Het-1A), NDBO (CP-A) and HGD (CP-B) cells following a ten minute pulse of bile salts at neutral (Bile salts) or acidified pH (Bile Acid), or acid alone. Cells were assayed using PamChip[®]4 PTK and STK arrays. CP-A BS PTK readings are at biological n=2, all others at biological n=3. Enriched REACTOME pathways were determined and hierarchically categorised from global (tier 1) to individual signalling (tier 3) categories to allow for comparisons across cell lines and conditions. This tier 2 view focusses on a subset of categories identified to be enriched in tier 1.

shared by numerous human disease states. Both databases also enrich for terms relating to external stimuli (KEGG: Environmental information processing, REACTOME: Cellular response to external stimuli), demonstrating that the changes in kinase activity seen in response to acid mirror those characterised from other environmental stressors.

These themes were explored in more detail in **Fig. 4.18** (KEGG) and **Fig. 4.19** (REACTOME). Analysis using the KEGG database highlights in particular the enrichment in response to acid and acidic bile salts of terms relating to a variety of cellular processes, including cell motility

and both growth and death. This supports the overrepresented GO terms, as does the enrichment of human disease terms that closely link to an immune response ('Immune diseases', 'Infectious diseases: bacterial'). It is noteworthy that two terms relating to cancers are similarly enriched within this dataset.

Further detail is also provided by REACTOME enrichment. This includes strong enrichment for immune and inflammatory pathways in response to acid and acidic bile salts, in addition to enrichment for RTK and MAPK signalling. Integrin and leptin signalling are also noted to decrease in response to the same stressors. In contrast, enrichment for a reduction in a number of haemostatic parameters is again identified for the Het-1A response to bile salts, as is enrichment for a reduction in RTK-derived signalling and immune processes. It is noteworthy that an enrichment for a reduction in potassium-channel activity and for a decrease in cell cycle progress is seen in both BO lines but not in the NSE Het-1A line.

Overall, and as seen with the overrepresented GO terms, the enrichment for KEGG and REACTOME terms in response to acid and acidic bile salts was remarkably similar across cell lines representing NSE, NDBO and HGD. Notable differences included the enrichment of mitochondrial biogenesis (REACTOME) processes in response to acidic bile salts in CP-A cells only, and the enrichment within only the CP-A response of pathways associated with neurodegenerative diseases (KEGG) and neuronal system processes (REACTOME).

4.4.2.7. The conserved response to acidic bile salts in BO

The data presented herein have pointed to a conserved response to acid amongst all cell lines, highlighting that this is minimally modulated by the addition of bile salts. In total, 61 peptides were significantly upregulated in response to both acid and acidic bile salts in both CP-A and CP-B cells. These were considered to reflect a consensus response to acidic bile salt treatment and were analysed separately.

4.4.2.7.1. A conserved signalling response to acidic bile salts centres on TK and CMGC kinase signalling

As shown in **Fig. 4.20.**, the conserved signalling response to acidic bile salts in BO cells centres on the TK and CMGC ePK groups. The former is characterised by increased activation of a considerable number of RTKs, albeit with the notable downregulation of EphA4 activity. Within the CMGC group, activation of the p38, ERK and JNK MAPKs is noted, as is activation of a number of cyclin dependent kinases. Beyond these major groupings, changes are also

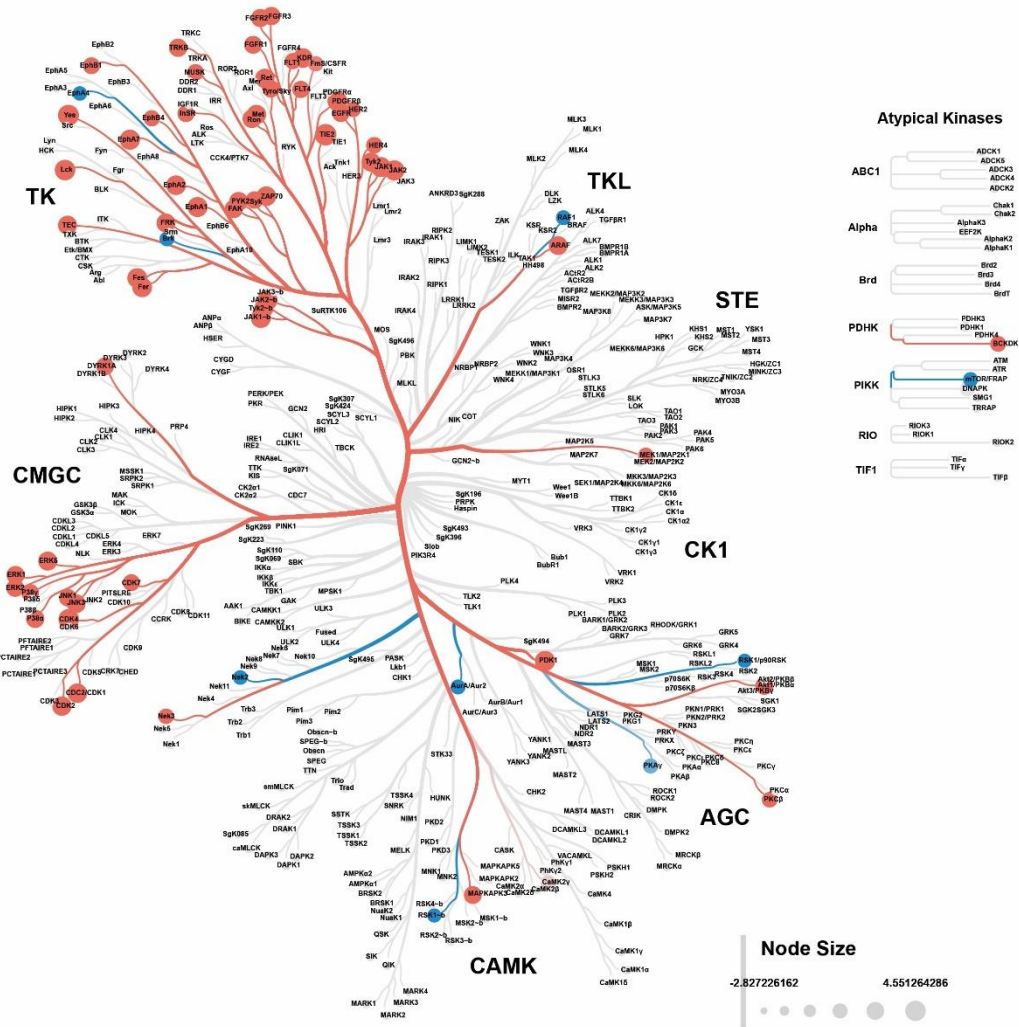


Figure 4.20. A kinome map visualisation of the NDBO (CP-A) response to a ten minute pulse of acidified bile salts. Cells were assayed using PamChip®4 PTK and STK arrays. CP-A BS PTK readings are at biological n=2, all others at biological n=3. Statistical analyses were undertaken using ANOVA with post-hoc Tukey correction for multiple significance testing. Kinases are subdivided by eukaryotic protein kinase (ePK) group. Branch and node colour represent change in kinase activity (red = increase, blue = decrease, grey = no significant change). Node size represents log₂-fold change in kinase activity.

seen in the TKL, CK1, AGC and CAMK ePK groups, as well as activation of the atypical branched chain keto acid dehydrogenase kinase (BCKDK) protein and inactivation of the atypical mTOR protein.

The impact of the significant RTK activation demonstrated in **Fig. 4.20** is clear from **Fig. 4.21.**, which summarises the relationships between non-redundant GO BP terms for the conserved signalling response to acidic bile salts. Here, the role of RTKs in regulating the response to the acidic bile salt stimulus is clear, with a wide variety of impacts on the cell that include many metabolic, signalling and developmental processes (as outlined in **4.4.2.6.**). The extent

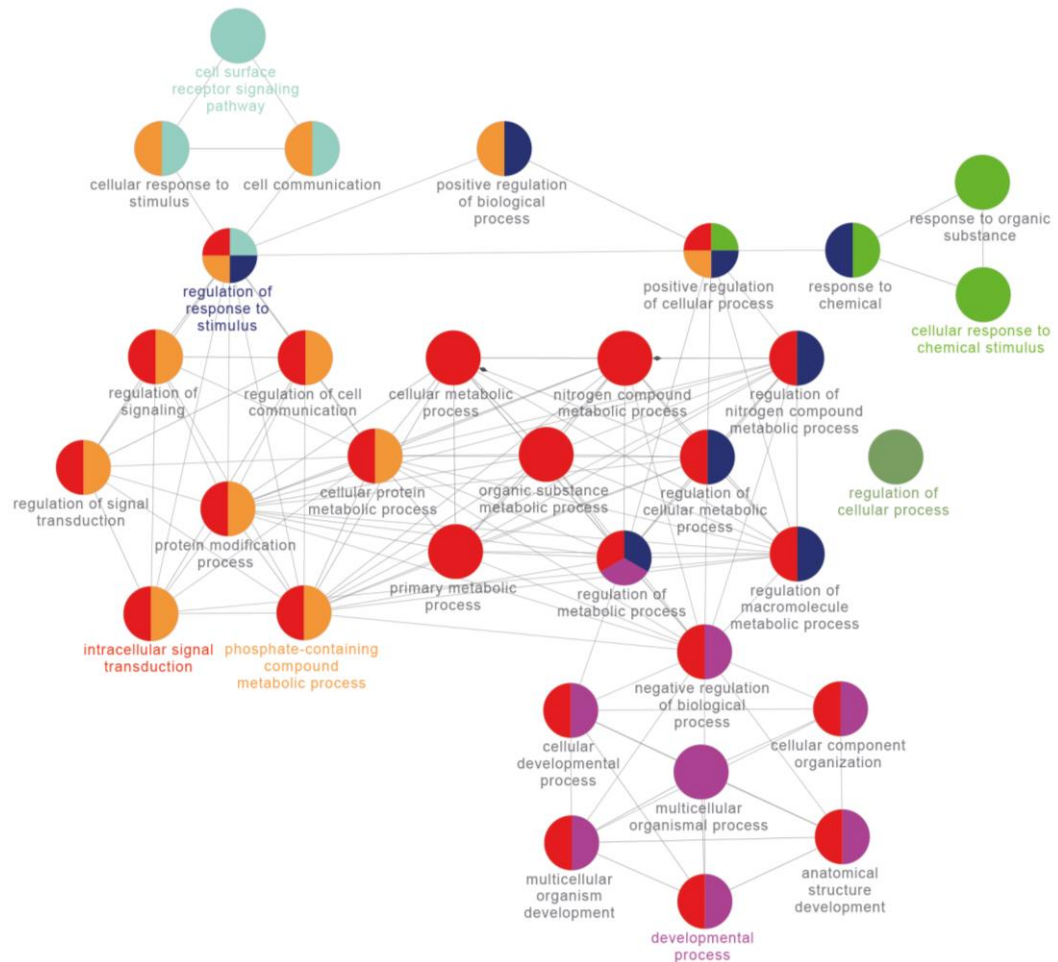


Figure 4.21. Functional grouping of non-redundant over-represented Gene Ontology (GO) Biological Process (BP) terms in peptides that significantly increased in phosphorylation in both NDBO (CP-A) and HGD (CP-B) cells in response to a ten minute pulse of acidic bile salts. Cells were assayed using PamChip®4 PTK and STK arrays. CP-A BS PTK readings are at biological n=2, all others at biological n=3. Statistical analyses were undertaken using ANOVA with post-hoc Tukey correction for multiple significance testing. The above representation was generated using Cytoscape ClueGo, which uses kappa statistics to identify relationships between terms based on the similarity of their associated genes. Dominant GO BP terms are expressed in colour and nodes that group within these share the same colour. Nodes represented by two or more colours are grouped with two or more GO BP terms.

to which these processes are interlinked is also apparent, suggesting that RTKs sit as a mediator of a significant network signalling response.

4.4.2.7.2. Network topology reveals four major signalling hubs that modulate the BO response to acidic bile salts

The interlinked GO BP terms summarised in **Fig. 4.21** suggest that signalling pathways that respond to acidic bile salts are significantly interlinked. This is of considerable interest from a therapeutic perspective given that kinases with high degrees of connectivity offer the most effective drug targets (and may also serve as useful biomarkers).⁽⁵³⁸⁾ We therefore utilised a topological approach to outline the signalling network responding to acidic bile salt

treatment. In brief, proteins for which phosphorylation had significantly increased were analysed for network topology using Cytoscape, and organised into communities using the GLayer clustering algorithm.

As shown in **Fig. 4.22.**, four major signalling hubs were identified, as follows: (i) a cluster led by the EGFR family proteins EGFR, erbB-2 and erbB-4, as well as beta-catenin (CTNNB1); (ii)

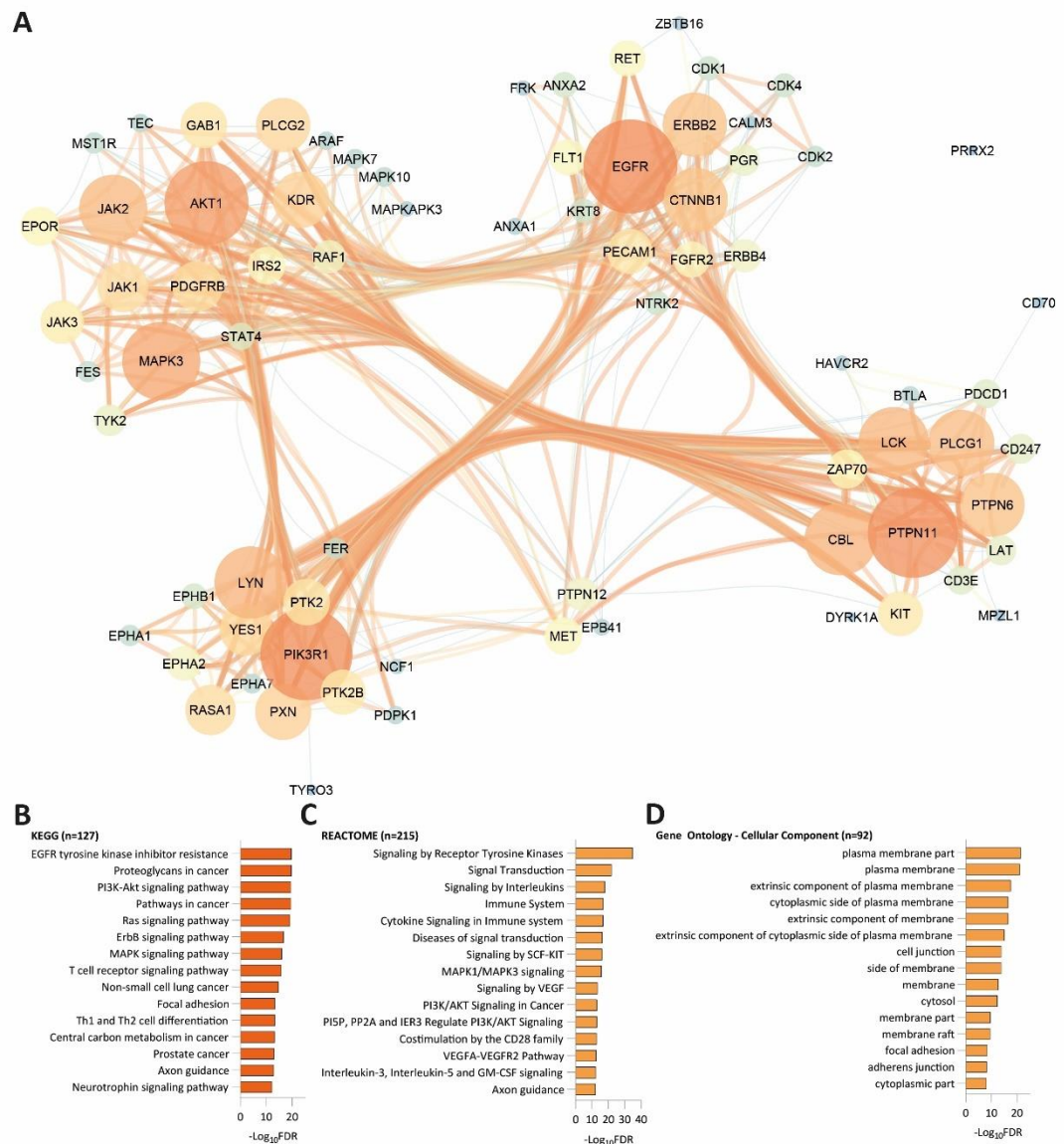


Figure 4.22. Conserved signalling response to acidic bile salts in Barrett's epithelia. Data are shown for peptides which significantly increased in phosphorylation in both NDBO (CP-A) and HGD (CP-B) cells in response to a ten minute exposure to an equimolar 100µM mix of bile salts at pH 4.0. Cells were assayed using PamChip®4 PTK and STK arrays and all readings are at biological n=3. Statistical analyses were undertaken using ANOVA with post-hoc Tukey correction for multiple significance testing. **(A)** Direct protein interaction network generated using Cytoscape StringApp. Edges are coloured by interaction confidence score, with only interactions of 0.4 or greater included. Node colour and size indicate the number of directed edges relating to each node (larger, brighter nodes have more edges). Nodes are clustered using the GLayer algorithm in Cytoscape. **(B,C)** The top 10 most significantly enriched pathways by KEGG and REACTOME analysis. **(D)** The top 10 over-represented Gene Ontology (GO) terms for relating to the cellular components mediating the cellular response to acidic bile salts. FDR: false discovery rate.

a cluster led by the tyrosine-protein phosphatases SHP2 (PTPN11) and SHP1 (PTPN6), as well as PLC γ 1 and the ubiquitin ligase CBL; (iii) a cluster led by phosphatidylinositol 3-kinase (PIK3R1) and the protein tyrosine kinase LYN; and (iv) a cluster led by MAPK, Akt and JAK kinase signalling. It is notable that RTKs feature in – and can therefore modulate signalling from – each of the clusters.

The importance of RTKs to the kinase response to acidic bile salts is supported by KEGG (**Fig. 4.22B**) and REACTOME (**Fig. 4.22C**) enrichment, which both identify an RTK signalling process as their most significantly enriched term. This is somewhat additionally corroborated by enrichment of multiple GO Cellular Component (CC) terms relating to the plasma membrane (**Fig. 4.22D**). Specific RTK responses enriched by KEGG and REACTOME include those relating to EGFR, which supports its placement within a major signalling hub,

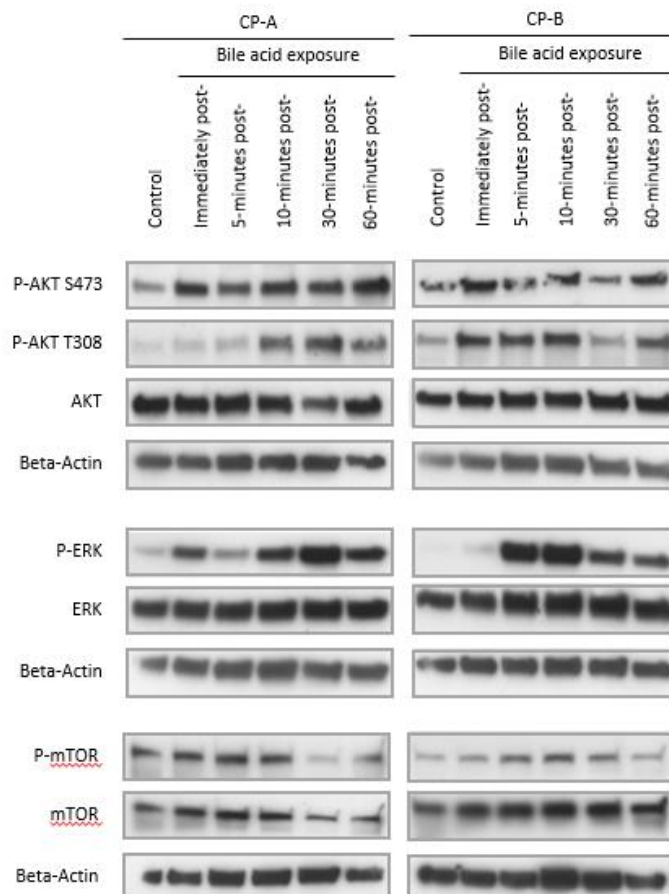


Figure 4.23. Representative immunoblots detailing the change in PI3K/Akt, mTOR and MAPK activity in NDBO CP-A and HGD CP-B cells during the 60 minute period following a 10-minute exposure to acidic bile salts. Cells were exposed for ten minutes to an equimolar 100 μ M mix of bile salts at pH 4.0 and then either immediately lysed for phosphorylation analyses or cultured in neutral serum-free media for up to a period of one hour. Phosphorylated epitopes are shown with the relevant total protein comparators and a β -actin loading control. $n \geq 2$ for all analyses.

and both VEGFR2 and KIT. Downstream of these RTKs, the MAPK and PI3K/Akt pathways are also enriched.

Functional enrichment analysis by KEGG and REACTOME also identified a number of immune pathways. Relating to this, cluster (ii) identifies a number of immune-related proteins, including CD3E, LAT, CD247, PDCD1, CD70, BTLA, HAVCR2 and ZAP70. This suggests a relationship between the immune response to acidic bile salts and the RTK-derived signalling process, seemingly led by EGFR in cluster (i), that mediate cellular kinase activity following acidic bile salt withdrawal. In support of this, and linking with data presented in **Chapter 3**, phosphorylation of the p50 subunit containing NF- κ B p105 subunit significantly increased in HGD CP-B cells in response to acidic bile salts (LFC 0.44; $p=0.01$).

4.4.3. Validation of temporal changes in NDBO (CP-A) and HGD (CP-B) MAPK and PI3K/Akt/mTOR pathway phosphorylation in response to acidic bile salts

In order to validate involvement of the MAPK and PI3K/Akt pathways in the BO response to acidic bile salts, we assessed phosphorylation of ERK as well as Akt at both serine 473 (S473) and threonine (T308). As shown in **Fig. 4.23.**, in both NDBO CP-A and HGD CP-B cells, acidic bile salt treatment resulted in significant upregulation of all three phosphorylated epitopes. There were however differences between the cell lines in the intensity and timing of phosphorylation. Phosphorylation of T308 residues was, for instance, seen later for CP-A than for CP-B cells, whereas an earlier but bimodal change in ERK phosphorylation was seen in CP-A cells.

Despite significant enrichment of these pathways, data from the kinome array suggest that mTOR phosphorylation changes minimally in response to acidic bile salt treatment (LFC -0.11; $p=0.694$ in CP-A and LFC -0.07; $p=0.86$ in CP-B cells). We therefore also assayed mTOR phosphorylation in order to validate this negative finding. As is shown in **Fig. 4.23.**, minimal change and an eventual decrease was seen in mTOR phosphorylation in CP-A cells for up to an hour following acidic bile salt treatment. Phosphorylation of mTOR in CP-B cells also demonstrated little change, with a modest increase in the representative blot shown here likely to be mostly attributable to an increase in total mTOR expression.

4.4.4. An exploration of the relative impact of bile salts on signalling

Activation of the MAPK and PI3K/Akt pathways in response to bile salts delivered at a neutral pH has previously been described in the literature. This is not supported by the data shown

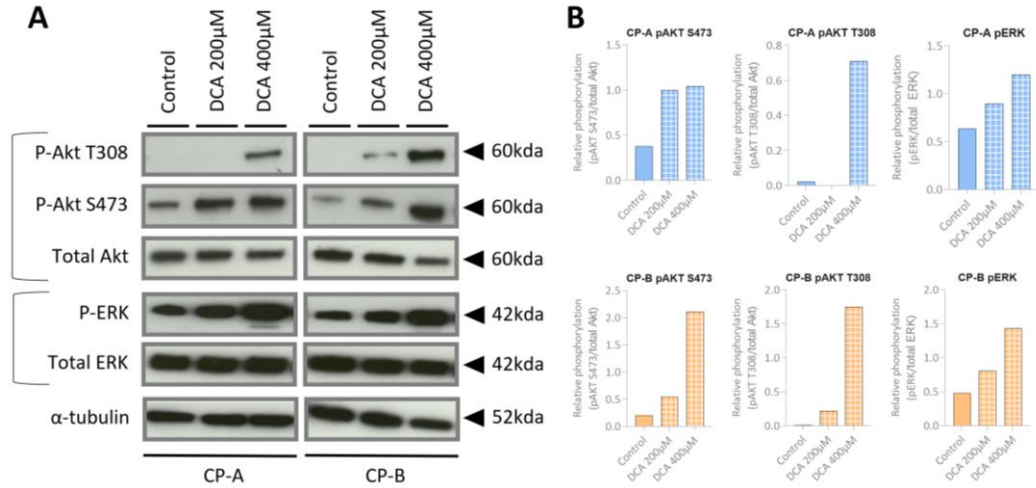


Figure 4.24. An immunoblot demonstrating change in phosphorylation of the S473 and T308 Akt epitopes in response to 24 hours exposure to DCA. Cells were continuously exposed to either vehicle or DCA at a 200µM or 400µM concentration for 24 hours then lysed for determination of total protein concentrations and protein phosphorylation. An immunoblot is presented in (A), with α-tubulin shown as a loading control. Corresponding densitometry is presented in (B). n=1.

here, which may relate to both the lower molar concentration of bile salts used and the relatively short (but more physiological) time period over which they were applied. To determine if this is the case, we continuously exposed NDBO CP-A and HGD CP-B cells to

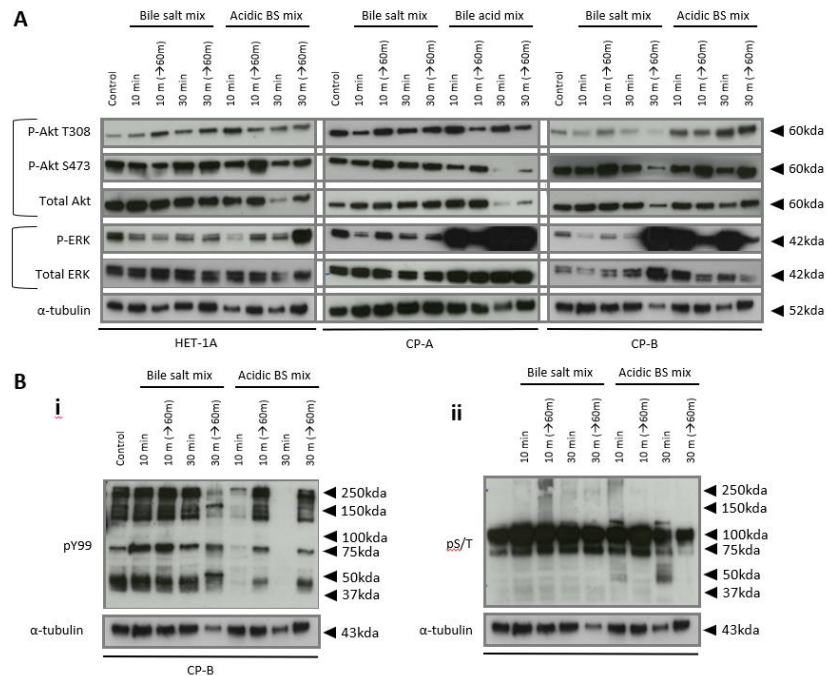


Figure 4.25. Immunoblots detailing changes in the phosphorylation of (A) ERK, and both the S473 and T308 Akt epitopes, and (B) total tyrosine and serine/threonine residues, in response to bile salts at both neutral and acidic pH. Cells were exposed to either vehicle or an equimolar 100µM mix of bile salts at neutral or acidic pH 10 or 30 minutes then either immediately lysed or cultured within serum-free media for a further hour prior to lysis. Relative protein phosphorylation was determined by immunoblot and is compared to total protein levels for the protein from which the phosphorylated epitope derived. A β-actin loading control is also shown. This is representative of multiple n=1.

supraphysiological (200 μ M and 400 μ M) doses of DCA for a period of 24 hours. This reflects an exposure commonly used within the literature and, as shown in **Fig. 4.24.**, results in a dose-dependent increase in phosphorylation of the T308 and S473 Akt epitopes, as well as of ERK phosphorylation.

Next, we evaluated the relative impact of a short (10 minute) and more prolonged, supraphysiological (30 minute), exposure to the more physiological equimolar mix of bile salts used in this work, which was delivered at either neutral or acidic pH. This included assessment of immediate phosphorylation and phosphorylation following a 60 minute period of recovery in neutral, bile-salt free media. As demonstrated in **Fig. 4.25A.**, a 30 minute exposure to bile salts had minimal impact on signalling, much as with a 10 minute exposure. Interestingly, prolonged exposure to acidic bile salts did not substantially change phosphorylation when compared to a ten minute pulse, which is in keeping with a direct suppressive effect of acid, with a process of acid withdrawal promoting signalling. This was explored in more detail in HGD CP-B cells (**Fig. 4.25B**), where prolonged acid suppression can be seen to result in increased suppression of tyrosine signalling but a similar intensity of tyrosine signalling 'recovery'.

4.4.5. Upstream mediators of signalling in response to acid and acidic bile salts

Given that acid withdrawal is the key driver for kinase activity, we sought to determine the potential upstream mediators of this. The presence of ROS within the inflammatory BO environment is well described and is suggested to modulate signalling responses to

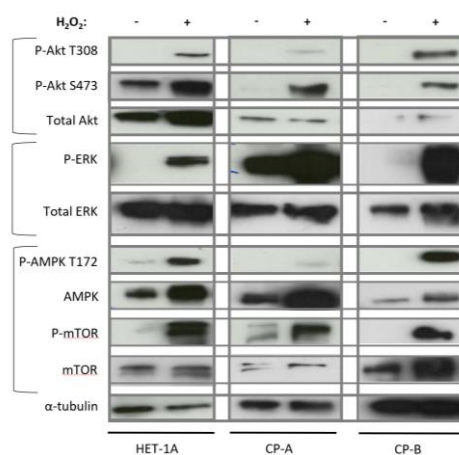


Figure 4.26. Immunoblots detailing changes in the phosphorylation of the S473 and T308 Akt epitopes, ERK, and both AMPK T172 and mTOR in response to a 10 minute pulse of hydrogen peroxide in NSE (Het-1A), NDBO (CP-A) and HGD (CP-B) cells. Cells were exposed to either vehicle or 300 μ M mix hydrogen peroxide for a period of ten minutes followed by protein lysis. Relative protein phosphorylation was determined by immunoblot and is compared to total protein levels for the protein from which the phosphorylated epitope derived. An α -tubulin loading control is also shown. n=2. H₂O₂: hydrogen peroxide.

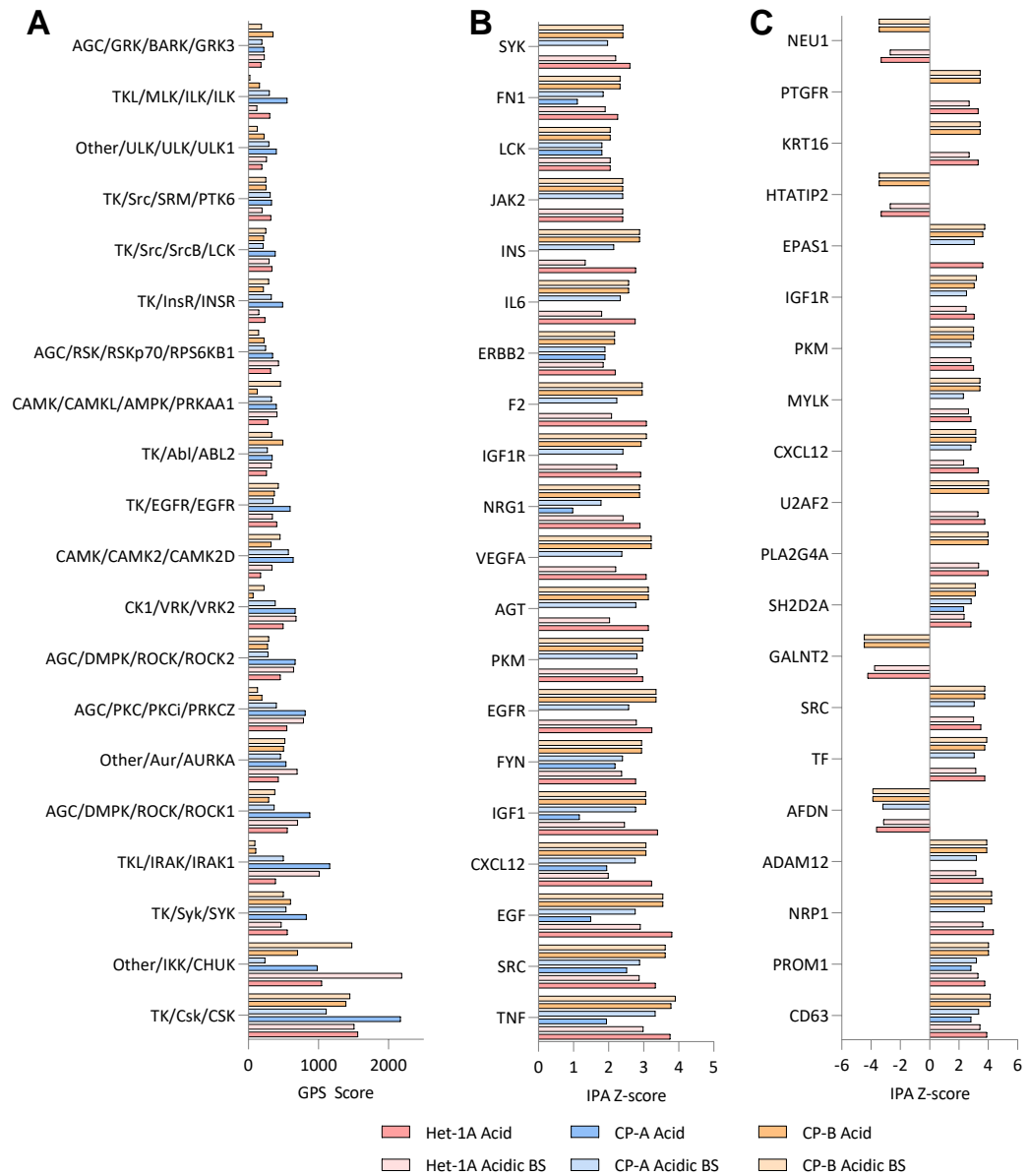


Figure 4.27. Corresponding upstream mediators of the NSE (Het-1A), NDBO (CP-A) and HGD (CP-B) kinomic response to a ten-minute exposure of acid or acidified bile salts (BS). All cells were treated with the same equimolar 100 μ M mix of bile salts at pH 4.0, or with acidified media at pH 4.0. Cells were assayed using PamChip[®]4 PTK and STK arrays and all readings are at biological n=3. Statistical analyses were undertaken using ANOVA with post-hoc Tukey correction for multiple significance testing. **(A)** Cognate protein kinases predicted by Group-Based Prediction system. **(B)** Upstream regulators predicted by Ingenuity Upstream Regulator Analysis in Ingenuity Pathway Analysis (IPA). **(C)** Causal Network Analysis by IPA, detailing potential upstream regulators that are not directly connected to targets within the studied dataset.

acid.(115) We therefore sought to determine whether similar signalling responses would be seen following ROS exposure. **Fig. 4.26** suggests not, with a ten minute exposure to the ROS-causative agent hydrogen peroxide causing an immediate upregulation of PI3K/Akt signalling, as well as activation of AMPK/mTOR autophagy-promoting signalling that was not seen in the kinase array or the immunoblots shown above. Further, and as will be outlined

in **Chapter 5**, there is no evidence for an increase in ROS following ten minutes of acid treatment.

We therefore utilised complementary bioinformatic programmes (IPA and GPS, as outlined in **4.3.3.4.4.**) to respectively predict upstream signalling regulators and, specifically cognate kinases, for the kinomic response profiled in this work. In keeping with the outputs of the functional enrichment, predicted regulators (**Fig. 4.27**) included a multitude of pro-inflammatory molecules (such as CHUK, IRAK1, TNF, CCL12, CD63) as well as both a number of RTKs (EGFR, INSR, ERBB2, IGF1R), their ligands (VEGFA, IGF1, EGF) and their downstream mediators (FYN, SRC, LCK, CSK, SYK).

4.5. Discussion

In **Chapter 3**, exposure to a ten minute pulse of acidic bile salts resulted in a DEG response that enriched for processes relating to EMT, migration and inflammation. Further work described in **Chapter 3** demonstrated that acidic bile salts cause a small degree of rapid cell death that is compensated for by a proliferative response that results in a stable overall cell number. In addition, a number of transcription factors were revealed as potential mediators of the cellular response to acidic bile salts, including NF- κ B, KLF5, AP1 and FOXM1. Enrichment of the DEGs also highlighted a potential upstream contribution from MAPK, PI3K/Akt and RTK-derived signalling processes. However, despite these inferences, this work did not specifically delineate the pathways that are activated in response to acidic bile salt exposure, nor the cellular processes that these drive independently of changes in genetic expression. The relative contribution made by an acidic environment as opposed to bile salts was also not determined by this work, nor was any potential change in the cellular response to microenvironmental stress between different stages of BO.

We therefore sought to determine the relative impact of bile salts, both at neutral and acidic pH, as well as acid alone, on the kinome of cells representing NSE (or at least, as outlined in **Chapter 3**, a dysplastic squamous phenotype), NDBO and HGD. We also sought to compare the basal signalling phenotype of these cells. Pertinently, prior to this work there has been only one previous systematic appraisal of kinome signalling in BO, which is a historical study that analysed the basal signalling of a small number of samples using a relatively primitive kinase array.⁽³²⁵⁾ Further, previous analyses of the impact of bile salts and acid have focussed on a small number of target molecules and have used varying concentrations of bile salts and acid (**Table 3.1.**)

Overall, the work outlined here demonstrates that the basal kinome of cell lines representing NSE (Het-1A), NDBO (CP-A) and HGD (CP-B) varies substantially. Surprisingly, NDBO CP-A cells are more kinase active than their HGD CP-B counterparts. This relatively elevated activity is associated with enrichment for immune processes, migratory terms and RTK signalling within CP-A cells. In contrast, the contested Het-1A cell line was enriched for terms relating to the circulatory system. Importantly, when the BO CP-A and CP-B cells were compared, CP-A enriched both for MAPK and PI3K/Akt signalling processes, for pathways associated with the development of cancer, and for signalling derived from EGFR family members.

We also show that acid suppresses tyrosine kinase signalling, but that acid withdrawal (i.e. a normalisation in extracellular pH) results in a rapid induction in tyrosine kinase activity and a subsequent increase in serine/threonine kinase activity. These were mapped using a kinase array, which was able to monitor in real-time the change in PTK, as well as STK, signalling as the cellular pH returned to neutral. This revealed that the intensity (i.e. amplitude) of the gain in the tyrosine kinase signal is greatest for NDBO CP-A cells and broadly equivalent for NSE Het-1A and HGD CP-B cells. Bile salts, in contrast, result in minimal changes in PTK or STK activity when used alone. They do however modulate the acid signal when delivered as acidic bile salts, though not to a degree that alters the cellular functions driven by the dominant acid response. The cellular response to acid is nevertheless variable across cell lines, though a consensus response to acid and therefore acidic bile salts is demonstrable across the BO cell lines.

When characterised, this shared cellular response to acid can be separated in to four separate signalling hubs, which are dominated by RTKs and in particular EGFR and its related family members. This, and the enrichment for PI3K/Akt and MAPK signalling, corroborates two key upstream predictions made on the basis of RNA-seq data in **Chapter 3**. Importantly, this signalling network is dependent on, and modulated by, a number of other RTKs, such that the outputs are likely to be contingent on the activity of the RTK network as a whole. Further, a signalling hub that interacts closely with the EGFR-dominant signalling group features a number of pro-inflammatory mediators, which raises the exciting possibility of acid-responsive RTKs acting to modulate the pro-inflammatory signalling that is known to define BO dysplastic progression. The demonstration within the kinase array that NF- κ B is activated in HGD CP-B cells in the acute response to acidic bile salts, and evidence from **Chapter 3** of increased NF- κ B binding in response to acidic bile salts, seems to support this

suggestion. The relevance of these multiple conclusions, and their relationship to current literature, is outlined in full here.

Firstly, a previous comparison of patient kinome profiles by *Van Baal et al.* suggested that NDBO has similarities with squamous epithelium but that NDBO tissue demonstrated lower Src protein family activity than was seen in NSE.(325) This is surprising given the predominance of Src-derived pathways in the NDBO CP-A cells described here, though the HGD CP-B lines broadly fit the same pattern. It is of course important to recall that the 'NSE' Het-1A cells used here demonstrate a number of dysplastic features, though these would broadly be expected to increase their relative signalling activity. EGFR signalling was also found to be lower in patient NDBO samples than in NSE.(325) In keeping with the findings outlined here, it was nevertheless raised when compared to gastric cardia, and EGF signalling was enriched. It is, however, challenging to directly compare these findings with those presented in this work given the use of a single cell line here, and the use of whole patient biopsies in the existing study. These are likely to incorporate a significant degree of stromal and inflammatory tissue, and as *Van Baal* and colleagues outlined, 'the direct evaluation of epithelial cells...' – which has been undertaken in this study - '...would be of interest'. Further, there was no evaluation in *Van Baal* and colleague's work of the impact on signalling of gastric refluxate contents. It is nevertheless reassuring that significant enrichment of EGF-led processes was seen both in the existing analysis of patient samples, and in the work described here.

It is also of note that in addition to EGFR-signalling pathways, when compared with HGD CP-B cells the NDBO CP-A cell line enriched for neurotrophin signalling processes. There are limited data on the neurotrophin tyrosine kinase receptors (NTRKs) in BO but they have been implicated in the development of colorectal cancers, albeit after the development of gene fusion events.(539) Similar fusions are not commonly seen in BO but there is very recent evidence that NTRK-led signalling processes contribute to early dysplastic processes in the basal crypts of gastrointestinal epithelia.(540,541) It is therefore possible that these drive early dysplastic processes in BO.

Secondly, whilst the overall impact of bile salts is modest, ten minutes exposure to the equimolar bile salt mix used in this study did result in upregulation of PLC γ 1 activity in NSE cells. A PLC-dependent pathway has previously been implicated in the progression of BO but has not been extensively explored in the context of NSE and the risk of transdifferentiation.(542) However, PLC activity is known to be inhibited by aspirin.(543)

This drug notably reduces the risk of the development of multiple gastrointestinal cancers, including those of the oesophagus.(544) It has also recently been shown, through the AspECT trial, to prevent deaths and HGD in BO.(101) It is then possible that the chemopreventative action of aspirin is at least in part attributable to a reduction in bile salt-induced increases in PLC γ 1 activity within NSE cells with the potential to transdifferentiate. It is, however, unclear what the relative importance of this would be alongside the significant role aspirin plays in reducing inflammation propagated by the COX enzymes.(397,422) It otherwise appears that bile salts play a very limited role in propagating signalling during short periods of exposure. This is in contrast to prolonged bile salt exposures, which are described within the literature as resulting in significant upregulation of MAPK and PI3K/Akt activity; a finding we replicate here. Despite this, manometry and continuous oesophageal sampling studies have shown no evidence for exposures as long as those required to induce MAPK and PI3K/Akt activity here.(119,471,473) Instead, it is likely that bile salts induce harm through direct genotoxicity.(190)

Thirdly, and accordingly, it is clear that acid is the main driver for changes in cellular kinase activity. In particular, we show that direct acid exposure results in a reduction in tyrosine phosphorylation, with longer exposures to acid seemingly resulting in greater suppression of tyrosine phosphorylation. There are, to our knowledge, no previous reports demonstrating a suppression in tyrosine kinase activity in response to acid exposure. It is even more remarkable that this occurs in the presence of minimal changes in serine/threonine phosphorylation. This may indicate activation of a tyrosine-specific phosphatase that has not been identified through this work. This appears to be inactivated once normal extracellular pH has returned, with a predominantly growth factor-driven process then driving the diverse mitogenic, pro-inflammatory pathways that have been outlined here, and that are also known to characterise progressive BO (outlined in **1.1.2.5**).

Crucially, this finding would in theory mean that it is the change in extracellular pH, rather than the direct impact of acid itself, that would be deleterious for patients with BO. As such, the overall time over which patients with BO are exposed to reflux is likely to be less important than the number of reflux episodes they are exposed to. This is supported by clinical data. In a prospective case-control study of 256 patients with Barrett's and 229 patients with non-erosive GORD, *Avidan et al.* demonstrated that the number of reflux episodes was the only reflux-related factor that associated with increased BO severity.(545) Intriguingly, the authors concluded that, in light of a lack of an association between disease severity and factors such as oesophageal pH and total acid-exposure time, their data

highlighted a role for extra-acid factors in driving progression. This perhaps ignores the possibility – demonstrated in the data reported here - that it is the change in pH, rather than the lowered pH itself, that is a risk factor for progression.

Further clinical support for these data, and for acid exposure being of greater importance to dysplastic progression than bile salts, is provided by the AspECT trial. This confirmed that PPI therapy, which both normalises and reduces fluctuations in pH, results in reduced progression to HGD amongst patients with NDBO.(101) It is also of note that an 'acid pocket' can remain in the proximal stomach despite PPI therapy, and that the half-life (around 90-120 minutes in serum) and duration of effect of PPI therapy (6-18 hours) is such that even patients on maximum acid-suppression therapy are likely to be exposed to fluctuations in pH.(546) The signalling resulting from 'acid withdrawal' may therefore explain why patients on PPI therapy, and who are less exposed to acid, still develop BO.

Fourthly, the response to acid withdrawal characterised here was of greater intensity in NDBO CP-A cells than in NSE Het-1A and HGD CP-B cells. However, similar pathways and processes were driven by acid withdrawal in NSE Het-1A and HGD CP-B cells. It is possible that the increased intensity of signalling seen in NDBO CP-A cells results from greater expression of RTKs implicated in the acid withdrawal response. This would mean that all cells demonstrate a similar response to acid withdrawal, but that the intensity of this, and therefore potentially the extent to which it impacts on cell phenotype, is shaped by overexpression of acid-responsive RTKs. This might include RTK-control of inflammatory signalling, as supported by the increased NF- κ B component phosphorylation identified in response to acidic bile salts in the HGD CP-B cells described here.

This theory may not, however, entirely address why a signalling mechanism conserved across all stages of BO and NSE would be implicated in BO dysplastic progression. It is tempting to suggest that the NSE cells, which appear to represent a dysplastic squamous population, simply do not reflect the normal cellular response of NSE tissue. However, given the sheer extent of the similarities in the signalling processes established across all three cell lines, this seems unlikely. Instead, it is possible that the acid withdrawal-signalling process identified here augments other processes involved in BO progression. This may for instance include the direct genotoxicity of bile salts, with this and the enhanced activity of mitogenic pathways from acid withdrawal coupling together to increase cellular instability.(190) It also follows that the pro-inflammatory changes established in direct response to acid withdrawal

may modulate stromal inflammation, and that this may impact differently on BO and NSE tissue.(212)

As well as these pro-inflammatory processes, the acidic bile salt kinase response was enriched for cell death and migratory terms related to EMT. The former supports the data outlined in **3.4.2.1.**, where moderate early cell death was seen within two hours of acidic bile salt exposure. Given a strong concomitant pro-proliferative signature amongst DEGs (**3.4.4.2.**), it appears that a direct signalling response results in cell death, followed by a pro-proliferative transcriptional response that results in the cellular population remaining stable in number. It is not clear why some and not all cells would die on the basis of the data presented here, but it is possible that those at the edge of a cellular sheet are more susceptible to pH change.

Finally, it is of interest that acidic bile salts resulted in a significant reduction in the activity of CFTR and AR within NDBO CP-A cells. The genes encoding for both of these proteins increased in response to the same stressor when assessed by RNA-seq. The increase in expression could therefore be seen as a compensatory response to a loss of activity but it is unclear what impact these molecules are having on cellular processes (explored in **5.1.**).

4.5.1. Strengths & limitations

This work uses a kinase activity assay to deliver a high-throughput analysis of the impact on tyrosine kinase and serine/threonine kinase signalling of exposure to three extracellular conditions applied to three cell lines. As such, it provides a sensitive, statistically-competent model from which to identify the relative impact of bile salts, acid and acidic bile salts. It additionally allows for the kinetic analysis of PTK signalling, but unfortunately not STK phosphorylation events. Reassuringly, a number of processes and pathways enriched by this kinome analysis in NDBO CP-A cells exposed to acidic bile salts correlate with those predicted based on the differential expression of genes in CP-A cells following exposure to the same stressor (as outlined in **Chapter 3**). Through directly analysing cellular signalling events, the kinase activity assay also provides an advantage over solely analysing differential gene expression, which is a more common approach to analysing cellular behaviour, in facilitating a more comprehensive characterisation of the upstream mediators of cellular signalling. This was strengthened still further in this analysis by the concomitant use of a specific cognate kinase prediction system, GPS, and IPA. Specific phosphorylated motifs were used as inputs for both bioinformatic approaches, providing a more specific dataset against which to query databases than simply inputting protein names.

There are, however, a number of limitations to the kinase assay approach used here. Firstly, phosphatase activity was not assessed and kinase activity was determined in the presence of phosphatase inhibitors. This may therefore interpret a greater level of kinase activity than would normally be exhibited by a cell. Secondly, the kinase activity assay is restricted to tyrosine and serine/threonine signalling. This accounts for a majority of cellular signalling events but, unlike alternative approaches such as phosphoproteomics, the kinase activity assay here provides a less global overview of cellular phosphorylation events, including those relating to lipids. Despite this, we have validated the key pathways implicated by the kinase activity assay using more established immunoblotting, which indicates that the data it provides can be interpreted with a relatively high degree of confidence. Finally, though the kinase activity does provide an opportunity to identify upstream mediators of signalling, their relative importance remains uncertain. This is explored in further detail in **Chapter 5**.

4.6. Conclusions & further work

We demonstrate that acid, rather than bile salts, drives cellular signalling in response to the components of gastric refluxate in both normal squamous epithelial and Barrett's cells. Remarkably, direct cellular exposure to acid results in a significant reduction in tyrosine phosphorylation, which is reversed upon acid withdrawal. The ensuing tyrosine kinase hyperactivity drives a plethora of pro-inflammatory, pro-migratory signalling processes and is substantially mediated by a network RTK response. These are enriched for MAPK and PI3K/Akt signalling pathways, reflecting considerable serine/threonine kinase activity. There is in addition evidence within BO cells of direct phosphorylation of components of NF- κ B, which was implicated in the regulomic response to acidic bile salts in **Chapter 3**.

Whilst MAPK and PI3K/Akt-dominant signalling forms the mainstay of a consensus response to acid withdrawal in both NSE and Barrett's, in the assay undertaken here the magnitude of the increase in intensity of the acid withdrawal signal was significantly greater for NDBO CP-A than both NSE Het-1A and HGD CP-B cells. NDBO CP-A cells additionally demonstrated a higher degree of basal activity than HGD CP-B cells. EGFR signalling was enriched both following acid and acidic bile salt treatment, which in keeping with findings in **Chapter 3**, and when comparing NDBO CP-A cells to their HGD CP-B equivalents. A number of other RTKs are implicated in both contexts, including Erb-B2 and the NTRKs. It is, however, unclear to what extent one or more of these maintain basal and stress-responsive signalling at different stages of Barrett's dysplastic progression, and in basal and stressed conditions. This will be explored in further detail in **Chapter 5**.

Chapter 5

Delineating the RTK-mediated Response to Micro-Environmental Stress in Barrett's Oesophagus

5.1. Background

5.1.1. Overview

In **Chapter 3**, RTKs were identified as key mediators of the cellular transcriptomic response to microenvironmental stressors in BO. This was supported by work undertaken in **Chapter 4**, which identified RTKs as determining kinase activity in response to cellular exposure to an acidic pH. Prior to this work, the evidence for a role for RTKs in the BO cellular response to microenvironmental stressors, or in propagating BO dysplastic progression, has been limited. Co-amplification of RTKs is nevertheless described as 'almost ubiquitous' in OAC, and there is evidence of a correlation between BO dysplastic progression and the protein overexpression of a number of RTKs.(236,430)

Emerging evidence from *in vitro* analyses suggests that changes in RTK expression during BO progression may be mirrored by an increase in their activity, and that this may be instigated by microenvironmental stressors. This is supported by the recognition of a role in the BO kinomic response to acid-stress for the MAPK and PI3K/AKT pathways; both of which are downstream of RTKs.(297,525) Despite this, a majority of RTK-focussed studies evaluate genomic amplification or changes in protein overexpression, with few evaluating the mechanisms through which RTKs interact with microenvironmental stressors and contribute to BO dysplastic progression.(297,430) They are in addition limited by a narrow and somewhat biased focus on a handful of better characterised RTKs.(430,431)

This work focusses on the contribution made by RTKs both to the BO cellular response to microenvironmental stressors, and to the development and progression of dysplasia.

Class I: EGFR receptor family		Class VII: NGF receptor family		Class XI: TIE receptor family	
EGFR (erbB-1)	[EGFR]	TRKA (NGFR, NTRK1)	[NTRK1]	TIE (TIE1)	[TIE1]
erbB-2 (HER2)	[ERBB2]	TRKB (BDNF, NTRK2)	[NTRK2]	TEK (TIE2)	[TEK]
erbB-3 (HER3)	[ERBB3]	TRKC (NTRK3)	[NTRK3]	Class XII: RYK receptor family	
erbB-4 (HER4)	[ERBB4]	Class VIII: HGF receptor family		RYK	[RYK]
Class II: INSR receptor family		c-Met (HGFR/SFR)	[MET]	Class XIII: DDR receptor family	
INSR (CD220)	[INSR]	MSPR (RON, PTK8)	[MST1R]	DDR1 (CAK, HGK2)	[DDR1]
IGF1R (CD221)	[IGF1R]	Class IX: EPH receptor family		DDR2 (NTRK3, TYRO10)	[DDR2]
IRR	[INSRR]	EphA1 (EPH TK 1)	[EPHA1]	Class XIV: RET receptor family	
Class III: PDGFR receptor family		EphA2 (ECK)	[EPHA2]	c-Ret (CDHF12)	[RET]
PDGFR α	[PDGFRA]	EphA3 (HEK, TYRO4)	[EPHA3]	Class XV: ROS receptor family	
PDGFR β	[PDGFRB]	EPHA4 (TYRO1, SEK)	[EPHA4]	c-Ros (MCF3)	[ROS1]
CSF-1R (MCSFR)	[CSF1R]	EPHA5 (BSK, EHK1)	[EPHA5]	Class XVI: LTK receptor family	
SCFR (c-Kit)	[KIT]	EPHA6 (EHK2, hEK12)	[EPHA6]	LTKR (TYK1)	[LTK]
FLT3 (FLK2/STK1)	[FLT3]	EPHA7 (EHK3, hEK11)	[EPHA7]	ALK	[ALK]
Class IV: VEGFR receptor family		EPHA8 (EK3, hEK3)	[EPHA8]	Class XVII: ROR receptor family	
VEGFR1 (FLT1)	[FLT1]	EPHA10	[EPHA10]	ROR1 (NTRKR1)	[ROR1]
VEGFR2 (FLK1, KDR)	[KDR]	EPHB1 (ELK, hEK6)	[EPHB1]	ROR2 (NTRKR2)	[ROR2]
VEGFR3 (FLT4)	[FLT4]	EPHB2 (hEK5, TYRO5)	[EPHB2]	Class XVIII: MuSK receptor family	
Class V: FGFR receptor family		EPHB3 (hEK2, TYRO6)	[EPHB3]	MuSK	[MUSK]
FGFR1 (FLT2)	[FGFR1]	EPHB4 (TYRO11)	[EPHB4]	Class XIX: LMR receptor family	
FGFR2 (KGFR)	[FGFR2]	EPHB6 (HEP, EPH6)	[EPHB6]	LMTK1 (AATYK)	[AATK]
FGFR3	[FGFR3]	Class X: AXL receptor family		LMTK2 (AATYK2, CPRK)	[LMTK2]
FGFR4	[FGFR4]	AXL (tyrosine PK UFO)	[AXL]	LMTK3	[LMTK3]
Class VI: CCK receptor family		MER (c-Mer, MerTK)	[MERTK]	Class XX: STYK1 receptor family	
PTK7 (CCK4)	[PTK7]	TYRO3 (BYK, DTK)	[TYRO3]	STYK1 (NOK)	[STYK1]

Table 5.1. A list of RTKs encoded by the human genome, by receptor subfamily.(525) Recommended protein names are presented on the left hand side of each column, with commonly used alternative names listed in rounded brackets. Gene names are shown in square brackets.

5.1.2. Cell signalling by RTKs

The human genome encodes 58 RTKs.(525) These highly-conserved, high-affinity cell surface single-pass transmembrane receptors transduce signals from the extracellular environment to the cytoplasm; mediating a variety of cellular processes that include proliferation, survival, angiogenesis, metabolism, differentiation and migration. They are together characterised by the presence of an extracellular ligand-binding domain, a transmembrane helix, and a cytoplasmic protein tyrosine kinase (PTK) domain that is flanked by juxtamembranous regulatory regions. Twenty subfamilies are recognised (**Table 5.1**), each of which is characterised by a considerably different extracellular domain sequence as well as less dramatic changes to the cytoplasmic RTK tail.

RTK activation classically results from the binding of cognate ligand, stabilised as a dimer, to the extracellular RTK ligand binding domain. This results in the formation of a stable receptor homo- or hetero- dimer in which cytoplasmic PTK domains are juxtaposed, causing *trans*-autophosphorylation of tyrosine residues in the RTK activation loop and other membranous regions. The RTK undergoes conformational change as a result and stabilises in an active

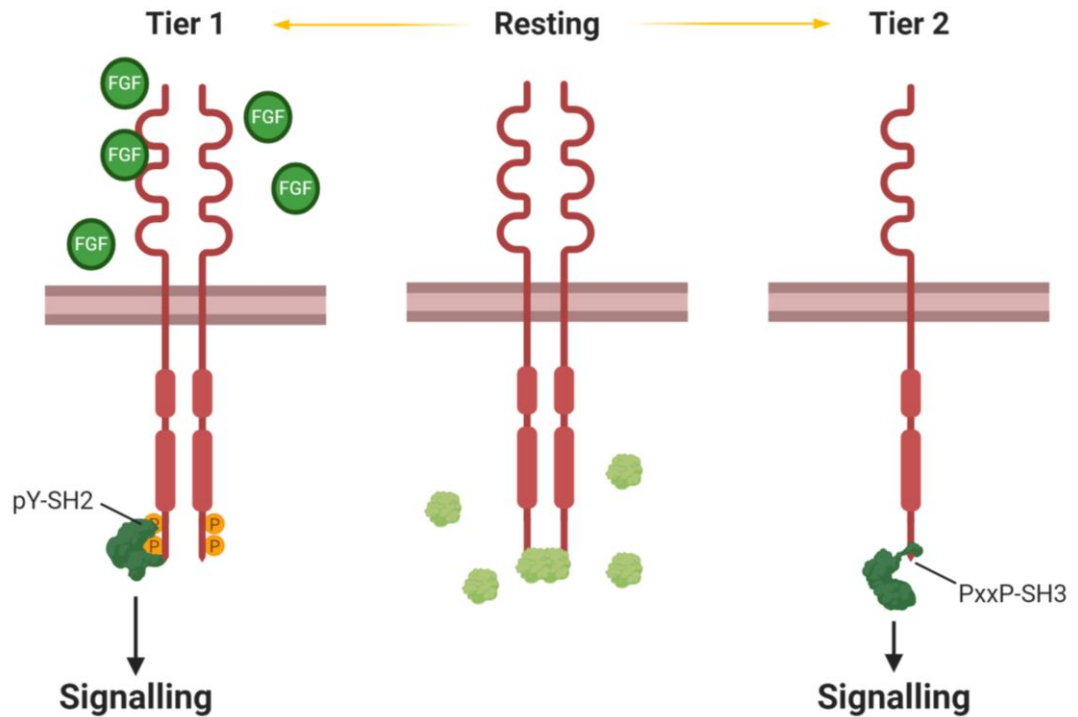


Figure 5.1. A schematic demonstrating mechanisms of RTK activation. RTKs, illustrated here in red (with FGFR2 used as an exemplar), exist as monomers, homodimers or heterodimers in the plasma membrane of a cell. When not bound by ligand many RTKs form heterotetramers with two molecules of GRB2 (shown in light green).(547) Ligand binding results in transphosphorylation of tyrosine residues in the cytoplasmic tail of the RTK, providing a docking site for SH2 and PTB domains of intracellular proteins (shown in dark green) that in turn become activated. In the absence of ligand, a subset of RTKs with proline-rich motifs within their cytoplasmic tail region appear to interact with SH3-domain containing intracellular proteins (shown in dark green), instigating signalling as a result.(532,533) FGF: fibroblast growth factor.

state, with cytoplasmic pTyr residues forming a docking site for the binding and subsequent SH2 or PTB-domain mediated activation of downstream signalling proteins. This pTyr-transduced 'Tier 1' RTK-derived signalling is supplemented by a second tier of signalling mediated by non-catalytic RTKs such as ErbB3, or by non-pTyr signalling instigated by RTKs that nevertheless do have catalytic capacity. A pertinent example of this tier 2 signalling is the recent recognition that in the absence of ligand binding and subsequent tyrosine phosphorylation, proline-rich (PxxP) motifs in the cytoplasmic tail region of a subset of RTKs act as docking sites for SH3-domain mediated binding and subsequent activation of intracellular proteins.(532,533)

Dysregulation of RTKs is a frequent feature of a number of cancers.(525,548) This commonly results from the presence of mutations that render RTKs constitutively active, an increase in ligand availability or processes such as genomic amplification and copy number variation that result in an increase in RTK protein expression.(548) Monoclonal antibodies specific to the extracellular region of RTKs or small molecule tyrosine kinase inhibitors are frequently used as methods for abrogating RTK signalling. This includes in OAC, in which therapies

directed against EGFR, ErbB2, the VEGFRs and c-Met have been trialled in various phase I-III studies, including in combination with radiotherapy.(2) Many of these have however been disappointing, which is at least in part attributed to frequent co-amplification of RTKs, which appears to also feature in BO.(236,430)

The impact of receptor co-activation in BO points to the considerable cross-talk between RTKs, which across all cells converge on a relatively limited, and highly-conserved, set of processes that are characterised by their redundancy.(525) The gain or loss of signalling from a single RTK can nevertheless considerably impact on cell phenotype and does confer some signalling specificity. It is however of note that as a consequence of the hundreds of interactions resulting from the activation of a single RTK, it has not proven possible to undertake comprehensive deterministic modelling of the reactions induced by individual RTKs.(525,549)

5.1.3. RTKs in Barrett's and OAC

5.1.3.1. Expression

Genomic amplification of RTKs is common in OAC and is seen in over half of all tumours. The most frequently amplified RTKs are *EGFR*, *ERBB2*, *FGFR2* and *MET*; with co-amplification of their downstream pathways also seen.(236) These copy number variations translate to an increase in protein expression, as has also been demonstrated in a number of clinicopathologic series that incorporate samples of BO.(236,430,431)

A summary of RTKs known to be overexpressed at the protein level in BO and OAC is provided in **Table 5.2**. In a recent targeted analysis, Paterson and colleagues demonstrated protein overexpression of at least one of EGFR, erbB-2, erbB-3, FGFR2 or c-Met in 51% of OAC cases, whilst 11% overexpressed more than one of these RTKs.(430) In contrast, 70% of all BO segments demonstrated overexpression of one of the same array of RTKs; with overexpression featuring in 25% of NDBO cases but increasing to over 60% in LGD and HGD.(430) Providing further evidence for protein co-overexpression of RTKs, Gockel and colleagues published a series in which 94% of OACs expressed at least four of the six RTKs (EGFR, VEGFRs 1-3, PDGFR α , PDGFR β) they studied.(431) Within these broad patterns, there are nuances in the disease stages at which RTKs are both over-expressed and co-expressed.

Protein overexpression of EGFR appears to occur late, for instance, with significant increases seen across multiple series between LGD and HGD, and from HGD to OAC.(430,550–552) Similarly, *EGFR* amplification and copy number variation is recognised to be a late feature of

RTK	Protein overexpression by stage of disease progression						Refs.
	NSE	Barrett's	NDBO	LGD	HGD	OAC	
Class I: EGFR family							
EGFR	-	5-14%	1%	3-5%	4-35%	10-97%	(430,431,550,551)
erbB-2	0%	3-19%	3-15%	11-41%	5-41%	0-54%	(330,430,551,553-555)
erbB-3	-	6-33%	2%	4-9%	5-47%	0.3-67%	(430,551)
Class II: INSR family							
IGF1R	0%	-	23-100%	52%	0-64%	47-82%	(556-559)
Class III: PDGFR family							
PDGFR α	-	-	-	-	-	91%	(431)
PDGFR β	-	-	-	-	-	85%	(431)
Class IV: VEGFR family							
VEGFR1	-	-	-	-	-	97%	(431)
VEGFR2	-	-	-	-	-	94%	(431)
VEGFR3	-	-	-	-	-	93%	(431)
Class V: FGFR family							
FGFR2	0%	63%	23%	49%	32-55%	34-65%	(430)
Class XVIII: HGF family							
c-MET	-	10%	4-40%	8-37%	8-100%	9-100%	(430,551,560,561)
Class X: AXL family							
AXL	-	-	-	-	-	55%	(562)

Table 5.2. A list of RTKs for which protein overexpression in NSE, BO or OAC has previously been reported, grouped by receptor subfamily. The range of protein overexpression as outlined in the current literature is shown, though it is important to note that some of this variation may result from the use of different experimental methods across studies.

BO dysplastic progression and is thought to occur after *TP53* loss.(563,564) The protein expression of EGFR is nevertheless higher at all stages of BO than it is in NSE and in at least one series protein expression correlates poorly with levels of *EGFR* genomic amplification.(565) Interestingly, acid treatment and both neutral and acidic bile salts are reported to drive an increase in EGFR mRNA expression in NSE and BO cells *in vitro*.(550,566) EGFR expression in OAC is also reported to be driven by the inflammatory mediator phospholipase A2, and in a rat model of reflux was higher following PPI treatment.(567,568) OACs that arise from cardiac-type mucosa (i.e. via a non-SIM dysplastic pathway) additionally appear to be more likely to feature EGFR overexpression.(569)

The EGFR family member erbB-2 is similarly present in BO at a higher protein level than in NSE.(410,430,553,554,570) In the Paterson series, half of all patients with erbB2-overexpressed OAC had overexpression prior to HGD.(430) This and multiple other series have BO demonstrated an increase in the protein expression of erbB-2 with the onset of dysplasia, and as dysplasia progresses towards OAC.(553,554,568,570-575) There is in addition some evidence that erbB-2 expression is higher in well-differentiated OACs, though

interpretation of protein levels can be complicated by marked intra-tumour heterogeneity.(576,577)

As with *EGFR*, *HER2* amplification has been reported to occur late and may follow the loss of a functional *TP53* product.(563) It is unclear how early *HER2* amplification is seen, with reports conflicting with respect to its presence in NDBO.(430,571) Increased *HER2* copy number and amplification is nevertheless recognised to distinguish dysplasia from non-dysplasia, and *HER2* amplification is commonly seen in OAC.(578–582) Underlining the strength of its association with malignancy, *HER2* amplification is in addition recognised as a feature of both the OE19 and OE33 OAC cell lines.(583) Despite at least one series reporting more frequent amplification of *HER2* than erbB-2 protein overexpression, there is evidence of a strong correlation between erbB-2 protein expression and *HER2* gene amplification.(430,555,570,572,574) Amplification of *HER2* in OAC additionally correlates with hyperinsulinaemia, whilst erbB-2 positive OACs are more common in men and those who smoke.(220,580,584) As with *EGFR*, protein expression of erbB-2 may be driven by secretory phospholipase A2.(568)

There are few, if any, reports of erbB-4 expression in BO and OAC, whilst erbB-3 overexpression has been reported at less than 1% in OAC and BO, or as high as 67% in OAC and 47% in HGD.(430,551,585) In at least one series, the expression of erbB-3 increased significantly between LGD and HGD.(551) Whilst *EGFR* and erbB-2 are principally considered to form homodimers when overexpressed in OAC, both RTKs also commonly form heterodimers with *HER3*, which has no intrinsic catalytic activity.(586) Heterodimers formed from erbB-2 and *IGF1R* are also reported in BO and are suggested to promote neoplastic progression.(584)

As with *EGFR* family members, *IGF1R* expression is very low in NSE.(556) However, expression is high in NDBO, with reports of up to 100% positivity, which may reflect a role for this RTK in early disease pathogenesis.(556) It is however unclear how expression links to dysplastic progression, with lower expression seen in HGD than NDBO in one study, but higher expression in HGD than LGD in another.(556,559) Genomic amplification of *IGF1R* appears rare in OAC, though copy number gains have been reported in as many as 33% of cases.(581,587) Environmental factors also appear to impact on *IGF1R* expression, with higher levels of the receptor seen in obesity, though not in diabetes.(556,588)

FGFR2 and c-Met are similarly mostly absent in NSE but present from early in BO progression.(430,560) In the Paterson series, most patients with *FGFR2* overexpression in

OAC had overexpression prior to HGD, with the most marked increase in expression occurring between NDBO and LGD.(430) c-Met overexpression also appears to occur early, with significant increases seen when progressing from LGD to HGD.(551,561) COX-2 is thought to drive c-Met expression, as is the lncRNA LINC00857.(561,589) As with other RTKs, FGFR2 expression in tumours is heterogenous.(590) c-Met is commonly co-overexpressed with EGFR in OAC.(430)

There is in addition limited evidence for changes in expression during Barrett's progression of a handful of other RTKs. These include the ephrin receptor EphB4, which is present at higher protein levels in BO and OAC than NSE, and the expression of which correlates with OAC stage.(591,592) Interestingly, EphB4 and EphB6 mRNA expression are both upregulated in response to BO cellular exposure to low pH.(592) ROR2 overexpression is also recognised to be higher in OAC than BO and NSE, whilst PDGFR α positivity in OAC correlates with age.(366,593) Finally, AXL is overexpressed in around half of all OACs and appears to be downstream of CDK9.(594)

5.1.3.2. Activity

There is a scarcity of studies outlining the induced activity of RTKs in BO and OAC in response to microenvironmental stressors, and equally few comparing basal RTK activity at different stages of disease progression. This relative paucity of information is at least partly abrogated by a number of studies focussed on expression levels for the ligands that interact with and activate RTKs. Activating mutations of RTKs have additionally been observed in a small proportion of cases of dysplastic BO and OAC.

The activity of EGFR is perhaps the most studied of all the RTKs in the context of BO progression. Though relatively rare, activating mutations of EGFR have been reported in up to 12% of patients with OAC and 14% with BO.(595,596) There is in addition evidence for high levels of the EGFR ligands EGF and TGF α in the BO mucosa, though conversely the expression of EGF in saliva appears relatively lower in patients with BO when compared with healthy controls.(196,597,598)

The activity of EGFR may be dynamically modulated by microenvironmental stressors. *Bhat* and colleagues have for instance demonstrated *in vitro* that apurinic/apyrimidinic endonuclease 1 (APE1) activates an EGFR-STAT3 signalling axis in response to acidic bile salts in BO cells.(331) A link between EGFR activation and exposure to acidic bile salts has been supported by at least one additional study, albeit in NSE cells. (599) Nitric oxide also

appears to result in EGFR activation in BO.(600) Potentially providing a mechanistic basis for some of these findings, IGF binding protein 2 (IGFBP2) stabilises and activates an EGFR-DNA-PKcs signalling axis in response to acidic bile salts.(601)

The insulin signalling axis is also suggested to contribute to OAC progression, with a number of IGF1R polymorphisms associated with increased risk of invasive disease.(602,603) There is however no association between IGF-I levels and OAC risk.(604) In contrast, hyperinsulinaemia contributes to an increased risk of Barrett's development, and in a rat model of GORD contributed to the development of OAC.(584,605) There is also evidence that the IGF1R/INSR axis becomes more active during BO progression. Phosphorylation of IRS1, which is downstream of IGF1R/INSR, is for instance recognised to increase from 44% of patients with NDBO to 47% and 70% of patients with dysplastic BO and OAC respectively.(221) This increase correlates with increased phosphorylation of AKT and mTOR.(221) Intriguingly, this increase in receptor activity is suggested to be independent of serum IGF-1, insulin or IGFBP concentration, though all three are upregulated during BO dysplastic progression.(606,607) These may instead act to upregulate the IGF1R receptor, the expression of which is reported to associate with hyperinsulinaemia in a rat model of OAC carcinogenesis.(584) It is noteworthy given the link between BO and the metabolic syndrome that IGF levels are higher in obese patients.(607) The IGF-1 transport proteins, IGFBPs, have also been studied and are inversely associated with BO risk but upregulated in association with BO dysplastic progression.(605,606)

There is scant evidence for factors influencing the activation of the other 56 RTKs encoded by the human genome. The EGFR family member erbB-2 is, like EGFR, linked to STAT3 activation but the conditions in which it is activated are unclear.(608) Given that it does not bind ligand, it is possible that erbB-2 activation mirrors that of EGFR, with which it commonly heterodimerises. It is also recognised that a high methylated subtype of OAC exists in which frequent ErbB2 activation is seen.(609) Expression of the VEGFR2 ligand VEGF-A increases with dysplastic progression in tissue sampled from various stages of the BO metaplasia-dysplasia-OAC sequence, indicating increased VEGFR2 activity.(210,610) *In vitro* evidence drawn from experiments in NSE BAR-T cells also indicates that acidic bile salts cause a rapid and prolonged elevation in VEGF-A expression, though it does not appear to be the sole driver for VEGFR2 activation in these cells.(480) As with other tissues, VEGFR2 signals via a pathway dependent on PLCy1 and P-ERK in both BO and OAC. (480,542)

There is in addition indirect evidence for increased FGFR2 activity during the development of OAC, with FGF expression seen to increase during dysplastic BO progression.(611) There may also be FGFR2 CpG island hypomethylation in OAC but this is not as yet certain.(612) Where FGFR2 is activated, *in vitro* evidence points to it working with GATA6 to promote anchorage-independent cell growth.(613) Reflecting further epigenetic control of RTKs, hypermethylation of NTRK2 and NTRK3 is reported in patients with BO who smoke, though the significance of this is unclear.(266)Conflictingly, histological analysis of OAC with pan-TRK antibodies has demonstrated NTRK expression in gastric glands and tumour adjacent tissue but not in the malignant cells themselves, so whether NTRKs play a significant role in BO neoplastic transformation remains uncertain.(541) There is also evidence for a potential role for the ephrins - the largest RTK family – in dictating malignant phenotype; EphB4 promotes the growth of OAC by acting via its downstream mediator p125FAK.(591)

High levels of c-MET activation are seen in OAC, but less activation in HGD.(561) It is nevertheless implicated in BO progression and the development of EMT in particular, with HGF treatment in BO cells resulting in a short-term reduction in E-cadherin and a simultaneous increase in nuclear β -catenin.(560) c-MET activation is also associated with an increase in pathways associated with invasive growth, such as MMPs and osteopontin.(614) Correspondingly, HGF levels are higher in Barrett's than NSE.(560) AXL, which can cooperate with MET in signalling responses, mediates invasion of OAC cells through upregulation of lysosomes, secretion of lactate via NF- κ B dependent MCT-1 regulation and resultant extracellular acidification, which mediates cell invasion.(615) It is also recognised to upregulate c-Myc and c-Abl, with the latter function dependent on EIF4E phosphorylation.(562,616) AXL also regulates DISC in OAC, thereby promoting resistance to DNA-damaging therapies.(617) Finally, AXL may act as a key node in RTK cross-talk in OAC, where it has been seen to facilitate RTK phosphorylation.(618)

5.1.3.3. Impact

There is a growing body of evidence for a role for RTKs in modulating BO dysplastic progression. EGFR is again a key example yet, conflictingly, SNPs that result in an increase in EGF production and SNPs that result in reduced EGF production have both been associated with increase rates of BO progression and OAC development.(619,620) However, in a recently published rat model of oesophagitis, cross-talk between EGFR, COX-2 and pro-inflammatory cytokines was implicated in the progression of chronic oesophagitis to BO and OAC.(412) Increased expression of EGFR in response to TGF β has also been associated with expansion of EMT in BO via a pathway involving ZEB transcription factors.(621) A number of

other studies support a role for EGFR in modulating CDX2 and thereby BO cellular differentiation.(311,600) Further insights into the role of EGFR have been provided by NSE and OAC cells and tissue. In the former, EGFR activation results in resistance to cell death following exposure to acidic bile salts, though it is also reported to protect from DNA damage.(566,601) In OAC, EGFR overexpression is associated with poorer survival, de-differentiation and a more advanced T-stage.(430,622)

In contrast, erbB-2 overexpression is associated with the presence of moderately to well differentiated OAC tissue.(430) It also frequently correlates with overexpression of the oncogenic driver GRB7 and the tumour suppressor p53.(623,624) The impact of erbB-2 overexpression and *HER2* amplification/copy number variation is however less clear, with studies variously claiming a corresponding survival benefit, a survival detriment or no impact on survival at all.(430,555,573,580) Therapies targeted against erbB-2 have nevertheless resulted in a survival benefit in the clinic.(625) The results of strategies to inhibit EGFR have in contrast been less promising.(2) The impact of FGFR2 is also contested, with Paterson and colleagues reporting no impact on survival from protein overexpression whilst others have highlighted worse survival from *FGFR2* amplification.(430,590) However, evidence that in OAC an increase in the protein levels of the cognate FGFR2 ligands FGF8 and FGF18 impacts negatively on survival, and that the FGFR2 IIIb isoform correlates with the presence of lymph node metastases, suggests that higher activity reduces survival.(608,626) It does not however contribute to a change in tumour mutational burden.(627)

High expression of IGF1R is more clearly associated with poorer survival, though in one study it also increased the likelihood of proceeding to curative resection.(556,557,588) *In vitro* analyses demonstrate that IGF1R activation contributes to OAC cell proliferation.(221,607) Germline variation in genes encoding IGF1R has been shown to influence risk of developing BO, as have serum IGF-1 levels.(605,628) Amplification of *MET* and overexpression of its protein product is additionally associated with worse survival and contributes to tissue invasion and metastasis.(560,561,589,590,629–632) The contribution of c-Met to disease behaviour does however appear partly dependent on erbB-2. (632–634) Overexpression of EphB4 and AXL is also thought to negatively impact on survival, with AXL c-ABL co-overexpression portending an even worse prognosis.(562,591,618)

The expression or action of a small number of RTKs is in contrast associated with a survival benefit. This includes PDGFR α , increased levels of which appear to result in longer survival, albeit in a mixed cohort of OACs and OSCCs.(593) EphB3 may also act in a tumour suppressor

capacity in OAC.(635) Further, *in vitro* treatment of OAC OE33 cells with the ROR2 ligand WNT5A suppresses proliferation, survival and migration.(366)

In Barrett's, HGD lesions that progress to OAC feature higher expression of EGFR and erbB-2.(551,555) Time to dysplastic progression is also shorter in Barrett's segments in which erbB2 is overexpressed, whilst *HER2* polysomy is recognised to predict malignant progression.(570,636) Both are implicated in the Barrett's cell cycle; high expression of the EGFR ligand TGF α correlates with Barrett's proliferation indices, whilst erbB-2 overexpression is associated with an increase in the cell cycle component Cyclin D1.(637,638)

5.2. Aims

In this work, the role of RTKs in maintaining and propagating the viability and dysplastic phenotype of BO cells will be explored under the conditions outlined in **Chapter 3**; namely, (i) under basal, unstressed and pro-proliferative conditions, (ii) under serum-starved, quiescent pro-autophagic conditions, and (iii) following exposure to the contents of gastric refluxate. The determinants of RTK activation following exposure to the contents of gastric refluxate will also be explored.

5.3. Methods

5.3.1. Experimental outline

In order to determine the extent to which RTK activation differs by stressor and cell line, a phospho-RTK array and immunoblotting was used to outline the pattern of RTK activation immediately following acidic bile salt exposure. In order to assess the mechanism of RTK activation, the NSE Het-1A, NDBO CP-A and HGD CP-B cellular response to acid was then analysed by determining ROS production and intracellular pH change over the 10 minute treatment period. The specific RTKs responsible for maintaining the basal phenotype and viability of NSE Het-1A, NDBO CP-A and HGD CP-B and CP-D cells was then determined using a functional genomics short interfering RNA (siRNA)-based screen targeted against all 58 RTKs encoded by the human genome. A candidate list of stress-responsive and basal-signalling RTKs was derived from these experiments and their functional relevance explored using an established RNA-seq dataset drawn from patient samples.

Reagents and plasticware were sourced as outlined in **2.2.** and **Appendix A.** Unless otherwise stated, all reagents and chemicals were obtained from Merck KGaA or its

subsidiary, MilliporeSigma, and all plasticware sourced from Corning® Incorporated. Cell culture, immunoblotting, qRT-PCR and kinase activity assay analyses were undertaken as respectively outlined in **2.3.**, **2.4.3.**, **2.5.** and **4.3.3.3.**, supported by **Appendices E** through to **G**. Statistical analyses and data representation were undertaken as outlined in **2.9**.

5.3.2. Phospho-RTK array

5.3.2.1. Principle

The Proteome Profiler Human Phospho-RTK Array Kit [ARY001B, R&D Systems] was used to determine the relative phosphorylation of RTKs in NSE Het1-A, NDBO CP-A and HGD CP-B cells following exposure to bile salts, at acidic or neutral pH, and acid alone. This nitrocellulose membrane-based sandwich immunoassay incorporates antibodies specific to the phosphorylation sites of 49 of the 58 RTKs encoded by the human genome (see **Appendix H** for details), each of which is spotted in duplicate. These capture relevant phosphorylation sites, with a relative phosphorylation signal provided by the addition of a HRP-linked pan-phosphotyrosine antibody.

5.3.2.2. Method

Each array was blocked in 1.5ml Array Buffer 1 for one hour on a rocking platform held at room temperature. A total of 50µg lysate, suspended in 1.5ml Array Buffer 1, was then added and each array incubated overnight at 4°C. Arrays were subsequently washed three times in 20ml Wash Buffer prior to the addition of 1.5ml Detection Antibody, with which they were incubated for two hours on a rocking platform held at room temperature. Arrays were washed a further three times and developed as outlined for immunoblots in **2.4.3.2**.

5.3.3. Intracellular pH measurement

5.3.3.1. Principle

Intracellular pH was determined using the Molecular Probes™ pHrodo™ Red AM intracellular pH indicator [P35372, TFS]. This fluorogenic probe is made lipophilic through the addition of acetoxymethyl ester groups that through rendering the probe uncharged facilitate free entry into cells. Once in the cytoplasm, the ester side-chains are removed by non-specific esterases, causing the probe to be retained within the cell. The pK_a of 6.5 nears normal cytoplasmic pH (6.8-7.4) and the probe is weakly fluorescent at neutral pH. However, decreases in pH result in increased fluorescence and increases in decreased fluorescence which, coupled with the photostable properties of the probes, enables for the dynamic

assessment of pH changes. The pH can be quantified by calibration against a standard curve generated by clamping the intracellular pH with extracellular buffer using the Molecular Probes™ Intracellular pH Calibration Buffer Kit [P35379, TFS].

5.3.3.2. Method

Cells were seeded in a 96-well plate, as outlined in **2.3.3.3**. One hour prior to pH sampling, each well was washed once in 100µl Live Cell Imaging Solution (LCIS [A14291DJ, TFS]). The pH sensitive pHrodo™ red AM probe was prepared through addition of 10µl probe solution to 100µl PowerLoad™ concentrate. This was diluted in 10ml LCIS to make a working solution, from which a volume of 100µl was added to each well. Plates were subsequently incubated at 37°C for 30 minutes then washed again in LCIS prior to experimentation or serum-starvation as outlined in **2.3.3.3**. and **3.3.2.**, respectively.

As per manufacturer instructions, fluorescence intensity was measured at 560_{EX}/580_{EM} nm. For cells exposed to serum-starvation, pH was measured at the end of the 48 hour starvation period and compared to a control cell population maintained in proliferative media. The pH of cells treated with acid was measured prior to treatment, at 2 minute intervals during 10 minutes of acid exposure and for 10 minutes after neutral pH media was restored using a BioTek™ Synergy™ H1 multifunctional microplate reader, with cells cultured at 37°C in air. Following the measurement of pH during these experimental conditions, a BioTek™ Synergy™ H1 multifunctional microplate reader was used to measure fluorescence intensity whilst the same cell populations were sequentially exposed to buffers representing pH 4.5, 5.5, 6.5, 7.5. This allowed for the generation of a standard curve from which experimental changes in pH could be derived.

5.3.4. Oxidative stress detection

5.3.4.1. Principle

The CellROX™ Green Reagent [C10444, TFS] was used for live cell measurements of oxidative stress. This cell-permeant fluorogenic dye fluoresces weakly in its reduced form but exhibits bright green fluorescence, with absorption/emission maxima of 485_{EX}/520_{EM} nm, when oxidised by ROS.

5.3.4.2. Methods

Cells were seeded in a 96-well plate and treated or exposed to serum starvation, as outlined in **2.3.3.3**. and **3.3.2**. respectively. At the pre-defined sampling points, CellROX® Green

Reagent was added to existing media in each well at a final concentration of 5 μ M and cells incubated for 30 minutes at 37°C in a humidified atmosphere comprising 5% CO₂/95% air. The media was subsequently aspirated and cells washed three times in PBS prior to measurement of fluorescence at 485_{EX}/520_{EM}nm using a BioTek™ Synergy™ H1 multifunctional microplate reader.

5.3.5. An siRNA-based functional genomics screen

5.3.5.1. Statement of contribution

The functional genomics screen was undertaken in collaboration with Dr Jacquelyn Bond (Leeds Institute of Medical Research at St James's, University of Leeds). I devised and planned this screen, purchased all materials, prepared the cell lines and both analysed and interpreted all of the data, including any relating to quality control and normalisation processes. The practical experimental work (i.e. loading siRNAs and cells on to plates, and high-throughput microscopy) was undertaken by Dr Bond through a relevant core facility.

5.3.5.2. Overview

An siRNA-based functional genomics screen was used to determine the relative contribution made by RTKs to the viability and phenotype of NSE (Het-1A), NDBO (CP-A) and HGD (CP-B, CP-D) cells. This was explored under both pro-proliferative conditions and the conditions of serum-starvation characterised in **Chapter 3**. As summarised in **Fig. 5.2.**, a reverse

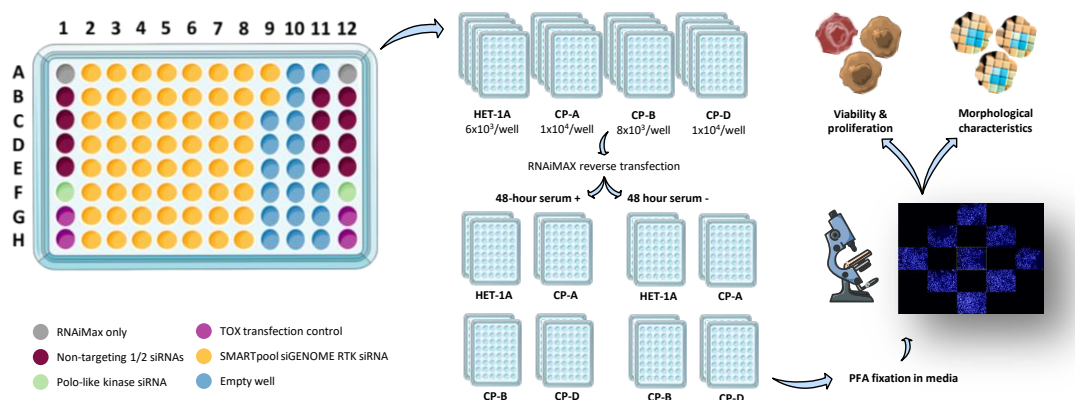


Figure 5.2. A schematic demonstrating the targeted siRNA screen used to determine receptor tyrosine kinase (RTK) contribution to cellular phenotype and viability in NSE (HET-1A), NDBO (CP-A) and HGD (CP-B, CP-D) cells. Briefly, four SMARTpool siGENOME siRNA duplexes were used to target each of the 58 RTKs encoded by the human genome via a reverse transfection protocol, in the presence of negative (non-targeting 1/2), positive (polo-like kinase, TOX transfection control) and mock (RNAiMax only) controls. Cells were subsequently maintained in proliferative and serum-starved media for a period of 48 hours and the impact of RTK gene knockdown assessed using high-throughput microscopy to determine cell number and markers of BO morphology. Cell, cytoplasm and nuclear boundaries were demarcated through the use of DAPI and TOTO-3 stains.

transfection approach was used to deploy siRNAs targeted against all 58 RTKs encoded by the human genome, with appropriate positive and negative controls, for NSE (Het-1A), NDBO (CP-A) and HGD (CP-B, CP-D) cells maintained under pro-proliferative and starvation conditions. Cells were fixed after a 48 hour period, stained and assessed by high-throughput imaging in order to determine the impact on cellular phenotype. This was assessed by determining changes in cell number and a panel of morphological characteristics identified by literature review to vary by grade of BO dysplasia and EMT.

5.3.5.3. Screening method

5.3.5.3.1. Plate set-up

A custom human SMARTpool siGENOME siRNA library [Dharmacon] consisting of 232 individual siRNA duplexes targeted against all 58 RTKs encoded by the human genome was used, as summarised in **Appendix I**. Four duplexes were deployed per well in columns 2-8 A-H and 9 A-B (see **Fig. 5.2.**) of a 96-well View Plate [PerkinElmer]. Two additional mock transfection wells in columns 1 and 12 comprised of transfection reagent (Lipofectamine™ RNAiMax Transfection Reagent) only. Negative controls (siGENOME Non-Targeting Pool #1 [D-001206-13-05, Dharmacon] and siGENOME Non-Targeting Pool #2 [D-001206-14-05, Dharmacon]) were used in eight and four wells, respectively, in columns 1 (B-D), 11 (B-D) and 12 (B-D). Each plate consisted of two positive control SMARTpool siGENOME siRNAs, which were targeted against polo-like kinase (PLK) 1 [M-003290-01-0005, Dharmacon] and thymocyte selection associated high mobility group box (TOX) [M-020339-01-0005, Dharmacon]. All siRNAs were aliquoted into View Plates using a Bravo Automated Liquid Handling Platform [Agilent]. Reconstituted plates were stored at -80°C prior to use.

5.3.5.3.2. Reverse transfection

A reverse transfection approach was used with 6 pmol of each siRNA duplex suspended in 100µl Opti-MEM I medium in each relevant well of the View Plate. A total volume of 1µl Lipofectamine RNAiMAX was then added to each well and the contents gently mixed on a rotary shaker for 10-20 minutes at room temperature. A final siRNA concentration of 10nM was achieved through the addition of 500µl proliferative media (see **2.3.3.1.**) containing cells maintained using constant magnetic stirring in a uniform suspension at the following pre-optimised concentrations: Het-1A (6×10^3 /well), CP-A (1×10^4 /well), CP-B (8×10^3 /well), CP-D

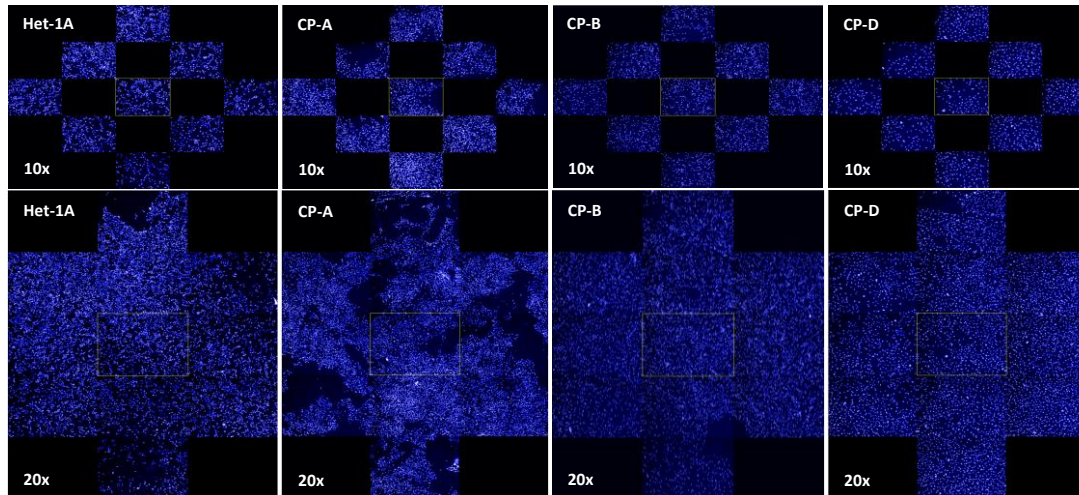


Figure 5.3. Representative images detailing growth patterns of DAPI-stained NSE (Het-1A), NDBO (CP-A) and HGD (CP-B, CP-D) cells imaged using an Operetta® microscope at 10x and 20x magnification. Each row shows cells within a single well imaged over either nine fields of view (10x magnification) or 11 fields of view (20x magnification).

(1×10^4 /well). Edge effects were limited by allowing cell-transfection complexes to rest in a laminar flow hood for one hour prior to incubation in normal cell culture conditions.

5.3.5.3.3. Culture, fixation & staining for imaging

Once plated, cells were grown for 48 hours then suspended in fresh proliferation (see **2.3.3.1.**) or starvation (see **2.3.3.2.**) media for a further 48 hours prior to fixation in PFA. Cells were then stained with $1 \mu\text{g/ml}$ DAPI (4',6-diamidino-2-phenylindole) [TFS] and 500nm TOTO®-3 [TFS] by incubation for one hour at room temperature in the dark in order to identify cell, cytoplasm and nuclear boundaries. A minimum of two repeats were obtained for each cell line in each serum condition, with one repeat using cells at a low passage (<10) and the other at a higher passage (>10). Experiments were undertaken in, and analyses carried out within, specific batches.

5.3.5.3.4. Staining, fixation & high-throughput imaging

Following fixing and staining, plates were imaged using an Operetta® High Content Imaging microscope [PerkinElmer]. Plates were loaded using a Plate Handler II robotic arm operated through Plateworks [PerkinElmer] software. Each plate was identified by a barcode prior to loading. As shown in **Fig. 5.3.**, 20x magnification risked artificially undercounting CP-A cells due to their patchy growth. Six fields of view were therefore obtained per well at 10x magnification. Fluorescent images for DAPI and TOTO3 were respectively obtained at $6 \mu\text{m}$ and $7 \mu\text{m}$ above the well surface for 60ms and 500ms.

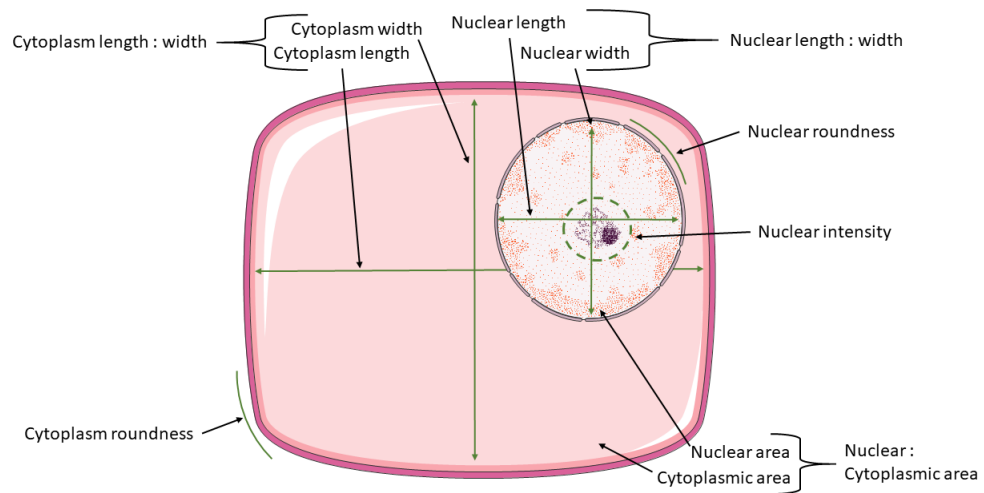


Figure 5.4. A schematic demonstrating morphological parameters analysed from the high-throughput siRNA screen. Each studied parameter was selected following a literature review for cellular parameters that change with the grade of dysplasia in BO.

Obtained images were then analysed using Columbus Image Data Management System. DAPI and TOTO-3 staining was used to segmentate cells in to nuclei (blue-fluorescent staining) and cytoplasm (far-red fluorescent regions surrounding blue-fluorescent regions). Border objects were excluded. Modified analysis algorithms were generated to provide outputs relating to the number of cells (segmented using DAPI and TOTO-3 staining) and the proportion of dead cells. It is in addition recognised that a number of morphological changes accompany dysplastic change, including alterations in nuclear size and shape, nuclear/nucleolar enlargement, an increase in the nuclear : cytoplasmic ratio and hyperchromatism. These parameters were therefore also assessed, as is summarised in **Fig. 5.4.**

5.3.5.4. Analysis

5.3.5.4.1. Robust z-score

The statistical significance of siRNA-mediated knockdown of the 58 candidate genes in each of the studied cell lines and serum conditions was assessed through the calculation of robust Z-scores. This measure accounts for different scale and variability effects as well as plate effects, and as such is less likely to produce biased scores of outlying values of highly active compounds. Of note, robust measures are recommended in instances where replicates may not be available.(639) The first plate batch consisted of the first replicate for each cell line and serum condition. The second batch consisted of the second replicate for each cell line and serum condition. A third batch consisted of a replicate for each serum condition for Het-

1A. Given the difference in serum availability, the negative controls for each cell line within each batch were considered separately. As such, individual data points were normalised to the plate median and robust z-scores calculated from the median and median absolute deviation (MAD) of the negative data population (mock transfection controls + NT1 controls + NT2 controls) for each output in each plate, as follows:

$$\text{Robust } Z = \frac{x - \mu}{MAD}$$

Where: μ = median, and MAD = median absolute deviation, of the given negative population for the given output, and x = raw value for that output.

The MAD is the median value of the absolute deviation of each of the data points X_i to n from the median for the entire dataset, as follows:

$$MAD = 1.4826 * (\text{median}(|X_i - \text{median } X_1 \dots n|))$$

The constant 1.4826 is applied so that MAD approximates standard deviation when the values are normally distributed.

5.3.5.4.2. Plate QC

In a process repeated for all studied outputs, each plate was colour coded and the results manually assessed for sources of systematic bias such as drift, row or edge effects. The Strictly Standardised Mean Difference (SSMD) was used to assess the performance of positive and negative controls. Briefly, SSMD is a measure of effect size and as the equation shown below illustrates, reflects the difference between positive and negative controls:

$$SSMD = \frac{Pcont - Ncont}{Pstdev - Nstdev}$$

Where: Pcont = Mean of positive controls, Ncont = Mean of negative controls, Pstdev = Standard deviation of positive controls and Nstdev = Standard deviation of negative controls.

A SSMD of ≥ 1 is considered acceptable in the context of a moderate positive control. SSMD was calculated for each plate for both PLK1 and TOX. For each plate, the highest SSMD value was used to pass or fail the plate, with values less than 1 deemed to reflect plate failure.

5.3.5.4.3. Correlation coefficients

Pearson correlation coefficient was determined for each output by comparing the z-scores of the two repeats for that output.

5.3.5.4.4. Hit selection

Upper and lower thresholds for hit selection were determined for each output in each plate as determined by the MAD using all sample values for that output in that plate and the following formula:

$$\text{Hit threshold (upper and lower limits)} = \text{Median} \pm r * \text{MAD}$$

Thus, any output with a value above the median plate value + 4MADs is regarded as a hit, as is any output with a value below the median plate value – 4 MADs. In comparison to the more conventional standard deviation-based z-score method, the MAD method is more robust to outliers and any violation of the assumption that data are normally distributed. Where two replicates were available, hits were chosen if present in both replicates, or if present in one replicate and indeterminate (i.e. not a hit in the opposing direction) in the other plate. If a positive hit existed in one replicate but was negative in the second plate, it was not considered a hit in either direction.

5.3.6. Sphingomyelinase assays

5.3.6.1. Acid sphingomyelinase activity assay

The fluorometric Abcam Acidic Sphingomyelinase Assay Kit [ab190554] was used to determine acid sphingomyelinase (ASMase) activity, with all assays undertaken in line with manufacturer instructions. Briefly, cells were maintained in sphingomyelin working solution for two hours following lysis. The enzyme mix was then reconstituted in manufacturer-supplied assay buffer, after which it was maintained on ice throughout use. This was mixed with AbRed, added to sphingomyelinase assay mixture and, following an incubation period, fluorescence was read at 540_{EX}/590_{EM}nm using a BioTek™ Synergy™ H1 multifunctional microplate reader.

5.3.6.2. Inhibition of acid sphingomyelinase and neutral sphingomyelinase activity

Imipramine [IO899] was used at a concentration of 100μM and GW4869 [D1692] at a 20μM concentration for three hours in order to respectively inhibit ASMase and neutral sphingomyelinase (NSMase).

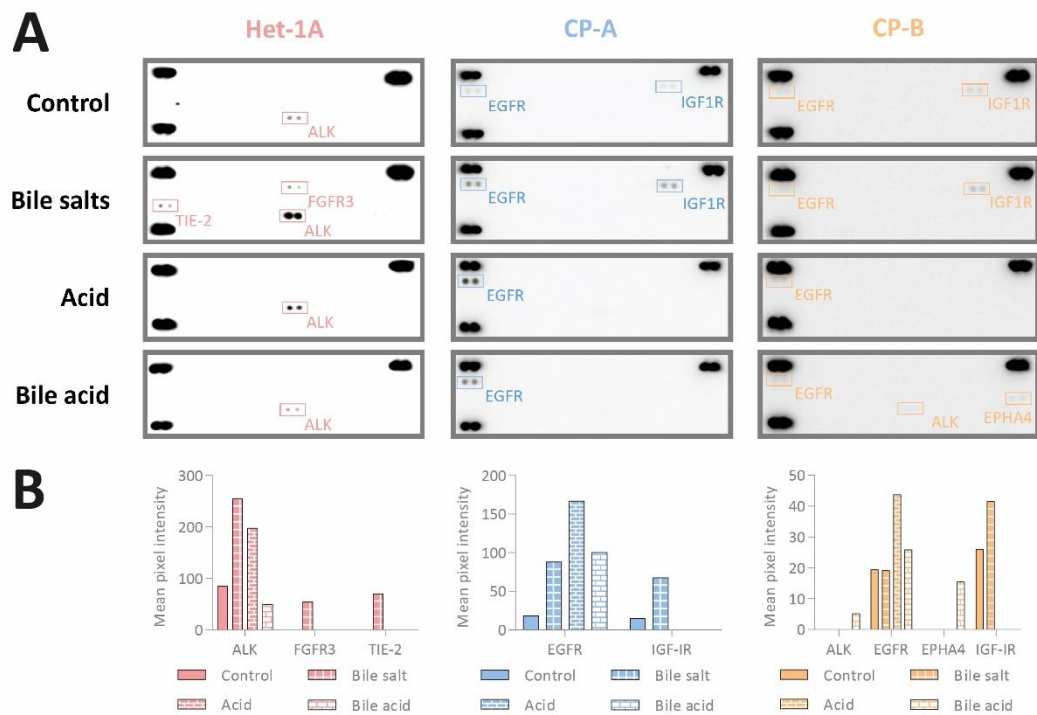


Figure 5.5. Phospho-RTK array profiling of phosphorylated RTKs in NSE (Het-1A), NDBO (CP-A) and HGD (CP-B) cells following a ten minute pulse of bile salts at neutral (Bile salts) or acidified pH (Bile Acid), or acid alone. (A) Unprocessed phospho-RTK arrays with spots revealing phosphorylated RTKs highlighted. The double spots shown in three corners of each array are control spots. Arrays were exposed simultaneously for each cell line, enabling the parallel comparison of relative RTK phosphorylation within columns (i.e. within cell lines) but not across rows (i.e. for the same condition across different cell lines). **(B)** Densitometric summary of RTK phosphorylation by cell line and treatment condition.

5.4. Results

5.4.1. RTK activation under conditions of refluxate-exposure

The data outlined in **Chapters 3** and **4**, coupled with the existing literature summarised in **5.1.**, indicate a probable role for RTKs in mediating cellular response to acid and, potentially, bile salts. In particular, and as summarised in **Fig. 4.22**, a kinase activity assay has revealed a probable RTK network response to acidic bile salt exposure. It is however unclear whether any one, or multiple, RTKs act as early activators of this BO network, and whether similar RTK activation is seen in NSE Het-1A cells. We sought to explore this in greater detail and, in particular, to determine the extent to which exposure to neutral and acidic bile salts, and acid alone, results in RTK activation across NSE Het-1A, NDBO CP-A and HGD CP-B cell lines.

5.4.1.1. EGFR is phosphorylated under conditions of bile salt and acid exposure in BO but not NSE cells

The relative phosphorylation of RTKs was determined in parallel using a phospho-RTK array following exposure of NSE Het-1A, NDBO CP-A and HGD CP-B cells to bile salts, at either neutral or acidic pH, or acid alone. As is outlined in **Fig. 5.5.**, the pattern of relative RTK phosphorylation following bile salt exposure was identical for NDBO CP-A and HGD CP-B

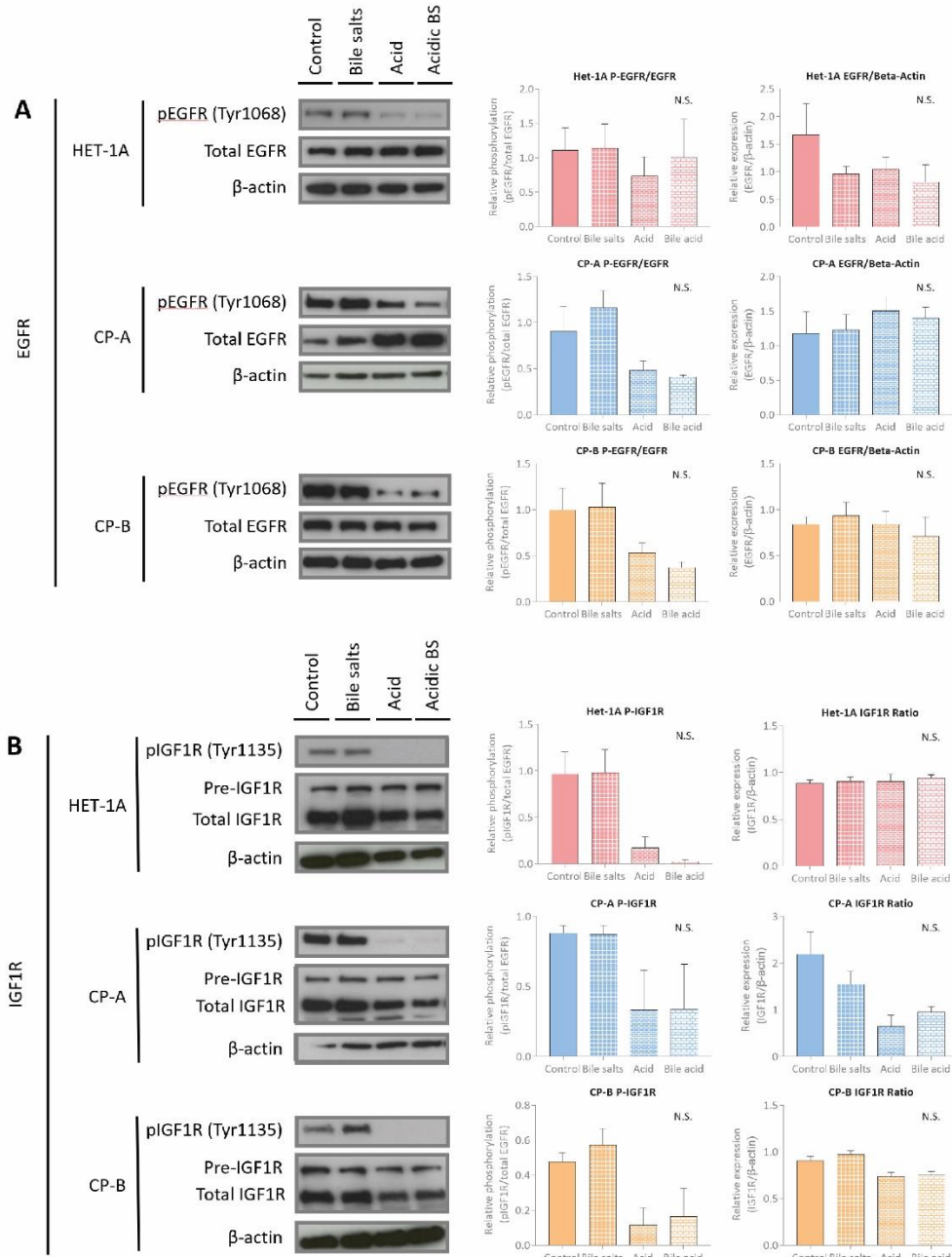


Figure 5.6. Immunoblots demonstrating changes in (A) EGFR and (B) IGF1R activation loop phosphorylation immediately following a 10 minute exposure to bile salts, at acidic and neutral pH, and acid alone, in NDBO (CP-A) and HGD (CP-B) cells. Cells were exposed to a 100μM equimolar mix of bile salts at pH 4.0 or neutral pH, or acid at pH 4.0 alone, for ten minutes then immediately sampled. Cells treated with vehicle only within serum-free media are used as a control population. Blots are shown alongside densitometry for relative phosphorylated activation loop epitope intensity and relative total RTK expression. A β-actin loading control is also shown. Statistical analyses were undertaken using the Kruskal-Wallis test with Dunn’s post-hoc correction. n=3.

cells, with activation of both EGFR and IGF1R seen. In both cell lines, treatment with acid entirely abrogated IGF1R phosphorylation, with EGFR activation clearly exceeding that of any other RTK under conditions of direct acid exposure. Interestingly, the addition of bile

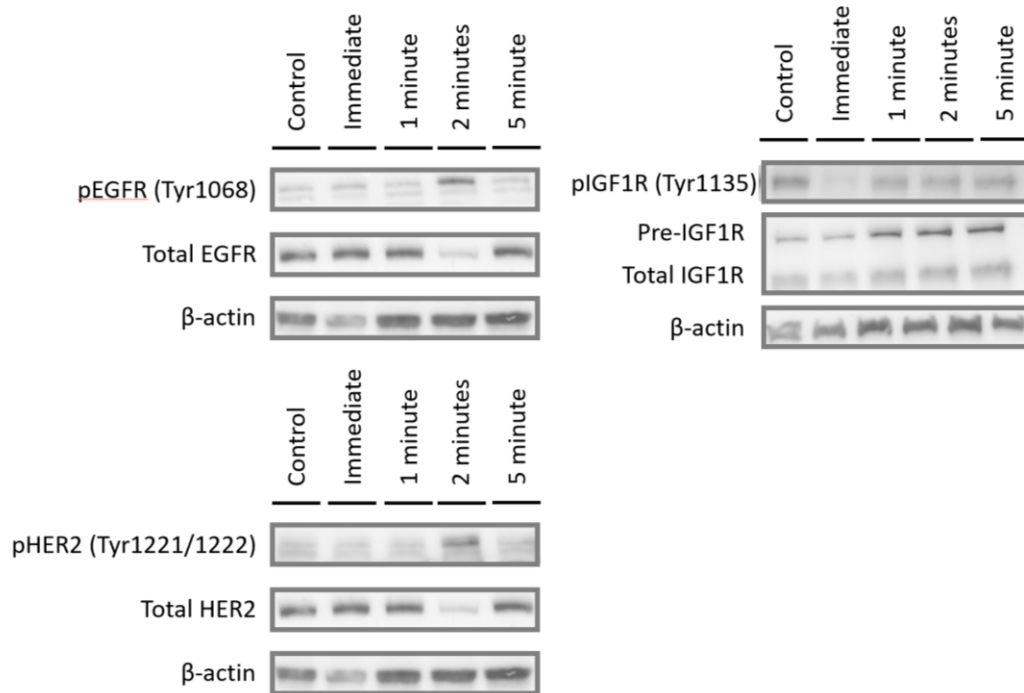


Figure 5.7. Immunoblots demonstrating changes in EGFR, IGF1R and HER2 activation loop phosphorylation in NDBO (CP-A) cells during the five minute period following a 10 minute exposure to acidic bile salts. Cells were exposed to a 100 μ M equimolar mix of bile salts at pH 4.0 for ten minutes then either immediately sampled or washed and placed in neutral pH serum-free media and samples after a 1, 2 or 5 minute period had elapsed. Cells treated with vehicle only within serum-free media are used as a control population. Representative of n=2.

salts to acid had no additional impact on RTK phosphorylation in NDBO CP-A cells, but resulted in the additional increased relative activation of ALK and EPHA4 in HGD CP-B cells. In contrast, the Het-1A cells were dominated by ALK phosphorylation across all four studied conditions, with bile salts also resulting in phosphorylation of TIE-2 and FGFR3.

We sought to validate the phospho-RTK data for EGFR and IGF1R using immunoblotting. As shown in **Fig. 5.6.**, data for IGF1R signalling exactly mirrored that for the phospho-RTK screen for acid and acidic bile salts, though there was no appreciable increase in phosphorylation in response to bile salts. The phosphorylation of EGFR, in contrast, was lower in conditions of acid and acidic bile salts than for control, though there was nevertheless demonstrably still phosphorylation present at the immediate end of 10 minutes of acid exposure.

We hypothesised on the basis of this result that EGFR phosphorylation would increase rapidly following the restoration of neutral media (i.e. 'acid withdrawal', a concept described in **Chapter 4**). This was assessed by immunoblotting (**Fig. 5.6.**), which demonstrated an increase in EGFR activation within two minutes of acid withdrawal. As also shown in **Fig. 5.6.**, this time point coincided with an increase in phosphorylation of Erb-B2 (HER2), which was demonstrated in **Chapter 4** to share the same signalling 'hub' as EGFR. In contrast, IGF1R

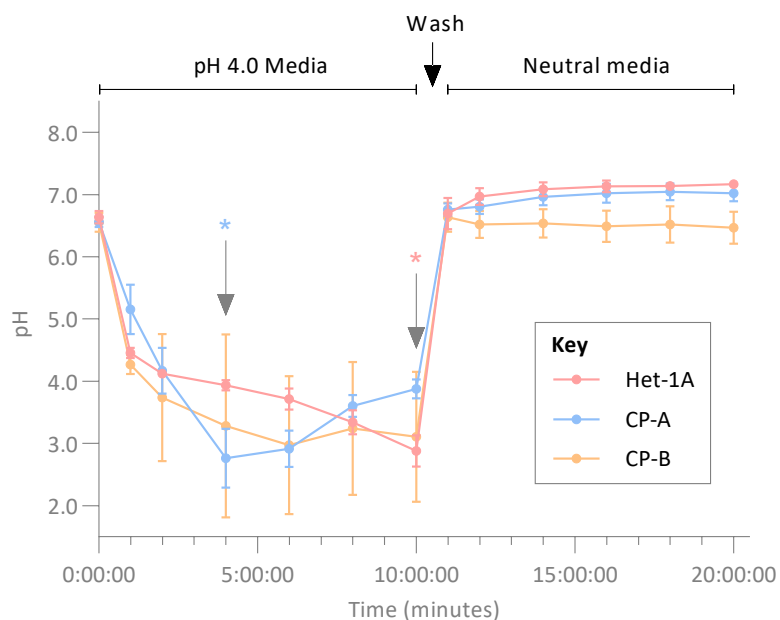


Figure 5.8. A graph plotting intracellular pH against time for NSE (Het-1A), NDBO (CP-A) and HGD (CP-B) cells exposed to pH 4.0 and then neutral media. Intracellular pH was detected using the Molecular Probes™ pHrodo™ Red AM intracellular pH indicator. Data are shown as mean \pm SEM. Statistical analyses are undertaken using the Kruskal-Wallis test with post-hoc Dunn's correction for multiple significance testing. pH values at each time point were compared to basal pH (time 0). Statistically significant changes in pH are highlighted by an asterisk (*, representing $p < 0.05$) in the relevant cell line colour. $n = 4$.

phosphorylation appears to return to rapidly return to baseline but does not increase relative to control conditions.

5.4.1.2. EGFR is catalytically active at a low intracellular pH and in the absence of significant ROS production

Given that EGFR appears catalytically active at the immediate end of a ten minute exposure to an extracellular pH of 4.0, we sought to quantify temporal changes in the intracellular pH of the NSE Het-1A, NDBO CP-A and HGD CP-B cell lines in response to exposure to acidic media, as well as its subsequent withdrawal (**Fig. 5.8.**). All three cell lines demonstrated a rapid and substantial reduction in pH once cells were exposed to acidic media, with intracellular pH at least equilibrating with that of the surrounding media by two minutes of treatment. Beyond this second minute, a further fall in pH was seen in all three cell lines with an approximate pH of 3 reached by NSE Het-1A and HGD CP-B cell lines by the tenth minute of acid exposure. Interestingly, NDBO CP-A pH reached a nadir at four minutes and rose thereafter. Once acidic media was removed and replaced with neutral pH media, all three cell lines rapidly recovered to their baseline pH.

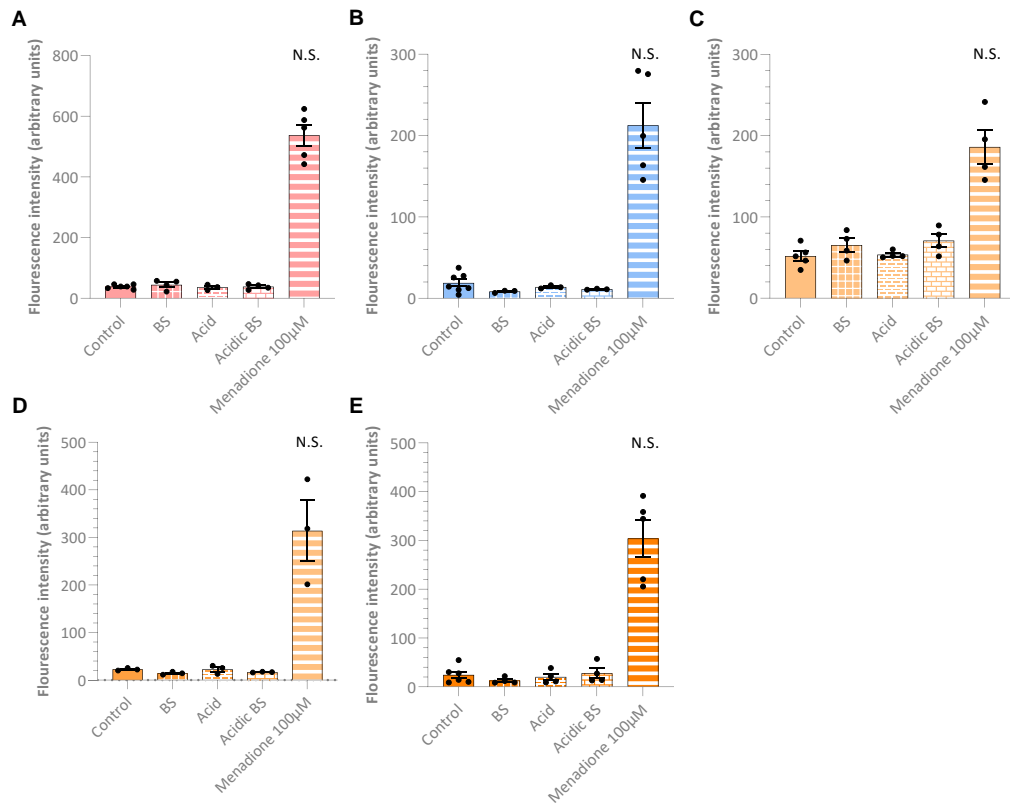


Figure 5.9. Reactive oxygen species (ROS) production following a 10 minute exposure to bile salts, at acidic (Acidic BS) or neutral pH (BS), acid alone, or positive control (Menadiione) in NSE (Het-1A), NDBO (CP-A) and HGD (CP-B, CP-C, CP-D) cells. Cells were exposed to a 100µM equimolar mix of bile salts at either pH 4.0 or neutral pH, or to acidic media (pH 4.0) alone, for ten minutes. A control cell population was instead exposed to 100µM of the known ROS inducing agent, Menadiione. ROS as measured immediately following the end of the ten minute experimental period. Statistical analysis was undertaken using the Kruskal-Wallis test with post-hoc Dunn’s correction for multiple significance testing. $n \geq 3$ for all comparisons. N.S.: non-significant.

As outlined in **1.1.2.2.1.** and **1.1.2.5.**, a number of previous reports have linked cellular signalling following gastric refluxate exposure to an increase in ROS. We therefore sought to determine whether the ten minute treatment period used here would cause a change in levels of ROS within NSE Het-1A, NDBO CP-A and HGD CP-B, CP-C and CP-D cells. As shown in **Fig. 5.9.**, no increase was seen with bile salts, either at neutral or acidic pH, or acid alone.

5.4.1.3. Neither single nor multiple repeated pulses of bile salts, at neutral or acidic pH, or acid alone, result in upregulation of EGFR, IGF1R, EPHA4 or FGFR3 in NSE Het-1A, NDBO CP-A or HGD CP-B cells

In earlier work, activation of EGFR and inactivation of IGF1R was shown in NDBO CP-A and HGD CP-B cells in response to acidic bile salts. Activation of FGFR3 and EPHA4 were also shown in response to acidic bile salts, albeit respectively in only NSE Het-1A and HGD CP-B

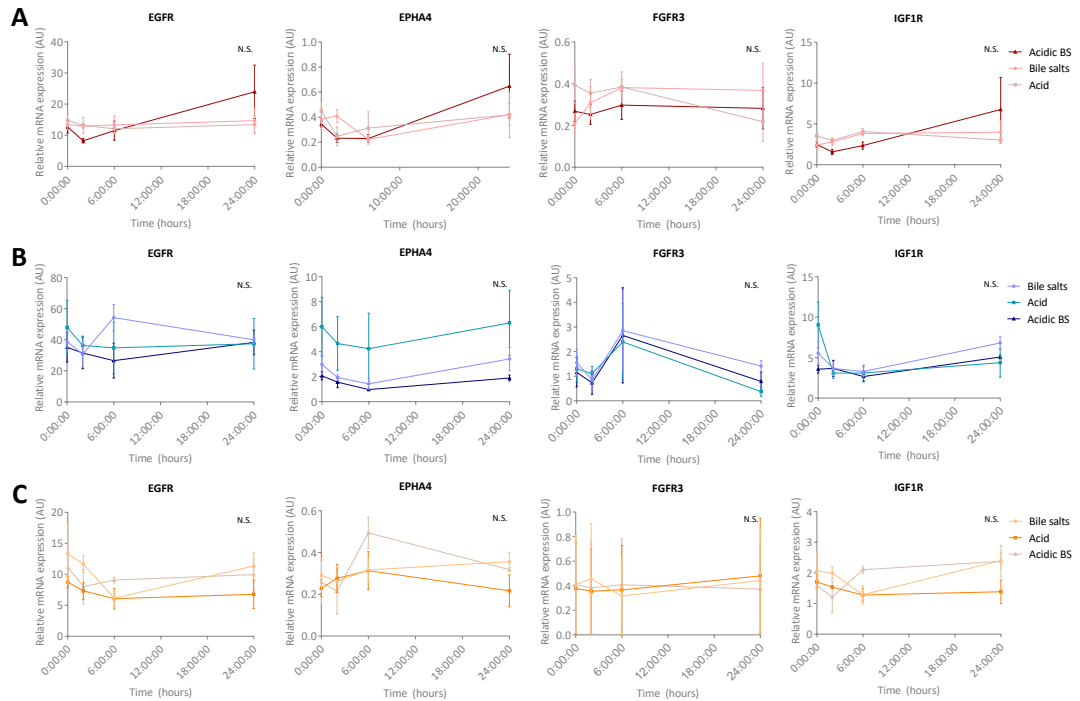


Figure 5.10. Change in mRNA expression of EGFR, EPHA4, FGFR3 and IGF1R over the 24 hour period following a 10 minute exposure to bile salts at acidic (Acidic BS) or neutral pH (BS), and acid alone. Cells were exposed to a 100 μ M equimolar mix of bile salts at either pH 4.0 or neutral pH, or to acidic media (pH 4.0) alone, for ten minutes. mRNA expression of each of the four assessed RTKs was determined by qPCR at baseline (0 hours), and at 2, 6 and 24 hours after treatment. Statistical analyses were undertaken using the Kruskal-Wallis test with post-hoc Dunn’s correction. n \geq 3 for all time points. N.S.: non-significant.

cells. Expression of a number of RTKs, including EGFR and IGF1R, has been reported to increase during BO dysplastic progression, as outlined in 5.1.3.1. We hypothesised on the basis of this that the change in phosphorylation of EGFR, IGF1R, EPHA4 and FGFR3 in response to acidic bile salts would be associated with a change in their expression.

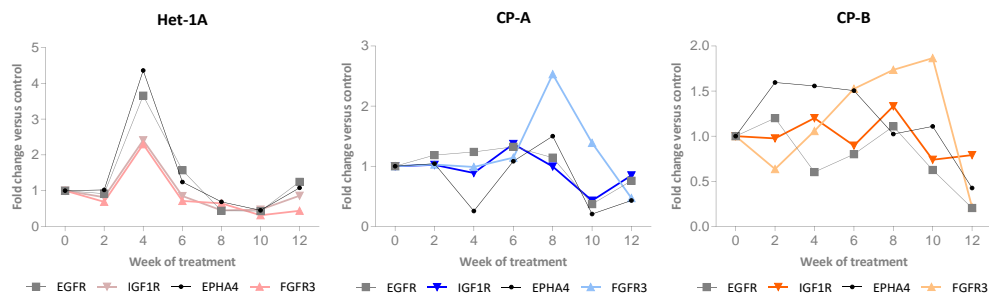


Figure 5.11. Fold change in the expression of EGFR, IGF1R, EPHA4 and FGFR3 in cells representing NSE (Het-1A), NDBO (CP-A) and HGD (CP-B) that are repeatedly exposed to acidic bile salts over a period of twelve weeks. Cells were exposed to an equimolar 100 μ M mix of bile salts at pH 4.0 or vehicle for ten minutes on five days a week for twelve weeks. Fold-change in mRNA expression of each gene is shown for acidic bile salt treatment relative to control. n=1.

Consequently, the change in RTK mRNA expression in the 24 hour period following a pulse of bile salts, at neutral or acidic pH, or acid alone was studied by qRT-PCR in NSE Het-1A, NDBO CP-A and HGD CP-B cells (**Fig. 5.11.**). The relative mRNA expression of these same RTKs was also studied in these same cells following daily exposure to acidic bile salts or vehicle on five days a week for twelve weeks (**Fig. 5.12**). None of the applied cellular conditions significantly altered short-term changes in mRNA RTK expression, though a trend towards an increase in EGFR expression in response to acidic bile salts was seen for both NSE Het-1A and NDBO CP-A cells.

In the long-term, NSE Het-1A cells demonstrated a small early peak in the expression of all four studied RTKs but, appreciating the limitations of interpreting from a single repeat, there was no appreciable long-term change in RTK expression. Similarly, all four RTKs had returned to their approximate baseline following 12 weeks of acidic bile salt exposure in NDBO CP-A cells. This did, however, contrast with the downward trend seen for EGFR, EPHA4 and FGFR3 at twelve weeks of acidic bile salt exposure.

5.4.1.4. Acid sphingomyelinase regulates EGFR signalling in response to acid and regulates cell death

As shown in **Fig. 3.18C**, acidic bile salt treatment of NDBO CP-A cells led to enrichment of cholesterol biosynthetic processes. Acid sphingomyelinase (ASMase) and neutral sphingomyelinase (NSMase) catalyse the conversion of sphingomyelin to ceramide and phosphorylcholine, and are key mediators of intracellular cholesterol transport.⁽⁶⁴⁰⁾ Intriguingly, cholesterol levels are reported to be inversely proportional to ASMase activity.⁽⁶⁴¹⁾ ASMase is also known to be activated at a lower pH and is a mediator of both tissue injury and the inflammasome.⁽⁶⁴⁰⁾ Pertinently, increased ASMase activity was recently identified as a modulator of the activity of RTKs and their downstream signalling pathways in cancer cells, including for MET and IGF1R.^(641,642) Further, it is known that tricyclic antidepressants, which as outlined in **Chapter 1** are a risk factor for BO progression, act as functional inhibitors of ASMase (FIASMA).⁽⁶⁴³⁾ We therefore hypothesised that ASMase activity would increase in response to the acid exposure used in this study, and that this would contribute to the change in RTK phosphorylation seen in response to acidic bile salt exposure.

As is outlined in **Fig. 5.12A.**, and though data are exploratory only given that they are presented as a single 'n' number, NDBO CP-A ASMase activity increased markedly during a ten minute period of extracellular acid exposure. We therefore undertook to determine the

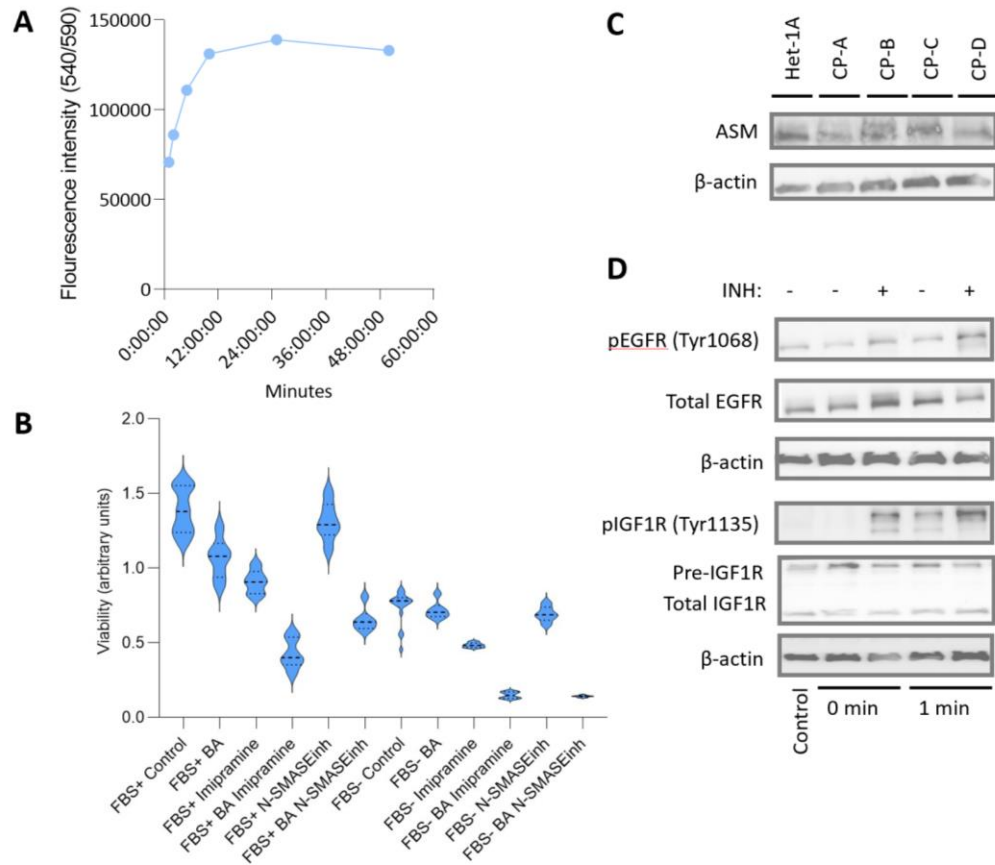


Figure 5.12. A panel figure illustrating (A) the activity of acid sphingomyelinase (ASMase) in response to cellular acid exposure and (B-D) the impact of ASMase inhibition on cellular viability and signalling. (A) NDBO (CP-A) ASMase activity was determined by a fluorometric assay for which fluorescence intensity is proportional to ASMase activity. **(B)** Viability of NDBO (CP-A) cells was determined following inhibition of ASMase using 100µM imipramine for three hours and inhibition of neutral sphingomyelinase (NSMase) using 20µM GW4869 for three hours; with viability compared in the basal state (Control) and following a ten minute exposure to a 100µM mix of bile salts at pH 4.0 (BA). **(C)** Protein expression of ASMase across NSE (Het-1A), NDBO (CP-A) and HGD (CP-B, CP-C, CP-D) cell lines. **(D)** Impact of ASMase inhibition using 100µM imipramine for three hours on activation loop EGFR and IGF1R phosphorylation.

impact of a loss of both ASMase and NSMase activity on NDBO CP-A cellular viability following exposure to a ten minute pulse of acidic bile salts, both in the presence and absence of exogenous growth factor (i.e. from FBS, in order to determine any additional impact from the loss of growth-factor derived signalling). Data are again presented as exploratory at n=1, but there appears to a significant loss of viability in response to inhibition of ASMase (using imipramine) and, to a lesser extent, NSMase. Reassuringly, ASMase expression was confirmed across all five studied cell lines used in this work, with higher protein expression seen in the HGD CP-B and CP-C cells.

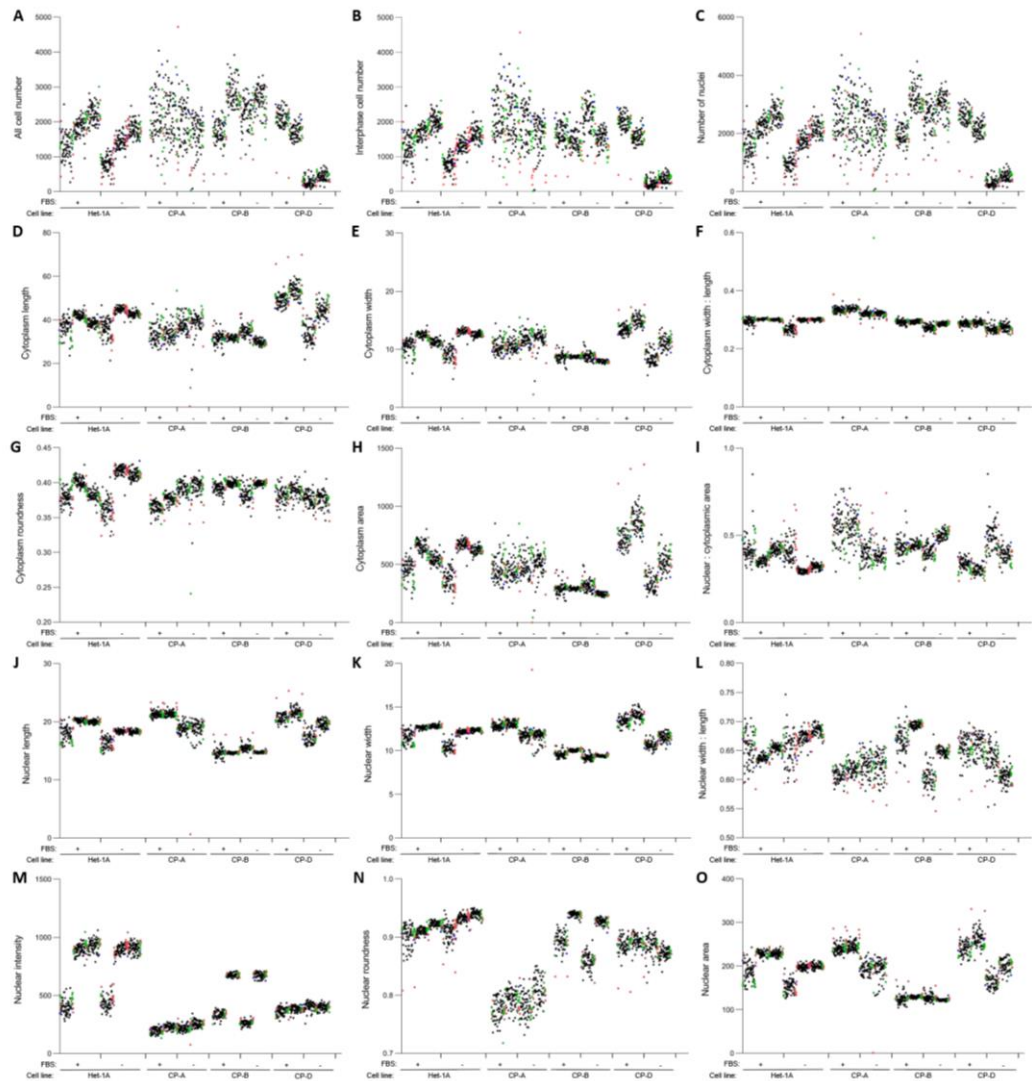


Figure 5.13. Plate-well scatter plots for all siRNA screen outputs. The x-axis comprises of ordered wells across the plates and the y-axis comprises of raw output values. Positive and negative controls are shown in red and green respectively. Mock transfection wells are shown in blue. Raw values per output are shown in black, as follows; A: All cell number; B: Interphase cell number; C: Number of nuclei; D: Cytoplasm length; E: Cytoplasm width; F: Cytoplasm width : length; G: Cytoplasm roundness; H: Cytoplasm area; I: Nuclear : cytoplasmic area; J: Nuclear length; K: Nuclear width; L: Nuclear width : length; M: Nuclear intensity; N: Nuclear roundness; O: Nuclear area.

5.4.2. RTK activity under stressed serum-starvation and basal proliferative conditions

5.4.2.1. Functional genomics screen

In addition to their putative role in mediating the cellular response to acid and acidic bile salts, RTKs such as EGFR and the NTRKs were over-represented in the signalling processes controlling the basal phenotype of NDBO CP-A cells. Surprisingly, ‘cellular response to growth factor stimulus’ was a key enriched term in NDBO CP-A cells exposed to serum-starvation. We therefore sought to evaluate whether, and which, RTKs mediate the basal proliferative, and serum-starvation stress-induced, phenotype of NDBO CP-A cells. Given the

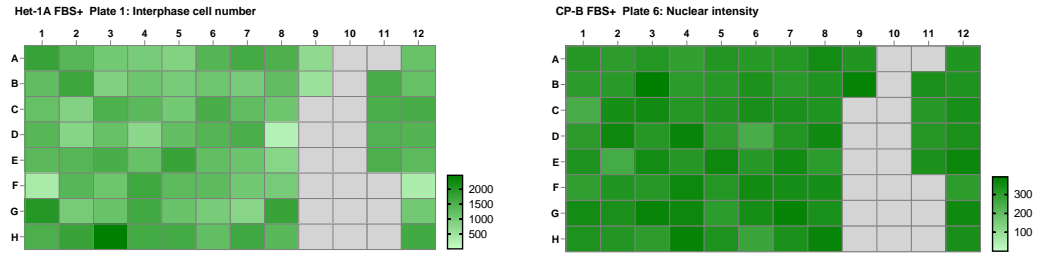


Figure 5.14. Representative plate maps for interphase cell number in NSE (Het-1A) cells and nuclear intensity in HGD (CP-B) cells; both of which were maintained in proliferative media.

known RTK overexpression in HGD, we additionally sought to evaluate whether the relative importance of each RTK varied by stage of BO dysplastic progression through comparing with HGD CP-B and CP-D cells. The relative importance of RTKs in each of these cell lines, and in control NSE Het-1A cells, was determined by high-throughput functional genomic siRNA-mediated knockdown of each RTK. Analysed endpoints included cellular number, as a surrogate of proliferation and viability, and changes in BO morphology; reflecting evidence for a plastic BO ‘phenotype space’.(462)

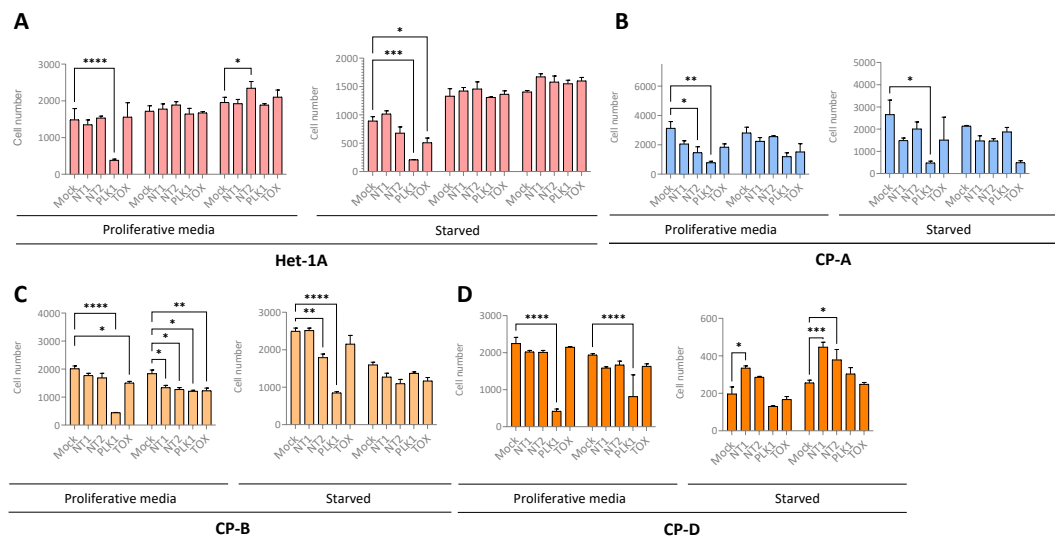


Figure 5.15. A summary of positive and negative control outputs per plate for interphase cell number in (A) NSE (Het-1A), (B) NDBO (CP-A) and (C,D) HGD (CP-B, CP-D) cells. Each graph includes results for a mock (RNAiMAX transfection reagent only) control well, negative control SMARTpool siGENOME siRNAs (NT1: siGENOME Non-Targeting Pool #1; NT2: siGENOME Non-Targeting Pool #2) and positive control SMARTpool siGENOME siRNAs (PLK polo-like kinase 1; TOX: thymocyte selection associated high mobility group box). Three repeats were undertaken for Het-1A (A) and are shown, and two for all other graphs. Data are shown as mean \pm SEM. Analyses were undertaken using ANOVA with post-hoc Tukey correction for multiple significance testing, with all values compared to the mock control. Comparisons that reached pre-defined significance thresholds are highlighted, and are distinguished as follows: * $p \leq 0.05$; ** $p \leq 0.01$, *** $p \leq 0.001$; **** $p \leq 0.0001$.

5.4.2.1.1. Quality control

Functional genomic screens undertaken using siRNAs are susceptible to edge effects, resulting in values ‘drifting’ across a plate. These were assessed for using a combination of plate-wells scatter plots (Fig. 5.13) and plate heatmaps (Fig. 5.14). Amongst some of the studied output values, drift was seen, including for instance for all cell number (Fig. 5.13A). However, other features such as nuclear intensity (Fig. 5.13M) demonstrated little apparent change across the same studied plates. Given the small number of genes knocked down in this screen, we postulated that much of the apparent drift is attributable to the significant variation in the impact of their knockdown. This was confirmed by individual analyses of plate heatmaps which, as reflected in the representative heatmaps shown in Fig. 5.14, demonstrated no obvious edge effects.

Plates were then analysed for the efficacy of positive control-mediated impact on cell number, as shown in Fig. 5. 15. At least one negative control demonstrating a significant reduction in cell number was available for one Het-1A, one CP-A, two CP-B and two CP-D

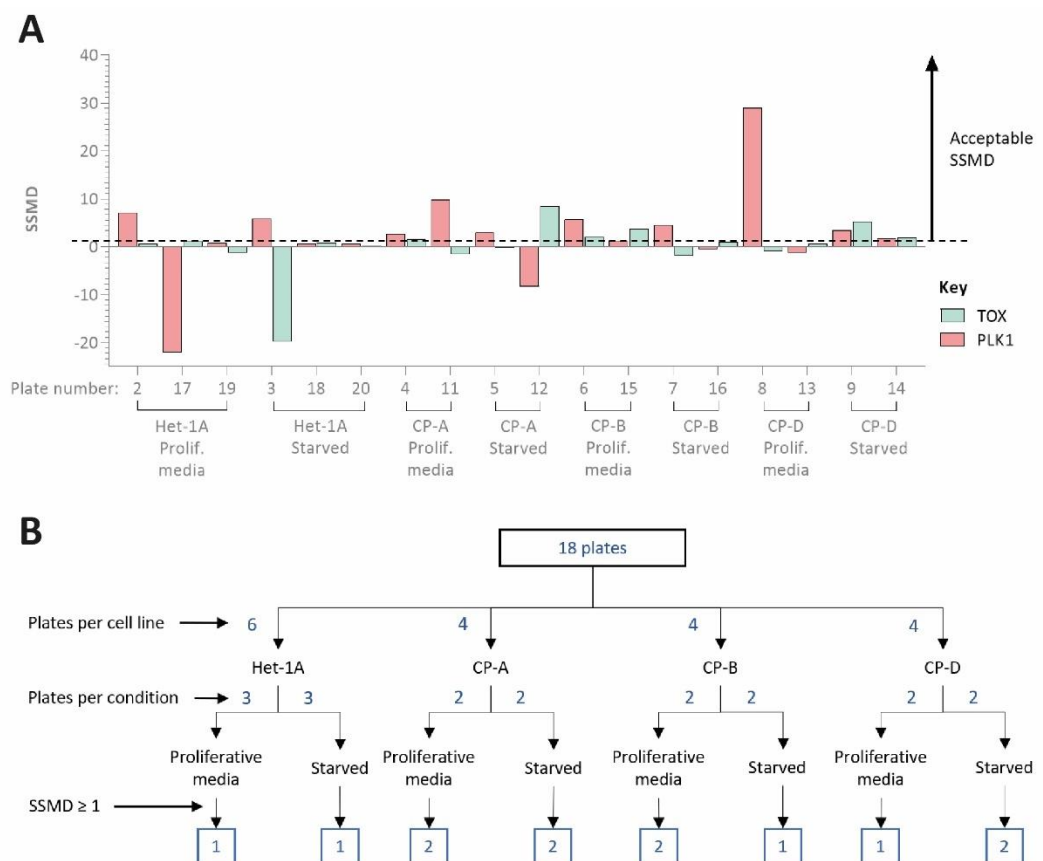


Figure 5.16. A panel illustrating (A) strictly standardised mean difference (SSMD) values for interphase cell number for each replicate (B) their impact on the selection of plates for analysis. In (B) ‘active’ plate numbers at each stage of the quality assessment workflow are shown in blue. The final number of plates (i.e. repeat plates) used for each condition is shown in the blue square box at the end of the flow diagram.

plates assayed within proliferative media, and for one Het-1A, one CP-A, one CP-B and one CP-D plate analysed in serum-starved conditions. This therefore meant the screen passed pre-determined selection criteria with at least one plate demonstrating a successful positive control available for each cell line in each assayed condition. There was, nevertheless, marked variability in the efficacy of the two studied positive controls, and these were therefore regarded to represent ‘moderate’ controls in the context of this screen.

The SSMD was then used as a statistically rigorous means to addressing the limitations of the use of moderate controls, as outlined in *Birmingham et al* and shown in **Fig. 5.16**.(644) As summarised in **5.3.5.4.**, for each plate the highest SSMD value was used to pass or fail the plate, with values less than 1 deemed to reflect plate failure. **Fig. 5.16B** shows the number of plates remaining for output analyses once these quality control criteria had been applied. Briefly, two repeats were available for NDBO CP-A cells cultured in proliferative conditions and conditions of serum-starvation, and two plates were available for HGD CP-B cells cultured in proliferative media and HGD CP-D cells cultured under conditions of serum-starvation. Robust Z-score cut-offs for output analysis were then determined for each studied parameter, as outlined in **5.3.5.4.1.** and summarised in **Fig. 5.17**.

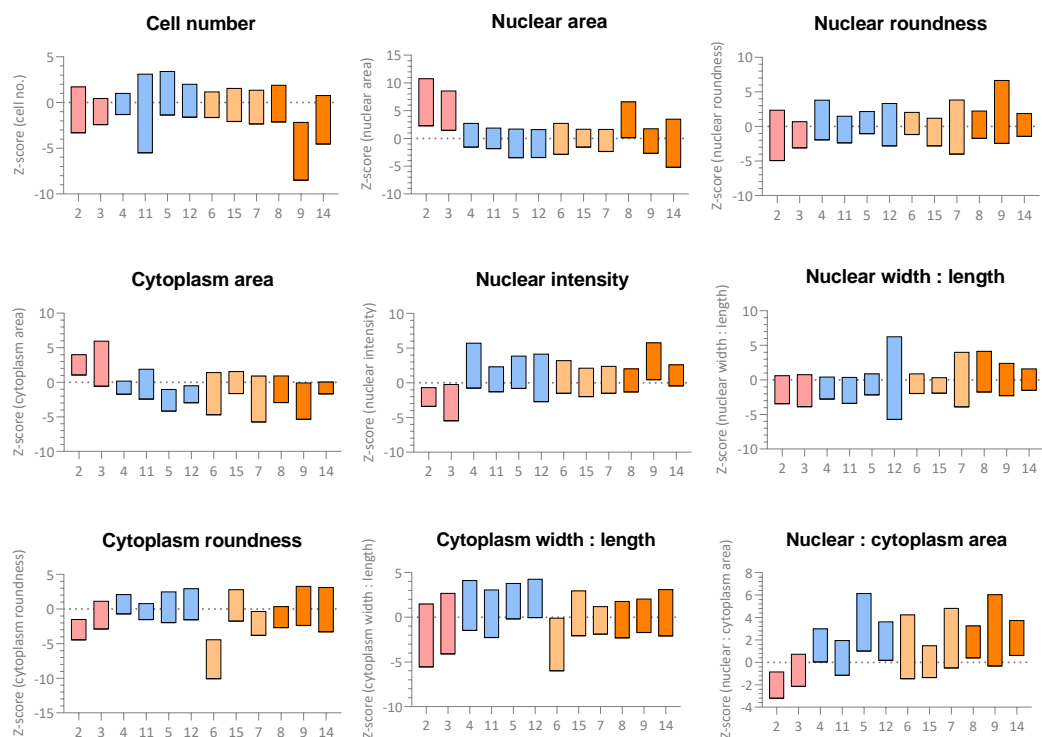


Figure 5.17. Robust Z-score cut-off values for each output per cell line, condition and plate. NSE (Het-1A) cells are shown in pink, NDBO (CP-A) in blue and HGD (CP-B, CP-D) in light (CP-B) and dark (CP-D) orange. Plates 2, 4, 5, 6, 15 and 8 were maintained in proliferative media. Plates 3, 11, 12, 7, 9 and 14 were serum starved.

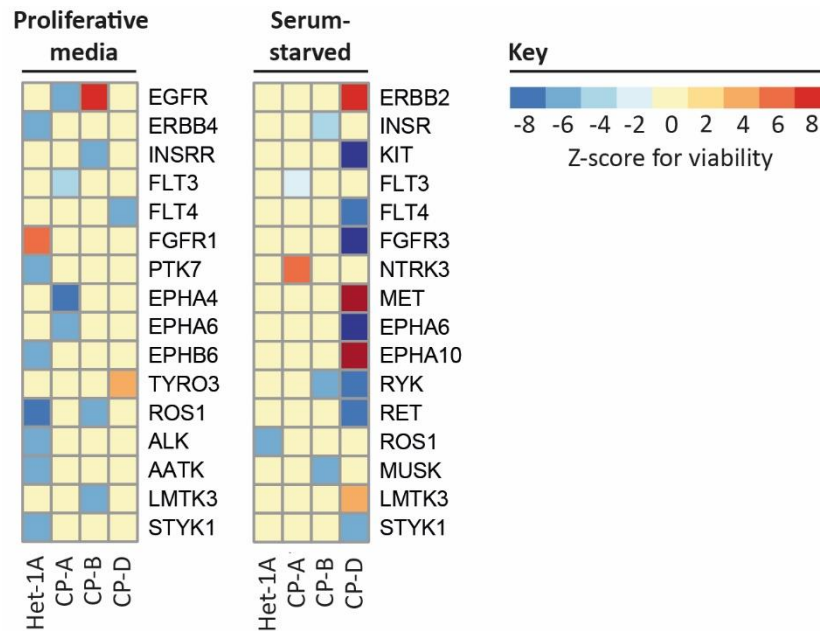


Figure 5.18. Heatmaps demonstrating the impact on cellular viability of siRNA-mediated knockdown of receptor tyrosine kinases (RTKs) under proliferative and serum-starved conditions for NSE (Het-1A), NDBO (CP-A) and HGD (CP-B, CP-D) cells. Z-scores are shown for all values that exceeded plate-specific Z-score cut-off values (as illustrated in Fig. 5.6).

5.4.2.1.2. Viability

Cellular proliferation and viability was determined by final cell number following a 48-hour culture period in proliferative conditions or conditions of serum-starvation. A summary of the ‘hits’ from this screen are shown in Fig. 5.18. A large number of negative hits (meaning a reduced cell number following RTK knockdown) were seen for Het-1A cells cultured in proliferative conditions, and for HGD CP-B cells cultured in serum-starved conditions. Interestingly, knockdown of EGFR led to a reduced cell number in NDBO CP-A cells, but enhanced cell number in HGD CP-B cells. There were few RTKs that had a similar effect across cell lines and surprisingly few shared hits between HGD CP-B and CP-D cells. A number of ephrins were identified to be hits in both culture conditions but this is in the context of this being the largest group of RTKs, so its overrepresentation amongst this list would likely be expected.

5.4.2.1.3. Morphology

BO is known to be maintained in a plastic ‘phenotype space’. We hypothesised that this would be maintained during proliferative and serum-starved conditions by specific RTKs, and that selective knockdown of these RTKs would result in a change in the BO phenotype to a more ‘fibroblastic’, dysplastic-like morphology, or a more epithelial-like morphology.

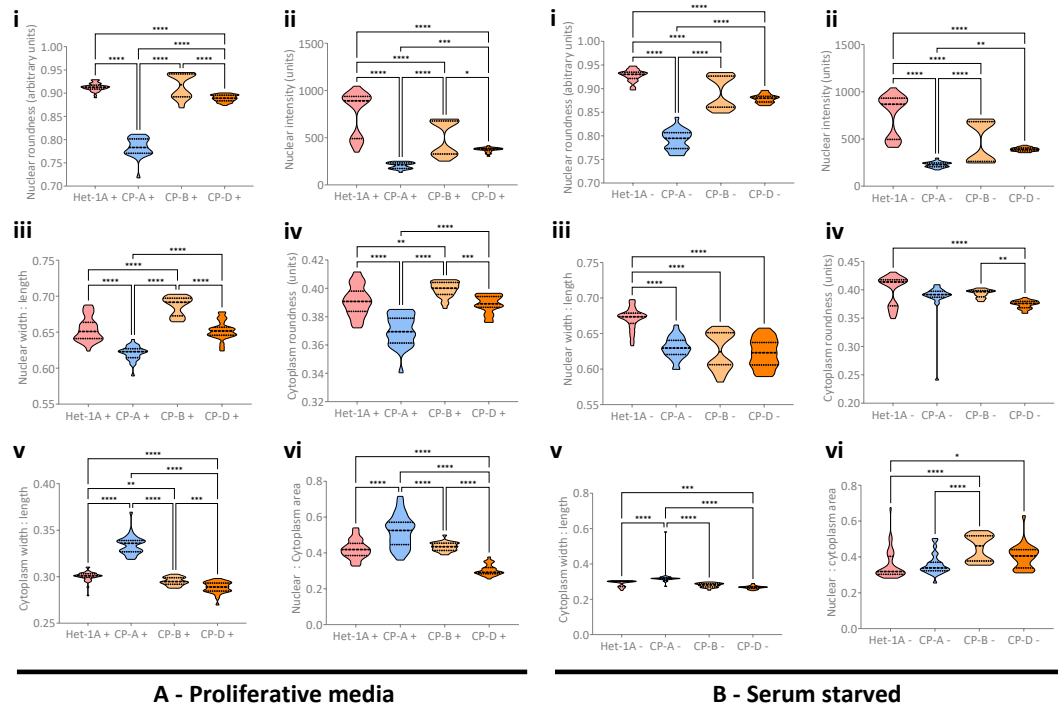


Figure 5.19. Violin plots demonstrating the differences in baseline morphological characteristics between NSE (Het-1A), NDBO (CP-A) and HGD (CP-B, CP-D) cells maintained in (A) proliferative and (B) serum-starved media. (i) Nuclear roundness; (ii) Nuclear intensity; (iii) Nuclear width : length; (iv) Cytoplasm roundness; (v) Cytoplasm width : length; (vi) Nuclear : cytoplasm area. Analyses were undertaken using ANOVA with post-hoc Tukey correction for multiple significance testing. Comparisons that reached pre-defined significance thresholds are highlighted, and are distinguished as follows: * $p \leq 0.05$; ** $p \leq 0.01$; *** $p \leq 0.001$; **** $p \leq 0.0001$.

To assess this, we identified a panel of morphological characteristics that are known to change as BO progresses. These are summarised in **Fig. 5.19.**, which compares each characteristic across NSE Het-1A, NDBO CP-A and HGD CP-B and CP-D cells. As can be seen, most characteristics individually discriminated NDBO from the two HGD lines. We then evaluated the impact of each RTK knockdown on each of these features, characterising ‘hits’ that changed cellular morphology in the ‘direction’ of increased dysplasia (i.e. established a more fibroblastic-like phenotype) or that changed morphology in the direction of decreased dysplasia (i.e. established a less fibroblastic-like phenotype). The outcomes of this analysis are shown in **Fig. 5.20** and summarised in **Table 5.1**.

Interestingly, EGFR is again strongly represented in NDBO CP-A cells, both in proliferative conditions and conditions of serum-starvation. Otherwise, a surprising number of RTKs appeared to be active and essential for maintaining BO phenotype even under conditions of serum-starvation.

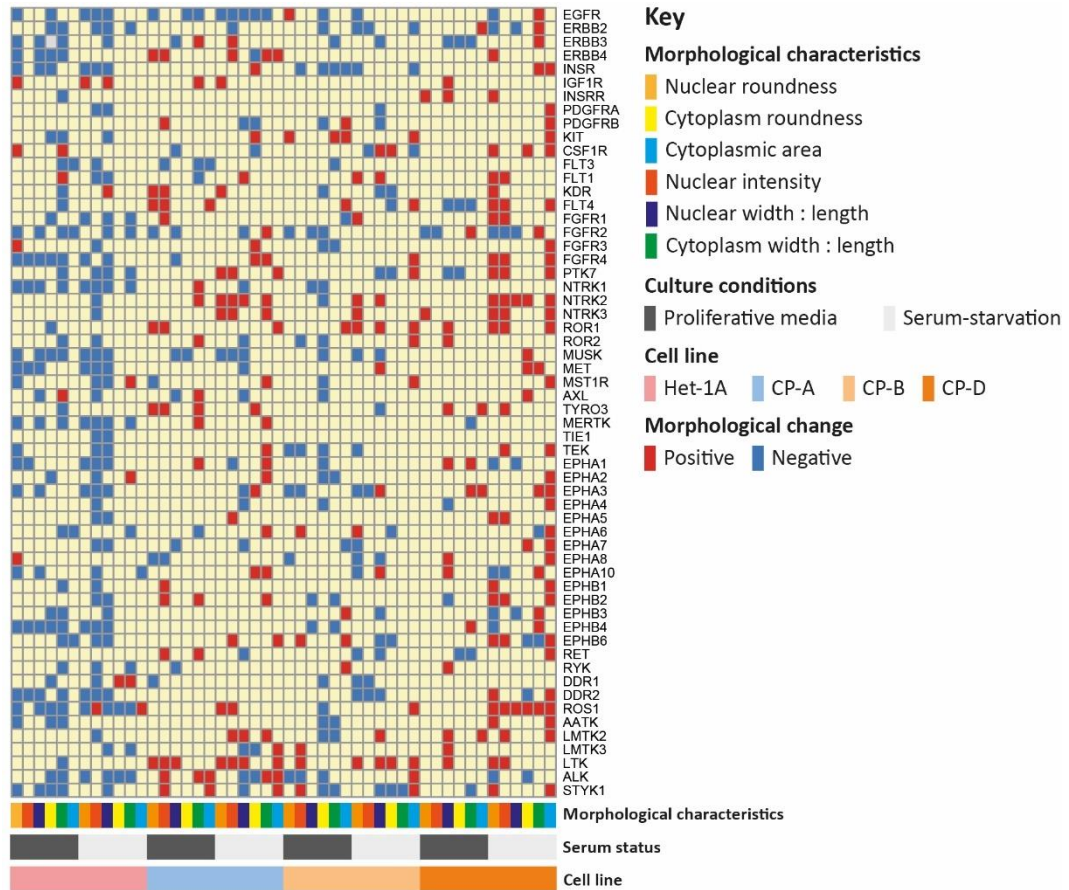


Figure 5.20. A heatmap demonstrating enriched morphological term ‘hits’ following siRNA-mediated knockdown of all 58 RTKs encoded by the human genome in NSE (Het-1A), NDBO (CP-A) and HGD (CP-B, CP-D) cell lines. RTKs are presented, grouped by class, in the right hand-column. Morphological data have been manually curated and grouped by cell line, serum-status (i.e. cultured in proliferative media vs. culture in conditions of serum-starvation) and the morphological characteristic under assessment; as highlighted by the graphical key provided below the heatmap. ‘Positive’ morphological change (i.e. that resulting in the cell adopting a higher-grade dysplastic BO phenotype in response to RTK knockdown) is presented in red. ‘Negative’ morphological change (i.e. that resulting in the cell adopting a lower-grade dysplastic phenotype in response to RTK knockdown) is presented in blue.

	CP-A		CP-B		CP-D	
	+	-	+	-	+	-
Proliferative media	FLT4 TYRO3 LTK ALK	EGFR FLT3	KIT	FGFR2 TEK ALK INSR		ERBB3 FLT4
Serum-starvation	NTRK2 LTK PTK7 NTRK3 LMTK2	MUSK EGFR	LTK ROR1	ERBB2 DDR2	ROS1 NTRK2 CSF1R FLT4 FGFR4 PTK7 NTRK3 ROR1 EPHB2	

Table 5.3. Aggregated data showing the direction of morphological change following RTK knockdown in BO cell lines. RTKs were included if they had three or more terms that following RTK knockdown by siRNA reflected either a (+) more dysplastic or (-) less dysplastic phenotype under both pro-proliferative conditions and conditions of serum-starvation.

5.4.3. ROS generation under conditions of serum-starvation

Given that increased ROS generation has been associated with increased RTK activity in BO under conditions of stress, we sought to quantify ROS after a 48-hour period of serum-starvation. As shown in **Fig. 5.21.**, a significant increase in ROS was seen in all conditions.

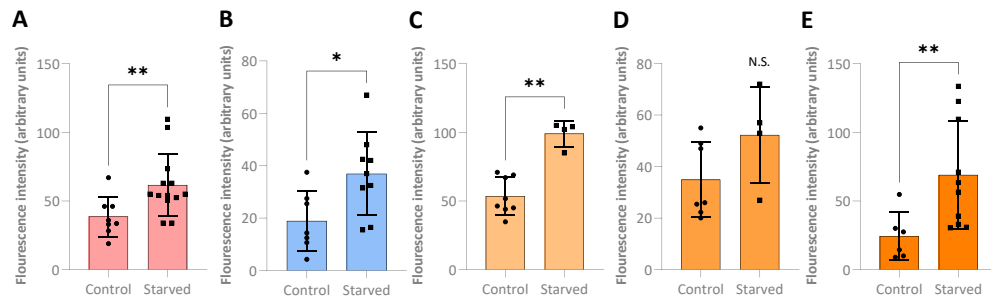


Figure 5.21. Reactive oxygen species (ROS) production following a 48-hour culture period within proliferation media (Control) or conditions of serum-starvation (Starved). Statistical analysis was undertaken using the Mann-Whitney test. Comparisons that reached pre-defined significance thresholds are highlighted, and are distinguished as follows: * $p \leq 0.05$; ** $p \leq 0.01$. N.S.: non-significant. $n \geq 4$ for all comparisons.

5.4.4. Expression of RTKs implicated in mediating the BO basal and stress-responsive phenotype in NSE (Het-1A), NDBO (CP-A) and HGD (CP-B) cells, and matched patient samples

Finally, we sought to validate any potential role in BO progression for RTKs highlighted in **Chapters 2-5** by determining protein expression, and its change, in NSE, BO dysplasia and OAC using both the cell lines studied here and patient samples. A subset of RTKs identified in the siRNA screen were used for this analysis so as to determine the extent to which the outcomes of the siRNA screen were impacted by the expression of genes rather than the importance of their activity. We also sought to quantify any post-translational processing of RTKs by determining both protein and mRNA expression of a subset of RTKs most frequently identified in this work.

As seen in **Fig. 5.22.**, NDBO CP-A cells exhibited higher protein and mRNA expression of EGFR, IGF1R, FGFR3 and EPHA4 than HGD or NSE cells. They also demonstrated higher expression of IR and c-Met. Intriguingly, expression of KIT was very low in CP-B cells despite appearing as a 'hit' in the siRNA screen. These differences broadly compared to those seen in patient samples (**Fig. 5.23**), albeit with higher levels of a number of RTKs seen in NSE.

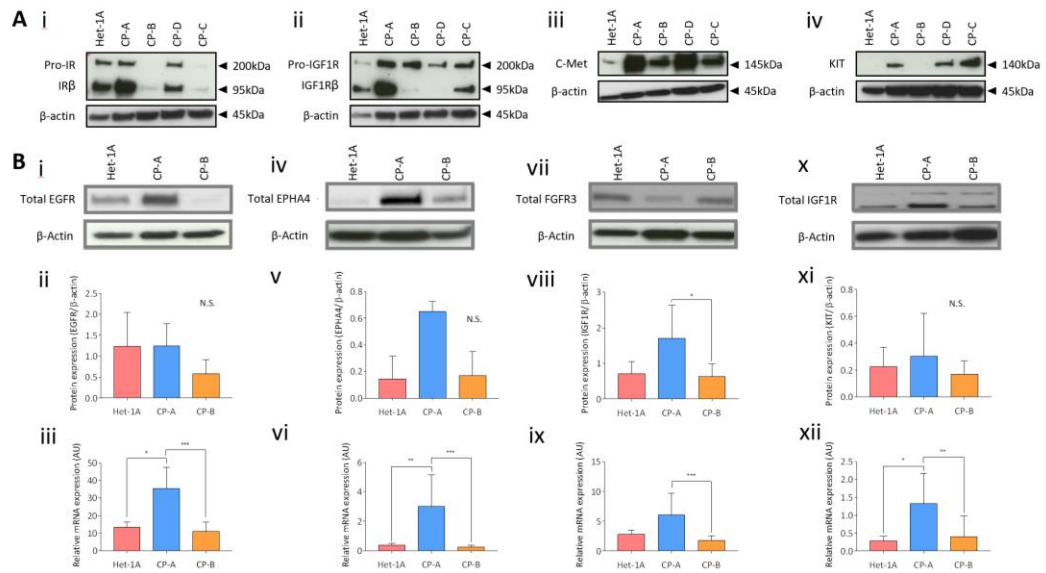


Figure 5.22. The relative expression of receptor tyrosine kinases in NSE Het-1A, NDBO CP-A and HGD CP-B, CP-C and CP-D cell lines. (A) Relative protein expression of (i) insulin receptor (IR), (ii) IGF1R, (iii) c-Met and (iv) KIT was assessed by immunoblot using NSE (Het-1A), NDBO (CP-A) and HGD (CP-B, CP-C and CP-D) cell lines. **(B)** The relative protein (i, ii, iv, v, vii, viii, x, xi) and mRNA (iii, vi, ix, xii) expression across NSE (Het-1A), NDBO (CP-A) and HGD (CP-B) cell lines. N.B. Two sets of experimental analyses, undertaken at different times, are presented for IGF1R. A, n=1. B, n=3 for all protein analyses and n=6 for all mRNA analyses. Samples were analysed using the Kruskal-Wallis test with post-hoc Dunnet's correction for multiple significance testing. Significant comparisons are highlighted as follows: * p<0.05; ** p<0.01.

5.5. Discussion

The results outlined in Chapters 3 and 4 suggested that RTKs play an important role in mediating signalling, genetic expression and, in turn, the phenotype of BO cells maintained in pro-proliferative conditions, as well as in response to serum-starvation and acidic bile salt-induced stress. In this chapter, we used a variety of techniques to explore the specific RTKs responsible for mediating signalling in each of these conditions, as well as to evaluate possible mechanisms for their activation.

5.5.1. RTK activation under conditions of reflux-mediated stress

In order to explore the context in which RTK activation occurs, we determined changes in the cytoplasmic pH of NSE Het-1A, NDBO CP-A and HGD CP-B cells in response to the extracellular application of pH 4.0 media. All three studied cell lines demonstrated a substantial reduction in pH during the ten minute acid exposure period, though CP-A cells appeared to begin to compensate for this and had the highest pH value whilst still exposed

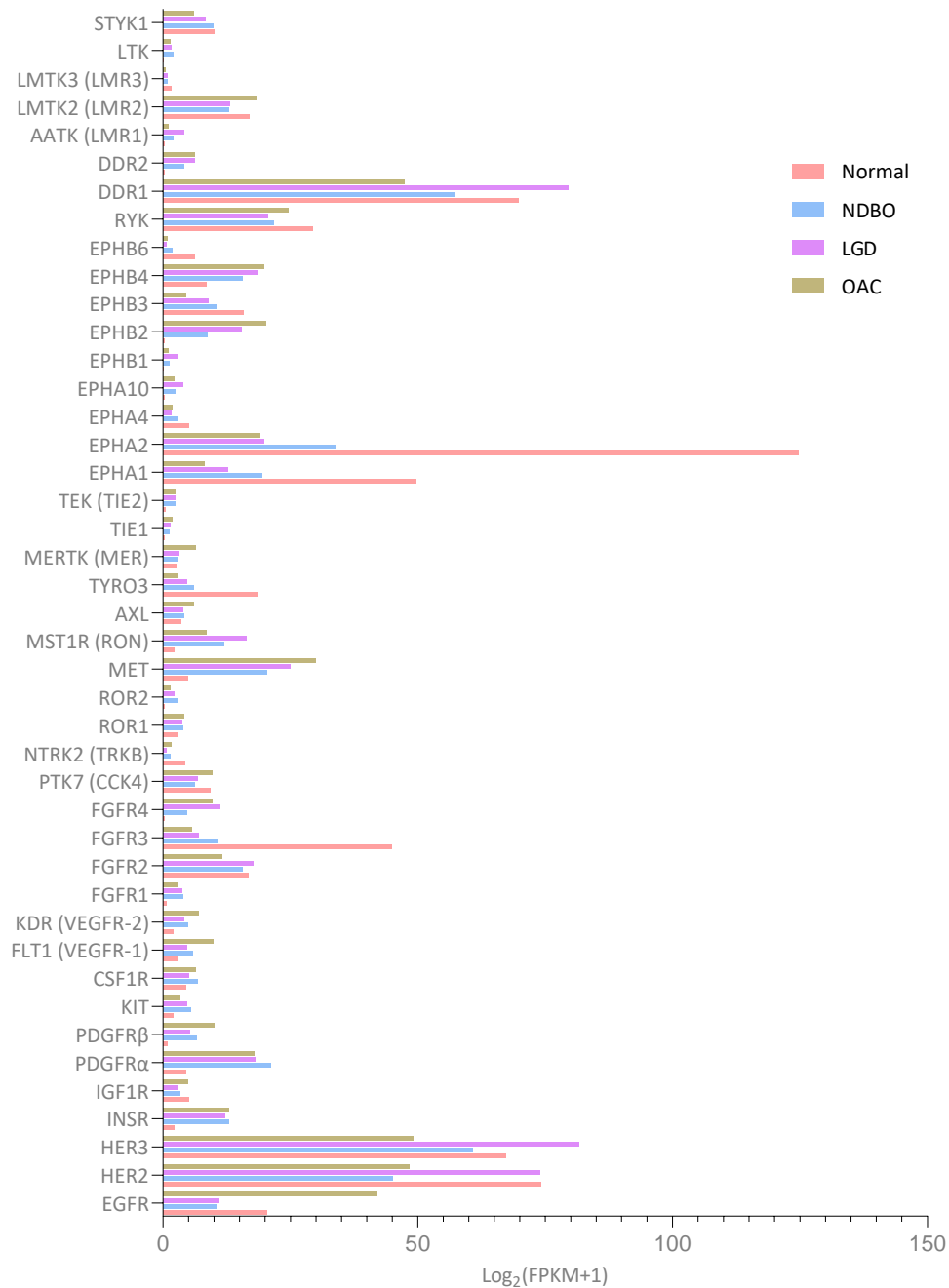


Figure 5.23. The total mRNA expression of RTKs in normal, NDBO, LGD and OAC tissues in a patient dataset cultivated by Maag et al. (486) RTKs for which FPKM values were less than 1 across all tissue types are unlikely to be expressed and were removed from the graph.

to acidic media. Once neutral media was restored, the intracellular pH of all three cell lines rapidly recovered.

It has been suggested previously that BO cells might represent a cellular population that is better adapted for the reflux-rich lower oesophageal environment. It is tempting to suggest that this is reflected by the apparent ability of the NDBO CP-A cells to begin to buffer against the pH change induced by external acid exposure. However, the relative impact of acid on

changes in, and the absolute, cytoplasmic pH of NSE or BO, or even between stages of BO, cannot be reliably concluded on the basis of the results demonstrated here from a cell line grown in 2D. Rather, any such conclusions should be drawn from 3D modelling that allows for cells to generate and maintain a protective luminal surface, AJCs and the multiple other protective factors previously outlined in **1.1.2.2.1**. Instead, the changes in cytoplasmic pH outlined here serve to highlight the conditions in which the early signalling changes and RTK phosphorylation mapped here and in **Chapter 4**, occur.

With this aside, it is interesting to note that the cytosolic pH fell below that of the extracellular media in which cells were cultured. *In vivo*, extracellular pH is slightly alkaline, at around 7.3-7.4.(645) Despite this, the cytoplasm has a tendency to acidify and cytoplasmic pH generally remains below that of extracellular fluid. This is partly due to the generation of acidic metabolites through processes such as mitochondrial oxidative phosphorylation, and partly a consequence of the negative electrical membrane potential, which results in the cellular uptake of positive ions. Oxidative phosphorylation likely increases in response to an acidic cytoplasmic pH due to a lower dependence on oxygen.(646) These processes may therefore have continued to drive the cytosolic pH below that of the applied acid stressor within the studied cell lines.

The compensatory mechanisms for intracellular acidification include acid-extruding bicarbonate transporters, lactate-H⁺ co-transporters, alkali cation-H⁺ exchangers and acid-loading transporters.(645,647,648) This latter group utilises Cl⁻-HCO₃⁻ exchange, which is mediated by anion exchangers and SLC26A proteins.(645) In **Chapter 3**, CFTR expression was seen to significantly increase in response to acidic bile salts, whereas in **Chapter 4**, a reduction in CFTR activity followed exposure to the same stressor. CFTR regulates the activity of SLC26A proteins as well as acting as conducting ATP-mediated Cl⁻ and HCO₃⁻ exchange.(649) It may then be that CFTR activity reduced as a compensatory response to significantly reduced cytosolic pH (i.e. preserving buffering HCO₃⁻ within the cytoplasm) but its expression increased as a mechanism to exert greater control over SLC26A proteins.

It is significant that EGFR phosphorylation persisted in NDBO CP-A and CP-B cells despite this low pH, and that EGFR exhibited relatively higher levels of phosphorylation than any other assessed RTK. Overall, this supports the significant role for EGFR signalling in responding to acid outlined in **Chapters 3** and **4**, suggesting that early changes in EGFR phosphorylation drive a network response in which multiple RTKs are phosphorylated. These include HER2,

which was identified within the acidic bile salt responsive EGFR signalling 'hub' in **Chapter 4**, and the phosphorylation of which is seen here to increase at a similar time to that of EGFR.

Remarkably, and though this is caveated by the availability of only a single repeat, a ten minute pulse of acidic bile salts substantially increases activity of ASMase. This is required for cellular viability following acidic bile salt exposure, as is – albeit to a lesser extent – NSMase. It is unclear what function in particular it drives to maintain viability, but the data suggest that ASMase reduces the increase in EGFR and IGF1R phosphorylation seen following acidic bile salt withdrawal. This is likely a consequence of this enzyme's function in generating lipid rafts, and it is possible that other RTKs or signalling molecules are sequestered away from EGFR and IGF1R as a consequence of ASMase activity, which would then prevent their phosphorylation. This is an interesting area to study in further work, not least given the link between FIASMAs such as imipramine and the risk of progression of BO. In particular, it would be helpful to visualise RTKs and identify their relative presence within or outside of lipid rafts whilst responding to acidic bile salts, both with and without the presence of an ASMase inhibitor.

5.5.2. RTK control of cellular viability and morphology under basal and serum-starved conditions

Enrichment of genes responding to serum-starvation in **Chapter 3** highlighted a role for growth factor-led signalling in maintaining the pro-survival, pro-quiescence, pro-autophagic phenotype it creates. This is unexpected given that serum-starvation is likely to result in a reduction in exogenous growth factor availability, though data provided in **Chapter 3** did also demonstrate upregulation of a number of RTK ligands in response to serum-starvation. In light of this, we elected to determine the impact of selective RTK knockdown on BO viability and phenotype, hypothesising that as cells are maintained in a 'phenotype space', it would be possible to determine which RTKs most strongly contribute to pro- or anti-dysplastic features.

As outlined here, a surprising number of RTKs are active in the serum-starved state. It is possible that these are responding to the autocrine or paracrine production of growth factors. Equally, it may be that non-classical RTK-derived signalling mechanisms are operating under conditions of serum-starvation, including for example via interactions between the proline-rich motifs present on a number of RTKs with the SH3 domains of intracellular proteins. It was beyond the scope of this work to explore to what extent these

typical and atypical mechanisms underpin the autophagic state of BO, but given its importance in maintaining the viability of BO cells which may harbour genomic change, this would be of considerable interest from the point of identifying novel cancer promotion mechanisms.

A number of the RTKs identified as potential regulators of both morphology and viability have previously been linked with BO dysplastic progression, including for instance EGFR and erbB-2. There are however a number of novel targets, including most pertinently the NTRKs, which were also identified in the kinase activity assay outlined in **Chapter 4**. Interestingly, there was very little concordance in identified hits even amongst the two HGD cell lines. This may be a consequence of the significant differences seen in RTK expression between cell lines, as has also been shown here. This does not, however, act to undermine this analysis. Rather, whilst a hit may be more likely to occur if the RTK is strongly expressed in that cell line, the occurrence of the hit still points to a potential role for that particular RTK in maintaining viability or, for example, dysplastic features. In further work, this will allow for a candidate list of potential RTK predictors and mediators of BO progression to be evaluated.

5.5.3. Limitations

The use of a phospho-RTK screen and immunoblotting has allowed for the further validation of the kinase assay and, reassuringly, points to the activity of similar RTKs. It is, however, important to note that neither this analysis nor that outlined in **Chapters 3 and 4** provides a definitive readout of the function of the RTKs identified to respond to acidic bile salts. This is likely to be difficult to determine in full given that any contribution to BO dysplastic progression will be seen over years, rather than minutes. We will explore this in further work using the OCCAMS dataset, through which we will be able to correlate the expression of EGFR and other RTKs identified as stress-responsive with known mediators of dysplastic progression such as members of inflammatory pathways and key transcription factors.

Further, whilst the siRNA screening approach used here benefits from high-throughput imaging, the identification of morphology hits as a surrogate for dysplastic progression is crude. In further work, the images obtained from the screen will be subject to an unbiased analysis using artificial intelligence, from which it will be possible to categorise RTK function by the 'cellular type' attributed to images following each RTK's knockdown. It will also be important to fully validate the screen hits identified here, both through their evaluation in

patient data as outlined above, and through a planned second siRNA screen that uses different chemistries.

5.6. Conclusions & future work

This work has again highlighted EGFR as a mediator of the response to acidic bile salt withdrawal in BO, identifying that its activation loop phosphorylation is relatively higher than all other RTKs in both NDBO CP-A and HGD CP-B cells. EGFR phosphorylation appears to increase rapidly from this start point following this start point in a process that may be mediated by ASMase. The importance of sphingolipid signalling has also been confirmed, whilst an unbiased functional genomic screen has provided a candidate list of RTKs to be explored further for their potential role in mediating autophagic stress and, crucially, both the viability and the cell cycle exit and entry of NDBO CP-A and HGD CP-B and CP-D cell. The wider context of these findings and planned future work are outlined in **Chapter 6**.

Chapter 6

Discussion & conclusions

6.1. Discussion

The incidence of BO has increased dramatically over recent decades.(42–44) This is attributed to environmental influences that include GORD, obesity and smoking; which together account for between 70-80% of cases of OAC.(73,99) However, despite significant evidence for their role in both the development and the dysplastic progression of OAC, the mechanisms through which risk factors such as GORD contribute to neoplastic transformation have remained unclear. Nevertheless, it is increasingly apparent that OAC arises not through the development of a small number of driving genetic aberrations, but as a consequence of multiple small changes and, crucially, a breakdown in gene-regulatory control.(258)

This work has utilised integrated analyses of cellular signalling, chromatin accessibility and the resultant transcriptome to explore the impact of stressors common to the BO microenvironment on gene regulation, and to delineate their upstream mediators. Using a cell line model that we validate to reflect at least two distinct stages of BO progression, we identify RTKs as key mediators of the BO cellular stress response. We also demonstrate that whilst direct acid exposure suppresses tyrosine phosphorylation, its withdrawal leads to significant upregulation in PTK activity that is led by a network RTK response for which EGFR is a key mediator, and which is shared across NSE, NDBO and HGD cells. A number of other RTKs are also implicated in this cellular response to acid as well as in controlling cellular viability and proliferation, and the BO dysplastic phenotype space, under conditions of serum-starvation. Amongst others, these include multiple other members of the EGFR family, NTRK2 and FGFR2. Fascinatingly, a number of these exert significant control over cellular viability, proliferation and phenotype even in the absence of exogenous ligand;

demonstrating either significant autocrine and paracrine signalling, or prevalent signalling processes mediated by catalytically active RTKs, such as through proline-rich motif-SH3 domain mediated interactions.

Interestingly, amongst these multiple RTKs, IGF1R was noted to decrease in phosphorylation (and thereby activation) in response to acidic bile salts. This is of particular interest given the relationship of the metabolic syndrome (and thereby hyperinsulinaemia) with the development and dysplastic progression of BO. It is, however, unclear what the direct phenotypic impact would be of a reversal of the reduction of IGF1R phosphorylation, or the increase in EGFR phosphorylation, that is seen in response to acidic bile salts. It is however interesting to note that EGFR is considered likely to act independently of ligand in CP-A cells (i.e. in conditions of serum-starvation), and that its phosphorylation persists to an intracellular pH of 4. It is possible, as outlined in **Chapter 5**, that this relates either to either a tendency to greater autophosphorylation at lower pH, or to changes in the membrane localisation of EGFR, such as that mediated by acid sphingomyelinase, that can result in the formation of signalling facilitative lipid rafts.

The findings outlined here must, however, be viewed in the context of both the strengths and the limitations of this study. Firstly, the bulk of the data presented here draw from an *in vitro* 2D model incorporating five cells derived from NSE, NDBO and HGD. As outlined in **Chapter 3**, the NDBO CP-A and HGD CP-B, CP-C and CP-D cells are separated by a number of morphological and phenotypic features that indicate these derive from clearly different stages of BO dysplastic progression. However, in the absence of characterised parent cells for these lines, and without an effective biomarker for dysplastic progression, this cannot be confirmed. It is also noteworthy that the NSE Het-1A cell line lacks a number of features that would be expected for NSE tissue and, as others have highlighted, is likely to reflect a dysplastic squamous cell type.⁽⁴⁹¹⁾ Given the close correlation in the cellular response to acid across the studied cell lines, it is unlikely that the dysplastic phenotype of the Het-1A cells has significantly impacted on the conclusions drawn here. Nevertheless, it is important that the analyses outlined here are repeated in a cell line that is more representative of NSE.

The limitations of immortalised 2D cell lines, particularly those held in monoculture, for modelling physiological events are well described within the literature.⁽⁶⁵⁰⁾ These include genetic drift over multiple passages, abnormal or non-representative gene expression, a lack of cellular heterogeneity and the absence of cell-cell interaction with a stromal compartment and other cells. Some of these aspects can be controlled for, such as the

approach we have taken here to use a combination of 'high' and 'low' passage cells in each 'omics' analysis in order to control for any passage-related genetic drift. It is also possible to co-culture the cells used here, and it would be of interest to determine whether stromal constituents, or culture with inflammatory cells, alters kinase activity or gene regulation. Even so, the 2D model does not recapitulate normal tissue architecture and cell-cell interactions, nor normal intercellular heterogeneity. This is of particular importance when considering the role of intercellular junctions and the AJC in maintaining the pH of epithelial cells exposed to acid within the oesophagus.(124,125,138) It is, for example, surprising that the data outlined in **Chapter 5** indicate a dramatic fall in intracellular pH despite evidence that BO (but not NSE) cells *in vivo* are able to limit pH changes in response to luminal acid exposure.(137)

For some disease sites faced with the same concerns, animal research provides an alternative model in which data can be validated. However, and as has been outlined here, there are no animal models in which OAC spontaneously develops, nor any that faithfully recapitulate both the biology and anatomy of human tumours.(142) Instead, patient-derived organoids (PDOs) offer an alternative *in vitro* model that recapitulates inter-cellular heterogeneity and 3D cellular interactions. Whilst in the past, these proved technically challenging to derive in BO, a number of groups have demonstrated that it is feasible to generate a living biobank of BO PDOs.(465,467) This includes the Fitzgerald Group (Cambridge), who now have an established pipeline for the generation of both OAC and BO PDOs (personal communication). It would then be interesting to compare the kinase activity and transcriptomic responses to cellular stress that are seen here in the BO PDO models.

Using this cell line model, we established stressors that led to the differential expression of genes enriched for processes known to associate with the dysplastic progression of BO. This includes a pro-autophagic response to serum-starvation, and a pro-inflammatory/migratory EMT response to acidic bile salts. It is a strength of this work that the viability of the studied cells in response to these stressors was confirmed and their phenotypic impacts analysed using orthogonal approaches. This work is in addition strengthened by the extensive *a priori* analyses of existing literature used to define a near-physiological acidic bile salt exposure. However, *in vivo*, patients with severe BO or GORD may be exposed to in excess of 100 episodes of reflux over a period of 24 hours, with reflux persisting for the many years over which BO dysplastic change is known to occur. The relative impact of a single pulse of acidic bile salts versus over 100 pulses per day for multiple weeks is unclear. Unsatisfactorily, the attempted long-term treatment of cells in this work has not been repeated, and it was not

practical to treat the cells for in excess of a single pulse a day for five days a week. However, recent improvements in microfluidics technology would now provide an opportunity to study cellular signalling and gene regulatory control in response to repeated, automated, acidic bile salt exposures and should be explored.(651) It would be particularly interesting to evaluate the impact of a patient's own refluxate on *ex vivo* tissue held within a microfluidics device; including through the use of single-cell RNA sequencing to analyse the impact of this stressor on different cellular populations within the tissue segment.

Serum-starvation was used as an additional stressor, with enrichment of differentially enriched genes suggesting that this results in a quiescent, pro-autophagic phenotype. It is known that there are significant cellular populations of cells that are quiescent or that have undergone autophagy in BO tissue.(483,517) This is, however, an underdeveloped area of research in BO despite the putative importance both of autophagy for regulating survival in response to stress, and of the exit and entry of cells in to the proliferating compartment. It is, after all, only when proliferating that cells can exhibit a majority of the cancer hallmarks.(432) Application of a simple and reproducible cellular stress, such as serum-starvation, may therefore provide for new approaches to study different populations of cells in BO. However, the gene enrichment here should be confirmed through the analysis of the protein expression of specific markers of autophagy.

Nevertheless, within this cell line model we utilised analyses of intracellular kinase activity, gene expression and chromatin accessibility, coupled with a functional genomic screen, to determine the impact of exposures on gene-regulatory control and its upstream mediators. This integrated analysis is a particular strength of this work, but it is associated with a number of limitations. Most pertinently, technical failure of an ATAC-seq repeat means that data on chromatin accessibility are presented as exploratory only, and a second control reading is needed to definitively conclude on patterns of chromatin accessibility in response to the studied stressors. It is also noteworthy that the impact on chromatin accessibility of neither bile salts nor acid alone was sampled, though it seems unlikely that their individual contribution would differ much beyond that suggested by the kinase array.

Indeed, a particular strength of the kinome analyses undertaken here is the use of a versatile, statistically-powered system that allowed for the high-throughput analysis of multiple PTK and STK signalling outcomes in multiple samples that could then be compared with one another. Whilst this was very much appropriate for this work, there are multiple cellular kinase events, not to mention myriad PTMs, that would not have been evaluated

within the kinase activity assay. A wider exploration of these could be undertaken using more sophisticated proteomics approaches, particularly now given that these could be targeted towards the use of a single exposure (acidic bile salts) at a single stage of BO dysplastic progression.

Finally, the functional genomic screen is limited by the lack of a validation screen. It does nevertheless provide a unique approach for identifying cellular components that sustain, inhibit or propagate the BO dysplastic phenotype space. In order to expand this further, validation of intracellular protein endpoints should be undertaken to support the outputs of the screen. This may, for example, include analysing E-cadherin and N-cadherin protein expression in cells that appear to trend towards a greater EMT phenotype in response to gene knockdown. It would also be of interest to undertake an unbiased analysis of the phenotypes generated by RTK knockdown using an automated intelligence (AI) approach such as that offered by the open-source software, CellProfiler. This may allow for the more sophisticated subcategorization of the impacts of knockdown of each of the studied RTKs.(652)

Despite these limitations, it is satisfying that each of the four screens implicated the same RTK (EGFR) as a key driver of the BO cellular response in NDBO CP-A cells. It is also reassuring that many of the processes enriched from the DEGs identified by RNA-seq following acidic bile salt exposure were also enriched in analyses of the pathways upstream of the transcriptional response. This lends considerable support to the approach taken here, which has a number of potential clinical implications.

Firstly, the identification of EGFR and a number of other RTKs as potential mediators of the BO cellular response warrants their exploration as predictive biomarkers for dysplastic progression; either alone or in combination. Depending on their functional impact, which requires further analysis, it is in addition possible that one or a number of these RTKs could form the basis for new chemopreventative or chemotherapeutic strategies, including through the use of already available tyrosine kinase inhibitors. Secondly, it seems likely that the cellular signalling response to acidic bile salts shown here also occurs in OAC. If so, this may be impacting on the efficacy of both systemic anti-cancer therapy and radiotherapy; not least given that patients must lie supine, increasing their exposure to refluxate, to receive the latter. Thirdly, bile salts/acids (at neutral pH) are implicated in the development of other malignancies of the gastrointestinal tract, including pancreatic adenocarcinoma, hepatocellular carcinoma and colorectal cancer.(653–655) The data shown here should

prompt an analysis of the potential for PLCy1-mediated signalling to drive these cancers in response to acidic bile salt exposure. Fourthly, the signalling shown to derive from changes in pH here may well occur across cell types throughout the body, particularly in cancerous conditions in which pH changes follow increased metabolic activity. This should be explored as a potential ubiquitous driver of anti-cancer therapy resistance.

Finally, this work has, above all, demonstrated the importance of a systemic analysis of gene regulatory control mechanisms to understand the drivers of BO progression. It is, for instance, apparent that different cellular stressors (in this case acidic bile salts versus serum-starvation) can drive entirely different transcriptional profiles in the presence of a fixed genotype. The impact of these varying transcriptional responses on increasing cellular instability risks being missed through fixed analyses of genetic change at each stage of BO progression.

6.2. Conclusions & further work

Using analyses of chromatin accessibility and gene expression, we demonstrate that the exposure of NDBO CP-A cells to acidic bile salts and serum-starvation recapitulates gene-regulatory and phenotypic changes that are associated with BO dysplastic progression. These include enrichment with both conditions of RTK-mediated signalling. Using a kinase activity assay, we demonstrate that direct acid exposure suppresses PTK, but not STK, signalling across NSE, NDBO and HGD cell lines. This is restored on withdrawal of acid, with a conserved RTK-led signalling response leading a significant upregulation in the activity of MAPK and PI3K/Akt pathways, which in turn mediate a pro-migratory, pro-inflammatory Th1-cytokine type response. This includes direct activation of the NF- κ B pathway, consensus chromatin sequences for which are identified at 24 and 48 hours post acidic bile salt exposure. In contrast, we demonstrate that serum-starvation results in a pro-quiescent, pro-autophagic cell signature. Using siRNA-mediated functional genomic screening, we determine a subset of RTKs that control both BO viability under conditions of stress, and the BO phenotype (i.e. dysplastic) space. Reflecting these different stressors, a number of chromatin sites that open in response to acidic bile salts were closed with serum-starvation, and vice-versa. The consensus site for KLF5 binding, which has recently been implicated in BO progression, was however open in response to both stressors. We propose on the basis of these data that RTKs act to mediate stress response in BO and drive signalling that may catalyse dysplastic progression. This has important consequences for the clinic, including the potential for one or a number of RTKs to be used as predictive biomarkers for BO

progression, and for these same molecules to form the basis for chemopreventative and chemotherapeutic treatment strategies.

This will be analysed in further work, including through correlating the expression and co-expression of RTKs identified here with both BO dysplastic progression, and its known inflammatory and proliferative mediators. It will also be important to repeat and thereby confirm the results of the chromatin accessibility assays shown here, and to undertake knockdown analyses to validate the phenotypic impact of RTKs highlighted in this analysis on BO cellular behaviour.

List of References

1. Kamangar F, Nasrollahzadeh D, Safiri S, Sepanlou SG, Fitzmaurice C, Ikuta KS, et al. The global, regional, and national burden of oesophageal cancer and its attributable risk factors in 195 countries and territories, 1990–2017: a systematic analysis for the Global Burden of Disease Study 2017. *Lancet Gastroenterol Hepatol*. 2020 Jun 1;5(6):582–97.
2. Smyth EC, Lagergren J, Fitzgerald RC, Lordick F, Shah MA, Lagergren P, et al. Oesophageal Cancer. *Nat Rev Dis Primer*. 2017 Jul 27;3:17048.
3. Arnold M, Lavrsanne M, Brown LM, Devesa SS, Bray F. Predicting the Future Burden of Esophageal Cancer by Histological Subtype: International Trends in Incidence up to 2030. *Am J Gastroenterol*. 2017 Aug;112(8):1247–55.
4. Offman J, Pesola F, Sasieni P. Trends and projections in adenocarcinoma and squamous cell carcinoma of the oesophagus in England from 1971 to 2037. *Br J Cancer*. 2018 May;118(10):1391–8.
5. Arnold M, Ferlay J, van Berge Henegouwen MI, Soerjomataram I. Global burden of oesophageal and gastric cancer by histology and subsite in 2018. *Gut*. 2020 Sep;69(9):1564–71.
6. Edgren G, Adami H-O, Weiderpass E, Weiderpass Vainio E, Nyrén O. A global assessment of the oesophageal adenocarcinoma epidemic. *Gut*. 2013 Oct;62(10):1406–14.
7. Blüher M. Obesity: global epidemiology and pathogenesis. *Nat Rev Endocrinol*. 2019 May;15(5):288–98.
8. Dirac MA, Safiri S, Tsoi D, Adedoyin RA, Afshin A, Akhlaghi N, et al. The global, regional, and national burden of gastro-oesophageal reflux disease in 195 countries and territories, 1990–2017: a systematic analysis for the Global Burden of Disease Study 2017. *Lancet Gastroenterol Hepatol*. 2020 Jun 1;5(6):561–81.
9. Maret-Ouda J, Markar SR, Lagergren J. Gastroesophageal Reflux Disease: A Review. *JAMA*. 2020 Dec 22;324(24):2536–47.
10. Haggitt RC, Tryzelaar J, Ellis FH, Colcher H. Adenocarcinoma Complicating Columnar Epithelium-lined (Barrett's) Esophagus. *Am J Clin Pathol*. 1978 Jul 1;70(1):1–5.
11. Curtius K, Rubenstein JH, Chak A, Inadomi JM. Computational modelling suggests that Barrett's oesophagus may be the precursor of all oesophageal adenocarcinomas. *Gut*. 2020; Nov 24 [epub ahead of print].
12. Sawas T, Killcoyne S, Iyer PG, Wang KK, Smyrk TC, Kisiel JB, et al. Identification of Prognostic Phenotypes of Esophageal Adenocarcinoma in 2 Independent Cohorts. *Gastroenterology*. 2018;155(6):1720-1728.e4.
13. Holmberg D, Ness-Jensen E, Mattsson F, El-Serag HB, Lagergren J. Risk of oesophageal adenocarcinoma in individuals with Barrett's oesophagus. *Eur J Cancer*. 2017 Apr 1;75:41–6.
14. Morgan E, Soerjomataram I, Gavin AT, Rutherford MJ, Gatenby P, Bardot A, et al. International trends in oesophageal cancer survival by histological subtype between 1995 and 2014. *Gut*. 2021; 70(2):234-242.
15. Launoy G, Bossard N, Castro C, Manfredi S, Group the GE-5 W. Trends in net survival from esophageal cancer in six European Latin countries: results from the SUDCAN population-based study. *Eur J Cancer Prev*. 2017 Jan;26:S24.

16. Dubecz A, Gall I, Solymosi N, Schweigert M, Peters JH, Feith M, et al. Temporal trends in long-term survival and cure rates in esophageal cancer: a SEER database analysis. *J Thorac Oncol Off Publ Int Assoc Study Lung Cancer*. 2012 Feb;7(2):443–7.
17. Lordick F, Mariette C, Haustermans K, Obermannová R, Arnold D, ESMO Guidelines Committee. Oesophageal cancer: ESMO Clinical Practice Guidelines for diagnosis, treatment and follow-up. *Ann Oncol Off J Eur Soc Med Oncol*. 2016 Sep;27(suppl 5):v50–7.
18. Ajani JA, D’Amico TA, Bentrem DJ, Chao J, Corvera C, Das P, et al. Esophageal and Esophagogastric Junction Cancers, Version 2.2019, NCCN Clinical Practice Guidelines in Oncology. *J Natl Compr Cancer Netw JNCCN*. 2019 01;17(7):855–83.
19. Allum WH, Blazeby JM, Griffin SM, Cunningham D, Jankowski JA, Wong R, et al. Guidelines for the management of oesophageal and gastric cancer. *Gut*. 2011 Nov 1;60(11):1449–72.
20. Lao-Sirieix P, Fitzgerald RC. Screening for oesophageal cancer. *Nat Rev Clin Oncol*. 2012 May;9(5):278–87.
21. Fléjou J-F. Barrett’s oesophagus: from metaplasia to dysplasia and cancer. *Gut*. 2005 Mar 1;54(suppl 1):i6–12.
22. Peters Y, Al-Kaabi A, Shaheen NJ, Chak A, Blum A, Souza RF, et al. Barrett oesophagus. *Nat Rev Dis Primer*. 2019 May 23;5(1):35.
23. Paull A, Trier JS, Dalton MD, Camp RC, Loeb P, Goyal RK. The histologic spectrum of Barrett’s esophagus. *N Engl J Med*. 1976 Aug 26;295(9):476–80.
24. Kerkhof M, van Dekken H, Steyerberg EW, Meijer GA, Mulder AH, de Bruïne A, et al. Grading of dysplasia in Barrett’s oesophagus: substantial interobserver variation between general and gastrointestinal pathologists. *Histopathology*. 2007 Jun;50(7):920–7.
25. American Gastroenterological Association, Spechler SJ, Sharma P, Souza RF, Inadomi JM, Shaheen NJ. American Gastroenterological Association medical position statement on the management of Barrett’s esophagus. *Gastroenterology*. 2011 Mar;140(3):1084–91.
26. Smith RR, Hamilton SR, Boitnott JK, Rogers EL. The spectrum of carcinoma arising in Barrett’s esophagus. A clinicopathologic study of 26 patients. *Am J Surg Pathol*. 1984 Aug;8(8):563–73.
27. Skinner DB, Walther BC, Riddell RH, Schmidt H, Iascone C, DeMeester TR. Barrett’s esophagus. Comparison of benign and malignant cases. *Ann Surg*. 1983 Oct;198(4):554–65.
28. Bhat SK, McManus DT, Coleman HG, Johnston BT, Cardwell CR, McMenamin U, et al. Oesophageal adenocarcinoma and prior diagnosis of Barrett’s oesophagus: a population-based study. *Gut*. 2015 Jan;64(1):20–5.
29. Fitzgerald RC, di Pietro M, Ragunath K, Ang Y, Kang J-Y, Watson P, et al. British Society of Gastroenterology guidelines on the diagnosis and management of Barrett’s oesophagus. *Gut*. 2014 Jan;63(1):7–42.
30. Brown IS, Whiteman DC, Lauwers GY. Foveolar type dysplasia in Barrett esophagus. *Mod Pathol Off J U S Can Acad Pathol Inc*. 2010 Jun;23(6):834–43.
31. Mahajan D, Bennett AE, Liu X, Bena J, Bronner MP. Grading of gastric foveolar-type dysplasia in Barrett’s esophagus. *Mod Pathol*. 2010 Jan;23(1):1–11.
32. Takubo K, Aida J, Naomoto Y, Sawabe M, Arai T, Shiraishi H, et al. Cardiac rather than intestinal-type background in endoscopic resection specimens of minute Barrett adenocarcinoma. *Hum Pathol*. 2009 Jan;40(1):65–74.

33. Kelty CJ, Gough MD, Van Wyk Q, Stephenson TJ, Ackroyd R. Barrett's oesophagus: intestinal metaplasia is not essential for cancer risk. *Scand J Gastroenterol*. 2007 Nov;42(11):1271–4.
34. Lavery DL, Martinez P, Gay LJ, Cereser B, Novelli MR, Rodriguez-Justo M, et al. Evolution of oesophageal adenocarcinoma from metaplastic columnar epithelium without goblet cells in Barrett's oesophagus. *Gut*. 2016 Jun 1;65(6):907–13.
35. Schellnegger R, Quante A, Rospleszcz S, Schernhammer M, Höhl B, Tobiasch M, et al. Goblet Cell Ratio in Combination with Differentiation and Stem Cell Markers in Barrett Esophagus Allow Distinction of Patients with and without Esophageal Adenocarcinoma. *Cancer Prev Res Phila Pa*. 2017 Jan;10(1):55–66.
36. Global cancer statistics 2018: GLOBOCAN estimates of incidence and mortality worldwide for 36 cancers in 185 countries - Bray - 2018 - CA: A Cancer Journal for Clinicians - Wiley Online Library [Internet]. [cited 2020 Dec 10]. Available from: <https://acsjournals.onlinelibrary.wiley.com/doi/10.3322/caac.21492>.
37. Wong MCS, Hamilton W, Whiteman DC, Jiang JY, Qiao Y, Fung FDH, et al. Global Incidence and mortality of oesophageal cancer and their correlation with socioeconomic indicators temporal patterns and trends in 41 countries. *Sci Rep*. 2018 Mar 14;8(1):4522.
38. Thrift AP, Whiteman DC. The incidence of esophageal adenocarcinoma continues to rise: analysis of period and birth cohort effects on recent trends. *Ann Oncol Off J Eur Soc Med Oncol*. 2012 Dec;23(12):3155–62.
39. Steevens J, Botterweck AAM, Dirx MJM, van den Brandt PA, Schouten LJ. Trends in incidence of oesophageal and stomach cancer subtypes in Europe. *Eur J Gastroenterol Hepatol*. 2010 Jun;22(6):669–78.
40. Vaughan TL, Fitzgerald RC. Precision prevention of oesophageal adenocarcinoma. *Nat Rev Gastroenterol Hepatol*. 2015 Apr;12(4):243–8.
41. Oesophageal cancer statistics [Internet]. Cancer Research UK. 2015 [cited 2018 Dec 18]. Available from: <https://www.cancerresearchuk.org/health-professional/cancer-statistics/statistics-by-cancer-type/oesophageal-cancer>
42. Soest EM van, Dieleman JP, Siersema PD, Sturkenboom MCJM, Kuipers EJ. Increasing incidence of Barrett's oesophagus in the general population. *Gut*. 2005 Aug 1;54(8):1062–6.
43. Conio M, Cameron AJ, Romero Y, Branch CD, Schleck CD, Burgart LJ, et al. Secular trends in the epidemiology and outcome of Barrett's oesophagus in Olmsted County, Minnesota. *Gut*. 2001 Mar 1;48(3):304–9.
44. Coleman HG, Bhat S, Murray LJ, McManus D, Gavin AT, Johnston BT. Increasing incidence of Barrett's oesophagus: a population-based study. *Eur J Epidemiol*. 2011 Sep;26(9):739–45.
45. Prach AT, MacDonald TA, Hopwood DA, Johnston DA. Increasing incidence of Barrett's oesophagus: education, enthusiasm, or epidemiology? *Lancet Lond Engl*. 1997 Sep 27;350(9082):933.
46. Ronkainen J, Aro P, Storskrubb T, Johansson S-E, Lind T, Bolling-Sternevald E, et al. Prevalence of Barrett's esophagus in the general population: an endoscopic study. *Gastroenterology*. 2005 Dec;129(6):1825–31.
47. Zagari RM, Fuccio L, Wallander M-A, Johansson S, Fiocca R, Casanova S, et al. Gastro-oesophageal reflux symptoms, oesophagitis and Barrett's oesophagus in the general population: the Loiano–Monghidoro study. *Gut*. 2008 Oct 1;57(10):1354–9.
48. Ward EM, Wolfsen HC, Achem SR, Loeb DS, Krishna M, Hemminger LL, et al. Barrett's esophagus is common in older men and women undergoing screening colonoscopy regardless of reflux symptoms. *Am J Gastroenterol*. 2006 Jan;101(1):12–7.

49. Rex DK, Cummings OW, Shaw M, Cumings MD, Wong RKH, Vasudeva RS, et al. Screening for Barrett's esophagus in colonoscopy patients with and without heartburn. *Gastroenterology*. 2003 Dec;125(6):1670–7.
50. Gerson LB, Shetler K, Triadafilopoulos G. Prevalence of Barrett's esophagus in asymptomatic individuals. *Gastroenterology*. 2002 Aug;123(2):461–7.
51. Rubenstein JH, Morgenstern H, Appelman H, Scheiman J, Schoenfeld P, McMahon LF, et al. Prediction of Barrett's esophagus among men. *Am J Gastroenterol*. 2013 Mar;108(3):353–62.
52. Masclee GMC, Coloma PM, de Wilde M, Kuipers EJ, Sturkenboom MCJM. The incidence of Barrett's oesophagus and oesophageal adenocarcinoma in the United Kingdom and The Netherlands is levelling off. *Aliment Pharmacol Ther*. 2014 Jun;39(11):1321–30.
53. Ho KY. From GERD to Barrett's esophagus: is the pattern in Asia mirroring that in the West? *J Gastroenterol Hepatol*. 2011 May;26(5):816–24.
54. Shiota S, Singh S, Anshasi A, El-Serag HB. Prevalence of Barrett's Esophagus in Asian Countries: A Systematic Review and Meta-analysis. *Clin Gastroenterol Hepatol Off Clin Pract J Am Gastroenterol Assoc*. 2015 Nov;13(11):1907–18.
55. Hvid-Jensen F, Pedersen L, Drewes AM, Sørensen HT, Funch-Jensen P. Incidence of adenocarcinoma among patients with Barrett's esophagus. *N Engl J Med*. 2011 Oct 13;365(15):1375–83.
56. Franklin J, Jankowski J. Recent advances in understanding and preventing oesophageal cancer. *F1000Research*. 2020;9:F1000.
57. Bhat S, Coleman HG, Yousef F, Johnston BT, McManus DT, Gavin AT, et al. Risk of malignant progression in Barrett's esophagus patients: results from a large population-based study. *J Natl Cancer Inst*. 2011 Jul 6;103(13):1049–57.
58. Peters Y, Honing J, Kievit W, Kestens C, Pestman W, Nagtegaal ID, et al. Incidence of Progression of Persistent Nondysplastic Barrett's Esophagus to Malignancy. *Clin Gastroenterol Hepatol Off Clin Pract J Am Gastroenterol Assoc*. 2019;17(5):869-877.e5.
59. Sharma P, Falk GW, Weston AP, Reker D, Johnston M, Sampliner RE. Dysplasia and cancer in a large multicenter cohort of patients with Barrett's esophagus. *Clin Gastroenterol Hepatol Off Clin Pract J Am Gastroenterol Assoc*. 2006 May;4(5):566–72.
60. de Jonge PJF, van Blankenstein M, Looman CWN, Casparie MK, Meijer GA, Kuipers EJ. Risk of malignant progression in patients with Barrett's oesophagus: a Dutch nationwide cohort study. *Gut*. 2010 Aug;59(8):1030–6.
61. Bird-Lieberman EL, Dunn JM, Coleman HG, Lao-Sirieix P, Oukrif D, Moore CE, et al. Population-based study reveals new risk-stratification biomarker panel for Barrett's esophagus. *Gastroenterology*. 2012 Oct;143(4):927-935.e3.
62. Lim YC, Fitzgerald RC. Diagnosis and treatment of Barrett's oesophagus. *Br Med Bull*. 2013 Sep 1;107(1):117–32.
63. Thrift AP, Kramer JR, Qureshi Z, Richardson PA, El-Serag HB. Age at Onset of GERD Symptoms Predicts Risk of Barrett's Esophagus. *Am J Gastroenterol*. 2013 Jun;108(6):915–22.
64. To H, Clemons NJ, Duong CP, Trainer AH, Phillips WA. The Genetics of Barrett's Esophagus: A Familial and Population-Based Perspective. *Dig Dis Sci*. 2016 Jul 1;61(7):1826–34.
65. Findlay JM, Middleton MR, Tomlinson I. Genetic susceptibility to Barrett's oesophagus: Lessons from early studies. *United Eur Gastroenterol J*. 2016 Aug;4(4):485–92.
66. Contino G, Vaughan TL, Whiteman D, Fitzgerald RC. The Evolving Genomic Landscape of Barrett's Esophagus and Esophageal Adenocarcinoma. *Gastroenterology*. 2017 Sep;153(3):657-673.e1.

67. Krishnamoorthi R, Singh S, Ragunathan K, Visrodia K, Wang KK, Katzka DA, et al. Factors Associated With Progression of Barrett's Esophagus: A Systematic Review and Meta-analysis. *Clin Gastroenterol Hepatol*. 2018 Jul 1;16(7):1046-1055.e8.
68. Cook MB, Wild CP, Forman D. A Systematic Review and Meta-Analysis of the Sex Ratio for Barrett's Esophagus, Erosive Reflux Disease, and Nonerosive Reflux Disease. *Am J Epidemiol*. 2005 Dec 1;162(11):1050-61.
69. Brown CS, Lapin B, Goldstein JL, Linn JG, Talamonti MS, Carbray J, et al. Predicting Progression in Barrett's Esophagus: Development and Validation of the Barrett's Esophagus Assessment of Risk Score (BEAR Score). *Ann Surg*. 2018;267(4):716-20.
70. Gatenby P, Bhattacharjee S, Wall C, Caygill C, Watson A. Risk stratification for malignant progression in Barrett's esophagus: Gender, age, duration and year of surveillance. *World J Gastroenterol*. 2016 Dec 28;22(48):10592-600.
71. Abrams JA, Fields S, Lightdale CJ, Neugut AI. Racial and ethnic disparities in the prevalence of Barrett's esophagus among patients who undergo upper endoscopy. *Clin Gastroenterol Hepatol Off Clin Pract J Am Gastroenterol Assoc*. 2008 Jan;6(1):30-4.
72. Jung KW, Talley NJ, Romero Y, Katzka DA, Schleck CD, Zinsmeister AR, et al. Epidemiology and natural history of intestinal metaplasia of the gastroesophageal junction and Barrett's esophagus: a population-based study. *Am J Gastroenterol*. 2011 Aug;106(8):1447-55; quiz 1456.
73. Olsen CM, Pandeya N, Green AC, Webb PM, Whiteman DC, Australian Cancer Study. Population attributable fractions of adenocarcinoma of the esophagus and gastroesophageal junction. *Am J Epidemiol*. 2011 Sep 1;174(5):582-90.
74. Lagergren J, Bergström R, Lindgren A, Nyrén O. Symptomatic gastroesophageal reflux as a risk factor for esophageal adenocarcinoma. *N Engl J Med*. 1999 Mar 18;340(11):825-31.
75. Taylor JB, Rubenstein JH. Meta-analyses of the effect of symptoms of gastroesophageal reflux on the risk of Barrett's esophagus. *Am J Gastroenterol*. 2010 Aug;105(8):1729, 1730-7; quiz 1738.
76. Singh S, Sharma AN, Murad MH, Buttar NS, El-Serag HB, Katzka DA, et al. Central adiposity is associated with increased risk of esophageal inflammation, metaplasia, and adenocarcinoma: a systematic review and meta-analysis. *Clin Gastroenterol Hepatol Off Clin Pract J Am Gastroenterol Assoc*. 2013 Nov;11(11):1399-1412.e7.
77. Kubo A, Cook MB, Shaheen NJ, Vaughan TL, Whiteman DC, Murray L, et al. Sex-specific associations between body mass index, waist circumference and the risk of Barrett's oesophagus: a pooled analysis from the international BEACON consortium. *Gut*. 2013 Dec;62(12):1684-91.
78. Andrici J, Tio M, Cox MR, Eslick GD. Hiatal hernia and the risk of Barrett's esophagus. *J Gastroenterol Hepatol*. 2013 Mar;28(3):415-31.
79. Pohl H, Wrobel K, Bojarski C, Voderholzer W, Sonnenberg A, Rösch T, et al. Risk factors in the development of esophageal adenocarcinoma. *Am J Gastroenterol*. 2013 Feb;108(2):200-7.
80. Cronin-Fenton DP, Murray LJ, Whiteman DC, Cardwell C, Webb PM, Jordan SJ, et al. Reproductive and sex hormonal factors and oesophageal and gastric junction adenocarcinoma: a pooled analysis. *Eur J Cancer Oxf Engl 1990*. 2010 Jul;46(11):2067-76.
81. Iyer PG, Borah BJ, Heien HC, Das A, Cooper GS, Chak A. Association of Barrett's esophagus with type II Diabetes Mellitus: results from a large population-based case-control study. *Clin Gastroenterol Hepatol Off Clin Pract J Am Gastroenterol Assoc*. 2013 Sep;11(9):1108-1114.e5.

82. Petrick JL, Li N, Anderson LA, Bernstein L, Corley DA, Serag HBE, et al. Diabetes in relation to Barrett's esophagus and adenocarcinomas of the esophagus: A pooled study from the International Barrett's and Esophageal Adenocarcinoma Consortium. *Cancer*. 2019;125(23):4210–23.
83. Chandar AK, Devanna S, Lu C, Singh S, Greer K, Chak A, et al. Association of Serum Levels of Adipokines and Insulin With Risk of Barrett's Esophagus: A Systematic Review and Meta-Analysis. *Clin Gastroenterol Hepatol Off Clin Pract J Am Gastroenterol Assoc*. 2015 Dec;13(13):2241-2255.e1-4; quiz e179.
84. Wang Z, Shaheen NJ, Whiteman DC, Anderson LA, Vaughan TL, Corley DA, et al. Helicobacter pylori Infection Is Associated With Reduced Risk of Barrett's Esophagus: An Analysis of the Barrett's and Esophageal Adenocarcinoma Consortium. *Am J Gastroenterol*. 2018;113(8):1148–55.
85. Eröss B, Farkas N, Vincze Á, Tinusz B, Szapáry L, Garami A, et al. Helicobacter pylori infection reduces the risk of Barrett's esophagus: A meta-analysis and systematic review. *Helicobacter*. 2018 Aug;23(4):e12504.
86. Chak A, Ochs-Balcom H, Falk G, Grady WM, Kinnard M, Willis JE, et al. Familiality in Barrett's esophagus, adenocarcinoma of the esophagus, and adenocarcinoma of the gastroesophageal junction. *Cancer Epidemiol Biomark Prev Publ Am Assoc Cancer Res Cosponsored Am Soc Prev Oncol*. 2006 Sep;15(9):1668–73.
87. Westra WM, Lutzke LS, Mostafavi NS, Roes AL, Calpe S, Wang KK, et al. Smokeless Tobacco and Cigar and/or Pipe Are Risk Factors for Barrett Esophagus in Male Patients With Gastroesophageal Reflux Disease. *Mayo Clin Proc*. 2018;93(9):1282–9.
88. Andrici J, Cox MR, Eslick GD. Cigarette smoking and the risk of Barrett's esophagus: a systematic review and meta-analysis. *J Gastroenterol Hepatol*. 2013 Aug;28(8):1258–73.
89. Behrens G, Jochem C, Keimling M, Ricci C, Schmid D, Leitzmann MF. The association between physical activity and gastroesophageal cancer: systematic review and meta-analysis. *Eur J Epidemiol*. 2014 Mar;29(3):151–70.
90. Hilal J, El-Serag HB, Ramsey D, Ngyuen T, Kramer JR. Physical activity and the risk of Barrett's esophagus. *Dis Esophagus Off J Int Soc Dis Esophagus*. 2016 Apr;29(3):248–54.
91. Singh S, Garg SK, Singh PP, Iyer PG, El-Serag HB. Acid-suppressive medications and risk of oesophageal adenocarcinoma in patients with Barrett's oesophagus: a systematic review and meta-analysis. *Gut*. 2014 Aug;63(8):1229–37.
92. Nguyen DM, Richardson P, El-Serag HB. Medications (NSAIDs, statins, proton pump inhibitors) and the risk of esophageal adenocarcinoma in patients with Barrett's esophagus. *Gastroenterology*. 2010 Jun;138(7):2260–6.
93. Kambhampati S, Tieu AH, Lubber B, Wang H, Meltzer SJ. Risk Factors for Progression of Barrett's Esophagus to High Grade Dysplasia and Esophageal Adenocarcinoma. *Sci Rep*. 2020 Mar 17;10(1):4899.
94. Lagergren J, Bergström R, Adami HO, Nyrén O. Association between medications that relax the lower esophageal sphincter and risk for esophageal adenocarcinoma. *Ann Intern Med*. 2000 Aug 1;133(3):165–75.
95. Fortuny J, Johnson CC, Bohlke K, Chow W-H, Hart G, Kucera G, et al. Use of anti-inflammatory drugs and lower esophageal sphincter-relaxing drugs and risk of esophageal and gastric cancers. *Clin Gastroenterol Hepatol Off Clin Pract J Am Gastroenterol Assoc*. 2007 Oct;5(10):1154-1159.e3.
96. Ranka S, Gee JM, Johnson IT, Skinner J, Hart AR, Rhodes M. Non-steroidal anti-inflammatory drugs, lower oesophageal sphincter-relaxing drugs and oesophageal cancer. A case-control study. *Digestion*. 2006;74(2):109–15.

97. Enestvedt BK, Lugo R, Guarner-Argente C, Shah P, Falk GW, Furth E, et al. Location, location, location: does early cancer in Barrett's esophagus have a preference? *Gastrointest Endosc.* 2013 Sep;78(3):462–7.
98. Cassani L, Sumner E, Slaughter JC, Yachimski P. Directional distribution of neoplasia in Barrett's esophagus is not influenced by distance from the gastroesophageal junction. *Gastrointest Endosc.* 2013 Jun;77(6):877–82.
99. Engel LS, Chow W-H, Vaughan TL, Gammon MD, Risch HA, Stanford JL, et al. Population attributable risks of esophageal and gastric cancers. *J Natl Cancer Inst.* 2003 Sep 17;95(18):1404–13.
100. Chow WH, Finkle WD, McLaughlin JK, Frankl H, Ziel HK, Fraumeni JF. The relation of gastroesophageal reflux disease and its treatment to adenocarcinomas of the esophagus and gastric cardia. *JAMA.* 1995 Aug 9;274(6):474–7.
101. Jankowski JAZ, Caestecker J de, Love SB, Reilly G, Watson P, Sanders S, et al. Esomeprazole and aspirin in Barrett's oesophagus (AspECT): a randomised factorial trial. *The Lancet.* 2018 Aug 4;392(10145):400–8.
102. Collen MJ, Lewis JH, Benjamin SB. Gastric acid hypersecretion in refractory gastroesophageal reflux disease. *Gastroenterology.* 1990 Mar;98(3):654–61.
103. Mulholland MW, Reid BJ, Levine DS, Rubin CE. Elevated gastric acid secretion in patients with Barrett's metaplastic epithelium. *Dig Dis Sci.* 1989 Sep;34(9):1329–34.
104. Rubenstein JH, Taylor JB. Meta-analysis: the association of oesophageal adenocarcinoma with symptoms of gastro-oesophageal reflux. *Aliment Pharmacol Ther.* 2010 Nov;32(10):1222–7.
105. Ayazi S, Hagen JA, Chan LS, DeMeester SR, Lin MW, Ayazi A, et al. Obesity and gastroesophageal reflux: quantifying the association between body mass index, esophageal acid exposure, and lower esophageal sphincter status in a large series of patients with reflux symptoms. *J Gastrointest Surg Off J Soc Surg Aliment Tract.* 2009 Aug;13(8):1440–7.
106. Wu JC-Y, Mui L-M, Cheung CM-Y, Chan Y, Sung JJ-Y. Obesity is associated with increased transient lower esophageal sphincter relaxation. *Gastroenterology.* 2007 Mar;132(3):883–9.
107. Cornier M-A, Dabelea D, Hernandez TL, Lindstrom RC, Steig AJ, Stob NR, et al. The metabolic syndrome. *Endocr Rev.* 2008 Dec;29(7):777–822.
108. Ryan AM, Healy LA, Power DG, Byrne M, Murphy S, Byrne PJ, et al. Barrett esophagus: prevalence of central adiposity, metabolic syndrome, and a proinflammatory state. *Ann Surg.* 2008 Jun;247(6):909–15.
109. Drahos J, Ricker W, Parsons R, Pfeiffer RM, Warren JL, Cook MB. Metabolic syndrome increases risk of Barrett's esophagus in the absence of gastroesophageal reflux: An analysis of SEER-Medicare data. *J Clin Gastroenterol.* 2015 Apr;49(4):282–8.
110. Drahos J, Ricker W, Pfeiffer RM, Cook MB. Metabolic syndrome and risk of esophageal adenocarcinoma in elderly patients in the United States: An analysis of SEER-Medicare data. *Cancer.* 2017 Feb 15;123(4):657–65.
111. Kauppila JH, Mattsson F, Brusselaers N, Lagergren J. Prognosis of oesophageal adenocarcinoma and squamous cell carcinoma following surgery and no surgery in a nationwide Swedish cohort study. *BMJ Open.* 2018 May 1;8(5):e021495.
112. Corley DA, Mehtani K, Quesenberry C, Zhao W, De Boer J, Weiss NS. Impact of Endoscopic Surveillance on Mortality From Barrett's Esophagus-Associated Esophageal Adenocarcinomas. *Gastroenterology.* 2013 Aug;145(2):312-319.e1.
113. Verbeek RE, Leenders M, Ten Kate FJW, van Hillegersberg R, Vleggaar FP, van Baal JWPM, et al. Surveillance of Barrett's esophagus and mortality from esophageal

- adenocarcinoma: a population-based cohort study. *Am J Gastroenterol*. 2014 Aug;109(8):1215–22.
114. Whiteman DC. Does a prior diagnosis of Barrett's oesophagus influence risk of dying from oesophageal adenocarcinoma? *Gut*. 2015 Jan;64(1):5–6.
 115. Reid BJ, Li X, Galipeau PC, Vaughan TL. Barrett's oesophagus and oesophageal adenocarcinoma: time for a new synthesis. *Nat Rev Cancer*. 2010 Feb;10(2):87–101.
 116. Pearson JP, Parikh S. Review article: Nature and properties of gastro-oesophageal and extra-oesophageal refluxate | Request PDF. *Aliment Pharmacol Ther*. 2011;33 (Suppl. 1):1–71.
 117. Mittal RK, Goyal RK. Sphincter mechanisms at the lower end of the esophagus. *GI Motil Online* [Internet]. 2006 May 16 [cited 2020 Dec 21]; Available from: <https://www.nature.com/gimo/contents/pt1/full/gimo14.html>
 118. Sarosiek J, McCallum RW. Mechanisms of oesophageal mucosal defence. *Best Pract Res Clin Gastroenterol*. 2000 Oct 1;14(5):701–17.
 119. Zerbib F, des Varannes SB, Roman S, Poudroux P, Artigue F, Chaput U, et al. Normal values and day-to-day variability of 24-h ambulatory oesophageal impedance-pH monitoring in a Belgian-French cohort of healthy subjects. *Aliment Pharmacol Ther*. 2005 Nov 15;22(10):1011–21.
 120. Blevins CH, Iyer PG, Vela MF, Katzka DA. The Esophageal Epithelial Barrier in Health and Disease. *Clin Gastroenterol Hepatol Off Clin Pract J Am Gastroenterol Assoc*. 2018 May;16(5):608–17.
 121. Sarosiek J, McCallum RW. What is the secretory potential of submucosal mucous glands within the human gullet in health and disease? *Digestion*. 1995;56 Suppl 1:15–23.
 122. Badgery H, Chong L, Ilich E, Huang Q, Georgy SR, Wang DH, et al. Recent insights into the biology of Barrett's esophagus. *Ann N Y Acad Sci*. 2020 Dec;1481(1):198–209.
 123. Younes ZH, Duncan MD, Harmon JW. Role of growth factors in oesophageal mucosal healing: A work in progress. *J Gastroenterol Hepatol*. 1998 Nov;13(S3):S156–60.
 124. Furuse M, Hata M, Furuse K, Yoshida Y, Haratake A, Sugitani Y, et al. Claudin-based tight junctions are crucial for the mammalian epidermal barrier: a lesson from claudin-1-deficient mice. *J Cell Biol*. 2002 Mar 18;156(6):1099–111.
 125. Chen Y, Merzdorf C, Paul DL, Goodenough DA. COOH terminus of occludin is required for tight junction barrier function in early *Xenopus* embryos. *J Cell Biol*. 1997 Aug 25;138(4):891–9.
 126. Liu Y, Nusrat A, Schnell FJ, Reaves TA, Walsh S, Pochet M, et al. Human junction adhesion molecule regulates tight junction resealing in epithelia. *J Cell Sci*. 2000 Jul;113 (Pt 13):2363–74.
 127. Sandilands A, Sutherland C, Irvine AD, McLean WHI. Filaggrin in the frontline: role in skin barrier function and disease. *J Cell Sci*. 2009 May 1;122(Pt 9):1285–94.
 128. Orlando RC, Lacy ER, Tobey NA, Cowart K. Barriers to paracellular permeability in rabbit esophageal epithelium. *Gastroenterology*. 1992 Mar;102(3):910–23.
 129. Bass BL, Schweitzer EJ, Harmon JW, Kraimer J. H⁺ back diffusion interferes with intrinsic reactive regulation of esophageal mucosal blood flow. *Surgery*. 1984 Aug;96(2):404–13.
 130. Souza RF. Reflux Esophagitis and Its Role in the Pathogenesis of Barrett's Metaplasia. *J Gastroenterol*. 2017 Jul;52(7):767–76.
 131. Farré R, van Malenstein H, De Vos R, Geboes K, Depoortere I, Vanden Berghe P, et al. Short exposure of oesophageal mucosa to bile acids, both in acidic and weakly acidic

- conditions, can impair mucosal integrity and provoke dilated intercellular spaces. *Gut*. 2008 Oct;57(10):1366–74.
132. Orlando RC. The integrity of the esophageal mucosa. Balance between offensive and defensive mechanisms. *Best Pract Res Clin Gastroenterol*. 2010 Dec;24(6):873–82.
 133. Tobey NA, Orlando RC. Mechanisms of acid injury to rabbit esophageal epithelium. Role of basolateral cell membrane acidification. *Gastroenterology*. 1991 Nov;101(5):1220–8.
 134. Jimenez P, Lanas A, Piazuolo E, Esteva F. Effects of extracellular pH on restitution and proliferation of rabbit oesophageal epithelial cells. *Aliment Pharmacol Ther*. 1999 Apr;13(4):545–52.
 135. Tsuji H, Fuse Y, Kawamoto K, Fujino H, Kodama T. Healing process of experimental esophageal ulcers induced by acetic acid in rats. *Scand J Gastroenterol Suppl*. 1989;162:6–10.
 136. Slack JMW. Metaplasia and transdifferentiation: from pure biology to the clinic. *Nat Rev Mol Cell Biol*. 2007 May;8(5):369–78.
 137. Lao-Sirieix P, Corovic A, Jankowski J, Lowe A, Triadafilopoulos G, Fitzgerald RC. Physiological and molecular analysis of acid loading mechanisms in squamous and columnar-lined esophagus. *Dis Esophagus Off J Int Soc Dis Esophagus*. 2008;21(6):529–38.
 138. Jovov B, Van Itallie CM, Shaheen NJ, Carson JL, Gambling TM, Anderson JM, et al. Claudin-18: a dominant tight junction protein in Barrett's esophagus and likely contributor to its acid resistance. *Am J Physiol Gastrointest Liver Physiol*. 2007 Dec;293(6):G1106-1113.
 139. Dixon J, Strugala V, Griffin SM, Welfare MR, Dettmar PW, Allen A, et al. Esophageal mucin: an adherent mucus gel barrier is absent in the normal esophagus but present in columnar-lined Barrett's esophagus. *Am J Gastroenterol*. 2001 Sep;96(9):2575–83.
 140. Tobey NA, Argote CM, Vanegas XC, Barlow W, Orlando RC. Electrical parameters and ion species for active transport in human esophageal stratified squamous epithelium and Barrett's specialized columnar epithelium. *Am J Physiol Gastrointest Liver Physiol*. 2007 Jul;293(1):G264-270.
 141. Ostrowski J, Mikula M, Karczmarski J, Rubel T, Wyrwicz LS, Bragoszewski P, et al. Molecular defense mechanisms of Barrett's metaplasia estimated by an integrative genomics. *J Mol Med Berl Ger*. 2007 Jul;85(7):733–43.
 142. Kapoor H, Lohani KR, Lee TH, Agrawal DK, Mittal SK. Animal Models of Barrett's Esophagus and Esophageal Adenocarcinoma-Past, Present, and Future. *Clin Transl Sci*. 2015 Dec;8(6):841–7.
 143. Quante M, Bhagat G, Abrams JA, Marache F, Good P, Lee MD, et al. Bile acid and inflammation activate gastric cardia stem cells in a mouse model of Barrett-like metaplasia. *Cancer Cell*. 2012 Jan 17;21(1):36–51.
 144. Leedham SJ, Preston SL, McDonald S a. C, Elia G, Bhandari P, Poller D, et al. Individual crypt genetic heterogeneity and the origin of metaplastic glandular epithelium in human Barrett's oesophagus. *Gut*. 2008 Aug;57(8):1041–8.
 145. Integrated genomic characterization of oesophageal carcinoma. *Nature*. 2017 Jan 12;541(7636):169–75.
 146. Boch JA, Shields HM, Antonioli DA, Zwas F, Sawhney RA, Trier JS. Distribution of cytokeratin markers in Barrett's specialized columnar epithelium. *Gastroenterology*. 1997 Mar;112(3):760–5.

147. Jiang M, Li H, Zhang Y, Yang Y, Lu R, Liu K, et al. Transitional basal cells at the squamous-columnar junction generate Barrett's oesophagus. *Nature*. 2017 Oct 26;550(7677):529–33.
148. Seery JP. Stem cells of the oesophageal epithelium. *J Cell Sci*. 2002 May 1;115(Pt 9):1783–9.
149. Hutchinson L, Stenstrom B, Chen D, Piperdi B, Levey S, Lyle S, et al. Human Barrett's adenocarcinoma of the esophagus, associated myofibroblasts, and endothelium can arise from bone marrow-derived cells after allogeneic stem cell transplant. *Stem Cells Dev*. 2011 Jan;20(1):11–7.
150. Minacapelli CD, Bajpai M, Geng X, Cheng CL, Chouthai AA, Souza R, et al. Barrett's metaplasia develops from cellular reprogramming of esophageal squamous epithelium due to gastroesophageal reflux. *Am J Physiol Gastrointest Liver Physiol*. 2017 Jun 1;312(6):G615–22.
151. Ling FC, Khochfar J, Baldus SE, Brabender J, Drebber U, Bollschweiler E, et al. HIF-1 α protein expression is associated with the environmental inflammatory reaction in Barrett's metaplasia. *Dis Esophagus Off J Int Soc Dis Esophagus*. 2009;22(8):694–9.
152. Colleypriest BJ, Burke ZD, Griffiths LP, Chen Y, Yu W-Y, Jover R, et al. Hnf4 α is a key gene that can generate columnar metaplasia in oesophageal epithelium. *Differ Res Biol Divers*. 2017;93:39–49.
153. O'Riordan JM, Abdel-latif MM, Ravi N, McNamara D, Byrne PJ, McDonald GSA, et al. Proinflammatory cytokine and nuclear factor kappa-B expression along the inflammation-metaplasia-dysplasia-adenocarcinoma sequence in the esophagus. *Am J Gastroenterol*. 2005 Jun;100(6):1257–64.
154. Moons LMG, Kusters JG, van Delft JHM, Kuipers EJ, Gottschalk R, Geldof H, et al. A pro-inflammatory genotype predisposes to Barrett's esophagus. *Carcinogenesis*. 2008 May;29(5):926–31.
155. Milano F, van Baal JWPM, Buttar NS, Rygiel AM, de Kort F, DeMars CJ, et al. Bone morphogenetic protein 4 expressed in esophagitis induces a columnar phenotype in esophageal squamous cells. *Gastroenterology*. 2007 Jun;132(7):2412–21.
156. Chen H, Fang Y, Tevebaugh W, Orlando RC, Shaheen NJ, Chen X. Molecular Mechanism of Barrett's Esophagus. *Dig Dis Sci*. 2011 Dec;56(12):3405–20.
157. Kong J, Crissey MAS, Stairs DB, Sepulveda AR, Lynch JP. Cox2 and β -Catenin/T-cell Factor Signaling Intestinalize Human Esophageal Keratinocytes When Cultured under Organotypic Conditions. *Neoplasia N Y N*. 2011 Sep;13(9):792–805.
158. Murata-Kamiya N, Kurashima Y, Teishikata Y, Yamahashi Y, Saito Y, Higashi H, et al. Helicobacter pylori CagA interacts with E-cadherin and deregulates the beta-catenin signal that promotes intestinal transdifferentiation in gastric epithelial cells. *Oncogene*. 2007 Jul 12;26(32):4617–26.
159. Wang DH, Clemons NJ, Miyashita T, Dupuy AJ, Zhang W, Szczepny A, et al. Aberrant epithelial-mesenchymal Hedgehog signaling characterizes Barrett's metaplasia. *Gastroenterology*. 2010 May;138(5):1810–22.
160. Yamanaka Y, Shiotani A, Fujimura Y, Ishii M, Fujita M, Matsumoto H, et al. Expression of Sonic hedgehog (SHH) and CDX2 in the columnar epithelium of the lower oesophagus. *Dig Liver Dis Off J Ital Soc Gastroenterol Ital Assoc Study Liver*. 2011 Jan;43(1):54–9.
161. Wang DH, Tiwari A, Kim ME, Clemons NJ, Regmi NL, Hodges WA, et al. Hedgehog signaling regulates FOXA2 in esophageal embryogenesis and Barrett's metaplasia. *J Clin Invest*. 2014 Sep;124(9):3767–80.
162. Vega ME, Giroux V, Natsuzaka M, Liu M, Klein-Szanto AJ, Stairs DB, et al. Inhibition of Notch signaling enhances transdifferentiation of the esophageal squamous

- epithelium towards a Barrett's-like metaplasia via KLF4. *Cell Cycle Georget Tex*. 2014;13(24):3857–66.
163. Morrow DJ, Avissar NE, Toia L, Redmond EM, Watson TJ, Jones C, et al. Pathogenesis of Barrett's esophagus: bile acids inhibit the Notch signaling pathway with induction of CDX2 gene expression in human esophageal cells. *Surgery*. 2009 Oct;146(4):714–21; discussion 721–722.
 164. Menke V, van Es JH, de Lau W, van den Born M, Kuipers EJ, Siersema PD, et al. Conversion of metaplastic Barrett's epithelium into post-mitotic goblet cells by gamma-secretase inhibition. *Dis Model Mech*. 2010 Feb;3(1–2):104–10.
 165. Lao-Sirieix P, Fitzgerald RC. Role of the micro-environment in Barrett's carcinogenesis. *Biochem Soc Trans*. 2010 Apr 1;38(2):327–30.
 166. Monaco L, Brillantino A, Torelli F, Schettino M, Izzo G, Cosenza A, et al. Prevalence of bile reflux in gastroesophageal reflux disease patients not responsive to proton pump inhibitors. *World J Gastroenterol WJG*. 2009 Jan 21;15(3):334–8.
 167. Rohof WO, Bennink RJ, Boeckxstaens GE. Proton pump inhibitors reduce the size and acidity of the acid pocket in the stomach. *Clin Gastroenterol Hepatol Off Clin Pract J Am Gastroenterol Assoc*. 2014 Jul;12(7):1101–1107.e1.
 168. Das KM, Kong Y, Bajpai M, Kulkarni D, Geng X, Mishra P, et al. Transformation of benign Barrett's epithelium by repeated acid and bile exposure over 65 weeks: a novel in vitro model. *Int J Cancer*. 2011 Jan 15;128(2):274–82.
 169. Miwa K, Sahara H, Segawa M, Kinami S, Sato T, Miyazaki I, et al. Reflux of duodenal or gastro-duodenal contents induces esophageal carcinoma in rats. *Int J Cancer*. 1996 Jul 17;67(2):269–74.
 170. Nehra D, Howell P, Williams CP, Pye JK, Beynon J. Toxic bile acids in gastro-oesophageal reflux disease: influence of gastric acidity. *Gut*. 1999 May;44(5):598–602.
 171. Kauer WK, Peters JH, DeMeester TR, Feussner H, Ireland AP, Stein HJ, et al. Composition and concentration of bile acid reflux into the esophagus of patients with gastroesophageal reflux disease. *Surgery*. 1997 Nov;122(5):874–81.
 172. Vaezi MF, Richter JE. Role of acid and duodenogastroesophageal reflux in gastroesophageal reflux disease. *Gastroenterology*. 1996 Nov;111(5):1192–9.
 173. Nemeth J, Varro A, Bridson J, Walker R, Dockray GJ. Increased tissue concentrations of the gastrin precursor in patients treated with omeprazole. *Eur J Clin Invest*. 1992 Oct;22(10):638–44.
 174. Fitzgerald RC, Abdalla S, Onwuegbusi BA, Sirieix P, Saeed IT, Burnham WR, et al. Inflammatory gradient in Barrett's oesophagus: implications for disease complications. *Gut*. 2002 Sep;51(3):316–22.
 175. Picardo SL, Maher SG, O'Sullivan JN, Reynolds JV. Barrett's to oesophageal cancer sequence: a model of inflammatory-driven upper gastrointestinal cancer. *Dig Surg*. 2012;29(3):251–60.
 176. Tselepis C, Perry I, Dawson C, Hardy R, Darnton SJ, McConkey C, et al. Tumour necrosis factor-alpha in Barrett's oesophagus: a potential novel mechanism of action. *Oncogene*. 2002 Sep 5;21(39):6071–81.
 177. Chemnitzer O, Götzel K, Maurer L, Dietrich A, Eichfeld U, Lyros O, et al. Response to TNF- α Is Increasing Along with the Progression in Barrett's Esophagus. *Dig Dis Sci*. 2017 Dec;62(12):3391–401.
 178. Garcia JM, Splenser AE, Kramer J, Alsarraj A, Fitzgerald S, Ramsey D, et al. Circulating Inflammatory Cytokines and Adipokines are Associated With Barrett's Esophagus: a Case–Control Study. *Clin Gastroenterol Hepatol Off Clin Pract J Am Gastroenterol Assoc*. 2014 Feb;12(2):229–238.e3.

179. Nguyen T, Tang Z, Younes M, Alsarraj A, Ramsey D, Fitzgerald S, et al. Esophageal COX-2 expression is increased in Barrett's esophagus, obesity, and smoking. *Dig Dis Sci*. 2015 Jan;60(1):65–73.
180. Nguyen GH, Schetter AJ, Chou DB, Bowman ED, Zhao R, Hawkes JE, et al. Inflammatory and microRNA gene expression as prognostic classifier of Barrett's-associated esophageal adenocarcinoma. *Clin Cancer Res Off J Am Assoc Cancer Res*. 2010 Dec 1;16(23):5824–34.
181. Zhang HY, Zhang Q, Zhang X, Yu C, Huo X, Cheng E, et al. Cancer-related inflammation and Barrett's carcinogenesis: interleukin-6 and STAT3 mediate apoptotic resistance in transformed Barrett's cells. *Am J Physiol Gastrointest Liver Physiol*. 2011 Mar;300(3):G454-460.
182. Dvorakova K, Payne CM, Ramsey L, Holubec H, Sampliner R, Dominguez J, et al. Increased expression and secretion of interleukin-6 in patients with Barrett's esophagus. *Clin Cancer Res Off J Am Assoc Cancer Res*. 2004 Mar 15;10(6):2020–8.
183. Dvorak K, Chavarria M, Payne CM, Ramsey L, Crowley-Weber C, Dvorakova B, et al. Activation of the interleukin-6/STAT3 antiapoptotic pathway in esophageal cells by bile acids and low pH: relevance to barrett's esophagus. *Clin Cancer Res Off J Am Assoc Cancer Res*. 2007 Sep 15;13(18 Pt 1):5305–13.
184. Gaj P, Mikula M, Wyrwicz LS, Regula J, Ostrowski J. Barrett's esophagus associates with a variant of IL23R gene. *Acta Biochim Pol*. 2008;55(2):365–9.
185. Kohata Y, Fujiwara Y, Machida H, Okazaki H, Yamagami H, Tanigawa T, et al. Role of Th-2 cytokines in the development of Barrett's esophagus in rats. *J Gastroenterol*. 2011 Jul;46(7):883–93.
186. Lagisetty KH, McEwen DP, Nancarrow DJ, Schiebel JG, Ferrer-Torres D, Ray D, et al. Immune determinants of Barrett's progression to esophageal adenocarcinoma. *JCI Insight*. 2020 Dec 8;
187. Lao-Sirieix P, Roy A, Worrall C, Vowler SL, Gardiner S, Fitzgerald RC. Effect of acid suppression on molecular predictors for esophageal cancer. *Cancer Epidemiol Biomark Prev Publ Am Assoc Cancer Res Cosponsored Am Soc Prev Oncol*. 2006 Feb;15(2):288–93.
188. Fitzgerald RC, Omary MB, Triadafilopoulos G. Altered sodium-hydrogen exchange activity is a mechanism for acid-induced hyperproliferation in Barrett's esophagus. *Am J Physiol*. 1998 Jul;275(1):G47-55.
189. Fitzgerald RC, Omary MB, Triadafilopoulos G. Dynamic effects of acid on Barrett's esophagus. An ex vivo proliferation and differentiation model. *J Clin Invest*. 1996 Nov 1;98(9):2120–8.
190. Jenkins GJS, D'Souza FR, Suzen SH, Eltahir ZS, James SA, Parry JM, et al. Deoxycholic acid at neutral and acid pH, is genotoxic to oesophageal cells through the induction of ROS: The potential role of anti-oxidants in Barrett's oesophagus. *Carcinogenesis*. 2007 Jan;28(1):136–42.
191. Jenkins GJS, Cronin J, Alhamdani A, Rawat N, D'Souza F, Thomas T, et al. The bile acid deoxycholic acid has a non-linear dose response for DNA damage and possibly NF-kappaB activation in oesophageal cells, with a mechanism of action involving ROS. *Mutagenesis*. 2008 Sep;23(5):399–405.
192. Dvorak K, Watts GS, Ramsey L, Holubec H, Payne CM, Bernstein C, et al. Expression of bile acid transporting proteins in Barrett's esophagus and esophageal adenocarcinoma. *Am J Gastroenterol*. 2009 Feb;104(2):302–9.

193. Clemons NJ, McColl KEL, Fitzgerald RC. Nitric oxide and acid induce double-strand DNA breaks in Barrett's esophagus carcinogenesis via distinct mechanisms. *Gastroenterology*. 2007 Oct;133(4):1198–209.
194. Winter JW, Paterson S, Scobie G, Wirz A, Preston T, McColl KEL. N-nitrosamine generation from ingested nitrate via nitric oxide in subjects with and without gastroesophageal reflux. *Gastroenterology*. 2007 Jul;133(1):164–74.
195. Iijima K, Henry E, Moriya A, Wirz A, Kelman AW, McColl KEL. Dietary nitrate generates potentially mutagenic concentrations of nitric oxide at the gastroesophageal junction. *Gastroenterology*. 2002 May;122(5):1248–57.
196. Yandrapu H, Marcinkiewicz M, Poplawski C, Namiot Z, Zbroch T, Sarosiek J. A distinct salivary secretory response mediated by the esophago-salivary reflex in patients with Barrett's esophagus: its potential pathogenetic implications. *Adv Med Sci*. 2014 Sep;59(2):281–7.
197. Snider EJ, Compres G, Freedberg DE, Khiabani H, Nobel YR, Stump S, et al. Alterations to the Esophageal Microbiome Associated with Progression from Barrett's Esophagus to Esophageal Adenocarcinoma. *Cancer Epidemiol Biomark Prev Publ Am Assoc Cancer Res Cosponsored Am Soc Prev Oncol*. 2019 Oct;28(10):1687–93.
198. Lv J, Guo L, Liu J-J, Zhao H-P, Zhang J, Wang J-H. Alteration of the esophageal microbiota in Barrett's esophagus and esophageal adenocarcinoma. *World J Gastroenterol*. 2019 May 14;25(18):2149–61.
199. Bobryshev YV, Tran D, Killingsworth MC, Buckland M, Lord RVN. Dendritic cells in Barrett's esophagus and esophageal adenocarcinoma. *J Gastrointest Surg Off J Soc Surg Aliment Tract*. 2009 Jan;13(1):44–53.
200. Bobryshev YV, Freeman AK, Botelho NK, Tran D, Levert-Mignon AJM, Lord RVN. Expression of the putative stem cell marker Musashi-1 in Barrett's esophagus and esophageal adenocarcinoma. *Dis Esophagus Off J Int Soc Dis Esophagus*. 2010 Sep;23(7):580–9.
201. Bobryshev YV, Tran D, Killingsworth MC, Buckland M, Lord RVN. Dendritic cell-associated immune inflammation of cardiac mucosa: a possible factor in the formation of Barrett's esophagus. *J Gastrointest Surg Off J Soc Surg Aliment Tract*. 2009 Mar;13(3):442–50.
202. Moons LMG, Kusters JG, Bultman E, Kuipers EJ, van Dekken H, Tra WMW, et al. Barrett's oesophagus is characterized by a predominantly humoral inflammatory response. *J Pathol*. 2005 Nov;207(3):269–76.
203. Berndt U, Philipsen L, Bartsch S, Hu Y, Röcken C, Bertram W, et al. Comparative Multi-Epitope-Ligand-Cartography reveals essential immunological alterations in Barrett's metaplasia and esophageal adenocarcinoma. *Mol Cancer*. 2010 Jul 6;9:177.
204. Salmela MT, Karjalainen-Lindsberg ML, Puolakkainen P, Saarialho-Kere U. Upregulation and differential expression of matrilysin (MMP-7) and metalloelastase (MMP-12) and their inhibitors TIMP-1 and TIMP-3 in Barrett's oesophageal adenocarcinoma. *Br J Cancer*. 2001 Aug 3;85(3):383–92.
205. Onwuegbusi BA, Aitchison A, Chin S, Kranjac T, Mills I, Huang Y, et al. Impaired transforming growth factor β signalling in Barrett's carcinogenesis due to frequent SMAD4 inactivation. *Gut*. 2006 Jun;55(6):764–74.
206. Onwuegbusi BA, Rees JRE, Lao-Sirieix P, Fitzgerald RC. Selective Loss of TGF β Smad-Dependent Signalling Prevents Cell Cycle Arrest and Promotes Invasion in Oesophageal Adenocarcinoma Cell Lines. *PLoS ONE*. 2007;2(1):e177.
207. Ebbing EA, van der Zalm AP, Steins A, Creemers A, Hermsen S, Rentenaar R, et al. Stromal-derived interleukin 6 drives epithelial-to-mesenchymal transition and therapy

- resistance in esophageal adenocarcinoma. *Proc Natl Acad Sci U S A*. 2019 Feb 5;116(6):2237–42.
208. Liu D, Zhang R, Wu J, Pu Y, Yin X, Cheng Y, et al. Interleukin-17A promotes esophageal adenocarcinoma cell invasiveness through ROS-dependent, NF- κ B-mediated MMP-2/9 activation. *Oncol Rep*. 2017 Mar;37(3):1779–85.
209. Auvinen MI, Sihvo EIT, Ruohtula T, Salminen JT, Koivistoinen A, Siivola P, et al. Incipient angiogenesis in Barrett's epithelium and lymphangiogenesis in Barrett's adenocarcinoma. *J Clin Oncol Off J Am Soc Clin Oncol*. 2002 Jul 1;20(13):2971–9.
210. Griffiths EA, Pritchard SA, McGrath SM, Valentine HR, Price PM, Welch IM, et al. Increasing expression of hypoxia-inducible proteins in the Barrett's metaplasia–dysplasia–adenocarcinoma sequence. *Br J Cancer*. 2007 May 7;96(9):1377–83.
211. Botelho NK, Schneiders FI, Lord SJ, Freeman AK, Tyagi S, Nancarrow DJ, et al. Gene expression alterations in formalin-fixed, paraffin-embedded Barrett esophagus and esophageal adenocarcinoma tissues. *Cancer Biol Ther*. 2010 Jul 15;10(2):172–9.
212. Saadi A, Shannon NB, Lao-Sirieix P, O'Donovan M, Walker E, Clemons NJ, et al. Stromal genes discriminate preinvasive from invasive disease, predict outcome, and highlight inflammatory pathways in digestive cancers. *Proc Natl Acad Sci U S A*. 2010 Feb 2;107(5):2177–82.
213. Grimm M, Lazariotou M, Kircher S, Stuermer L, Reiber C, Höfelmayr A, et al. MMP-1 is a (pre-)invasive factor in Barrett-associated esophageal adenocarcinomas and is associated with positive lymph node status. *J Transl Med*. 2010 Oct 14;8:99.
214. Clemons NJ, Shannon NB, Abeyratne LR, Walker CE, Saadi A, O'Donovan ML, et al. Nitric oxide-mediated invasion in Barrett's high-grade dysplasia and adenocarcinoma. *Carcinogenesis*. 2010 Sep;31(9):1669–75.
215. Lagarde SM, ten Kate FJW, Richel DJ, Offerhaus GJA, van Lanschot JJB. Molecular prognostic factors in adenocarcinoma of the esophagus and gastroesophageal junction. *Ann Surg Oncol*. 2007 Feb;14(2):977–91.
216. Konturek PC, Burnat G, Rau T, Hahn EG, Konturek S. Effect of adiponectin and ghrelin on apoptosis of Barrett adenocarcinoma cell line. *Dig Dis Sci*. 2008 Mar;53(3):597–605.
217. Ogunwobi O, Mutungi G, Beales ILP. Leptin stimulates proliferation and inhibits apoptosis in Barrett's esophageal adenocarcinoma cells by cyclooxygenase-2-dependent, prostaglandin-E2-mediated transactivation of the epidermal growth factor receptor and c-Jun NH2-terminal kinase activation. *Endocrinology*. 2006 Sep;147(9):4505–16.
218. Beales ILP, Ogunwobi OO. Leptin synergistically enhances the anti-apoptotic and growth-promoting effects of acid in OE33 oesophageal adenocarcinoma cells in culture. *Mol Cell Endocrinol*. 2007 Aug 15;274(1–2):60–8.
219. Rubenstein JH, Morgenstern H, McConell D, Scheiman JM, Schoenfeld P, Appelman H, et al. Associations of diabetes mellitus, insulin, leptin, and ghrelin with gastroesophageal reflux and Barrett's esophagus. *Gastroenterology*. 2013 Dec;145(6):1237–1244.e1–5.
220. Arcidiacono D, Antonello A, Fassan M, Nucci D, Morbin T, Agostini M, et al. Insulin promotes HER2 signaling activation during Barrett's Esophagus carcinogenesis. *Dig Liver Dis Off J Ital Soc Gastroenterol Ital Assoc Study Liver*. 2017 Jun;49(6):630–8.
221. Greer KB, Kresak A, Bednarchik B, Dawson D, Li L, Chak A, et al. Insulin/Insulin-Like Growth Factor-1 Pathway in Barrett's Carcinogenesis. *Clin Transl Gastroenterol*. 2013 Mar;4(3):e31.

222. Yandrapu H, Marcinkiewicz M, Poplawski C, Han K, Zbroch T, Goldin G, et al. Role of saliva in esophageal defense: implications in patients with nonerosive reflux disease. *Am J Med Sci*. 2015 May;349(5):385–91.
223. Kauppi J, Räsänen J, Sihvo E, Nieminen U, Arkkila P, Ahotupa M, et al. Increased Oxidative Stress in the Proximal Stomach of Patients with Barrett's Esophagus and Adenocarcinoma of the Esophagus and Esophagogastric Junction. *Transl Oncol*. 2016 Aug;9(4):336–9.
224. Underwood TJ, Hayden AL, Derouet M, Garcia E, Noble F, White MJ, et al. Cancer-associated fibroblasts predict poor outcome and promote periostin-dependent invasion in oesophageal adenocarcinoma. *J Pathol*. 2015 Feb;235(3):466–77.
225. Trevellin E, Scarpa M, Carraro A, Lunardi F, Kotsafti A, Porzionato A, et al. Esophageal adenocarcinoma and obesity: peritumoral adipose tissue plays a role in lymph node invasion. *Oncotarget*. 2015 May 10;6(13):11203–15.
226. Corley DA, Levin TR, Habel LA, Weiss NS, Buffler PA. Surveillance and survival in Barrett's adenocarcinomas: a population-based study. *Gastroenterology*. 2002 Mar;122(3):633–40.
227. Weston AP, Sharma P, Topalovski M, Richards R, Cherian R, Dixon A. Long-term follow-up of Barrett's high-grade dysplasia. *Am J Gastroenterol*. 2000 Aug;95(8):1888–93.
228. Bytzer P, Christensen PB, Damkier P, Vinding K, Seersholm N. Adenocarcinoma of the esophagus and Barrett's esophagus: a population-based study. *Am J Gastroenterol*. 1999 Jan;94(1):86–91.
229. Ross-Innes CS, Becq J, Warren A, Cheetham RK, Northen H, O'Donovan M, et al. Whole-genome sequencing provides new insights into the clonal architecture of Barrett's esophagus and esophageal adenocarcinoma. *Nat Genet*. 2015 Sep;47(9):1038–46.
230. Gregson EM, Bornschein J, Fitzgerald RC. Genetic progression of Barrett's oesophagus to oesophageal adenocarcinoma. *Br J Cancer*. 2016 Aug;115(4):403–10.
231. Verbeek RE, Spittuler LF, Peute A, van Oijen MGH, Ten Kate FJ, Vermeijden JR, et al. Familial clustering of Barrett's esophagus and esophageal adenocarcinoma in a European cohort. *Clin Gastroenterol Hepatol Off Clin Pract J Am Gastroenterol Assoc*. 2014 Oct;12(10):1656-1663.e1.
232. Dong J, Levine DM, Buas MF, Zhang R, Onstad L, Fitzgerald RC, et al. Interactions Between Genetic Variants and Environmental Factors Affect Risk of Esophageal Adenocarcinoma and Barrett's Esophagus. *Clin Gastroenterol Hepatol Off Clin Pract J Am Gastroenterol Assoc*. 2018 Oct;16(10):1598-1606.e4.
233. Lee E, Stram DO, Ek WE, Onstad LE, MacGregor S, Gharahkhani P, et al. Pleiotropic analysis of cancer risk loci on esophageal adenocarcinoma risk. *Cancer Epidemiol Biomark Prev Publ Am Assoc Cancer Res Cosponsored Am Soc Prev Oncol*. 2015 Nov;24(11):1801–3.
234. Nones K, Waddell N, Wayte N, Patch A-M, Bailey P, Newell F, et al. Genomic catastrophes frequently arise in esophageal adenocarcinoma and drive tumorigenesis. *Nat Commun*. 2014 Oct 29;5(1):5224.
235. Frankell AM, Jammula S, Li X, Contino G, Killcoyne S, Abbas S, et al. The landscape of selection in 551 esophageal adenocarcinomas defines genomic biomarkers for the clinic. *Nat Genet*. 2019 Mar;51(3):506–16.
236. Secrier M, Li X, de Silva N, Eldridge MD, Contino G, Bornschein J, et al. Mutational signatures in esophageal adenocarcinoma define etiologically distinct subgroups with therapeutic relevance. *Nat Genet*. 2016 Oct;48(10):1131–41.

237. Weaver JM, Ross-Innes CS, Shannon N, Lynch AG, Forshew T, Barbera M, et al. Ordering of mutations in preinvasive disease stages of esophageal carcinogenesis. *Nat Genet.* 2014 Aug;46(8):837–43.
238. Stachler MD, Taylor-Weiner A, Peng S, McKenna A, Agoston AT, Odze RD, et al. Paired exome analysis of Barrett's esophagus and adenocarcinoma. *Nat Genet.* 2015 Sep;47(9):1047–55.
239. Patman G. Tracing the genetic pathway to oesophageal cancer. *Nat Rev Gastroenterol Hepatol.* 2015 Oct;12(10):551.
240. Olliver JR, Hardie LJ, Dexter S, Chalmers D, Wild CP. DNA damage levels are raised in Barrett's oesophageal mucosa relative to the squamous epithelium of the oesophagus. *Biomark Biochem Indic Expo Response Susceptibility Chem.* 2003 Dec;8(6):509–21.
241. Jolly AJ, Wild CP, Hardie LJ. Acid and bile salts induce DNA damage in human oesophageal cell lines. *Mutagenesis.* 2004 Jul;19(4):319–24.
242. Bhardwaj V, Horvat A, Korolkova O, Washington MK, El-Rifai W, Dikalov SI, et al. Prevention of DNA damage in Barrett's esophageal cells exposed to acidic bile salts. *Carcinogenesis.* 2016 Dec;37(12):1161–9.
243. Huo X, Juergens S, Zhang X, Rezaei D, Yu C, Strauch ED, et al. Deoxycholic acid causes DNA damage while inducing apoptotic resistance through NF- κ B activation in benign Barrett's epithelial cells. *Am J Physiol Gastrointest Liver Physiol.* 2011 Aug;301(2):G278–286.
244. Theisen J, Peters JH, Fein M, Hughes M, Hagen JA, Demeester SR, et al. The mutagenic potential of duodeno-esophageal reflux. *Ann Surg.* 2005 Jan;241(1):63–8.
245. Dvorakova K, Payne CM, Ramsey L, Bernstein H, Holubec H, Chavarria M, et al. Apoptosis resistance in Barrett's esophagus: ex vivo bioassay of live stressed tissues. *Am J Gastroenterol.* 2005 Feb;100(2):424–31.
246. Barrett MT, Sanchez CA, Galipeau PC, Neshat K, Emond M, Reid BJ. Allelic loss of 9p21 and mutation of the CDKN2/p16 gene develop as early lesions during neoplastic progression in Barrett's esophagus. *Oncogene.* 1996 Nov 7;13(9):1867–73.
247. Bian Y-S, Osterheld M-C, Fontollet C, Bosman FT, Benhattar J. p16 inactivation by methylation of the CDKN2A promoter occurs early during neoplastic progression in Barrett's esophagus. *Gastroenterology.* 2002 Apr;122(4):1113–21.
248. Stachler MD, Camarda ND, Deitrick C, Kim A, Agoston AT, Odze RD, et al. Detection of Mutations in Barrett's Esophagus Before Progression to High-Grade Dysplasia or Adenocarcinoma. *Gastroenterology.* 2018 Jul;155(1):156–67.
249. Martincorena I, Fowler JC, Wabik A, Lawson ARJ, Abascal F, Hall MWJ, et al. Somatic mutant clones colonize the human esophagus with age. *Science.* 2018 Nov 23;362(6417):911–7.
250. Maley CC, Galipeau PC, Finley JC, Wongsurawat VJ, Li X, Sanchez CA, et al. Genetic clonal diversity predicts progression to esophageal adenocarcinoma. *Nat Genet.* 2006 Apr;38(4):468–73.
251. Martinez P, Timmer MR, Lau CT, Calpe S, Sancho-Serra MDC, Straub D, et al. Dynamic clonal equilibrium and predetermined cancer risk in Barrett's oesophagus. *Nat Commun.* 2016 Aug 19;7:12158.
252. Li X, Paulson TG, Galipeau PC, Sanchez CA, Liu K, Kuhner MK, et al. Assessment of Esophageal Adenocarcinoma Risk Using Somatic Chromosome Alterations in Longitudinal Samples in Barrett's Esophagus. *Cancer Prev Res Phila Pa.* 2015 Sep;8(9):845–56.

253. Li X, Galipeau PC, Paulson TG, Sanchez CA, Arnaudo J, Liu K, et al. Temporal and spatial evolution of somatic chromosomal alterations: a case-cohort study of Barrett's esophagus. *Cancer Prev Res Phila Pa.* 2014 Jan;7(1):114–27.
254. Scott SJ, Li X, Jammula S, Devonshire G, Lindon C, Fitzgerald RC, et al. Evidence that polyploidy in esophageal adenocarcinoma originates from mitotic slippage caused by defective chromosome attachments. *Cell Death Differ.* 2021 Mar 1;
255. Dulak AM, Stojanov P, Peng S, Lawrence MS, Fox C, Stewart C, et al. Exome and whole-genome sequencing of esophageal adenocarcinoma identifies recurrent driver events and mutational complexity. *Nat Genet.* 2013 May;45(5):478–86.
256. Srivastava A, Golden KL, Sanchez CA, Liu K, Fong PY, Li X, et al. High Goblet Cell Count Is Inversely Associated with Ploidy Abnormalities and Risk of Adenocarcinoma in Barrett's Esophagus. *PLoS One.* 2015;10(7):e0133403.
257. Paulson T, Galipeau P, Oman K, Sanchez C, Kuhner M, Smith L, et al. Somatic whole genome dynamics of precancer in Barrett's Esophagus. *Res Sq Prepr [Internet].* 2021 Mar 2 [cited 2021 Mar 9]; Available from: <https://www.researchsquare.com/article/rs-257949/v1>.
258. Killcoyne S, Gregson E, Wedge DC, Woodcock DJ, Eldridge MD, de la Rue R, et al. Genomic copy number predicts esophageal cancer years before transformation. *Nat Med.* 2020 Nov;26(11):1726–32.
259. Allis CD, Jenuwein T. The molecular hallmarks of epigenetic control. *Nat Rev Genet.* 2016 Aug;17(8):487–500.
260. Anastasiadou E, Jacob LS, Slack FJ. Non-coding RNA networks in cancer. *Nat Rev Cancer.* 2018 Jan;18(1):5–18.
261. Talens RP, Christensen K, Putter H, Willemsen G, Christiansen L, Kremer D, et al. Epigenetic variation during the adult lifespan: cross-sectional and longitudinal data on monozygotic twin pairs. *Aging Cell.* 2012 Aug;11(4):694–703.
262. Agarwal A, Polineni R, Hussein Z, Vigoda I, Bhagat TD, Bhattacharyya S, et al. Role of epigenetic alterations in the pathogenesis of Barrett's esophagus and esophageal adenocarcinoma. *Int J Clin Exp Pathol.* 2012;5(5):382–96.
263. Kaz AM, Wong C-J, Luo Y, Virgin JB, Washington MK, Willis JE, et al. DNA methylation profiling in Barrett's esophagus and esophageal adenocarcinoma reveals unique methylation signatures and molecular subclasses. *Epigenetics.* 2011 Dec;6(12):1403–12.
264. Kaz AM, Grady WM, Stachler MD, Bass AJ. Genetic and Epigenetic Alterations in Barrett's Esophagus and Esophageal Adenocarcinoma. *Gastroenterol Clin North Am.* 2015 Jun;44(2):473–89.
265. Xu E, Gu J, Hawk ET, Wang KK, Lai M, Huang M, et al. Genome-wide methylation analysis shows similar patterns in Barrett's esophagus and esophageal adenocarcinoma. *Carcinogenesis.* 2013 Dec;34(12):2750–6.
266. Kaz AM, Wong C-J, Varadan V, Willis JE, Chak A, Grady WM. Global DNA methylation patterns in Barrett's esophagus, dysplastic Barrett's, and esophageal adenocarcinoma are associated with BMI, gender, and tobacco use. *Clin Epigenetics.* 2016;8:111.
267. Luebeck EG, Curtius K, Hazelton WD, Maden S, Yu M, Thota PN, et al. Identification of a key role of widespread epigenetic drift in Barrett's esophagus and esophageal adenocarcinoma. *Clin Epigenetics.* 2017;9:113.
268. Kuester D, Dar AA, Moskaluk CC, Krueger S, Meyer F, Hartig R, et al. Early involvement of death-associated protein kinase promoter hypermethylation in the carcinogenesis of Barrett's esophageal adenocarcinoma and its association with clinical progression. *Neoplasia N Y N.* 2007 Mar;9(3):236–45.

269. Jin Z, Hamilton JP, Yang J, Mori Y, Oлару A, Sato F, et al. Hypermethylation of the AKAP12 promoter is a biomarker of Barrett's-associated esophageal neoplastic progression. *Cancer Epidemiol Biomark Prev Publ Am Assoc Cancer Res Cosponsored Am Soc Prev Oncol*. 2008 Jan;17(1):111–7.
270. Wang JS, Guo M, Montgomery EA, Thompson RE, Cosby H, Hicks L, et al. DNA promoter hypermethylation of p16 and APC predicts neoplastic progression in Barrett's esophagus. *Am J Gastroenterol*. 2009 Sep;104(9):2153–60.
271. Smith E, De Young NJ, Pavey SJ, Hayward NK, Nancarrow DJ, Whiteman DC, et al. Similarity of aberrant DNA methylation in Barrett's esophagus and esophageal adenocarcinoma. *Mol Cancer*. 2008 Oct 2;7:75.
272. Clément G, Braunschweig R, Pasquier N, Bosman FT, Benhattar J. Methylation of APC, TIMP3, and TERT: a new predictive marker to distinguish Barrett's oesophagus patients at risk for malignant transformation. *J Pathol*. 2006 Jan;208(1):100–7.
273. Jin Z, Cheng Y, Oлару A, Kan T, Yang J, Paun B, et al. Promoter hypermethylation of CDH13 is a common, early event in human esophageal adenocarcinogenesis and correlates with clinical risk factors. *Int J Cancer*. 2008 Nov 15;123(10):2331–6.
274. Wong DJ, Barrett MT, Stöger R, Emond MJ, Reid BJ. p16INK4a promoter is hypermethylated at a high frequency in esophageal adenocarcinomas. *Cancer Res*. 1997 Jul 1;57(13):2619–22.
275. Peng DF, Razvi M, Chen H, Washington K, Roessner A, Schneider-Stock R, et al. DNA hypermethylation regulates the expression of members of the Mu-class glutathione S-transferases and glutathione peroxidases in Barrett's adenocarcinoma. *Gut*. 2009 Jan;58(1):5–15.
276. Lee O-J, Schneider-Stock R, McChesney PA, Kuester D, Roessner A, Vieth M, et al. Hypermethylation and loss of expression of glutathione peroxidase-3 in Barrett's tumorigenesis. *Neoplasia N Y N*. 2005 Sep;7(9):854–61.
277. Jin Z, Mori Y, Yang J, Sato F, Ito T, Cheng Y, et al. Hypermethylation of the nel-like 1 gene is a common and early event and is associated with poor prognosis in early-stage esophageal adenocarcinoma. *Oncogene*. 2007 Sep 20;26(43):6332–40.
278. Hamilton JP, Sato F, Jin Z, Greenwald BD, Ito T, Mori Y, et al. Reprimo methylation is a potential biomarker of Barrett's-Associated esophageal neoplastic progression. *Clin Cancer Res Off J Am Assoc Cancer Res*. 2006 Nov 15;12(22):6637–42.
279. Zou H, Molina JR, Harrington JJ, Osborn NK, Klatt KK, Romero Y, et al. Aberrant methylation of secreted frizzled-related protein genes in esophageal adenocarcinoma and Barrett's esophagus. *Int J Cancer*. 2005 Sep 10;116(4):584–91.
280. Tischoff I, Hengge UR, Vieth M, Ell C, Stolte M, Weber A, et al. Methylation of SOCS-3 and SOCS-1 in the carcinogenesis of Barrett's adenocarcinoma. *Gut*. 2007 Aug;56(8):1047–53.
281. Jin Z, Mori Y, Hamilton JP, Oлару A, Sato F, Yang J, et al. Hypermethylation of the somatostatin promoter is a common, early event in human esophageal carcinogenesis. *Cancer*. 2008 Jan 1;112(1):43–9.
282. Jin Z, Oлару A, Yang J, Sato F, Cheng Y, Kan T, et al. Hypermethylation of tachykinin-1 is a potential biomarker in human esophageal cancer. *Clin Cancer Res Off J Am Assoc Cancer Res*. 2007 Nov 1;13(21):6293–300.
283. Jammula S, Katz-Summercorn AC, Li X, Linossi C, Smyth E, Killcoyne S, et al. Identification of Subtypes of Barrett's Esophagus and Esophageal Adenocarcinoma Based on DNA Methylation Profiles and Integration of Transcriptome and Genome Data. *Gastroenterology*. 2020 May;158(6):1682-1697.e1.

284. Seder CW, Hartojo W, Lin L, Silvers AL, Wang Z, Thomas DG, et al. INHBA overexpression promotes cell proliferation and may be epigenetically regulated in esophageal adenocarcinoma. *J Thorac Oncol Off Publ Int Assoc Study Lung Cancer*. 2009 Apr;4(4):455–62.
285. Kailasam A, Mittal SK, Agrawal DK. Epigenetics in the Pathogenesis of Esophageal Adenocarcinoma. *Clin Transl Sci*. 2015 Aug;8(4):394–402.
286. Feber A, Xi L, Luketich JD, Pennathur A, Landreneau RJ, Wu M, et al. MicroRNA expression profiles of esophageal cancer. *J Thorac Cardiovasc Surg*. 2008 Feb;135(2):255–60; discussion 260.
287. Clark RJ, Craig MP, Agrawal S, Kadakia M. microRNA involvement in the onset and progression of Barrett's esophagus: a systematic review. *Oncotarget*. 2018 Jan 30;9(8):8179–96.
288. Abraham JM, Meltzer SJ. Long Noncoding RNAs in the Pathogenesis of Barrett's Esophagus and Esophageal Carcinoma. *Gastroenterology*. 2017 Jul;153(1):27–34.
289. Wu W, Bhagat TD, Yang X, Song JH, Cheng Y, Agarwal R, et al. Hypomethylation of noncoding DNA regions and overexpression of the long noncoding RNA, AFAP1-AS1, in Barrett's esophagus and esophageal adenocarcinoma. *Gastroenterology*. 2013 May;144(5):956-966.e4.
290. Fitzgerald RC, Omary MB, Triadafilopoulos G. Acid modulation of HT29 cell growth and differentiation. An in vitro model for Barrett's esophagus. *J Cell Sci*. 1997 Mar;110 (Pt 5):663–71.
291. Kaur BS, Ouatu-Lascar R, Omary MB, Triadafilopoulos G. Bile salts induce or blunt cell proliferation in Barrett's esophagus in an acid-dependent fashion. *Am J Physiol Gastrointest Liver Physiol*. 2000 Jun;278(6):G1000-1009.
292. Boonstra JJ, van Marion R, Beer DG, Lin L, Chaves P, Ribeiro C, et al. Verification and unmasking of widely used human esophageal adenocarcinoma cell lines. *J Natl Cancer Inst*. 2010 Feb 24;102(4):271–4.
293. Morrison DK. MAP Kinase Pathways. *Cold Spring Harb Perspect Biol*. 2012;4(11):a011254.
294. Braicu C, Buse M, Busuioc C, Drula R, Gulei D, Raduly L, et al. A Comprehensive Review on MAPK: A Promising Therapeutic Target in Cancer. *Cancers*. 2019;11(10):1618.
295. Hemmings BA, Restuccia DF. PI3K-PKB/Akt pathway. *Cold Spring Harb Perspect Biol*. 2012 Sep 1;4(9):a011189.
296. Castellano E, Downward J. RAS Interaction with PI3K. *Genes Cancer*. 2011 Mar;2(3):261–74.
297. Clemons NJ, Phillips WA, Lord RV. Signaling pathways in the molecular pathogenesis of adenocarcinomas of the esophagus and gastroesophageal junction. *Cancer Biol Ther*. 2013 Sep;14(9):782–95.
298. Lord RV, O'Grady R, Sheehan C, Field AF, Ward RL. K-ras codon 12 mutations in Barrett's oesophagus and adenocarcinomas of the oesophagus and oesophagogastric junction. *J Gastroenterol Hepatol*. 2000 Jul;15(7):730–6.
299. Galiana C, Lozano JC, Bancel B, Nakazawa H, Yamasaki H. High frequency of Ki-ras amplification and p53 gene mutations in adenocarcinomas of the human esophagus. *Mol Carcinog*. 1995 Dec;14(4):286–93.
300. Trautmann B, Wittekind C, Strobel D, Meixner H, Keymling J, Gossner L, et al. K-ras point mutations are rare events in premalignant forms of Barrett's oesophagus. *Eur J Gastroenterol Hepatol*. 1996 Aug;8(8):799–804.

301. Sommerer F, Vieth M, Markwarth A, Röhrich K, Vomschloss S, May A, et al. Mutations of BRAF and KRAS2 in the development of Barrett's adenocarcinoma. *Oncogene*. 2004 Jan 15;23(2):554–8.
302. Beales ILP, Ogunwobi O, Cameron E, El-Amin K, Mutungi G, Wilkinson M. Activation of Akt is increased in the dysplasia-carcinoma sequence in Barrett's oesophagus and contributes to increased proliferation and inhibition of apoptosis: a histopathological and functional study. *BMC Cancer*. 2007 Jun 8;7:97.
303. Sagatys E, Garrett CR, Boulware D, Kelley S, Malafa M, Cheng JQ, et al. Activation of the serine/threonine protein kinase Akt during the progression of Barrett neoplasia. *Hum Pathol*. 2007 Oct;38(10):1526–31.
304. Zhang X, Yu C, Wilson K, Zhang HY, Melton SD, Huo X, et al. Malignant transformation of non-neoplastic Barrett's epithelial cells through well-defined genetic manipulations. *PLoS One*. 2010 Sep 30;5(9).
305. Souza RF, Shewmake K, Terada LS, Spechler SJ. Acid exposure activates the mitogen-activated protein kinase pathways in Barrett's esophagus. *Gastroenterology*. 2002 Feb;122(2):299–307.
306. Souza RF, Shewmake K, Pearson S, Sarosi GA, Feagins LA, Ramirez RD, et al. Acid increases proliferation via ERK and p38 MAPK-mediated increases in cyclooxygenase-2 in Barrett's adenocarcinoma cells. *Am J Physiol Gastrointest Liver Physiol*. 2004 Oct;287(4):G743-748.
307. Sarosi GA, Jaiswal K, Herndon E, Lopez-Guzman C, Spechler SJ, Souza RF. Acid increases MAPK-mediated proliferation in Barrett's esophageal adenocarcinoma cells via intracellular acidification through a Cl⁻/HCO₃⁻ exchanger. *Am J Physiol Gastrointest Liver Physiol*. 2005 Dec;289(6):G991-997.
308. Keswani RN, Chumsangsri A, Mustafi R, Delgado J, Cohen EEW, Bissonnette M. Sorafenib inhibits MAPK-mediated proliferation in a Barrett's esophageal adenocarcinoma cell line. *Dis Esophagus Off J Int Soc Dis Esophagus*. 2008;21(6):514–21.
309. Delgado J-S, Mustafi R, Yee J, Cerda S, Chumsangsri A, Dougherty U, et al. Sorafenib triggers antiproliferative and pro-apoptotic signals in human esophageal adenocarcinoma cells. *Dig Dis Sci*. 2008 Dec;53(12):3055–64.
310. Jaiswal K, Lopez-Guzman C, Souza RF, Spechler SJ, Sarosi GA. Bile salt exposure increases proliferation through p38 and ERK MAPK pathways in a non-neoplastic Barrett's cell line. *Am J Physiol Gastrointest Liver Physiol*. 2006 Feb;290(2):G335-342.
311. Avissar NE, Toia L, Hu Y, Watson TJ, Jones C, Raymond DP, et al. Bile acid alone, or in combination with acid, induces CDX2 expression through activation of the epidermal growth factor receptor (EGFR). *J Gastrointest Surg Off J Soc Surg Aliment Tract*. 2009 Feb;13(2):212–22.
312. Vona-Davis L, Frankenberry K, Cunningham C, Riggs DR, Jackson BJ, Szwerz MF, et al. MAPK and PI3K inhibition reduces proliferation of Barrett's adenocarcinoma in vitro. *J Surg Res*. 2005 Jul 1;127(1):53–8.
313. Harris JC, Clarke PA, Awan A, Jankowski J, Watson SA. An antiapoptotic role for gastrin and the gastrin/CCK-2 receptor in Barrett's esophagus. *Cancer Res*. 2004 Mar 15;64(6):1915–9.
314. Ogunwobi OO, Beales ILP. Glycine-extended gastrin stimulates proliferation via JAK2- and Akt-dependent NF-kappaB activation in Barrett's oesophageal adenocarcinoma cells. *Mol Cell Endocrinol*. 2008 Dec 16;296(1–2):94–102.

315. Ogunwobi OO, Beales ILP. Globular adiponectin, acting via adiponectin receptor-1, inhibits leptin-stimulated oesophageal adenocarcinoma cell proliferation. *Mol Cell Endocrinol.* 2008 Mar 26;285(1–2):43–50.
316. Jaiswal K, Tello V, Lopez-Guzman C, Nwariaku F, Anthony T, Sarosi GA. Bile salt exposure causes phosphatidyl-inositol-3-kinase-mediated proliferation in a Barrett's adenocarcinoma cell line. *Surgery.* 2004 Aug;136(2):160–8.
317. Song S, Guha S, Liu K, Buttar NS, Bresalier RS. COX-2 induction by unconjugated bile acids involves reactive oxygen species-mediated signalling pathways in Barrett's oesophagus and oesophageal adenocarcinoma. *Gut.* 2007 Nov;56(11):1512–21.
318. Looby E, Abdel-Latif MMM, Athié-Morales V, Duggan S, Long A, Kelleher D. Deoxycholate induces COX-2 expression via Erk1/2-, p38-MAPK and AP-1-dependent mechanisms in esophageal cancer cells. *BMC Cancer.* 2009 Jun 17;9:190.
319. Morgan C, Alazawi W, Sirieix P, Freeman T, Coleman N, Fitzgerald R. In vitro acid exposure has a differential effect on apoptotic and proliferative pathways in a Barrett's adenocarcinoma cell line. *Am J Gastroenterol.* 2004 Feb;99(2):218–24.
320. Schmidt MK, Meurer L, Volkweis BS, Edelweiss MI, Schirmer CC, Kruehl CDP, et al. c-Myc overexpression is strongly associated with metaplasia-dysplasia-adenocarcinoma sequence in the esophagus. *Dis Esophagus Off J Int Soc Dis Esophagus.* 2007;20(3):212–6.
321. Mariette C, Piessen G, Leteurtre E, Hémon B, Triboulet J-P, Van Seuning I. Activation of MUC1 mucin expression by bile acids in human esophageal adenocarcinomatous cells and tissues is mediated by the phosphatidylinositol 3-kinase. *Surgery.* 2008 Jan;143(1):58–71.
322. Mariette C, Perrais M, Leteurtre E, Jonckheere N, Hémon B, Pigny P, et al. Transcriptional regulation of human mucin MUC4 by bile acids in esophageal cancer cells is promoter-dependent and involves activation of the phosphatidylinositol 3-kinase signalling pathway. *Biochem J.* 2004 Feb 1;377(Pt 3):701–8.
323. Song S, Byrd JC, Guha S, Liu K-F, Koul D, Bresalier RS. Induction of MUC5AC mucin by conjugated bile acids in the esophagus involves the phosphatidylinositol 3-kinase/protein kinase C/activator protein-1 pathway. *Cancer.* 2011 Jun 1;117(11):2386–97.
324. Souza RF, Shewmake KL, Shen Y, Ramirez RD, Bullock JS, Hladik CL, et al. Differences in ERK activation in squamous mucosa in patients who have gastroesophageal reflux disease with and without Barrett's esophagus. *Am J Gastroenterol.* 2005 Mar;100(3):551–9.
325. van Baal JWPM, Diks SH, Wanders RJA, Rygiel AM, Milano F, Joore J, et al. Comparison of kinome profiles of Barrett's esophagus with normal squamous esophagus and normal gastric cardia. *Cancer Res.* 2006 Dec 15;66(24):11605–12.
326. Park SY, Lee YJ, Cho EJ, Shin CY, Sohn UD. Intrinsic resistance triggered under acid loading within normal esophageal epithelial cells: NHE1- and ROS-mediated survival. *J Cell Physiol.* 2015 Jul;230(7):1503–14.
327. Thomas SJ, Snowden JA, Zeidler MP, Danson SJ. The role of JAK/STAT signalling in the pathogenesis, prognosis and treatment of solid tumours. *Br J Cancer.* 2015 Jul 28;113(3):365–71.
328. Beales ILP, Ogunwobi OO. Glycine-extended gastrin inhibits apoptosis in Barrett's esophageal and esophageal adenocarcinoma cells through JAK2/STAT3 activation. *J Mol Endocrinol.* 2009 Apr;42(4):305–18.

329. Duggan SP, Garry C, Behan FM, Phipps S, Kudo H, Kirca M, et al. siRNA Library Screening Identifies a Druggable Immune-Signature Driving Esophageal Adenocarcinoma Cell Growth. *Cell Mol Gastroenterol Hepatol*. 2018;5(4):569–90.
330. Timme S, Ihde S, Fichter CD, Waehle V, Bogatyreva L, Atanasov K, et al. STAT3 expression, activity and functional consequences of STAT3 inhibition in esophageal squamous cell carcinomas and Barrett's adenocarcinomas. *Oncogene*. 2014 Jun 19;33(25):3256–66.
331. Bhat AA, Lu H, Soutto M, Capobianco A, Rai P, Zaika A, et al. Exposure of Barrett's and esophageal adenocarcinoma cells to bile acids activates EGFR-STAT3 signaling axis via induction of APE1. *Oncogene*. 2018 Nov;37(46):6011–24.
332. Bray SJ. Notch signalling in context. *Nat Rev Mol Cell Biol*. 2016 Nov;17(11):722–35.
333. Scoville DH, Sato T, He XC, Li L. Current view: intestinal stem cells and signaling. *Gastroenterology*. 2008 Mar;134(3):849–64.
334. Chen X, Jiang K, Fan Z, Liu Z, Zhang P, Zheng L, et al. Aberrant expression of Wnt and Notch signal pathways in Barrett's esophagus. *Clin Res Hepatol Gastroenterol*. 2012 Oct;36(5):473–83.
335. Kunze B, Wein F, Fang H-Y, Anand A, Baumeister T, Strangmann J, et al. Notch Signaling Mediates Differentiation in Barrett's Esophagus and Promotes Progression to Adenocarcinoma. *Gastroenterology*. 2020 Aug;159(2):575–90.
336. Song S, Maru DM, Ajani JA, Chan C-H, Honjo S, Lin H-K, et al. Loss of TGF- β adaptor β 2SP activates notch signaling and SOX9 expression in esophageal adenocarcinoma. *Cancer Res*. 2013 Apr 1;73(7):2159–69.
337. Mendelson J, Song S, Li Y, Maru DM, Mishra B, Davila M, et al. Dysfunctional TGF- β signaling with constitutively active Notch signaling in Barrett's esophageal adenocarcinoma. *Cancer*. 2011 Aug 15;117(16):3691–702.
338. Tamagawa Y, Ishimura N, Uno G, Yuki T, Kazumori H, Ishihara S, et al. Notch signaling pathway and Cdx2 expression in the development of Barrett's esophagus. *Lab Investig J Tech Methods Pathol*. 2012 Jun;92(6):896–909.
339. Dickson I. Another Notch in the mechanism of Barrett oesophagus progression. *Nat Rev Gastroenterol Hepatol*. 2020 Jul;17(7):381.
340. Carballo GB, Honorato JR, de Lopes GPF, Spohr TCL de SE. A highlight on Sonic hedgehog pathway. *Cell Commun Signal CCS*. 2018 Mar 20;16(1):11.
341. Berman DM, Karhadkar SS, Maitra A, Montes De Oca R, Gerstenblith MR, Briggs K, et al. Widespread requirement for Hedgehog ligand stimulation in growth of digestive tract tumours. *Nature*. 2003 Oct 23;425(6960):846–51.
342. Clemons NJ, Wang DH, Croagh D, Tikoo A, Fennell CM, Murone C, et al. Sox9 drives columnar differentiation of esophageal squamous epithelium: a possible role in the pathogenesis of Barrett's esophagus. *Am J Physiol Gastrointest Liver Physiol*. 2012 Dec 15;303(12):G1335-1346.
343. van Baal JWPM, Milana F, Rygiel AM, Sondermeijer CMT, Spek CA, Bergman JJGHM, et al. A comparative analysis by SAGE of gene expression profiles of esophageal adenocarcinoma and esophageal squamous cell carcinoma. *Cell Oncol Off J Int Soc Cell Oncol*. 2008;30(1):63–75.
344. Castillo D, Puig S, Iglesias M, Seoane A, de Bolós C, Munitiz V, et al. Activation of the BMP4 pathway and early expression of CDX2 characterize non-specialized columnar metaplasia in a human model of Barrett's esophagus. *J Gastrointest Surg Off J Soc Surg Aliment Tract*. 2012 Feb;16(2):227–37; discussion 237.

345. Rizvi S, Demars CJ, Comba A, Gainullin VG, Rizvi Z, Almada LL, et al. Combinatorial chemoprevention reveals a novel smoothed-independent role of GLI1 in esophageal carcinogenesis. *Cancer Res.* 2010 Sep 1;70(17):6787–96.
346. Ng CK, Ma K, Cheng Y, Miyashita T, Harmon JW, Meltzer SJ. Krüppel-like Factor 5 Promotes Sonic Hedgehog Signaling and Neoplasia in Barrett's Esophagus and Esophageal Adenocarcinoma. *Transl Oncol.* 2019 Nov;12(11):1432–41.
347. Kelly RJ, Ansari AM, Miyashita T, Zahurak M, Lay F, Ahmed AK, et al. Targeting the Hedgehog Pathway Using Itraconazole to Prevent Progression of Barrett's Esophagus to Invasive Esophageal Adenocarcinoma. *Ann Surg.* 2019 Jul 8;
348. Huang J, Liu H, Sun T, Fang J-Y, Wang J, Xiong H. Omeprazole prevents CDX2 and SOX9 expression by inhibiting hedgehog signaling in Barrett's esophagus cells. *Clin Sci Lond Engl 1979.* 2019 Feb 14;133(3):483–95.
349. Wang Y, Ding Q, Yen C-J, Xia W, Izzo JG, Lang J-Y, et al. The crosstalk of mTOR/S6K1 and Hedgehog pathways. *Cancer Cell.* 2012 Mar 20;21(3):374–87.
350. MacDonald BT, Tamai K, He X. Wnt/beta-catenin signaling: components, mechanisms, and diseases. *Dev Cell.* 2009 Jul;17(1):9–26.
351. Wanchai V, Jin J, Bircan E, Eng C, Orloff M. Genome-wide tracts of homozygosity and exome analyses reveal repetitive elements with Barrets esophagus/esophageal adenocarcinoma risk. *BMC Bioinformatics.* 2019 Mar 14;20(Suppl 2):98.
352. Götzl K, Chemnitzer O, Maurer L, Dietrich A, Eichfeld U, Lyros O, et al. In-depth characterization of the Wnt-signaling/ β -catenin pathway in an in vitro model of Barrett's sequence. *BMC Gastroenterol.* 2019 Mar 6;19(1):38.
353. Bian YS, Osterheld MC, Bosman FT, Fontolliet C, Benhattar J. Nuclear accumulation of beta-catenin is a common and early event during neoplastic progression of Barrett esophagus. *Am J Clin Pathol.* 2000 Oct;114(4):583–90.
354. Osterheld M-C, Bian Y-S, Bosman FT, Benhattar J, Fontolliet C. Beta-catenin expression and its association with prognostic factors in adenocarcinoma developed in Barrett esophagus. *Am J Clin Pathol.* 2002 Mar;117(3):451–6.
355. Krishnadath KK, Tilanus HW, van Blankenstein M, Hop WC, Kremers ED, Dinjens WN, et al. Reduced expression of the cadherin-catenin complex in oesophageal adenocarcinoma correlates with poor prognosis. *J Pathol.* 1997 Jul;182(3):331–8.
356. Moyes LH, McEwan H, Radulescu S, Pawlikowski J, Lamm CG, Nixon C, et al. Activation of Wnt signalling promotes development of dysplasia in Barrett's oesophagus. *J Pathol.* 2012 Sep;228(1):99–112.
357. Lyros O, Rafiee P, Nie L, Medda R, Jovanovic N, Otterson MF, et al. Wnt/ β -Catenin Signaling Activation beyond Robust Nuclear β -Catenin Accumulation in Nondysplastic Barrett's Esophagus: Regulation via Dickkopf-1. *Neoplasia N Y N.* 2015 Jul;17(7):598–611.
358. Bailey T, Biddlestone L, Shepherd N, Barr H, Warner P, Jankowski J. Altered cadherin and catenin complexes in the Barrett's esophagus-dysplasia-adenocarcinoma sequence: correlation with disease progression and dedifferentiation. *Am J Pathol.* 1998 Jan;152(1):135–44.
359. Corn PG, Heath EI, Heitmiller R, Fogt F, Forastiere AA, Herman JG, et al. Frequent hypermethylation of the 5' CpG island of E-cadherin in esophageal adenocarcinoma. *Clin Cancer Res Off J Am Assoc Cancer Res.* 2001 Sep;7(9):2765–9.
360. Jethwa P, Naqvi M, Hardy RG, Hotchin N-A, Roberts S, Spychal R, et al. Overexpression of Slug is associated with malignant progression of esophageal adenocarcinoma. *World J Gastroenterol.* 2008 Feb 21;14(7):1044–52.

361. Heuberger J, Kosel F, Qi J, Grossmann KS, Rajewsky K, Birchmeier W. Shp2/MAPK signaling controls goblet/paneth cell fate decisions in the intestine. *Proc Natl Acad Sci U S A*. 2014 Mar 4;111(9):3472–7.
362. Choi YW, Heath EI, Heitmiller R, Forastiere AA, Wu TT. Mutations in beta-catenin and APC genes are uncommon in esophageal and esophagogastric junction adenocarcinomas. *Mod Pathol Off J U S Can Acad Pathol Inc*. 2000 Oct;13(10):1055–9.
363. Clément G, Braunschweig R, Pasquier N, Bosman FT, Benhattar J. Alterations of the Wnt signaling pathway during the neoplastic progression of Barrett’s esophagus. *Oncogene*. 2006 May 18;25(21):3084–92.
364. Clément G, Guilleret I, He B, Yagui-Beltrán A, Lin Y-C, You L, et al. Epigenetic alteration of the Wnt inhibitory factor-1 promoter occurs early in the carcinogenesis of Barrett’s esophagus. *Cancer Sci*. 2008 Jan;99(1):46–53.
365. Lyros O, Lamprecht A-K, Nie L, Thieme R, Götzl K, Gasparri M, et al. Dickkopf-1 (DKK1) promotes tumor growth via Akt-phosphorylation and independently of Wnt-axis in Barrett’s associated esophageal adenocarcinoma. *Am J Cancer Res*. 2019;9(2):330–46.
366. Lyros O, Nie L, Moore T, Medda R, Otterson M, Behmaram B, et al. Dysregulation of WNT5A/ROR2 Signaling Characterizes the Progression of Barrett-Associated Esophageal Adenocarcinoma. *Mol Cancer Res MCR*. 2016 Jul;14(7):647–59.
367. Taniguchi K, Karin M. NF- κ B, inflammation, immunity and cancer: coming of age. *Nat Rev Immunol*. 2018 May;18(5):309–24.
368. El Jamal SM, Yaseen AA, Alatassi H, Slone S, Bishop BJ, Fraig M. Strong NF κ B Expression is Associated With High-grade Dysplasia in Barrett’s Esophagus. *Appl Immunohistochem Mol Morphol AIMM*. 2017 Jun;25(5):329–33.
369. Doak SH, Jenkins GJS, Parry EM, D’Souza FR, Griffiths AP, Toffazal N, et al. Chromosome 4 hyperploidy represents an early genetic aberration in premalignant Barrett’s oesophagus. *Gut*. 2003 May;52(5):623–8.
370. Yen C-J, Izzo JG, Lee D-F, Guha S, Wei Y, Wu T-T, et al. Bile Acid Exposure Up-regulates Tuberos Sclerosis Complex 1/Mammalian Target of Rapamycin Pathway in Barrett’s-Associated Esophageal Adenocarcinoma. *Cancer Res*. 2008 Apr 15;68(8):2632–40.
371. Cronin J, Alhamdani A, Griffiths AP, Baxter JN, Brown T, Jenkins GJS. In vitro and ex vivo models of extended reflux exposure demonstrate that weakly acidic mixed reflux heightens NF- κ B-mediated gene expression. *Dis Esophagus Off J Int Soc Dis Esophagus*. 2011 Jul;24(5):360–70.
372. Si J, Fu X, Behar J, Wands J, Beer DG, Souza RF, et al. NADPH oxidase NOX5-S mediates acid-induced cyclooxygenase-2 expression via activation of NF- κ B in Barrett’s esophageal adenocarcinoma cells. *J Biol Chem*. 2007 Jun 1;282(22):16244–55.
373. Feng C, Luo Y, Nian Y, Liu D, Yin X, Wu J, et al. Diallyl Disulfide Suppresses the Inflammation and Apoptosis Resistance Induced by DCA Through ROS and the NF- κ B Signaling Pathway in Human Barrett’s Epithelial Cells. *Inflammation*. 2017 Jun;40(3):818–31.
374. McAdam E, Haboubi HN, Forrester G, Eltahir Z, Spencer-Harty S, Davies C, et al. Inducible nitric oxide synthase (iNOS) and nitric oxide (NO) are important mediators of reflux-induced cell signalling in esophageal cells. *Carcinogenesis*. 2012 Nov;33(11):2035–43.
375. Rawat N, Alhamdani A, McAdam E, Cronin J, Eltahir Z, Lewis P, et al. Curcumin abrogates bile-induced NF- κ B activity and DNA damage in vitro and suppresses NF- κ B activity whilst promoting apoptosis in vivo, suggesting chemopreventative potential in

- Barrett's oesophagus. *Clin Transl Oncol Off Publ Fed Span Oncol Soc Natl Cancer Inst Mex.* 2012 Apr;14(4):302–11.
376. Burnat G, Majka J, Konturek PC. Bile acids are multifunctional modulators of the Barrett's carcinogenesis. *J Physiol Pharmacol Off J Pol Physiol Soc.* 2010 Apr;61(2):185–92.
377. Jenkins GJS, Harries K, Doak SH, Wilmes A, Griffiths AP, Baxter JN, et al. The bile acid deoxycholic acid (DCA) at neutral pH activates NF-kappaB and induces IL-8 expression in oesophageal cells in vitro. *Carcinogenesis.* 2004 Mar;25(3):317–23.
378. Peng D-F, Hu T-L, Soutto M, Belkhiri A, El-Rifai W. Glutathione Peroxidase 7 Suppresses Bile Salt-Induced Expression of Pro-Inflammatory Cytokines in Barrett's Carcinogenesis. *J Cancer.* 2014 Jun 10;5(7):510–7.
379. von Knethen A, Callsen D, Brüne B. NF-κB and AP-1 Activation by Nitric Oxide Attenuated Apoptotic Cell Death in RAW 264.7 Macrophages. *Mol Biol Cell.* 1999 Feb;10(2):361–72.
380. Duggan SP, Behan FM, Kirca M, Smith S, Reynolds JV, Long A, et al. An integrative genomic approach in oesophageal cells identifies TRB3 as a bile acid responsive gene, downregulated in Barrett's oesophagus, which regulates NF-kappaB activation and cytokine levels. *Carcinogenesis.* 2010 May;31(5):936–45.
381. Verbeek RE, Siersema PD, Ten Kate FJ, Fluiter K, Souza RF, Vleggaar FP, et al. Toll-like receptor 4 activation in Barrett's esophagus results in a strong increase in COX-2 expression. *J Gastroenterol.* 2014 Jul;49(7):1121–34.
382. Konturek PC, Nikiforuk A, Kania J, Raithel M, Hahn EG, Mühldorfer S. Activation of NFkappaB represents the central event in the neoplastic progression associated with Barrett's esophagus: a possible link to the inflammation and overexpression of COX-2, PPARgamma and growth factors. *Dig Dis Sci.* 2004 Aug;49(7–8):1075–83.
383. Peng D-F, Hu T-L, Soutto M, Belkhiri A, El-Rifai W. Loss of glutathione peroxidase 7 promotes TNF-α-induced NF-κB activation in Barrett's carcinogenesis. *Carcinogenesis.* 2014 Jul;35(7):1620–8.
384. Aiyer HS, Li Y, Harper N, Myers SR, Martin RCG. Molecular changes in the esophageal epithelium after a subchronic exposure to cigarette smoke in the presence of bile-acid reflux. *Inhal Toxicol.* 2011 Apr;23(5):304–11.
385. Hong J, Li D, Wands J, Souza R, Cao W. Role of NADPH oxidase NOX5-S, NF-κB, and DNMT1 in acid-induced p16 hypermethylation in Barrett's cells. *Am J Physiol Cell Physiol.* 2013 Nov 15;305(10):C1069-1079.
386. Li D, Hong J, Cao W. Silencer-of-Death Domain Mediates Acid-Induced Decrease in Cell Apoptosis in Barrett's Associated Esophageal Adenocarcinoma Cells. *J Pharmacol Exp Ther.* 2017 Jan;360(1):14–22.
387. Yamada T, Osawa S, Ikuma M, Kajimura M, Sugimoto M, Furuta T, et al. Guggulsterone, a plant-derived inhibitor of NF-TB, suppresses CDX2 and COX-2 expression and reduces the viability of esophageal adenocarcinoma cells. *Digestion.* 2014;90(3):208–17.
388. Huo X, Zhang X, Yu C, Cheng E, Zhang Q, Dunbar KB, et al. Aspirin Prevents NF-κB Activation and CDX2 Expression Stimulated by Acid and Bile Salts in Oesophageal Squamous Cells of Barrett's Oesophagus Patients. *Gut.* 2018 Apr;67(4):606–15.
389. Kazumori H, Ishihara S, Rumi M a. K, Kadowaki Y, Kinoshita Y. Bile acids directly augment caudal related homeobox gene Cdx2 expression in oesophageal keratinocytes in Barrett's epithelium. *Gut.* 2006 Jan;55(1):16–25.

390. Ojima E, Fujimura T, Oyama K, Tsukada T, Kinoshita J, Miyashita T, et al. Chemoprevention of esophageal adenocarcinoma in a rat model by ursodeoxycholic acid. *Clin Exp Med*. 2015 Aug;15(3):343–50.
391. Huo X, Zhang HY, Zhang XI, Lynch JP, Strauch ED, Wang J-Y, et al. Acid and bile salt-induced CDX2 expression differs in esophageal squamous cells from patients with and without Barrett's esophagus. *Gastroenterology*. 2010 Jul;139(1):194-203.e1.
392. Dang T, Meng X, Modak C, Wu J, Chang Z, Che N, et al. Overexpression of CCN1 in Het1A cells attenuates bile-induced esophageal metaplasia through suppressing non-canonical NFκB activation. *Cytokine*. 2019 Apr;116:61–9.
393. Wilson KT, Fu S, Ramanujam KS, Meltzer SJ. Increased expression of inducible nitric oxide synthase and cyclooxygenase-2 in Barrett's esophagus and associated adenocarcinomas. *Cancer Res*. 1998 Jul 15;58(14):2929–34.
394. Shirvani VN, Ouatu-Lascar R, Kaur BS, Omary MB, Triadafilopoulos G. Cyclooxygenase 2 expression in Barrett's esophagus and adenocarcinoma: Ex vivo induction by bile salts and acid exposure. *Gastroenterology*. 2000 Mar;118(3):487–96.
395. Morris CD, Armstrong GR, Bigley G, Green H, Attwood SE. Cyclooxygenase-2 expression in the Barrett's metaplasia-dysplasia-adenocarcinoma sequence. *Am J Gastroenterol*. 2001 Apr;96(4):990–6.
396. Benoit V, de Moraes E, Dar NA, Taranchon E, Bours V, Hautefeuille A, et al. Transcriptional activation of cyclooxygenase-2 by tumor suppressor p53 requires nuclear factor-kappaB. *Oncogene*. 2006 Sep 21;25(42):5708–18.
397. Kaur BS, Khamnehei N, Irvani M, Namburu SS, Lin O, Triadafilopoulos G. Rofecoxib inhibits cyclooxygenase 2 expression and activity and reduces cell proliferation in Barrett's esophagus. *Gastroenterology*. 2002 Jul;123(1):60–7.
398. Taddei A, Fabbroni V, Pini A, Lucarini L, Ringressi MN, Fantappiè O, et al. Cyclooxygenase-2 and inflammation mediators have a crucial role in reflux-related esophageal histological changes and Barrett's esophagus. *Dig Dis Sci*. 2014 May;59(5):949–57.
399. Zampeli E, Karamanolis G, Morfopoulos G, Xirouchakis E, Kalampoki V, Michopoulos S, et al. Increased expression of VEGF, COX-2, and Ki-67 in Barrett's esophagus: does the length matter? *Dig Dis Sci*. 2012 May;57(5):1190–6.
400. Ling FC, Baldus SE, Khochfar J, Xi H, Neiss S, Brabender J, et al. Association of COX-2 expression with corresponding active and chronic inflammatory reactions in Barrett's metaplasia and progression to cancer. *Histopathology*. 2007 Jan;50(2):203–9.
401. Shimizu D, Vallböhmer D, Kuramochi H, Uchida K, Schneider S, Chandrasoma PT, et al. Increasing cyclooxygenase-2 (cox-2) gene expression in the progression of Barrett's esophagus to adenocarcinoma correlates with that of Bcl-2. *Int J Cancer*. 2006 Aug 15;119(4):765–70.
402. Jiménez P, Piazuelo E, Cebrian C, Ortego J, Strunk M, García-Gonzalez MA, et al. Prostaglandin EP2 receptor expression is increased in Barrett's oesophagus and oesophageal adenocarcinoma. *Aliment Pharmacol Ther*. 2010 Feb 1;31(3):440–51.
403. Moons LMG, Kuipers EJ, Rygiel AM, Groothuismink AZM, Geldof H, Bode WA, et al. COX-2 CA-haplotype is a risk factor for the development of esophageal adenocarcinoma. *Am J Gastroenterol*. 2007 Nov;102(11):2373–9.
404. Kristinsson JO, van Westerveld P, te Morsche RHM, Roelofs HMJ, Wobbes T, Witteman BJM, et al. Cyclooxygenase-2 polymorphisms and the risk of esophageal adeno- or squamous cell carcinoma. *World J Gastroenterol*. 2009 Jul 28;15(28):3493–7.
405. Ferguson HR, Wild CP, Anderson LA, Murphy SJ, Johnston BT, Murray LJ, et al. Cyclooxygenase-2 and inducible nitric oxide synthase gene polymorphisms and risk of

- reflux esophagitis, Barrett's esophagus, and esophageal adenocarcinoma. *Cancer Epidemiol Biomark Prev Publ Am Assoc Cancer Res Cosponsored Am Soc Prev Oncol*. 2008 Mar;17(3):727–31.
406. Abdalla SI, Sanderson IR, Fitzgerald RC. Effect of inflammation on cyclooxygenase (COX)-2 expression in benign and malignant oesophageal cells. *Carcinogenesis*. 2005 Sep;26(9):1627–33.
407. Zhang F, Altorki NK, Wu YC, Soslow RA, Subbaramaiah K, Dannenberg AJ. Duodenal reflux induces cyclooxygenase-2 in the esophageal mucosa of rats: evidence for involvement of bile acids. *Gastroenterology*. 2001 Dec;121(6):1391–9.
408. Lurje G, Vallbohmer D, Collet PH, Xi H, Baldus SE, Brabender J, et al. COX-2 mRNA expression is significantly increased in acid-exposed compared to nonexposed squamous epithelium in gastroesophageal reflux disease. *J Gastrointest Surg Off J Soc Surg Aliment Tract*. 2007 Sep;11(9):1105–11.
409. Zhang F, Subbaramaiah K, Altorki N, Dannenberg AJ. Dihydroxy bile acids activate the transcription of cyclooxygenase-2. *J Biol Chem*. 1998 Jan 23;273(4):2424–8.
410. Bajpai M, Liu J, Geng X, Souza RF, Amenta PS, Das KM. Repeated exposure to acid and bile selectively induces colonic phenotype expression in a heterogeneous Barrett's epithelial cell line. *Lab Investig J Tech Methods Pathol*. 2008 Jun;88(6):643–51.
411. Liu F-X, Wang W-H, Wang J, Li J, Gao P-P. Effect of *Helicobacter pylori* infection on Barrett's esophagus and esophageal adenocarcinoma formation in a rat model of chronic gastroesophageal reflux. *Helicobacter*. 2011 Feb;16(1):66–77.
412. Majka J, Wierdak M, Szlachcic A, Magierowski M, Targosz A, Urbanczyk K, et al. Interaction of epidermal growth factor with COX-2 products and peroxisome proliferator-activated receptor- γ system in experimental rat Barrett's esophagus. *Am J Physiol Gastrointest Liver Physiol*. 2020 Mar 1;318(3):G375–89.
413. Zhou X, Li D, Resnick MB, Wands J, Cao W. NADPH Oxidase NOX5-S and Nuclear Factor κ B1 Mediate Acid-Induced Microsomal Prostaglandin E Synthase-1 Expression in Barrett's Esophageal Adenocarcinoma Cells. *Mol Pharmacol*. 2013 May;83(5):978–90.
414. Möbius C, Stein HJ, Spiess C, Becker I, Feith M, Theisen J, et al. COX2 expression, angiogenesis, proliferation and survival in Barrett's cancer. *Eur J Surg Oncol J Eur Soc Surg Oncol Br Assoc Surg Oncol*. 2005 Sep;31(7):755–9.
415. von Rahden BHA, Stein HJ, Hartl SA, Theisen J, Stigler B, Siewert JR, et al. Expression of prostaglandin E synthase in Barrett's cancer. *Dis Esophagus Off J Int Soc Dis Esophagus*. 2008;21(4):304–8.
416. Souza RF, Shewmake K, Beer DG, Cryer B, Spechler SJ. Selective inhibition of cyclooxygenase-2 suppresses growth and induces apoptosis in human esophageal adenocarcinoma cells. *Cancer Res*. 2000 Oct 15;60(20):5767–72.
417. Cheong E, Ivory K, Doleman J, Parker ML, Rhodes M, Johnson IT. Synthetic and naturally occurring COX-2 inhibitors suppress proliferation in a human oesophageal adenocarcinoma cell line (OE33) by inducing apoptosis and cell cycle arrest. *Carcinogenesis*. 2004 Oct;25(10):1945–52.
418. Buttar NS, Wang KK, Anderson MA, Dierkhising RA, Pacifico RJ, Krishnadath KK, et al. The effect of selective cyclooxygenase-2 inhibition in Barrett's esophagus epithelium: an in vitro study. *J Natl Cancer Inst*. 2002 Mar 20;94(6):422–9.
419. Piazuelo E, Jiménez P, Strunk M, Santander S, García A, Esteva F, et al. Effects of selective PGE2 receptor antagonists in esophageal adenocarcinoma cells derived from Barrett's esophagus. *Prostaglandins Other Lipid Mediat*. 2006 Dec;81(3–4):150–61.
420. Santander S, Cebrián C, Esquivias P, Conde B, Esteva F, Jiménez P, et al. Cyclooxygenase inhibitors decrease the growth and induce regression of human

- esophageal adenocarcinoma xenografts in nude mice. *Int J Oncol.* 2012 Feb;40(2):527–34.
421. Oyama K, Fujimura T, Ninomiya I, Miyashita T, Kinami S, Fushida S, et al. A COX-2 inhibitor prevents the esophageal inflammation-metaplasia-adenocarcinoma sequence in rats. *Carcinogenesis.* 2005 Mar;26(3):565–70.
422. Heath EI, Canto MI, Piantadosi S, Montgomery E, Weinstein WM, Herman JG, et al. Secondary chemoprevention of Barrett's esophagus with celecoxib: results of a randomized trial. *J Natl Cancer Inst.* 2007 Apr 4;99(7):545–57.
423. Qiao D, Gaitonde SV, Qi W, Martinez JD. Deoxycholic acid suppresses p53 by stimulating proteasome-mediated p53 protein degradation. *Carcinogenesis.* 2001 Jun;22(6):957–64.
424. Zaika E, Wei J, Yin D, Andl C, Moll U, El-Rifai W, et al. p73 protein regulates DNA damage repair. *FASEB J Off Publ Fed Am Soc Exp Biol.* 2011 Dec;25(12):4406–14.
425. Feagins LA, Zhang H-Y, Hormi-Carver K, Quinones MH, Thomas D, Zhang X, et al. Acid has antiproliferative effects in nonneoplastic Barrett's epithelial cells. *Am J Gastroenterol.* 2007 Jan;102(1):10–20.
426. Roman S, Pétré A, Thépot A, Hautefeuille A, Scoazec J-Y, Mion F, et al. Downregulation of p63 upon exposure to bile salts and acid in normal and cancer esophageal cells in culture. *Am J Physiol Gastrointest Liver Physiol.* 2007 Jul;293(1):G45–53.
427. Zaika E, Bhardwaj V, Wei J, Washington MK, Souza R, El-Rifai W, et al. Proinflammatory cytokines and bile acids upregulate Δ Np73 protein, an inhibitor of p53 and p73 tumor suppressors. *PLoS One.* 2013;8(5):e64306.
428. Lee S-W, Lien H-C, Lin C-C, Wen M-C, Chang C-S. Low Expression of Transforming Growth Factor β in the Epithelium of Barrett's Esophagus. *Gastroenterol Res.* 2018 Jun;11(3):189–94.
429. Barrett MT, Galipeau PC, Sanchez CA, Emond MJ, Reid BJ. Determination of the frequency of loss of heterozygosity in esophageal adenocarcinoma by cell sorting, whole genome amplification and microsatellite polymorphisms. *Oncogene.* 1996 May 2;12(9):1873–8.
430. Paterson AL, O'Donovan M, Provenzano E, Murray LJ, Coleman HG, Johnson BT, et al. Characterization of the timing and prevalence of receptor tyrosine kinase expression changes in oesophageal carcinogenesis. *J Pathol.* 2013 May;230(1):118–28.
431. Gockel I, Moehler M, Frerichs K, Drescher D, Trinh TT, Duenschede F, et al. Co-expression of receptor tyrosine kinases in esophageal adenocarcinoma and squamous cell cancer. *Oncol Rep.* 2008 Oct;20(4):845–50.
432. Hanahan D, Weinberg RA. Hallmarks of cancer: the next generation. *Cell.* 2011 Mar 4;144(5):646–74.
433. Nowell PC. The clonal evolution of tumor cell populations. *Science.* 1976 Oct 1;194(4260):23–8.
434. García-Nieto PE, Morrison AJ, Fraser HB. The somatic mutation landscape of the human body. *Genome Biol.* 2019 Dec 24;20(1):298.
435. Balmain A. The critical roles of somatic mutations and environmental tumor-promoting agents in cancer risk. *Nat Genet.* 2020 Nov;52(11):1139–43.
436. Engström W, Darbre P, Eriksson S, Gulliver L, Hultman T, Karamouzian MV, et al. The potential for chemical mixtures from the environment to enable the cancer hallmark of sustained proliferative signalling. *Carcinogenesis.* 2015 Jun;36 Suppl 1:S38–60.

437. Stoner GD, Kaighn ME, Reddel RR, Resau JH, Bowman D, Naito Z, et al. Establishment and characterization of SV40 T-antigen immortalized human esophageal epithelial cells. *Cancer Res.* 1991 Jan 1;51(1):365–71.
438. Palanca-Wessels MC, Barrett MT, Galipeau PC, Rohrer KL, Reid BJ, Rabinovitch PS. Genetic analysis of long-term Barrett's esophagus epithelial cultures exhibiting cytogenetic and ploidy abnormalities. *Gastroenterology.* 1998 Feb;114(2):295–304.
439. Bolger AM, Lohse M, Usadel B. Trimmomatic: a flexible trimmer for Illumina sequence data. *Bioinformatics.* 2014 Aug 1;30(15):2114–20.
440. Leggett RM, Ramirez-Gonzalez RH, Clavijo BJ, Waite D, Davey RP. Sequencing quality assessment tools to enable data-driven informatics for high throughput genomics. *Front Genet [Internet].* 2013 Dec 17 [cited 2021 Jan 13];4. Available from: <https://www.ncbi.nlm.nih.gov/pmc/articles/PMC3865868/>
441. Dobin A, Davis CA, Schlesinger F, Drenkow J, Zaleski C, Jha S, et al. STAR: ultrafast universal RNA-seq aligner. *Bioinforma Oxf Engl.* 2013 Jan 1;29(1):15–21.
442. Trapnell C, Williams BA, Pertea G, Mortazavi A, Kwan G, van Baren MJ, et al. Transcript assembly and quantification by RNA-Seq reveals unannotated transcripts and isoform switching during cell differentiation. *Nat Biotechnol.* 2010 May;28(5):511–5.
443. Corces MR, Trevino AE, Hamilton EG, Greenside PG, Sinnott-Armstrong NA, Vesuna S, et al. An improved ATAC-seq protocol reduces background and enables interrogation of frozen tissues. *Nat Methods.* 2017 Oct;14(10):959–62.
444. Britton E, Rogerson C, Mehta S, Li Y, Li X, OCCAMS consortium, et al. Open chromatin profiling identifies AP1 as a transcriptional regulator in oesophageal adenocarcinoma. *PLoS Genet.* 2017 Aug;13(8):e1006879.
445. Zhang Y, Liu T, Meyer CA, Eeckhoutte J, Johnson DS, Bernstein BE, et al. Model-based analysis of ChIP-Seq (MACS). *Genome Biol.* 2008;9(9):R137.
446. Trapnell C, Roberts A, Goff L, Pertea G, Kim D, Kelley DR, et al. Differential gene and transcript expression analysis of RNA-seq experiments with TopHat and Cufflinks. *Nat Protoc.* 2012 Mar 1;7(3):562–78.
447. Mootha VK, Lindgren CM, Eriksson K-F, Subramanian A, Sihag S, Lehar J, et al. PGC-1 α -responsive genes involved in oxidative phosphorylation are coordinately downregulated in human diabetes. *Nat Genet.* 2003 Jul;34(3):267–73.
448. Subramanian A, Tamayo P, Mootha VK, Mukherjee S, Ebert BL, Gillette MA, et al. Gene set enrichment analysis: a knowledge-based approach for interpreting genome-wide expression profiles. *Proc Natl Acad Sci U S A.* 2005 Oct 25;102(43):15545–50.
449. Scala G, Serra A, Marwah VS, Saarimäki LA, Greco D. FunMappOne: a tool to hierarchically organize and visually navigate functional gene annotations in multiple experiments. *BMC Bioinformatics.* 2019 Feb 15;20(1):79.
450. García-Jiménez C, Goding CR. Starvation and Pseudo-Starvation as Drivers of Cancer Metastasis through Translation Reprogramming. *Cell Metab.* 2019 Feb 5;29(2):254–67.
451. Chaffer CL, Brueckmann I, Scheel C, Kaestli AJ, Wiggins PA, Rodrigues LO, et al. Normal and neoplastic nonstem cells can spontaneously convert to a stem-like state. *Proc Natl Acad Sci U S A.* 2011 May 10;108(19):7950–5.
452. Beerling E, Seinstra D, de Wit E, Kester L, van der Velden D, Maynard C, et al. Plasticity between Epithelial and Mesenchymal States Unlinks EMT from Metastasis-Enhancing Stem Cell Capacity. *Cell Rep.* 2016 Mar 15;14(10):2281–8.
453. Gupta PB, Fillmore CM, Jiang G, Shapira SD, Tao K, Kuperwasser C, et al. Stochastic state transitions give rise to phenotypic equilibrium in populations of cancer cells. *Cell.* 2011 Aug 19;146(4):633–44.

454. Huang RY-J, Wong MK, Tan TZ, Kuay KT, Ng AHC, Chung VY, et al. An EMT spectrum defines an anoikis-resistant and spheroidogenic intermediate mesenchymal state that is sensitive to e-cadherin restoration by a src-kinase inhibitor, saracatinib (AZD0530). *Cell Death Dis.* 2013 Nov 7;4:e915.
455. Quail DF, Joyce JA. Microenvironmental regulation of tumor progression and metastasis. *Nat Med.* 2013 Nov;19(11):1423–37.
456. Tsai JH, Donaher JL, Murphy DA, Chau S, Yang J. Spatiotemporal regulation of epithelial-mesenchymal transition is essential for squamous cell carcinoma metastasis. *Cancer Cell.* 2012 Dec 11;22(6):725–36.
457. Zhao Z, Zhu X, Cui K, Mancuso J, Federley R, Fischer K, et al. In Vivo Visualization and Characterization of Epithelial-Mesenchymal Transition in Breast Tumors. *Cancer Res.* 2016 Apr 15;76(8):2094–104.
458. Hoek KS, Goding CR. Cancer stem cells versus phenotype-switching in melanoma. *Pigment Cell Melanoma Res.* 2010 Dec;23(6):746–59.
459. Dankort D, Curley DP, Carlidge RA, Nelson B, Karnezis AN, Damsky WE, et al. Braf(V600E) cooperates with Pten loss to induce metastatic melanoma. *Nat Genet.* 2009 May;41(5):544–52.
460. Kreso A, O’Brien CA, van Galen P, Gan OI, Notta F, Brown AMK, et al. Variable clonal repopulation dynamics influence chemotherapy response in colorectal cancer. *Science.* 2013 Feb 1;339(6119):543–8.
461. Rosen JM, Jordan CT. The increasing complexity of the cancer stem cell paradigm. *Science.* 2009 Jun 26;324(5935):1670–3.
462. McDonald SAC, Graham TA, Lavery DL, Wright NA, Jansen M. The Barrett’s Gland in Phenotype Space. *Cell Mol Gastroenterol Hepatol.* 2015 Jan;1(1):41–54.
463. Jolly MK, Tripathi SC, Jia D, Mooney SM, Celiktas M, Hanash SM, et al. Stability of the hybrid epithelial/mesenchymal phenotype. *Oncotarget.* 2016 May 10;7(19):27067–84.
464. Zhang J, Tian X-J, Zhang H, Teng Y, Li R, Bai F, et al. TGF- β -induced epithelial-to-mesenchymal transition proceeds through stepwise activation of multiple feedback loops. *Sci Signal.* 2014 Sep 30;7(345):ra91.
465. Sato T, Stange DE, Ferrante M, Vries RGJ, Van Es JH, Van den Brink S, et al. Long-term expansion of epithelial organoids from human colon, adenoma, adenocarcinoma, and Barrett’s epithelium. *Gastroenterology.* 2011 Nov;141(5):1762–72.
466. Bus P, Siersema PD, van Baal JWPM. Cell culture models for studying the development of Barrett’s esophagus: a systematic review. *Cell Oncol Dordr.* 2012 Jun;35(3):149–61.
467. Li X, Francies HE, Secrier M, Perner J, Miremadi A, Galeano-Dalmau N, et al. Organoid cultures recapitulate esophageal adenocarcinoma heterogeneity providing a model for clonality studies and precision therapeutics. *Nat Commun.* 2018 Jul 30;9(1):2983.
468. Attwood SE, Harrison L-A, Preston SL, Jankowski JA. Esophageal adenocarcinoma in ‘mice and men’: back to basics! *Am J Gastroenterol.* 2008 Sep;103(9):2367–72.
469. Wang X, Ouyang H, Yamamoto Y, Kumar PA, Wei TS, Dagher R, et al. Residual embryonic cells as precursors of a Barrett’s-like metaplasia. *Cell.* 2011 Jun 24;145(7):1023–35.
470. Rokkas T, Sladen GE. Ambulatory esophageal pH recording in gastroesophageal reflux: relevance to the development of esophagitis. *Am J Gastroenterol.* 1988 Jun;83(6):629–32.
471. Neumann CS, Cooper BT. Oesophageal pH monitoring in Barrett’s oesophagus. *Gut.* 2003 Jan;52(1):153–4.

472. Savarino E, Zentilin P, Frazzoni M, Cuoco DL, Pohl D, Dulbecco P, et al. Characteristics of gastro-esophageal reflux episodes in Barrett's esophagus, erosive esophagitis and healthy volunteers. *Neurogastroenterol Motil Off J Eur Gastrointest Motil Soc.* 2010 Oct;22(10):1061-e280.
473. Wiener GJ, Morgan TM, Copper JB, Wu WC, Castell DO, Sinclair JW, et al. Ambulatory 24-hour esophageal pH monitoring. Reproducibility and variability of pH parameters. *Dig Dis Sci.* 1988 Sep;33(9):1127-33.
474. Ouatu-Lascar R, Fitzgerald RC, Triadafilopoulos G. Differentiation and proliferation in Barrett's esophagus and the effects of acid suppression. *Gastroenterology.* 1999 Aug;117(2):327-35.
475. Theisen J, Nehra D, Citron D, Johansson J, Hagen JA, Crookes PF, et al. Suppression of gastric acid secretion in patients with gastroesophageal reflux disease results in gastric bacterial overgrowth and deconjugation of bile acids. *J Gastrointest Surg Off J Soc Surg Aliment Tract.* 2000 Feb;4(1):50-4.
476. Iftikhar SY, Ledingham S, Steele RJ, Evans DF, Lendrum K, Atkinson M, et al. Bile reflux in columnar-lined Barrett's oesophagus. *Ann R Coll Surg Engl.* 1993 Nov;75(6):411-6.
477. Reid BJ, Sanchez CA, Blount PL, Levine DS. Barrett's esophagus: cell cycle abnormalities in advancing stages of neoplastic progression. *Gastroenterology.* 1993 Jul;105(1):119-29.
478. Tamagawa Y, Ishimura N, Uno G, Aimi M, Oshima N, Yuki T, et al. Bile acids induce Delta-like 1 expression via Cdx2-dependent pathway in the development of Barrett's esophagus. *Lab Investig J Tech Methods Pathol.* 2016 Mar;96(3):325-37.
479. Kestens C, Siersema PD, Offerhaus GJA, van Baal JWPM. BMP4 Signaling Is Able to Induce an Epithelial-Mesenchymal Transition-Like Phenotype in Barrett's Esophagus and Esophageal Adenocarcinoma through Induction of SNAIL2. *PloS One.* 2016;11(5):e0155754.
480. Zhang Q, Agoston AT, Pham TH, Zhang W, Zhang X, Huo X, et al. Acidic Bile Salts Induce Epithelial to Mesenchymal Transition via VEGF Signaling in Non-Neoplastic Barrett's Cells. *Gastroenterology.* 2019 Jan;156(1):130-144.e10.
481. Cardoso J, Mesquita M, Dias Pereira A, Bettencourt-Dias M, Chaves P, Pereira-Leal JB. CYR61 and TAZ Upregulation and Focal Epithelial to Mesenchymal Transition May Be Early Predictors of Barrett's Esophagus Malignant Progression. *PloS One.* 2016;11(9):e0161967.
482. Penfield JD, Anderson M, Lutzke L, Wang KK. The role of cellular senescence in the gastrointestinal mucosa. *Gut Liver.* 2013 May;7(3):270-7.
483. Kong J, Whelan KA, Laczko D, Dang B, Caro Monroig A, Soroush A, et al. Autophagy levels are elevated in barrett's esophagus and promote cell survival from acid and oxidative stress. *Mol Carcinog.* 2016 Nov;55(11):1526-41.
484. Bhutia SK, Mukhopadhyay S, Sinha N, Das DN, Panda PK, Patra SK, et al. Autophagy: cancer's friend or foe? *Adv Cancer Res.* 2013;118:61-95.
485. den Hoed CM, van Blankenstein M, Dees J, Kuipers EJ. The minimal incubation period from the onset of Barrett's oesophagus to symptomatic adenocarcinoma. *Br J Cancer.* 2011 Jul 12;105(2):200-5.
486. Maag JLV, Fisher OM, Levert-Mignon A, Kaczorowski DC, Thomas ML, Hussey DJ, et al. Novel Aberrations Uncovered in Barrett's Esophagus and Esophageal Adenocarcinoma Using Whole Transcriptome Sequencing. *Mol Cancer Res MCR.* 2017 Nov;15(11):1558-69.

487. Zhou Y, Zhou B, Pache L, Chang M, Khodabakhshi AH, Tanaseichuk O, et al. Metascape provides a biologist-oriented resource for the analysis of systems-level datasets. *Nat Commun.* 2019 Apr 3;10(1):1523.
488. Loh C-Y, Chai JY, Tang TF, Wong WF, Sethi G, Shanmugam MK, et al. The E-Cadherin and N-Cadherin Switch in Epithelial-to-Mesenchymal Transition: Signaling, Therapeutic Implications, and Challenges. *Cells.* 2019 Sep 20;8(10).
489. Han H, Cho J-W, Lee S, Yun A, Kim H, Bae D, et al. TRRUST v2: an expanded reference database of human and mouse transcriptional regulatory interactions. *Nucleic Acids Res.* 2018 Jan 4;46(D1):D380–6.
490. Rogerson C, Ogden S, Britton E, OCCAMS Consortium, Ang Y, Sharrocks AD. Repurposing of KLF5 activates a cell cycle signature during the progression from a precursor state to oesophageal adenocarcinoma. *eLife.* 2020 Sep 3;9.
491. Underwood TJ, Derouet MF, White MJ, Noble F, Moutasim KA, Smith E, et al. A comparison of primary oesophageal squamous epithelial cells with HET-1A in organotypic culture. *Biol Cell.* 2010 Dec;102(12):635–44.
492. Valcourt JR, Lemons JMS, Haley EM, Kojima M, Demuren OO, Collier HA. Staying alive: metabolic adaptations to quiescence. *Cell Cycle Georget Tex.* 2012 May 1;11(9):1680–96.
493. Ratjen F, Bell SC, Rowe SM, Goss CH, Quittner AL, Bush A. Cystic fibrosis. *Nat Rev Dis Primer.* 2015 May 14;1:15010.
494. Gharahkhani P, Fitzgerald RC, Vaughan TL, Palles C, Gockel I, Tomlinson I, et al. Genome-wide association studies in oesophageal adenocarcinoma and Barrett's oesophagus: a large-scale meta-analysis. *Lancet Oncol.* 2016 Oct;17(10):1363–73.
495. Meltzer SJ. Leaky transporters and sphincters in Barrett's oesophagus? *Lancet Oncol.* 2016 Oct;17(10):1336–7.
496. Woodley FW, Machado RS, Hayes D, Di Lorenzo C, Kaul A, Skaggs B, et al. Children with cystic fibrosis have prolonged chemical clearance of acid reflux compared to symptomatic children without cystic fibrosis. *Dig Dis Sci.* 2014 Mar;59(3):623–30.
497. Ghisa M, Marinelli C, Savarino V, Savarino E. Idiopathic pulmonary fibrosis and GERD: links and risks. *Ther Clin Risk Manag.* 2019;15:1081–93.
498. Fox CA, Sapinoso LM, Zhang H, Zhang W, McLeod HL, Petroni GR, et al. Altered Expression of TFF-1 and CES-2 in Barrett's Esophagus and Associated Adenocarcinomas. *Neoplasia N Y N.* 2005 Apr;7(4):407–16.
499. Zhang Z, Chen C, Fang Y, Li S, Wang X, Sun L, et al. Development of a prognostic signature for esophageal cancer based on nine immune related genes. *BMC Cancer.* 2021 Feb 4;21(1):113.
500. Babar M, Ryan AW, Anderson LA, Segurado R, Turner G, Murray LJ, et al. Genes of the interleukin-18 pathway are associated with susceptibility to Barrett's esophagus and esophageal adenocarcinoma. *Am J Gastroenterol.* 2012 Sep;107(9):1331–41.
501. O'Farrell NJ, Feighery R, Picardo SL, Lynam-Lennon N, Biniecka M, McGarrigle SA, et al. Changes in mitochondrial stability during the progression of the Barrett's esophagus disease sequence. *BMC Cancer.* 2016 Jul 19;16:497.
502. Cooper SC, Trudgill NJ. Subjects with prostate cancer are less likely to develop esophageal cancer: analysis of SEER 9 registries database. *Cancer Causes Control CCC.* 2012 Jun;23(6):819–25.
503. Cooper SC, Croft S, Day R, Thomson CS, Trudgill NJ. Patients with prostate cancer are less likely to develop oesophageal adenocarcinoma: could androgens have a role in the aetiology of oesophageal adenocarcinoma? *Cancer Causes Control CCC.* 2009 Oct;20(8):1363–8.

504. Palethorpe HM, Drew PA, Smith E. Androgen Signaling in Esophageal Adenocarcinoma Cell Lines In Vitro. *Dig Dis Sci*. 2017 Dec;62(12):3402–14.
505. Debruyne PR, Witek M, Gong L, Birbe R, Chervoneva I, Jin T, et al. Bile acids induce ectopic expression of intestinal guanylyl cyclase C Through nuclear factor-kappaB and Cdx2 in human esophageal cells. *Gastroenterology*. 2006 Apr;130(4):1191–206.
506. Dibb M, Han N, Choudhury J, Hayes S, Valentine H, West C, et al. The FOXM1-PLK1 axis is commonly upregulated in oesophageal adenocarcinoma. *Br J Cancer*. 2012 Nov 6;107(10):1766–75.
507. Levine DM, Ek WE, Zhang R, Liu X, Onstad L, Sather C, et al. A genome-wide association study identifies new susceptibility loci for esophageal adenocarcinoma and Barrett's esophagus. *Nat Genet*. 2013 Dec;45(12):1487–93.
508. Su Z, Gay LJ, Strange A, Palles C, Band G, Whiteman DC, et al. Common variants at the MHC locus and at chromosome 16q24.1 predispose to Barrett's esophagus. *Nat Genet*. 2012 Oct;44(10):1131–6.
509. Tavares ALP, Brown JA, Ulrich EC, Dvorak K, Runyan RB. RUNX2-I is an early regulator of epithelial-mesenchymal cell transition in the chick embryo. *Dev Dyn Off Publ Am Assoc Anat*. 2018 Mar;247(3):542–54.
510. Lv J, Guo L, Wang J-H, Yan Y-Z, Zhang J, Wang Y-Y, et al. Biomarker identification and trans-regulatory network analyses in esophageal adenocarcinoma and Barrett's esophagus. *World J Gastroenterol*. 2019 Jan 14;25(2):233–44.
511. Wu L, Zhao JC, Kim J, Jin H-J, Wang C-Y, Yu J. ERG is a critical regulator of Wnt/LEF1 signaling in prostate cancer. *Cancer Res*. 2013 Oct 1;73(19):6068–79.
512. Gregorieff A, Stange DE, Kujala P, Begthel H, van den Born M, Korving J, et al. The ets-domain transcription factor Spdef promotes maturation of goblet and paneth cells in the intestinal epithelium. *Gastroenterology*. 2009 Oct;137(4):1333-1345.e1-3.
513. Jones DL, Meridew JA, Link PA, Ducharme MT, Lydon KL, Choi KM, et al. ZNF416 is a pivotal transcriptional regulator of fibroblast mechanoactivation. *J Cell Biol*. 2021 May 3;220(5).
514. Duggan SP, Kirca M, Behan FM, Kelleher DP. S1635 Loss of Bile Acid Responsive Gene Retinoic Acid Receptor-Related Orphan Receptor A (Rora) in Barrett's Metaplasia, Implications for Refluxed Induced Signaling in Esophageal Cells. *Gastroenterology*. 2010 May;138(5):S-243.
515. Soslow RA, Petersen CG, Remotti H, Altorki N. Acidic fibroblast growth factor is expressed sequentially in the progression from Barrett's esophagus to esophageal adenocarcinoma. *Dis Esophagus Off J Int Soc Dis Esophagus*. 2001;14(1):23–7.
516. Soslow RA, Nabeya Y, Ying L, Blundell M, Altorki NK. Acidic fibroblast growth factor is progressively increased in the development of oesophageal glandular dysplasia and adenocarcinoma. *Histopathology*. 1999 Jul;35(1):31–7.
517. Saxena R, Klochkova A, Murray MG, Kabir MF, Samad S, Beccari T, et al. Roles for Autophagy in Esophageal Carcinogenesis: Implications for Improving Patient Outcomes. *Cancers*. 11(11):1697.
518. Rask K, Thörn M, Pontén F, Kraaz W, Sundfeldt K, Hedin L, et al. Increased expression of the transcription factors CCAAT-enhancer binding protein-beta (C/EBBbeta) and C/EBzeta (CHOP) correlate with invasiveness of human colorectal cancer. *Int J Cancer*. 2000 May 1;86(3):337–43.
519. Manning G, Whyte DB, Martinez R, Hunter T, Sudarsanam S. The protein kinase complement of the human genome. *Science*. 2002 Dec 6;298(5600):1912–34.
520. Cooper JA, Sefton BM, Hunter T. Detection and quantification of phosphotyrosine in proteins. *Methods Enzymol*. 1983;99:387–402.

521. Cohen P. The regulation of protein function by multisite phosphorylation--a 25 year update. *Trends Biochem Sci.* 2000 Dec;25(12):596–601.
522. Sharma K, D'Souza RCJ, Tyanova S, Schaab C, Wiśniewski JR, Cox J, et al. Ultradeep human phosphoproteome reveals a distinct regulatory nature of Tyr and Ser/Thr-based signaling. *Cell Rep.* 2014 Sep 11;8(5):1583–94.
523. Sacco F, Perfetto L, Castagnoli L, Cesareni G. The human phosphatase interactome: An intricate family portrait. *FEBS Lett.* 2012 Aug 14;586(17):2732–9.
524. Chen MJ, Dixon JE, Manning G. Genomics and evolution of protein phosphatases. *Sci Signal.* 2017 Apr 11;10(474).
525. Lemmon MA, Schlessinger J. Cell signaling by receptor tyrosine kinases. *Cell.* 2010 Jun 25;141(7):1117–34.
526. Zhang J, Yang PL, Gray NS. Targeting cancer with small molecule kinase inhibitors. *Nat Rev Cancer.* 2009 Jan;9(1):28–39.
527. Cantwell-Dorris ER, O'Leary JJ, Sheils OM. BRAFV600E: implications for carcinogenesis and molecular therapy. *Mol Cancer Ther.* 2011 Mar;10(3):385–94.
528. Kuchenov D, Ziebell F, Salopiata F, Citir M, Klingmueller U, Huber W, et al. A combinatorial extracellular code tunes the intracellular signaling network activity to distinct cellular responses. *bioRxiv.* 2018 Jun 14;346957.
529. Mace K, Krakowiak J, El-Samad H, Pincus D. Multi-kinase control of environmental stress responsive transcription. *PLoS One.* 2020;15(3):e0230246.
530. Tan H-Y, Wang N, Lam W, Guo W, Feng Y, Cheng Y-C. Targeting tumour microenvironment by tyrosine kinase inhibitor. *Mol Cancer.* 2018 Feb 19;17(1):43.
531. Wilson LJ, Linley A, Hammond DE, Hood FE, Coulson JM, MacEwan DJ, et al. New Perspectives, Opportunities, and Challenges in Exploring the Human Protein Kinome. *Cancer Res.* 2018 Jan 1;78(1):15–29.
532. Timsah Z, Ahmed Z, Ivan C, Berrout J, Gagea M, Zhou Y, et al. Grb2 depletion under non-stimulated conditions inhibits PTEN, promotes Akt-induced tumor formation and contributes to poor prognosis in ovarian cancer. *Oncogene.* 2016 Apr 28;35(17):2186–96.
533. Ahmed Z, Timsah Z, Suen KM, Cook NP, Lee GR, Lin C-C, et al. Grb2 monomer-dimer equilibrium determines normal versus oncogenic function. *Nat Commun.* 2015 Jun 24;6:7354.
534. Cheng P, Li J-S, Gong J, Zhang L-F, Chen R-Z. Effects of refluxate pH values on duodenogastroesophageal reflux-induced esophageal adenocarcinoma. *World J Gastroenterol.* 2011 Jul 7;17(25):3060–5.
535. Johnson SA, Hunter T. Kinomics: methods for deciphering the kinome. *Nat Methods.* 2005 Jan;2(1):17–25.
536. Wang C, Xu H, Lin S, Deng W, Zhou J, Zhang Y, et al. GPS 5.0: An Update on the Prediction of Kinase-specific Phosphorylation Sites in Proteins. *Genomics Proteomics Bioinformatics.* 2020 Feb;18(1):72–80.
537. Xue Y, Liu Z, Cao J, Ma Q, Gao X, Wang Q, et al. GPS 2.1: enhanced prediction of kinase-specific phosphorylation sites with an algorithm of motif length selection. *Protein Eng Des Sel PEDS.* 2011 Mar;24(3):255–60.
538. Azevedo H, Moreira-Filho CA. Topological robustness analysis of protein interaction networks reveals key targets for overcoming chemotherapy resistance in glioma. *Sci Rep.* 2015 Nov 19;5:16830.
539. Chou A, Fraser T, Ahadi M, Fuchs T, Sioson L, Clarkson A, et al. NTRK gene rearrangements are highly enriched in MLH1/PMS2 deficient, BRAF wild-type colorectal

- carcinomas-a study of 4569 cases. *Mod Pathol Off J U S Can Acad Pathol Inc.* 2020 May;33(5):924–32.
540. Kim JH, Hong JH, Choi Y-L, Lee JA, Seo M, Lee M-S, et al. NTRK oncogenic fusions are exclusively associated with the serrated neoplasia pathway in the colorectum and begin to occur in sessile serrated lesions. *medRxiv.* 2021 Mar 30;2021.03.29.21253871.
541. Arnold A, Daum S, von Winterfeld M, Berg E, Hummel M, Horst D, et al. Analysis of NTRK expression in gastric and esophageal adenocarcinoma (AGE) with pan-TRK immunohistochemistry. *Pathol Res Pract.* 2019 Nov;215(11):152662.
542. Zhang Q, Yu C, Peng S, Xu H, Wright E, Zhang X, et al. Autocrine VEGF signaling promotes proliferation of neoplastic Barrett's epithelial cells through a PLC-dependent pathway. *Gastroenterology.* 2014 Feb;146(2):461-472.e6.
543. Bomalaski JS, Hirata F, Clark MA. Aspirin inhibits phospholipase C. *Biochem Biophys Res Commun.* 1986 Aug 29;139(1):115–21.
544. Rothwell PM, Fowkes FGR, Belch JFF, Ogawa H, Warlow CP, Meade TW. Effect of daily aspirin on long-term risk of death due to cancer: analysis of individual patient data from randomised trials. *Lancet Lond Engl.* 2011 Jan 1;377(9759):31–41.
545. Avidan B, Sonnenberg A, Schnell TG, Sontag SJ. Acid reflux is a poor predictor for severity of erosive reflux esophagitis. *Dig Dis Sci.* 2002 Nov;47(11):2565–73.
546. Kahrilas PJ. Management of the Acid Pocket. *Gastroenterol Hepatol.* 2014 Sep;10(9):587–9.
547. Lin C-C, Melo FA, Ghosh R, Suen KM, Stagg LJ, Kirkpatrick J, et al. Inhibition of basal FGF receptor signaling by dimeric Grb2. *Cell.* 2012 Jun 22;149(7):1514–24.
548. Du Z, Lovly CM. Mechanisms of receptor tyrosine kinase activation in cancer. *Mol Cancer.* 2018 Feb 19;17(1):58.
549. Lazzara MJ, Lauffenburger DA. Quantitative modeling perspectives on the ErbB system of cell regulatory processes. *Exp Cell Res.* 2009 Feb 15;315(4):717–25.
550. Cronin J, McAdam E, Danikas A, Tselepis C, Griffiths P, Baxter J, et al. Epidermal growth factor receptor (EGFR) is overexpressed in high-grade dysplasia and adenocarcinoma of the esophagus and may represent a biomarker of histological progression in Barrett's esophagus (BE). *Am J Gastroenterol.* 2011 Jan;106(1):46–56.
551. Ecker BL, Taylor L, Zhang PJ, Furth EE, Ginsberg GG, McMillan MT, et al. HER3 Expression Is a Marker of Tumor Progression in Premalignant Lesions of the Gastroesophageal Junction. *PLoS One.* 2016;11(8):e0161781.
552. Li Y, Wo JM, Ray MB, Jones W, Su RR, Ellis S, et al. Cyclooxygenase-2 and epithelial growth factor receptor up-regulation during progression of Barrett's esophagus to adenocarcinoma. *World J Gastroenterol.* 2006 Feb 14;12(6):928–34.
553. Almhanna K, Rosa M, Henderson-Jackson E, Jiang K, Shamekh R, Sayegh Z, et al. Her-2 Expression in Gastroesophageal Intestinal Metaplasia, Dysplasia, and Adenocarcinoma. *Appl Immunohistochem Mol Morphol AIMM.* 2016 Oct;24(9):633–8.
554. Mokrowiecka A, Wierzchniewska-Lawska A, Smolarz B, Romanowicz-Makowska H, Lochowski M, Kozak J, et al. Amplification of Her-2/neu oncogene in GERD - Barrett's metaplasia – dysplasia - adenocarcinoma sequence. *Hepatogastroenterology.* 2013 Aug;60(125):1063–6.
555. Yoon HH, Shi Q, Sukov WR, Wiktor AE, Khan M, Sattler CA, et al. Association of HER2/ErbB2 expression and gene amplification with pathologic features and prognosis in esophageal adenocarcinomas. *Clin Cancer Res Off J Am Assoc Cancer Res.* 2012 Jan 15;18(2):546–54.

556. De Bruijn K, Biermann K, Shapiro J, Dogan F, Spaander M, Janssen J, et al. Absence or low IGF-1R-expression in esophageal adenocarcinoma is associated with tumor invasiveness and radicality of surgical resection. *J Surg Oncol*. 2015 Jun;111(8):1047–53.
557. Kalinina T, Bockhorn M, Kaifi JT, Thielges S, Güngör C, Effenberger KE, et al. Insulin-like growth factor-1 receptor as a novel prognostic marker and its implication as a cotarget in the treatment of human adenocarcinoma of the esophagus. *Int J Cancer*. 2010 Oct 15;127(8):1931–40.
558. Nagaraja V, Eslick GD. Forthcoming prognostic markers for esophageal cancer: a systematic review and meta-analysis. *J Gastrointest Oncol*. 2014 Feb;5(1):67–76.
559. Irvani S, Zhang HQ, Yuan ZQ, Cheng JQ, Karl RC, Jove R, et al. Modification of insulin-like growth factor 1 receptor, c-Src, and Bcl-XL protein expression during the progression of Barrett's neoplasia. *Hum Pathol*. 2003 Oct;34(10):975–82.
560. Anderson MR, Harrison R, Atherfold PA, Campbell MJ, Darnton SJ, Obszynska J, et al. Met receptor signaling: a key effector in esophageal adenocarcinoma. *Clin Cancer Res Off J Am Assoc Cancer Res*. 2006 Oct 15;12(20 Pt 1):5936–43.
561. Herrera LJ, El-Hefnawy T, Queiroz de Oliveira PE, Raja S, Finkelstein S, Gooding W, et al. The HGF receptor c-Met is overexpressed in esophageal adenocarcinoma. *Neoplasia N Y N*. 2005 Jan;7(1):75–84.
562. Hong J, Abid F, Phillips S, Salaria SN, Revetta FL, Peng D, et al. Co-overexpression of AXL and c-ABL predicts a poor prognosis in esophageal adenocarcinoma and promotes cancer cell survival. *J Cancer*. 2020;11(20):5867–79.
563. Ooi A, Zen Y, Ninomiya I, Tajiri R, Suzuki S, Kobayashi H, et al. Gene amplification of ERBB2 and EGFR in adenocarcinoma in situ and intramucosal adenocarcinoma of Barrett's esophagus. *Pathol Int*. 2010 Jun;60(6):466–71.
564. Rygiel AM, Milano F, Ten Kate FJ, Schaap A, Wang KK, Peppelenbosch MP, et al. Gains and amplifications of c-myc, EGFR, and 20.q13 loci in the no dysplasia-dysplasia-adenocarcinoma sequence of Barrett's esophagus. *Cancer Epidemiol Biomark Prev Publ Am Assoc Cancer Res Cosponsored Am Soc Prev Oncol*. 2008 Jun;17(6):1380–5.
565. Rossi E, Villanacci V, Danesino C, Donato F, Nascimbeni R, Bassotti G. Epidermal growth factor receptor overexpression/amplification in adenocarcinomas arising in the gastrointestinal tract. *Rev Espanola Enfermedades Dig Organo Of Soc Espanola Patol Dig*. 2011 Dec;103(12):632–9.
566. Goldman A, Chen HDR, Roesly HB, Hill KA, Tome ME, Dvorak B, et al. Characterization of squamous esophageal cells resistant to bile acids at acidic pH: implication for Barrett's esophagus pathogenesis. *Am J Physiol Gastrointest Liver Physiol*. 2011 Feb;300(2):G292–302.
567. Nasr AO, Dillon MF, Conlon S, Downey P, Chen G, Ireland A, et al. Acid suppression increases rates of Barrett's esophagus and esophageal injury in the presence of duodenal reflux. *Surgery*. 2012 Mar;151(3):382–90.
568. Halpern AL, Kohtz PD, White AM, Houk AK, Rehring JF, Hanson L, et al. Secretory Phospholipase A2 Ila Mediates Expression of Growth Factor Receptors in Esophageal Adenocarcinoma. *Dig Dis Sci*. 2020 Apr 10;
569. Demicco EG, Farris AB, Baba Y, Agbor-Etang B, Bergethon K, Mandal R, et al. The dichotomy in carcinogenesis of the distal esophagus and esophagogastric junction: intestinal-type vs cardiac-type mucosa-associated adenocarcinoma. *Mod Pathol Off J U S Can Acad Pathol Inc*. 2011 Sep;24(9):1177–90.
570. Rossi E, Grisanti S, Villanacci V, Della Casa D, Cengia P, Missale G, et al. HER-2 overexpression/amplification in Barrett's oesophagus predicts early transition from

- dysplasia to adenocarcinoma: a clinico-pathologic study. *J Cell Mol Med.* 2009 Sep;13(9B):3826–33.
571. Fassan M, Mastracci L, Grillo F, Zagonel V, Bruno S, Battaglia G, et al. Early HER2 dysregulation in gastric and oesophageal carcinogenesis. *Histopathology.* 2012 Nov;61(5):769–76.
572. Hu Y, Bandla S, Godfrey TE, Tan D, Luketich JD, Pennathur A, et al. HER2 amplification, overexpression and score criteria in esophageal adenocarcinoma. *Mod Pathol Off J U S Can Acad Pathol Inc.* 2011 Jul;24(7):899–907.
573. Schoppmann SF, Jesch B, Friedrich J, Wrba F, Schultheis A, Pluschnig U, et al. Expression of Her-2 in carcinomas of the esophagus. *Am J Surg Pathol.* 2010 Dec;34(12):1868–73.
574. Geddert H, Zeriuoh M, Wolter M, Heise JW, Gabbert HE, Sarbia M. Gene amplification and protein overexpression of c-erb-b2 in Barrett carcinoma and its precursor lesions. *Am J Clin Pathol.* 2002 Jul;118(1):60–6.
575. al-Kasspoles M, Moore JH, Orringer MB, Beer DG. Amplification and overexpression of the EGFR and erbB-2 genes in human esophageal adenocarcinomas. *Int J Cancer.* 1993 May 8;54(2):213–9.
576. Walch A, Bink K, Gais P, Stangl S, Hutzler P, Aubele M, et al. Evaluation of c-erbB-2 overexpression and Her-2/neu gene copy number heterogeneity in Barrett's adenocarcinoma. *Anal Cell Pathol J Eur Soc Anal Cell Pathol.* 2000;20(1):25–32.
577. Yoshida K, Yasui W, Ito H, Tahara E. Growth factors in progression of human esophageal and gastric carcinomas. *Exp Pathol.* 1990;40(4):291–300.
578. Allan EAG, Miller R, Going JJ. Aneusomy detected by fluorescence in-situ hybridization has high positive predictive value for Barrett's dysplasia. *Histopathology.* 2015 Oct;67(4):451–6.
579. Rossi E, Villanacci V, Bassotti G, Donato F, Festa A, Cengia G, et al. TOPOIIalpha and HER-2/neu overexpression/amplification in Barrett's oesophagus, dysplasia and adenocarcinoma. *Histopathology.* 2010 Jul;57(1):81–9.
580. Nagaraja V, Shaw N, Morey AL, Cox MR, Eslick GD. HER2 expression in oesophageal carcinoma and Barrett's oesophagus associated adenocarcinoma: An Australian study. *Eur J Surg Oncol J Eur Soc Surg Oncol Br Assoc Surg Oncol.* 2016 Jan;42(1):140–8.
581. Miller CT, Moy JR, Lin L, Schipper M, Normolle D, Brenner DE, et al. Gene amplification in esophageal adenocarcinomas and Barrett's with high-grade dysplasia. *Clin Cancer Res Off J Am Assoc Cancer Res.* 2003 Oct 15;9(13):4819–25.
582. Reichelt U, Duesedau P, Tsourlakis MC, Quaas A, Link BC, Schurr PG, et al. Frequent homogeneous HER-2 amplification in primary and metastatic adenocarcinoma of the esophagus. *Mod Pathol Off J U S Can Acad Pathol Inc.* 2007 Jan;20(1):120–9.
583. Dahlberg PS, Jacobson BA, Dahal G, Fink JM, Kratzke RA, Maddaus MA, et al. ERBB2 amplifications in esophageal adenocarcinoma. *Ann Thorac Surg.* 2004 Nov;78(5):1790–800.
584. Arcidiacono D, Dedja A, Giacometti C, Fassan M, Nucci D, Francia S, et al. Hyperinsulinemia Promotes Esophageal Cancer Development in a Surgically-Induced Duodeno-Esophageal Reflux Murine Model. *Int J Mol Sci.* 2018 Apr 14;19(4).
585. Nishigaki H, Wada K, Tatsuguchi A, Sueoka N, Futagami S, Gudis K, et al. ErbB2 without erbB3 expression in metaplastic columnar epithelium of Barrett's esophagus. *Digestion.* 2004;70(2):95–102.
586. Fichter CD, Timme S, Braun JA, Gudernatsch V, Schöpflin A, Bogatyreva L, et al. EGFR, HER2 and HER3 dimerization patterns guide targeted inhibition in two histotypes of esophageal cancer. *Int J Cancer.* 2014 Oct 1;135(7):1517–30.

587. Albrecht B, Hausmann M, Zitzelsberger H, Stein H, Siewert JR, Hopt U, et al. Array-based comparative genomic hybridization for the detection of DNA sequence copy number changes in Barrett's adenocarcinoma. *J Pathol.* 2004 Jul;203(3):780–8.
588. Donohoe CL, Doyle SL, McGarrigle S, Cathcart MC, Daly E, O'Grady A, et al. Role of the insulin-like growth factor 1 axis and visceral adiposity in oesophageal adenocarcinoma. *Br J Surg.* 2012 Mar;99(3):387–96.
589. Su W, Wang L, Niu F, Zou L, Guo C, Wang Z, et al. LINC00857 knockdown inhibits cell proliferation and induces apoptosis via involving STAT3 and MET oncogenic proteins in esophageal adenocarcinoma. *Aging.* 2019 May 13;11(9):2812–21.
590. Betts G, Valentine H, Pritchard S, Swindell R, Williams V, Morgan S, et al. FGFR2, HER2 and cMet in gastric adenocarcinoma: detection, prognostic significance and assessment of downstream pathway activation. *Virchows Arch Int J Pathol.* 2014 Feb;464(2):145–56.
591. Hasina R, Mollberg N, Kawada I, Mutreja K, Kanade G, Yala S, et al. Critical role for the receptor tyrosine kinase EPHB4 in esophageal cancers. *Cancer Res.* 2013 Jan 1;73(1):184–94.
592. Liersch-Löhn B, Slavova N, Buhr HJ, Bennani-Baiti IM. Differential protein expression and oncogenic gene network link tyrosine kinase ephrin B4 receptor to aggressive gastric and gastroesophageal junction cancers. *Int J Cancer.* 2016 Mar 1;138(5):1220–31.
593. Goscinski MA, Larsen SG, Giercksky K-E, Nesland JM, Suo Z. PDGFR- α and CD117 Expression Pattern in Esophageal Carcinomas. *Anticancer Res.* 2015 Jul;35(7):3793–9.
594. Veeranki OL, Tong Z, Dokey R, Mejia A, Zhang J, Qiao Y, et al. Targeting cyclin-dependent kinase 9 by a novel inhibitor enhances radiosensitization and identifies Axl as a novel downstream target in esophageal adenocarcinoma. *Oncotarget.* 2019 Jul 23;10(45):4703–18.
595. Pühringer-Oppermann FA, Stein HJ, Sarbia M. Lack of EGFR gene mutations in exons 19 and 21 in esophageal (Barrett's) adenocarcinomas. *Dis Esophagus Off J Int Soc Dis Esophagus.* 2007;20(1):9–11.
596. Kwak EL, Jankowski J, Thayer SP, Lauwers GY, Brannigan BW, Harris PL, et al. Epidermal growth factor receptor kinase domain mutations in esophageal and pancreatic adenocarcinomas. *Clin Cancer Res Off J Am Assoc Cancer Res.* 2006 Jul 15;12(14 Pt 1):4283–7.
597. Jankowski J, Coghil G, Tregaskis B, Hopwood D, Wormsley KG. Epidermal growth factor in the oesophagus. *Gut.* 1992 Nov;33(11):1448–53.
598. Jankowski J, McMenemin R, Hopwood D, Penston J, Wormsley KG. Abnormal expression of growth regulatory factors in Barrett's oesophagus. *Clin Sci Lond Engl* 1979. 1991 Nov;81(5):663–8.
599. Ghatak S, Reveiller M, Toia L, Ivanov A, Godfrey TE, Peters JH. Bile acid at low pH reduces squamous differentiation and activates EGFR signaling in esophageal squamous cells in 3-D culture. *J Gastrointest Surg Off J Soc Surg Aliment Tract.* 2013 Oct;17(10):1723–31.
600. Kusaka G, Uno K, Iijima K, Endo H, Asano N, Koike T, et al. The role of nitric oxide in the induction of caudal-type homeobox 2 through epidermal growth factor receptor in the development of Barrett's esophagus. *Scand J Gastroenterol.* 2012 Oct;47(10):1148–58.
601. Zhou Z, Lu H, Zhu S, Goma A, Chen Z, Yan J, et al. Activation of EGFR-DNA-PKcs pathway by IGF2BP2 protects esophageal adenocarcinoma cells from acidic bile salts-induced DNA damage. *J Exp Clin Cancer Res CR.* 2019 Jan 9;38(1):13.

602. MacDonald K, Porter GA, Guernsey DL, Zhao R, Casson AG. A polymorphic variant of the insulin-like growth factor type I receptor gene modifies risk of obesity for esophageal adenocarcinoma. *Cancer Epidemiol.* 2009 Jul;33(1):37–40.
603. McElholm AR, McKnight A-J, Patterson CC, Johnston BT, Hardie LJ, Murray LJ, et al. A population-based study of IGF axis polymorphisms and the esophageal inflammation, metaplasia, adenocarcinoma sequence. *Gastroenterology.* 2010 Jul;139(1):204–212. e3.
604. Siahpush SH, Vaughan TL, Lampe JN, Freeman R, Lewis S, Odze RD, et al. Longitudinal study of insulin-like growth factor, insulin-like growth factor binding protein-3, and their polymorphisms: risk of neoplastic progression in Barrett's esophagus. *Cancer Epidemiol Biomark Prev Publ Am Assoc Cancer Res Cosponsored Am Soc Prev Oncol.* 2007 Nov;16(11):2387–95.
605. Greer KB, Thompson CL, Brenner L, Bednarchik B, Dawson D, Willis J, et al. Association of insulin and insulin-like growth factors with Barrett's oesophagus. *Gut.* 2012 May;61(5):665–72.
606. Di Martino E, Wild CP, Rotimi O, Darnton JS, Olliver RJ, Hardie LJ. IGFBP-3 and IGFBP-10 (CYR61) up-regulation during the development of Barrett's oesophagus and associated oesophageal adenocarcinoma: potential biomarkers of disease risk. *Biomark Biochem Indic Expo Response Susceptibility Chem.* 2006 Dec;11(6):547–61.
607. Doyle SL, Donohoe CL, Finn SP, Howard JM, Lithander FE, Reynolds JV, et al. IGF-1 and its receptor in esophageal cancer: association with adenocarcinoma and visceral obesity. *Am J Gastroenterol.* 2012 Feb;107(2):196–204.
608. Schoppmann SF, Jesch B, Friedrich J, Jomrich G, Maroske F, Birner P. Phosphorylation of signal transducer and activator of transcription 3 (STAT3) correlates with Her-2 status, carbonic anhydrase 9 expression and prognosis in esophageal cancer. *Clin Exp Metastasis.* 2012 Aug;29(6):615–24.
609. Yu M, Maden SK, Stachler M, Kaz AM, Ayers J, Guo Y, et al. Subtypes of Barrett's oesophagus and oesophageal adenocarcinoma based on genome-wide methylation analysis. *Gut.* 2019 Mar;68(3):389–99.
610. Vallböhmer D, Peters JH, Kuramochi H, Oh D, Yang D, Shimizu D, et al. Molecular determinants in targeted therapy for esophageal adenocarcinoma. *Arch Surg Chic Ill 1960.* 2006 May;141(5):476–81; discussion 481–482.
611. Lord RVN, Park JM, Wickramasinghe K, DeMeester SR, Oberg S, Salonga D, et al. Vascular endothelial growth factor and basic fibroblast growth factor expression in esophageal adenocarcinoma and Barrett esophagus. *J Thorac Cardiovasc Surg.* 2003 Feb;125(2):246–53.
612. Dilworth MP, Nieto T, Stockton JD, Whalley CM, Tee L, James JD, et al. Whole Genome Methylation Analysis of Nondysplastic Barrett Esophagus that Progresses to Invasive Cancer. *Ann Surg.* 2019 Mar;269(3):479–85.
613. Lin L, Bass AJ, Lockwood WW, Wang Z, Silvers AL, Thomas DG, et al. Activation of GATA binding protein 6 (GATA6) sustains oncogenic lineage-survival in esophageal adenocarcinoma. *Proc Natl Acad Sci U S A.* 2012 Mar 13;109(11):4251–6.
614. Miller CT, Lin L, Casper AM, Lim J, Thomas DG, Orringer MB, et al. Genomic amplification of MET with boundaries within fragile site FRA7G and upregulation of MET pathways in esophageal adenocarcinoma. *Oncogene.* 2006 Jan 19;25(3):409–18.
615. Maacha S, Hong J, von Lersner A, Zijlstra A, Belkhiri A. AXL Mediates Esophageal Adenocarcinoma Cell Invasion through Regulation of Extracellular Acidification and Lysosome Trafficking. *Neoplasia N Y N.* 2018 Oct;20(10):1008–22.

616. Hong J, Maacha S, Belkhiri A. Transcriptional upregulation of c-MYC by AXL confers epirubicin resistance in esophageal adenocarcinoma. *Mol Oncol.* 2018 Dec;12(12):2191–208.
617. Hong J, Belkhiri A. AXL mediates TRAIL resistance in esophageal adenocarcinoma. *Neoplasia N Y N.* 2013 Mar;15(3):296–304.
618. Hector A, Montgomery EA, Karikari C, Canto M, Dunbar KB, Wang JS, et al. The Axl receptor tyrosine kinase is an adverse prognostic factor and a therapeutic target in esophageal adenocarcinoma. *Cancer Biol Ther.* 2010 Nov 15;10(10):1009–18.
619. Menke V, Pot RGJ, Moons LMG, van Zoest KPM, Hansen B, van Dekken H, et al. Functional single-nucleotide polymorphism of epidermal growth factor is associated with the development of Barrett's esophagus and esophageal adenocarcinoma. *J Hum Genet.* 2012 Jan;57(1):26–32.
620. Lanuti M, Liu G, Goodwin JM, Zhai R, Fuchs BC, Asomaning K, et al. A functional epidermal growth factor (EGF) polymorphism, EGF serum levels, and esophageal adenocarcinoma risk and outcome. *Clin Cancer Res Off J Am Assoc Cancer Res.* 2008 May 15;14(10):3216–22.
621. Ohashi S, Natsuzaka M, Wong GS, Michaylira CZ, Grugan KD, Stairs DB, et al. Epidermal growth factor receptor and mutant p53 expand an esophageal cellular subpopulation capable of epithelial-to-mesenchymal transition through ZEB transcription factors. *Cancer Res.* 2010 May 15;70(10):4174–84.
622. Marx AH, Zielinski M, Kowitz C-M, Dancau A-M, Thielges S, Simon R, et al. Homogeneous EGFR amplification defines a subset of aggressive Barrett's adenocarcinomas with poor prognosis. *Histopathology.* 2010 Sep;57(3):418–26.
623. Rauser S, Weis R, Braselmann H, Feith M, Stein HJ, Langer R, et al. Significance of HER2 low-level copy gain in Barrett's cancer: implications for fluorescence in situ hybridization testing in tissues. *Clin Cancer Res Off J Am Assoc Cancer Res.* 2007 Sep 1;13(17):5115–23.
624. Tanaka T, Fujimura A, Ichimura K, Yanai H, Sato Y, Takata K, et al. Clinicopathological characteristics of human epidermal growth factor receptor 2-positive Barrett's adenocarcinoma. *World J Gastroenterol.* 2012 Nov 21;18(43):6263–8.
625. Bang Y-J, Van Cutsem E, Feyereislova A, Chung HC, Shen L, Sawaki A, et al. Trastuzumab in combination with chemotherapy versus chemotherapy alone for treatment of HER2-positive advanced gastric or gastro-oesophageal junction cancer (ToGA): a phase 3, open-label, randomised controlled trial. *Lancet Lond Engl.* 2010 Aug 28;376(9742):687–97.
626. Yoshino M, Ishiwata T, Watanabe M, Matsunobu T, Komine O, Ono Y, et al. Expression and roles of keratinocyte growth factor and its receptor in esophageal cancer cells. *Int J Oncol.* 2007 Oct;31(4):721–8.
627. Klempner SJ, Madison R, Pujara V, Ross JS, Miller VA, Ali SM, et al. FGFR2-Altered Gastroesophageal Adenocarcinomas Are an Uncommon Clinicopathologic Entity with a Distinct Genomic Landscape. *The Oncologist.* 2019 Nov;24(11):1462–8.
628. Dighe SG, Chen J, Yan L, He Q, Gharahkhani P, Onstad L, et al. Germline variation in the insulin-like growth factor pathway and risk of Barrett's esophagus and esophageal adenocarcinoma. *Carcinogenesis.* 2020 Dec 10;
629. Catenacci DVT, Ang A, Liao W-L, Shen J, O'Day E, Loberg RD, et al. MET tyrosine kinase receptor expression and amplification as prognostic biomarkers of survival in gastroesophageal adenocarcinoma. *Cancer.* 2017 May 15;123(6):1061–70.

630. Ren JL, Wu HF, Wang WJ, Hu GM, Gu B, Zhang M, et al. C-Met as a potential novel prognostic marker in squamous cell carcinoma and adenocarcinoma of esophagus: evidence from a meta-analysis. *Panminerva Med.* 2017 Mar;59(1):97–106.
631. Tuynman JB, Lagarde SM, Ten Kate FJW, Richel DJ, van Lanschot JJB. Met expression is an independent prognostic risk factor in patients with oesophageal adenocarcinoma. *Br J Cancer.* 2008 Mar 25;98(6):1102–8.
632. Hassan MS, Williams F, Awasthi N, Schwarz MA, Schwarz RE, Li J, et al. Combination effect of lapatinib with foretinib in HER2 and MET co-activated experimental esophageal adenocarcinoma. *Sci Rep.* 2019 Nov 26;9(1):17608.
633. Goltsov AA, Fang B, Pandita TK, Maru DM, Swisher SG, Hofstetter WL. HER2 Confers Resistance to Foretinib Inhibition of MET-Amplified Esophageal Adenocarcinoma Cells. *Ann Thorac Surg.* 2018 Feb;105(2):363–70.
634. Shah MA, Cho J-Y, Tan IB, Tebbutt NC, Yen C-J, Kang A, et al. A Randomized Phase II Study of FOLFOX With or Without the MET Inhibitor Onartuzumab in Advanced Adenocarcinoma of the Stomach and Gastroesophageal Junction. *The Oncologist.* 2016 Sep;21(9):1085–90.
635. Schauer MC, Stoecklein NH, Theisen J, Kröpil F, Baldus S, Hoelscher A, et al. The simultaneous expression of both ephrin B3 receptor and E-cadherin in Barrett's adenocarcinoma is associated with favorable clinical staging. *Eur J Med Res.* 2012 May 14;17:10.
636. Brankley SM, Halling KC, Jenkins SM, Timmer MR, Iyer PG, Smyrk TC, et al. Fluorescence in situ hybridization identifies high risk Barrett's patients likely to develop esophageal adenocarcinoma. *Dis Esophagus Off J Int Soc Dis Esophagus.* 2016 Aug;29(6):513–9.
637. Jankowski J, McMenemin R, Yu C, Hopwood D, Wormsley KG. Proliferating cell nuclear antigen in oesophageal diseases; correlation with transforming growth factor alpha expression. *Gut.* 1992 May;33(5):587–91.
638. Trudgill NJ, Suvarna SK, Royds JA, Riley SA. Cell cycle regulation in patients with intestinal metaplasia at the gastro-oesophageal junction. *Mol Pathol MP.* 2003 Dec;56(6):313–7.
639. Zhang XD. Illustration of SSMD, z score, SSMD*, z* score, and t statistic for hit selection in RNAi high-throughput screens. *J Biomol Screen.* 2011 Aug;16(7):775–85.
640. Li C, Guo S, Pang W, Zhao Z. Crosstalk Between Acid Sphingomyelinase and Inflammasome Signaling and Their Emerging Roles in Tissue Injury and Fibrosis. *Front Cell Dev Biol.* 2019;7:378.
641. Kuzu OF, Gowda R, Noory MA, Robertson GP. Modulating cancer cell survival by targeting intracellular cholesterol transport. *Br J Cancer.* 2017 Aug 8;117(4):513–24.
642. Zhu L, Xiong X, Kim Y, Okada N, Lu F, Zhang H, et al. Acid sphingomyelinase is required for cell surface presentation of Met receptor tyrosine kinase in cancer cells. *J Cell Sci.* 2016 Nov 15;129(22):4238–51.
643. Kornhuber J, Tripal P, Reichel M, Mühle C, Rhein C, Muehlbacher M, et al. Functional Inhibitors of Acid Sphingomyelinase (FIASMA): a novel pharmacological group of drugs with broad clinical applications. *Cell Physiol Biochem Int J Exp Cell Physiol Biochem Pharmacol.* 2010;26(1):9–20.
644. Birmingham A, Selfors LM, Forster T, Wrobel D, Kennedy CJ, Shanks E, et al. Statistical Methods for Analysis of High-Throughput RNA Interference Screens. *Nat Methods.* 2009 Aug;6(8):569–75.
645. Casey JR, Grinstein S, Orlowski J. Sensors and regulators of intracellular pH. *Nat Rev Mol Cell Biol.* 2010 Jan;11(1):50–61.

646. Wilson DF, Harrison DK, Vinogradov SA. Oxygen, pH, and mitochondrial oxidative phosphorylation. *J Appl Physiol Bethesda Md* 1985. 2012 Dec 15;113(12):1838–45.
647. Cordat E, Casey JR. Bicarbonate transport in cell physiology and disease. *Biochem J*. 2009 Jan 15;417(2):423–39.
648. Halestrap AP, Meredith D. The SLC16 gene family—from monocarboxylate transporters (MCTs) to aromatic amino acid transporters and beyond. *Pflugers Arch*. 2004 Feb;447(5):619–28.
649. Fong P. CFTR–SLC26 transporter interactions in epithelia. *Biophys Rev*. 2012 Feb 15;4(2):107–16.
650. Duval K, Grover H, Han L-H, Mou Y, Pegoraro AF, Fredberg J, et al. Modeling Physiological Events in 2D vs. 3D Cell Culture. *Physiology*. 2017 Jul;32(4):266–77.
651. Scheler O, Postek W, Garstecki P. Recent developments of microfluidics as a tool for biotechnology and microbiology. *Curr Opin Biotechnol*. 2019 Feb;55:60–7.
652. Carpenter AE, Jones TR, Lamprecht MR, Clarke C, Kang IH, Friman O, et al. CellProfiler: image analysis software for identifying and quantifying cell phenotypes. *Genome Biol*. 2006;7(10):R100.
653. Nguyen TT, Ung TT, Kim NH, Jung YD. Role of bile acids in colon carcinogenesis. *World J Clin Cases*. 2018 Nov 6;6(13):577–88.
654. Feng H-Y, Chen Y-C. Role of bile acids in carcinogenesis of pancreatic cancer: An old topic with new perspective. *World J Gastroenterol*. 2016 Sep 7;22(33):7463–77.
655. Sun L, Beggs K, Borude P, Edwards G, Bhushan B, Walesky C, et al. Bile acids promote diethylnitrosamine-induced hepatocellular carcinoma via increased inflammatory signaling. *Am J Physiol Gastrointest Liver Physiol*. 2016 Jul 1;311(1):G91–104.

List of Abbreviations

95%CI	95% confidence interval
AJC	Apical junction complex
Akt	Serine/threonine protein kinase B
ALK	Anaplastic lymphoma kinase
ANOVA	Analysis of variance
AP-1	Activator protein 1
APE1	Apurinic/aprimidinic endonuclease 1 enzyme
ATAC-seq	Assay for transposase-accessible chromatin using sequencing
ATCC	American Type Culture Collection
ATOH1	Protein analog homolog 1
ATP	Adenosine triphosphate
AU	Arbitrary units
B2SP	β 2-spectrin
BCA	Bicinchoninic acid
BCKDK	Branched chain keto acid dehydrogenase kinase
Bcl-2	B-cell lymphoma 2
BEACON	Barrett's and Esophageal Adenocarcinoma Consortium
BMI	Body mass index
BMP	Bone morphogenetic protein
BO	Barrett's oesophagus
BP	Biological process
BPE	Bovine pituitary extract
BSA	Bovine serum albumin
BSG	British Society for Gastroenterology
CAF	Cancer-associated fibroblast
cAMP	Cyclic adenosine monophosphate
CC	Cellular component
CCD	Charge-coupled device
CCK	Chemokine
CDK	Cyclin dependent kinase
cDNA	Complimentary DNA
CO ₂	Carbon dioxide
COX	Cyclooxygenase
COVID-19	Coronavirus disease 2019
CREB	cAMP response element-binding protein
Ct	Cycle threshold
CV	Coefficient of variation
DALY	Disability-adjusted life year
DCA	Deoxycholic acid
dCT	Delta cycle threshold
DEG	Differentially expressed gene
DKK	Dkkopf-related protein
DDR	DNA-damage repair
DNA	Deoxyribosenucleic acid

DNA-PK	DNA-dependent protein kinase
DIS	Dilated intracellular space
DM	Diabetes mellitus
DMSO	Dimethyl sulfoxide
DNA	Deoxyribonucleic acid
dNTP	Deoxynucleotide triphosphate
Dsh	Dishevelled
DTT	Dithiothreitol
EAGLE	Esophageal Adenocarcinoma Consortium
ECACC	European Collection of Authenticated Cell Cultures
ECL	Electrochemiluminescence
ECM	Extracellular matrix
EDTA	Ethylenediaminetetraacetic acid
EGF	Epidermal growth factor
EGFR	Epidermal growth factor receptor
EMT	Epithelial mesenchymal transition
EPHA-	Ephrin receptor A-
EPHB-	Ephrin receptor B-
ERK	Extracellular signal-related kinase
FBS	Foetal bovine serum
FC	Fold change
FGFR	Fibroblast growth factor receptor
FLT-	Fms related tyrosine kinase-
FOXO	Forkhead transcription factors
FPKM	Fragments per kilobase of transcript per million mapped reads
Fz	Frizzled
GATA6	GATA binding protein 6
GCA	Glycolic acid
GCDCA	Glycochenodeoxycholic acid
GDCA	Glycodeoxycholic acid
GLI1	Zinc finger protein GLI1
GO	Gene Ontology
GOJ	Gastro-oesophageal junction
GORD	Gastroesophageal reflux disease
GPCR	G-protein coupled receptor
GPS	Group-based Prediction System
GRB2	Growth factor receptor bound protein 2
GSEA	Gene set enrichment analysis
GWAS	Genome-wide association study
H. Pylori	Helicobacter pylori
H2RA	Histamine 2 receptor antagonist
HCL	Hydrochloric acid
HEPES	4-(2-hydroxyethyl)-1-piperazineethanesulfonic acid
HER2	Receptor tyrosine-protein kinase erbB-2 (ERBB2)
HES1	Transcription factor HES-1
HGD	High grade dysplasia

HIF	Hypoxia inducible factor
HNF	Hepatocyte nuclear factor
IFN	Interferon
IGF1R	Insulin-like growth factor-1 receptor
IκB	Inhibitor of κB proteins
IKK	IκB kinase
IL	Interleukin
INSR	Insulin receptor
INSRR	Insulin-receptor related receptor
IP	Immunoprecipitation
IPA	Ingenuity pathway analysis
IRS	Insulin receptor substrate
JAK	Janus kinase
JNK	c-Jun N-terminal kinase
KEGG	Kyoto Encyclopedia of Genes and Genomes
KD	Knockdown
KLF	Krüepel-like factor
KSFM	Keratinocyte serum-free medium
LEF	Lymphoid enhancer-binding factor 1
LGD	Low grade dysplasia
lncRNA	Long non-coding RNA
LoH	Loss of heterozygosity
LOS	Lower oesophageal sphincter
MACS	Model-based Analysis of CHIP-Seq
MAD	Median absolute deviation
MAPK	Mitogen activated protein kinase
Mb	Megabase
MF	Molecular function
miRNA	Micro RNA
MLE	Multi-layered epithelium
mRNA	Messenger RNA
MSigDB	Molecular Signatures Database
mTORC1	Mammalian target of rapamycin complex 1
MTT	3-(4,5-dimethylthiazol-2-yl)-2,5-diphenyltetrazolium bromide
Myc	c-Myc proto-oncogene protein
N2	Nitrogen
ncRNA	Non-coding RNA
NDBO	Non-dysplastic Barrett's oesophagus
NF-κB	Nuclear factor kappa-light-chain-enhancer of activated B cells
NFW	Nuclease-free water
nm	Nano-metres
NOX5	NADPH oxidase, EF-hand calcium binding domain 5
NSAID	Non-steroidal anti-inflammatory drug
NSE	Normal squamous epithelium
NT	Non-targeting
NTRK3	Neurotrophic receptor tyrosine kinase 3

O ₂	Oxygen
OCCAMS	Oesophageal Cancer Clinical & Molecular Stratification Network
OAC	Oesophageal adenocarcinoma
OR	Odds ratio
OSCC	Oesophageal squamous cell carcinoma
p53	Cellular tumour antigen p53
p63	Tumour protein 63
PAGE	Polyacrylamide gel electrophoresis
PANTHER	Protein Analysis Through Evolutionary Relationships
PAX9	Paired box protein Pax-9
PBS	Phosphate buffered saline
PCA	Principle component analysis
PCC	Pearson's correlation coefficient
PCR	Polymerase chain reaction
PKD1	Phosphoinositide-dependent protein kinase 1
PGE	Prostaglandin E
PGES	Prostaglandin E synthase
PI3K	Phosphatidylinositol 3-kinase
PIP2/3	Phosphatidylinositol di/tri-phosphate
piRNA	Piwi-interacting RNA
PPI	Proton pump inhibitor
PRAS40	Proline-rich Akt substrate of 40kDa
PTCH1	Patched-1
PTEN	Phosphate and tensin homolog
PTK	Protein tyrosine kinase
PVDF	Polyvinylidene difluoride
PTM	Post-translational modification
PVP	Polyvinylpyrrolidone
pY	Phosphotyrosine
qRT-PCR	Quantitative polymerase chain reaction
REVIGO	Reduce & Visualise Gene Ontology
RNA	Ribonucleic acid
RNA-seq	RNA sequencing
ROR	RTK-like orphan receptor
ROS	Reactive oxygen species
RPM	Revolutions per minute
RR	Relative risk
RTK	Receptor tyrosine kinase
RR	Relative risk
RSV	Rous sarcoma virus
s	Seconds
SDS	Sodium dodecyl sulphate
SEER	Surveillance, Epidemiology and End Results
Ser	Serine
SEM	Standard error of the mean
SHH	Sonic hedgehog

SIM	Specialised intestinal metaplasia
siRNA	Short interfering ribonucleic acid
Smo	Smoothened
SOS	Son-of-sevenless
Src	Tyrosine protein kinase Src
SSMD	Strictly standardised mean difference
SSRI	Selective serotonin reuptake inhibitor
SV40	Simian virus 40
STAT	Signal transducer and activator of proteins
STK	Serine/Threonine kinase
STRING	Search Tool for the Retrieval of Interacting Genes
SWI/SNF	SWItch/Sucrose Non-fermentable
TBS	Tris-buffered saline
TCA	Taurocholic acid
TCF	T-cell related factor
TGF	Transforming growth factor
T _h 1/2	T-helper 1/2
Thr	Threonine
TLR	Toll-like receptor
T _m	Melting temperature
TNF	Tumour necrosis factor
TRB	Tribbles homolog
TSC	Tuberous sclerosis protein
UK	United Kingdom
USA	United States of America
VEGF	Vascular endothelial growth factor
v/v	Volume /Volume
w/v	Weight/Volume
WIF	Wnt inhibitory factor
WT	Wild type
WTCC2	Wellcome Trust Case Control Consortium 2

Appendix A

List of suppliers & manufacturers

Shortened supplier name	Full name of supplier	Location
Abcam®	Abcam®	Cambridge, UK
Agilent	Agilent	Santa Clara, USA
ATCC®	American Type Culture Collection	Virginia, USA
Beckman Coulter	Beckman Coulter Life Sciences	High Wycombe, UK
Bio-Rad	Bio-Rad Laboratories Ltd.	Hertfordshire, UK
BioServ UK	BioServ UK, Ltd.	Sheffield, UK
BioTek™	BioTek™ Instruments, Inc.	Vermont, USA
Caltag Medsystems Ltd.	Caltag Medsystems Ltd.	Buckingham, USA
CST	Cell Signalling Technology	London, UK
Corning®	Corning® Inc.	New York, USA
Dharmacon	Dharmacon, Inc.	Lafayette, USA
ECACC	European Collection of Authenticated Cell Cultures	Salisbury, UK
IDT	Integrated DNA Technologies	Leuven, Belgium
Illumina®	Illumina®, Inc.	California, USA
Insight Biotechnology	Insight Biotechnology Ltd.	Middlesex, UK
Merck	Merck KGaA	Dorset, UK
MilliporeSigma	MilliporeSigma	Dorset, UK
MP Biomedicals	MP Biomedicals	California, USA
NCBI	National Centre for Biotechnology Information	Bethesda, USA
NEB	New England Biolabs	Hitchin, UK
NIH	National Institutes of Health	Bethesda, USA
PamGene	PamGene International B.V.,	BJ's-Hertogenbosch, NL
PerkinElmer	PerkinElmer, Inc.	Waltham, USA
Promega	Promega Corporation	Hampshire, UK
PROTEC	PROTEC GmbH & Co. KG	Oberstenfeld, Germany
QIAGEN	QIAGEN	Hilden, Germany
R&D Systems	R&D Systems, Inc.	Minneapolis, USA
Syngene	Syngene	Cambridge, UK
TFS	Thermo Fisher Scientific	Loughborough, UK

Key

NL: The Netherlands; UK: United Kingdom; USA: United States of America.

Appendix B

List of antibodies for immunoblotting

Target (total/phospho-epitope)	Species	Supplier	Code	Dilution
Primary antibodies				
Phospho-(Ser/Thr; phospho-S/T)	Rabbit	CST	#9631	1:1000-2500
Phospho-(Tyr; phospho-Y99)	Mouse	SCB	sc-7020	1:1000-2500
β-Actin	Rabbit	NEB	#4970	1:2500
AKT (total)	Rabbit	CST	#9272	1:1000
AKT (phospho-Ser473)	Rabbit	CST	#9271	1:1000
AKT (phospho-Thr308)	Rabbit	CST	#4056	1:1000
ALK (total)	Mouse	TFS	#354300	1:500
AMPK (total)	Rabbit	CST	#2532	1:1000
AMPK (phospho-Thr172)	Rabbit	CST	#2535	1:1000
ASM (total)	Rabbit	IB	GTX114782	1:1000
E-Cadherin (total)	Rabbit	CST	#3195	1:1000
N-Cadherin (total)	Rabbit	CST	#4061	1:1000
EGFR (total)	Rabbit	NEB	#2232	1:1000
EGFR (phospho-Tyr1068)	Rabbit	CST	#2234	1:1000
EPHA4 (total)	Mouse	TFS	#371600	1:200
ERK1/2 (total)	Rabbit	CST	#9102	1:1000
ERK1/2 (phospho-Thr202/Tyr204)	Rabbit	CST	#9101	1:1000-1:5000
FGFR2 (total: D4H9)	Rabbit	CST	#11835	1:1000
HER2 (total)	Rabbit	CST	#2165	1:1000
HER2 (phospho-Tyr1221/1222)	Rabbit	CST	#2243	1:500
IGF1R (total)	Mouse	SCB	Sc-81464	1:1000
IGF1R (phospho-Tyr1135)	Rabbit	CST	#3918	1:500-1000
Insulin receptor β (total: 4B8)	Rabbit	CST	#3025	1:1000
KLF5	Mouse	SCB	sc-398470	1:1000
MET (total)	Rabbit	CST	#8198	1:1000
Cleaved PARP (total)	Rabbit	CST	#9541	1:1000
PDGFRα (total)	Rabbit	CST	#3174	1:1000
PDGFRβ (total)	Rabbit	CST	#3169	1:1000
mTOR (total)	Rabbit	CST	#2972	1:1000
ULK1 (total)	Rabbit	Sigma	A7481	1:1000
ULK1 (phospho-Ser555)	Rabbit	CST	#5869	1:1000
ULK1 (phospho-Ser467)	Rabbit	CST	#4634	1:500
VEGFR2 (total)	Mouse	SCB	sc-393163	1:1000
Secondary antibodies				
Mouse	Horse (HRP-linked)	CST	#7076	1:2500
Rabbit	Goat (HRP-linked)	CST	#7074	1:2500

Notes

All primary antibodies were raised against human epitopes.

Key

CST: cell signalling technology; IB: Insight Biotechnology; NEB: New England Biolabs; SCB: Santa Cruz Biotechnology; TFS: Thermo Fisher Scientific.

Appendix C

List of primers for qRT-PCR analyses

Gene	Accession	Forward primer	Reverse primer
<i>ALK</i>	Q9UM73	5'-CGATGTGTCTGACAGGTTCTG-3'	5'-GTCCAGGCTGATGGAGATATTG-3'
<i>CDX2</i>	Q99626	5'-TCGGCAGCCAAGTGAAG-3'	5'-GATGGTGATGTAGCGACTGTAG-3'
<i>EGFR</i>	P00533	5'-CAAGGAAGCCAAGCCAAATG-3'	5'-CCGTGGTCATGCTCCAATAA-3'
<i>EPHA4</i>	P54764	5'-AGTCCTTCTGGTCTCTGTCTC-3'	5'-CCGCTTCTGTTTGGCTTTAC-3'
<i>FGFR3</i>	P22607	5'-CTGAAAGACGATGCCACTGA-3'	5'-CCCAGCAGGTTGATGATGT-3'
<i>GAPDH</i>	P04406		
<i>IGF1R</i>	P08069	5'-ATTCCAGCAGTCCCAGTTATG-3'	5'-CTGCTTAGCCCAGGAAATGA-3'
<i>KRT4</i>	P19013	5'-AAGAGACGATAGAGGAGACGAG-3'	5'-AGACAGAGGATGGAGGTGAA-3'
<i>KRT7</i>	P08729	5'-GTGGTGCTGAAGAAGGATGT-3'	5'-AGGGTCTGAGGAAGTTGAT-3'
<i>KRT8</i>	P05787	5'-GCAGATCAAGACCCTCAACA-3'	5'-CACTTGGTCTCCAGCATCTT-3'
<i>KRT18</i>	P05783	5'-GACCTGGACTCCATGAGAAATC-3'	5'-GTTGAGCTGCTCCATCTGTA-3'
<i>KRT19</i>	P08727	5'-GGGACAGGAAGATCACTACAAC-3'	5'-CCAGAAGACACCCTCAAAG-3'
<i>KRT20</i>	P35900	5'-CTGAATAAGGTCTTTGATGACC-3'	5'-ATGCTTGTGTAGGCCATCGA-3'
<i>MUC2</i>	Q02817	5'-GCGAGCAGTGTGTCTGTAA-3'	5'-GAAGGTGTACGTCTCCCATC-3'
<i>SOX9</i>	P48436	5'-TGACCTATCCAAGCGCATTAC-3'	5'-GCTTGCTCTGAAGAGGGTTTA-3'
<i>TEK</i>	Q02763	5'-TTGAAGTGGAGAGAAGGTCTG-3'	5'-GTTGACTCTAGCTCGGACCAC-3'
<i>TP63</i>	Q9H3D4	5'-TCCTCAGGGAGCTGTTATCC-3'	5'-ATTCACGGCTCAGCTCATGG-3'
<i>VIL1</i>	P09327	5'-AGCCAGATCACTGCTGAGGT-3'	5'-TGGACAGGTGTTCTCTCTTC-3'

Notes

All primers were sourced from IDT.

Appendix D

Tyrosine Kinase PamChip®4 Microarray List of Peptide Substrates

(PamGene® Category Number 86402)

No.	ID	Sequence	Tyr	Accession	Description
1	EFS_246_258	GGTDEGIYDVPLL	[253]	O43281	Embryonal Fyn-associated substrate (HEFS).
2	41_654_666	LDGENIYIRHSNL	[660]	P11171	Protein 4.1 (Band 4.1) (P4.1) (EPB4.1) (4.1R).
3	ACHD_383_395	YISKAEYFLLKS	[383, 390]	Q07001	Acetylcholine receptor subunit delta precursor.
4	AMPE_5_17	EREGSKRYCIQTK	[12]	Q07075	Glutamyl aminopeptidase (EC 3.4.11.7) (EAP) (Aminopeptidase A) (APA) (Differentiation antigen gp160) (CD249 antigen).
5	ANXA2_17_29	HSTPPSAYGSVKA	[24]	P07355	Annexin A2 (Annexin-2) (Lipocortin II) (Calpactin I heavy chain) (Chromobindin-8) (p36) (Protein I) (Placental anticoagulant protein IV).
6	ART_004_EAIYAAPF AKKKXC	EAIYAAPFAKKK	NA	NA	NA
7	B3AT_39_51	TEATATDYHTTSH	[46]	P02730	Band 3 anion transport protein (Anion exchange protein 1) (AE 1) (Solute carrier family 4 member 1) (CD233 antigen).
8	C1R_199_211	TEASGYISSLEYP	[204, 210]	P00736	Complement C1r subcomponent precursor (EC 3.4.21.41) (Complement component 1, r subcomponent) [Contains: Complement C1r subcomponent heavy chain; Complement C1r subcomponent light chain].
9	CALM_93_105	FDKDGNGYISAAE	[100]	P0DP23	Calmodulin (CaM).
10	CALM_95_107	KDGNGYISAAELR	[100]	P0DP23	Calmodulin (CaM).
11	CBL_693_705	EGEEDTEYMT PSS	[700]	P22681	E3 ubiquitin-protein ligase CBL (EC 6.3.2.-) (Signal transduction protein CBL) (Proto-oncogene c-CBL) (Casitas B-lineage lymphoma proto-oncogene) (RING finger protein 55).
12	CD3Z_116_128	KDKMAEAYSEIGM	[123]	P20963	T-cell surface glycoprotein CD3 zeta chain precursor (T-cell receptorT3 zeta chain) (CD247 antigen).
13	CD3Z_146_158	STATKDTYDALHM	[153]	P20963	T-cell surface glycoprotein CD3 zeta chain precursor (T-cell receptorT3 zeta chain) (CD247 antigen).
14	ART_003_EAI(pY)AA PFAKKXC	EAI(pY)AAPFAKKK	NA	NA	NA
15	CDK2_8_20	EKIGEGTYGVVYK	[15, 19]	P24941	Cyclin-dependent kinase 2 (EC:2.7.11.22) Cell division protein kinase 2 (EC 2.7.11.22) (p33 protein kinase).
16	CDK7_157_169	GLAKSFGSPNRAY	[169]	P50613	Cyclin-dependent kinase 7 (EC:2.7.11.22, EC:2.7.11.23) Cell division protein kinase 7 (EC 2.7.11.22) (EC 2.7.11.23) (CDK-activating kinase) (TFIIH basal transcription factor complex kinase subunit) (39 kDa protein kinase) (P39 Mo15)
17	CRK_214_226	GPPEPGPYAQPSV	[221]	P46108	Proto-oncogene C-crk (p38) (Adapter molecule crk).
18	CTNB1_79_91	VADIDGQYAMTRA	[86]	P35222	Catenin beta-1 (Beta-catenin).
19	DCX_67_79	GIVYAVSSDRFRS	[70]	O43602	Neuronal migration protein doublecortin (Lissencephalin-X) (Lis-X) (Doublin).

No.	ID	Sequence	Tyr	Accession	Description
20	DDR1_506_518	LLLSNPAYRLLLA	[513]	Q08345	Epithelial discoidin domain-containing receptor 1 precursor (EC 2.7.10.1) (Epithelial discoidin domain receptor 1) (Tyrosine kinase DDR) (Discoidin receptor tyrosine kinase) (Tyrosine-protein kinase CAK) (Cell adhesion kinase) (TRK E) (Protein-tyrosine kinase RTK 6) (HGK2) (CD167a antigen).
21	DYR1A_212_224	KHDTEMKYYIVHL	[219, 220]	Q13627	Dual specificity tyrosine-phosphorylation-regulated kinase 1A (EC 2.7.12.1) (Protein kinase mini brain homolog) (MNBH) (HP86) (Dual specificity YAK1-related kinase) (hMNB).
22	DYR1A_312_324	CQLGQRIYQYIQS	[319, 321]	Q13627	Dual specificity tyrosine-phosphorylation-regulated kinase 1A (EC 2.7.12.1) (Protein kinase minibrain homolog) (MNBH) (HP86) (Dual specificity YAK1-related kinase) (hMNB).
22	DYR1A_312_324	CQLGQRIYQYIQS	[319, 321]	Q13627	Dual specificity tyrosine-phosphorylation-regulated kinase 1A (EC 2.7.12.1) (Protein kinase mini brain homolog) (MNBH) (HP86) (Dual specificity YAK1-related kinase) (hMNB).
23	EGFR_1062_1074	EDSFLQRYSSDPT	[1069]	P00533	Epidermal growth factor receptor precursor (EC 2.7.10.1) (Receptor tyrosine-protein kinase ErbB-1).
24	EGFR_1103_1115	GSVQNPVYHNQPL	[1110]	P00533	Epidermal growth factor receptor precursor (EC 2.7.10.1) (Receptor tyrosine-protein kinase ErbB-1).
25	EGFR_1118_1130	APSRDPHYQDPHS	[1125]	P00533	Epidermal growth factor receptor precursor (EC 2.7.10.1) (Receptor tyrosine-protein kinase ErbB-1).
26	EGFR_1190_1202	STAENAEYLRVAP	[1197]	P00533	Epidermal growth factor receptor precursor (EC 2.7.10.1) (Receptor tyrosine-protein kinase ErbB-1).
27	EGFR_862_874	LGAEKEYHAEGG	[869]	P00533	Epidermal growth factor receptor precursor (EC 2.7.10.1) (Receptor tyrosine-protein kinase ErbB-1).
28	EGFR_908_920	MTFGSKPYDGIPA	[915]	P00533	Epidermal growth factor receptor precursor (EC 2.7.10.1) (Receptor tyrosine-protein kinase ErbB-1).
29	EPHA1_774_786	LDDFDGTYETQGG	[781]	P21709	Ephrin type-A receptor 1 precursor (EC 2.7.10.1) (Tyrosine-protein kinase receptor EPH).
30	EPHA2_581_593	QLKPLKTYVDPHT	[588]	P29317	Ephrin type-A receptor 2 precursor (EC 2.7.10.1) (Tyrosine-protein kinase receptor ECK) (Epithelial cell kinase).
31	EPHA2_765_777	EDDPEATYTTSGG	[772]	P29317	Ephrin type-A receptor 2 precursor (EC 2.7.10.1) (Tyrosine-protein kinase receptor ECK) (Epithelial cell kinase).
32	EPHA4_589_601	LNQGVRTYVDPFT	[596]	P54764	Ephrin type-A receptor 4 precursor (EC 2.7.10.1) (Tyrosine- protein kinase receptor SEK) (Receptor protein-tyrosine kinase HEK8) (Tyrosine-protein kinase TYRO1).
33	EPHA4_921_933	QAIKMDRYKDNFT	[928]	P54764	Ephrin type-A receptor 4 precursor (EC 2.7.10.1) (Tyrosine- protein kinase receptor SEK) (Receptor protein-tyrosine kinase HEK8) (Tyrosine-protein kinase TYRO1).
34	EPHA7_607_619	TYIDPETYEDPNR	[608, 614]	Q15375	Ephrin type-A receptor 7 precursor (EC 2.7.10.1) (Tyrosine- protein kinase receptor EHK-3) (EPH homology kinase 3) (Receptor protein-tyrosine kinase HEK11).
35	EPHB1_771_783	DDTSDPTYTSSLG	[778]	P54762	Ephrin type-B receptor 1 precursor (EC 2.7.10.1) (Tyrosine-protein kinase receptor EPH-2) (NET) (HEK6) (ELK).
36	EPHB1_921_933	SAIKMVQYRDSFL	[928]	P54762	Ephrin type-B receptor 1 precursor (EC 2.7.10.1) (Tyrosine-protein kinase receptor EPH-2) (NET) (HEK6) (ELK).
37	EPHB4_583_595	IGHGTKVYIDPFT	[590]	P54760	Ephrin type-B receptor 4 precursor (EC 2.7.10.1) (Tyrosine-protein kinase receptor HTK) (Tyrosine-protein kinase TYRO11).
38	EPOR_361_373	SEHAQDTYLVLDK	[368]	P19235	Erythropoietin receptor precursor (EPO-R).
39	ERBB2_870_882	LDIDETEHADGG	[877]	P04626	Receptor tyrosine-protein kinase erbB-2 precursor (EC 2.7.10.1) (p185erbB2) (C-erbB-2) (NEU proto-oncogene) (Tyrosine kinase-type cell surface receptor HER2) (MLN 19) (CD340 antigen).
40	ERBB4_1181_1193	QALDNPEYHNASN	[1188]	Q15303	Receptor tyrosine-protein kinase erbB-4 precursor (EC 2.7.10.1) (p180erbB4) (Tyrosine kinase-type cell surface receptor HER4)
41	EFS_246_258_Y253F	GGTDEGIFDVPLL	[]	O43281	Embryonal Fyn-associated substrate (HEFS).

No.	ID	Sequence	Tyr	Accession	Description
42	FABPH_13_25	DSKNFDDYMKSLG	[20]	P05413	Fatty acid-binding protein, heart (H-FABP) (Heart-type fatty acid-binding protein) (Muscle fatty acid-binding protein) (M-FABP) (Mammary-derived growth inhibitor) (MDGI).
43	FAK1_569_581	RYMEDSTYYKASK	[570, 576, 577]	Q05397	Focal adhesion kinase 1 (EC 2.7.10.2) (FADK 1) (pp125FAK) (Protein-tyrosine kinase 2).
44	FAK2_572_584	RYIEDEDYYKASV	[573, 579, 580]	Q14289	Protein tyrosine kinase 2 beta (EC 2.7.10.2) (Focal adhesion kinase 2) (FADK 2) (Proline-rich tyrosine kinase 2) (Cell adhesion kinase beta) (CAK beta) (Calcium-dependent tyrosine kinase) (CADTK) (Related adhesion focal tyrosine kinase) (RAFTK).
45	FER_707_719	RQEDGGVYSSSGL	[714]	P16591	Proto-oncogene tyrosine-protein kinase FER (EC 2.7.10.2) (p94-FER) (c-FER) (Tyrosine kinase 3).
46	FES_706_718	REEADGVYAASGG	[713]	P07332	Proto-oncogene tyrosine-protein kinase Fes/Fps (EC 2.7.10.2) (C-Fes).
47	FGFR3_641_653	DVHNLDDYYKTTN	[647, 648]	P22607	Fibroblast growth factor receptor 3 precursor (EC 2.7.10.1) (FGFR-3) (CD333 antigen).
48	FRK_380_392	KVDNEDIYERHE	[387]	P42685	Tyrosine-protein kinase FRK (EC 2.7.10.2) (FYN-related kinase) (Nuclear tyrosine protein kinase RAK).
49	INSR_1348_1360	SLGFKRSYEEHIP	[1355]	P06213	Insulin receptor precursor (EC 2.7.10.1) (IR) (CD220 antigen)[Contains: Insulin receptor subunit alpha; Insulin receptor subunit beta].
50	INSR_992_1004	YASSNPEYLSASD	[992, 999]	P06213	Insulin receptor precursor (EC 2.7.10.1) (IR) (CD220 antigen)[Contains: Insulin receptor subunit alpha; Insulin receptor subunit beta].
51	JAK1_1027_1039	AIETDKEYYTVKD	[1034,1035]	P23458	Tyrosine-protein kinase JAK1 (EC 2.7.10.2) (Janus kinase 1) (JAK-1).
52	JAK2_563_577	VRREVGDYGQLHETE	[570]	O60674	Tyrosine-protein kinase JAK2 (EC 2.7.10.2) (Janus kinase 2) (JAK-2).
53	K2C6B_53_65	GAGFGSRSLYGLG	[62]	P04259	Keratin, type II cytoskeletal 6B (Cytokeratin-6B) (CK 6B) (K6bkeratin).
54	K2C8_425_437	SAYGGLTSPGLSY	[427, 437]	P05787	Keratin, type II cytoskeletal 8 (Cytokeratin-8) (CK-8) (Keratin-8) (K8).
55	LAT_194_206	MESIDDDYVNPES	[200]	O43561	Linker for activation of T-cells family member 1 (36 kDa phospho-tyrosine adapter protein) (pp36) (p36-38).
56	LAT_249_261	EEGAPDYENLQEL	[255]	O43561	Linker for activation of T-cells family member 1 (36 kDa phospho-tyrosine adapter protein) (pp36) (p36-38).
57	LCK_387_399	RLIEDNEYTAREG	[394]	P06239	Proto-oncogene tyrosine-protein kinase LCK (EC 2.7.10.2) (p56-LCK) (Lymphocyte cell-specific protein-tyrosine kinase) (LSK) (T cell-specific protein-tyrosine kinase).
58	MBP_198_210	ARTAHYGSLPQKS	[203]	P02686	Myelin basic protein (MBP) (Myelin A1 protein) (Myelin membrane encephalitogenic protein).
59	MBP_259_271	FGYGGRASDYKSA	[261, 268]	P02686	Myelin basic protein (MBP) (Myelin A1 protein) (Myelin membrane encephalitogenic protein).
60	MBP_263_275	GRASDYKSAHKGKGF	[268]	P02686	Myelin basic protein (MBP) (Myelin A1 protein) (Myelin membrane encephalitogenic protein).
61	MET_1227_1239	RDMYDKEYYSVHN	[1230, 1234, 1235]	P08581	Hepatocyte growth factor receptor precursor (EC 2.7.10.1) (HGF receptor) (Scatter factor receptor) (SF receptor) (HGF/SF receptor) (Met proto-oncogene tyrosine kinase) (c-Met).
62	MK01_180_192	HTGFLTEYVATRW	[187]	P28482	Mitogen-activated protein kinase 1 (EC 2.7.11.24) (Extracellular signal-regulated kinase 2) (ERK-2) (Mitogen-activated protein kinase 2) (MAP kinase 2) (MAPK 2) (p42-MAPK) (ERT1).
63	MK01_198_210	IMLNSKGYTKSID	[205]	P28482	Mitogen-activated protein kinase 1 (EC 2.7.11.24) (Extracellular signal-regulated kinase 2) (ERK-2) (Mitogen-activated protein kinase 2) (MAP kinase 2) (MAPK 2) (p42-MAPK) (ERT1).
64	MK07_212_224	AEHQYFMTEYVAT	[216,221]	Q13164	Mitogen-activated protein kinase 7 (EC 2.7.11.24) (Extracellular signal-regulated kinase 5) (ERK-5) (ERK4) (BMK1 kinase)
65	MK10_216_228	TSFMMPYVVVTRY	[223, 228]	P53779	Mitogen-activated protein kinase 10 (EC 2.7.11.24) (Stress-activated protein kinase JNK3) (c-Jun N-terminal kinase 3) (MAP kinase p49 3F12).

No.	ID	Sequence	Tyr	Accession	Description
66	NCF1_313_325	QRSRKRLSQDAYR	[324]	P14598	Neutrophil cytosol factor 1 (NCF-1) (Neutrophil NADPH oxidase factor1) (47 kDa neutrophil oxidase factor) (p47-phox) (NCF-47K) (47 kDa autosomal chronic granulomatous disease protein) (Nox organizer 2) (Nox-organizing protein 2) (SH3 and PX domain-containing protein 1A).
67	NPT2A_501_513	AKALGKRTAKYRW	[511]	Q06495	Sodium-dependent phosphate transport protein 2A (Sodium/phosphate cotransporter 2A) (Na ⁺)/Pi cotransporter 2A) (Sodium-phosphate transport protein 2A) (Na ⁺)-dependent phosphate cotransporter 2A) (NaPi-2a) (Solute carrier family 34 member 1) (NaPi-3).
68	NTRK1_489_501	HIIENPQYFSDAC	[496]	P04629	High affinity nerve growth factor receptor precursor (EC 2.7.10.1) (Neurotrophic tyrosine kinase receptor type 1) (TRK1-transforming tyrosine kinase protein) (p140-TrkA) (Trk-A).
69	NTRK2_509_521	PVIENPQYFGITN	[516]	Q16620	BDNF/NT-3 growth factors receptor precursor (EC 2.7.10.1) (Neurotrophic tyrosine kinase receptor type 2) (TrkB tyrosine kinase) (GP145-TrkB) (Trk-B).
70	NTRK2_696_708	GMSRDVYSTDYR	[702, 706,707]	Q16620	BDNF/NT-3 growth factors receptor precursor (EC 2.7.10.1) (Neurotrophic tyrosine kinase receptor type 2) (TrkB tyrosine kinase) (GP145-TrkB) (Trk-B).
71	ODPAT_291_303	SMSDPGVSYRTRE	[299]	P29803	Pyruvate dehydrogenase E1 component subunit alpha, testis-specific form, mitochondrial precursor (EC 1.2.4.1) (PDHE1-A type II).
72	PAXI_111_123	VGEEHVYSFPNK	[118]	P49023	Paxillin.
73	PAXI_24_36	FLSEETPYSYPTG	[31, 33]	P49023	Paxillin.
74	PDPK1_2_14	ARTTSQLYDAVPI	[9]	O15530	3-phosphoinositide-dependent protein kinase 1 (EC 2.7.11.1) (hPDK1).
75	PECA1_706_718	KKDTETVYSEVRK	[713]	P16284	Platelet endothelial cell adhesion molecule precursor (PECAM-1) (EndoCAM) (GPIIA') (CD31 antigen).
76	PERI_458_470	QRSELDKSSAHSY	[470]	P41219	Peripherin.
77	PGFRB_1002_1014	LDTSSVLYTAVQP	[1009]	P09619	Beta-type platelet-derived growth factor receptor precursor(EC 2.7.10.1) (PDGF-R-beta) (CD140b antigen).
78	PGFRB_709_721	RPPSAELYSNALP	[716]	P09619	Beta-type platelet-derived growth factor receptor precursor(EC 2.7.10.1) (PDGF-R-beta) (CD140b antigen).
79	PGFRB_768_780	SSNYMAPYDNYVP	[771, 775,778]	P09619	Beta-type platelet-derived growth factor receptor precursor(EC 2.7.10.1) (PDGF-R-beta) (CD140b antigen).
80	PGFRB_771_783	YMAPYDNYVPSAP	[771, 775,778]	P09619	Beta-type platelet-derived growth factor receptor precursor(EC 2.7.10.1) (PDGF-R-beta) (CD140b antigen).
81	PLCG1_1246_1258	EGSFESRYQQPFE	[1253]	P19174	1-phosphatidylinositol-4,5-bisphosphate phosphodiesterase gamma-1(EC 3.1.4.11) (Phosphoinositide phospholipase C) (PLC-gamma-1) (Phospholipase C-gamma-1) (PLC-II) (PLC-148).
82	PLCG1_764_776	IGTAEPDYGALYE	[771, 775]	P19174	1-phosphatidylinositol-4,5-bisphosphate phosphodiesterase gamma-1(EC 3.1.4.11) (Phosphoinositide phospholipase C) (PLC-gamma-1) (Phospholipase C-gamma-1) (PLC-II) (PLC-148).
83	PRGR_545_557	LRPDSEASQSPQY	[557]	P06401	Progesterone receptor (PR) (Nuclear receptor subfamily 3 group C member 3).
84	PRGR_786_798	EQRMKESFYSLC	[795]	P06401	Progesterone receptor (PR) (Nuclear receptor subfamily 3 group C member 3).
85	PP2AB_297_309	EPHVTRRTPDYFL	[307]	P62714	Serine/threonine-protein phosphatase 2A catalytic subunit beta isoform(EC 3.1.3.16) (PP2A-beta).
86	PRRX2_202_214	WTASSPYSTVPPY	[208, 214]	Q99811	Paired mesoderm homeobox protein 2 (PRX-2) (Paired-related homeoboxprotein 2).

No.	ID	Sequence	Tyr	Accession	Description
87	PTN11_539_551	SKRRKGHEYTNIKY	[546, 551]	Q06124	Tyrosine-protein phosphatase non-receptor type 11 (EC 3.1.3.48) (Protein-tyrosine phosphatase 2C) (PTP-2C) (PTP-1D) (SH-PTP3) (SH-PTP2) (SHP-2) (Shp2).
88	RB_804_816	IYISPLKSPYKIS	[805, 813]	P06400	Retinoblastoma-associated protein (PP110) (P105-RB) (RB).
89	RBL2_99_111	VPTVSKGTVEGNY	[111]	Q08999	Retinoblastoma-like protein 2 (130 kDa retinoblastoma-associated protein) (p130) (PRB2) (RBR-2).
90	RET_1022_1034	TPSDSLIYDDGLS	[1029]	P07949	Proto-oncogene tyrosine-protein kinase receptor ret precursor (EC 2.7.10.1) (C-ret).
91	RET_680_692	AQAFPVSYSSSGA	[687]	P07949	Macrophage-stimulating protein receptor precursor (EC 2.7.10.1) (MSP receptor) (p185-Ron) (CD136 antigen) (CDw136) [Contains: Macrophage-stimulating protein receptor alpha chain; Macrophage-Stimulating protein receptor beta chain].
92	RON_1346_1358	SALLGDHYVQLPA	[1353]	Q04912	Signal transducer and activator of transcription 5A.
93	STAT1_694_706	DGPKGTGYIKTEL	[701]	P42224	Signal transducer and activator of transcription 1-alpha/beta (Transcription factor ISGF-3 components p91/p84).
94	STAT3_698_710	DPGSAAPYLKTKF	[705]	P40763	Signal transducer and activator of transcription 3 (Acute-phase response factor).
95	STAT4_686_698	TERGDKGYVPSVF	[693]	Q14765	Proto-oncogene tyrosine-protein kinase receptor ret precursor (EC 2.7.10.1) (C-ret).
96	STAT4_714_726	PSDLLPMSPSVYA	[725]	Q14765	Signal transducer and activator of transcription 4.
97	STA5A_687_699	LAKAVDGYVKPQI	[694]	P42229	Signal transducer and activator of transcription 4.
98	STAT6_634_646	MGKDGRGYVPATI	[641]	P42226	Signal transducer and activator of transcription 6 (IL-4 Stat).
99	RAF1_332_344	PRGQRDSSYYWEI	[340, 341]	P04049	RAF proto-oncogene serine/threonine-protein kinase (EC 2.7.11.1) (Raf-1) (C-RAF) (cRaf).
100	RASA1_453_465	TVDGKEIYNTIRR	[460]	P20936	Ras GTPase-activating protein 1 (GTPase-activating protein) (GAP) (Rasp21 protein activator) (p120GAP) (RasGAP).
101	TNNT1_2_14	SDTEEQEYEEEQP	[9]	P13805	Troponin T, slow skeletal muscle (TnTs) (Slow skeletal muscle troponinT) (sTnT).
102	TYRO3_679_691	KIYSGDYRRQGCA	[681, 685, 686]	Q06418	Tyrosine-protein kinase receptor TYRO3 precursor (EC 2.7.10.1) (Tyrosine-protein kinase RSE) (Tyrosine-protein kinase SKY) (Tyrosine-protein kinase DTK) (Protein-tyrosine kinase byk).
103	VGFR1_1040_1052	DFGLARDIYKNPD	[1048]	P17948	Vascular endothelial growth factor receptor 1 precursor (EC 2.7.10.1) (VEGFR-1) (Vascular permeability factor receptor) (Tyrosine-protein kinase receptor FLT) (Flt-1) (Tyrosine-protein kinase FRT) (Fms-like tyrosine kinase 1).
104	VGFR1_1046_1058_Y1048F	DIFKNPDYVRKGD	[1053]	P17948	Vascular endothelial growth factor receptor 1 precursor (EC 2.7.10.1) (VEGFR-1) (Vascular permeability factor receptor) (Tyrosine-protein kinase receptor FLT) (Flt-1) (Tyrosine-protein kinase FRT) (Fms-like tyrosine kinase 1).
105	VGFR1_1049_1061	KNPDYVRKGDTRL	[1053]	P17948	Vascular endothelial growth factor receptor 1 precursor (EC 2.7.10.1) (VEGFR-1) (Vascular permeability factor receptor) (Tyrosine-protein kinase receptor FLT) (Flt-1) (Tyrosine-protein kinase FRT) (Fms-like tyrosine kinase 1).
106	VGFR1_1162_1174	VQQDGKDYIPINA	[1169]	P17948	Vascular endothelial growth factor receptor 1 precursor (EC 2.7.10.1) (VEGFR-1) (Vascular permeability factor receptor) (Tyrosine-protein kinase receptor FLT) (Flt-1) (Tyrosine-protein kinase FRT) (Fms-like tyrosine kinase 1).
107	VGFR1_1206_1218	GSSDDVRYVNAFK	[1213]	P17948	Vascular endothelial growth factor receptor 1 precursor (EC 2.7.10.1) (VEGFR-1) (Vascular permeability factor receptor) (Tyrosine-protein kinase receptor FLT) (Flt-1) (Tyrosine-protein kinase FRT) (Fms-like tyrosine kinase 1).
108	VGFR2_1046_1058	DFGLARDIYKDPD	[1054]	P35968	Vascular endothelial growth factor receptor 2 precursor (EC 2.7.10.1) (VEGFR-2) (Kinase insert domain receptor) (Protein-tyrosine kinase receptor Flk-1) (CD309 antigen).
109	VGFR2_1207_1219_C1208S	VSDPKFHYDNTAG	[1214]	P35968	Vascular endothelial growth factor receptor 2 precursor (EC 2.7.10.1) (VEGFR-2) (Kinase insert domain receptor) (Protein-tyrosine kinase receptor Flk-1) (CD309 antigen).

No. ID	Sequence	Tyr	Accession	Description
110 VGFR2_944_956	RFRQKGKDYVGAIP	[951]	P35968	Vascular endothelial growth factor receptor 2 precursor (EC 2.7.10.1) (VEGFR-2) (Kinase insert domain receptor) (Protein-tyrosine kinase receptor Flk-1) (CD309 antigen).
111 VGFR2_989_1001	EEAPEDLYKDFLT	[996]	P35968	Vascular endothelial growth factor receptor 2 precursor (EC 2.7.10.1) (VEGFR-2) (Kinase insert domain receptor) (Protein-tyrosine kinase receptor Flk-1) (CD309 antigen).
112 VGFR3_1061_1073	DIYKDPDYVRKGS	[1063, 1068]	P35916	Vascular endothelial growth factor receptor 3 precursor (EC 2.7.10.1) (VEGFR-3) (Tyrosine-protein kinase receptor FLT4).
113 VINC_815_827	KSFLDSGYRILGA	[822]	P18206	Vinculin (Metavinculin).
114 ZAP70_485_497	ALGADDSYYTARS	[492, 493]	P43403	Tyrosine-protein kinase ZAP-70 (EC 2.7.10.2) (70 kDa zeta-associated protein) (Syk-related tyrosine kinase).
115 ZBT16_621_633	LRTHNGASPYQCT	[630]	Q05516	Zinc finger and BTB domain-containing protein 16 (Zinc finger protein PLZF) (Promyelocytic leukemia zinc finger protein) (Zinc-finger protein 145).
116 FGFR1_761_773	TSNQEYLDLSMPL	[766]	P11362	Basic fibroblast growth factor receptor 1 precursor (EC 2.7.10.1) (FGFR-1) (bFGF-R) (Fms-like tyrosine kinase 2) (c-fgr) (CD331 antigen).
117 PGFRB_1014_1028	PNEGDNNDYIPLPDP	[1021]	P09619	Beta-type platelet-derived growth factor receptor precursor (EC 2.7.10.1) (PDGF-R-beta) (CD140b antigen).
118 ERBB2_1241_1253	PTAENPEYLGLDV	[1248]	P04626	Receptor tyrosine-protein kinase erbB-2 precursor (EC 2.7.10.1) (p185erbB2) (C-erbB-2) (NEU proto-oncogene) (Tyrosine kinase-type cell surface receptor HER2) (MLN 19) (CD340 antigen).
119 KSYK_518_530	ALRADENYYKAQT	[525, 526]	P43405	Tyrosine-protein kinase SYK (EC 2.7.10.2) (Spleen tyrosine kinase).
120 MK12_178_190	ADSEMGTGVVTRW	[185]	P53778	Mitogen-activated protein kinase 12 (EC 2.7.11.24) (Extracellular signal-regulated kinase 6) (ERK-6) (ERK5) (Stress-activated protein kinase 3) (Mitogen-activated protein kinase p38 gamma) (MAP kinase p38 gamma).
121 MK14_173_185	RHTDDEMGTGVAT	[182]	Q16539	Mitogen-activated protein kinase 14 (EC 2.7.11.24) (Mitogen-activated protein kinase p38 alpha) (MAP kinase p38 alpha) (Cytokine suppressive anti-inflammatory drug-binding protein) (CSAID-binding protein) (CSBP) (MAX-interacting protein 2) (MAPkinase MXI2) (SAPK2A).
122 PGFRB_572_584	VSSDGHEYIYVDP	[579, 581]	P09619	Beta-type platelet-derived growth factor receptor precursor (EC 2.7.10.1) (PDGF-R-beta) (CD140b antigen).
123 TEC_512_524	RYFLDDQYTSSSG	[513, 519]	P42680	Tyrosine-protein kinase Tec (EC 2.7.10.2).
124 VGFR1_1235_1247	ATSMFDDYQGDSS	[1242]	P17948	Vascular endothelial growth factor receptor 1 precursor (EC 2.7.10.1) (VEGFR-1) (Vascular permeability factor receptor) (Tyrosine-protein kinase receptor FLT) (Flt-1) (Tyrosine-protein kinase FRT) (Fms-like tyrosine kinase 1).
125 VGFR2_1168_1180	AQQDGKDYIVLPI	[1175]	P35968	Vascular endothelial growth factor receptor 2 precursor (EC 2.7.10.1) (VEGFR-2) (Kinase insert domain receptor) (Protein-tyrosine kinase receptor Flk-1) (CD309 antigen).
126 ANXA1_14_26	IENEEQEYVQTVK	[21]	P04083	Annexin A1 (Annexin-1) (Annexin I) (Lipocortin I) (Calpactin II) (Chromobindin-9) (p35) (Phospholipase A2 inhibitory protein).
127 EGFR_1165_1177	ISLDNPDYQQDFF	[1172]	P00533	Epidermal growth factor receptor precursor (EC 2.7.10.1) (Receptor tyrosine-protein kinase ErbB-1).
128 EPOR_419_431	ASAASFYETILDLP	[426]	P19235	Erythropoietin receptor precursor (EPO-R).
129 ERBB4_1277_1289	IVAENPEYLSEFS	[1284]	Q15303	Receptor tyrosine-protein kinase erbB-4 precursor (EC 2.7.10.1) (p180erbB4) (Tyrosine kinase-type cell surface receptor HER4).
130 FGFR2_762_774	TLTNEEYLDLSQ	[769]	P21802	Fibroblast growth factor receptor 2 precursor (EC 2.7.10.1) (FGFR-2) (Keratinocyte growth factor receptor 2) (CD332 antigen).
131 FGFR3_753_765	TVTSTDEYLDLSA	[760]	P22607	Fibroblast growth factor receptor 3 precursor (EC 2.7.10.1) (FGFR-3) (CD333 antigen).

No.	ID	Sequence	Tyr	Accession	Description
132	P85A_600_612	NENTEDQYSLVED	[607]	P27986	Phosphatidylinositol 3-kinase regulatory subunit alpha (PI3-kinase p85subunit alpha) (PtdIns-3-kinase p85-alpha) (PI3K).
133	PDPK1_369_381	DEDICYGNYDNLLS	[373, 376]	O15530	3-phosphoinositide-dependent protein kinase 1 (EC 2.7.11.1) (hPDK1).
134	AKT1_170_182	KATGRYYAMKILK	[175, 176]	P31749	RAC-alpha serine/threonine-protein kinase (EC:2.7.11.1) (PKB, RAC)
135	AKT1_309_321_C310S	FSGTPEYLAVEVL	[315]	P31749	RAC-alpha serine/threonine-protein kinase (EC:2.7.11.1) (PKB, RAC)
136	AKT1_320_332	VLEDNDYGRAVDW	[326]	P31749	RAC-alpha serine/threonine-protein kinase (EC:2.7.11.1) (PKB, RAC)
137	ARAF_297_307	RDSGYWVEVPP	[301, 302]	P10398	Serine/threonine-protein kinase A-Raf (EC:2.7.11.1),(ARAF1, PKS, PKS2)
138	BTLA_252_262	KPGIVYASLNH	[257]	Q7Z6A9	B- and T-lymphocyte attenuator, B- and T-lymphocyte-associated protein,CD272
139	CD28_185_197	RLLHSDYMNMTPR	[191]	P10747	T-cell-specific surface glycoprotein CD28, TP44, CD28
140	CD28_203_215	RKHYPYAPPRDF	[206, 209]	P10747	T-cell-specific surface glycoprotein CD28, TP44, CD28
141	CD3E_182_194	PVPNPDYEPIRKG	[188]	P07766	T-cell surface glycoprotein CD3 epsilon chain, T-cell surface antigen T3/Leu-4 epsilon chain, CD3e
142	CD3E_193_205	KGQRDLYSGLNQR	[199]	P07766	T-cell surface glycoprotein CD3 epsilon chain, T-cell surface antigen T3/Leu-4 epsilon chain, CD3e
143	CD3Z_135_147	KGHDGLYQGLSTA	[142]	P20963	T-cell surface glycoprotein CD3 zeta chain precursor (T-cell receptorT3 zeta chain) (CD247 antigen).
144	CD3Z_146_158	TATKDTYDALHMQ	[153]	P20963	T-cell surface glycoprotein CD3 zeta chain precursor (T-cell receptorT3 zeta chain) (CD247 antigen).
145	CD70_9_21_C17S	SVRRRYPGSVLRA	[15]	P32970	CD70 antigen, CD27 ligand, Tumor necrosis factor ligand superfamily member 7
146	CDK1_9_21	KIGEGTYGVVYKG	[15, 19]	P06493	Cyclin-dependent kinase 1 (EC:2.7.11.22, EC:2.7.11.23), Cell division protein kinase 1, Cell division control protein 2 homolog, (p34 protein kinase) (CDK1)
147	CDK4_11_23	EIGVGAYGTVYKA	[17, 21]	P11802	Cyclin-dependent kinase 4 (EC:2.7.11.22) ,Cell division protein kinase 4 (PSK-J3)
148	ERBB3_1283_1295	PASEQGYEEMRAF	[1289]	P21860	Receptor tyrosine-protein kinase erbB-3 (EC:2.7.10.1), Proto- oncogene-like protein c-ErbB-3 , Tyrosine kinase-type cell surface receptor HER3
149	FYN_525_537	TATEPQYQGENL	[531]	P06241	Tyrosine-protein kinase Fyn (EC:2.7.10.2), Proto-oncogene Syn, Proto-oncogene c-Fyn, Src-like kinase
150	GAB2_638_648	DEKVDYVQVDK	[643]	Q9UQC2	GRB2-associated-binding protein 2, GRB2-associated binder 2, Growth factor receptor bound protein 2-associated protein 2
151	GSK3B_210_222_C218S	GEPNVSYISSRY	[216, 221,222]	P49841	Glycogen synthase kinase-3 beta (EC:2.7.11.26), Serine/threonine-protein kinase GSK3B (EC:2.7.11.1)
152	IRS2_626_638	HPYPEDYGDIEIG	[628, 632]	Q9Y4H2	Insulin receptor substrate 2
153	JAK1_214_226	DISYKRYIPETLN	[217, 220]	P23458	Tyrosine-protein kinase JAK1 (EC 2.7.10.2) (Janus kinase 1) (JAK-1).
154	JAK2_1001_1013	LPQDKKEYKVKKEP	[1007, 1008]	O60674	Tyrosine-protein kinase JAK2 (EC 2.7.10.2) (Janus kinase 2) (JAK-2).
155	JAK3_974_986	LPLDKDYVVREP	[980, 981]	P52333	Tyrosine-protein kinase JAK3 (EC:2.7.10.2) (Janus kinase 3) (JAK-3).
156	KIT_930_942_C942S	ESTNHIYSNLANS	[936]	P10721	Mast/stem cell growth factor receptor Kit (EC:2.7.10.1), CD117
157	LYN_391_403	VIEDNEYTAREGA	[397]	P07948	Tyrosine-protein kinase Lyn (EC:2.7.10.2)
158	LYN_501_512	YTATEGQYQQQP	[501, 508]	P07948	Tyrosine-protein kinase Lyn (EC:2.7.10.2)
159	MAPK3_198_210_C203S	ALQTPSYTPYYVA	[204, 207, 208]	Q16644	MAP kinase-activated protein kinase 3 (EC:2.7.11.1)

No.	ID	Sequence	Tyr	Accession	Description
160	MET_1228_1240	DMYDKEYYSVHNK	[1230, 1234, 1235]	P08581	Hepatocyte growth factor receptor precursor (EC 2.7.10.1) (HGF receptor) (Scatter factor receptor) (SF receptor) (HGF/SF receptor) (Met proto-oncogene tyrosine kinase) (c-Met).
161	MET_1360_1370_C1 361S	KSVAPYPSLLS	[1365]	P08581	Hepatocyte growth factor receptor precursor (EC 2.7.10.1) (HGF receptor) (Scatter factor receptor) (SF receptor) (HGF/SF receptor) (Met proto-oncogene tyrosine kinase) (c-Met).
162	MK01_200_209	LNSKGYTKSI	[205]	P28482	Mitogen-activated protein kinase 1 (EC 2.7.11.24) (Extracellular signal-regulated kinase 2) (ERK-2) (Mitogen-activated protein kinase 2) (MAP kinase 2) (MAPK 2) (p42-MAPK) (ERT1).
163	MK03_199_208	GFLTEYVATR	[204]	P27361	Mitogen-activated protein kinase 3 (EC:2.7.11.24), (Extracellular signal-regulated kinase 1) (ERK-1) (Mitogen-activated protein kinase 3) (MAP kinase 3) (MAPK 3) (p44-MAPK) (ERT2)
164	MK08_181_191	MMPYVVTRY	[185, 190, 191]	P45983	Mitogen-activated protein kinase 8 (EC 2.7.11.24) (MAP kinase 8) (MAPK 8)
165	MK12_180_189_M1 82B	SEBTGYVVTR	[185]	P53778	Mitogen-activated protein kinase 12 (EC 2.7.11.24) (Extracellular signal-regulated kinase 6) (ERK-6) (ERK5) (Stress- activated proteinkinase 3) (Mitogen-activated protein kinase p38 gamma) (MAP kinase p38gamma).
166	MK14_177_187	DEMTGYVATRW	[182]	Q16539	Mitogen-activated protein kinase 14 (EC 2.7.11.24) (Mitogen- activated protein kinase p38 alpha) (MAP kinase p38 alpha) (Cytokine suppressive anti-inflammatory drug-binding protein) (CSAID-binding protein) (CSBP) (MAX-interacting protein 2) (MAP kinase MXI2) (SAPK2A).
167	PDCD1_221_229_FS 219_220KK	KKVDYGELDFQ	[223]	Q15116	Programmed cell death protein 1, (Protein PD-1) (CD279)
168	PECA1_708_718	DTVYSEVRK	[713]	P16284	Platelet endothelial cell adhesion molecule precursor (PECAM-1) (EndoCAM) (GPIIA') (CD31 antigen).
169	PLCG1_777_789	GRNPGFYVEANPM	[783]	P19174	1-phosphatidylinositol-4,5-bisphosphate phosphodiesterase gamma-1(EC 3.1.4.11) (Phosphoinositide phospholipase C) (PLC-gamma-1) (Phospholipase C-gamma-1) (PLC-II) (PLC-148).
170	PLCG2_1211_1223	NNQLFLYDTHQNL	[1217]	P16885	1-phosphatidylinositol 4,5-bisphosphate phosphor-diesterase gamma- 2 (EC:3.1.4.11) (Phosphoinositide phospholipase C-gamma-2) (PLC-IV) (Phospholipase C-gamma-2) (PLC-gamma 2)
171	PTN11_541_551	RKGHEYTNIKY	[546, 551]	Q06124	Tyrosine-protein phosphatase non-receptor type 11 (EC 3.1.3.48) (Protein-tyrosine phosphatase 2C) (PTP-2C) (PTP-1D) (SH-PTP3) (SH-PTP2) (SHP-2) (Shp2).
172	PTN11_57_67	QNTGDYYDLYG	[62, 63, 66]	Q06124	Tyrosine-protein phosphatase non-receptor type 11 (EC 3.1.3.48) (Protein-tyrosine phosphatase 2C) (PTP-2C) (PTP-1D) (SH-PTP3) (SH-PTP2) (SHP-2) (Shp2).
173	PTN6_531_541	GQESEYGNITY	[536, 541]	P29350	Tyrosine-protein phosphatase non-receptor type 6 (EC:3.1.3.48)
174	PTN6_558_570	KHKEDVYENLHTK	[564]	P29350	Tyrosine-protein phosphatase non-receptor type 6 (EC:3.1.3.48)
175	SHC1_309_321	ELRFKQYLRNPPK	[315]	P29353	SHC-transforming protein 1
176	SRC_524_536	TSTEPQYQPGENL	[530]	P12931	Proto-oncogene tyrosine-protein kinase Src (EC:2.7.10.2) (Proto- oncogene c-Src) (pp60c-src) (p60-Src)
177	STAT2_684_696	LQERRKYLKHRLI	[690]	P52630	Signal transducer and activator of transcription 2 (p113)
178	TIE2_986_998	SRGQEVYVKKTMG	[992]	Q02763	Angiopoietin-1 receptor (EC:2.7.10.1)
179	TYK2_1048_1060	VPEGHEYRVRED	[1054, 1055]	P29597	Non-receptor tyrosine-protein kinase TYK2 (EC:2.7.10.2)

No.	ID	Sequence	Tyr	Accession	Description
180	VGFR1_1320_1332_ C1320K/C1321K	KKSPPPDYNVSVL	[1327]	P17948	Vascular endothelial growth factor receptor 1 precursor (EC 2.7.10.1) (VEGFR-1) (Vascular permeability factor receptor) (Tyrosine-protein kinase receptor FLT) (Flt-1) (Tyrosine-protein kinase FRT) (Fms-liketyrosine kinase 1).
181	VISTA_260_270	RHPLSYVAQRQ	[265]	Q9H7M9	V-type immunoglobulin domain-containing suppressor of T-cell activation
182	YES_420_432	LIEDNEYTARQGA	[426]	P07947	Tyrosine-protein kinase Yes (EC:2.7.10.2) (Proto-oncogene c-Yes) (p61-Yes)
183	CD79A_181_193	EYEDENLYEGLNL	[182, 188]	P11912	B-cell antigen receptor complex-associated protein alpha- chain precursor (Ig-alpha) (MB-1 membrane glycoprotein) (Surface IgM-associated protein) (Membrane-bound immunoglobulin-associated protein) (CD79a antigen).
184	CD3Z_77_89	LGRREEYDVLDKR	[83]	P20963	T-cell surface glycoprotein CD3 zeta chain precursor (T-cell receptorT3 zeta chain) (CD247 antigen).
185	CD3Z_105_117	NPQEGLYNELQKD	[111]	P20963	T-cell surface glycoprotein CD3 zeta chain precursor (T-cell receptorT3 zeta chain) (CD247 antigen).
186	CD3Z_117_129	DKMAEAYSEIGMK	[123]	P20963	T-cell surface glycoprotein CD3 zeta chain precursor (T-cell receptorT3 zeta chain) (CD247 antigen).
187	MUSK_548_560	LHPNPMYQRMPLL	[554]	O15146	Muscle, skeletal receptor tyrosine-protein kinase (EC:2.7.10.1)
188	ODBA_340_352_D34 OK	KDSSAYRSVDEVN	[345]	P12694	2-oxoisovalerate dehydrogenase subunit alpha, mitochondrial (EC:1.2.4.4) (BCKDE1A)
189	GAB1_622_632	DKQVEYLDLIDL	[627]	Q13480	GRB2-associated-binding protein 1, GRB2-associated binder 1, Growth factor receptor bound protein 2-associated protein 1
190	HAVR2_257_267	GIRSEENIYTI	[265]	Q8TDQ0	Hepatitis A virus cellular receptor 2, T-cell immunoglobulin and mucin domain-containing protein 3, T-cell membrane protein 3
191	IRS1_890_902	PKSPGEYVNIEFG	[896]	P35568	Insulin receptor substrate 1
192	ZAP70_313_325	SVYESPYSDPEEL	[315, 319]	P43403	Tyrosine-protein kinase ZAP-70 (EC 2.7.10.2) (70 kDa zeta-associated protein) (Syk-related tyrosine kinase).
193	MPZL1_236_246	QGPVIYAQLDH	[241]	O95297	Myelin protein zero-like protein 1
194	PLCG2_1191_1203_ C1200S	ESEELYSSSRQL	[1197]	P16885	1-phosphatidylinositol 4,5-bisphosphate phosphodiesterase gamma- 2 (EC:3.1.4.11) (Phosphoinositide phospholipase C-gamma-2) (PLC-IV) (Phospholipase C-gamma-2) (PLC-gamma-2)
195	PTN11_580_590	SARVYENVGLM	[584]	Q06124	Tyrosine-protein phosphatase non-receptor type 11 (EC 3.1.3.48) (Protein-tyrosine phosphatase 2C) (PTP-2C) (PTP-1D) (SH-PTP3) (SH-PTP2) (SHP-2) (Shp2).
196	ENOG_37_49	SGASTGIYEAL	[44]	P09104	Gamma-enolase (EC 4.2.1.11) (2-phospho-D-glycerate hydro-lyase) (Neural enolase) (Neuron-specific enolase) (NSE) (Enolase 2).

Appendix E

Serine/Threonine Kinase PamChip®4 Microarray List of Peptide Substrates

(PamGene® Category Number 87102)

No.	ID	Sequence	Ser	Thr	Accession	Description
1	pTY3H_64_78	RFIGRRQ(pS)LIEDARK	[71]	[]	P07101	Tyrosine 3-monooxygenase (EC 1.14.16.2) (Tyrosine 3-hydroxylase) (TH).
2	ATF2_47_59	VADQTPTPTRFLK	[]	[51, 53, 55]	P15336	Cyclic AMP-dependent transcription factor ATF-2 (Activating transcription factor 2) (cAMP response element-binding protein CRE-BP1) (HB16).
3	CDN1A_139_151	GRKRRQTSMTDFY	[146]	[145, 148]	P38936	Cyclin-dependent kinase inhibitor 1 (p21) (CDK-interacting protein 1) (Melanoma differentiation-associated protein 6) (MDA-6).
4	FIBA_569_581	EFPSRGKSSSYSK	[572, 576, 577, 578, 580]	[]	P02671	Fibrinogen alpha chain precursor [Contains: Fibrinopeptide A].
5	IKKB_173_185_C179A	LDQGLSATSFGVT	[177, 181]	[180, 185]	O14920	Inhibitor of nuclear factor kappa-B kinase subunit beta (I-kappa-B-kinase beta) (IkbKB) (IKK-beta) (IKK-B) (EC=2.7.11.10) (I-kappa-B kinase 2) (IKK2) (Nuclear factor NF-kappa-B inhibitor kinase beta) (NFKBIKB).
6	LIPS_944_956	GFHPRRSSQGATQ	[950, 951]	[955]	Q05469	Hormone-sensitive lipase (HSL) (EC=3.1.1.79).
7	MYBB_513_525	DNTPHTPTPFKNA	[]	[515, 518, 520]	P10244	Myb-related protein B (B-Myb).
8	PLEK_106_118	GQKFARKSTRRSI	[113, 117]	[114]	P08567	Pleckstrin (Platelet p47 protein).
9	RBL2_632_644	DEICIAGSPLTPR	[639]	[642]	Q08999	Retinoblastoma-like protein 2 (130 kDa retinoblastoma-associated protein) (p130) (PRB2) (RBR-2).
10	VIGLN_289_301	EEKKKKTTTIAVE	[]	[295, 296, 297]	Q00341	Vigilin (High density lipoprotein-binding protein) (HDL-binding protein).
11	GRIK2_708_720	FMSSRRQSVLVKS	[710, 711, 715, 720]	[]	Q13002	Glutamate receptor, ionotropic kainate 2 precursor (Glutamate receptor6) (GluR-6) (GluR6) (Excitatory amino acid receptor 4) (EAA4).
12	RADI_559_569	RDKYKTLRQIR	[]	[564]	P35241	Radixin.
13	ACM1_421_433	CNKAFRDTFRLLL	[]	[428]	P11229	Muscarinic acetylcholine receptor M1.
14	ATM_1972_1984	KRSLAFEEGSQST	[1974, 1981, 1983]	[1984]	Q13315	Serine-protein kinase ATM (EC=2.7.11.1) (Ataxia telangiectasia mutated) (A-T, mutated).
15	CDN1B_151_163	IRKRPATDDSSSTQ	[160, 161]	[157, 162]	P46527	Cyclin-dependent kinase inhibitor 1B (Cyclin-dependent kinase inhibitor p27) (p27Kip1).
16	FOXO3_25_37	QSRPRCTWPLQR	[26, 30]	[32]	O43524	Forkhead box protein O3 (Forkhead in rhabdomyosarcoma-like 1) (AF6q21 protein).

No.	ID	Sequence	Ser	Thr	Accession	Description
17	IKKB_686_698	QLMSQPSTASNSL	[689, 692, 695, 697]	[693]	O14920	Inhibitor of nuclear factor kappa-B kinase subunit beta (I-kappa-B-kinase beta) (IkBKB) (IKK-beta) (IKK-B) (EC=2.7.11.10) (I-kappa-B kinase 2) (IKK2) (Nuclear factor NF-kappa-B inhibitor kinase beta) (NFKBKB).
18	LMNA_192_204	DAENRLQTMKEEL	[]	[199]	P02545	Lamin-A/C (70 kDa lamin) (Renal carcinoma antigen NY-REN-32).
19	MYC_51_63	KKFELLPTPPLSP	[62]	[58]	P01106	Myc proto-oncogene protein (c-Myc) (Transcription factor p64).
20	PP2AB_297_309	EPHVTRRTPDYFL	[]	[301, 304]	P62714	Serine/threonine-protein phosphatase 2A catalytic subunit beta isoform (EC 3.1.3.16) (PP2A-beta).
21	RBL2_655_667	GLGRSITSPTTLY	[659, 662]	[661, 664, 665]	Q08999	Retinoblastoma-like protein 2 (130 kDa retinoblastoma-associated protein) (p130) (PRB2) (RBR-2).
22	YAP1_121_133	QHVRAHSSPASLQ	[127, 128, 131]	[]	P46937	65 kDa Yes-associated protein (YAP65).
23	KAP2_92_104	SRFNRRVSVCAET	[92, 99]	[104]	P13861	cAMP-dependent protein kinase type II-alpha regulatory subunit.
24	RS6_228_240	IAKRRRLSSLRAS	[235, 236, 240]	[]	P62753	40S ribosomal protein S6 (Phosphoprotein NP33).
25	ACM1_444_456	KIPKRPGSVHRTP	[451]	[455]	P11229	Muscarinic acetylcholine receptor M1.
26	BAD_112_124	RELRRMSDEFVDS	[118, 124]	[]	Q92934	Bcl2 antagonist of cell death (BAD) (Bcl-2-binding component 6) (Bcl-XL/Bcl-2-associated death promoter) (Bcl-2-like 8 protein).
27	CENPA_1_14	MGPRRRSRKPEAPR	[7]	[]	P49450	Histone H3-like centromeric protein A (Centromere protein A) (CENP-A)(Centromere autoantigen A).
28	FRAP_2443_2455	RTRTDSYSAGQSV	[2448, 2450, 2454]	[2444, 2446]	P42345	FKBP12-rapamycin complex-associated protein (FK506-binding protein 12-rapamycin complex-associated protein 1) (Rapamycin target protein) (RAPT1) (Mammalian target of rapamycin) (mTOR).
29	K6PL_766_778	LEHVTRRTLMDK	[775]	[770, 773]	P17858	6-phosphofructokinase, liver type (EC 2.7.1.11) (Phosphofructokinase1) (Phospho-hexokinase) (Phosphofructo-1-kinase isozyme B) (PFK-B).
30	LMNB1_16_28	GGPTTLPSPTRL	[23, 28]	[19, 20, 25]	P20700	Lamin-B1.
31	NEK2_172_184	FAKTFVGTPTYMS	[184]	[175, 179]	P51955	Serine/threonine-protein kinase Nek2 (EC 2.7.11.1) (NimA-related protein kinase 2) (NimA-like protein kinase 1) (HSPK21).
32	PPR1A_28_40	QIRRRRPTPATLV	[]	[35, 38]	Q13522	Protein phosphatase 1 regulatory subunit 1A (Protein phosphatase inhibitor 1) (IPP-1) (I-1).
33	RBL2_959_971	DRTSRDSSPVMRS	[962, 965, 966, 971]	[961]	Q08999	Retinoblastoma-like protein 2 (130 kDa retinoblastoma-associated protein) (p130) (PRB2) (RBR-2).
34	ADRB2_338_350	ELLCLRSSLKAY	[345, 346]	[]	P07550	Beta-2 adrenergic receptor (Beta-2 adrenoceptor) (Beta-2adrenoreceptor).
35	KCC2G_278_289	VASMMHRQETVE	[280]	[287]	Q13555	Calcium/calmodulin-dependent protein kinase type II gamma chain (EC 2.7.11.17) (CaM-kinase II gamma chain) (CaM kinase II subunit gamma) (CaMK-II subunit gamma).
36	RYR1_4317_4329	VRRLRLTAREAA	[]	[4324]	P21817	Ryanodine receptor 1 (Skeletal muscle-type ryanodine receptor) (RyR1)(RYR-1) (Skeletal muscle calcium release channel).
37	ACM4_456_468	CNATFKKTRHLL	[]	[459, 463]	P08173	Muscarinic acetylcholine receptor M4.
38	BAD_69_81	IRSRHSSYPAGTE	[71, 74, 75]	[80]	Q92934	Bcl2 antagonist of cell death (BAD) (Bcl-2-binding component 6) (Bcl-XL/Bcl-2-associated death promoter) (Bcl-2-like 8 protein).

No.	ID	Sequence	Ser	Thr	Accession	Description
39	COF1_17_29	DMKVRKSSTPEEV	[23, 24]	[25]	P23528	Cofilin-1 (Cofilin, non-muscle isoform) (18 kDa phosphoprotein) (p18).
40	FRAP_2475_2487	VPESIHFIGDGL	[2478, 2481]	[]	P42345	FKBP12-rapamycin complex-associated protein (FK506-binding protein 12-rapamycin complex-associated protein 1) (Rapamycin target protein) (RAPT1) (Mammalian target of rapamycin) (mTOR).
41	KAPCG_192_206	VKGRWTLCGTPEYL	[]	[196, 198, 202]	P22612	cAMP-dependent protein kinase catalytic subunit gamma (EC 2.7.11.11)(PKA C-gamma).
42	MARCS_152_164	KKKKRFSFKKSF	[159, 163]	[]	P29966	Myristoylated alanine-rich C-kinase substrate (MARCKS) (Protein kinaseC substrate, 80 kDa protein, light chain) (PKCSL) (80K-L protein).
43	NEK3_158_170	FACTYVGTPLYVP	[]	[161, 165]	P51956	Serine/threonine-protein kinase Nek3 (EC 2.7. 11.1) (NimA-related protein kinase 3) (HSPK36)
44	PRKDC_2618_2630	TRTQEGSLARWP	[2624, 2626]	[2618, 2620]	P78527	DNA-dependent protein kinase catalytic subunit (DNA-PK catalytic subunit) (DNA-PKcs) (EC=2.7.11.1) (DNPk1) (p460).
45	REL_260_272	KMQLRRPSDQEV	[267, 272]	[]	Q04864	C-Rel proto-oncogene protein (C-Rel protein).
46	ART_025_CXGLRRWSL GGLRRWS	GLRRWSLGLRRWSL	NA	NA	NA	NA
47	KCNA1_438_450	DSDLRRSSTMS	[439, 442, 445, 446, 447, 450]	[448]	Q09470	Potassium voltage-gated channel subfamily A member 1 (Voltage-gatedpotassium channel subunit Kv1.1) (HUKI)(HBK1).
48	SCN7A_898_910	KNGCRRGSSLGQI	[905, 906]	[]	Q01118	Sodium channel protein type 7 subunit alpha (Sodium channel proteintype VII subunit alpha) (Putative voltage-gated sodium channel subunitalpha Nax) (Sodium channel protein cardiac and skeletal muscle subunitalpha).
49	ACM5_494_506	CYALCNRTFRKTF	[]	[501, 505]	P08912	Muscarinic acetylcholine receptor M5.
50	BAD_93_105	FRGRSRAPPNLW	[97, 99]	[]	Q92934	BAD (Bcl-2-binding component 6) (Bcl-XL/Bcl-2-associated death promoter) (Bcl-2-like 8 protein).
51	CSF1R_701_713	NIHLEKKVRRDS	[713]	[]	P07333	Macrophage colony-stimulating factor 1 receptor precursor(EC 2.7.10.1) (CSF-1-R) (Fms proto-oncogene) (c-fms) (CD115 antigen).
52	GPR6_349_361	QSKVPFRSRPSE	[350, 356, 358, 360]	[]	P46095	Sphingosine 1-phosphate receptor GPR6 (G-protein coupled receptor 6).
53	KCNA2_442_454	PDLKKSRSASTIS	[447, 449, 451, 454]	[452]	P16389	Potassium voltage-gated channel subfamily A member 2 (Voltage-gatedpotassium channel subunit Kv1.2) (HBK5) (NGK1) (HUKIV).
54	MARCS_160_172	FKKFKLSGFSFK	[163, 167, 170]	[]	P29966	Myristoylated alanine-rich C-kinase substrate (MARCKS) (Protein kinaseC substrate, 80 kDa protein, light chain) (PKCSL) (80K-L protein).
55	NMDZ1_890_902	SFKRRRSSKDTST	[890, 896, 897, 901]	[900, 902]	Q05586	Glutamate [NMDA] receptor subunit zeta-1 precursor (N-methyl-D-aspartate receptor subunit NR1).
56	PTK6_436_448	ALRERLSSFTSYE	[442, 443, 446]	[445]	Q13882	Tyrosine-protein kinase 6 (EC 2.7.10.2) (Breast tumor kinase)(Tyrosine-protein kinase BRK).
57	SRC_413_425	LIEDNEYARQGA	[]	[420]	P12931	Proto-oncogene tyrosine-protein kinase Src (EC 2.7.10.2) (p60-Src) (c-Src) (pp60c-src).

No. ID	Sequence	Ser	Thr	Accession	Description
58 CAC1C_1974_1986	ASLGRRASFHLEC	[1975, 1981]	[]	Q13936	Voltage-dependent L-type calcium channel subunit alpha- 1C (Voltage-gated calcium channel subunit alpha Cav1.2) (Calcium channel, L type,alpha-1 polypeptide, isoform 1, cardiac muscle).
59 KPB1_1011_1023	QVEFRRLSISAES	[1018, 1020, 1023]	[]	P46020	Phosphorylase b kinase regulatory subunit alpha, skeletal muscleisoform (Phosphorylase kinase alpha M subunit).
60 SRC8_CHICK_423_435	KTPSSPVYQDAVS	[426, 427, 435]	[424]	Q01406	Src substrate protein p85 (p80) (Cortactin).
61 ACM5_498_510	CNRTFRKTFKMLL	[]	[501, 505]	P08912	Muscarinic acetylcholine receptor M5.
62 BCKD_45_57	ERSKTVTSFYNQS	[47, 52, 57]	[49, 51]	O14874	[3-methyl-2-oxobutanoate dehydrogenase [lipoamide]] kinase,mitochondrial precursor (EC 2.7.11.4) (Branched- chain alpha-keto acid dehydrogenase kinase) (BCKDHKIN) (BCKD-kinase).
63 CSK21_355_367	ISSVPTPSPLGPL	[356, 357, 362]	[360]	P68400	Casein kinase II subunit alpha (EC 2.7.11.1) (CK II).
64 GPSM2_394_406	PKLGRRHSMENME	[401]	[]	P81274	G-protein-signaling modulator 2 (Mosaic protein LGN).
65 KCNA3_461_473	EELRKARSNSTLS	[468, 470, 473]	[471]	P22001	Potassium voltage-gated channel subfamily A member 3 (Voltage-gatedpotassium channel subunit Kv1.3) (HPCN3) (HGK5) (HuKIII) (HLK3).
66 MBP_222_234	HFFKNIVTPRTPP	[]	[229, 232]	P02686	Myelin basic protein (MBP) (Myelin A1 protein) (Myelin membrane encephalitogenic protein).
67 NOS3_1171_1183	SRIRTQSFSLQER	[1171, 1177, 1179]	[1175]	P29474	Nitric oxide synthase, endothelial (EC=1.14.13.39) (Endothelial NOS) (eNOS) (EC-NOS) (NOS type III) (NOSIII) (Constitutive NOS) (cNOS).
68 RAB1A_187_199	KSNVKIQSTPVKQ	[188, 194]	[195]	P62820	Ras-related protein Rab-1A (YPT1-related protein).
69 STK6_283_295	SSRRTTLCGTLDY	[283, 284]	[287, 288, 292]	O14965	Serine/threonine-protein kinase 6 (EC 2.7.11.1) (Aurora kinase A)(Aurora-A) (Serine/threonine kinase 15) (Aurora/IPL1-related kinase 1)(Aurora-related kinase 1) (hARK1) (Breast tumor-amplified kinase).
70 CFTR_730_742	EPLERRLSLVPDS	[737, 742]	[]	P13569	Cystic fibrosis transmembrane conductance regulator (CFTR) (cAMP-dependent chloride channel) (ATP-binding cassette transporter sub-family C member 7).
71 MYPC3_268_280	LSAFRRSLAGGG	[269, 275]	[274]	Q14896	Myosin-binding protein C, cardiac-type (Cardiac MyBP-C) (C-protein,cardiac muscle isoform).
72 VASP_271_283	LARRRKATQVGEK	[]	[278]	P50552	Vasodilator-stimulated phosphoprotein (VASP).
73 ADDB_696_708	GSPSKSPSKKKKK	[697, 699, 701, 703]	[]	P35612	Beta-adducin (Erythrocyte adducin subunit beta)
74 BRCA1_1451_1463	EKAULTSQKSSEY	[1457, 1460, 1461]	[1456]	P38398	Breast cancer type 1 susceptibility protein (RING finger protein 53).
75 DCX_49_61	HFDERDKTSRNMR	[57]	[56]	O43602	Neuronal migration protein doublecortin (Lissencephalin-X) (Lis-X)(Doublin).
76 GSUB_61_73	KKPRRKDTPALHI	[]	[68]	O96001	G-substrate.
77 KCNB1_489_501	KWTKRTLSETSSS	[496, 499, 500, 501]	[491, 494, 498]	Q14721	Potassium voltage-gated channel subfamily B member 1 (Voltage-gatedpotassium channel subunit Kv2.1) (h-DRK1).
78 MK10_214_226	AGTSMMPYVVT	[217]	[216, 221, 226]	P53779	Mitogen-activated protein kinase 10 (EC 2.7.11.24) (Stress- activated protein kinase JNK3) (c-Jun N-terminal kinase 3) (MAP kinase p49 3F12).

No.	ID	Sequence	Ser	Thr	Accession	Description
79	NR4A1_344_356	GRRGRLPSKPKQP	[351]	[]	P22736	Nuclear receptor subfamily 4 group A member 1 (Orphan nuclear receptor HMR) (Early response protein NAK1) (TR3 orphan receptor) (ST-59).
80	RAF1_253_265	QRQRSTSTPNVHM	[257, 259]	[258, 260]	P04049	RAF proto-oncogene serine/threonine-protein kinase (EC 2.7.11.1) (Raf-1) (C-RAF) (cRaf).
81	STMN2_90_102	AAGERRKSQEAQV	[97]	[]	Q93045	Stathmin-2 (Protein SCG10) (Superior cervical ganglion-10 protein).
82	CGHB_109_121	QCALCRRSTTDCG	[116]	[117, 118]	P01233	Choriogonadotropin subunit beta precursor (CG-beta) (Chorionic gonadotrophin chain beta).
83	NCF1_296_308	RGAPRRSSIRNA	[303, 304]	[]	P14598	Neutrophil cytosol factor 1 (NCF-1) (Neutrophil NADPH oxidase factor1) (47 kDa neutrophil oxidase factor) (p47- phox) (NCF-47K) (47 kDa autosomal chronic granulomatous disease protein) (Nox organizer 2)(Nox-organizing protein 2) (SH3 and PX domain-containing protein 1A).
84	VTNC_390_402	NQNSRRPSRATWL	[393, 397]	[400]	P04004	Vitronectin precursor (Serum-spreading factor) (S-protein) (V75)[Contains: Vitronectin V65 subunit; Vitronectin V10 subunit;Somatomedin-B].
85	ADDB_706_718	KKKFRTPSFLKKS	[713, 718]	[711]	P35612	Beta-adducin (Erythrocyte adducin subunit beta)
86	C1R_201_213	ASGYISSLEYPRS	[202, 206, 207, 213]	[]	P00736	Complement C1r subcomponent EC=3.4.21.41)
87	ELK1_356_368	LLPHTLTPVLLT	[]	[359, 361, 363, 368]	P19419	ETS domain-containing protein Elk-1.
88	GYS2_1_13	MLRGRSLSVTSLG	[6, 8, 11]	[10]	P54840	Glycogen [starch] synthase, liver (EC 2.4.1.11).
89	KIF11_919_931	LDIPTGTPQRKS	[931]	[923, 925, 926]	P52732	Kinesin-like protein KIF11 (Kinesin-related motor protein Eg5)(Kinesin-like spindle protein HKSP) (Thyroid receptor-interacting protein 5) (TRIP-5) (Kinesin-like protein 1).
90	MP2K1_281_293	GDAAEPPRPRTTP	[]	[286, 292]	Q02750	Dual specificity mitogen-activated protein kinase kinase 1(EC 2.7.12.2) (MAP kinase kinase 1) (MAPKK 1) (ERK activator kinase 1)(MAPK/ERK kinase 1) (MEK1).
91	NTRK3_824_836	LHALGKATPIYLD	[]	[831]	Q16288	NT-3 growth factor receptor precursor (EC 2.7.10.1) (Neurotrophic tyrosine kinase receptor type 3) (TrkC tyrosine kinase) (GP145-TrkC)(Trk-C).
92	RAP1B_172_184	PGKARKKSSCQLL	[179, 180]	[]	P61224	Ras-related protein Rap-1b precursor (GTP-binding protein smg p21B).
93	TAU_524_536	GSRRTPLSPTPP	[525, 527, 531]	[529, 534]	P10636	Microtubule-associated protein tau (Neurofibrillary tangle protein)(Paired helical filament-tau) (PHF-tau).
94	CREB1_126_138	EILSRPSYRKIL	[129, 133]	[]	P16220	cAMP response element-binding protein (CREB).
95	NCF1_321_333	QDAYRRNSVRFLQ	[328]	[]	P14598	Neutrophil cytosol factor 1 (NCF-1) (Neutrophil NADPH oxidase factor1) (47 kDa neutrophil oxidase factor) (p47- phox) (NCF-47K) (47 kDa autosomal chronic granulomatous disease protein) (Nox organizer 2)(Nox-organizing protein 2) (SH3 and PX domain-containing protein 1A).
96	CFTR_761_773	LQARRRQSVLNLM	[768]	[]	P13569	Cystic fibrosis transmembrane conductance regulator (CFTR) (cAMP-dependent chloride channel) (ATP-binding cassette transporter sub-family C member 7).
97	AKT1_301_313	KDGATMKTFCGTP	[]	[305, 308, 312]	P31749	RAC-alpha serine/threonine-protein kinase (EC 2.7.11.1) (RAC-PK-alpha)(Protein kinase B) (PKB) (C-AKT).

No.	ID	Sequence	Ser	Thr	Accession	Description
98	CA2D1_494_506	LEDIKRLTPRFTL	[]	[501, 505]	P54289	Voltage-dependent calcium channel subunit alpha-2/delta- 1 precursor(Voltage-gated calcium channel subunit alpha- 2/delta-1) [Contains: Voltage-dependent calcium channel subunit alpha-2-1; Voltage-dependent calcium channel subunit delta-1].
99	ELK1_410_422	ISVDGLSTPVVLS	[411, 416, 422]	[417]	P19419	ETS domain-containing protein Elk-1.
100	H2B1B_27_40	GKKRRKRSRKESYSI	[33, 37, 39]	[]	P33778	Histone H2B type 1-B (H2B.f) (H2B/f) (H2B.1).
101	KIF2C_105_118_S106 G	EGLRSRSTRMSTVS	[109, 111, 115, 118]	[112, 116]	Q99661	Kinesin-like protein KIF2C (Mitotic centromere-associated kinesin) (MCAK) (Kinesin-like protein 6).
102	MP2K1_287_299	PPRPRTPGRPLSS	[298, 299]	[292]	Q02750	Dual specificity mitogen-activated protein kinase kinase 1(EC 2.7.12.2) (MAP kinase kinase 1) (MAPKK 1) (ERK activator kinase 1)(MAPK/ERK kinase 1) (MEK1).
103	P53_12_24	PPLSQETFSDLWK	[15, 20]	[18]	P04637	Cellular tumor antigen p53 (Tumor suppressor p53) (Phosphoprotein p53)(Antigen NY-CO-13).
104	RB_242_254	AVIPINGSPRTPR	[249]	[252]	P06400	Retinoblastoma-associated protein (PP110) (P105-RB)
105	TLE2_246_258	EPPSPATTPCGKV	[249]	[252, 253]	Q04725	Transducin-like enhancer protein 2 (ESG2).
106	DESP_2842_2854	RSGSRRGSFDATG	[2843, 2845, 2849]	[2853]	P15924	Desmoplakin (DP) (250/210 kDa paraneoplastic pemphigus antigen).
107	NFKB1_330_342	FVQLRRKSDLETS	[337, 342]	[341]	P19838	Nuclear factor NF-kappa-B p105 subunit (DNA-binding factor KBF1) (EBP-1) [Contains: Nuclear factor NF-kappa-B p50 subunit].
108	F263_454_466	NPLMRRNSVTPLA	[461]	[463]	Q16875	6-phosphofructo-2-kinase/fructose-2,6-biphosphatase 3 (6PF-2-K/Fru-2,6-P2ASE brain/placenta-type isozyme) (iPFK-2) (Renal carcinoma antigen NY-REN-56) [Includes: 6- phosphofructo-2-kinase (EC .7.1.105);Fructose-2,6-bisphosphatase (EC 3.1.3.46)].
109	ANDR_785_797	VRMRHLSQEFQWL	[791]	[]	P10275	Androgen receptor (Dihydrotestosterone receptor) (Nuclear receptor subfamily 3 group C member 4).
110	CD27_212_224	HQRKRYRSNKGES	[219, 224]	[]	P26842	CD27 antigen precursor (CD27L receptor) (T-cell activation antigenCD27) (T14) (Tumor necrosis factor receptor superfamily member 7).
111	ERBB2_679_691	QQKIRKYTMRRLL	[]	[686]	P04626	Receptor tyrosine-protein kinase erbB-2 precursor (EC 2.7.10.1)(p185erbB2) (C-erbB-2) (NEU proto-oncogene) (Tyrosine kinase-type cell surface receptor HER2) (MLN 19) (CD340 antigen).
112	H32_3_18	RTKQTARKSTGGKAPR	[11]	[4, 7, 12]	Q71DI3	Histone H3.2 (H3/m) (H3/o).
113	KPCB_19_31_A25S	RFARKGSLRQKNV	[25]	[]	P05771	Protein kinase C beta type (EC 2.7.11.13) (PKC-beta) (PKC-B).
114	MPH6_140_152	EDENGDITPIKAK	[]	[147]	Q99547	M-phase phosphoprotein 6.
115	P53_308_323	LPNNTSSSPQPKKKPL	[313, 314, 315]	[312]	P04637	Cellular tumor antigen p53 (Tumor suppressor p53) (Phosphoprotein p53)(Antigen NY-CO-13).
116	RB_350_362	SFETQRTPRKSNL	[350, 360]	[353, 356]	P06400	Retinoblastoma-associated protein (PP110) (P105-RB)
117	TOP2A_1463_1475	RRKRKPSSTDDSD	[1469, 1471, 1474]	[1470]	P11388	DNA topoisomerase 2-alpha (EC=5.99.1.3) (DNA topoisomerase II, alpha isozyme).
118	E1A_ADE05_212_224	AILRRPTSPVSRE	[219, 222]	[218]	P03255	Early E1A 32 kDa protein.

No. ID	Sequence	Ser	Thr	Accession	Description
119 PLM_76_88	EEGTFRSSIRRLS	[82, 83, 88]	[79]	O00168	Phospholemmann precursor (FXVD domain-containing ion transport regulator 1).
120 KAP3_107_119	NRFTRRASVCAEA	[114]	[110]	P31323	cAMP-dependent protein kinase type II-beta regulatory subunit.
121 ANXA1_209_221	AGERRRKGDVNVF	[]	[216]	P04083	Annexin A1 (Annexin-1) (Annexin I) (Lipocortin I) (Calpactin II)(Chromobindin-9) (p35) (Phospholipase A2 inhibitory protein).
122 CDC2_154_169	GIPIRVYTHEVVTLWY	[]	[161, 166]	P06493	Cell division control protein 2 homolog (EC 2.7.11.22/23) (p34 protein kinase) (Cyclin-dependent kinase 1) (CDK1).
123 ERF_519_531	GEAGGPLTPRRVS	[531]	[526]	P50548	ETS domain-containing transcription factor ERF (Ets2 repressor factor).
124 IF4E_203_215	TATKSGSTTKNRF	[207, 209]	[203, 205, 210, 211]	P06730	Eukaryotic translation initiation factor 4E (eIF-4E) (eIF4E) (mRNA cap-binding protein) (eIF-4F 25 kDa subunit).
125 KPCB_626_639	AENFRFFTRHPPV	[]	[634]	P05771-2	Protein kinase C beta type (EC 2.7.11.13) (PKC-beta) (PKC-B).
126 MPIP1_172_184	FTQRQNSAPARML	[178]	[173]	P30304	M-phase inducer phosphatase 1 (EC=3.1.3.48) (Dual specificity phosphatase Cdc25A).
127 PDE5A_95_107	GTPTRKISASEFD	[102, 104]	[96, 98]	O76074	cGMP-specific 3',5'-cyclic phosphodiesterase (EC 3.1.4.35) (CGB-PDE)(cGMP-binding cGMP-specific phosphodiesterase).
128 RB_774_786	TRPPTLSPIHIP	[780]	[774, 778]	P06400	Retinoblastoma-associated protein (PP110) (P105-RB)
129 VASP_150_162	EHIERRVSNAGGP	[157]	[]	P50552	Vasodilator-stimulated phosphoprotein (VASP).
130 EPB42_241_253	LLNKRKRSVPILR	[248]	[]	P16452	Erythrocyte membrane protein band 4.2 (Erythrocyte protein 4.2)(P4.2).
131 PTN12_32_44	FMRLRRLSTKYRT	[39]	[40, 44]	Q05209	Tyrosine-protein phosphatase non-receptor type 12 (EC 3.1.3.48)(Protein-tyrosine phosphatase G1) (PTPG1) (PTP-PEST).
132 KCNA6_504_516	ANRERRPSYLPTP	[511]	[515]	P17658	Potassium voltage-gated channel subfamily A member 6 (Voltage-gatedpotassium channel subunit Kv1.6) (HBK2).
133 pVASP_150_164	EHIERRV(pS)NAGGPPA	[157]	[]	P50552	Vasodilator-stimulated phosphoprotein (VASP).
134 CDK7_163_175	GSPNRAYTHQVVT	[164]	[170, 175]	P50613	Cell division protein kinase 7 (EC 2.7.11.22) (EC 2.7.11.23) (CDK-activating kinase) (CAK) (TFIIH basal transcription factor complexkinase subunit) (39 kDa protein kinase) (P39 Mo15) (STK1) (CAK1).
135 ESR1_160_172	GGRRERLASTNDKG	[167]	[168]	P03372	Estrogen receptor (ER) (Estradiol receptor) (ER-alpha) (Nuclearreceptor subfamily 3 group A member 1).
136 IKBA_26_38	LDDRHDSDLDSMK	[32, 36]	[]	P25963	NF-kappa-B inhibitor alpha (I-kappa-B-alpha) (IkappaBalpha) (Ikb-alpha) (Major histocompatibility complex enhancer-binding protein MAD3).
137 KS6A1_374_386	QLFRGFSFVATGL	[380]	[384]	Q15418	Ribosomal protein S6 kinase alpha-1 (S6K-alpha 1) (EC=2.7.11.1 (90 kDa ribosomal protein S6 kinase 1) (p90-RSK 1) (pp90RSK1) (p90S6K) (Ribosomal S6 kinase 1) (RSK-1) (MAP kinase-activated protein kinase 1a)
138 MPIP3_208_220	RSGLYRSPMPEN	[209, 214, 216]	[]	P30307	M-phase inducer phosphatase 3 (EC 3.1.3.48) (Dual specificity phosphatase Cdc25C).
139 PDPK1_27_39	SMVRTQTESSTPP	[27, 35, 36]	[31, 33, 37]	O15530	3-phosphoinositide-dependent protein kinase 1 (EC 2.7.11.1) (hPDK1).
140 RB_803_815	NIYISPLKSPYKI	[807, 811]	[]	P06400	Retinoblastoma-associated protein (PP110) (P105-RB)
141 VASP_232_244	GAKLRKVKQEAA	[239]	[]	P50552	Vasodilator-stimulated phosphoprotein (VASP).
142 GBRB2_427_439	SRLRRRASQLKIT	[427, 434]	[439]	P47870	Gamma-aminobutyric acid receptor subunit beta-2 precursor (GABA(A)receptor subunit beta-2).

No. ID	Sequence	Ser	Thr	Accession	Description
143 PYGL_8_20	QEKRRQISIRGIV	[15]	[]	P06737	Glycogen phosphorylase, liver form (EC 2.4.1.1).
144 TY3H_65_77	FIGRRQSLIEDAR	[71]	[]	P07101	Tyrosine 3-monooxygenase (EC 1.14.16.2) (Tyrosine 3-hydroxylase) (TH).

Appendix F

PamGene® Evolve pTyr (PTK) Software Protocol

pTyr Evolve Protocol: 1200PTKlysv03.PS12Protocol	
Step	Action
1	Load disposable (PamChip®4 module at 30°C)
2	Pump 30 cycles, 30 seconds
3	Quick aspirate 5 seconds, pump up 15 seconds
4	Prime fluid2
5	Quick wash (dispense fluid 2 30µl, Quick Wash.Pump 1 cycles 30 sec, Quick Wash/Quick Aspirate 5 sec, Pump Up 15 sec)
6	Quick wash (dispense fluid 2 30µl, Quick Wash.Pump 1 cycles 30 sec, Quick Wash/Quick Aspirate 5 sec, Pump Up 15 sec)
7	Quick wash (dispense fluid 2 30µl, Quick Wash.Pump 1 cycles 30 sec, Quick Wash/Quick Aspirate 5 sec, Pump Up 15 sec)
8	Manual dispense
9	Pump 2 cycles 60 sec
10	Read MultEx filter1: 10msec filter1: 50 msec filter1: 200 msec
11	Read Kinetic MultEx/Read by Cycles MultEx every 5 cycles, filter1: 10 msec filter1: 50 msec filter1: 200 msec Read Kinetic MultEx/Pump 60 cycles 60 sec
12	Quick Aspirate 5 sec PumpUp 60 sec
13	Prime fluid2
14	Quick Wash(Dispense fluid2 30 µl Quick Wash/Pump 1 cycles 60 sec Quick Wash/Quick Aspirate 5 sec PumpUp 60 sec)
15	Dispense fluid2 30 µl
16	Pump 2 cycles 60 sec
17	Read MultEx filter1: 10 msec filter1: 20 msec filter1: 50 msec filter1: 100 msec filter1: 200 msec
18	Quick Aspirate 5 sec PumpUp 60 sec
19	Unload Disposable

Appendix G

PamGene® Evolve pSer/pThr (STK) Software Protocol

pSer/Thr Evolve Protocol: 1300STKlysv08.PS12Protocol	
Step no.	Action
1	Load disposable (PamChip®4 module at 30°C)
2	Pump 30 cycles, 30 seconds
3	Quick aspirate 5 seconds, pump up 15 seconds
4	Prime fluid2
5	Quick wash (dispense fluid 2 30µl, Quick Wash.Pump 1 cycles 30 sec, Quick Wash/Quick Aspirate 5 sec, Pump Up 15 sec)
6	Quick wash (dispense fluid 2 30µl, Quick Wash.Pump 1 cycles 30 sec, Quick Wash/Quick Aspirate 5 sec, Pump Up 15 sec)
7	Quick wash (dispense fluid 2 30µl, Quick Wash.Pump 1 cycles 30 sec, Quick Wash/Quick Aspirate 5 sec, Pump Up 15 sec)
8	Manual dispense
9	Pump 60 cycles 60 sec
10	Quick Aspirate 5 sec PumpUp 60 sec
11	Prime fluid2
12	Quick Wash(Dispense fluid2 30 µl Quick Wash/Pump 1 cycles 60 sec Quick Wash/Quick Aspirate 5 sec PumpUp 60 sec)
13	Quick Wash(Dispense fluid2 30 µl Quick Wash/Pump 1 cycles 60 sec Quick Wash/Quick Aspirate 5 sec PumpUp 60 sec)
14	Quick Wash(Dispense fluid2 30 µl Quick Wash/Pump 2 cycles 60 sec Quick Wash/Quick Aspirate 5 sec PumpUp 60 sec)
15	Manual Dispense
16	Pump 2 cycles 60 sec
17	Read MultEx filter1: 10 msec filter1: 50 msec filter1: 200 msec
18	Read Kinetic MultEx/Read by Cycles MultEx every 5 cycles, filter1: 10 msec filter1: 50 msec filter1: 200 msec Read Kinetic MultEx/Pump 30 cycles 60 sec
19	Quick Aspirate 5 sec PumpUp 60 sec
20	Prime fluid2
21	Quick Wash(Dispense fluid2 30 µl Quick Wash/Pump 1 cycles 60 sec Quick Wash/Quick Aspirate 5 sec PumpUp 60 sec)
22	Dispense fluid2 30 µl
23	Pump 2 cycles 60 sec
24	Read MultEx filter1: 10 msec filter1: 20 msec filter1: 50 msec filter1: 100 msec filter1: 200 msec
25	Unload Disposable

Appendix H

Proteome Profiler Human Phospho-RTK Array Kit

Coordinates	Receptor family	RTK
A1,A2 A23, A24 F1, F2	Reference spots	Reference spots
F23, F24	Negative control	Negative control
B1, B2 B3, B4 B5, B6 B7, B8	Class I: EGFR	EGFR ERBB2/HER2 ERBB3/HER3 ERBB4/HER4
B17, B18 B19, B20	Class II: IR	IR IGF1R
C7, C8 C9, C10 C11, C12 C13, C14 C15, C16	Class III: PDGFR	PDGFR α PDGFR β KIT (SCFR) FLK2 (FLT-3) CSF1R (M-CSFR)
D9, D10 D11, D12 D13, D14	Class IV: VEGFR	VEGFR1 VEGFR2 VEGFR3
B9, B10 B11, B12 B13, B14 B15, B16	Class V: FGFR	FGFR1 FGFR2 α FGFR3 FGFR4
D3, D4 D5, D6 D7, D8	Class VII: NGFR	TRKA TRKB TRKC
C3, C4 C5, C6	Class VIII: HGFR	MET (HGFR) MST1R (MSPR)
D17, D18 D19, D20 D21, D22 D23, D24 E19, E20 E1, E2 E3, E4 E21, E22 E5, E6 E7, E8 F5, F6 E9, E10 E11, E12	Class IX: EPHR	EPHA1 EPHA2 EPHA3 EPHA4 EPHA5 EPHA6 EPHA7 EPHA10 EPHB1 EPHB2 EPHB3 EPHB4 EPHB6
B21, B22 B23, B24 C1, C2	Class X: AXL	AXL DTK (TYRO3) MER
C23, C24 D1, D2	Class XI: TIE	TIE-1 TIE-2
F7, F8	Class XII: RYK	RYK
E15, E16 E17, E18	Class XIII: DDR	DDR1 DDR2
C17, C18	Class XIV: RET	C-RET

Coordinates	Receptor family	RTK
E13, E14	Class XVI: LTK	ALK
C19, C20 C21, C22	Class XVII: ROR	ROR1 ROR2
D15, D16	Class XVIII: MuSK	MuSK

Appendix I

siGENOME SMARTpool siRNA targeting sequences

Gene		SMARTpool construct		
Name	Accession	Catalogue number	Catalogue number	Target sequence
EGFR	NM_201283	M-003114-03	D-003114-32	CCGCAAUUCGAGACGAA
			D-003114-33	CAAAGUGUGUACGGAAUA
			D-003114-34	GUAACAAGCUCACGCAGUU
			D-003114-35	GAGGAAUUAUGUACUACGA
ERBB2	NM_004448	M-003126-04	D-003126-05	GGACGAAUUCGCACAAUG
			D-003126-06	GACGAAUUCGCACAAUGG
			D-003126-07	CUACAACACAGACAGUUU
			D-003126-08	AGACGAAGCAUACGUGAUG
ERBB3	NM_001005915	M-003127-03	D-003127-08	GCAGUGGAUUCGAGAAGUG
			D-003127-22	AGAUUGUCUCACGGGACA
			D-003127-23	GUGGAUUCGAGAAGUGACA
			D-003127-24	GCGAUGCUGAGAACCAUA
ERBB4	NM_001042599	M-003128-03	D-003128-06	GCAGGAAACAUCUAUUA
			D-003128-07	GAUCACAACUGCUCUUA
			D-003128-09	GCUCUGGAGUGUAUACA
			D-003128-22	GGAAUCCAACGCGAGAAA
INSR	NM_001079817	M-003014-02	D-003014-05	GGAAGACGUUUGAGGAUUA
			D-003014-06	GAACAAGGCCUCCGAGAGU
			D-003014-07	GGAGAGACCUUGGAAUUG
			D-003014-08	GGACGGAACCCACCUAUUU
IGF1R	NM_000875	M-003012-05	D-003012-06	GGCCAGAAUUGGAGAAUUA
			D-003012-08	GCAGACACCUACAACAUC
			D-003012-17	GGACUCAGUACGCCGUUA
			D-003012-18	GUGGGAGGUUGGUGAUUA
INSRR	NM_014215	M-005332-00	D-005332-01	CCAAUUGGCUGGUGAGAUU
			D-005332-02	GGACAGCCUCAUCAAGGA
			D-005332-03	GAACAAGGCUGAGAUCAAC
			D-005332-04	GAGCAGAUUCGAUAAUCC
PDGFRA	NM_006206	M-003162-04	D-003162-08	CAUCAGAGCUGGAUCUAGA
			D-003162-09	GGCCUUAUUUUAUUGGAU
			D-003162-10	GAGCUUACCUAUAAGUU
			D-003162-23	CCUCUAGGAUUGACGGAUU
PDGFRB	NM_002609	M-003163-03	D-003163-05	GAAAGGAGACGUCAAUAU
			D-003163-06	GGAAUGAGGUGGUCAACU
			D-003163-07	CAACGAGUCUCCAGUGCUA
			D-003163-09	UGACAACGACUAUAUCAUC
KIT	NM_001093772	M-003150-02	D-003150-05	AAACACGGCUUAAGCAAUU
			D-003150-06	GAACAGAACCUACUGAU
			D-003150-07	GGGAAGCCUCAUGUCUGA
			D-003150-08	GCAAUCCAUAUUAUGUGUU
CSF1R	NM_005211	M-003109-03	D-003109-06	CAACAACGUACCUUCCAA
			D-003109-07	CCACGCAGCUGCCUACAA
			D-003109-09	GGAGAGAGCGGGACUAUAC
			D-003109-22	GGACAUUCAACACGGCUC
FLT3	NM_004119	M-003137-02	D-003137-05	GAAGGCAUCUACACCAUUA
			D-003137-06	GAAGGAGUCUGGAUAGAA
			D-003137-07	GAAUUUAAGUCGUGUGUUC
			D-003137-08	GGAAUCAUUUCACUCUGA

Name	Accession	Catalogue number	Catalogue number	Target sequence
FLT1	NM_002019	M-003136-03	D-003136-05	GAGCAAACGUGACUUUUU
			D-003136-06	CCAAUUGGGUUUCAUGUUA
			D-003136-07	CAACAAGGAUGCAGCACUA
			D-003136-09	GCCGGAAGUUGUAUGGUUA
KDR	NM_002253	M-003148-01	D-003148-05	GGAAUUCUCUUGCAAGCUA
			D-003148-06	GAUUACAGAUCUCCAUUUA
			D-003148-07	GCAGACAGAUCUACGUUUG
			D-003148-08	GCGAUGGCCUCUCUGUAA
FLT4	NM_002020	M-003138-02	D-003138-05	GCAAGAACGUGCAUCUGUU
			D-003138-06	GCGAAUACCGUCCUACGA
			D-003138-07	GAAGACAUUUGAGGAAUUC
			D-003138-08	GAGCAGCCAUUCAACA
FGFR1	NM_023108	M-003131-03	D-003131-09	AUUCAAACCGACCACAGA
			D-003131-22	CCACAGAAUUGGAGGCUAC
			D-003131-23	CCGCACAUCAGUGGCUAA
			D-003131-24	ACGUGGAGUUCAUGUGUAA
FGFR2	NM_000141	M-003132-04	D-003132-05	CCAAUUCUCUACACCAGAA
			D-003132-06	GAACAGUAUUCACCUAGUU
			D-003132-07	GGCCAACACUGUCAAGUUU
			D-003132-08	GUGAAGAUUGUAGAAAGAU
FGFR3	NM_000142	M-003133-01	D-003133-05	UGUCGGACCUGGUGUCUGA
			D-003133-06	GCAUCAAGCUGCGGAUCA
			D-003133-07	GGACGGCACACCCUACGUU
			D-003133-08	UGCACAACCUAGCUACUA
FGFR4	NM_002011	M-003134-02	D-003134-05	GCACUGGAGUCUCGUGAUG
			D-003134-09	CCUCGAAUAGGCACAGUUA
			D-003134-10	AUAACUACCGCUAGAUGU
			D-003134-11	GCAUUCGGCUGCGCAUCA
PTK7	NM_152881	M-003167-03	D-003167-09	GAGCAUAGUGGGCUGUAUU
			D-003167-10	ACACUUCGUUGCCACAUUG
			D-003167-11	GCGGUAACUGCCUGGUCA
			D-003167-25	ACGUGGUAGUAGCGAGGUA
NTRK1	NM_001007792	M-003159-02	D-003159-05	GGACAACCCUUCGAGUUC
			D-003159-06	CCAGUGACCUCACAGGAA
			D-003159-07	CCACAAUACUUCAGUGAUG
			D-003159-08	GAAGAGUGGUCUCGGUUC
NTRK2	NM_001018064	M-003160-02	D-003160-05	GAACAGAAGUAAUGAAAUC
			D-003160-06	GUAAUGCUGUUUCUGCUUA
			D-003160-07	GCAAGACACUCCAAGUUUG
			D-003160-08	GAAAGUCUAUCAUUAUC
NTRK3	NM_002530	M-003161-02	D-003161-08	GAAUAUCACUCCAUCAC
			D-003161-21	ACGCUGAGUCUUCGGAAU
			D-003161-22	UUUCCAGAGAGCACGGAUA
			D-003161-23	AAGUGUAGUUUCUGGCGGA
ROR1	NM_001083592	M-003171-02	D-003171-08	GAGAAUGUCCUGUGUCAA
			D-003171-21	UGACUUGUGUCGCGAUGAA
			D-003171-22	CGGAUUAGAAACCUCGACA
			D-003171-23	GCGUGGCAACAACGGCAA
ROR2	NM_004560	M-003172-01	D-003172-05	GGAACUCGUCGUCGCCUUA
			D-003172-06	GCAGGUGCCUCCUGAUG
			D-003172-07	GCAAUGUGCUAGUGUACGA
			D-003172-08	GAAGACAGAAUUGGUUCA
MUSK	NM_005592	M-003158-01	D-003158-05	GAAGAAGCCUCGCGAGUA
			D-003158-06	GUAAUAAUCUCCAUCAUGU
			D-003158-07	GGAAUGAACUGAAAGUAGU
			D-003158-08	GAGAUUCCUGGACUAGAA

Name	Accession	Catalogue number	Catalogue number	Target sequence
MET	NM_000245	M-003156-02	D-003156-09	GAAGAU CAGUUUCCUAAUU
			D-003156-10	CCAGAGACAUGUAUGAUAA
			D-003156-11	GAACAGAAUCACUGACAUAA
			D-003156-12	GAAACUGUAUGCUGGAUGA
MST1R	NM_002447	M-003157-04	D-003157-10	GUGGAGCGCUGUUGUGAAU
			D-003157-11	GACAGGGAGUACUUAUGUG
			D-003157-12	CGACCCACCUUCAGAGUAC
			D-003157-13	UAGAGGAGUUUGAGUGUGA
AXL	NM_001699	M-003104-03	D-003104-06	GAAAGAAGGAGACCCGUUA
			D-003104-07	CCAAGAAGAUUCUACA AUGG
			D-003104-08	GGAACUGCAUGCUGAAUGA
			D-003104-09	GAAGGAGACCCGUUAUGGA
TYRO3	NM_006293	M-003183-02	D-003183-06	ACGCUGAGAUUUACAACUA
			D-003183-07	GGAUUGCCUCCUUUGUGAAA
			D-003183-08	GAGAGGAACUACGAAGAUC
			D-003183-09	GCGCAUCGAGGCCACAUUG
MERTK	NM_006343	M-003155-02	D-003155-05	GAACUUACCUUACAUAGCU
			D-003155-06	GGACCUGCAUACUUA CUUA
			D-003155-21	GAGAUUUAGCUGCUCGAAA
			D-003155-22	GAUUUACAGUGGCGAUUUAU
TIE1	NM_005424	M-003179-02	D-003179-06	GGGACAGCCUCUACCCUUA
			D-003179-07	GAAGUUCUGUGCAAAUUGG
			D-003179-08	CAACAUUGGCCUCAGAACUG
			D-003179-21	UCGAAACUGUGACGAUGAA
TEK	NM_000459	M-003178-03	D-003178-05	GAAAGAAUAUGCCUCCAAA
			D-003178-07	UGAAGUACCUGAUUUCUA
			D-003178-08	CGAAAGACCUACGUGAAUA
			D-003178-09	GUGCAGAACUCUACGAGAA
EPHA1	NM_005232	M-003115-03	D-003115-01	AGGAAGUUACUCUGAUGGA
			D-003115-02	AGAAAGAACCAGGCAACU
			D-003115-04	AGACUGUGGCCAUUAAGAC
			D-003115-09	GCGCAUUCUUUGCAGUAUU
EPHA2	NM_004431	M-003116-02	D-003116-06	GCAGCAAGGUGCAGGAAUU
			D-003116-08	GAAGUUCACUACCGAGAUC
			D-003116-21	UGAAUGACAUGCCGUAUCUA
			D-003116-22	GCAACGUGAUGUCUGGCCGA
EPHA3	NM_182644	M-003117-03	D-003117-05	GAUCGGACCUCCAGAAAUA
			D-003117-06	GAACUCAGCUCAGAAGAUU
			D-003117-08	GAGCAUCAGUUUACAAGA
			D-003117-09	AAAUUGGGUGGAAUAUA
EPHA4	NM_004438	M-003118-02	D-003118-05	GGUCUGGGAUGAAGUAUUU
			D-003118-07	GAACUUGGGUGGAUAGCAA
			D-003118-21	GCAAUUGCCUAUCGUAAA
			D-003118-22	UGUUGAAUGCGAACGAAUA
EPHA5	NM_182472	M-005315-03	D-005315-01	GGAAAGACGUGUCAUAUUA
			D-005315-02	GAGAAUGGCUCUUUAGAU
			D-005315-03	GAACAGCCUUAAGAAUG
			D-005315-20	UGGACAAGCUGAUACGUAA
EPHA6	NM_173655	M-005313-03	D-005313-01	GGAAUAUACUGGUCAAUAG
			D-005313-03	AAACAUCAUUCGCCUAGAA
			D-005313-04	CCACAUGGAUCGGCAAAGA
			D-005313-05	GAUCCAGUUGCCAUUAAA
EPHA7	NM_004440	M-003119-02	D-003119-06	CUAGAUGCCUCCUGUAUUA
			D-003119-07	AGAAGAAGGUUAUCGUUUA
			D-003119-08	UAGCAAAGCUGACCAAGAA
			D-003119-21	AGACUGGAUUAGAGGAUAA

Name	Accession	Catalogue number	Catalogue number	Target sequence
EPHA8	NM_001006943	M-003120-03	D-003120-09	GCGCGUCUAUGCUGAGAUC
			D-003120-22	GGGACACACCCAAGAUGUA
			D-003120-23	ACACGUACCAGGUUUGCAA
			D-003120-24	UCUACUACCUGGAGUCGGA
EPHA10	NM_173641	M-005325-01	D-005325-13	GGACUGCACUGCCAAGUAA
			D-005325-14	GCGGGUACCUGCAAGGAGA
			D-005325-15	GUAAUGGGUGGGAGGAGAU
			D-005325-16	UGGGUGAGCGCAAGAUGAA
EPHB1	NM_004441	M-003121-02	D-003121-05	GCGAU AAGCUCCAGCAUUA
			D-003121-06	GAAACGGGCUUUAUGCAA
			D-003121-07	GGAUGAAGAUCUACA UUGA
			D-003121-08	GCACGUCUCUGUCAACAUC
EPHB2	NM_017449	M-003122-03	D-003122-07	GGAAAGCAAUGACUGUUCU
			D-003122-08	CGGACAAGCUGCAACACUA
			D-003122-25	GCUUUAACACGGUGGACGA
			D-003122-26	CCAAAUUGUCAACACGCUA
EPHB3	NM_004443	M-003123-02	D-003123-09	GGAAUGAAGGUUUUAUUG
			D-003123-10	GAUCCUACCUCACCAGUU
			D-003123-11	GAAGACCUGCUCGUAUUG
			D-003123-12	CACAAUAACUUCUACCGUG
EPHB4	NM_004444	M-003124-02	D-003124-05	GGACAAACACGGACAGUAU
			D-003124-06	GUACUAAGGUCUACAUCGA
			D-003124-07	GGAGAGAAGCAGAAUUAUC
			D-003124-08	GCCAAUAGCCACUCUAACA
EPHB6	NM_004445	M-003125-02	D-003125-05	GGAAGUCGAUCCUGCUUUAU
			D-003125-06	GGACCAAGGUGGACACAAU
			D-003125-07	UGUGGGAAGUGAUGAGUUA
			D-003125-08	CGGGAGACCUACCCUUU
RET	NM_020630	M-003170-02	D-003170-05	GCAAAGACCUAGGAGAAGAU
			D-003170-06	GCACACGGCUGCAUGAGAA
			D-003170-08	UUAAAUGGAUGGCAAUUGA
			D-003170-21	GCGAGGAGAU GUACCGCCU
RYK	NM_002958	M-003174-03	D-003174-05	GAAAGAUUGGUUACCGAAUA
			D-003174-08	GGUGAAGGAUUAUGCAAUA
			D-003174-09	CGAAGUCCAAGGUUGAAUA
			D-003174-22	AGUAAUAUUUCUGUAGCA
DDR1	NM_013994	M-003111-04	D-003111-08	UGAAAGAGGUGAAGAUCAU
			D-003111-09	GGGACACCCUUUGCUGGUA
			D-003111-10	GAAUGUCGCUUCCGCGGUG
			D-003111-24	UGGUUACUCUUCAGCGAAA
DDR2	NM_006182	M-003112-04	D-003112-06	GAACGAGAGUGCCACCAAU
			D-003112-09	GACUACGAUCGCAUCUUU
			D-003112-23	GAUCAAUACAGUCGGGAU
			D-003112-24	AGGUCAUGGCAUCGAGUUU
ROS1	NM_002944	M-003173-01	D-003173-05	GAGGAGACCUUCUACUUA
			D-003173-06	UUACAGAGGUUCAGGAUUA
			D-003173-07	GAACAAACCUAAGCAUGAA
			D-003173-08	GAAAGAGCACUUCAAAUAA
AATK	NM_001080395	M-005301-03	D-005301-02	GUACAGAGAGGACUACUUC
			D-005301-03	GGUACGAGGUGAUGCAGUU
			D-005301-04	UCAGUGGCCUCAACGAGAA
			D-005301-05	GCAAGUACAGAGAGGACUA
LMTK2	NM_014916	M-003149-02	D-003149-05	GAAAUUCUCUCAACUGAUG
			D-003149-06	GCAGAGGUCUUCACACUUU
			D-003149-07	UAAAU GAUCUUCAGACAGA
			D-003149-21	CGGCGAUGACUUCGAGACA

Name	Accession	Catalogue number	Catalogue number	Target sequence
LMTK3	NM_001080434	M-005338-03	D-005338-01	GAACAGCGAGCAGAUCAAA
			D-005338-05	AGAAGACGCCCGAGAGUUG
			D-005338-06	GCAAGAUGGUCUCCUCCA
			D-005338-07	CGAGAUGCCACGACUUAUC
LTK	NM_206961	M-003152-02	D-003152-06	GUGGCAACCUAACACUGA
			D-003152-07	GGAGCUAGCUGUGGAU AAC
			D-003152-08	GCAAGUUUCGCCAUCAGAA
			D-003152-21	CCAGCAUCUUGGAGCGUCU
ALK	NM_004304	M-003103-02	D-003103-05	GACAAGAUCCUGCAGAAUA
			D-003103-06	GGAAGAGUCUGGCAGUUGA
			D-003103-07	GCACGUGGCUCGGGACAUU
			D-003103-09	GGUCAUAGCUCCUUGGAAU
STYK1	NM_018423	M-003113-01	D-003113-05	CCUAGAAGCUGCCAUUAAA
			D-003113-06	GAUUAGGCCUGGCUUAUGA
			D-003113-07	CCCAGUAGCUGCACACAU A
			D-003113-08	GGUGGUACCUGAACUGUAU